JOHANNES GUTENBERG
UNIVERSITÄT MAINZ

JG|U

The Power of Factorization: Resummation of Super-Leading Logarithms & Weak Annihilation Amplitudes

Dissertation zur Erlangung des Grades

Doktor der Naturwissenschaften

am Fachbereich Physik, Mathematik und Informatik der
Johannes Gutenberg-Universität in Mainz

Michel Stillger

geboren in Hadamar, Deutschland

Mainz, den 29.08.2024

The Power of Factorization: Resummation of Super-Leading Logarithms & Weak Annihilation Amplitudes

Betreuer und erster Gutachter:	Prof. Dr. Matthias Neubert	(JGU Mainz)
Zweiter Gutachter:	Prof. Dr. Stefan Weinzierl	(JGU Mainz)
Dritter Gutachter:	Prof. Dr. Gavin Salam	(University of Oxford)
Tag der mündlichen Prüfung:	10. Februar 2025	
Prüfungskommission:	Prof. Dr. Matthias Neubert	(JGU Mainz)
	Prof. Dr. Stefan Weinzierl	(JGU Mainz)
	Prof. Dr. Gavin Salam	(University of Oxford)
	Prof. Dr. Lucia Masetti	(JGU Mainz)
	J-Prof. Dr. Jamir Marino	(JGU Mainz)
Prüfungsvorsitz:	Prof. Dr. Peter Spichtinger	(JGU Mainz)

Abstract

Factorization of physics associated with different scales is a powerful tool that enhances our understanding of high-energy processes. This thesis applies this concept within the framework of soft-collinear effective theory (SCET) to two different scenarios.

In the first part, a factorization theorem for non-global observables is derived, consisting of a hard function that captures physics at the high scale Q of the order of the partonic center-of-mass energy, convoluted with a low-energy matrix element that describes physics relevant at the soft veto scale Q_0. On the example of gap-between-jet cross sections, the leading double-logarithmic corrections, known as super-leading logarithms, are resummed to all orders in perturbation theory by solving the renormalization-group equation of the hard function. It is shown that they give sizable contributions to partonic $2 \to 2$ scattering processes, but play a subdominant role for vector or Higgs boson production in association with one or no jet. In a second step, the analysis is extended to also include the imaginary parts of the large logarithms. We demonstrate that this "Glauber series", which in the low-energy effective theory arises from Glauber-gluon exchanges between initial-state partons and collinear emissions from these partons, is parametrically suppressed with respect to the leading double-logarithmic corrections. Numerically, it suffices to consider up to four such exchanges to capture the relevant contribution to the cross section. For large N_c, we resum the Glauber series in closed form.

In the second part, we study weak annihilation contributions to exclusive non-leptonic B-meson decay amplitudes. By performing a systematic two-step matching of the relevant operators in the weak effective Hamiltonian on SCET-2, we identify several new partially endpoint-divergent contributions and so far unknown four- and five-particle distribution amplitudes of the B meson. We show how the endpoint divergences cancel between the standard QCD factorization contributions and some of these newly discovered ones. Therefore, this work establishes a subleading power factorization theorem for weak-annihilation amplitudes.

Zusammenfassung

Die Faktorisierung von Physik, die mit unterschiedlichen Skalen verknüpft ist, stellt ein leistungsfähiges Werkzeug zur Verbesserung unseres Verständnisses von Hochenergieprozessen dar. Diese Arbeit wendet dieses Konzept im Rahmen der soft-kollinearen effektiven Theorie (SCET) auf zwei verschiedene Szenarien an.

Im ersten Teil wird ein Faktorisierungstheorem für nicht-globale Observablen hergeleitet. Dieses besteht aus einer harten Funktion, die die Physik an der hohen Skala Q, welche von der Größenordnung der partonischen Schwerpunktsenergie ist, erfasst, gefaltet mit einem Niederenergiematrixelement, das die Physik an der soften Veto-Skala Q_0 beschreibt. Am Beispiel von Gap-between-Jet-Wirkungsquerschnitten werden die führenden Doppellogarithmen, bekannt als "super-leading logarithms", durch die Lösung der Renormierungsgruppengleichung der harten Funktion zu allen Ordnungen in Störungstheorie resummiert. Es wird gezeigt, dass sie nicht zu vernachlässigende Beiträge zu partonischen $2 \to 2$ Streuungsprozessen geben, aber eine untergeordnete Rolle bei der Produktion von Vektor- oder Higgs-Bosonen in Verbindung mit einem oder keinem Jet spielen. Im zweiten Schritt wird die Analyse um die Imaginärteile der großen Logarithmen erweitert. Wir zeigen, dass diese "Glauber-Reihe", die in der Niederenergietheorie durch Glauber-Gluon-Austausche zwischen Partonen im Anfangszustand und kollinearen Emissionen von diesen entsteht, relativ zu den führenden doppel-logarithmischen Korrekturen parametrisch unterdrückt ist. Numerisch reicht es aus, die ersten vier solcher Austausche zu betrachten, um den relevanten Beitrag zum Wirkungsquerschnitt zu erfassen. Für große N_c resummieren wir die Glauber-Reihe in geschlossener Form.

Im zweiten Teil untersuchen wir "Weak-Annihilation-Beiträge" zu exklusiven nicht-leptonischen B-Meson-Zerfallsamplituden. Durch ein systematisches, zweistufiges Matching der relevanten Operatoren im schwachen effektiven Hamiltonian auf SCET-2 identifizieren wir mehrere neue, teilweise endpunkt-divergente Beiträge und bisher unbekannte vier- und fünf-Teilchen-Verteilungsamplituden des B-Mesons. Wir zeigen, wie sich die Endpunkt-Divergenzen zwischen den bekannten QCD-Faktorisierungsbeiträgen und einigen der neu entdeckten Beiträgen aufheben. Dadurch etabliert diese Arbeit ein Faktorisierungstheorem in nächstführender Ordnung für exklusive nicht-leptonischen B-Meson-Zerfallsamplituden.

List of Publications

This thesis is mostly based on the following publications

[1] T. Becher, M. Neubert, D.Y. Shao and M. Stillger, *Factorization of Non-Global LHC Observables and Resummation of Super-Leading Logarithms*, *JHEP* **12** (2023) 116 [2307.06359],

[2] P. Böer, M. Neubert and M. Stillger, *Glauber Phases in Non-Global LHC Observables: Resummation for Quark-Initiated Processes*, *JHEP* **10** (2023) 075 [2307.11089],

[3] P. Böer, P. Hager, M. Neubert, M. Stillger and X. Xu, *Glauber Phases in Non-Global LHC Observables: Resummation for Gluon-Initiated Processes*, *JHEP* **02** (2024) 109 [2311.18811],

[4] P. Böer, P. Hager, M. Neubert, M. Stillger and X. Xu, *Renormalization-Group Improved Resummation of Super-Leading Logarithms*, *JHEP* **08** (2024) 035 [2405.05305],

[5] P. Böer, P. Hager, M. Neubert, M. Stillger and X. Xu, *Resummation of Glauber Phases in Non-Global LHC Observables for Large N_c*, *JHEP* **08** (2024) 036 [2407.01691],

and work to appear

[6] P. Böer, M. Neubert and M. Stillger, *in preparation*.

Contents

Part II: Weak Annihilation Amplitudes in Non-Leptonic B-Meson Decays

Epilogue

Chapter 1

Introduction

The progression of modern physics is marked by a dynamic interplay between theoretical advancements and experimental discoveries. With the High-Luminosity Large Hadron Collider (HL-LHC) starting to operate in the near future, experimental measurements will reach unprecedented precision. Therefore, theorists are compelled to refine their models and enhance the accuracy of their predictions to keep pace.

A powerful tool for refining theoretical predictions are effective field theories (EFTs), as they separate physics at different energy (length) scales. This scale separation goes under the name of *factorization* and allows one to distinguish the ultraviolet (UV) behavior of a theory, associated with high energy scales, from its infrared (IR) behavior, linked to low energy scales. In the "standard" EFT approach, heavy fields are systematically integrated out, retaining only the relevant light degrees of freedom. This results in a simplified theory that accurately describes low-energy phenomena while including UV corrections through higher-dimensional operators suppressed by the heavy mass scale.

The prime example of an EFT frequently used in high-energy physics is SMEFT. Here, the standard model of particle physics (SM) is considered to be an EFT of an unknown UV theory and is extended by higher-dimensional operators compatible with the $SU(3)_c \times SU(2)_L \times U(1)_Y$ symmetry group. The Wilson coefficients of these operators need to be determined either from fits to experimental data or by matching to an UV model. This allows, for example, for the description of Majorana neutrino masses by the so-called Weinberg operator. In contrast, considering the SM as UV theory and working at low energies, beta decays in nuclear physics can be described by Fermi theory. Integrating out the heavy W boson results in flavor changing four-fermion operators, describing these types of decays on a partonic level. However, the application of EFTs is not limited to particle physics. General relativity is nowadays considered as an EFT of an unknown quantum theory of gravity and BCS theory in solid-state physics, an effective theory for phonons, describes superconductivity.

While many EFTs, including the aforementioned ones, assume that UV physics can be completely integrated out, this is not always feasible for high-energy processes. For instance, outgoing partons in colliders have small virtualities but still carry large energies comparable to the center-of-mass energy. In such cases, the EFT framework can still be used to separate physics at different energy scales. The appropriate theory for this is soft-collinear effective theory (SCET), which will be applied to collider and B physics in this thesis.

This thesis is structured as follows: First, we introduce the basic concepts of SCET as an effective theory of quantum chromodynamics (QCD).[1] In Part I this EFT is then applied to derive a factorization theorem for non-global observables at hadron colliders and to resum appearing large logarithms. Part II is dedicated to the study of subleading power corrections to non-leptonic B-meson decay amplitudes, in particular to weak annihilation contributions.

[1] It has also been successfully applied to quantum electrodynamics (QED) and gravity.

Soft-Collinear Effective Theory

Chapter 2

An EFT on the Light Cone

Many high-energy processes feature several widely separated scales. At particle colliders, the highest scale Q is typically associated with the partonic center-of-mass energy $\sqrt{\hat{s}}$, while for B physics it is given by the b-quark mass m_b. Lower energy scales are characterized through a power-counting parameter λ as $\lambda^a Q$ with $a > 0$ and are related to experimental vetoes on radiation, small transverse momenta, the QCD confinement scale Λ_{QCD}, etc. As the expansion parameter for the perturbative series of an observable for such processes is $\alpha_s \ln \lambda \sim 1$, with α_s the strong coupling, large logarithms $\ln \lambda \gg 1$ cause the breakdown of perturbation theory. An EFT description separating different scales allows one to resum these large logarithms using renormalization-group (RG) methods. This is discussed in great detail for non-global observables in Part I.

Particles in high-energy processes often carry momenta of virtuality Q^2, it is thus not possible to remove physics at this scale by integrating out heavy fields in the standard EFT approach. However, assigning different scalings to these momenta and performing an expansion in λ, it is possible to achieve the desired scale separation. On a technical level, this procedure is called *method of regions*. It was proposed by Beneke and Smirnov over 25 years ago in [7] and allows for an asymptotic expansion of Feynman integrals with multiple distinct scales. Even though it has been applied successfully in many cases, only recently a first proof for the specific scenario of an "on-shell expansion" was presented in [8]. The general idea is to expand the integrand of a Feynman integral for different λ scalings of the loop momenta. The integral for each of these "regions" is often simpler to evaluate and – more importantly – depends only on a *single* scale. Evaluating them in $d = 4 - 2\epsilon$ dimensions and adding up the contributions from all regions, one recovers the full result of the UV theory expanded order by order in λ. Some examples can be found in [9].

As many particles in high-energy processes have (nearly) light-like momenta, it is convenient to decompose all momenta p in a light-cone basis

$$p^\mu = n\cdot p\,\frac{\bar{n}^\mu}{2} + \bar{n}\cdot p\,\frac{n^\mu}{2} + p_\perp^\mu \equiv (n\cdot p, \bar{n}\cdot p, p_\perp^\mu)\,, \tag{2.1}$$

with light-like vectors ($n^2 = \bar{n}^2 = 0$)

$$n^\mu = (1, \boldsymbol{n})\,, \qquad\qquad \bar{n}^\mu = (1, -\boldsymbol{n})\,, \tag{2.2}$$

such that $n\cdot\bar{n} = 2$ and $p_\perp$ is transverse to n and $\bar{n}$. When applying the method of regions, one encounters momenta with different scaling in their light-cone components as well as with different virtuality. The most relevant virtualities are *hard* with $p^2 \sim Q^2$, *(anti-)hard-collinear* with $p^2 \sim \lambda^2 Q^2$ and *soft* or *(anti-)collinear* both with $p^2 \sim$

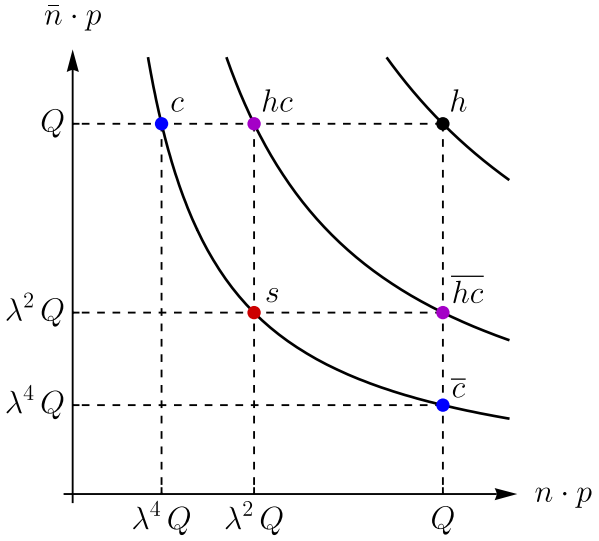

Figure 2.1: Modes in SCET. (Anti-)collinear modes have the same virtuality as soft ones, while (anti-)hard-collinear modes have a higher virtuality.

$\lambda^4 Q^2$.[1] Their light-cone components scale as follows

$$\begin{aligned} p_h^\mu &\sim (1,1,1)\,Q\,, \qquad & p_{hc}^\mu &\sim (\lambda^2,1,\lambda)\,Q\,, \qquad & p_c^\mu &\sim (\lambda^4,1,\lambda^2)\,Q\,, \\ & & p_{\overline{hc}}^\mu &\sim (1,\lambda^2,\lambda)\,Q\,, \qquad & p_{\bar{c}}^\mu &\sim (1,\lambda^4,\lambda^2)\,Q\,, \\ & & & & p_s^\mu &\sim (\lambda^2,\lambda^2,\lambda^2)\,Q\,. \end{aligned} \tag{2.3}$$

From here on we drop the hard scale Q in such relations. Figure 2.1 shows the position of these modes in the $(n\cdot p, \bar{n}\cdot p)$ plane. Modes with the same virtuality lie on a hyperbola.

SCET was constructed to reproduce the method-of-regions results by introducing separate fields for each mode. In general, one needs to include all modes in (2.3) (and maybe more) to reproduce the full result of the UV theory, see the example in Section 2 of [11]. However, in many physical processes not all of them contribute. The effective theory, called *SCET-1*, developed in the seminal papers [12–15] contains only hard-collinear and soft modes, i.e. modes with different virtuality. This theory is appropriate to describe e.g. Drell-Yan production close to the threshold, as soft modes have a smaller virtuality [16]. In contrast, in exclusive B-meson decays, studied in Part II, both the collinear final-state mesons and the soft spectator quark have virtuality $\Lambda_{\rm QCD}^2$. The appropriate theory containing soft and collinear modes is called *SCET-2*. The situation for non-global observables at hadron colliders is more complicated, as will be discussed in Part I.

[1] Depending on the process under consideration, many more/different modes can contribute. For example, Glauber modes with scaling $p_g^\mu \sim (\lambda^4,\lambda^2,\lambda^2)$ can mediate interactions between collinear and soft modes which otherwise is forbidden by momentum conservation [10].

2.1 Field Decomposition

Combining (hard-)collinear and anti-(hard-)collinear modes yields hard ones, which are integrated out in the EFT. This implies that there cannot be any interactions between different (hard-)collinear sectors and they can be constructed separately. Therefore, the construction of SCET with one (hard-)collinear direction is explained in the following.

As explained above, the effective theory must contain separate fields for all relevant modes. The only exception are hard modes, their effect is captured by non-trivial Wilson coefficients of operators. We start by constructing SCET-1 and postpone the construction of SCET-2 to the next chapter.

For SCET-1 the relevant decompositions for fermions and gauge bosons read

$$\psi(x) \to \xi_{hc}(x) + \eta_{hc}(x) + q_s(x)\,, \qquad A(x) \to A_{hc}(x) + A_s(x)\,. \tag{2.4}$$

We use the notation $A \coloneqq A^a\,t^a$ with t^a a generator in the fundamental representation of $SU(N_c)$ normalized to $\mathrm{tr}(t^a\,t^b) = T_F\,\delta^{ab}$ with $T_F = \frac{1}{2}$. Derivatives of these fields scale like the associated momenta, i.e.

$$\partial^\mu \phi_{hc} \sim (\lambda^2, 1, \lambda)\,\phi_{hc}\,, \qquad \partial^\mu \phi_s \sim (\lambda^2, \lambda^2, \lambda^2)\,\phi_s\,, \tag{2.5}$$

where $\phi_{hc} \in \{\xi_{hc}, \eta_{hc}, A_{hc}\}$ and $\phi_s \in \{q_s, A_s\}$. As derivatives $\bar{n}\cdot\partial\phi_{hc}$ are $\mathcal{O}(1)$ in the power expansion, one has to include an arbitrary number of them when constructing operators in the effective theory. This yields non-local operators of the form

$$\phi_{hc}(x + t\bar{n}) = \sum_{i=0}^{\infty} \frac{t^i}{i!}\,(\bar{n}\cdot\partial)^i\,\phi_{hc}(x)\,, \tag{2.6}$$

with Wilson coefficients depending on the $\mathcal{O}(1)$ variable t. In momentum space, this translates to a dependence on the large momentum components of the hard-collinear fields. This feature will be discussed in detail in Part II. The hard-collinear fermion is split into two components $\psi_{hc} = \xi_{hc} + \eta_{hc}$ which are defined by

$$\xi_{hc}(x) \coloneqq \frac{\not{n}\bar{\not{n}}}{4}\,\psi_{hc}(x)\,, \qquad \eta_{hc}(x) \coloneqq \frac{\bar{\not{n}}\not{n}}{4}\,\psi_{hc}(x)\,. \tag{2.7}$$

They fulfill the important projection properties $\not{n}\,\xi_{hc} = \bar{\not{n}}\,\eta_{hc} = 0$. The λ-scaling of these fields can be determined by considering their propagators. For the hard-collinear fermions, one finds

$$\langle 0|\mathrm{T}\,\xi_{hc}(x)\,\bar{\xi}_{hc}(y)|0\rangle = \frac{\not{n}\bar{\not{n}}}{4}\,\langle 0|\mathrm{T}\,\psi_{hc}(x)\,\bar{\psi}_{hc}(y)|0\rangle\,\frac{\bar{\not{n}}\not{n}}{4} = \int \frac{d^4p}{(2\pi)^4}\,\frac{\not{n}}{2}\,\frac{i\,\bar{n}\cdot p}{p^2 + i0}\,e^{-ip\cdot(x-y)} \tag{2.8}$$

and a similar result with $n \leftrightarrow \bar{n}$ for η_{hc}. Here, T denotes the time-ordering of fields on the right of it. While for the soft fermion the propagator remains unchanged

$$\langle 0|\mathrm{T}\,q_s(x)\,\bar{q}_s(y)|0\rangle = \int \frac{d^4p}{(2\pi)^4}\,\frac{i(\not{p} + m)}{p^2 - m^2 + i0}\,e^{-ip\cdot(x-y)}\,, \tag{2.9}$$

with a mass $m \sim \lambda^2$. One can directly infer the scaling of the fermion fields

$$\xi_{hc} \sim \lambda\,, \qquad \eta_{hc} \sim \lambda^2\,, \qquad q_s \sim \lambda^3\,. \tag{2.10}$$

As η_{hc} is subleading compared to ξ_{hc}, it will be integrated out below using its equation of motion. For the gluon fields, one needs to consider their propagator in R_ξ gauge

$$\langle 0|\mathrm{T}\, A_i^\mu(x)\, A_i^\nu(y)|0\rangle = \int \frac{d^4p}{(2\pi)^4}\, \frac{-i}{p^2+i0}\left(\eta^{\mu\nu} - (1-\xi)\,\frac{p^\mu p^\nu}{p^2}\right) e^{-ip\cdot(x-y)}\,. \tag{2.11}$$

After contracting with n, $\bar n$ or projecting onto the $\perp$-components, one finds the following scaling for the components of the gluon fields

$$A_{hc}^\mu \sim (\lambda^2, 1, \lambda)\,, \qquad A_s^\mu \sim (\lambda^2, \lambda^2, \lambda^2)\,. \tag{2.12}$$

The appearance of an unsuppressed field $\bar n\cdot A_{hc}$ is problematic because such fields can be inserted arbitrarily often into operators. This can be dealt with using Wilson lines as explained below.

2.2 Gauge Symmetry and Multipole Expansion

In this work, we focus on high-energy processes that are dominated by the strong interaction, i.e. by QCD. The construction of SCET has to respect the $SU(N_c)$ gauge symmetry of the underlying full theory. Decomposing the quark and gluon fields according to (2.4) also decomposes the gauge group into a hard-collinear and soft part. Soft fields cannot transform under hard-collinear gauge transformations, as this would turn them into hard-collinear fields. The soft gluon field transforms as a background field for hard-collinear fields. The decomposed gauge transformations are [14]

$$\begin{aligned}
\text{hard-collinear:}\quad & A_{hc} \to U_{hc}\, A_{hc}\, U_{hc}^\dagger + \frac{1}{g_s}\, U_{hc}\big[iD_s, U_{hc}^\dagger\big]\,, && \xi_{hc} \to U_{hc}\,\xi_{hc}\,,\\
& A_s \to A_s\,, && q_s \to q_s\,,\\
\text{soft:}\quad & A_{hc} \to U_s\, A_{hc}\, U_s^\dagger\,, && \xi_{hc} \to U_s\,\xi_{hc}\,,\\
& A_s \to U_s\, A_s\, U_s^\dagger + \frac{1}{g_s}\, U_s\big[i\partial, U_s^\dagger\big]\,, && q_s \to U_s\, q_s\,,
\end{aligned} \tag{2.13}$$

where the covariant derivative is $iD_s := i\partial + g_s A_s$. Here and in the following, we use the convention that fields without argument are evaluated at x. The hard-collinear gauge transformations are not homogeneous in λ for $\bar n\cdot A_{hc}$ and $A_{hc}^\perp$, as they contain the soft gluon field. A second source of inhomogeneity is the requirement $p\cdot x \sim 1$ implying in generic hard-collinear-soft interactions $x \sim (1, \lambda^{-2}, \lambda^{-1})$. Therefore, one has

$$\phi_{hc}^2(x)\,\phi_s(x) = \phi_{hc}^2(x)\left(1 + x_\perp\cdot\partial + x_+\cdot\partial + \frac{1}{2}\, x_\perp^\mu x_\perp^\nu \partial_\mu\partial_\nu + \mathcal{O}(\lambda^3)\right)\phi_s(x_-)\,, \tag{2.14}$$

where $x_- := \bar n\cdot x\,\frac{n}{2}$ and $x_+ := n\cdot x\,\frac{\bar n}{2}$. The derivatives are taken before setting the soft field to $x = x_-$. Thus one has to *multipole expand* soft fields around $x = x_-$ to obtain homogeneous hard-collinear-soft interactions.

It is essential to work with objects homogeneous in λ to control the underlying power expansion in SCET. Therefore, the effective theory should be built from hard-collinear fields $\hat{A}_{hc}$, $\hat{\xi}_{hc}$ which have the following homogeneous gauge transformations

$$\begin{aligned}
\text{hard-collinear:}\quad & \hat{A}_{hc} \to U_{hc}\,\hat{A}_{hc}\,U_{hc}^\dagger + \frac{1}{g_s}\,U_{hc}\big[i\hat{D}_s(x_-), U_{hc}^\dagger\big]\,, && \hat{\xi}_{hc} \to U_{hc}\,\hat{\xi}_{hc}\,,\\
& A_s \to A_s\,, && q_s \to q_s\,,\\
\text{soft:}\quad & \hat{A}_{hc} \to U_s(x_-)\,\hat{A}_{hc}\,U_s^\dagger(x_-)\,, && \hat{\xi}_{hc} \to U_s(x_-)\,\hat{\xi}_{hc}\,,\\
& A_s \to U_s\,A_s\,U_s^\dagger + \frac{1}{g_s}\,U_s\big[i\partial, U_s^\dagger\big]\,, && q_s \to U_s\,q_s\,,
\end{aligned} \tag{2.15}$$

where $i\hat{D}_s(x_-) \coloneqq i\partial + g_s\,n\cdot A_s(x_-)\,\frac{\bar{n}}{2}$. The new fields $\hat{A}_{hc}$, $\hat{\xi}_{hc}$ are connected to the old ones by the R_s Wilson line defined in Appendix A.1

$$\hat{\xi}_{hc} \coloneqq R_s^\dagger\,\xi_{hc}\,, \qquad\qquad \hat{A}_{hc} \coloneqq R_s^\dagger\,A_{hc}\,R_s\,, \tag{2.16}$$

which moves the soft gauge transformation of hard-collinear fields from x to x_- [15].

Chapter 3

The Lagrangian

After the above discussion of field decomposition, gauge invariance and multipole expansion, we are now ready to derive the SCET-1 Lagrangian. The starting point is the QCD Lagrangian

$$\mathcal{L}_{\text{QCD}} = \bar{\psi}(i\not{D} - m)\psi - \frac{1}{2}\operatorname{tr} F_{\mu\nu} F^{\mu\nu}\,, \tag{3.1}$$

with covariant derivative $iD \coloneqq i\partial + g_s A$ and field strength tensor $ig_s F^{\mu\nu} \coloneqq [iD^\mu, iD^\nu]$. In the following, we focus on the quark part, a discussion including the Yang-Mills part can be found in [15].

First, we insert the field split (2.4) in (3.1) and drop momentum-conservation violating terms, i.e. terms containing only one hard-collinear field. Fixing hard-collinear light-cone gauge (HCLCG) $\bar{n}\cdot A_{hc} = 0$ allows us to eliminate the unsuppressed gluon component in (2.12). Second, the suppressed quark component η_{hc} is integrated out using its equation of motion [14]

$$\eta_{hc} = -\frac{1}{i\bar{n}\cdot D_s + i0}\frac{\bar{\not{n}}}{2}\Big((i\not{D}_\perp - m)\xi_{hc} + g_s \not{A}^\perp_{hc}\, q_s\Big)\,. \tag{3.2}$$

In the following, we omit the $i0$ prescription. Third, before substituting the old fields A_{hc} and ξ_{hc} with the new ones, we "unfix" HCLCG [17] by replacing $\hat{A}_{hc}$ and $\hat{\xi}_{hc}$ in (2.16) with

$$\hat{\mathcal{A}}_{hc} \coloneqq \hat{W}^\dagger_{hc}\, g_s \hat{A}_{hc}\, \hat{W}_{hc} + \hat{W}^\dagger_{hc}\big[i\hat{D}_s(x_-), W_{hc}\big]\,, \qquad \hat{\mathcal{X}}_{hc} \coloneqq \hat{W}^\dagger_{hc}\,\hat{\xi}_{hc}\,, \tag{3.3}$$

respectively. Here, the hard-collinear Wilson line is defined in Appendix A.1. The composite building blocks $\hat{\mathcal{A}}_{hc}$ and $\hat{\mathcal{X}}_{hc}$ are invariant under hard-collinear gauge transformations and related to the elementary fields $\hat{A}_{hc}$ and $\hat{\xi}_{hc}$ by a gauge transformation $U_{hc} = \hat{W}^\dagger_{hc}$. Therefore, the unsuppressed gluon component only appears through Wilson lines ensuring gauge invariance. After the substitution, soft fields in interactions with hard-collinear ones split into a homogenous background field $n\cdot A_s(x_-)$, appearing only through $i\hat{D}_s(x_-)$, and the gauge-covariant fields [18]

$$\mathcal{A}_s \coloneqq R^\dagger_s\Big(g_s A_s - g_s n\cdot A_s(x_-)\frac{\bar{n}}{2}\Big)R_s + R^\dagger_s\big[i\hat{D}_s(x_-), R_s\big]\,, \qquad \mathcal{Q}_s \coloneqq R^\dagger_s\, q_s\,. \tag{3.4}$$

They fulfill the fixed-line gauge condition $(x - x_-)\cdot\mathcal{A}_s(x) = 0$. Finally, one finds for the SCET-1 Lagrangian

$$\begin{aligned}\mathcal{L}_{\text{SCET-1}} = \mathcal{L}_{\text{YM}} &+ \bar{q}_s(i\not{D}_s - m)q_s + \bar{\mathcal{X}}_{hc}\big(in\cdot D_s(x_-) + n\cdot\mathcal{A}_{hc} + n\cdot\mathcal{A}_s\big)\frac{\bar{\not{n}}}{2}\mathcal{X}_{hc} \\ &+ \bar{\mathcal{X}}_{hc}\big(i\not{\partial}_\perp + \not{\mathcal{A}}^\perp_{hc} + \not{\mathcal{A}}^\perp_s - m\big)\frac{1}{i\bar{n}\cdot\partial + \bar{n}\cdot\mathcal{A}_s}\big(i\not{\partial}_\perp + \not{\mathcal{A}}^\perp_{hc} + \not{\mathcal{A}}^\perp_s + m\big)\frac{\bar{\not{n}}}{2}\mathcal{X}_{hc} \\ &- \bar{\mathcal{Q}}_s\not{\mathcal{A}}^\perp_{hc}\frac{1}{i\bar{n}\cdot\partial + \bar{n}\cdot\mathcal{A}_s}\frac{\bar{\not{n}}}{2}\not{\mathcal{A}}^\perp_{hc}\mathcal{Q}_s + \bar{\mathcal{X}}_{hc}\Big(n\cdot\mathcal{A}_{hc}\frac{\bar{\not{n}}}{2} + \not{\mathcal{A}}^\perp_{hc}\Big)\mathcal{Q}_s\end{aligned}$$

$$+\,\bar{\mathcal{X}}_{hc}\,\frac{\bar{n}\!\!\!/}{2}\left(i\partial\!\!\!/_\perp+\mathcal{A}\!\!\!/^\perp_{hc}+\mathcal{A}\!\!\!/^\perp_s+m\right)\frac{1}{i\bar{n}\cdot\partial+\bar{n}\cdot\mathcal{A}_s}\,\mathcal{A}\!\!\!/^\perp_{hc}\,\mathcal{Q}_s+\text{h.c.}\,, \tag{3.5}$$

where the hermitian conjugate only refers to the last two terms. Here and in the following, we omit hats as objects without them will not appear anymore. Let us summarize the main features of Lagrangian (3.5):

- It is exact to all orders in λ.
- As explained in Section 3.4 of [14], it does not renormalize, i.e. all matching coefficients retain their tree-level values and the strong coupling g_s evolves with the standard QCD β-function.
- As a remnant of the Lorentz invariance of the full theory, the Lagrangian is invariant under linear combinations of [19]

$$\begin{aligned}
&\text{(I):}\quad && n^\mu\to n^\mu+\delta^\mu_\perp\,, && \bar{n}^\mu\to\bar{n}^\mu\,,\\
&\text{(II):}\quad && n^\mu\to n^\mu\,, && \bar{n}^\mu\to\bar{n}^\mu+\delta^\mu_\perp\,,\\
&\text{(III):}\quad && n^\mu\to\zeta\,n^\mu\,, && \bar{n}^\mu\to\zeta^{-1}\,\bar{n}^\mu\,,
\end{aligned} \tag{3.6}$$

  where $\zeta=\mathcal{O}(1)$, $\delta_\perp=\mathcal{O}(\lambda)$ and $n\cdot\delta_\perp=\bar{n}\cdot\delta_\perp=0$. Naturally, the EFT must be independent of the choice of the reference vectors n and $\bar{n}$ as long as $n^2=\bar{n}^2=0$ and $n\cdot\bar{n}=2$. This symmetry is referred to as *reparametrization invariance* (RPI) and restricts the form of possible operators in SCET. Type (III) is exploited in Part II to construct a basis of SCET-1 operators.
- If the mass scales like $m\sim\lambda$, the soft quark field is not dynamical.

3.1 Leading Power

All terms in (3.5) containing the soft building blocks (3.4) need to be multipole expanded to obtain terms homogenous in λ. This expansion is most conveniently performed by expressing them through field strength tensors [15]

$$\begin{aligned}
n\cdot\mathcal{A}_s(x)&=\int_0^1 dt\;(x-x_-)^\mu\,n^\nu\left(R_s^\dagger\,g_s\,F^s_{\mu\nu}\,R_s\right)\left(x_-+t(x-x_-)\right),\\
\mathcal{A}^\perp_{s,\nu}(x)&=\int_0^1 dt\;t\,(x-x_-)^\mu\left(R_s^\dagger\,g_s\,F^s_{\mu\nu_\perp}\,R_s\right)\left(x_-+t(x-x_-)\right),\\
\bar{n}\cdot\mathcal{A}_s(x)&=\int_0^1 dt\;t\,(x-x_-)^\mu\,\bar{n}^\nu\left(R_s^\dagger\,g_s\,F^s_{\mu\nu}\,R_s\right)\left(x_-+t(x-x_-)\right),
\end{aligned} \tag{3.7}$$

where $F^s_{\mu\nu}$ is the standard QCD field strength tensor with only soft gluons. As we show below, all these objects start at $\mathcal{O}(\lambda^3)$ in the expansion and, therefore, do not contribute to the leading-power Lagrangian. It is thus given by the sum of

$$\begin{aligned}
\mathcal{L}^{(0)}_{hc}&=\bar{\mathcal{X}}_{hc}\left(in\cdot D_s(x_-)+n\cdot\mathcal{A}_{hc}\right)\frac{\bar{n}\!\!\!/}{2}\,\mathcal{X}_{hc}\\
&\quad+\bar{\mathcal{X}}_{hc}\left(i\partial\!\!\!/_\perp+\mathcal{A}\!\!\!/^\perp_{hc}\right)\frac{1}{i\bar{n}\cdot\partial}\left(i\partial\!\!\!/_\perp+\mathcal{A}\!\!\!/^\perp_{hc}\right)\frac{\bar{n}\!\!\!/}{2}\,\mathcal{X}_{hc}-\frac{1}{2}\,\text{tr}\,\mathcal{F}^{hc}_{\mu\nu}\,\mathcal{F}^{\mu\nu}_{hc}
\end{aligned} \tag{3.8}$$

and the soft part

$$\mathcal{L}_s = \bar{q}_s (i \not{D}_s - m) q_s - \frac{1}{2} \operatorname{tr} F^s_{\mu\nu} F_s^{\mu\nu} \,. \tag{3.9}$$

Here and in the following, we assume the mass to scale as $m \sim \lambda^2$. The hard-collinear field strength tensor is defined by

$$\mathcal{F}^{\mu\nu}_{hc} \coloneqq \frac{1}{i g_s} \left[i D^\mu_s(x_-) + \mathcal{A}^\mu_{hc}, i D^\nu_s(x_-) + \mathcal{A}^\nu_{hc} \right] \tag{3.10}$$

As soon as hard-collinear fields are present, the measure in the action is $\mathcal{O}(\lambda^{-4})$ compensating the $\mathcal{O}(\lambda^4)$ of the leading-power Lagrangian (3.8). The purely soft Lagrangian (3.9) is of $\mathcal{O}(\lambda^8)$ which is compensated by $d^4x \sim \mathcal{O}(\lambda^{-8})$ in the action. At leading power, the SCET-1 Lagrangian contains only the hard-collinear-soft eikonal interaction through the soft gluon field $n \cdot A_s(x_-)$. These unsuppressed interactions can be removed at the Lagrangian level by a *decoupling transformation*, explained in Appendix A.2.

3.2 Subleading Power

Besides the leading parts (3.8) and (3.9), the SCET-1 Lagrangian contains an infinite tower of subleading terms

$$\mathcal{L}_{\text{SCET}-1} = \mathcal{L}_s + \sum_{n=0}^{\infty} \mathcal{L}^{(n)}_{hc} + \mathcal{L}^{(n+1)}_{hc,s} \,, \tag{3.11}$$

where the superscript indicates the suppression relative to the leading Lagrangian. They either contain the small mass m or arise from multipole expanding the soft fields (3.4). The terms in these expansions relevant for the first and second subleading Lagrangian are [15]

$$\begin{aligned} n \cdot \mathcal{A}_s &= x_\perp^\mu \, n^\nu \, g_s F^s_{\mu\nu}(x_-) + x_+^\mu \, n^\nu \, g_s F^s_{\mu\nu}(x_-) + \frac{1}{2} \, x_\perp^\mu \, x_{\perp\varrho} \, n^\nu \left[D^\varrho_s, g_s F^s_{\mu\nu} \right](x_-) + \mathcal{O}(\lambda^5) \,, \\ \mathcal{Q}_s &= q_s(x_-) + x_{\perp\mu} \left[D^\mu_s \, q_s \right](x_-) + \mathcal{O}(\lambda^5) \,, \end{aligned} \tag{3.12}$$

where the first term in both cases is of $\mathcal{O}(\lambda^3)$, and

$$\mathcal{A}^\perp_{s,\nu} = \frac{1}{2} \, x^\mu_\perp \, g_s F^s_{\mu\nu_\perp}(x_-) + \mathcal{O}(\lambda^4) \,, \qquad \bar{n} \cdot \mathcal{A}_s = \mathcal{O}(\lambda^3) \,. \tag{3.13}$$

The different components of the soft gluon field are suppressed with different powers of λ relative to the hard-collinear one. As consequence, we need the $\mathcal{O}(\lambda^3)$ and $\mathcal{O}(\lambda^4)$ terms in the expansion of $n \cdot \mathcal{A}_s$ but only the first term for $\mathcal{A}_s^\perp$. The component $\bar{n} \cdot \mathcal{A}_s$ only contributes to $\mathcal{L}^{(3)}_{hc}$ and higher terms.

At subleading power, one finds a new interaction between soft quarks and hard-collinear fields. It is suppressed relative to the leading-power Lagrangian by at least one power of λ and its first term reads

$$\mathcal{L}^{(1)}_{hc,s} = \bar{q}_s(x_-) \not{\mathcal{A}}^\perp_{hc} \, \mathcal{X}_{hc} + \bar{\mathcal{X}}_{hc} \not{\mathcal{A}}^\perp_{hc} \, q_s(x_-) \,. \tag{3.14}$$

The soft quark at x_- is the leading contribution from the second line of (3.12). At the same power, there also exist interaction terms of hard-collinear fields and soft gluons. The associated Lagrangian is

$$\begin{aligned}\mathcal{L}^{(1)}_{hc} &= \mathcal{L}^{(1)}_{\text{YM}} + \bar{\mathcal{X}}_{hc}\, x_\perp^\mu\, n^\nu\, g_s F^s_{\mu\nu}(x_-)\, \frac{\bar{n}\!\!\!/}{2}\, \mathcal{X}_{hc} \\ &\quad + m\, \bar{\mathcal{X}}_{hc}\Big(\big(i\partial\!\!\!/_\perp + \mathcal{A}\!\!\!/^\perp_{hc}\big)\, \frac{1}{i\bar{n}\cdot\partial} - \frac{1}{i\bar{n}\cdot\partial}\, \big(i\partial\!\!\!/_\perp + \mathcal{A}\!\!\!/^\perp_{hc}\big)\Big)\, \frac{\bar{n}\!\!\!/}{2}\, \mathcal{X}_{hc}\,,\end{aligned} \tag{3.15}$$

where the Yang-Mills part is given in [15] and the first term is part of the multipole expansion of $n\cdot\mathcal{A}_s$ in (3.12).

The by two powers of λ suppressed interaction terms featuring soft quarks are

$$\begin{aligned}\mathcal{L}^{(2)}_{hc,s} &= \bar{q}_s(x_-)\Big(n\cdot\mathcal{A}_{hc} + \mathcal{A}\!\!\!/^\perp_{hc}\, \frac{1}{i\bar{n}\cdot\partial}\, \big(i\partial\!\!\!/_\perp + \mathcal{A}\!\!\!/^\perp_{hc}\big)\Big)\, \frac{\bar{n}\!\!\!/}{2}\, \mathcal{X}_{hc} \\ &\quad + \bar{\mathcal{X}}_{hc}\, \frac{\bar{n}\!\!\!/}{2}\Big(n\cdot\mathcal{A}_{hc} + \big(i\partial\!\!\!/_\perp + \mathcal{A}\!\!\!/^\perp_{hc}\big)\, \frac{1}{i\bar{n}\cdot\partial}\, \mathcal{A}\!\!\!/^\perp_{hc}\Big)\, q_s(x_-) \\ &\quad + \big[\bar{q}_s\, \overleftarrow{D}^\mu_s\big](x_-) x_{\perp\mu}\, \mathcal{A}\!\!\!/^\perp_{hc}\, \mathcal{X}_{hc} + \bar{\mathcal{X}}_{hc}\, \mathcal{A}\!\!\!/^\perp_{hc}\, x_{\perp\mu} \big[D^\mu_s\, q_s\big](x_-)\,,\end{aligned} \tag{3.16}$$

where the last line is the second term in the multipole expansion of $\mathcal{Q}_s$. Expressing this Lagrangian in a covariant form through A_{hc}, ξ_{hc} and employing the soft equation of motion, one finds a term $-m\,\bar{q}_s(x_-)\, W^\dagger_{hc}\, \xi_{hc}$. In HCLCG this term would be dropped by momentum conservation. However, dropping momentum conservation violating terms in the covariant Lagrangian is *not* hard-collinear gauge-invariant. Gauge invariance is only restored after applying the soft equation of motion in physical transition amplitudes [17]. The interaction terms without soft quarks are

$$\begin{aligned}\mathcal{L}^{(2)}_{hc} &= \mathcal{L}^{(2)}_{\text{YM}} - m^2\, \bar{\mathcal{X}}_{hc}\, \frac{1}{i\bar{n}\cdot\partial}\, \frac{\bar{n}\!\!\!/}{2}\, \mathcal{X}_{hc} \\ &\quad + \bar{\mathcal{X}}_{hc}\Big(x_+^\mu\, n^\nu\, g_s F^s_{\mu\nu}(x_-) + \frac{1}{2}\, x_\perp^\mu\, x_{\perp\varrho}\, n^\nu \big[D^\varrho_s, g_s F^s_{\mu\nu}\big](x_-)\Big)\, \frac{\bar{n}\!\!\!/}{2}\, \mathcal{X}_{hc} \\ &\quad + \frac{1}{2}\, \bar{\mathcal{X}}_{hc}\Big(\big(i\partial\!\!\!/_\perp + \mathcal{A}\!\!\!/^\perp_{hc}\big)\, \frac{1}{i\bar{n}\cdot\partial}\, x_\perp^\mu\, \gamma_\perp^\nu\, g_s F^s_{\mu\nu}(x_-) \\ &\qquad\qquad + x_\perp^\mu\, \gamma_\perp^\nu\, g_s F^s_{\mu\nu}(x_-)\, \frac{1}{i\bar{n}\cdot\partial}\, \big(i\partial\!\!\!/_\perp + \mathcal{A}\!\!\!/^\perp_{hc}\big)\Big)\, \frac{\bar{n}\!\!\!/}{2}\, \mathcal{X}_{hc}\,,\end{aligned} \tag{3.17}$$

where the Yang-Mills part is again given in [15]. This subleading Lagrangian also contains terms from the multipole expansion of $\mathcal{A}^\perp_s$ in (3.13).

Chapter 4

SCET-2

For many interesting processes, e.g. for weak annihilation discussed in Part II, external fields are described by collinear instead of hard-collinear modes. In these cases the appropriate theory is SCET-2 and we discuss its construction in this chapter, following closely reference [11].

In a first step, one decomposes quark and gluon fields similar to (2.4) in

$$\psi(x) \to \xi_c(x) + \eta_c(x) + q_s(x)\,, \qquad A(x) \to A_c(x) + A_s(x)\,, \tag{4.1}$$

where the components of the collinear quark field are defined by projections in complete analogy to (2.7). The scaling of the soft fields is the same as in SCET-1. Analyzing the propagators of the collinear fields, one finds

$$\xi_c \sim \lambda^2\,, \qquad \eta_c \sim \lambda^4\,, \qquad A_c^\mu \sim (\lambda^4, 1, \lambda^2)\,. \tag{4.2}$$

Similar to the unsuppressed component and derivative for hard-collinear modes, one can deal with $\bar{n}\cdot A_c$ and $\bar{n}\cdot\partial_c$ by introducing Wilson lines and non-local operators, respectively. By momentum conservation, interactions of two collinear and one soft or one collinear and two soft fields are forbidden. Therefore, the gauge symmetry of SCET-2 is just the same as in full QCD for each sector

$$\begin{aligned}
\text{collinear:}\quad & A_c \to U_c\, A_c\, U_c^\dagger + \frac{1}{g_s}\, U_c\big[i\partial, U_c^\dagger\big]\,, && \xi_c \to U_c\,\xi_c\,,\\
& A_s \to A_s\,, && q_s \to q_s\,,\\
\text{soft:}\quad & A_c \to A_c\,, && \xi_c \to \xi_c\,,\\
& A_s \to U_s\, A_s\, U_s^\dagger + \frac{1}{g_s}\, U_s\big[i\partial, U_s^\dagger\big]\,, && q_s \to U_s\, q_s\,.
\end{aligned} \tag{4.3}$$

As these transformations are already homogeneous in λ, there is no need for a field redefinition as in (2.16). The interaction of two collinear and two soft fields *is* allowed by momentum conservation. However, as in these interactions $x \sim (1, \lambda^{-2}, \lambda^{-2})$, one needs to multipole expand both collinear and soft fields to avoid inhomogeneities according to [11]

$$\begin{aligned}
\phi_c(x) &= \Big(1 + x_-\cdot\partial + \mathcal{O}(\lambda^4)\Big)\,\phi_c(x_+ + x_\perp)\,,\\
\phi_s(x) &= \Big(1 + x_+\cdot\partial + \mathcal{O}(\lambda^4)\Big)\,\phi_s(x_- + x_\perp)\,,
\end{aligned} \tag{4.4}$$

where the derivatives are taken before setting the fields to $x = x_\pm + x_\perp$.

4.1 The Lagrangian

The Lagrangian of SCET-2 can also be organized as power series in λ. Taking into account that $d^4x \sim \mathcal{O}(\lambda^{-8})$ for purely soft and purely collinear terms but $d^4x \sim \mathcal{O}(\lambda^{-6})$

in soft-collinear interactions terms, one can show that these interactions are power suppressed [11, 20]. Therefore, the Lagrangian takes the form

$$\mathcal{L}_{\text{SCET}-2} = \mathcal{L}_s + \mathcal{L}_c + \sum_{n=0}^{\infty} \mathcal{L}_{c,s}^{(n+2)} \,. \tag{4.5}$$

However, if incoming and outgoing fields in the same collinear direction exist, soft and collinear fields can interact at leading power through *Glauber gluons*. They are responsible for the existence of the super-leading logarithms discussed in Part I. Following the same step as in Chapter 3, one can show that the soft part of the Lagrangian is the same as in SCET-1, see (3.9), and the collinear part is

$$\begin{aligned} \mathcal{L}_c = {} & \bar{\mathcal{X}}_c \big(in\cdot\partial + n\cdot\mathcal{A}_c \big) \frac{\bar{n}\!\!\!/}{2} \, \mathcal{X}_c \\ & + \bar{\mathcal{X}}_c \big(i\partial\!\!\!/_\perp + \mathcal{A}\!\!\!/_c^\perp - m \big) \frac{1}{i\bar{n}\cdot\partial} \big(i\partial\!\!\!/_\perp + \mathcal{A}\!\!\!/_c^\perp + m \big) \frac{\bar{n}\!\!\!/}{2} \, \mathcal{X}_c - \frac{1}{2} \operatorname{tr} \mathcal{F}_{c\,\mu\nu}^{c} \, \mathcal{F}_c^{\mu\nu} \,, \end{aligned} \tag{4.6}$$

where the collinear field strength tensor is defined by

$$\mathcal{F}_c^{\mu\nu} \coloneqq \frac{1}{ig_s} \left[i\partial^\mu + \mathcal{A}_c^\mu, i\partial^\nu + \mathcal{A}_c^\nu \right] . \tag{4.7}$$

Similar to above, we use gauge-invariant building blocks for the collinear fields. They are defined by

$$\mathcal{A}_c \coloneqq W_c^\dagger \, g_s A_c \, W_c + W_c^\dagger \left[i\partial, W_c \right] , \qquad\qquad \mathcal{X}_c \coloneqq W_c^\dagger \, \xi_c \,, \tag{4.8}$$

where the collinear Wilson line is defined in Appendix A.1. Both the soft and the collinear part of (4.5) are equivalent to the full QCD Lagrangian (3.1). The Lagrangian does not renormalize and has the same RPI as in SCET-1. However, as soon as one includes heavy quarks, see Chapter 5, $\mathcal{L}_c$ receives power corrections from integrating out heavy-quark loops [11].

The first subleading term in the Lagrangian $\mathcal{L}_{c,s}^{(2)}$ is given in [11]. In soft-collinear interactions, it is most convenient to also use gauge-invariant building blocks for the soft fields

$$\mathcal{A}_{s,n} \coloneqq S_n^\dagger \, g_s A_s \, S_n + S_n^\dagger \left[i\partial, S_n \right] , \qquad\qquad \mathcal{Q}_{s,n} \coloneqq S_n^\dagger \, q_s \,, \tag{4.9}$$

with soft Wilson lines defined in Appendix A.1. The building blocks (4.8) and (4.9) will be used in Part II to construct gauge invariant operators.

4.2 Matching from SCET-1

As combining soft and (anti-)collinear modes yields (anti-)hard-collinear ones, the matching process on SCET-2 contains two steps [11, 21–25]. In a first step, one matches QCD on SCET-1 by integrating out hard modes at a scale $\mu_h \sim Q$. The Wilson coefficients arising in this first matching step are called *hard functions*. In a second step, one then matches on SCET-2 by integrating out (anti-)hard-collinear modes.

This second matching step happens at an intermediate jet scale $\mu_j \sim \lambda Q$ and results in so-called *jet functions*.

The matching from SCET-1 to SCET-2 is most conveniently done using a theory with hard-collinear, collinear and soft modes [11, 23, 24]. It is called *SCET(hc,c,s)* in [11]. First, one performs a decoupling transformation in SCET-1, as described in Appendix A.2, for each hard-collinear sector. As a consequence, operators in the EFT contain products of soft Wilson lines in different directions, and soft fields only appear in their gauge invariant form (4.9). For a single (hard-)collinear direction, this is equivalent to working in soft light-cone gauge $n \cdot A_s = 0$. In a second step, the decoupled hard-collinear fields in each sector are matched separately using SCET(hc,c,s). Employing (hard-)collinear light-cone gauge $\bar{n} \cdot A_{hc} = \bar{n} \cdot A_c = 0$ avoids dealing with unsuppressed field components. The SCET(hc,c,s) Lagrangian – in light-cone gauge and without leading power interactions between different sectors – is obtained by replacing

$$\xi_{hc}^{(0)} \to \xi_{hc}^{(0)} + \xi_c \,, \qquad\qquad A_{hc}^{(0)} \to A_{hc}^{(0)} + A_c \tag{4.10}$$

and dropping all momentum-conservation violating terms. Integrating out the hard-collinear modes in this theory yields, at tree level, relations of the form

$$\xi_{hc}^{(0)} \to f\big(\xi_c, A_c, \mathcal{Q}_{s,n}, \mathcal{A}_{s,n}\big) \,, \qquad\qquad A_{hc}^{(0)} \to f\big(\xi_c, A_c, \mathcal{Q}_{s,n}, \mathcal{A}_{s,n}\big) \,, \tag{4.11}$$

where the right-hand sides are power series in λ. Finally, gauge invariance is restored by replacing collinear fields with the gauge-invariant building blocks in (4.8). At tree level, integrating out hard-collinear modes is equivalent to solving equations of motions for $\xi_{hc}^{(0)}$ and $A_{hc}^{(0)}$. Using this method, the expansion of the right-hand sides in (4.11) to $\mathcal{O}(\lambda^4)$ and partially $\mathcal{O}(\lambda^5)$ was obtained in [11]. The trivial terms are

$$\mathcal{X}_{hc}^{(0)} \to \mathcal{X}_c + \mathcal{O}(\lambda^3) \,, \qquad\qquad \mathcal{A}_{hc}^{(0)\perp} \to \mathcal{A}_c^{\perp} + \mathcal{O}(\lambda^3) \,. \tag{4.12}$$

The subleading corrections will be studied in detail in Part II. Lastly, we note that there is no need to consider the small components $n \cdot \mathcal{A}_{hc}$ and $n \cdot \mathcal{A}_c$ when constructing operators in the EFT as they can be removed using equations of motion [26].

Chapter 5

Heavy Quark Effective Theory

In SCET, only quark masses up to $\mathcal{O}(\lambda)$ can be considered, as they do not change the light-like character of momenta. When dealing with B-meson decays in Part II, one also has to take into account the bottom quark mass $m_b \sim \mathcal{O}(1)$. The appropriate effective theory to describe such heavy quarks is *heavy quark effective theory* (HQET) [27, 28].

A heavy quark inside a heavy meson, such as the b-quark inside the B-meson, carries almost the full meson momentum. Therefore, its momentum can be split according to

$$p_b^\mu = m_b v^\mu + k^\mu \,, \tag{5.1}$$

where v is the velocity ($v^2 = 1$) of the heavy meson and $k \sim \Lambda_{\rm QCD} \sim \mathcal{O}(\lambda^2)$ a residual soft momentum. The full QCD b-quark field is decomposed as

$$b(x) = e^{-i m_b v\cdot x} \left[b_v(x) + B_v(x) \right] , \tag{5.2}$$

where the two HQET fields b_v and B_v carry only the residual soft momentum and the meson velocity v appears as a label on these fields. In complete analogy to the hard-collinear quark fields in (2.7), the two fields are obtained by different projections

$$b_v(x) \coloneqq e^{i m_b v\cdot x}\, P_+\, b(x) \,, \qquad\qquad B_v(x) \coloneqq e^{i m_b v\cdot x}\, P_-\, b(x) \,, \tag{5.3}$$

with projector $P_\pm \coloneqq (1 \pm \slashed{v})/2$ and $\slashed{v}\, b_v = b_v$. For the two-point correlation function, one finds

$$\langle 0|\mathrm{T}\, b_v(x)\, \bar b_v(y)|0\rangle = \int \frac{d^4k}{(2\pi)^4}\, \frac{i}{v\cdot k + i0}\, P_+\, e^{-ik\cdot(x-y)} \,. \tag{5.4}$$

Here we used that $P_\pm \gamma^\mu P_\pm = \pm v^\mu P_\pm$. From a similar relation for B_v, one can infer the power counting of the two HQET fields

$$b_v \sim \lambda^3 \,, \qquad\qquad B_v \sim \lambda^4 \,. \tag{5.5}$$

The large component b_v has the same power counting as a light soft quark in SCET. The small component B_v, describing hard fluctuations, can be integrated out at tree-level by applying its equation of motion

$$B_v = \frac{1}{2m_b + i v\cdot D_s - i0}\, i\not{D}_s^\perp\, b_v \,, \tag{5.6}$$

with covariant derivative $iD_s = i\partial + g_s A_s$ and $v\cdot D_s^\perp = 0$. In the following we omit the $i0$ prescription.

Inserting (5.2) in the QCD Lagrangian and applying the equation of motion for B_v, one finds

$$\mathcal{L}_{\rm HQET} = \bar b_v \left(i v\cdot D_s + i\not{D}_s^\perp\, \frac{1}{2m_b + i v\cdot D_s}\, i\not{D}_s^\perp \right) b_v \,. \tag{5.7}$$

In contrast to SCET, the HQET Lagrangian does receive contributions from integrating out hard loops, i.e. it renormalizes. Taking the heavy-quark limit $m_b \to \infty$, i.e. considering only the first term in the power expansion, one finds

$$\mathcal{L}^{(0)}_{\text{HQET}} = \bar{b}_v \, i v \cdot D_s \, b_v \,. \tag{5.8}$$

As this Lagrangian is independent of m_b and has a trivial Dirac structure, QCD has a *spin-flavor symmetry* in the heavy quark limit [29, 30]. This symmetry is broken by subleading terms starting at $\mathcal{O}(1/m_b)$. The first terms are given by

$$\mathcal{L}^{(1)}_{\text{HQET}} = \frac{1}{2m_b} \bar{b}_v \left(iD_s^\perp\right)^2 b_v + \frac{i}{8m_b} \bar{b}_v \left[\gamma_\perp^\mu, \gamma_\perp^\nu\right] g_s F^s_{\mu\nu} \, b_v \tag{5.9}$$

and are referred to as kinetic and chromo-magnetic operator, respectively.

Similar to (3.6) in SCET, the Lagrangian (5.7) has a RPI. The split of the heavy quark momentum (5.1) is not unique and can be changed by

$$v^\mu \to v^\mu - \frac{q^\mu}{m_b} \,, \qquad k^\mu \to k^\mu + q^\mu \,, \tag{5.10}$$

where $q \sim \Lambda_{\text{QCD}} \sim \lambda^2$, without altering the effective theory. This reparameterization connects terms with different power counting, e.g. the leading-power Lagrangian and the kinetic operator. Therefore, the first term in the power expansion that has a non-trivial matching coefficient is the chromo-magnetic operator [31]. Splitting the heavy quark momentum is not the only ambiguity in the HQET construction. As quarks are always confined in hadrons, there exists no canonical definition of the heavy quark mass m_b. This problem can be solved by introducing a *residual mass term*, see [32] for more details.

There is an important detail regarding the normalization of meson states in HQET. Such a state is described in the effective theory by a velocity v and a residual soft momentum k. It is convenient to normalize them in a mass-independent way, i.e.

$$\left\langle B_{v'}(k') \middle| B_v(k) \right\rangle = 2v^0 \, \delta_{vv'} \, (2\pi)^3 \, \delta^{(3)}(\boldsymbol{k} - \boldsymbol{k}') \,, \tag{5.11}$$

to avoid difficulties when taking the heavy quark limit. The connection to QCD states is then

$$\left| B(p) \right\rangle = \sqrt{m_B} \Big(\left| B_v(k) \right\rangle + \mathcal{O}(1/m_b) \Big) \,, \tag{5.12}$$

with meson mass $m_B \sim m_b$.

Appendix

A.1 Wilson Lines

As Wilson lines play an important role in SCET, we list their definitions and most important properties in this appendix. In Parts I and II of this work, more than one (hard-)collinear direction is relevant. Therefore, in most cases we also give the expressions associated with an anti-hard-collinear sector.

The Wilson lines used to transform A_{hc} and ξ_{hc} to HCLCG are defined by

$$\begin{aligned} W_{hc}(x) &\coloneqq \mathrm{P}\exp\left[ig_s\int_{-\infty}^{0} dt\; \bar{n}\cdot A_{hc}(x+t\bar{n})\right], \\ W_{\overline{hc}}(x) &\coloneqq \mathrm{P}\exp\left[ig_s\int_{-\infty}^{0} dt\; n\cdot A_{\overline{hc}}(x+tn)\right], \end{aligned} \tag{A.1.1}$$

where P denotes that the fields in the exponential are path-ordered. In the redefinition (2.16) of the old hard-collinear fields, the R_s Wilson line is defined by

$$R_s(x) \coloneqq \mathrm{P}\;\exp\left[ig_s\int_{-\infty}^{0} dt\,(x-x_-)_\mu\, A_s^\mu\big(x_- + t(x-x_-)\big)\right]. \tag{A.1.2}$$

This Wilson line transforms soft fields into fixed-line gauge with $U_s = R_s^\dagger$. In an anti-collinear sector, the redefinition is performed using the same Wilson line with x_- replaced by x_+.

Similar to the Wilson lines (A.1.1), one can define

$$\begin{aligned} S_n(x) &\coloneqq \mathrm{P}\exp\left[ig_s\int_{-\infty}^{0} dt\; n\cdot A_s(x+tn)\right], \\ S_{\bar{n}}(x) &\coloneqq \mathrm{P}\exp\left[ig_s\int_{-\infty}^{0} dt\; \bar{n}\cdot A_s(x+t\bar{n})\right]. \end{aligned} \tag{A.1.3}$$

They transform soft fields to light-cone gauge and are used to perform the decoupling transformation, see Appendix A.2.

Under the homogeneous gauge transformations (2.15), these Wilson lines transform according to

$$\begin{aligned} &\text{hard-collinear:} && W_{hc} \to U_{hc}\, W_{hc}\,, && R_s \to R_s\,, && S_n \to S_n\,, \\ &\text{soft:} && W_{hc} \to U_s(x_-)\, W_{hc}\, U_s^\dagger(x_-)\,, && R_s \to U_s\, R_s\, U_s^\dagger(x_-)\,, && S_n \to U_s\, S_n\,. \end{aligned} \tag{A.1.4}$$

Remember that fields without argument live at x. Form the first column, it is obvious that the building blocks (3.3) are invariant under hard-collinear gauge transformations, whereas from the second column, one can infer that the fields (3.4) transform covariantly with $U_s(x_-)$ under soft gauge transformations.

The covariant derivative along their direction vanishes [9]. The most relevant relations for us are

$$\big[i\bar{n}\cdot D_{hc}\, W_{hc}\big] = 0\,, \qquad\qquad \big[in\cdot D_s\, S_n\big] = 0\,, \tag{A.1.5}$$

where $iD_{hc} \coloneqq i\partial + g_s A_{hc}$. Similar relations hold in the anti-hard-collinear sector, i.e. for $n \leftrightarrow \bar{n}$. The square brackets indicate that the derivatives only act on the Wilson lines. Exploiting this property, it is easy to show that the hard-collinear building blocks (3.3) for the gluon fields are indeed in HCLCG.

In SCET-2 an additional type of Wilson lines appear. These collinear Wilson lines encode the $\mathcal{O}(1)$ component of the collinear gluon field and are defined by

$$\begin{aligned} W_c(x) &\coloneqq \mathrm{P}\exp\left[ig_s\int_{-\infty}^{0} dt\; \bar{n}\cdot A_c(x+t\bar{n})\right], \\ W_{\bar{c}}(x) &\coloneqq \mathrm{P}\exp\left[ig_s\int_{-\infty}^{0} dt\; n\cdot A_{\bar{c}}(x+tn)\right]. \end{aligned} \tag{A.1.6}$$

They only transform under gauge transformations according to

$$\text{collinear:}\quad W_c \to U_c\, W_c\,, \qquad\qquad \text{soft:}\quad W_c \to W_c \tag{A.1.7}$$

and, therefore, the building blocks (4.8) are indeed invariant. Similar to (A.1.5), they turn covariant derivatives to ordinary ones

$$\big[i\bar{n}\cdot D_c\, W_c\big] = 0\,, \tag{A.1.8}$$

where $iD_c \coloneqq i\partial + g_s A_c$.

A.2 Decoupling Transformation

In this appendix, we discuss the decoupling transformation removing the leading power interaction of soft and hard-collinear fields, see Section 3.1. Similar to Appendix A.1, we also include anti-hard-collinear fields in the discussion.

The leading-power SCET-1 Lagrangian (3.8) contains hard-collinear-soft interactions only through the soft gluon field $n\cdot A_s(x_-)$. It is possible to eliminate this interaction by redefining the (anti-)hard-collinear fields [13]

$$\begin{aligned} \xi^{(0)}_{hc}(x) &\coloneqq S_n^\dagger(x_-)\,\xi_{hc}(x)\,, & A^{(0)}_{hc}(x) &\coloneqq S_n^\dagger(x_-)\,A_{hc}(x)\,S_n(x_-)\,, \\ \xi^{(0)}_{\overline{hc}}(x) &\coloneqq S_{\bar{n}}^\dagger(x_+)\,\xi_{\overline{hc}}(x)\,, & A^{(0)}_{\overline{hc}}(x) &\coloneqq S_{\bar{n}}^\dagger(x_+)\,A_{\overline{hc}}(x)\,S_{\bar{n}}(x_+)\,, \end{aligned} \tag{A.2.1}$$

where the soft Wilson lines are defined in Appendix A.1. The multipole expansion of the soft Wilson lines ensures that only the components of the soft momenta which are commensurate with the small components of the hard-collinear or anti-hard-collinear momenta can propagate in these interactions. Under this redefinition the Wilson lines (A.1.1) transform as

$$W_{hc} = S_n(x_-)\,W^{(0)}_{hc}\,S_n^\dagger(x_-)\,, \qquad\qquad W_{\overline{hc}} = S_{\bar{n}}(x_+)\,W^{(0)}_{\overline{hc}}\,S_{\bar{n}}^\dagger(x_+)\,, \tag{A.2.2}$$

where the superscript $^{(0)}$ on the Wilson lines indicate that they contain the decoupled hard-collinear gluon fields. Using (A.1.5), it is possible to show that the building blocks (3.3) transform as

$$\begin{aligned} \mathcal{X}_{hc} &= S_n(x_-)\, \mathcal{X}_{hc}^{(0)}\,, \qquad \mathcal{A}_{hc} = S_n(x_-)\, \mathcal{A}_{hc}^{(0)}\, S_n^\dagger(x_-)\,, \\ \mathcal{X}_{\overline{hc}} &= S_{\bar n}(x_+)\, \mathcal{X}_{\overline{hc}}^{(0)}\,, \qquad \mathcal{A}_{\overline{hc}} = S_{\bar n}(x_+)\, \mathcal{A}_{\overline{hc}}^{(0)}\, S_{\bar n}^\dagger(x_+)\,, \end{aligned} \tag{A.2.3}$$

where we defined new soft *and* (anti-)hard-collinear gauge invariant building blocks

$$\begin{aligned} \mathcal{A}_{hc}^{(0)} &\coloneqq W_{hc}^{(0)\dagger}\, g_s A_{hc}^{(0)}\, W_{hc}^{(0)} + W_{hc}^{(0)\dagger}\left[i\partial, W_{hc}^{(0)}\right], \qquad \mathcal{X}_{hc}^{(0)} \coloneqq W_{hc}^{(0)\dagger}\, \xi_{hc}^{(0)}\,, \\ \mathcal{A}_{\overline{hc}}^{(0)} &\coloneqq W_{\overline{hc}}^{(0)\dagger}\, g_s A_{\overline{hc}}^{(0)}\, W_{\overline{hc}}^{(0)} + W_{\overline{hc}}^{(0)\dagger}\left[i\partial, W_{\overline{hc}}^{(0)}\right], \qquad \mathcal{X}_{\overline{hc}}^{(0)} \coloneqq W_{\overline{hc}}^{(0)\dagger}\, \xi_{\overline{hc}}^{(0)}\,. \end{aligned} \tag{A.2.4}$$

Finally, observing that

$$in\cdot D_s(x_-) + n\cdot\mathcal{A}_{hc} = S_n(x_-)\left(in\cdot\partial + n\cdot\mathcal{A}_{hc}^{(0)}\right) S_n^\dagger(x_-) \tag{A.2.5}$$

and inserting it in the SCET-1 Lagrangian, one finds that the leading-power interactions are gone. In contrast, performing the decoupling transformation in the subleading terms, see Section 3.2, transforms all soft fields to light-cone gauge. The respective Lagrangians can then be expressed through the building blocks (A.2.4) and (4.9). For example, the multipole term in the first subleading Lagrangian (3.15) becomes [33]

$$\mathcal{L}_{hc}^{(1)} \supset \bar{\mathcal{X}}_{hc}^{(0)}\, ix_\perp^\mu \left[in\cdot\partial \mathcal{A}_{s,n,\mu}^\perp(x_-)\right] \frac{\bar{n}\!\!\!/}{2}\, \mathcal{X}_{hc}^{(0)}\,, \tag{A.2.6}$$

whereas in the term proportional to m one just has to replace all hard-collinear fields by the decoupled ones.

Part I

Non-Global Observables at Hadron Colliders

Chapter 6

Non-Global Observables

Jet observables play an important role at high-energy colliders, as they closely mirror the underlying hard-scattering event and are used in a wide range of physics analyses. By providing a unique vantage point to study the strong interactions at the shortest distances, they allow for the search of new phenomena and precision tests of the SM. However, jet rates are among the most difficult observables to calculate theoretically, especially for hadron colliders as the LHC [34]. Defining M-jet cross sections involves clustering energetic radiation into jets and vetoing the remaining out-of-jet radiation, ensuring it to be soft, see Figure 6.1 for a graphical illustration. This veto in certain regions of phase space leads to *non-global* observables and to an intricate pattern of logarithmically enhanced corrections in perturbation theory.

The simplest example are gap-between-jet cross sections, where the radiation above a low scale Q_0 is vetoed outside the jets. As the jets itself carry large energy $Q \sim \sqrt{\hat{s}}$, the coefficients of the perturbative series for such an observable are enhanced by large logarithms $L = \ln(Q/Q_0) \gg 1$. For wide-angle jets at e^+e^- colliders, the leading logarithmic corrections are of the form $\alpha_s^n L^n$. They arise from soft gluon emissions of the primary partons produced in the collision and, as Dasgupta and Salam observed in [35], also from secondary soft gluon emissions inside the jets. The latter so-called *non-global logarithms* (NGLs) have an intricate structure, even at leading logarithmic accuracy, and the complexity of the involved color algebra renders their resummation highly non-trivial. In the large-N_c approximation, the leading NGLs can be resummed by solving a non-linear integro-differential equation derived in [36]. Using a map between the JIMWLK [37–39] and BK [40, 41] evolution equations for small-x dynamics, this BMS equation was generalized to finite N_c in [42] and numerical results for the leading NGLs at $N_c = 3$ were obtained in [43–46]. Advances in the development of finite-N_c parton showers made it possible to resum the NGLs numerically also in this framework [47–56]. Recently, also the resummation of next-to-leading NGLs was achieved [55–62].

At hadron colliders an additional subtlety arises. Soft interactions between the two initial-state partons, mediated by Glauber gluons, lead to complex phase factors, so-called *Glauber phases*.[1] They prevent the cancellation of soft+collinear singularities and lead to collinear factorization violation [63–65]. Consequently color coherence breaks down in higher orders of perturbation theory, leading to so-called *super-leading logarithms* (SLLs), an infinite tower of double logarithms $\alpha_s^{3+n} L^{3+2n}$ starting at four-loop order in perturbation theory [66–68]. As the SLLs are suppressed in the large-N_c limit, traditional probabilistic parton showers do not even capture the leading double-logarithmic corrections for gap-between-jet cross sections at hadron colliders.

For a long time, very little was known about the SLLs. The four- and five-loop terms, i.e. $\alpha_s^4 L^5$ and $\alpha_s^5 L^7$, were computed several years ago in [66–68] for different $2 \to 2$ hard-scattering processes without interference effects. In [69] it was shown that they can amount for corrections up to 15% for gap-between-jet cross sections.

[1] In the literature, these phase factors are also called Coulomb phases.

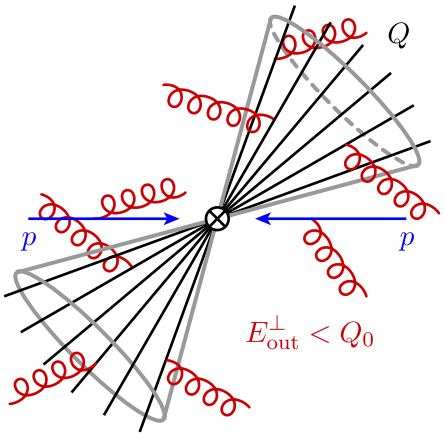

Figure 6.1: Graphical illustration of a $pp \to 2$ jet scattering process. Soft radiation is shown in red and initial-state hadrons (protons) in blue. The radiation outside of the jets is restricted by Q_0 whereas the jets (gray cones) carry large energy $Q \sim \sqrt{\hat{s}}$.

The gap-between-jet cross section for lepton colliders can be factorized into a hard function, describing the hard-scattering $e^+e^- \to m$ partons, and a soft function, a vacuum matrix element of m soft Wilson lines [70,71].[2] The NGLs are then resummed by solving RG equations. Using a similar factorization theorem for hadron colliders, the all-order resummation of the SLLs for quark-initiated scattering processes and for a fixed-coupling approximation has been recently accomplished in [73].

This part is structured as follows: In Chapter 7 we derive in detail the aforementioned factorization theorem for gap-between-jet cross sections at hadron colliders using SCET, including a derivation of the one-loop anomalous dimension governing the RG evolution of the hard function. The resummation of the SLLs is extended to processes with initial-state partons transforming under an arbitrary representation of $SU(N_c)$ and to RG-improved perturbation theory in Chapter 8. A full phenomenological analysis of the SLLs is beyond the scope of this work but we include a numerical analysis for all $2 \to 0$, $2 \to 1$ and $2 \to 2$ scattering processes relevant in QCD and investigate interference effects for partonic $qq \to qq$ scattering. In Chapter 9 we extend the resummation to subleading logarithmic corrections arising from multiple Glauber-gluon exchanges. For this *Glauber series*, we determine the all-order structure and perform (partial) resummations for two expansions and for large N_c. Finally, we present our conclusions in Chapter 10.

[2] It is also possible to include sequential jet clustering in this framework [72].

Chapter 7

Factorization Theorem

In this chapter, we discuss in detail – using the language of SCET – the leading power factorization theorem for gap-between-jet cross sections [1, 73, 74]

$$\sigma_{2\to M}(Q_0) = \int d\xi_1\, d\xi_2 \sum_{m=2+M}^{\infty} \left\langle \boldsymbol{\mathcal{H}}_m(\{\underline{n}\}, s, \xi_1, \xi_2, \mu) \otimes \boldsymbol{\mathcal{W}}_m(\{\underline{n}\}, Q_0, \xi_1, \xi_2, \mu) \right\rangle , \quad (7.1)$$

applicable for $2 \to M$ wide-angle scattering at hadron colliders. Furthermore, the anomalous dimension of the *hard function* $\boldsymbol{\mathcal{H}}_m$ is calculated and the cancellation of real and virtual collinear singularities is demonstrated. For the *low-energy matrix element* $\boldsymbol{\mathcal{W}}_m$ only the lowest order approximation is relevant in this work, but it deserves further studies in future. The various symbols in (7.1) are explained below.

7.1 Jets in SCET

The scattering of several energetic particles in SCET is described by the m-jet operator. As soft fields are power suppressed compared to hard-collinear ones, see Section 2.1, the leading power m-jet operator contains m hard-collinear fields, one for each direction of the jets [75,76]. At subleading power, soft fields as well as more than one hard-collinear field in each direction are allowed, see [26, 77] for more details on this subject.

Introducing m hard-collinear sectors for the directions of the jet, i.e. light-like vectors $n_i = (1, \boldsymbol{n}_i)$ and $\bar{n}_i = (1, -\boldsymbol{n}_i)$ such that $n_i \cdot \bar{n}_i = 2$, the relevant leading power Lagrangian contains m copies of $\mathcal{L}^{(0)}_{hc}$, derived in Chapter 3, and one soft Lagrangian $\mathcal{L}_s$. By momentum conservation, there cannot be any interactions among the different hard-collinear sectors, only the leading-power eikonal interactions with the soft field remain. Matching the full QCD jet operator onto SCET-1, one finds[1]

$$J_m(0) = \int \frac{dt_1}{2\pi} \cdots \frac{dt_m}{2\pi} \left[\widetilde{\mathcal{C}}_m\right]^{a_1\ldots a_m}_{\alpha_1\ldots\alpha_m}(t_1, \ldots, t_m, \mu) \prod_{i=1}^{m} \left[\Phi_i\right]^{a_i}_{\alpha_i}(t_i \bar{n}_i) , \quad (7.2)$$

with $\Phi_i \in \{\mathcal{X}_i, \bar{\mathcal{X}}_i, \mathcal{A}^{\perp}_i\}$ being the hard-collinear gauge invariant building block (3.3) in the n_i-collinear direction. The a_i are the color indices of these fields, either fundamental for (anti-)quarks or adjoint for gluons. Dirac and Lorentz indices of (anti-)quarks and gluons, respectively, are labeled by α_i. Showing all these indices explicitly makes the connection to the color-helicity-space formalism [78, 79], used throughout this part, more transparent. The hard-collinear fields in (7.2) are displaced along the light-cone, as derivatives $\bar{n}_i \cdot \partial$ are unsuppressed in SCET. This non-locality reflects in $\{\underline{t}\}$-dependent Wilson coefficients $\widetilde{\mathcal{C}}_m(\{\underline{t}\})$.

Performing the decoupling transformation, see Appendix A.2, for each hard-collinear sector transforms the fields in the jet operator according to

$$\left[\Phi_i\right]^{a_i}_{\alpha_i}(t_i \bar{n}_i) = \left[\boldsymbol{S}_i(n_i)\right]^{a_i b_i} \left[\Phi^{(0)}_i\right]^{b_i}_{\alpha_i}(t_i \bar{n}_i) . \quad (7.3)$$

[1] Evaluating the jet operator at $x = 0$ is sufficient, as the $d^d x$ integral only yields an overall δ-function.

All soft Wilson lines live at $x = 0$, which is why we drop this argument and prefer to indicate their directions. Using color-space notation, one can express the soft Wilson line for outgoing partons, $j > 2$, transforming under an arbitrary representation, as [9]

$$\boldsymbol{S}_j(n_j) = \mathbf{P} \exp\left[i g_s \int_0^\infty dt\; n_j \cdot A_s^a(t n_j)\, \boldsymbol{T}_j^a \right]. \tag{7.4}$$

For incoming partons, one has to integrate over $t \in (-\infty, 0)$.

In general the appropriate EFT to describe inclusive processes is SCET-1, where soft modes have a lower virtuality than collinear ones. However, imposing a veto on radiation outside the jets in non-global observables forces the transverse components of soft and collinear momenta to be of the same magnitude. Thus, the relevant theory for non-global observables is SCET-2. At leading power the matching of the decoupled hard-collinear SCET-1 fields $\Phi_i^{(0)}$ on SCET-2 is trivial, see Section 4.2, and they can be replaced by the collinear gauge invariant building blocks. In the following, we denote these fields also by $\Phi_i \in \{\mathcal{X}_i, \bar{\mathcal{X}}_i, \mathcal{A}_i^\perp\}$ and explicitly mention which type of collinear fields we refer to. For hadron colliders it is possible that one of the incoming partons becomes collinear to an outgoing one, i.e. $n_1 \parallel n_j$ or $n_2 \parallel n_j$, thus collinear and soft physics cannot be factorized. Interactions between these sectors mediated by Glauber gluons break collinear factorization [63–66, 80]. For lepton colliders, in contrast, the incoming partons are color-neutral ($\boldsymbol{S}_i(n_i) = \mathbf{1}$ for $i = 1, 2$) and, therefore, no such factorization breaking effects occur [70, 71]. Glauber-gluon exchanges are always associated with the initial state, see (7.37). For the final-state partons $j > 2$, one can thus evaluate the on-shell matrix elements of collinear fields in terms of on-shell spinors and polarization vectors [81]

$$\begin{aligned}
\big\langle p_j; a_j, s_j \big|\, \big[\mathcal{X}_j\big]_{\alpha_j}^{b_j}(t_j \bar{n}_j)\, \big|0\big\rangle &= \delta^{b_j a_j}\, v_{\alpha_j}(p_j; s_j)\, e^{+i t_j \bar{n}_j \cdot p_j}\,, \\
\big\langle p_j; a_j, s_j \big|\, \big[\bar{\mathcal{X}}_j\big]_{\alpha_j}^{b_j}(t_j \bar{n}_j)\, \big|0\big\rangle &= \delta^{a_j b_j}\, \bar{u}_{\alpha_j}(p_j; s_j)\, e^{+i t_j \bar{n}_j \cdot p_j}\,, \\
\big\langle p_j; a_j, s_j \big|\, \big[\mathcal{A}_j^\perp\big]_{\alpha_j}^{b_j}(t_j \bar{n}_j)\, \big|0\big\rangle &= \delta^{a_j b_j}\, \varepsilon_{\alpha_j}^*(p_j; s_j)\, e^{+i t_j \bar{n}_j \cdot p_j}\,,
\end{aligned} \tag{7.5}$$

where s_j labels the helicity of the parton. These relations do not receive loop corrections because all integrals containing only collinear modes vanish in dimensional regularization.

7.2 Derivation

The derivation of the factorization theorem (7.1) works similar to the one for e^+e^- colliders in [70, 71]. Nevertheless, the inclusion of color-charged initial-state partons leads to complications. Starting point is the cross section for the scattering of two hadrons H_1, H_2 into M jets

$$\begin{aligned}
\sigma_{2\to M}(Q_0) = \frac{1}{2s} \sum_{m=2+M}^{\infty} \sum_{\text{spin/color}} \prod_{j=3}^{m} \int \frac{d^{d-1}p_j}{(2\pi)^{d-1}} \frac{1}{2|\boldsymbol{p}_j|} \left|\mathcal{M}(H_1 H_2 \to 3 \ldots m)\right|^2 \\
\times (2\pi)^d\, \delta^{(d)}(\rho_1 + \rho_2 - p_{\text{tot}})\, \Theta_{\text{hard}}(\{\underline{n}\})\, \theta(Q_0 - E_{\text{out}}^\perp)\,,
\end{aligned} \tag{7.6}$$

where ρ_1, ρ_2 are the momenta of the two hadrons and p_{tot} is the total momentum of the final-state partons. The collection of all parton directions is abbreviated by $\{\underline{n}\} = \{n_1, \dots, n_m\}$. The sum over parton multiplicities m also contains the sum over all partonic final-state channels. As we are only interested in unpolarized hadron beams, the sum over final-state colors and helicities also includes an average over the hadron spins. The angular constraint $\Theta_{\text{hard}}(\{\underline{n}\}) = \theta_{\text{hard}}(n_1) \dots \theta_{\text{hard}}(n_m)$ defines the jet region. The total transverse momentum of the soft radiation outside the jets $E_{\text{out}}^{\perp} = \sum_i |p_i^{\perp}|$ is restricted by Q_0.[2] Here, $\perp$ denotes the $(d-2)$ components transverse to the beam directions n_1 and n_2. Of course, one could consider different restrictions. For example, at ATLAS the total transverse momentum of jets inside the veto region is constrained [82, 83]. In the leading-logarithmic approximation, one is only sensitive to the energy cutoff and the precise definition of the veto is irrelevant.

The scattering amplitude is connected to the m-jet operator (7.2) by

$$\mathcal{M}(H_1 H_2 \to 3 \dots m) = \big\langle \{p_3\} \dots \{p_m\}; X_s \big| J_m(0) \big| H_1(\rho_1) H_2(\rho_2) \big\rangle \,, \tag{7.7}$$

where $\{p_j\}$ denotes the set of momentum, helicity, and color of final-state parton j and X_s the soft final state restricted by Q_0 in the veto region. On the right-hand side, implicit sums over the hard-collinear fields $\Phi_i \in \{\mathcal{X}_i, \bar{\mathcal{X}}_i, \mathcal{A}_i^{\perp}\}$ for $i = 1, 2$ are understood. In the factorization theorem (7.1), they are also included in the sum over m. Evaluating the on-shell matrix elements for the final-state partons after decoupling and matching onto SCET-2 according to (7.5), the sum over final-state colors of the squared amplitude can be performed straightforwardly and the Wilson coefficients get Fourier transformed. Using translation invariance, one can perform all integrals except for

$$\begin{aligned} \int d\xi_1\, d\xi_2 \int \frac{dt_1}{2\pi}\, \frac{dt_2}{2\pi}\; \bar{n}_1 \cdot \rho_1\, \bar{n}_2 \cdot \rho_2\, e^{-i t_1 \xi_1\, \bar{n}_1 \cdot \rho_1}\, e^{-i t_2 \xi_2\, \bar{n}_2 \cdot \rho_2}\, \mathcal{C}_m(\{\underline{p}\}, \mu)\, \mathcal{C}_m^{\dagger}(\{\underline{p}\}, \mu) \\ \times \big[\text{final-state spinors/polarization vectors}\big] \dots \end{aligned} \tag{7.8}$$

where $\{\underline{p}\} = \{\xi_1\, \rho_1, \xi_2\, \rho_2, p_3, \dots, p_m\}$. The variable ξ_i can be interpreted as the momentum fraction carried by a parton of hadron H_i. To obtain the full spin- and color-summed squared matrix element in (7.6), one needs to add the hadronic matrix element, denoted by the ellipsis. As hadrons are color-neutral and we average over their spins τ_1 and τ_2, one finds for the matrix elements of the collinear fields

$$\begin{aligned} &\sum\!\!\!\!\!\!\int_{X_s} \sum_{\tau_1, \tau_2} \big\langle H_1(\rho_1, \tau_1) H_2(\rho_2, \tau_2) \big| \big[\bar{\Phi}_1\big]_{\bar{\alpha}_1}^{\bar{b}_1}(t_1 \bar{n}_1)\, \big[\bar{\Phi}_2\big]_{\bar{\alpha}_2}^{\bar{b}_2}(t_2 \bar{n}_2) \dots \big| X_s \big\rangle \\ &\qquad \times \big\langle X_s \big| \dots \big[\Phi_1\big]_{\alpha_1}^{b_1}(0)\, \big[\Phi_2\big]_{\alpha_2}^{b_2}(0) \big| H_1(\rho_1, \tau_1) H_2(\rho_2, \tau_2) \big\rangle \\ &= \sum\!\!\!\!\!\!\int_{X_s} \bigg(\prod_{i=1}^{2} \frac{1}{\mathcal{N}_i}\, \big[\overline{\mathcal{P}}^{(i)}\big]_{\alpha_i \bar{\alpha}_i}^{b_i \bar{b}_i}\, \big[\mathcal{P}^{(i)}\big]_{\bar{\beta}_i \beta_i}^{\bar{c}_i c_i} \bigg) \big\langle H_1(\rho_1) H_2(\rho_2) \big| \big[\bar{\Phi}_1\big]_{\bar{\beta}_1}^{\bar{c}_1}(t_1 \bar{n}_1)\, \big[\bar{\Phi}_2\big]_{\bar{\beta}_2}^{\bar{c}_2}(t_2 \bar{n}_2) \dots \big| X_s \big\rangle \\ &\qquad \times \big\langle X_s \big| \dots \big[\Phi_1\big]_{\beta_1}^{c_1}(0)\, \big[\Phi_2\big]_{\beta_2}^{c_2}(0) \big| H_1(\rho_1) H_2(\rho_2) \big\rangle \,, \end{aligned} \tag{7.9}$$

[2] We omit the phase-space integrals associated with the soft radiation in (7.6) to increase readability. They are denoted by $\sum\!\!\!\!\!\!\int_{X_s}$ below.

where the color- and spin-average factors for the initial-state fields are

$$\mathcal{N}_i = \begin{cases} 2N_c & \text{for } i = q, \bar{q}\,, \\ (d-2)(N_c^2-1) & \text{for } i = g\,. \end{cases} \tag{7.10}$$

The ellipses represent the (conjugate) soft Wilson lines from the decoupling in the (conjugate) amplitude. Contracting color and Dirac/Lorentz indices of the collinear fields with the projectors, one finds

$$\begin{aligned} \big[\mathcal{P}^{(i)}\big]^{\bar{a}a}_{\bar{\alpha}\alpha}\,\big[\bar{\mathcal{X}}_i\big]^{\bar{a}}_{\bar{\alpha}}(t_i\bar{n}_i)\,\big[\mathcal{X}_i\big]^{a}_{\alpha}(0) &= \bar{\mathcal{X}}_i(t_i\bar{n}_i)\,\frac{\bar{\not{n}}_i}{2}\,\mathcal{X}_i(0)\,, \\ \big[\mathcal{P}^{(i)}\big]^{\bar{a}a}_{\bar{\alpha}\alpha}\,\big[\mathcal{X}_i\big]^{\bar{a}}_{\bar{\alpha}}(t_i\bar{n}_i)\,\big[\bar{\mathcal{X}}_i\big]^{a}_{\alpha}(0) &= -\bar{\mathcal{X}}_i(0)\,\frac{\bar{\not{n}}_i}{2}\,\mathcal{X}_i(t_i\bar{n}_i)\,, \\ \big[\mathcal{P}^{(i)}\big]^{\bar{a}a}_{\bar{\alpha}\alpha}\,\big[\mathcal{A}_i^{\perp}\big]^{\bar{a}}_{\bar{\alpha}}(t_i\bar{n}_i)\,\big[\mathcal{A}_i^{\perp}\big]^{a}_{\alpha}(0) &= 2\,\mathrm{tr}\big[i\partial_{t_i}\,\mathcal{A}^{\perp}_{i,\mu}(t_i\bar{n}_i)\,\mathcal{A}_i^{\perp\mu}(0)\big]\,, \end{aligned} \tag{7.11}$$

where the minus sign in the second equation appears due to the Grassmann character of the fermionic fields. The leftover factors $\bar{n}_i\cdot\rho_i$ in (7.8) combine with the conjugate projectors to

$$\bar{n}_i\cdot\rho_i\,\big[\overline{\mathcal{P}}^{(i)}\big]^{a\bar{a}}_{\alpha\bar{\alpha}} = \frac{1}{\xi_i}\,\delta^{a\bar{a}}\sum_{s_i}\begin{cases} u_\alpha(\xi_i\,\rho_i;s_i)\,\bar{u}_{\bar{\alpha}}(\xi_i\,\rho_i;s_i) & \text{for } i=q\,, \\ \bar{v}_\alpha(\xi_i\,\rho_i;s_i)\,v_{\bar{\alpha}}(\xi_i\,\rho_i;s_i) & \text{for } i=\bar{q}\,, \\ \varepsilon_\alpha(\xi_i\,\rho_i;s_i)\,\varepsilon^*_{\bar{\alpha}}(\xi_i\,\rho_i;s_i) & \text{for } i=g\,. \end{cases} \tag{7.12}$$

Combining these spinors/polarization vectors for the initial-state partons with the ones of the final state in (7.8) yields together with the Wilson coefficients the *partonic* $1+2\to 3\ldots m$ scattering amplitude [81]

$$\mathcal{M}_m(\{\underline{p}\},\mu) = \mathcal{C}_m(\{\underline{p}\},\mu)\times\big[\text{spinors/polarization vectors}\big]\,, \tag{7.13}$$

where the implicit Dirac/Lorentz indices on the right-hand side are contracted. The two inverse factors ξ_1, ξ_2 combine with s from (7.6) to the partonic center-of-mass energy $\hat{s} = \xi_1\xi_2 s$. To prove relation (7.9) and the following, one can contract both sides with $\mathcal{P}^{(i)}$ and turn derivatives $-i\partial_{t_i}$ into $\xi_i\,\bar{n}_i\cdot\rho_i$ by integration by parts.

Finally, factorizing hard physics in the form of Wilson coefficients and soft+collinear physics encoded in the hadronic matrix elements, one obtains the factorization theorem (7.1). Using color-helicity-space formalism, see Appendix A.3, one can organize the contraction of indices in a convenient way. In this formalism the hard function is defined by

$$\begin{aligned} \boldsymbol{\mathcal{H}}_m \coloneqq \frac{1}{2\xi_1\xi_2 s}\prod_{j=3}^{m}\int\frac{dE_j\,E_j^{d-3}}{\tilde{c}^\epsilon\,(2\pi)^2}\,\big|\mathcal{M}_m(\{\underline{p}\},\mu)\big\rangle\big\langle\mathcal{M}_m(\{\underline{p}\},\mu)\big| \\ \times(2\pi)^d\,2\,\delta(\bar{n}_1\cdot p_{\text{tot}}-\xi_1\sqrt{s})\,\delta(\bar{n}_2\cdot p_{\text{tot}}-\xi_2\sqrt{s})\,\delta^{(d-2)}(p_{\text{tot}}^{\perp})\,\Theta_{\text{hard}}(\{\underline{n}\})\,, \end{aligned} \tag{7.14}$$

where the vectors n_i are chosen in the laboratory frame, i.e. $p_i = E_i\,n_i$ and the energies of the incoming partons are $E_1 = \xi_1\sqrt{s}/2$ and $E_2 = \xi_2\sqrt{s}/2$. This implies $n_1\cdot n_2 = 2$

and, therefore, n_1 is anti-collinear to n_2. The amplitude expressed as vector in color-helicity space is squared as density matrix. Here, we include a factor $\tilde{c} \coloneqq e^{\gamma_E}/\pi$ as explained below. The low-energy matrix element contains all soft+collinear physics and is given by the Fourier transformation

$$\boldsymbol{\mathcal{W}}_m(\{\underline{n}\}, Q_0, \xi_1, \xi_2, \mu) \coloneqq \int \frac{dt_1}{2\pi} \frac{dt_2}{2\pi} \, \widetilde{\boldsymbol{\mathcal{W}}}_m(\{\underline{n}\}, Q_0, t_1, t_2, \mu) \, e^{-it_1 \xi_1 \bar{n}_1 \cdot \rho_1} \, e^{-it_2 \xi_2 \bar{n}_2 \cdot \rho_2} \tag{7.15}$$

of

$$\begin{aligned} \widetilde{\boldsymbol{\mathcal{W}}}_m \coloneqq \sum\!\!\!\!\!\!\int_{X_s} \mathcal{P}^{(1)} \, \mathcal{P}^{(2)} \, \big\langle H_1(\rho_1) \, H_2(\rho_2) \big| \bar{\Phi}_1(t_1 \bar{n}_1) \, \bar{\Phi}_2(t_2 \bar{n}_2) \, \boldsymbol{S}_1^\dagger(n_1) \dots \boldsymbol{S}_m^\dagger(n_m) \big| X_s \big\rangle \\ \times \big\langle X_s \big| \boldsymbol{S}_1(n_1) \dots \boldsymbol{S}_m(n_m) \, \Phi_1(0) \, \Phi_2(0) \big| H_1(\rho_1) \, H_2(\rho_2) \big\rangle \, \theta(Q_0 - E_{\text{out}}^\perp) \,, \end{aligned} \tag{7.16}$$

with the projectors as in (7.11). It is thus a unit matrix in helicity space. In (7.1) the hard function and the low-energy matrix element are first combined and then integrated over the directions of the final-state partons n_j denoted by the $\otimes$ symbol. It is defined by

$$\begin{aligned} &\boldsymbol{\mathcal{H}}_m(\{\underline{n}\}, s, \xi_1, \xi_2, \mu) \otimes \boldsymbol{\mathcal{W}}_m(\{\underline{n}\}, Q_0, \xi_1, \xi_2, \mu) \\ &\coloneqq \prod_{j=3}^{m} \int [d\Omega_j] \, \boldsymbol{\mathcal{H}}_m(\{\underline{n}\}, s, \xi_1, \xi_2, \mu) \, \boldsymbol{\mathcal{W}}_m(\{\underline{n}\}, Q_0, \xi_1, \xi_2, \mu) \end{aligned} \tag{7.17}$$

with the $(d-2)$-dimensional angular integral

$$[d\Omega_j] \coloneqq \tilde{c}^\epsilon \, \frac{d^{d-2}\Omega_j}{2(2\pi)^{d-3}} \,. \tag{7.18}$$

In the combination of the hard function and angular integrals, the factors of $\tilde{c}^\epsilon$ cancel out, but prevent a proliferation of γ_E terms and logarithms of π in intermediate steps. The trace denoted by $\langle \dots \rangle$ contains the sum (average) over final-state (initial-state) color and helicity indices, i.e. it includes one factor (7.10) for each initial-state parton. The factorization theorem (7.1) for gap-between-jet cross sections at hadron colliders is depicted in Figure 7.1.

The low-energy matrix element in (7.16) is *not* factorized into a soft and a collinear part, because Glauber-gluon exchanges in the low-energy EFT still mediate interactions between the two sectors. The corresponding Glauber Lagrangian is derived in [10] for forward scattering. As the Glauber-gluon interactions are associated with the jet-veto scale Q_0, one can match below this scale onto an EFT involving only soft and collinear fields associated with the scale Λ_{QCD} of non-perturbative physics. We conjecture that the Glauber interactions cancel at this scale, similar to the mechanism for the Drell–Yan process [84–86].[3] As soon as Glauber interactions are absent, the low-energy matrix element factorizes into the usual collinear parton distribution functions (PDFs) for quarks and gluons inside the hadron H_i

$$f_i(\xi_i, \mu) = \int \frac{dt_i}{2\pi} \, e^{-it_i \xi_i \bar{n}_i \cdot \rho_i} \, \big\langle H_i(\rho_i) \big| \bar{\Phi}_i(t_i \bar{n}_i) \, \mathcal{P}^{(i)} \, \Phi_i(0) \big| H_i(\rho_i) \big\rangle \tag{7.19}$$

[3] Only recently, it was shown that up to three-loop level breaking of collinear factorization does *not* imply breaking of PDF factorization [87].

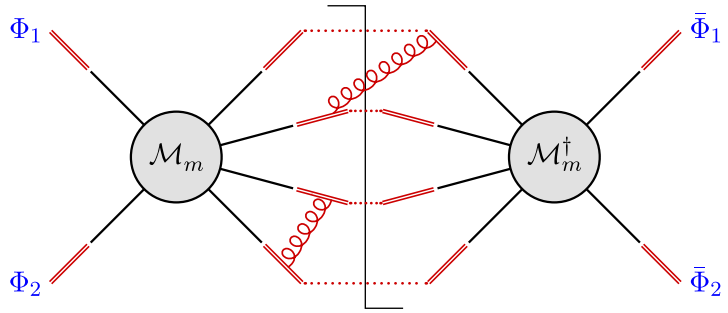

Figure 7.1: Graphical representation of the factorization theorem (7.1) for gap-between-jet cross sections at hadron colliders. Soft physics is indicated in red, the hard function $\boldsymbol{\mathcal{H}}_m$ is shown in black and collinear fields for the initial-state partons are shown in blue. The low-energy matrix element $\boldsymbol{\mathcal{W}}_m$ contains soft Wilson lines from the decoupling (double lines) as well as real and virtual soft gluons (curly lines).

and a vacuum matrix element containing only soft Wilson lines. To answer the question whether the loss of color coherence breaks collinear PDF factorization properly, one needs to study Glauber exchanges involving spectator partons.[4] At least for some observables they seem to be present [88–90] and also seem to be phenomenologically relevant [91]. This open issue will be addressed in future work. At the scale $\mu_s \sim Q_0$, the leading order form of the low-energy matrix element is

$$\boldsymbol{\mathcal{W}}_m(\{\underline{n}\}, Q_0, \xi_1, \xi_2, \mu_s) = f_1(\xi_1, \mu_s)\, f_2(\xi_2, \mu_s)\, \mathbf{1}_m + \mathcal{O}(\alpha_s)\,. \tag{7.20}$$

We show below, that the RG evolution creates double logarithms in the scale ratio Q/Q_0. As the low-energy theory naively only knows about a single scale Q_0, it must suffer from a collinear anomaly at higher orders in perturbation theory, producing rapidity logarithms [92,93]. These logarithms are a characteristic of processes involving Glauber gluons [10]. However, they need to have an intricate structure as the SLLs only start at four-loop order and deserve further studies in the future.

7.3 Anomalous Dimension

As the cross section is a physical observable, the dependence on the renormalization scale μ in (7.1) of hard function and low-energy matrix element needs to cancel. Therefore, their RG evolution is governed by the same anomalous dimension. The RG equation of the hard function reads [73]

$$\frac{d}{d\ln\mu}\,\boldsymbol{\mathcal{H}}_m(\{\underline{n}\}, s, \mu) = -\sum_{l=2+M}^{m} \boldsymbol{\mathcal{H}}_l(\{\underline{n}\}, s, \mu) * \boldsymbol{\Gamma}^H_{lm}(\{\underline{n}\}, s, \mu)\,, \tag{7.21}$$

where $\boldsymbol{\Gamma}^H$ is a matrix in color and multiplicity space. The anomalous dimension is an upper triangular matrix in multiplicity space, since virtual and real emissions can

[4] The authors of [80] state that the loss of coherence extends also to many *global* observables.

only map hard functions $\boldsymbol{\mathcal{H}}_l$ to $\boldsymbol{\mathcal{H}}_m$ with $m \geq l$. Its one loop form is

$$\boldsymbol{\Gamma}^H = \frac{\alpha_s}{4\pi} \begin{pmatrix} \boldsymbol{V}_{2+M} & \boldsymbol{R}_{2+M} & 0 & 0 & \dots \\ 0 & \boldsymbol{V}_{2+M+1} & \boldsymbol{R}_{2+M+1} & 0 & \dots \\ 0 & 0 & \boldsymbol{V}_{2+M+2} & \boldsymbol{R}_{2+M+2} & \dots \\ 0 & 0 & 0 & \boldsymbol{V}_{2+M+3} & \dots \\ \vdots & \vdots & \vdots & \vdots & \ddots \end{pmatrix} + \mathcal{O}(\alpha_s^2)\,, \tag{7.22}$$

where the virtual (real) entries on the (secondary) diagonal are determined in the following. The $*$ symbol in (7.21) indicates a convolution over the momentum fractions for each initial-state parton

$$(f * g)(\xi_i) \coloneqq \int_0^1 d\xi_i'\; f(\xi_i'\,\xi_i)\, g(\xi_i')\,. \tag{7.23}$$

It is thus convenient to omit the momentum-fraction arguments when using this notation. More details on the convolution over momentum fractions can be found at the end of Section 7.3.3. In contrast to e^+e^- colliders [70, 71], soft+collinear singularities related to the color-charged initial-state partons generate an explicit logarithm of the renormalization scale μ in the anomalous dimension. This logarithm is the source of the SLLs.

The hard function can be evolved from its characteristic scale $\mu_h \sim \sqrt{\hat{s}}$ down to the one of the low-energy matrix element $\mu_s \sim Q_0$ by solving the RG equation (7.21). A formal solution can be written in terms of the path-ordered exponential

$$\boldsymbol{U}(\{\underline{n}\}, s, \mu_h, \mu_s) = \mathbf{P} \exp\left[\int_{\mu_s}^{\mu_h} \frac{d\mu}{\mu}\, \boldsymbol{\Gamma}^H(\{\underline{n}\}, s, \mu)\right]. \tag{7.24}$$

It is defined by its series expansion[5,6]

$$\begin{aligned} \boldsymbol{\mathcal{H}}(\mu_s) &= \boldsymbol{\mathcal{H}}(\mu_h) * \boldsymbol{U}(\mu_h, \mu_s) \\ &= \boldsymbol{\mathcal{H}}(\mu_h) + \int_{\mu_s}^{\mu_h} \frac{d\mu_1}{\mu_1}\, \boldsymbol{\mathcal{H}}(\mu_h) * \boldsymbol{\Gamma}^H(\mu_1) \\ &\quad + \int_{\mu_s}^{\mu_h} \frac{d\mu_1}{\mu_1} \int_{\mu_s}^{\mu_1} \frac{d\mu_2}{\mu_2}\, \boldsymbol{\mathcal{H}}(\mu_h) * \boldsymbol{\Gamma}^H(\mu_1) * \boldsymbol{\Gamma}^H(\mu_2) + \dots\,, \end{aligned} \tag{7.25}$$

where the anomalous-dimension matrices on the right-hand side are ordered in the direction of decreasing scale values, i.e. $\mu_1 > \mu_2$ in the last line. By calculating this path-ordered exponential explicitly keeping only the leading-logarithmic terms in $\boldsymbol{\Gamma}^H$, one can resum the SLLs, see Chapter 8.

In the following, we derive in detail the one-loop anomalous dimension $\boldsymbol{\Gamma}^H$ of the hard function for hadron colliders and study the (non-)cancellation of (initial-) final-state collinear singularities.

[5] Here and in the following, we only indicate the – for the property studied – most relevant arguments to increase readability.

[6] As the $*$ convolution, defined in (7.23), is not associative, we use the convention that the leftmost product is convoluted first, i.e. $f * g * h \coloneqq (f * g) * h$.

7.3.1 Virtual Singularities

Infrared (IR) singularities of massless gauge amplitudes are a well studied subject [81, 94–98]. As shown in [81,94], the IR singularities of massless on-shell QCD amplitudes correspond to the ultraviolet (UV) singularities of soft and collinear loops in SCET and, therefore, can be renormalized with standard methods. The amplitudes renormalize multiplicatively

$$\left|\mathcal{M}_m(\{\underline{p}\},\mu)\right\rangle = \lim_{\epsilon\to 0} \boldsymbol{Z}^{-1}(\{\underline{p}\},\mu,\epsilon)\left|\mathcal{M}_m(\{\underline{p}\},\epsilon)\right\rangle . \tag{7.26}$$

The RG equation of the renormalized amplitude is determined by an anomalous dimension matrix, which is related to the $\boldsymbol{Z}$-factor by

$$\boldsymbol{\Gamma}^{\mathcal{M}}(\{\underline{p}\},\mu) = -\boldsymbol{Z}^{-1}(\{\underline{p}\},\mu,\epsilon)\,\frac{d}{d\ln\mu}\,\boldsymbol{Z}(\{\underline{p}\},\mu,\epsilon) . \tag{7.27}$$

This anomalous dimension takes into account all soft and collinear singularities and is up to two-loop order given by [94]

$$\boldsymbol{\Gamma}^{\mathcal{M}}(\{\underline{p}\},\mu) = \frac{1}{2}\sum_{(ij)} \boldsymbol{T}_i\cdot\boldsymbol{T}_j\,\gamma_{\text{cusp}}(\alpha_s)\,\ln\frac{\mu^2}{-s_{ij}} + \sum_{i=1}^{m}\gamma^i(\alpha_s)\,\mathbf{1} + \mathcal{O}(\alpha_s^3) , \tag{7.28}$$

where $s_{ij} \coloneqq 2\sigma_{ij}\,p_i\cdot p_j + i0$ and $\sigma_{ij} = +1$ if partons i,j are both incoming or both outgoing and $\sigma_{ij} = -1$ otherwise.[7] The first sum runs over all unordered pairs of partons with $i \neq j$, indicated by the symbol (ij). In the hard function $\boldsymbol{\mathcal{H}}_m$ the squared amplitude is integrated over the energies of the final-state partons taking phase-space constraints into account, see (7.14). The cusp logarithm in (7.28) depends on these energies through the s_{ij} and, therefore, one cannot immediately translate $\boldsymbol{\Gamma}^{\mathcal{M}}$ to the anomalous dimension of the hard function. Splitting angular and energy dependence of the cusp logarithm, one finds

$$\ln\frac{\mu^2}{-s_{ij}} = \ln\frac{2}{n_i\cdot n_j} + \ln\frac{\mu}{2E_i} + \ln\frac{\mu}{2E_j} + i\pi\,\Pi_{ij} , \tag{7.29}$$

where $2\Pi_{ij} = \sigma_{ij} + 1$. The last term is only present when partons i,j are both incoming or both outgoing and is related to the Glauber phases. Applying color conservation (A.3.7) for the two middle terms, the color structure simplifies

$$\begin{aligned}\boldsymbol{\Gamma}^{\mathcal{M}}(\{\underline{p}\},\mu) &= \frac{1}{2}\sum_{(ij)} \boldsymbol{T}_i\cdot\boldsymbol{T}_j\,\gamma_{\text{cusp}}(\alpha_s)\left(\ln\frac{2}{n_i\cdot n_j} + i\pi\,\Pi_{ij}\right)\\ &\quad + \sum_{i=1}^{m}\left(-C_i\,\gamma_{\text{cusp}}(\alpha_s)\,\ln\frac{\mu}{2E_i} + \gamma^i(\alpha_s)\right)\mathbf{1}\\ &= \boldsymbol{\Gamma}_s^{\mathcal{M}} + \sum_{i=1}^{m}\Gamma_{c,i}^{\mathcal{M}}\,\mathbf{1} ,\end{aligned} \tag{7.30}$$

[7] Remember that the momenta of the incoming partons are $p_1 = \xi_1\,\rho_1$ and $p_2 = \xi_2\,\rho_2$.

where C_i is the eigenvalue of the quadratic Casimir associated with the representation of parton i. The anomalous dimension splits into a purely soft part $\mathbf{\Gamma}_s^{\mathcal{M}}$ and m collinear parts $\Gamma_{c,i}^{\mathcal{M}}$, one for each parton.

Translating the anomalous dimension of the amplitude back into the $\boldsymbol{Z}$-factor, as for example described in Appendix B of [98], yields

$$\begin{aligned}\boldsymbol{Z}(\{\underline{p}\},\mu,\epsilon) = \mathbf{1} &- \frac{\alpha_s}{4\pi}\frac{1}{2\epsilon}\frac{1}{2}\sum_{(ij)} \boldsymbol{T}_i\cdot\boldsymbol{T}_j\,\gamma_0\left(\int\frac{d^2\Omega_k}{4\pi}\,\overline{W}_{ij}^k - i\pi\,\Pi_{ij}\right)\\ &- \frac{\alpha_s}{4\pi}\sum_{i=1}^{m}\left[C_i\,\gamma_0\left(\frac{1}{4\epsilon^2}+\frac{1}{2\epsilon}\ln\frac{\mu}{2E_i}\right)-\frac{\gamma_0^i}{2\epsilon}\right]\mathbf{1}+\mathcal{O}(\alpha_s^2)\,,\end{aligned} \tag{7.31}$$

where the non-trivial term in the first line regularizes the soft singularities and the term in the second line the collinear ones. Here, $\gamma_0 = 4$ is the first term in the expansion of the cusp anomalous dimension

$$\gamma_{\text{cusp}}(\alpha_s) = \sum_{n=0}^{\infty}\gamma_n\left(\frac{\alpha_s}{4\pi}\right)^{n+1} \tag{7.32}$$

and $\gamma_0^q = \gamma_0^{\bar{q}} = -3C_F$ and $\gamma_0^g = -\frac{11}{3}C_A + \frac{4}{3}T_F\,n_f$ are the first terms in a similar expansion of the quark and gluon anomalous dimensions, respectively. The one-loop coefficient of the cusp anomalous dimension can be found in Appendix A.4 and the number of quark flavors is denoted by n_f. In (7.31), we express the angular-dependent part of the cusp logarithm (7.29) as integral over the direction of the virtual gluon

$$\int\frac{d^2\Omega_k}{4\pi}\,\overline{W}_{ij}^k = \ln\frac{n_i\cdot n_j}{2}\,, \tag{7.33}$$

where the measure is the 4-dimensional version of (7.18) and the integrand is the soft dipole

$$W_{ij}^k := \frac{n_i\cdot n_j}{n_i\cdot n_k\,n_j\cdot n_k} \tag{7.34}$$

with subtracted collinear limits, i.e. $n_i \parallel n_k$ or $n_j \parallel n_k$,

$$\overline{W}_{ij}^k := W_{ij}^k - \frac{1}{n_i\cdot n_k}\,\delta(n_i-n_k) - \frac{1}{n_j\cdot n_k}\,\delta(n_j-n_k). \tag{7.35}$$

The soft dipole is given by the product of two eikonal factors summed over the spin of the virtual gluon. Subtracting the collinear limits is necessary as the associated singularities are already regularized by the second line in (7.31).

Soft limits: We are now ready to consider the soft limit of the hard function. At one loop, the associated virtual singularities are

$$\begin{aligned}\boldsymbol{\mathcal{H}}_m(\epsilon) = &-\frac{\alpha_s}{4\pi}\frac{1}{2\epsilon}\frac{1}{2}\sum_{(ij)}\gamma_0\left(\boldsymbol{T}_{i,L}\cdot\boldsymbol{T}_{j,L}+\boldsymbol{T}_{i,R}\cdot\boldsymbol{T}_{j,R}\right)\int\frac{d^2\Omega_k}{4\pi}\,\overline{W}_{ij}^k\,\boldsymbol{\mathcal{H}}_m(\mu)\\ &+\frac{\alpha_s}{4\pi}\frac{1}{2\epsilon}\,\gamma_0\,2i\pi\left(\boldsymbol{T}_{1,L}\cdot\boldsymbol{T}_{2,L}-\boldsymbol{T}_{1,R}\cdot\boldsymbol{T}_{2,R}\right)\boldsymbol{\mathcal{H}}_m(\mu)+\dots\,,\end{aligned} \tag{7.36}$$

where ellipsis denote terms that are free of soft singularities at one loop. The color matrices $\boldsymbol{T}_{i,L}$ ($\boldsymbol{T}_{i,R}$) act on the (conjugate) scattering amplitude and multiply the hard function from the left (right). The terms in the second line are purely imaginary and were simplified using color conservation (A.3.7)

$$\begin{aligned}\sum_{(ij)} \boldsymbol{T}_i\cdot\boldsymbol{T}_j\,\Pi_{ij} &= 2\,\boldsymbol{T}_1\cdot\boldsymbol{T}_2 + \sum_{i=3}^{m} \boldsymbol{T}_i\cdot(-\boldsymbol{T}_1-\boldsymbol{T}_2-\boldsymbol{T}_i)\\ &= 2\,\boldsymbol{T}_1\cdot\boldsymbol{T}_2 + (\boldsymbol{T}_1+\boldsymbol{T}_2)\cdot(\boldsymbol{T}_1+\boldsymbol{T}_2) - \sum_{i=3}^{m} C_i\\ &= 4\,\boldsymbol{T}_1\cdot\boldsymbol{T}_2 + C_1 + C_2 - \sum_{i=3}^{m} C_i\,.\end{aligned} \tag{7.37}$$

The constant imaginary part cancels between amplitude and its conjugate on the level of the anomalous dimension. The part proportional to $\boldsymbol{T}_1\cdot\boldsymbol{T}_2$ is only present if both incoming partons are color-charged, i.e. there are no Glauber phases for e^+e^- colliders and one can drop them in (7.36), see [71]. As the contribution of Glauber phases can always be moved to the initial state, our assumption leading to (7.5) is justified.

Collinear limits: When determining the contribution of collinear singularities, we need to worry about the integrals over the final-state energies in (7.14). Decomposing the hard function

$$\boldsymbol{\mathcal{H}}_m(\{\underline{n}\},s,\xi_1,\xi_2) = \int d\mathcal{E}_m\,\widetilde{\boldsymbol{\mathcal{H}}}_m(\{\underline{p}\}) \tag{7.38}$$

where $d\mathcal{E}_m$ denotes these integrals including phase-space constraints and flux factor, and defining an "unintegrated" hard function by

$$\widetilde{\boldsymbol{\mathcal{H}}}_m(\{\underline{p}\}) \coloneqq \big|\mathcal{M}_m(\{\underline{p}\})\big\rangle\big\langle\mathcal{M}_m(\{\underline{p}\})\big|\,, \tag{7.39}$$

allows one to simplify the notation in the following discussion. Note that the integral $d\mathcal{E}_m$ contains only $(m-2)$ energy integrals, one for each final-state parton. The one loop virtual collinear singularities are given by

$$\boldsymbol{\mathcal{H}}_m(\{\underline{p}\},\epsilon) = -\frac{\alpha_s}{4\pi}\int d\mathcal{E}_m \sum_{i=1}^{m}\left[C_i\,\gamma_0\left(\frac{1}{2\epsilon^2}+\frac{1}{\epsilon}\ln\frac{\mu}{2E_i}\right)-\frac{\gamma_0^i}{\epsilon}\right]\widetilde{\boldsymbol{\mathcal{H}}}_m(\{\underline{p}\},\mu)+\dots\,, \tag{7.40}$$

where ellipsis denote terms that are free of collinear singularities at one loop. Adding the contributions of the amplitude and its conjugate simply results in a factor 2 compared to (7.31), as virtual collinear singularities are associated with a trivial color structure.

7.3.2 Real Singularities

Similar to the virtual corrections studied in the previous section, real emissions develop singularities if the emitted parton becomes soft or collinear. As we are dealing with color-charged initial-state partons, we distinguish two types of collinear singularities

(i) time-like, originating from two final-state partons becoming collinear,

(ii) space-like, originating from one initial- and one final-state parton becoming collinear.

In the following, we study both of them in more detail.

Soft limits: In the soft limit, scattering amplitudes factorize according to

$$\left|\mathcal{M}_{m+1}(\{\underline{p},k\})\right\rangle = \varepsilon^*_\mu(k;s_k)\,\boldsymbol{J}^{\mu,a_k}(k)\left|\mathcal{M}_m(\{\underline{p}\})\right\rangle, \tag{7.41}$$

where momentum, color and spin of the soft gluon are labeled by k, a_k and s_k, respectively. The soft current at tree-level is given by

$$\boldsymbol{J}^{\mu,a_k}(k) = -g_s \sum_{i=1}^{m} \frac{n_i^\mu}{n_i\cdot k}\,\boldsymbol{T}_i^{a_k} \tag{7.42}$$

and the one- and two-loop results can be found in [99] and [100, 101], respectively. Performing the polarization sum for the emitted soft gluon, contained in $\langle\ldots\rangle$, on the level of the unintegrated hard function, one finds

$$\sum_{s_k}\widetilde{\boldsymbol{\mathcal{H}}}_{m+1}(\{\underline{p},k\},\epsilon) = -4\pi\alpha_s\,\tilde{\mu}^{2\epsilon}\sum_{(ij)}\frac{n_i\cdot n_j}{n_i\cdot k\,n_j\cdot k}\,\boldsymbol{T}_i^{a_k}\,\widetilde{\boldsymbol{\mathcal{H}}}_m(\{\underline{p}\},\mu)\,\boldsymbol{T}_j^{\bar{a}_k}, \tag{7.43}$$

where only the term $-\eta^{\mu\nu}$ of the polarization sum contributes by color conservation, and the strong coupling is renormalized in the $\overline{\text{MS}}$ scheme $\tilde{\mu}^2 \coloneqq \tilde{c}/4\,\mu^2$. As the momentum $k = E_k\,n_k$ of the gluon is soft, it is not part of the momentum conserving δ-functions in (7.14) and the integral over E_k can be evaluated straightforwardly. Isolating the soft divergence by introducing a cutoff, one finds [71, 102]

$$\sum_{s_k}\boldsymbol{\mathcal{H}}_{m+1}(\{\underline{p},k\},\epsilon) = \frac{\alpha_s}{\pi}\,\frac{1}{2\epsilon}\sum_{(ij)}\boldsymbol{T}_{i,L}\circ\boldsymbol{T}_{j,R}\,\overline{W}^k_{ij}\,\theta_{\text{hard}}(n_k)\,\boldsymbol{\mathcal{H}}_m(\{\underline{p}\},\mu)+\ldots, \tag{7.44}$$

where ellipsis denote terms that are free of soft singularities at one loop and the $\circ$ symbol describes the extension of the color space, now including the emitted collinear gluon. More details can be found in Appendix A.3. Here the soft dipole with subtracted collinear limits (7.35) appears as collinear singularities are treated separately below.

Time-like collinear limits: Similar to the factorization in the soft limit (7.41), the amplitude factorizes if two partons i, j become collinear. At tree level, one finds [103]

$$\left|\mathcal{M}_{m+1}(p_1,\ldots,p_i,p_j,\ldots,p_{m+1})\right\rangle = \mathbf{Sp}(p_i,p_j)\left|\mathcal{M}_m(p_1,\ldots,P,\ldots,p_{m+1})\right\rangle, \tag{7.45}$$

where explicit expressions for all tree-level splitting amplitudes $\mathbf{Sp}(p_i,p_j)$ can be found in [63]. This factorization formula holds for both time-like, i.e. $P\to i+j$ in the final state, and space-like, i.e. $i\to P+j$ in the initial state, splittings. As the splitting amplitudes are matrices in color-helicity space, the color *and* spin structure is different between left-hand and right-hand side.

Let us start with the time-like case (i). If both partons i, j are in the final state, one can parameterize their momenta as $p_i \approx \xi P$ and $p_j \approx (1-\xi)P$ where the momentum of

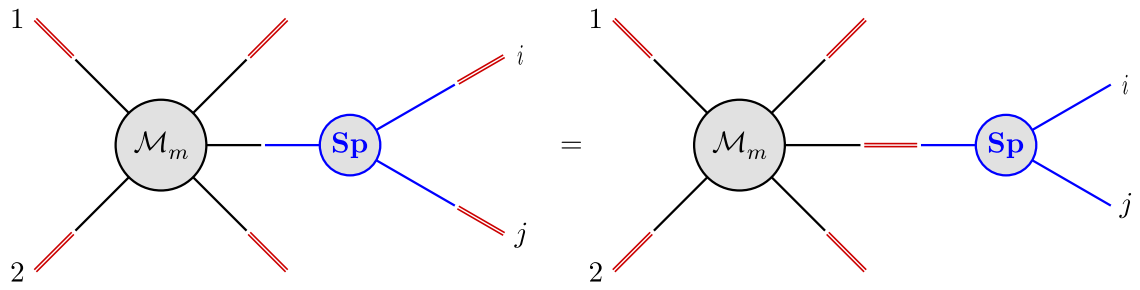

Figure 7.2: The amplitude factorizes if partons i and j become collinear. The associated soft Wilson lines (red double lines) combine into a single Wilson line for the parent parton.

the parent parton $P^2 \to 0$. The hard function $\boldsymbol{\mathcal{H}}_{m+1}$ in the factorization theorem (7.1) is multiplied from the left and right with soft Wilson lines contained in the low-energy matrix element $\boldsymbol{\mathcal{W}}_{m+1}$. If the final-state partons i, j become collinear, the two associated outgoing Wilson lines combine to a single Wilson line in the common direction n_P

$$\boldsymbol{S}_i(n_P)\,\boldsymbol{S}_j(n_P) = \boldsymbol{S}_{i+j}(n_P) = \mathbf{P}\exp\left[ig_s\int_0^\infty dt\; n_P\cdot A_s^a(tn_P)\big(\boldsymbol{T}_i^a + \boldsymbol{T}_j^a\big)\right]. \tag{7.46}$$

From color conservation, one can immediately infer that

$$\big(\boldsymbol{T}_i^a + \boldsymbol{T}_j^a\big)\,\mathbf{Sp}(p_i,p_j) = \mathbf{Sp}(p_i,p_j)\,\boldsymbol{T}_P^a\,, \tag{7.47}$$

which implies that the color state of the partons after the splitting corresponds to one of the parent parton [81, 103]. Consequently, we find an operator version of the usual QCD coherence

$$\begin{aligned}&\boldsymbol{S}_i(n_P)\,\boldsymbol{S}_j(n_P)\,\mathbf{Sp}(p_i,p_j)\,\big|\mathcal{M}_m(p_1,\dots,P,\dots,p_{m+1})\big\rangle\\ &= \mathbf{Sp}(p_i,p_j)\,\boldsymbol{S}_P(n_P)\,\big|\mathcal{M}_m(p_1,\dots,P,\dots,p_{m+1})\big\rangle\,,\end{aligned} \tag{7.48}$$

stating that the soft emissions from two collinear partons are the same as the collinear emissions from the parent parton. It is illustrated in Figure 7.2. Exploiting this on the level of the unintegrated hard function and the low-energy matrix element, one finds

$$\begin{aligned}&\big\langle\widetilde{\boldsymbol{\mathcal{H}}}_{m+1}(\{\underline{p}\},\epsilon)\,\boldsymbol{\mathcal{W}}_{m+1}(\{\underline{n}\},\epsilon)\big\rangle\\ &\xrightarrow[i\parallel j]{} \big\langle\mathbf{Sp}(p_i,p_j)\,\widetilde{\boldsymbol{\mathcal{H}}}_m(\{\underline{\hat{p}}\},\epsilon)\,\boldsymbol{\mathcal{W}}_m(\{\underline{\hat{n}}\},\epsilon)\,\mathbf{Sp}^\dagger(p_i,p_j)\big\rangle\\ &= 4\pi\alpha_s\,\tilde{\mu}^{2\epsilon}\,\frac{2}{s_{ij}}\,\mathcal{P}_{i+j\leftarrow P}(\xi)\,\big\langle\widetilde{\boldsymbol{\mathcal{H}}}_m(\{\underline{\hat{p}}\},\mu)\,\boldsymbol{\mathcal{W}}_m(\{\underline{\hat{n}}\},\mu)\big\rangle\,,\end{aligned} \tag{7.49}$$

where $s_{ij} = 2E_P^2\,\xi(1-\xi)\,n_i\cdot n_j$ and momenta $\{\underline{\hat{p}}\} = \{p_1,\dots,p_{i-1},P,p_{j+1},\dots,p_{m+1}\}$ and directions $\{\underline{\hat{n}}\} = \{n_1,\dots,n_{i-1},n_P,n_{j+1},\dots,n_{m+1}\}$ for time-like splittings. The trace $\langle\dots\rangle$ in the first two lines contains the sum over color and helicity indices of partons i, j and in the last line over the ones of parent parton P. Evaluating the squared splitting amplitudes under the trace is equivalent to averaging over their spin.

This yields the so-called splitting functions $\mathcal{P}_{i+j\leftarrow P}$, which can be found in (14–17) of [104] and are given by

$$\begin{aligned}
\mathcal{P}_{q+g\leftarrow q}(\xi) &= \mathcal{P}_{\bar{q}+g\leftarrow\bar{q}}(\xi) = C_F\left[\frac{1+\xi^2}{1-\xi} - \epsilon(1-\xi)\right],\\
\mathcal{P}_{g+q\leftarrow q}(\xi) &= \mathcal{P}_{g+\bar{q}\leftarrow\bar{q}}(\xi) = \mathcal{P}_{q+g\leftarrow q}(1-\xi)\,,\\
\mathcal{P}_{q+\bar{q}\leftarrow g}(\xi) &= \mathcal{P}_{\bar{q}+q\leftarrow g}(\xi) = T_F\left[1 - \frac{2\xi(1-\xi)}{1-\epsilon}\right],\\
\mathcal{P}_{g+g\leftarrow g}(\xi) &= 2C_A\left[\frac{\xi}{1-\xi} + \frac{1-\xi}{\xi} + \xi(1-\xi)\right].
\end{aligned} \tag{7.50}$$

The product of hard function and low-energy matrix element in (7.49) is integrated over $(m-1)$ directions of the final-state partons. Integrating over direction n_j, one encounters a collinear singularity

$$\int [d\Omega_j]\,\frac{1}{n_i\cdot n_j} = -\frac{1}{2\epsilon} + \mathcal{O}(\epsilon)\,. \tag{7.51}$$

The remaining angular integral can then be interpreted as the one over the direction of parent parton P, i.e. yielding the correct angular integrals for functions $\boldsymbol{\mathcal{H}}_m$ and $\boldsymbol{\mathcal{W}}_m$ of multiplicity m. The $(m-1)$ energy integrals can be split into an integral over the momentum fraction $\xi \in (0,1)$ and the $(m-2)$ energy integrals for these functions. Using that the measurement function is collinear safe, we find

$$\int d\mathcal{E}_{m+1}\,\frac{1}{E_P^2\,\xi(1-\xi)} = \int d\mathcal{E}_m\,\frac{E_P^{d-4}}{\tilde{c}^\epsilon(2\pi)^2}\int_0^1 d\xi\,\big[\xi(1-\xi)\big]^{d-4}\,. \tag{7.52}$$

Performing the momentum fraction integrals for the case that parent parton P is a (anti-)quark yields

$$\int_0^1 d\xi\,\big[\xi(1-\xi)\big]^{-2\epsilon}\,\frac{1}{2}\big[\mathcal{P}_{q+g\leftarrow q}(\xi) + \mathcal{P}_{g+q\leftarrow q}(\xi)\big] = C_F\left(-\frac{1}{\epsilon} - \frac{3}{2}\right) + \mathcal{O}(\epsilon)\,, \tag{7.53}$$

where one should average over the splittings $q\to q+g$ and $q\to g+q$ as they are both part of the same $(m+1)$-parton configuration. Of course, as the integral is symmetric under $\xi\to 1-\xi$ one could simply consider only one of the two channels. If the parent parton is a gluon, one also needs to take into account a factor $1/2$ for the splitting $g\to g+g$ to not over-count identical particles and sum over the flavors of the quark-anti-quark pair. We find in this case

$$\begin{aligned}
&\int_0^1 d\xi\,\big[\xi(1-\xi)\big]^{-2\epsilon}\,\frac{1}{2}\left(\mathcal{P}_{g+g\leftarrow g}(\xi) + \sum_q\big[\mathcal{P}_{q+\bar{q}\leftarrow g}(\xi) + \mathcal{P}_{\bar{q}+q\leftarrow g}(\xi)\big]\right)\\
&= C_A\left(-\frac{1}{\epsilon} - \frac{11}{6}\right) + \frac{2}{3}\,T_F\,n_f + \mathcal{O}(\epsilon)\,.
\end{aligned} \tag{7.54}$$

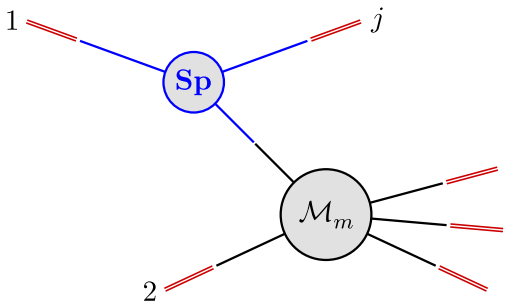

Figure 7.3: In the limit where initial-state parton 1 and final-state parton j become collinear, the amplitude still factorizes, but in contrast to the final-state collinear limit depicted in Figure 7.2, the soft Wilson lines associated with 1 and j do not combine.

Finally, combing the above results and summing over the splittings of all parent partons in the final-state, we find

$$\begin{aligned}&\int d\mathcal{E}_{m+1}\,\big\langle\widetilde{\boldsymbol{\mathcal{H}}}_{m+1}(\{\underline{p}\},\epsilon)\otimes\boldsymbol{\mathcal{W}}_{m+1}(\{\underline{n}\},\epsilon)\big\rangle \qquad (7.55)\\ &=\frac{\alpha_s}{4\pi}\int d\mathcal{E}_m\sum_{P=3}^{m}\left[C_P\,\gamma_0\left(\frac{1}{2\epsilon^2}+\frac{1}{\epsilon}\ln\frac{\mu}{2E_P}\right)-\frac{\gamma_0^P}{\epsilon}\right]\big\langle\widetilde{\boldsymbol{\mathcal{H}}}_m(\{\hat{\underline{p}}\},\mu)\otimes\boldsymbol{\mathcal{W}}_m(\{\hat{\underline{n}}\},\mu)\big\rangle+\dots\,,\end{aligned}$$

where ellipsis denote terms that are free of collinear final-state singularities at one loop.

Space-like collinear limits: Next, we study the case of collinear emission from an initial-state parton (ii). Without loss of generality, we restrict to splittings of initial-state parton 1. Instead of repeating the above derivation in this case, one can cross the momentum of parton i in the time-like result (7.49) to the initial state by replacing $p_i\to -p_1$.[8] To account also for the difference in kinematics, one needs to use $P\approx\xi\,p_1$ and $p_j\approx(1-\xi)p_1$, which implies we should also replace $\xi\to 1/\xi$. Even though (7.47) generalizes to partons in the initial state, it is not possible to commute and combine Wilson lines similar to (7.48). As already mentioned at the end of Section 3.1, the reason is that the soft Wilson line associated to parton 1 is incoming and the one associated to parton j is outgoing, see Figure 7.3. These two Wilson lines differ by their sign of the $i0$ prescription in the associated light-cone direction and, therefore, this effect is related to the Glauber phases in (7.37). On the level of the unintegrated hard function, the splitting factorization in the space-like case reads

$$\begin{aligned}&\big\langle\widetilde{\boldsymbol{\mathcal{H}}}_{m+1}(\{\underline{p}\},\epsilon)\,\boldsymbol{\mathcal{W}}_{m+1}(\{\underline{n}\},\epsilon)\big\rangle\\ &\xrightarrow[1\|j]{}4\pi\,\alpha_s\,\tilde{\mu}^{2\epsilon}\,\frac{2}{-s_{1j}}\,\frac{1}{\xi}\,\mathcal{P}_{1\to P}(\xi)\,\big\langle\boldsymbol{\mathcal{C}}_{1\to P}\,\widetilde{\boldsymbol{\mathcal{H}}}_m(\{\hat{\underline{p}}\},\mu)\,\boldsymbol{\mathcal{C}}^\dagger_{1\to P}\,\boldsymbol{\mathcal{W}}_{m+1}(\{\underline{n}\},\mu)\big\rangle\,,\end{aligned}\qquad (7.56)$$

where $s_{1j}=-2E_1^2\,(1-\xi)\,n_1\cdot n_j$ and $\{\hat{\underline{p}}\}=\{P,p_2,\dots,p_{j-1},p_{j+1},\dots,p_{m+1}\}$ for space-like splittings. Here $\mathcal{P}_{1\to P}$ are the unregularized DGLAP splitting functions. In con-

[8] At higher orders, careful analytic continuation is needed to correctly reproduce the complex phases in the amplitude when performing the crossing [63].

trast to the time-like case (7.50), it has become established to indicate only the incoming parton 1 and the parton P entering the hard scattering. From fermion flavor conservation, it is possible to infer the radiated collinear parton j. The extra factor $1/\xi$ compared to the time-like result (7.49) corrects the flux factor in the hard function to the one relevant for the scattering of the incoming parton P since $s_{P2} = \xi\, s_{12}$. The normalized color matrices of the space-like splitting amplitudes $\mathbf{Sp}(p_1, p_j)$ are denoted by $\boldsymbol{\mathcal{C}}_{1\to P}$. The explicit expressions for the different partonic channels can be found in Appendix A.3 and are illustrated in Figure 7.4. This object together with its conjugate maps the hard function from the m-parton color space before the splitting to the $(m+1)$-parton color space after it. The average factors (7.10), contained in $\langle \ldots \rangle$, differ between left- and right-hand side of (7.56) if parton 1 and P are not the same. Taking this into account, one finds after crossing that $\mathcal{P}_{1\to P} \equiv \mathcal{P}_{P+j\leftarrow 1}$ at one loop.

Similar to the time-like case (7.51), the integral over the $(m-1)$ directions of the final-state partons yields a collinear singularity. For the space-like case, one should interpret the splitting functions as singular distribution

$$\int [d\Omega_j]\, \frac{1}{n_1 \cdot n_j} = -\frac{1}{2\epsilon} \int [d\Omega_j]\, \delta(n_1 - n_j) + \mathcal{O}(\epsilon)\,. \tag{7.57}$$

Due to the change in the flux factor, the $(m-1)$ dimensional energy integral turns into

$$\int d\mathcal{E}_{m+1}\, \frac{1}{E_1^2\,(1-\xi)}\, \frac{1}{\xi} = \int_0^1 d\xi\, (1-\xi)^{d-4}\, \frac{E_1^{d-4}}{\tilde{c}^\epsilon (2\pi)^2} \int d\mathcal{E}_m\,, \tag{7.58}$$

where the energy of final-state parton j is parameterized by $E_j = E_1(1-\xi)$. As evident from (7.50), the splitting functions $\mathcal{P}_{q\to q}$ and $\mathcal{P}_{g\to g}$ suffer from a soft divergence if $\xi \to 1$. This divergence is regularized by the prefactor on the right-hand side of (7.58) and one can extract the pole by

$$(1-\xi)^{-1-2\epsilon} = -\frac{1}{2\epsilon}\delta(1-\xi) + \left[\frac{1}{1-\xi}\right]_+ + \mathcal{O}(\epsilon)\,, \tag{7.59}$$

with plus distribution $[\ldots]_+$ defined in (66) of [105]. In the following, we denote by $\overline{\mathcal{P}}_{1\to P}$ the splitting functions with removed singularity according to this prescription. If parton 1 and P are different, there is no soft singularity and $\overline{\mathcal{P}}_{1\to P} \equiv \mathcal{P}_{1\to P}$.

Summing over all different splittings, i.e. emitted partons j,[9] and including collinear emissions from initial-state parton 2, we find

$$\begin{aligned}
&\left\langle \boldsymbol{\mathcal{H}}_{m+1}(\{\underline{n}\}, \xi_1, \xi_2, \epsilon) \otimes \boldsymbol{\mathcal{W}}_{m+1}(\{\underline{n}\}, \xi_1, \xi_2, \epsilon) \right\rangle \\
&= \frac{\alpha_s}{4\pi} \int_0^1 d\xi_1' \left[C_1\, \gamma_0\, \delta(1-\xi_1') \left(\frac{1}{2\epsilon^2} + \frac{1}{\epsilon} \ln \frac{\mu}{2E_1} \right) \delta_{1P} - \frac{2}{\epsilon}\, \overline{\mathcal{P}}_{1\to P}(\xi_1') \right] \delta(n_1 - n_j) \\
&\quad \times \left\langle \boldsymbol{\mathcal{C}}_{1\to P}\, \boldsymbol{\mathcal{H}}_m(\{\hat{\underline{n}}\}, \xi_1'\, \xi_1, \xi_2, \mu)\, \boldsymbol{\mathcal{C}}_{1\to P}^\dagger \otimes \boldsymbol{\mathcal{W}}_{m+1}(\{\underline{n}\}, \xi_1, \xi_2, \mu) \right\rangle + (1 \leftrightarrow 2) + \ldots\,,
\end{aligned} \tag{7.60}$$

where ellipsis denote terms that are free of collinear initial-state singularities at one loop and for given partons $1, j$ one can infer the parton P by fermion flavor conservation. The term proportional to δ_{1P} only contributes if parton 1 and P are both

[9] We keep the sum over j implicit on the right-hand side of (7.60) as it is by definition part of the sum over multiplicities.

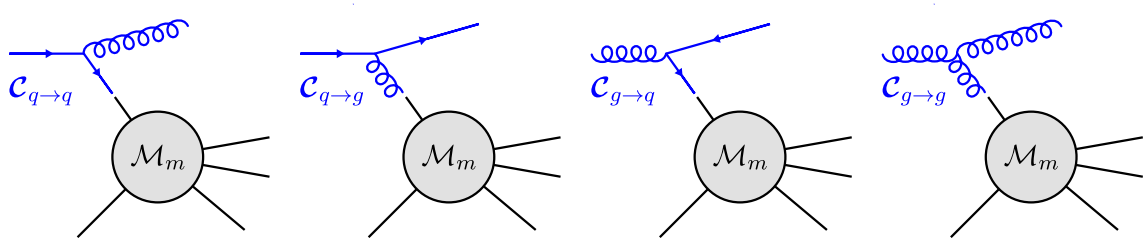

Figure 7.4: Color structures $\boldsymbol{\mathcal{C}}_{1\to P}$ for different collinear initial-state splittings. If the splitting includes quarks (first three cases), the color structure is given by the generator of the fundamental $SU(N_c)$ representation, appropriately contracted with the hard function. For the three gluon splitting (last case), it is given by the structure constant.

(anti-)quarks or both gluons, i.e. for the first and last splitting in Figure 7.4, and the hard function in the last line depends on $\{\underline{\hat{n}}\} = \{n_1, \dots, n_{j-1}, n_{j+1}, \dots, n_{m+1}\}$. Here, one recognizes the $*$ convolution defined in (7.23) over the momentum fractions of the initial-state partons.

7.3.3 (Non-)Cancellation of Collinear Singularities

Comparing the virtual collinear singularities of the hard function in (7.40) to the real ones in (7.55) and (7.60), we observe that the singularities associated with final-state partons exactly cancel. This cancellations takes place *before* the energy integrals, contained in the definition of the hard function (7.14), are carried out. For the collinear singularities associated with initial-state partons, the cancellation is spoiled by Glauber effects, as explained above, and therefore, they give rise to collinear anomalous dimensions $\boldsymbol{\Gamma}_i^C$. Virtual and real soft singularities in (7.36) and (7.44), respectively, give rise to a soft anomalous dimension $\boldsymbol{\Gamma}^S$ as well. Therefore, $\boldsymbol{\Gamma}^H$ contains three terms

$$\boldsymbol{\Gamma}^H(\xi_1,\xi_2) = \delta(1-\xi_1)\,\delta(1-\xi_2)\,\boldsymbol{\Gamma}^S + \boldsymbol{\Gamma}_1^C(\xi_1)\,\delta(1-\xi_2) + \delta(1-\xi_1)\,\boldsymbol{\Gamma}_2^C(\xi_2)\,, \tag{7.61}$$

where we omitted all arguments except for the momentum fractions. Since soft partons can only take away an insignificant amount of momentum, the corresponding part of the anomalous dimension $\boldsymbol{\Gamma}^S$ must come with $\delta(1-\xi_1)\,\delta(1-\xi_2)$.

Introducing a hard reference scale μ_h, one can separate soft+collinear and purely collinear terms

$$\ln\frac{\mu}{2E_i} = \ln\frac{\mu}{\mu_h} + \ln\frac{\mu_h}{2E_i} \tag{7.62}$$

for the initial-state singularities in (7.40) and (7.60). For the default choice $\mu_h \sim \sqrt{\hat{s}}$, the second logarithm is only there in the laboratory frame – as $2E_i = \sqrt{\hat{s}}$ in the partonic center-of-mass frame – and depends on the momentum fractions ξ_i.[10] Due to their trivial dependence on the momentum fractions, the terms with the large logarithm $\ln\frac{\mu}{\mu_h}$ are included in $\boldsymbol{\Gamma}^S$. This motivates the split [4]

$$\boldsymbol{\Gamma}^S = \gamma_{\text{cusp}}(\alpha_s)\left(\boldsymbol{\Gamma}^c \ln\frac{\mu^2}{\mu_h^2} + \boldsymbol{V}^G\right) + \frac{\alpha_s}{4\pi}\,\overline{\boldsymbol{\Gamma}} + \mathcal{O}(\alpha_s^2)\,, \tag{7.63}$$

[10] In [73] the hard function is defined in the partonic center-of-mass frame.

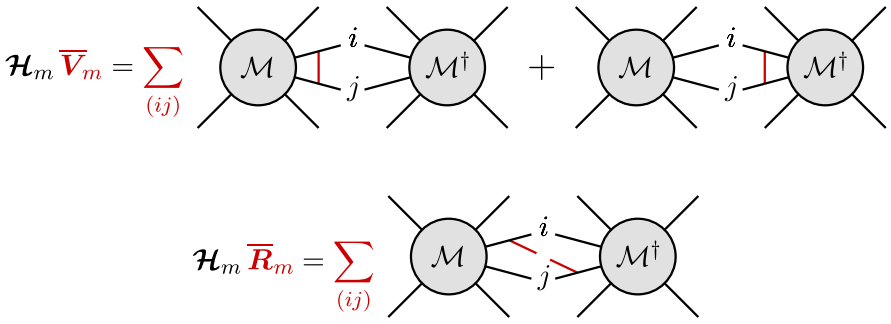

Figure 7.5: Action of the real-emission operator $\overline{\boldsymbol{R}}_m$ and the virtual piece $\overline{\boldsymbol{V}}_m$ on a hard function $\boldsymbol{\mathcal{H}}_m$.

where $\boldsymbol{\Gamma}^c$ contains the (real and virtual) soft+collinear terms and $\overline{\boldsymbol{\Gamma}}$ the purely soft ones. Note that the superscript ^{c} stands for cusp and is not to be confused with the superscript ^{C} in (7.61) meaning collinear. The Glauber phases (7.37) are of virtual origin only and included in $\boldsymbol{V}^G$.

To obtain explicit expressions, one can use that the one loop anomalous dimension is given by (-2) times the $1/\epsilon$ pole in the $\boldsymbol{Z}$-factor of the hard function. In multiplicity space, we find for the virtual and real purely collinear parts

$$\begin{aligned}
\boldsymbol{V}_i^C(\xi_i) &= -2\left(\gamma_0^i - C_i\,\gamma_0 \ln\frac{\mu_h}{2E_i}\right)\delta(1-\xi_i)\,\mathbf{1}\,,\\
\boldsymbol{R}_i^C(\xi_i) &= 2\left(2\overline{\mathcal{P}}_{i\to P}(\xi_i) - C_i\,\gamma_0\,\delta_{iP}\ln\frac{\mu_h}{2E_i}\,\delta(1-\xi_i)\right)\boldsymbol{\mathcal{C}}_{i\to P,L}\,\boldsymbol{\mathcal{C}}^\dagger_{i\to P,R}\,\delta(n_k-n_i)\,,
\end{aligned} \tag{7.64}$$

where, similar to (7.22), the one-loop coefficient $\frac{\alpha_s}{4\pi}$ is factored off. The real-emission operator $\boldsymbol{R}_i^C$ has different partonic channels $i \to P + k$. For example, if parton i is a quark and the operator acts on a hard function with multiplicity m and parton P being a quark (gluon), then it turns them into a function of multiplicity $(m+1)$ with initial-state quark and additional final-state gluon (quark). The logarithms in the real and virtual piece evaluate (modulo a sign) to the rapidity difference between the lab and the partonic center-of-mass frame for the deafult choice of μ_h. After convolution with the low-energy matrix element, this is an order one logarithm.

The purely soft terms $\overline{\boldsymbol{\Gamma}}$ know about the multiplicity m of the hard function multiplying them and are, at one loop, given by

$$\begin{aligned}
\overline{\boldsymbol{V}}_m &= 2\sum_{(ij)}\left(\boldsymbol{T}_{i,L}\cdot\boldsymbol{T}_{j,L} + \boldsymbol{T}_{i,R}\cdot\boldsymbol{T}_{j,R}\right)\int\frac{d^2\Omega_k}{4\pi}\,\overline{W}_{ij}^k\,,\\
\overline{\boldsymbol{R}}_m &= 4\sum_{(ij)}\boldsymbol{T}_{i,L}\circ\boldsymbol{T}_{j,R}\,\overline{W}_{ij}^k\,\theta_{\text{hard}}(n_k)\,.
\end{aligned} \tag{7.65}$$

Instead of performing the angular integral over $\overline{W}_{ij}^k$ in the virtual term using (7.33), it is convenient to keep it to show the cancellation of real and virtual contributions below. The real term describes the emission of a soft gluon in direction n_k and in the

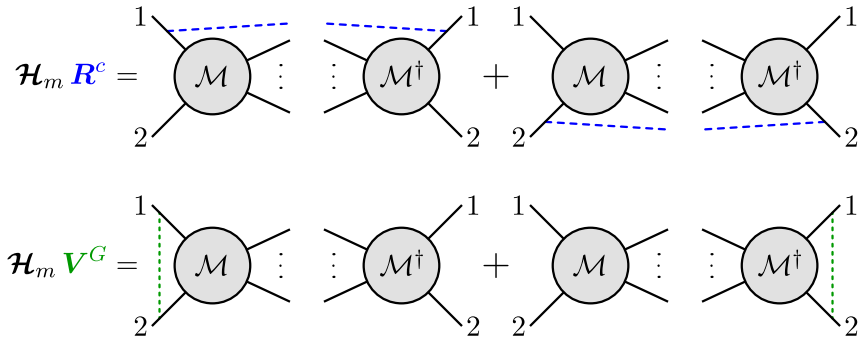

Figure 7.6: Action of the cusp operator $\boldsymbol{R}^c$ and the virtual piece $\boldsymbol{V}^G$ on a hard function $\boldsymbol{\mathcal{H}}_m$. The operator $\boldsymbol{R}^c$ adds an additional final-state leg (dashed blue line) along the direction of the incoming partons.

product $\boldsymbol{\mathcal{H}}_m\,\overline{\boldsymbol{R}}_m$ increases the multiplicity by one, see Figure 7.5. The corresponding angular integral is contained in the $\otimes$ with the low-energy matrix element $\boldsymbol{\mathcal{W}}_{m+1}$.

The Glauber term is proportional to the unit matrix in multiplicity space and reads

$$\boldsymbol{V}^G = -2i\pi\left(\boldsymbol{T}_{1,L}\cdot\boldsymbol{T}_{2,L} - \boldsymbol{T}_{1,R}\cdot\boldsymbol{T}_{2,R}\right) \tag{7.66}$$

In a slight abuse of notation, we denote both the matrix in multiplicity space and its entries by $\boldsymbol{V}^G$. The soft+collinear terms, proportional to the large logarithm, read

$$\boldsymbol{V}^c = \sum_{i=1,2} C_i\,\mathbf{1}\,, \qquad \boldsymbol{R}^c = -\sum_{i=1,2} \boldsymbol{T}_{i,L}\circ\boldsymbol{T}_{i,R}\,\delta(n_k - n_i)\,. \tag{7.67}$$

For the second term, we used $C_i\,\delta_{iP}\,\boldsymbol{\mathcal{C}}_{i\to P,L}\,\boldsymbol{\mathcal{C}}^\dagger_{i\to P,R} = \boldsymbol{T}_{i,L}\circ\boldsymbol{T}_{i,R}$, see Appendix A.3. In all real emission terms, n_k denotes the direction of the emitted parton. In Figure 7.6 we illustrate the action of $\boldsymbol{V}^G$ and $\boldsymbol{R}^C$ on a hard function.

Interestingly, the collinear RG evolution is *not* driven by the standard DGLAP kernels as real and virtual part in (7.64) have different color structure. For the same reason the two parts of $\boldsymbol{\Gamma}^c$ do not cancel and, therefore, the soft anomalous dimension (7.63) contains an extra logarithm leading to the SLLs. Turning the RG evolution of the hard functions into the one of the low-energy matrix element

$$\int d\xi_i\,\left\langle\left(\boldsymbol{\mathcal{H}} * \boldsymbol{\Gamma}^C_i\right)(\xi_i,\mu)\,\boldsymbol{\mathcal{W}}(\xi_i,\mu)\right\rangle = \int d\xi_i\,\left\langle\boldsymbol{\mathcal{H}}(\xi_i,\mu)\,\left(\boldsymbol{\Gamma}^C_i \star \boldsymbol{\mathcal{W}}\right)(\xi_i,\mu)\right\rangle, \tag{7.68}$$

where $\boldsymbol{\mathcal{H}}$ and $\boldsymbol{\mathcal{W}}$ are vectors in multiplicity space, one finds a standard Mellin convolution[11]

$$(f\star g)(\xi_i) \coloneqq \int d\xi_i'\,d\xi_i''\,\delta(\xi_i - \xi_i'\,\xi_i'')\,f(\xi_i')\,g(\xi_i'')\,. \tag{7.69}$$

At the soft scale $\mu\sim\mu_s$ the low-energy matrix element takes the form (7.20). Since the color structures $\boldsymbol{\mathcal{C}}_{i\to P}$ are normalized, the term with the extra logarithm $\ln\frac{\mu_h}{2E_i}$

[11] There exists an important relation between Mellin and $*$ convolution, $(f*g)*h = f*(g\star h)$. Therefore, it is possible to Mellin convolute several anomalous dimensions in (7.25) first and then combine them with the hard function.

cancels between real and virtual part of $\mathbf{\Gamma}_i^C$ in this case. The remaining terms yield the standard DGLAP evolution for the PDFs [105–107]

$$\begin{aligned} &\int d\xi_1\, f_1(\xi_1,\mu_s)\left\langle \left(\boldsymbol{\mathcal{H}} * \mathbf{\Gamma}_1^C\right)(\xi_1,\mu_s)\otimes \mathbf{1}\right\rangle \\ &= \int d\xi_1\, \frac{\alpha_s}{\pi}\left(\mathcal{P}_{1\to P}\star f_1\right)(\xi_1,\mu_s)\left\langle \boldsymbol{\mathcal{H}}(\xi_1,\mu_s)\otimes \mathbf{1}\right\rangle, \end{aligned} \tag{7.70}$$

where $\mathcal{P}_{1\to P}$ are now the *regularized* $\overline{\text{MS}}$ splitting kernels, e.g. given in (68–69) of [105].

Chapter 8

Resummation of Super-Leading Logarithms

The soft+collinear part $\mathbf{\Gamma}^c$ of the anomalous dimension comes together with an extra logarithm in the scale ratio μ/μ_h with hard scale of order the partonic center-of-mass energy $\mu_h \sim \sqrt{\hat{s}}$. Evaluating the factorization theorem (7.1) at the scale $\mu_s \sim Q_0$ and evolving the hard function down to this scale, the logarithm $L_s := \ln(\mu_h/\mu_s)$ becomes large. After the scale integration, it is turned into a double-logarithmic correction $\alpha_s L_s^2$ and needs to be resummed to all orders in perturbation theory.

To extract the logarithmically-enhanced terms, we compute the RG evolution of the hard function (7.25). Starting with the lowest multiplicity hard function for a given process, at Born level containing only a single entry $\boldsymbol{\mathcal{H}}_{2\to M} := (\boldsymbol{\mathcal{H}}_{2+M}, 0, 0, \dots)$, we multiply with powers of $\mathbf{\Gamma}^H$ and take the trace with the leading order low-energy matrix element (7.20). The evaluation of these products simplifies due to the simple structure of the anomalous dimension at one loop. Real-emission terms ($\overline{\boldsymbol{R}}_m$, $\boldsymbol{R}^c$ and $\boldsymbol{R}_i^C$) increase the multiplicity by one, while virtual contributions ($\overline{\boldsymbol{V}}_m$, $\boldsymbol{V}^G$, $\boldsymbol{V}^c$ and $\boldsymbol{V}_i^C$) leave it unchanged. To streamline the notation, all multiplicity indices are suppressed in the following and we work instead with matrices. Therefore, we combine real and virtual pieces of the soft anomalous dimension into [1]

$$
\begin{aligned}
\mathbf{\Gamma}^c &= \sum_{i=1,2} \left[C_i \, \mathbf{1} - \boldsymbol{T}_{i,L} \circ \boldsymbol{T}_{i,R} \, \delta(n_k - n_i) \right] , \\
\boldsymbol{V}^G &= -2i\pi \left(\boldsymbol{T}_{1,L} \cdot \boldsymbol{T}_{2,L} - \boldsymbol{T}_{1,R} \cdot \boldsymbol{T}_{2,R} \right) , \\
\overline{\mathbf{\Gamma}} &= 2 \sum_{(ij)} \left(\boldsymbol{T}_{i,L} \cdot \boldsymbol{T}_{j,L} + \boldsymbol{T}_{i,R} \cdot \boldsymbol{T}_{j,R} \right) \int \frac{d^2\Omega_k}{4\pi} \, \overline{W}_{ij}^k - 4 \sum_{(ij)} \boldsymbol{T}_{i,L} \circ \boldsymbol{T}_{j,R} \, \overline{W}_{ij}^k \, \theta_{\text{hard}}(n_k) ,
\end{aligned}
\tag{8.1}
$$

and for the collinear one as

$$
\begin{aligned}
\mathbf{\Gamma}_i^C(\xi_i) = \frac{\alpha_s}{4\pi} \Bigg[& 2 \left(2\overline{\mathcal{P}}_{i\to P}(\xi_i) - C_i \gamma_0 \ln \frac{\mu_h}{2E_i} \delta(1-\xi_i) \, \delta_{iP} \right) \delta(n_k - n_i) \, \boldsymbol{\mathcal{C}}_{i\to P} \, \boldsymbol{\mathcal{C}}_{i\to P}^\dagger \\
& - 2 \left(\gamma_0^i - C_i \gamma_0 \ln \frac{\mu_h}{2E_i} \right) \delta(1-\xi_i) \, \delta_{iP} \Bigg] .
\end{aligned}
\tag{8.2}
$$

These matrices in multiplicity space multiply the hard function from the right and their order matters. They also contain color matrices acting on the amplitude or its conjugate in each step, i.e. multiply the color indices of the hard function on the left or right. The real emissions generated by the real parts of the anomalous dimension are labeled with an index k_n, where $n = 0$ is the last (rightmost) emission, $n = 1$ the second to last, and so on.

The computation is greatly simplified for three reasons. First, color coherence implies that the sum of soft emissions from two collinear partons yields the same contri-

bution as a single soft emission from the parent parton, i.e.

$$\left[\mathbf{\Gamma}^C, \overline{\mathbf{\Gamma}}\right] = 0\,, \qquad \left[\mathbf{\Gamma}^c, \overline{\mathbf{\Gamma}}\right] = 0\,. \tag{8.3}$$

As for soft emissions from two collinear partons i, j, the anomalous dimension $\overline{\mathbf{\Gamma}}$ depends only on the sum of their colors

$$\boldsymbol{T}_{i,L} \circ \boldsymbol{T}_{q,R}\, \overline{W}^k_{iq} + \boldsymbol{T}_{j,L} \circ \boldsymbol{T}_{q,R}\, \overline{W}^k_{jq} = (\boldsymbol{T}_{i,L} + \boldsymbol{T}_{j,L}) \circ \boldsymbol{T}_{q,R}\, \overline{W}^k_{iq}\,, \tag{8.4}$$

with $\overline{W}^k_{iq} = \overline{W}^k_{jq}$, one can apply (7.47) to commute with $\mathbf{\Gamma}^c$ or $\mathbf{\Gamma}^C$, respectively. Second, due to collinear safety, singularities from real emissions cancel against the associated virtual singularities for a trivial low-energy matrix element. Third, complex Glauber phases also cancel in this case between amplitude and conjugate amplitude. In our formalism, these two properties are encoded in the cyclicity of the trace which implies

$$\left\langle \boldsymbol{\mathcal{H}}\, \mathbf{\Gamma}^c \otimes \mathbf{1} \right\rangle = 0\,, \qquad \left\langle \boldsymbol{\mathcal{H}}\, \boldsymbol{V}^G \otimes \mathbf{1} \right\rangle = 0\,. \tag{8.5}$$

The corresponding relation for $\mathbf{\Gamma}^C_i$ is (7.70) and ensures the standard PDF evolution. These relations hold for an arbitrary hard function.

The leading SLLs are obtained by inserting a maximal number of $\mathbf{\Gamma}^c$ in the series expansion (7.25) combined with the leading order low-energy matrix element (7.20) under the trace. The properties (8.3) and (8.5) imply that the two rightmost factors of $\mathbf{\Gamma}^H$ need to be proportional to $\boldsymbol{V}^G\,\overline{\mathbf{\Gamma}}$ to get a non-zero contribution. The insertion of this Glauber phase breaks color coherence [63–66, 80]. As tree-level QCD amplitudes do *not* contain any phase, it is possible to chose a basis such that the Born-level hard functions $\boldsymbol{\mathcal{H}}_{2\to M}$ are real [64]. To get a contribution to the cross section, a second Glauber phase is thus required.[1] Consequently, the SLLs are generated by the evolution operator [3, 4]

$$\begin{aligned}\boldsymbol{U}_{\text{SLL}}(\{\underline{n}\}, \mu_h, \mu_s) = \int_{\mu_s}^{\mu_h} \frac{d\mu_1}{\mu_1} \int_{\mu_s}^{\mu_1} \frac{d\mu_2}{\mu_2} \int_{\mu_s}^{\mu_2} \frac{d\mu_3}{\mu_3}\, \boldsymbol{U}^c(\mu_h, \mu_1)\, \gamma_{\text{cusp}}\big(\alpha_s(\mu_1)\big)\, \boldsymbol{V}^G \\ \times \boldsymbol{U}^c(\mu_1, \mu_2)\, \gamma_{\text{cusp}}\big(\alpha_s(\mu_2)\big)\, \boldsymbol{V}^G\, \frac{\alpha_s(\mu_3)}{4\pi}\, \overline{\mathbf{\Gamma}}\,,\end{aligned} \tag{8.6}$$

where we have defined the generalized Sudakov operator

$$\boldsymbol{U}^c(\mu_i, \mu_j) \coloneqq \exp\left[\mathbf{\Gamma}^c \int_{\mu_j}^{\mu_i} \frac{d\mu}{\mu}\, \gamma_{\text{cusp}}\big(\alpha_s(\mu)\big) \ln \frac{\mu^2}{\mu_h^2}\right]. \tag{8.7}$$

Here no path-ordering is required, since the matrix structure in the exponent is scale-independent. From (8.6) it is evident that the first double-logarithmic corrections arise at four-loop order in perturbation theory. As the SLLs are generated by the soft anomalous dimension only, the convolutions over momentum fractions are trivial. Their contribution to the $2 \to M$ jet cross section is

$$\sigma^{\text{SLL}}_{2\to M}(Q_0) = \sum_{\substack{\text{partonic}\\ \text{channels}}} \int d\xi_1\, d\xi_2\, f_1(\xi_1, \mu_s)\, f_2(\xi_2, \mu_s)\, \hat{\sigma}^{\text{SLL}}_{2\to M}(\xi_1, \xi_2, Q_0) \tag{8.8}$$

[1] In general, the hard function can develop non-trivial phases. In these cases, a second Glauber phase is not required. We discuss this in more detail in Chapter 9.

with partonic cross section

$$\hat{\sigma}^{\text{SLL}}_{2\to M}(\xi_1,\xi_2,Q_0) \coloneqq \left\langle \boldsymbol{\mathcal{H}}_{2\to M}(\{\underline{n}\},s,\xi_1,\xi_2,\mu_h)\,\boldsymbol{U}_{\text{SLL}}(\{\underline{n}\},\mu_h,\mu_s)\otimes \mathbf{1}\right\rangle, \tag{8.9}$$

where $\mu_h \sim \sqrt{\hat{s}}$ and $\mu_s \sim Q_0$. The partonic cross section depends on the specific scattering channel $1+2\to 3\ldots(M+2)$, over which one has to sum in (8.8). The hard functions are normalized such that their trace is equal to the contribution of the Born cross section, i.e.

$$\left\langle \boldsymbol{\mathcal{H}}_{2\to M}\otimes \mathbf{1}\right\rangle = \hat{\sigma}_{2\to M}\,. \tag{8.10}$$

The differential partonic cross section is obtained when not performing all angular integrals of $\otimes$.

8.1 All-Order Structure

It is instructive to study the all-order structure of the SLLs in detail. To do so, we expand the generalized Sudakov operators in (8.6) and find

$$\boldsymbol{U}_{\text{SLL}}(\mu_h,\mu_s) \subset \sum_{n=0}^{\infty}\int_{\mu_s}^{\mu_h}\frac{d\mu_1}{\mu_1}\int_{\mu_s}^{\mu_1}\frac{d\mu_2}{\mu_2}\cdots\int_{\mu_s}^{\mu_{n+2}}\frac{d\mu_{n+3}}{\mu_{n+3}}\,\boldsymbol{\Gamma}^S(\mu_1)\,\boldsymbol{\Gamma}^S(\mu_2)\,\ldots\,\boldsymbol{\Gamma}^S(\mu_{n+3})\,, \tag{8.11}$$

where the $\subset$ symbol indicates that not all terms on the right-hand side contribute to the SLLs and n denotes the number of $\boldsymbol{\Gamma}^c$ insertions. From the above considerations, it is clear that here the last two factors are $\boldsymbol{V}^G\,\overline{\boldsymbol{\Gamma}}$ and all others – except for one Glauber operator – are the cusp part $\boldsymbol{\Gamma}^c$ of the anomalous dimension. Factoring off the scale integrals, we conclude that the leading SLLs arise from the color traces [73]

$$C_{rn} \coloneqq \left\langle \boldsymbol{\mathcal{H}}_{2\to M}\,(\boldsymbol{\Gamma}^c)^r\,\boldsymbol{V}^G\,(\boldsymbol{\Gamma}^c)^{n-r}\,\boldsymbol{V}^G\,\overline{\boldsymbol{\Gamma}}\otimes\mathbf{1}\right\rangle, \tag{8.12}$$

where $0\le r\le n$. The dependence of the color traces on the partonic channels is kept implicit in our notation. The corresponding iterated scale integrals are

$$\begin{aligned} I_{rn}(\mu_h,\mu_s) \coloneqq \int_{\mu_s}^{\mu_h}\frac{d\mu_1}{\mu_1}\int_{\mu_s}^{\mu_1}\frac{d\mu_2}{\mu_2}\cdots\int_{\mu_s}^{\mu_{n+2}}\frac{d\mu_{n+3}}{\mu_{n+3}}\,\gamma_{\text{cusp}}\big(\alpha_s(\mu_1)\big)\,\ln\frac{\mu_1^2}{\mu_h^2}\,\ldots \\ \ldots\gamma_{\text{cusp}}\big(\alpha_s(\mu_r)\big)\,\ln\frac{\mu_r^2}{\mu_h^2}\,\gamma_{\text{cusp}}\big(\alpha_s(\mu_{r+1})\big)\,\gamma_{\text{cusp}}\big(\alpha_s(\mu_{r+2})\big)\,\ln\frac{\mu_{r+2}^2}{\mu_h^2}\,\ldots \\ \ldots\gamma_{\text{cusp}}\big(\alpha_s(\mu_{n+1})\big)\,\ln\frac{\mu_{n+1}^2}{\mu_h^2}\,\gamma_{\text{cusp}}\big(\alpha_s(\mu_{n+2})\big)\,\frac{\alpha_s(\mu_{n+3})}{4\pi}\,. \end{aligned} \tag{8.13}$$

The integrals over μ_1 to μ_r and μ_{r+2} to μ_{n+1} of this expression result from the r and $(n-r)$ insertions of $\boldsymbol{\Gamma}^c$ in (8.12), respectively. The contribution of the SLLs to the partonic cross section can hence be expressed as

$$\hat{\sigma}^{\text{SLL}}_{2\to M}(Q_0) = \sum_{n=0}^{\infty}\sum_{r=0}^{n} I_{rn}(\mu_h,\mu_s)\,C_{rn}\,. \tag{8.14}$$

In the following, we evaluate in detail first the color traces for arbitrary partonic scattering processes and second the process-independent iterated scale integrals.

8.1.1 Color Traces

Defining the abbreviation

$$\boldsymbol{\mathcal{H}} \coloneqq \boldsymbol{\mathcal{H}}_{2\to M}\,(\boldsymbol{\Gamma}^c)^r\,\boldsymbol{V}^G\,(\boldsymbol{\Gamma}^c)^{n-r}\,\boldsymbol{V}^G\,, \tag{8.15}$$

one finds for the insertion of the rightmost anomalous dimension in (8.12)

$$\big\langle \boldsymbol{\mathcal{H}}\,\overline{\boldsymbol{\Gamma}}\otimes\mathbf{1}\big\rangle = 4\sum_{(ij)}\big\langle \boldsymbol{\mathcal{H}}\,\boldsymbol{T}_i\cdot\boldsymbol{T}_j\otimes\mathbf{1}\big\rangle\int\frac{d^2\Omega_{k_0}}{4\pi}\,W_{ij}^{k_0}\,\theta_{\text{veto}}(n_{k_0})\,. \tag{8.16}$$

The sum over $i\neq j$ includes all up to $(M+n)$ partons contained in $\boldsymbol{\mathcal{H}}$. The $p\leq n$ collinear gluons from the n insertions of $\boldsymbol{\Gamma}^c$ are labeled by indices $k_1,\dots,k_p$ (from right to left) below. The angular integrals for the virtual and real soft wide-angle emissions k_0, contained in $\overline{\boldsymbol{V}}_{2+M+p}$ and the $\otimes$ symbol, respectively, combine as

$$\int\frac{d^2\Omega_{k_0}}{4\pi}\,\overline{W}_{ij}^{k_0}\big[1-\theta_{\text{hard}}(n_{k_0})\big] = \int\frac{d^2\Omega_{k_0}}{4\pi}\,W_{ij}^{k_0}\,\theta_{\text{veto}}(n_{k_0})\,, \tag{8.17}$$

where θ_{veto} restricts the emission to lie inside the veto region, i.e. outside the jets. In this region, we can replace the subtracted dipole (7.35) by the unsubtracted one. Exploiting the cyclicity of the trace, one can pull out $\boldsymbol{V}^G$ from (8.15) and finds

$$\big\langle \boldsymbol{\mathcal{H}}\,\boldsymbol{V}^G\,\overline{\boldsymbol{\Gamma}}\otimes\mathbf{1}\big\rangle = 16i\pi\sum_{j>2}J_j\,if^{abc}\big\langle \boldsymbol{\mathcal{H}}\,\boldsymbol{T}_1^a\,\boldsymbol{T}_2^b\,\boldsymbol{T}_j^c\otimes\mathbf{1}\big\rangle\,, \tag{8.18}$$

with angular integral

$$J_j \coloneqq \int\frac{d^2\Omega_{k_0}}{4\pi}\big[W_{1j}^{k_0}-W_{2j}^{k_0}\big]\,\theta_{\text{veto}}(n_{k_0})\,. \tag{8.19}$$

Clearly, the soft wide-angle emission must connect an initial-state parton in the amplitude with a final-state parton in the conjugate amplitude, or vice versa. All angular information of this emission is contained in the integral J_j. If the soft gluon is attached to a collinear one from $\boldsymbol{\Gamma}^c$, it needs to be collinear to an initial-state parton leading to

$$J_{12} \coloneqq J_2 = -J_1 = \int\frac{d^2\Omega_{k_0}}{4\pi}\,W_{12}^{k_0}\,\theta_{\text{veto}}(n_{k_0})\,. \tag{8.20}$$

Hence, there are $(M+1)$ independent kinematic structures in total. For the following discussion, it is convenient to label the appearing color structures. We define

$$\boldsymbol{X}_1 \coloneqq \sum_{j>2}J_j\,if^{abc}\,\boldsymbol{T}_1^a\,\boldsymbol{T}_2^b\,\boldsymbol{T}_j^c\,. \tag{8.21}$$

Note that both the angular integral J_j for $j>2$ and $if^{abc}\,\boldsymbol{T}_1^a\,\boldsymbol{T}_2^b$ are anti-symmetric under the exchange of partons $1\leftrightarrow 2$ and, therefore, $\boldsymbol{X}_1$ is invariant. Below, we also find color structures containing the symmetric integral J_{12}. This feature is exploited in Section 9.1 to construct a basis of color structures.

Pulling out the first factor $\mathbf{\Gamma}^c$ from (8.15), describing a collinear gluon k_1 emitted from one of the initial-state partons, one needs to calculate

$$\begin{aligned}\big\langle \boldsymbol{\mathcal{H}}\,\mathbf{\Gamma}^c\,\boldsymbol{X}_1\otimes\mathbf{1}\big\rangle = \sum_{i=1,2}\Bigg[{\sum_{j>2}}'\,J_j\,if^{abc}\big\langle C_i\,\boldsymbol{\mathcal{H}}\,\boldsymbol{T}_1^a\,\boldsymbol{T}_2^b\,\boldsymbol{T}_j^c\otimes\mathbf{1} - \boldsymbol{T}_i^d\,\boldsymbol{\mathcal{H}}\,\boldsymbol{T}_i^d\,\boldsymbol{T}_1^a\,\boldsymbol{T}_2^b\,\boldsymbol{T}_j^c\otimes\mathbf{1}\big\rangle \\ - J_i\,f^{abc}f^{cde}\big\langle\boldsymbol{T}_i^e\,\boldsymbol{\mathcal{H}}\,\boldsymbol{T}_i^d\,\boldsymbol{T}_1^a\,\boldsymbol{T}_2^b\otimes\mathbf{1}\big\rangle\Bigg]\,,\end{aligned} \tag{8.22}$$

where the prime on the sum in the first term indicates that $j\neq k_1$. The term with $j=k_1$ yields the result in the second line, the angular integral over the direction of the collinear gluon is already performed using the $\delta(n_{k_1}-n_i)$ in (8.1). Using the cyclicity of the trace to proceed, we commute the generators in the second term such that one can use $\boldsymbol{T}_i\cdot\boldsymbol{T}_i = C_i\,\mathbf{1}$ to cancel the first term. The commutator terms can then be simplified using

$$if^{abc}\,\boldsymbol{T}_i^a\,\boldsymbol{T}_i^b = -\frac{N_c}{2}\,\boldsymbol{T}_i^c\,. \tag{8.23}$$

Applying a similar strategy to the third term and translating the product of f-symbols to

$$\mathrm{tr}\big(F^a\,F^b\big) = N_c\,\delta^{ab}\,,\qquad \mathrm{tr}\big(F^a\,F^b\,F^c\big) = \frac{N_c}{2}\,if^{abc}\,, \tag{8.24}$$

where $(F^a)^{bc} = -if^{abc}$ is a generator of the adjoint representation, one can show that it vanishes. Physically, this means that the soft gluon k_0 does not attach to the collinear gluon k_1. Putting things together, we find

$$\big\langle\boldsymbol{\mathcal{H}}\,\mathbf{\Gamma}^c\boldsymbol{X}_1\otimes\mathbf{1}\big\rangle = N_c\,\big\langle\boldsymbol{\mathcal{H}}\,\boldsymbol{X}_1\otimes\mathbf{1}\big\rangle \tag{8.25}$$

where it is important to keep in mind that the implicit sum over $j>2$ on RHS does not contain gluon k_1 anymore. Repeating the same arguments for the collinear gluons $k_2,\dots,k_{n-r}$ leads to

$$\big\langle\boldsymbol{\mathcal{H}}\,(\mathbf{\Gamma}^c)^{n-r}\,\boldsymbol{V}^G\,\overline{\mathbf{\Gamma}}\otimes\mathbf{1}\big\rangle = 16i\pi\,N_c^{n-r}\big\langle\boldsymbol{\mathcal{H}}\,\boldsymbol{X}_1\otimes\mathbf{1}\big\rangle\,. \tag{8.26}$$

The second Glauber operator in (8.15) yields

$$\big\langle\boldsymbol{\mathcal{H}}\,\boldsymbol{V}^G\,\boldsymbol{X}_1\otimes\mathbf{1}\big\rangle = 2i\pi\,\big\langle\boldsymbol{\mathcal{H}}\,\big[\boldsymbol{T}_1\cdot\boldsymbol{T}_2,\boldsymbol{X}_1\big]\otimes\mathbf{1}\big\rangle = N_c\,i\pi\,\big\langle\boldsymbol{\mathcal{H}}\,\boldsymbol{X}_2\otimes\mathbf{1}\big\rangle\,, \tag{8.27}$$

where the new color structure is defined as

$$\boldsymbol{X}_2 \coloneqq \frac{1}{N_c}\sum_{j>2}J_j\,f^{abe}f^{cde}\big(\boldsymbol{T}_2^a\big\{\boldsymbol{T}_1^b,\boldsymbol{T}_1^c\big\} - \boldsymbol{T}_1^a\big\{\boldsymbol{T}_2^b,\boldsymbol{T}_2^c\big\}\big)\boldsymbol{T}_j^d\,. \tag{8.28}$$

The factor $1/N_c$ is chosen such that $\langle\boldsymbol{\mathcal{H}}_{2\to M}\,\boldsymbol{X}_2\rangle$ is at most $\mathcal{O}(1)$ in the large-N_c limit for all hard functions considered in Section 8.4. To arrive at this result, one can use

$$\boldsymbol{T}_i^a\,\boldsymbol{T}_i^b = \frac{1}{2}\,if^{abc}\,\boldsymbol{T}_i^c + \frac{1}{2}\big\{\boldsymbol{T}_i^a,\boldsymbol{T}_i^b\big\} \tag{8.29}$$

to symmetrize products of generators. The full color trace including the second Glauber operator then reads

$$\big\langle\boldsymbol{\mathcal{H}}\,\boldsymbol{V}^G\,(\mathbf{\Gamma}^c)^{n-r}\,\boldsymbol{V}^G\,\overline{\mathbf{\Gamma}}\otimes\mathbf{1}\big\rangle = -16\pi^2\,N_c^{n-r+1}\big\langle\boldsymbol{\mathcal{H}}\,\boldsymbol{X}_2\otimes\mathbf{1}\big\rangle\,, \tag{8.30}$$

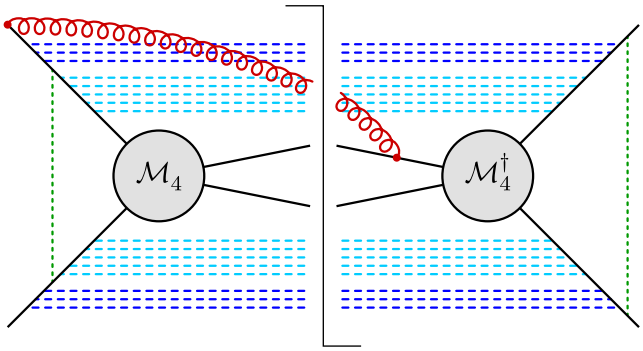

Figure 8.1: Example diagram for partonic $2 \to 2$ scattering giving rise to a color structure $\boldsymbol{X}_i$ with $i = 2, \ldots, 5$. In this case, the soft wide-angle emission (red) attaches to an initial-state leg and one final-state leg of the Born-level hard function. Glauber gluons (green) are exchanged between initial-state partons and collinear gluons (blue) are emitted from them. Darker colors indicate later emissions.

where $\boldsymbol{\mathcal{H}} \coloneqq \boldsymbol{\mathcal{H}}_{2\to M} \, (\boldsymbol{\Gamma}^c)^r$ contains only cusp anomalous dimensions.

Inserting the definition of $\boldsymbol{\Gamma}^c$ once again, we need to calculate

$$\begin{aligned}\big\langle \boldsymbol{\mathcal{H}} \, \boldsymbol{\Gamma}^c \, \boldsymbol{X}_2 \otimes \mathbf{1} \big\rangle = -\sum_{i=1,2} \Bigg[{\sum_{j>2}}' J_j \, \zeta^{abcd} \big\langle \boldsymbol{\mathcal{H}} \, \boldsymbol{T}_i^f \big[\boldsymbol{T}_2^a \big\{ \boldsymbol{T}_1^b, \boldsymbol{T}_1^c \big\} - \boldsymbol{T}_1^a \big\{ \boldsymbol{T}_2^b, \boldsymbol{T}_2^c \big\}, \boldsymbol{T}_i^f \big] \boldsymbol{T}_j^d \otimes \mathbf{1} \big\rangle \\ - J_i \, \zeta^{abcd} \, i f^{dfg} \big\langle \boldsymbol{\mathcal{H}} \, \boldsymbol{T}_i^f \big(\boldsymbol{T}_2^a \big\{ \boldsymbol{T}_1^b, \boldsymbol{T}_1^c \big\} - \boldsymbol{T}_1^a \big\{ \boldsymbol{T}_2^b, \boldsymbol{T}_2^c \big\} \big) \boldsymbol{T}_i^g \otimes \mathbf{1} \big\rangle \Bigg], \quad (8.31)\end{aligned}$$

with $N_c \, \zeta^{abcd} = f^{abe} f^{cde}$ and the prime indicates that $j \neq k_{n-r+1}$. The first line reproduces color structure $\boldsymbol{X}_2$ and three new structures with J_j, they read

$$\begin{aligned}\boldsymbol{X}_3 &\coloneqq \frac{1}{N_c} \sum_{j>2} J_j \, d^{ade} d^{bce} \big(\boldsymbol{T}_2^a \big\{ \boldsymbol{T}_1^b, \boldsymbol{T}_1^c \big\} - \boldsymbol{T}_1^a \big\{ \boldsymbol{T}_2^b, \boldsymbol{T}_2^c \big\} \big) \boldsymbol{T}_j^d \,, \\ \boldsymbol{X}_4 &\coloneqq \frac{1}{N_c^2} \sum_{j>2} J_j \big(\boldsymbol{T}_2^a \big\{ \boldsymbol{T}_1^a, \boldsymbol{T}_1^b \big\} - \boldsymbol{T}_1^a \big\{ \boldsymbol{T}_2^a, \boldsymbol{T}_2^b \big\} \big) \boldsymbol{T}_j^b \,, \qquad (8.32) \\ \boldsymbol{X}_5 &\coloneqq \frac{1}{N_c^2} \sum_{j>2} J_j \big(2C_1 \, \boldsymbol{T}_2 \cdot \boldsymbol{T}_j - 2C_2 \, \boldsymbol{T}_1 \cdot \boldsymbol{T}_j \big) \,,\end{aligned}$$

where the d-symbols are totally symmetric and traceless structure constants of $SU(N_c)$, see (8.56). In Figure 8.1 an example diagram yielding one of these color structures is shown. This time the second line does not vanish and yields color structure with angular integral J_{12}. We find

$$\begin{aligned}\boldsymbol{X}_6 &\coloneqq \frac{1}{N_c^3} \, J_{12} \, f^{abe} f^{cde} \big\{ \boldsymbol{T}_1^b, \boldsymbol{T}_1^c \big\} \big\{ \boldsymbol{T}_2^a, \boldsymbol{T}_2^d \big\} \,, \\ \boldsymbol{X}_7 &\coloneqq \frac{1}{N_c^3} \, J_{12} \, d^{ade} d^{bce} \big\{ \boldsymbol{T}_1^b, \boldsymbol{T}_1^c \big\} \big\{ \boldsymbol{T}_2^a, \boldsymbol{T}_2^d \big\} \,,\end{aligned}$$

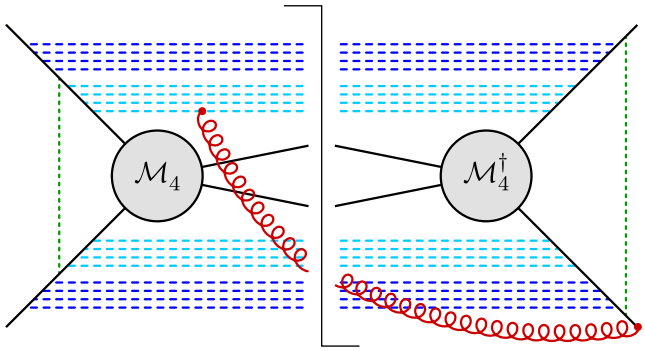

Figure 8.2: Example diagram for partonic $2 \to 2$ scattering giving rise to a color structure $\boldsymbol{X}_i$ with $i = 6, \dots, 11$. The colors have the same meaning as in Figure 8.1 but here the soft emission attaches to an initial-state leg and one of the early collinear emissions. Attachments to the later emissions (dark blue) do not contribute, as the second line in (8.22) vanishes.

$$\begin{aligned}
\boldsymbol{X}_8 &\coloneqq \frac{1}{N_c^3}\, J_{12}\, d^{ade} d^{bce} \Big[\boldsymbol{T}_2^a \left(\boldsymbol{T}_1^b \boldsymbol{T}_1^c \boldsymbol{T}_1^d\right)_+ + \boldsymbol{T}_1^a \left(\boldsymbol{T}_2^b \boldsymbol{T}_2^c \boldsymbol{T}_2^d\right)_+ \Big], \\
\boldsymbol{X}_9 &\coloneqq \frac{1}{N_c^2}\, J_{12} \left\{\boldsymbol{T}_1^a, \boldsymbol{T}_1^b\right\} \left\{\boldsymbol{T}_2^a, \boldsymbol{T}_2^b\right\}, \\
\boldsymbol{X}_{10} &\coloneqq \frac{1}{N_c}\, J_{12}\, \boldsymbol{T}_1 \cdot \boldsymbol{T}_2, \\
\boldsymbol{X}_{11} &\coloneqq J_{12}\, \boldsymbol{1}.
\end{aligned} \tag{8.33}$$

In (8.32) and (8.33) the factors $1/N_c$ are again chosen such that $\langle \boldsymbol{\mathcal{H}}_{2\to M}\, \boldsymbol{X}_i \rangle$ are at most $\mathcal{O}(1)$ in the large-N_c expansion. Color structure $\boldsymbol{X}_8$ contains the symmetrized product of three generators, defined by

$$\left(\boldsymbol{T}^{a_1} \dots \boldsymbol{T}^{a_k}\right)_+ \coloneqq \frac{1}{k!} \sum_{\sigma \in S_k} \boldsymbol{T}^{a_{\sigma(1)}} \dots \boldsymbol{T}^{a_{\sigma(k)}}, \tag{8.34}$$

where the sum is over all permutations of $\{1, 2, \dots, k\}$. A sample diagram giving rise to such a color structure is depicted in Figure 8.2. The action of $\boldsymbol{\Gamma}^c$ on the new structures (8.32) containing a sum over final-state partons can be calculated similar to (8.31) with

$$N_c^2\, \zeta^{abcd} = \begin{cases} N_c\, d^{ade} d^{bce} & \text{for } \boldsymbol{X}_3, \\ \delta^{ab}\delta^{cd} & \text{for } \boldsymbol{X}_4, \\ \delta^{ad}\delta^{bc} & \text{for } \boldsymbol{X}_5. \end{cases} \tag{8.35}$$

For new structures (8.33) without final-state generator, i.e. $i = 6, \dots, 11$, the action is

$$\left\langle \boldsymbol{\mathcal{H}}\, \boldsymbol{\Gamma}^c\, \boldsymbol{X}_i \otimes \boldsymbol{1} \right\rangle = -\left\langle \boldsymbol{\mathcal{H}}\, \boldsymbol{T}_1^a \left[\boldsymbol{X}_i, \boldsymbol{T}_1^a\right] \otimes \boldsymbol{1} \right\rangle - \left\langle \boldsymbol{\mathcal{H}}\, \boldsymbol{T}_2^a \left[\boldsymbol{X}_i, \boldsymbol{T}_2^a\right] \otimes \boldsymbol{1} \right\rangle, \tag{8.36}$$

because in this case $\boldsymbol{T}_{i,L} \circ \boldsymbol{T}_{i,R} = \boldsymbol{T}_{i,L} \cdot \boldsymbol{T}_{i,R}$. Remarkably, the set $\{\boldsymbol{X}_2, \dots, \boldsymbol{X}_{11}\}$ is closed under repeated application of $\boldsymbol{\Gamma}^c$. It is thus convenient to express its action as

a matrix $\mathbb{\Gamma}^c$ in the space of color structures defined by

$$\left\langle \boldsymbol{\mathcal{H}}\, \boldsymbol{\Gamma}^c \boldsymbol{X}_i \otimes \mathbf{1} \right\rangle =: \sum_{\tilde{\imath}} \left\langle \boldsymbol{\mathcal{H}}\, \boldsymbol{X}_{\tilde{\imath}} \otimes \mathbf{1} \right\rangle N_c \left(\mathbb{\Gamma}^c\right)_{\tilde{\imath}i} , \tag{8.37}$$

where we pulled out the factor N_c for convenience. Note that also here the implicit sum over $j > 2$ is different between left- and right-hand side. We find [4]

$$\mathbb{\Gamma}^c = \begin{pmatrix}
1 & 0 & 0 & 0 & 0 & 0 & 0 & 0 & 0 & 0 & 0 \\
0 & \frac{3}{2} & 0 & \frac{1}{N_c^2} & 0 & 0 & 0 & 0 & 0 & 0 & 0 \\
0 & \frac{1}{4} & 1 & 0 & 0 & 0 & 0 & 0 & 0 & 0 & 0 \\
0 & 1 & 0 & \frac{3}{2} & 0 & 0 & 0 & 0 & 0 & 0 & 0 \\
0 & 1 & 0 & 0 & \frac{1}{2} & 0 & 0 & 0 & 0 & 0 & 0 \\
0 & -\frac{N_c^2}{2} & 0 & -1 & 0 & 2 & 0 & 0 & 2 & 0 & 0 \\
0 & -\frac{N_c^2}{4} & 0 & 0 & 0 & \frac{1}{2} & 1 & 0 & 0 & 0 & 0 \\
0 & -\frac{N_c^2}{2} & 0 & 0 & 0 & 0 & 0 & 1 & 0 & 0 & 0 \\
0 & -1 & 0 & -\frac{1}{2} & 0 & \frac{2}{N_c^2} & 0 & 0 & 2 & 0 & 0 \\
0 & \frac{N_c^2+8}{6} - \frac{4(C_1+C_2)}{N_c} & 0 & \frac{N_c-C_1-C_2}{N_c} & \frac{C_1+C_2}{N_c} & 0 & 0 & 0 & 0 & 1 & 0 \\
0 & -\frac{4C_1C_2}{N_c^2} & 0 & 0 & \frac{2C_1C_2}{N_c^2} & \frac{8C_1C_2}{N_c^4} & 0 & 0 & 0 & 0 & 0
\end{pmatrix} , \tag{8.38}$$

where also $\boldsymbol{X}_1$ is included. The i-th column of this matrix (times N_c) describes the action of the cusp anomalous dimension on color structure $\boldsymbol{X}_i$.

To arrive at these results, one uses (8.29) to symmetrize products of generators. Contractions of several f- and d-symbols can then be simplified using (8.24) and the relations [108]

$$\begin{aligned}
&\mathrm{tr}\big(D^a F^b\big) = 0 , && \mathrm{tr}\big(D^a D^b F^c\big) = \frac{N_c^2-4}{2N_c}\, i f^{abc} , \\
&\mathrm{tr}\big(D^a D^b\big) = \frac{N_c^2-4}{N_c}\, \delta^{ab} , && \mathrm{tr}\big(D^a F^b F^c\big) = \frac{N_c}{2}\, d^{abc} ,
\end{aligned} \tag{8.39}$$

where $(D^a)^{bc} = d^{abc}$. Similar relations hold for traces of four and more f- and d-symbols. In our case, we need [108]

$$\begin{aligned}
\mathrm{tr}\big(F^a \big\{F^b, F^c\big\} F^d\big) &= 2\delta^{ad}\delta^{bc} + \big(\delta^{ab}\delta^{cd} + \delta^{ac}\delta^{bd}\big) + \frac{N_c}{2}\, d^{ade} d^{bce} , \\
\mathrm{tr}\big(F^a F^b D^c D^d\big) &= \frac{1}{2}\big(\delta^{ab}\delta^{cd} - \delta^{ac}\delta^{bd}\big) + \frac{N_c^2-8}{4N_c}\, f^{ade} f^{bce} + \frac{N_c}{4}\, d^{ade} d^{bce} .
\end{aligned} \tag{8.40}$$

For example, the first relation maps $f^{abe} f^{cde}$ in (8.31) to the three structures found in (8.35). Color structure $\boldsymbol{X}_8$ is obtained from anti-commutators by means of

$$d^{ade} d^{bce} \left(\boldsymbol{T}_i^b \boldsymbol{T}_i^c \boldsymbol{T}_i^d\right)_+ = \frac{1}{2}\, d^{ade} d^{bce} \left\{\boldsymbol{T}_i^b, \boldsymbol{T}_i^c\right\} \boldsymbol{T}_i^d - \frac{N_c^2-4}{12}\, \boldsymbol{T}_i^a , \tag{8.41}$$

which holds for generators in an arbitrary representation.

The color trace (8.12) associated with the SLLs can be written as

$$C_{rn} = -16\pi^2 N_c^{n+1} \sum_{i=2}^{11} c_i^{(r)} \left\langle \boldsymbol{\mathcal{H}}_{2\to M}\, \boldsymbol{X}_i \otimes \mathbf{1} \right\rangle , \tag{8.42}$$

where the coefficients $c_i^{(r)}$ are determined by recursive relations. Here, the $\otimes$ symbol only contains the angular integrals over the M final-state partons of the Born process. As this M has been kept arbitrary in the above derivation, our formalism allows for the study of processes with a single ($M = 1$) or even no ($M = 0$) final-state jet [73], see Section 8.4. So far, the literature on SLLs only discusses $2 \to 2$ hard-scattering processes [66–68]. As argued below (7.37), one needs (at least) two color-charged initial-state partons for non-trivial Glauber effects to arise. The same arguments can be applied to the final state where missing color-charged partons for $M = 0, 1$ are provided by collinear emissions from $\boldsymbol{\Gamma}^c$ (after the second insertion of the Glauber phase $\boldsymbol{V}^G$). For $M = 0$ the color structures (8.28) and (8.32) do not contribute and two such emissions are necessary, thus the SLLs start first at five-loop order. For $M = 1$ they start at four-loop order, as for $M \geq 2$, but the $n = 0$ terms does not contribute.

From (8.30), one can infer the boundary condition for the coefficients in (8.42)

$$c_i^{(0)} = \delta_{i2} \,. \tag{8.43}$$

The recursive relations for these coefficients can be read off from the i-th row of (8.38), we find for the structures with final-state generator

$$\begin{aligned} c_2^{(r+1)} &= \frac{3}{2}\, c_2^{(r)} + \frac{1}{N_c^2}\, c_4^{(r)} \,, & c_3^{(r+1)} &= \frac{1}{4}\, c_2^{(r)} + c_3^{(r)} \,, \\ c_4^{(r+1)} &= c_2^{(r)} + \frac{3}{2}\, c_4^{(r)} \,, & c_5^{(r+1)} &= c_2^{(r)} + \frac{1}{2}\, c_5^{(r)} \,, \end{aligned} \tag{8.44}$$

which can be solved to

$$\begin{aligned} c_2^{(r)} &= \frac{1}{2}\big(v_3^r + v_4^r\big) \,, & c_3^{(r)} &= -\frac{N_c^2}{2(N_c^2-4)}\, v_2^r + \frac{N_c}{4(N_c+2)}\, v_3^r + \frac{N_c}{4(N_c-2)}\, v_4^r \,, \\ c_4^{(r)} &= \frac{N_c}{2}\big(v_3^r - v_4^r\big) \,, & c_5^{(r)} &= -\frac{N_c^2}{N_c^2-1}\, v_1^r + \frac{N_c}{2(N_c+1)}\, v_3^r + \frac{N_c}{2(N_c-1)}\, v_4^r \,. \end{aligned} \tag{8.45}$$

The coefficients of the structures without final-state generator fulfill

$$\begin{aligned} c_6^{(r+1)} &= -\frac{N_c^2}{2}\, c_2^{(r)} - c_4^{(r)} + 2\, c_6^{(r)} + 2\, c_9^{(r)} \,, \\ c_7^{(r+1)} &= -\frac{N_c^2}{4}\, c_2^{(r)} + \frac{1}{2}\, c_6^{(r)} + c_7^{(r)} \,, \\ c_8^{(r+1)} &= -\frac{N_c^2}{2}\, c_2^{(r)} + c_8^{(r)} \,, \\ c_9^{(r+1)} &= -c_2^{(r)} - \frac{1}{2}\, c_4^{(r)} + \frac{2}{N_c^2}\, c_6^{(r)} + 2\, c_9^{(r)} \,, \end{aligned}$$

$$
\begin{aligned}
c_{10}^{(r+1)} &= \left[\frac{N_c^2+8}{6} - \frac{4(C_1+C_2)}{N_c}\right] c_2^{(r)} + \frac{N_c - C_1 - C_2}{N_c}\, c_4^{(r)} + \frac{C_1+C_2}{N_c}\, c_5^{(r)} + c_{10}^{(r)}\,, \\
c_{11}^{(r+1)} &= -\frac{4C_1C_2}{N_c^2}\, c_2^{(r)} + \frac{2C_1C_2}{N_c^2}\, c_5^{(r)} + \frac{8C_1C_2}{N_c^4}\, c_6^{(r)}\,.
\end{aligned} \tag{8.46}
$$

After inserting the solution (8.45), it is possible to solve these relations

$$
\begin{aligned}
c_6^{(r)} &= \frac{N_c^2}{2}\left(v_3^r + v_4^r - v_5^r - v_6^r\right), \\
c_7^{(r)} &= \frac{N_c^2}{4}\left[\frac{N_c}{N_c+2}\left(v_3^r - v_5^r\right) + \frac{N_c}{N_c-2}\left(v_4^r - v_6^r\right)\right], \\
c_8^{(r)} &= \frac{N_c^4}{N_c^2-4}\, v_2^r - \frac{N_c^2}{2}\left[\frac{N_c}{N_c+2}\, v_3^r + \frac{N_c}{N_c-2}\, v_4^r\right], \\
c_9^{(r)} &= \frac{N_c}{2}\left(v_3^r - v_4^r - v_5^r + v_6^r\right), \\
c_{10}^{(r)} &= (C_1+C_2)\left[\frac{2N_c}{N_c^2-1}\, v_1^r - \frac{N_c+2}{N_c+1}\, v_3^r + \frac{N_c-2}{N_c-1}\, v_4^r\right] \\
&\quad - \frac{N_c^2}{3}\left[v_2^r - \frac{N_c+4}{2N_c}\, v_3^r - \frac{N_c-4}{2N_c}\, v_4^r\right], \\
c_{11}^{(r)} &= \frac{2C_1C_2}{N_c^2}\left[\frac{2N_c^2}{N_c^2-1}\left(v_0^r - v_1^r\right) + \frac{N_c}{N_c+1}\left(v_3^r - v_5^r\right) + \frac{N_c}{N_c-1}\left(v_4^r - v_6^r\right)\right].
\end{aligned} \tag{8.47}
$$

Here and in (8.45), the solutions for the coefficients are expressed in terms of the eigenvalues of $\mathbb{\Gamma}^c$

$$
v_0 = 0\,, \qquad v_1 = \frac{1}{2}\,, \qquad v_2 = 1\,, \qquad v_{3,4} = \frac{3N_c \pm 2}{2N_c}\,, \qquad v_{5,6} = \frac{2(N_c \pm 1)}{N_c}\,, \tag{8.48}
$$

where v_3 and v_5 correspond to the plus signs. Eigenvalue v_0 contributes as $0^r = \delta_{0r}$.

Using the fact that the eigenvalues v_3 and v_4, as well as v_5 and v_6, coincide up to subleading terms in the large-N_c limit, one finds that the coefficients $c_i^{(r)}$ for $i = 6, 7, 8, 10$ contain "super-leading" terms in N_c. In order for these terms to cancel out in all predictions for physical quantities, the color operators $\boldsymbol{X}_6$ and $\boldsymbol{X}_7$, as well as $\boldsymbol{X}_8$ and $\boldsymbol{X}_{10}$, must satisfy the relations [4]

$$
\boldsymbol{X}_6 + \frac{1}{2}\,\boldsymbol{X}_7 = \mathcal{O}(1/N_c^2)\,, \qquad\qquad \boldsymbol{X}_8 - \frac{1}{3}\,\boldsymbol{X}_{10} = \mathcal{O}(1/N_c^2)\,. \tag{8.49}
$$

They can easily be proven for QCD, for example, by translating the structures $\boldsymbol{X}_i$ to the basis structures for quark-, quark-gluon- and gluon-initiated processes, developed in Section 9.1. As the color trace (8.42) is combined with the iterated scale integral (8.13), containing a factor α_s^{n+3}, and the super-leading terms in the coefficients cancel, the SLL contribute as $\alpha_s^2\,(N_c\,\alpha_s)^{n+1} = \mathcal{O}(1/N_c^2)$ and, therefore, are subleading in the large-N_c expansion.

Simplifications for QCD with Quarks and Gluons

In QCD only two types of fields are present, (anti-)quarks transforming in the fundamental and gluons transforming in the adjoint representation of $SU(N_c)$. Both their generators fulfill the useful relation

$$d^{ade}d^{bce}\left\{\boldsymbol{T}_i^b,\boldsymbol{T}_i^c\right\}\boldsymbol{T}_i^d = R_i\,\boldsymbol{T}_i^a\,, \tag{8.50}$$

where

$$R_q = R_{\bar{q}} = \frac{(N_c^2-4)^2}{2N_c^2}\,, \qquad R_g = \frac{N_c^2-4}{2}\,. \tag{8.51}$$

Applying this to (8.41), one finds

$$\boldsymbol{X}_8 = \left[\frac{R_1+R_2}{2N_c^2} - \frac{N_c^2-4}{6N_c^2}\right]\boldsymbol{X}_{10}\,. \tag{8.52}$$

Taking the large-N_c limit, one recovers the second consistency relation in (8.49). Exploiting this connection, one can remove the most complicated color structure $\boldsymbol{X}_8$ from our final result (8.42) by replacing

$$c_{10}^{(r)} \to c_{10}^{(r)} + c_8^{(r)}\left[\frac{R_1+R_2}{2N_c^2} - \frac{N_c^2-4}{6N_c^2}\right]. \tag{8.53}$$

For gluons, one finds by applying (8.39) twice

$$d^{ade}d^{bce}\left\{\boldsymbol{F}_i^b,\boldsymbol{F}_i^c\right\}\boldsymbol{F}_i^d = N_c\,d^{ade}\,\boldsymbol{D}_i^e\,\boldsymbol{F}_i^d = \frac{N_c^2-4}{2}\,\boldsymbol{F}_i^a\,, \tag{8.54}$$

which proves (8.50). Here and in the following, we denote generators by $\boldsymbol{F}_i$ if parton i is a gluon and define

$$\left[\mathbf{1}_i\right]^{a_ib_i} := \delta^{aa_ib_i}\,, \qquad \left[\boldsymbol{F}_i^a\right]^{a_ib_i} := -if^{aa_ib_i}\,, \qquad \left[\boldsymbol{D}_i^a\right]^{a_ib_i} := d^{aa_ib_i}\,. \tag{8.55}$$

In contrast, generators for (anti)-quarks are denoted by $\boldsymbol{t}_i$, see Appendix A.3 for their precise definition. Besides the standard commutation relation, they fulfill[2]

$$\left\{\boldsymbol{t}_i^a,\boldsymbol{t}_i^b\right\} = \frac{1}{N_c}\,\delta^{ab}\,\mathbf{1}_i + \sigma_i\,d^{abc}\,\boldsymbol{t}_i^c\,, \tag{8.56}$$

where $\sigma_i = -1$ $(+1)$ for an initial-state (anti-)quark. Relation (8.50) follows immediately

$$d^{ade}d^{bce}\left\{\boldsymbol{t}_i^b,\boldsymbol{t}_i^c\right\}\boldsymbol{t}_i^d = \frac{N_c^2-4}{2N_c}\,\sigma_i\,d^{ade}\left\{\boldsymbol{t}_i^e,\boldsymbol{t}_i^d\right\} = \frac{(N_c^2-4)^2}{2N_c^2}\,\boldsymbol{t}_i^a\,. \tag{8.57}$$

In Chapter 9, we apply (8.56) further to simply the color structures $\boldsymbol{X}_i$ for quark-initiated processes.

[2]Relation (8.56) can be understood as definition of the d-symbols.

8.1.2 Iterated Scale Integrals

The contribution of the SLLs to the partonic cross section consists of two parts, the color trace (8.12), simplified in the previous section, and the iterated scale integrals (8.13). When working in a strict double-logarithmic approximation one can ignore the running of the strong coupling, as it is a single-logarithmic effect. The iterated scale integral evaluates in this case to [73]

$$I_{rn}(\mu_h,\mu_s)\Big|_{\text{fixed}} = \left(\frac{\alpha_s}{4\pi}\right)^{n+3} \gamma_0^{n+2}\, \frac{(-4)^n n!}{(2n+3)!}\, \frac{(2r)!}{4^r (r!)^2}\, L_s^{2n+3}\,, \tag{8.58}$$

where $\alpha_s \coloneqq \alpha_s(\bar{\mu})$ and $\bar{\mu}$ is a fixed reference scale between μ_s and μ_h. A priori it is not clear which value one has to chose for $\bar{\mu}$ leading to a *scale uncertainty* when working with a fixed coupling. Here, we used the one-loop form of the cusp anomalous dimension (7.32) but including higher terms is straightforward

$$I_{rn}(\mu_h,\mu_s)\Big|_{\text{fixed}} = \frac{\alpha_s}{4\pi}\, \gamma_{\text{cusp}}^{n+2}(\alpha_s)\, \frac{(-4)^n n!}{(2n+3)!}\, \frac{(2r)!}{4^r (r!)^2}\, L_s^{2n+3}\,. \tag{8.59}$$

One can show these relations by changing variables in (8.13) to $L_i \coloneqq \ln(\mu_h/\mu_i) \geq 0$ and inverting the order of integration

$$\begin{aligned} I_{rn}(\mu_h,\mu_s)\Big|_{\text{fixed}} &= \frac{\alpha_s}{4\pi}\, \gamma_{\text{cusp}}^{n+2}(\alpha_s)\, (-2)^n \\ &\quad \times \int_0^{L_s} dL_{n+3} \cdots \int_0^{L_3} dL_2 \int_0^{L_2} dL_1 \left(\prod_{i=1}^{r} L_i\right)\left(\prod_{i=r+2}^{n+1} L_i\right) \\ &= \frac{\alpha_s}{4\pi}\, \gamma_{\text{cusp}}^{n+2}(\alpha_s)\, \frac{(-2)^n}{(2n+3)(2n+2)}\, \frac{1}{(2r)!!}\, \frac{(2r-1)!!}{(2n+1)!!}\, L_s^{2n+3}\,, \end{aligned} \tag{8.60}$$

where $n!! = n(n-2)\ldots$ denotes the double factorial. Expressing them through ordinary factorials, one obtains the above results.

When including a running coupling $\alpha_s(\mu)$, it is also possible to obtain explicit expressions for I_{rn} for given values of n and r. In this case, it is convenient to again change variables in (8.13) to $x_i \coloneqq \alpha_s(\mu_i)/\alpha_s(\mu_h) \geq 1$. For two-loop running, one can express the explicit scale logarithm as

$$\ln\frac{\mu_i^2}{\mu_h^2} = -2\int_{\alpha_s(\mu_i)}^{\alpha_s(\mu_h)} \frac{d\alpha}{\beta(\alpha)} = \frac{-4\pi}{\beta_0\,\alpha_h}\left[1 - \frac{1}{x_i} - \frac{\alpha_h}{4\pi}\,\frac{\beta_1}{\beta_0}\,\ln x_i + \mathcal{O}(\alpha_h^2)\right], \tag{8.61}$$

where $\alpha_h \coloneqq \alpha_s(\mu_h)$ and the expansion of the QCD β-function is

$$\beta(\alpha_s) = -2\alpha_s \sum_{n=0}^{\infty} \beta_n \left(\frac{\alpha_s}{4\pi}\right)^{n+1}, \tag{8.62}$$

with coefficients given in Appendix A.4. Using this result, we find

$$I_{rn}(\mu_h,\mu_s) = \gamma_0^{n+2}\left(\frac{1}{2\beta_0}\right)^{n+3}\left[\frac{-4\pi}{\beta_0\,\alpha_h}\right]^n \int_1^{x_s}\frac{dx_1}{x_1}\int_{x_1}^{x_s}\frac{dx_2}{x_2}\cdots\int_{x_{n+2}}^{x_s}\frac{dx_{n+3}}{x_{n+3}}$$

$$
\begin{aligned}
&\times \prod_{i=1}^{r} \left(1-\frac{1}{x_i}\right)\left\{1+\frac{\alpha_h}{4\pi}\left[\left(\frac{\gamma_1}{\gamma_0}-\frac{\beta_1}{\beta_0}\right)x_i+\frac{\beta_1}{\beta_0}\frac{x_i\,\ln x_i}{1-x_i}\right]+\mathcal{O}(\alpha_h^2)\right\} \\
&\times \left[1+\frac{\alpha_h}{4\pi}\left(\frac{\gamma_1}{\gamma_0}-\frac{\beta_1}{\beta_0}\right)x_{r+1}+\mathcal{O}(\alpha_h^2)\right] \\
&\times \prod_{i=r+2}^{n+1} \left(1-\frac{1}{x_i}\right)\left\{1+\frac{\alpha_h}{4\pi}\left[\left(\frac{\gamma_1}{\gamma_0}-\frac{\beta_1}{\beta_0}\right)x_i+\frac{\beta_1}{\beta_0}\frac{x_i\,\ln x_i}{1-x_i}\right]+\mathcal{O}(\alpha_h^2)\right\} \\
&\times \left[1+\frac{\alpha_h}{4\pi}\left(\frac{\gamma_1}{\gamma_0}-\frac{\beta_1}{\beta_0}\right)x_{n+2}+\mathcal{O}(\alpha_h^2)\right]\left[1-\frac{\alpha_h}{4\pi}\frac{\beta_1}{\beta_0}\,x_{r+1}+\mathcal{O}(\alpha_h^2)\right] \\
&=: \gamma_0^{n+2}\left(\frac{1}{2\beta_0}\right)^{n+3}\left[\frac{-4\pi}{\beta_0\,\alpha_h}\right]^n h_{nr}(x_s)\,.
\end{aligned}
\tag{8.63}
$$

At one loop ($\gamma_1 = \beta_1 = 0$), the functions h_{nr} are simple and only contain logarithms and polynomials. We find for the first three[3]

$$
\begin{aligned}
h_{00}(x) &= \frac{\ln^3 x}{6}\,, \qquad h_{10}(x) = \frac{\ln^4 x}{24}-\frac{\ln^2 x}{2}+\left(2+\frac{1}{x}\right)\ln x-3+\frac{3}{x}\,, \\
&\qquad\qquad h_{11}(x) = \frac{\ln^4 x}{24}-\frac{\ln^3 x}{6}+\frac{\ln^2 x}{2}-\ln x+1-\frac{1}{x}\,.
\end{aligned}
\tag{8.64}
$$

8.1.3 Partonic Cross Section

By combing the simplified color trace (8.42) and the iterated scale integrals with fixed (8.58) or running coupling (8.63), the contribution of the SLLs to the partonic cross section is fully determined. For a running coupling, we were not able to perform the iterated scale integrals in a closed form for arbitrary n and r and thus cannot perform the double sum in (8.14). However an alternative strategy, discussed in the next section, allows to express the resummed SLLs in RG-improved perturbation theory as a two-fold scale integral.

In the fixed coupling approximation, we find at the level of the partonic cross section [1]

$$
\begin{aligned}
\hat{\sigma}^{\text{SLL}}_{2\to M}(Q_0)\Big|_{\text{fixed}} &= \frac{4\alpha_s(\bar{\mu})\,L_s}{\pi\,N_c}\,w_\pi \sum_{n=0}^{\infty}(-w)^{n+1}\,\frac{4^n\,n!}{(2n+3)!} \\
&\quad\times \sum_{r=0}^{n}\frac{(2r)!}{4^r(r!)^2}\sum_{i=2}^{11} c_i^{(r)}\left\langle \boldsymbol{\mathcal{H}}_{2\to M}(\mu_h)\,\boldsymbol{X}_i\otimes\mathbf{1}\right\rangle
\end{aligned}
\tag{8.65}
$$

with parameters

$$
w := \frac{N_c\gamma_0}{4\pi}\,\alpha_s(\bar{\mu})\,L_s^2\,, \qquad\qquad w_\pi := \frac{N_c\gamma_0}{4\pi}\,\alpha_s(\bar{\mu})\,\pi^2\,. \tag{8.66}
$$

Here, the variable $L_s = \ln(\mu_h/\mu_s)$ depends on the ratio of the hard and soft matching scales and reduces to the variable L used in the introduction for the default scale

[3] In [1] we defined $x_s := \alpha_s(\mu_h)/\alpha_s(\mu_s) \leq 1$ and, therefore, one needs to replace $x \to 1/x$ in (8.64) to obtain our previous results.

choices $\mu_h = Q$ and $\mu_s = Q_0$. From this result its is obvious that the SLLs start at four-loop order, as the first non-vanishing term with $\mathbf{\Gamma}^c$ also requires the insertion of two Glauber operators and one soft anomalous dimension [73]. Furthermore, the series over n is alternating and, as we show in Section 8.4, resummation is crucial since strong cancellations take place.

The coefficients $c_i^{(r)}$ have a power-like dependence on r and can thus be decomposed

$$c_i^{(r)} = \sum_{j=0}^{6} v_j^r \, c_{ji} \,, \tag{8.67}$$

where the matrix c_{ji} can be read off from (8.45) and (8.47). One can then perform the nested double sum, thereby resumming the SLLs to all-orders. For the special case $v = 0$, one only needs to perform a single infinite sum and finds a generalized hypergeometric function [73]

$$\Sigma(0; w) \coloneqq \sum_{n=0}^{\infty} \frac{3!\, 4^n\, n!}{(2n+3)!} \, (-w)^n = {}_2F_2\big(1, 1; 2, \tfrac{5}{2}; -w\big) \,. \tag{8.68}$$

Here and below, we include a factor 3! in the definition of the Σ functions for convenience. For all other eigenvalues $v > 0$, we define

$$\Sigma(v; w) \coloneqq \sum_{n=0}^{\infty} \sum_{r=0}^{n} \frac{3!\, 4^n\, n!}{(2n+3)!} \, \frac{(2r)!}{4^r (r!)^2} \, v^r \, (-w)^n \,. \tag{8.69}$$

Separating the sums by replacing $n \to n + r$,

$$\Sigma(v; w) = \sum_{n=0}^{\infty} \sum_{r=0}^{\infty} \frac{(1)_{n+r} (1)_n \big(\frac{1}{2}\big)_r}{(2)_{n+r} \big(\frac{5}{2}\big)_{n+r}} \, \frac{(-w)^n \, (-vw)^r}{n!\, r!} \,, \tag{8.70}$$

where $(a)_n = \Gamma(a+n)/\Gamma(a)$ are Pochhammer symbols, one can show that these are Kampé de Fériet functions

$$\Sigma(v; w) = {}^{1+1}F_{2+0}\left(\begin{matrix} 1 : 1, \frac{1}{2} \\ 2, \frac{5}{2} : \end{matrix} ; -w, -vw \right) . \tag{8.71}$$

The arguments in the upper line indicate the Pochhammer symbols in the numerator, and the lower line corresponds to the ones in the denominator. These Σ functions are discussed in more detail in Section 8.3. The contribution of the resummed SLLs to the partonic cross section is given by

$$\hat{\sigma}^{\text{SLL}}_{2\to M}(Q_0)\Big|_{\text{fixed}} = -\frac{2\alpha_s(\bar{\mu})\, L_s}{3\pi\, N_c} \, w \, w_\pi \sum_{i=2}^{11} \sum_{j=0}^{6} \Sigma(v_j; w) \, c_{ji} \, \big\langle \boldsymbol{\mathcal{H}}_{2\to M}(\mu_h) \, \boldsymbol{X}_i \otimes \mathbf{1} \big\rangle \,. \tag{8.72}$$

Remarkably, it can be expressed through traces of only ten color structures $\boldsymbol{X}_i$ with the process dependent hard function $\boldsymbol{\mathcal{H}}_{2\to M}$ and seven Σ functions encoding the dependence on the leading double logarithms.

8.2 Resummation in RG-Improved Perturbation Theory

Including the running of the strong coupling, i.e. working in RG-improved perturbations theory, is an essential step in producing reliable predictions. However, it is not clear how to proceed from our all-order result for the color trace in the previous section, as the counterpart for the iterated scale integrals I_{rn} is not available in this case. Therefore, starting point for the resummation of the SLLs in RG-improved perturbation theory is (8.8) where all super-leading corrections are encoded in the evolution operator (8.6).

We now evaluate this operator under the trace with a trivial low-energy matrix element (7.20). From (8.18), one can directly conclude

$$\begin{aligned}
&\left\langle \boldsymbol{\mathcal{H}}_{2\to M}(\mu_h)\, \boldsymbol{U}_{\text{SLL}}(\mu_h,\mu_s) \otimes \mathbf{1} \right\rangle \\
&= 16i\pi \int_{\mu_s}^{\mu_h} \frac{d\mu_1}{\mu_1} \int_{\mu_s}^{\mu_1} \frac{d\mu_2}{\mu_2} \int_{\mu_s}^{\mu_2} \frac{d\mu_3}{\mu_3}\, \gamma_{\text{cusp}}\big(\alpha_s(\mu_1)\big)\, \gamma_{\text{cusp}}\big(\alpha_s(\mu_2)\big)\, \frac{\alpha_s(\mu_3)}{4\pi} \\
&\quad \times \left\langle \boldsymbol{\mathcal{H}}_{2\to M}(\mu_h)\, \boldsymbol{U}^c(\mu_h,\mu_1)\, \boldsymbol{V}^G\, \boldsymbol{U}^c(\mu_1,\mu_2)\, \boldsymbol{X}_1 \otimes \mathbf{1} \right\rangle .
\end{aligned} \tag{8.73}$$

The generalized Sudakov operator on the right-hand side evaluates to a scalar function, since $\boldsymbol{X}_1$ is eigenvector of $\boldsymbol{\Gamma}^c$ with eigenvalue N_c, see (8.25). Exploiting further that the Glauber operator maps color structure $\boldsymbol{X}_1$ according to (8.27), we find

$$\begin{aligned}
&16(i\pi)^2\, N_c \int_{\mu_s}^{\mu_h} \frac{d\mu_1}{\mu_1} \int_{\mu_s}^{\mu_1} \frac{d\mu_2}{\mu_2} \int_{\mu_s}^{\mu_2} \frac{d\mu_3}{\mu_3}\, \gamma_{\text{cusp}}\big(\alpha_s(\mu_1)\big)\, \gamma_{\text{cusp}}\big(\alpha_s(\mu_2)\big)\, \frac{\alpha_s(\mu_3)}{4\pi} \\
&\quad \times \left\langle \boldsymbol{\mathcal{H}}_{2\to M}(\mu_h)\, \boldsymbol{U}^c(\mu_h,\mu_1)\, \boldsymbol{X}_2 \otimes \mathbf{1} \right\rangle U^c(1;\mu_1,\mu_2)
\end{aligned} \tag{8.74}$$

where the scalar Sudakov function is

$$U^c(v;\mu_i,\mu_j) \coloneqq \exp\left[v\, N_c \int_{\mu_j}^{\mu_i} \frac{d\mu}{\mu}\, \gamma_{\text{cusp}}\big(\alpha_s(\mu)\big) \ln \frac{\mu^2}{\mu_h^2} \right] . \tag{8.75}$$

In general, v is equal to one of the eigenvalues of $\mathbb{\Gamma}^c$ and this function satisfies $0 < U^c(v;\mu_i,\mu_j) \leq 1$, where the value 1 is obtained only for $\mu_i = \mu_j$ or $v = 0$. Products of these function can be simplified using the identities

$$U^c(v;\mu_i,\mu_j)\, U^c(v;\mu_j,\mu_k) = U^c(v;\mu_i,\mu_k)\,, \qquad U^c(0;\mu_i,\mu_j) = 1\,. \tag{8.76}$$

The remaining generalized Sudakov operator can be evaluated using that the set $\{\boldsymbol{X}_2,\dots,\boldsymbol{X}_{11}\}$ is closed under repeated application of $\boldsymbol{\Gamma}^c$. By (8.37) it translates to a matrix exponential

$$\mathbb{U}^c(\mu_i,\mu_j) \coloneqq \exp\left[N_c\, \mathbb{\Gamma}^c \int_{\mu_j}^{\mu_i} \frac{d\mu}{\mu}\, \gamma_{\text{cusp}}\big(\alpha_s(\mu)\big) \ln \frac{\mu^2}{\mu_h^2} \right] . \tag{8.77}$$

Note that only the second column of this matrix exponential contributes. Since $\mathbb{\Gamma}^c$ is diagonalizable, the scale dependence of $\mathbb{U}^c(\mu_h,\mu_1)$ is encoded in linear combinations of the scalar functions (8.75) with eigenvalues given in (8.48). They can be combined with the factor $U^c(1;\mu_1,\mu_2)$ in (8.74) using the shorthand notation

$$U^c(v_{i_1},\dots,v_{i_l};\mu_h,\mu_1,\dots,\mu_l) \coloneqq U^c(v_{i_1};\mu_h,\mu_1)\, U^c(v_{i_2};\mu_1,\mu_2) \dots U^c(v_{i_l};\mu_{l-1},\mu_l)\,. \tag{8.78}$$

Finally, we find for the resummed partonic cross section

$$\hat{\sigma}^{\text{SLL}}_{2\to M}(Q_0) = \sum_{i=2}^{11} \left\langle \boldsymbol{\mathcal{H}}_{2\to M}(\mu_h)\, \boldsymbol{X}_i \otimes \mathbf{1} \right\rangle \varsigma_i^{\text{SLL}}(\mu_h, \mu_s)\,, \tag{8.79}$$

with $\mu_h \sim \sqrt{\hat{s}}$ and $\mu_s \sim Q_0$. The coefficient vector of the color structures is [4]

$$\begin{aligned}
\varsigma^{\text{SLL}}(\mu_h, \mu_s) \coloneqq -4\pi^2\, N_c \int_{\mu_s}^{\mu_h} \frac{d\mu_1}{\mu_1} \int_{\mu_s}^{\mu_1} \frac{d\mu_2}{\mu_2} \int_{\mu_s}^{\mu_2} \frac{d\mu_3}{\mu_3}\, \gamma_{\text{cusp}}\big(\alpha_s(\mu_1)\big)\, \gamma_{\text{cusp}}\big(\alpha_s(\mu_2)\big)\, \frac{\alpha_s(\mu_3)}{\pi} \\
\times \begin{pmatrix}
0 \\
\frac{1}{2}\big[U^c(v_3,1) + U^c(v_4,1)\big] \\
-\frac{N_c^2}{2(N_c^2-4)}\Big[U^c(1,1) - \frac{N_c-2}{2N_c}\,U^c(v_3,1) - \frac{N_c+2}{2N_c}\,U^c(v_4,1)\Big] \\
\frac{N_c}{2}\big[U^c(v_3,1) - U^c(v_4,1)\big] \\
-\frac{N_c^2}{N_c^2-1}\Big[U^c(\frac{1}{2},1) - \frac{N_c-1}{2N_c}\,U^c(v_3,1) - \frac{N_c+1}{2N_c}\,U^c(v_4,1)\Big] \\
\frac{N_c^2}{2}\big[U^c(v_3,1) + U^c(v_4,1) - U^c(v_5,1) - U^c(v_6,1)\big] \\
\frac{N_c^4}{4(N_c^2-4)}\Big[\frac{N_c-2}{N_c}\big(U^c(v_3,1) - U^c(v_5,1)\big) + \frac{N_c+2}{N_c}\big(U^c(v_4,1) - U^c(v_6,1)\big)\Big] \\
\frac{N_c^4}{N_c^2-4}\Big[U^c(1,1) - \frac{N_c-2}{2N_c}\,U^c(v_3,1) - \frac{N_c+2}{2N_c}\,U^c(v_4,1)\Big] \\
\frac{N_c}{2}\big[U^c(v_3,1) - U^c(v_4,1) - U^c(v_5,1) + U^c(v_6,1)\big] \\
\frac{2N_c(C_1+C_2)}{N_c^2-1}\Big[U^c(\frac{1}{2},1) - \frac{(N_c-1)(N_c+2)}{2N_c}\,U^c(v_3,1) + \frac{(N_c+1)(N_c-2)}{2N_c}\,U^c(v_4,1)\Big] \\
-\frac{N_c^2}{3}\Big[U^c(1,1) - \frac{N_c+4}{2N_c}\,U^c(v_3,1) - \frac{N_c-4}{2N_c}\,U^c(v_4,1)\Big] \\
\frac{4C_1C_2}{N_c^2-1}\Big[U^c(0,1) - U^c(\frac{1}{2},1) + \frac{N_c-1}{2N_c}\big(U^c(v_3,1) - U^c(v_5,1)\big) \\
+\frac{N_c+1}{2N_c}\big(U^c(v_4,1) - U^c(v_6,1)\big)\Big]
\end{pmatrix},
\end{aligned} \tag{8.80}$$

where for brevity we have dropped the three scale arguments of $U^c(v_i, 1; \mu_h, \mu_1, \mu_2)$. This vector describes the full scale dependence of the leading double-logarithmic corrections, independent of the partonic scattering process under consideration. The process dependence in (8.79) is encoded in the traces of the hard functions with the color structures.

In leading order RG-improved perturbation theory, one uses the one-loop approximation for the cusp anomalous dimension in the Glauber terms and rewrites the scale integrals μ_1, μ_2, μ_3 in terms of coupling integrals with the one-loop β-function. The first line in (8.80) becomes

$$\varsigma^{\text{SLL}}(\mu_h, \mu_s) = -\frac{2\pi^2\gamma_0^2}{\beta_0^3}\, N_c \int_1^{x_s} \frac{dx_2}{x_2}\, \ln\frac{x_s}{x_2} \int_1^{x_2} \frac{dx_1}{x_1}\, \dots\,, \tag{8.81}$$

where we already performed the x_3-integral and inverted the order of integrations. The remaining two-fold integral can be performed numerically without much effort. The ellipsis denote the 11-component vector containing the scalar evolution functions. For these functions, as evident from (8.61), one has to keep the two-loop approximations for the cusp anomalous dimension and the β-function. Expressed through the variables x_i, one finds

$$U^c(v;\mu_i,\mu_j) = \exp\left\{\frac{\gamma_0 v N_c}{2\beta_0^2}\left[\frac{4\pi}{\alpha_h}\left(\frac{1}{x_i}-\frac{1}{x_j}-\ln\frac{x_j}{x_i}\right)\right.\right. \\ \left.\left.+\left(\frac{\gamma_1}{\gamma_0}-\frac{\beta_1}{\beta_0}\right)\left(x_i-x_j+\ln\frac{x_j}{x_i}\right)+\frac{\beta_1}{2\beta_0}\left(\ln^2 x_j-\ln^2 x_i\right)\right]\right\}. \tag{8.82}$$

For the special case $\mu_i=\mu_h$ and $v=1$, this result reduces to the well-known expression for the Sudakov exponent encountered in applications of SCET [109]. In Appendix A.4 we generalize this expression for the case that the lower scale lies below the top-quark threshold ($\mu_j<\mu_t$). With the result (8.81) at hand, one can estimate the *perturbative uncertainty* in the standard way by varying the soft scale in the interval $Q_0/2<\mu_s<2Q_0$. In Section 8.4 we compare this uncertainty to the one arising by varying $\bar\mu$ in the fixed coupling approach.

8.3 Fixed-Coupling Results and Asymptotic Behavior

In the standard counting scheme $\alpha_s L_s=\mathcal{O}(1)$ the double logarithms scale as $\alpha_s L_s^2\sim 1/\alpha_s\gg 1$ and, therefore, the SLLs give parametrically large contributions to the cross section. It is thus important to understand the asymptotic behavior of the series (8.65). To study the double-logarithmic asymptotics, it is sufficient to work with a fixed coupling $\alpha_s(\bar\mu)$, since the scale dependence of the running coupling is a single-logarithmic effect.

It turns out that starting from the integral representation (8.80) is more convenient than from our fixed coupling result (8.72). In this way the analysis can be generalized to multiple Glauber-operator insertions in Chapter 9. Using the one-loop approximation for all cusp anomalous dimensions ($\gamma_0=4$) and changing variables, we find

$$\varsigma^{\rm SLL}(\mu_h,\mu_s)\Big|_{\rm fixed} = -4\pi^2 N_c\left(\frac{\alpha_s(\bar\mu)}{\pi}\right)^3\int_0^{L_s} dL_1\int_{L_1}^{L_s} dL_2\,(L_s-L_2)\ldots, \tag{8.83}$$

where we already performed the L_3 integral and the ellipsis denote the 11-component vector containing products of the scalar Sudakov functions. Changing variables once more $L_i=:z_i L_s$, they are given by

$$U^c(v;\mu_i,\mu_j)=\exp\left[v\,w\left(z_i^2-z_j^2\right)\right]. \tag{8.84}$$

To perform the double integral over the functions $U^c(v,1;\mu_h,\mu_1,\mu_2)$ in the coefficient vector, we invert the order of integration and define

$$\int_0^1 dz_2\,(1-z_2)\int_0^{z_2} dz_1\,U^c(v,1;\mu_h,\mu_1,\mu_2)=:\frac{1}{3!}\,\Sigma(v;w). \tag{8.85}$$

For $v = 0$, we simply recover the result (8.68). It is straightforward to further obtain [4]

$$\begin{aligned}
\Sigma(\tfrac{1}{2}; w) &= \frac{3\sqrt{2}}{w}\left[\ln(1+\sqrt{2}) + 2i\pi\, T\left(\sqrt{2w}, \frac{i}{\sqrt{2}}\right)\right] \\
&\quad - \frac{3\sqrt{2\pi}}{2w^{3/2}}\left[\operatorname{erf}\left(\sqrt{\frac{w}{2}}\right) - e^{-w}\operatorname{erfi}\left(\sqrt{\frac{w}{2}}\right)\right], \\
\Sigma(1; w) &= \frac{3}{w} - \frac{3\sqrt{\pi}}{2w^{3/2}}\operatorname{erf}\left(\sqrt{w}\right), \qquad (8.86) \\
\Sigma(v; w) &= \frac{3}{2z\sqrt{w}}\left[4\pi\, T\left(\sqrt{2}\, z, \frac{\sqrt{w}}{z}\right) - \pi + \pi\operatorname{erf}\left(\sqrt{w}\right)\operatorname{erf}(z)\right. \\
&\quad \left. + 2\arctan\left(\sqrt{v-1}\right) - \frac{\sqrt{\pi}\, z\operatorname{erf}\left(\sqrt{v\,w}\right)}{\sqrt{v}\, w} + \frac{\sqrt{\pi}\, e^{-w}\operatorname{erf}(z)}{\sqrt{w}}\right],
\end{aligned}$$

where the last line holds for $v > 1$ and $z = \sqrt{(v-1)w}$. The error functions are

$$\operatorname{erf}(z) = \frac{2}{\sqrt{\pi}}\int_0^z dx\, e^{-x^2}, \qquad \operatorname{erfi}(z) = \frac{2}{\sqrt{\pi}}\int_0^z dx\, e^{x^2}, \qquad (8.87)$$

and the Owen T-function is

$$T(z, a) = \frac{1}{2\pi}\int_0^a dt\, \frac{e^{-\frac{1}{2}z^2(1+t^2)}}{1+t^2}. \qquad (8.88)$$

By adding an $i0$ prescription to z in (8.86), one can analytically continue the result in the last line to $v \leq 1$. In this way, one recovers the results for $v = \frac{1}{2}$ and $v = 1$, see [4] for more details. Performing the sum over r in (8.69) in terms of a hypergeometric function, then using an integral representation for this function, and finally performing the sum over n in terms of an error function, one finds

$$\Sigma(v, w) = \int_0^1 dx\, \frac{3}{4\sqrt{x}}\left[\frac{2}{y^2(x)} - \frac{\sqrt{\pi}\operatorname{erf}\left(y(x)\right)}{y^3(x)}\right], \qquad (8.89)$$

with $y(x) = \sqrt{w(1+(v-1)x)}$. After evaluating the remaining integral over x, one reproduces the results (8.86). Therefore, the two definitions (8.69) and (8.85) are equivalent. In Figure 8.3 we show the w dependence of all relevant Σ functions for the eigenvalues in (8.48) with $N_c = 3$.

In the fixed coupling approximation, the coefficient vector in (8.79) is given by

$$\varsigma^{\mathrm{SLL}}(\mu_h, \mu_s)\Big|_{\mathrm{fixed}} = -\frac{2\alpha_s(\bar{\mu})\, L_s}{3\pi\, N_c}\, w\, w_\pi\, \ldots, \qquad (8.90)$$

where the ellipsis represent the vector in the second line of (8.80) with the simple replacement

$$U^c(v_i, 1; \mu_h, \mu_1, \mu_2) \to \Sigma(v_i; w). \qquad (8.91)$$

This result is of course equivalent to (8.72).

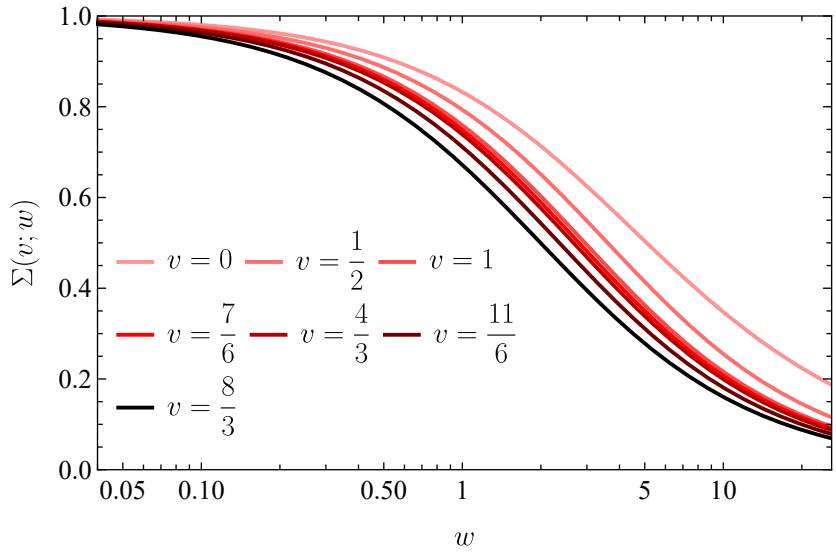

Figure 8.3: Behavior of the functions $\Sigma(v;w)$ for different values of v corresponding to the eigenvalues in (8.48). Darker colors correspond to larger values of v.

The asymptotic behavior for $w \gg 1$ of the Σ functions with $v > 0$ can be obtained from (8.85) by replacing the upper limit of the z_2 integral by infinity. We find

$$\begin{aligned}
\Sigma(\tfrac{1}{2};w) &= \frac{3\sqrt{2}\ln(1+\sqrt{2})}{w} - \frac{3\sqrt{\pi}}{\sqrt{2}\,w^{3/2}} + \mathcal{O}(e^{-\frac{w}{2}})\,, \\
\Sigma(1;w) &= \frac{3}{w} - \frac{3\sqrt{\pi}}{2w^{3/2}} + \mathcal{O}(e^{-w})\,, \\
\Sigma(v;w) &= \frac{3\arctan(\sqrt{v-1})}{\sqrt{v-1}\,w} - \frac{3\sqrt{\pi}}{2\sqrt{v}\,w^{3/2}} + \mathcal{O}(e^{-cw})\,,
\end{aligned} \tag{8.92}$$

where in the last line $c = \min(1, v)$. For the special case $v = 0$, we expand the generalized hypergeometric function in (8.68) and obtain

$$\Sigma(0;w) = \frac{3}{2}\,\frac{\ln(4w)+\gamma_E-2}{w} + \frac{3}{4w^2} + \mathcal{O}(w^{-3})\,. \tag{8.93}$$

Replacing the upper limit on z_2 by infinity in this case yields a divergent integral. Interestingly, the limits $w \gg 1$ and $v \to 0$ do not commute. In Figure 8.4 we compare the small-w and large-w expansion to the full result for the smallest and largest eigenvalue.

The leading asymptotic behavior of the resummed SLLs is given by

$$\hat{\sigma}^{\text{SLL}}_{2\to M}(Q_0) \sim \frac{\alpha_s L_s}{\pi N_c}\, w_\pi\, \ln(4w)\,. \tag{8.94}$$

In contrast to the standard exponential Sudakov suppression, the leading term for the SLLs is a constant or even logarithmically growing for $\Sigma(0;w)$. It will be interesting to contrast this asymptotic behavior to the one of subleading logarithmic terms. In Chapter 9, we study this for terms arising from multiple insertions of the Glauber operator $\boldsymbol{V}^G$.

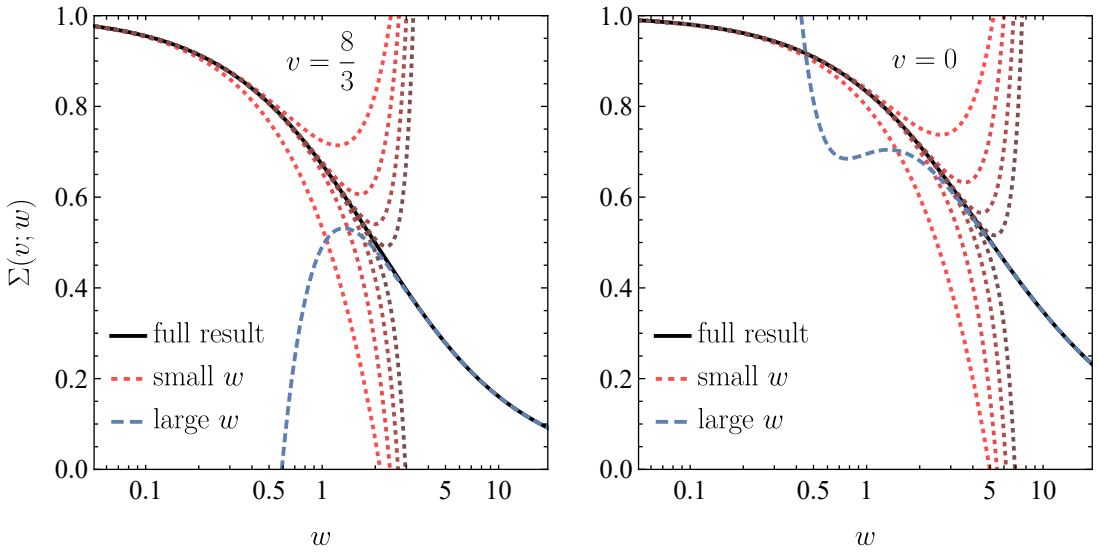

Figure 8.4: Plot of the function $\Sigma(v, w)$ for the largest parameter v_5 and the smallest value v_0. The full result is shown as a solid line. The red dotted lines show the perturbative expansion up to the eighth order in w. The blue dashed line is the large-w asymptotics.

8.4 Numerical Estimates

Scattering processes involving at most two ($M \leq 2$) hard final-state partons at Born level are of great phenomenological importance. In this section, we provide compact expressions for the SLL contribution to the partonic cross section (8.79) for all relevant partonic subprocesses and analyze their size. In order to compare the resummed effect in leading order RG-improved perturbation theory to the fixed coupling approximation, we replace

$$\alpha_s(\bar{\mu}) \to \left[1 + \frac{\gamma_1}{\gamma_0}\frac{\alpha_s(\bar{\mu})}{4\pi}\right]\alpha_s(\bar{\mu}) \tag{8.95}$$

in (8.90) to take the two-loop anomalous dimension approximately into account. We always evolve the strong coupling using `RunDec` [110] starting from $\alpha_s(m_Z) = 0.118$ with the two-loop β-function and with $n_f = 5$ active light quark flavors, see Appendix A.4 for more details.

8.4.1 Evaluation of Angular Integrals

To get numerical results, we need to evaluate the angular integrals J_j defined in (8.19). For concreteness, we consider a veto region $y_{\min} < y_{k_0} < y_{\max}$, where the rapidity y is defined with respect to the beam directions and particle 1 has rapidity $y_1 = +\infty$. The θ_{veto}-function in the definition restricts the integral to the veto region

$$J_j = \int_{y_{\min}}^{y_{\max}} dy_{k_0} \int_0^{2\pi} \frac{d\phi_{k_0}}{2\pi} \frac{\sinh(y_{k_0} - y_j)}{\cosh(y_{k_0} - y_j) - \cos(\phi_{k_0} - \phi_j)}\,, \tag{8.96}$$

where y_{k_0} and ϕ_{k_0} are the rapidity and azimuthal angle of the soft gluon and y_j and ϕ_j the ones of the hard parton along direction n_j. Carrying out the integrations leads

to the result [1]

$$J_j = -(y_{\max} - y_{\min}) \operatorname{sign}(y_j - y_{\max}) \,, \tag{8.97}$$

since the jets cannot be inside the veto region, i.e. $y_j \notin (y_{\min}, y_{\max})$. From this result it is obvious that the integrals J_j are invariant under boosts along the beam direction and only depend on the rapidity difference $\Delta Y \coloneqq y_{\max} - y_{\min}$, so that they are the same in the laboratory frame and the partonic center-of-mass frame.

Below we consider $2 \to M$ scattering processes with $M = 0, 1, 2$ color-charged partons in the final state. For the $2 \to 0$ case, for which all final-state particles are color-neutral, only the integral

$$J_{12} = J_2 = \Delta Y \tag{8.98}$$

is relevant. For forward scattering in a $2 \to 2$ process, the hard final-state particles have $y_3 > y_{\max}$ and $y_4 < y_{\min}$, which yields

$$J_3 = -\Delta Y \,, \qquad J_4 = +\Delta Y \,. \tag{8.99}$$

For backward scattering, these signs are opposite. Symmetric $2 \to 1$ scattering channels such as $gg \to g$ and $q\bar{q} \to g$ only involve the integral J_{12}, but for the $qg \to q$ channel also integral J_3 arises, with $J_3 = -\Delta Y$ for forward and opposite sign for backward scattering.

8.4.2 $2 \to 0$ Scattering Processes

Color-neutral final states are particularly interesting as they describe the production of one or several electroweak bosons (H, γ, $W^\pm$, Z^0) at hadron colliders via $q\bar{q}$ scattering or gluon fusion. Especially for Higgs and diboson production, it is experimentally often necessary to impose a jet veto to suppress background. Even though such jet-veto cross sections have been studied extensively, no analysis so far included the SLLs.

The leading order hard functions for the $q\bar{q} \to 0$ and $gg \to 0$ partonic scattering are

$$\begin{aligned} \big\langle a_1, a_2 \big| \boldsymbol{\mathcal{H}}_{q\bar{q}\to 0} \big| b_1, b_2 \big\rangle &= \big\langle \boldsymbol{\mathcal{H}}_{q\bar{q}\to 0} \big\rangle \, \frac{1}{N_c} \, \delta_{a_1 a_2} \, \delta_{b_1 b_2} \,, \\ \big\langle a_1, a_2 \big| \boldsymbol{\mathcal{H}}_{gg\to 0} \big| b_1, b_2 \big\rangle &= \big\langle \boldsymbol{\mathcal{H}}_{gg\to 0} \big\rangle \, \frac{1}{N_c^2 - 1} \, \delta^{a_1 a_2} \, \delta^{b_1 b_2} \,, \end{aligned} \tag{8.100}$$

where the trace on the right-hand side yields after angular integration the Born cross section (8.10). In the absence of color-charged final-state particles, the color structures $\boldsymbol{X}_i$ with $i = 2, \ldots, 5$ do not contribute and color conservation implies $\boldsymbol{T}_2 = -\boldsymbol{T}_1$. Thus one finds for the partonic cross sections in leading order RG-improved perturbation theory

$$\begin{aligned} \hat{\sigma}^{\text{SLL}}_{q\bar{q}\to 0}(Q_0) = -\hat{\sigma}_{q\bar{q}\to 0} \, \frac{64\pi^2}{\beta_0^3} \, C_F \, \Delta Y \int_1^{x_s} \frac{dx_2}{x_2} \, \ln \frac{x_s}{x_2} \int_1^{x_2} \frac{dx_1}{x_1} \\ \times \left[U^c(0,1) - 2\, U^c(\tfrac{1}{2}, 1) + U^c(1,1) \right] \end{aligned} \tag{8.101}$$

and

$$\begin{aligned}\hat{\sigma}^{\text{SLL}}_{gg\to 0}(Q_0) = -\hat{\sigma}_{gg\to 0}\,\frac{32\pi^2}{\beta_0^3}\,N_c\,\Delta Y\int_1^{x_s}\frac{dx_2}{x_2}\,\ln\frac{x_s}{x_2}\int_1^{x_2}\frac{dx_1}{x_1}\\ \times\Bigg\{\frac{8N_c^2}{N_c^2-1}\big[U^c(0,1)-U^c(\tfrac{1}{2},1)\big]\\ -\frac{N_c(N_c+3)}{N_c+1}\big[U^c(0,1)-2\,U^c(v_3,1)+U^c(v_5,1)\big]\\ +\frac{N_c(N_c-3)}{N_c-1}\big[U^c(0,1)-2\,U^c(v_4,1)+U^c(v_6,1)\big]\Bigg\}.\end{aligned} \tag{8.102}$$

Here and in the following, we drop the three scale arguments of $U^c(v_i,1;\mu_h,\mu_1,\mu_2)$ to increase readability. The fixed coupling versions can be obtained by the replacement described around (8.90).

For $2\to 0$ scattering the SLLs start at $\alpha_s^3 L_s^3\times(\alpha_s L_s^2)^2$ instead of four-loop order. To see this, we observe that the coefficients c_i of the functions $U^c(v_i,1)$ in (8.101) and (8.102) and, therefore, the coefficients of the Σ-functions in the fixed coupling approximation fulfill

$$\sum_{i=0}^{6} c_i = 0\,,\qquad \sum_{i=0}^{6} c_i\,v_i = 0\,. \tag{8.103}$$

Consequently, the first two terms in a Taylor expansion for small α_s vanish and the SLLs start at six-loop order.

In Figure 8.5 we study the SLL contributions to the total cross sections for $q\bar{q}\to 0$ (top row) and $gg\to 0$ (bottom row) as a function of the jet-veto scale Q_0. The soft and hard scales are chosen as $\mu_s = Q_0$ and $\mu_h = \sqrt{\hat{s}}$, respectively. We consider a fixed partonic center-of-mass energy $\sqrt{\hat{s}} = 1\,\text{TeV}$ and a gap region in rapidity with $\Delta Y = 2$.

The left panels show the resummed effect of the SLLs in leading-order RG-improved perturbation theory (black lines), see (8.81), and for a fixed coupling $\alpha_s(\bar{\mu})$ evaluated at the geometric mean $\bar{\mu} = \sqrt{QQ_0}$ (gray lines), see (8.90). The perturbative uncertainty from varying the soft scale between $Q_0/2 < \mu_s < 2Q_0$ in the running coupling approach is indicated by the yellow bands. The blue bands serve as an estimate for the scale ambiguity of choosing $\bar{\mu}\in(Q_0,Q)$ when working with a fixed coupling. As the running of the strong coupling is a single-logarithmic effect and we only resum the leading double-logarithmic corrections, both the perturbative and the scale uncertainties are very large. Interestingly, the running of the coupling is approximated well for a wide range of Q_0 values by evaluating the fixed coupling at the geometric mean.

The right panels show the contribution of the SLLs at $(3+n)$-th order in perturbation theory together with the resummed result, when working with a fixed coupling evaluated at $\bar{\mu} = \sqrt{QQ_0}$. As described above, the first two terms in this expansion vanish for $2\to 0$ processes and one can observe an alternating sign behavior. The absolute effect of the SLLs is very small $\mathcal{O}(0.1\%)$ for both $q\bar{q}\to 0$ and $gg\to 0$ scattering. However, for the gluonic case the individual contributions are huge, reaching up to 30% for small jet-veto scales, and strong cancellations take place. The biggest effects arise at seven-, eight- and nine-loop order ($n = 4,5,6$). In fact, the cancellations are so strong that the curves in the left-hand plot have a local maximum and change sign

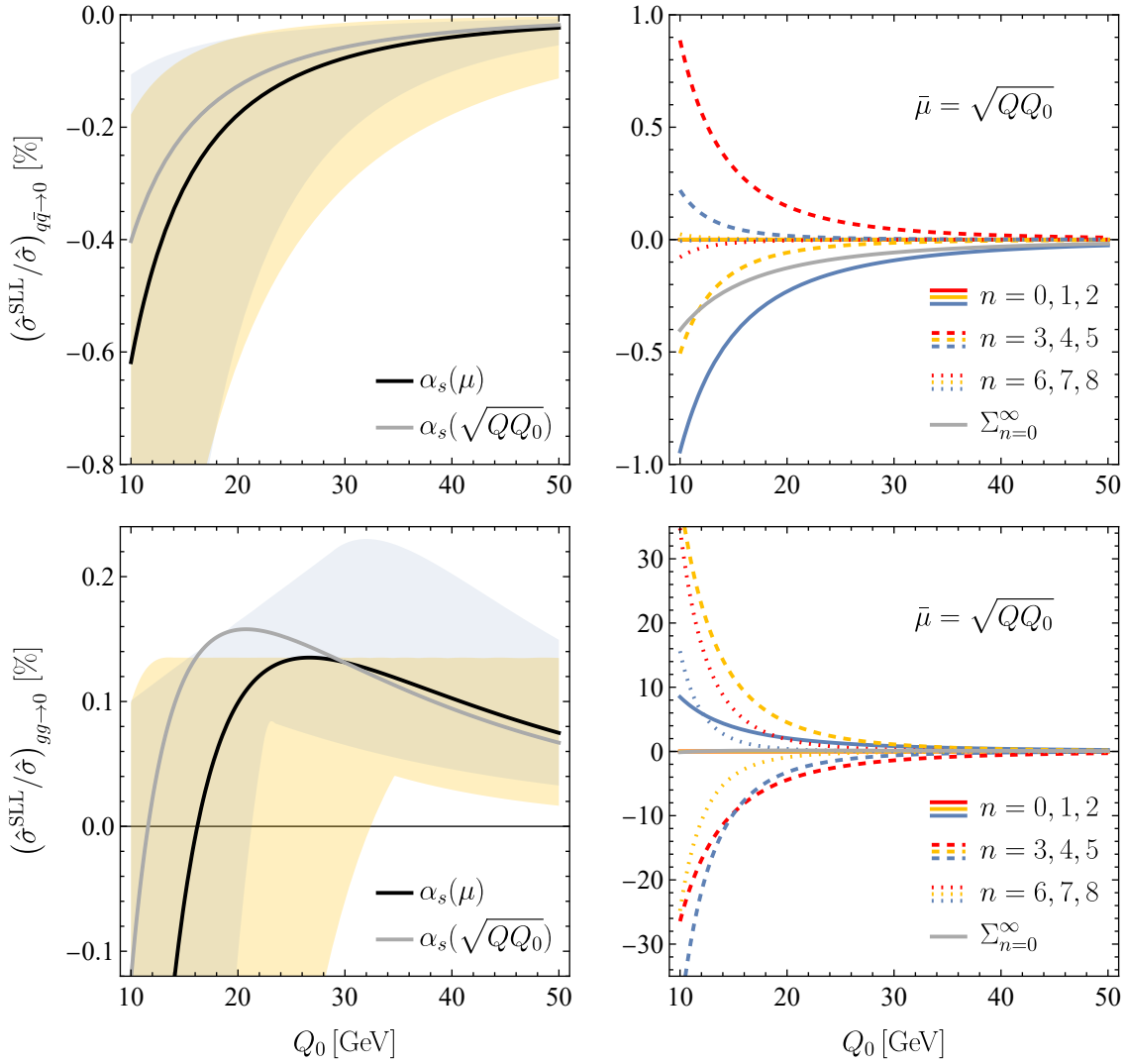

Figure 8.5: Numerical results for super-leading contributions to partonic $q\bar{q} \to 0$ scattering (top row) and $gg \to 0$ scattering (bottom row) as a function of the jet-veto scale Q_0, at fixed partonic center-of-mass energy $\sqrt{\hat{s}} = 1\,\mathrm{TeV}$ and for a central rapidity gap with $\Delta Y = 2$. The left plots show the resummed contribution of the SLLs with a running coupling $\alpha_s(\mu)$ (black lines) and for a fixed coupling $\alpha_s(\bar{\mu})$ with $\bar{\mu} = \sqrt{QQ_0}$ (gray lines). The perturbative uncertainties indicated by the yellow bands are obtained from the variation of the soft scale μ_s by a factor of 2 about its default value. The light-blue band shows the estimate of the scale uncertainty from varying $\bar{\mu} \in (Q_0, Q)$. The right plots show the individual contributions at $(3+n)$-th order in perturbation theory when working with a fixed coupling at $\bar{\mu} = \sqrt{QQ_0}$. The terms with $n = 0, 1$ vanish for $2 \to 0$ processes. The gray line depicts the infinite sum over all contributions and is the same in the left and right panels.

for scales below $Q_0 \approx 15\,\text{GeV}$. Without resumming the SLLs to all-orders, one could wrongly conclude that they play an important role in this case. For example, the contribution with $n = 4$ is of about 15% for $Q_0 \approx 15\,\text{GeV}$ which is a large five-loop effect. For $q\bar{q}$-scattering the individual contributions are way smaller, reaching at most 1%, and the cancellations are less pronounced.

These results suggest that SLLs play a subdominant role in electroweak boson production without additional jets. We stress, however, that a careful study of subleading logarithmic effects is necessary to verify this conclusion.

8.4.3 $2 \to 1$ Scattering Processes

Scattering processes with one color-charged final-state parton are also of great phenomenological importance since they include some benchmark Standard Model reactions such as $pp \to H + \text{jet}$ or $pp \to V + \text{jet}$, where $V = \gamma, W^\pm, Z^0$. In this case, the implicit sum over j for the color structures $\boldsymbol{X}_2, \dots, \boldsymbol{X}_5$ in (8.79) includes only a single term, and color conservation implies that $\boldsymbol{T}_3 = -\boldsymbol{T}_1 - \boldsymbol{T}_2$. The relevant partonic scattering reactions are $q\bar{q} \to g$, $gg \to g$, and $qg \to q$ with leading-order hard functions

$$\begin{aligned}
\big\langle a_1, a_2, a_3 \big| \boldsymbol{\mathcal{H}}_{q\bar{q}\to g} \big| b_1, b_2, b_3 \big\rangle &= \big\langle \boldsymbol{\mathcal{H}}_{q\bar{q}\to g} \big\rangle \, \frac{1}{C_F N_c} \, t^{a_3}_{a_2 a_1} \, t^{b_3}_{b_1 b_2} \,, \\
\big\langle a_1, a_2, a_3 \big| \boldsymbol{\mathcal{H}}_{gg\to g} \big| b_1, b_2, b_3 \big\rangle &= \big\langle \boldsymbol{\mathcal{H}}_{gg\to g} \big\rangle \, \frac{1}{N_c(N_c^2-1)} \, f^{a_1 a_2 a_3} \, f^{b_1 b_2 b_3} \,, \\
\big\langle a_1, a_2, a_3 \big| \boldsymbol{\mathcal{H}}_{qg\to q} \big| b_1, b_2, b_3 \big\rangle &= \big\langle \boldsymbol{\mathcal{H}}_{qg\to q} \big\rangle \, \frac{1}{C_F N_c} \, t^{a_2}_{a_3 a_1} \, t^{b_2}_{b_1 b_3} \,.
\end{aligned} \tag{8.104}$$

By momentum conservation, at least one color-neutral final-state parton needs to be present in these cases. This parton cannot interact with gluons and thus the hard function for $gg \to g$ starts at one loop. We ignore the presence of a second color structure proportional to $d^{a_1 a_2 a_3} \, d^{b_1 b_2 b_3}$ in this work and only consider the tree-level structure for simplicity. The SLL contribution to the partonic cross sections for the diagonal channels are

$$\begin{aligned}
\hat{\sigma}^{\text{SLL}}_{q\bar{q}\to g}(Q_0) = -\hat{\sigma}_{q\bar{q}\to g} \, \frac{32\pi^2}{\beta_0^3} \, N_c \, \Delta Y \int_1^{x_s} \frac{dx_2}{x_2} \, \ln\frac{x_s}{x_2} \int_1^{x_2} \frac{dx_1}{x_1} \\
\times \left[\frac{2C_F}{N_c} \, U^c(0,1) - \frac{N_c^2 - 2}{N_c^2} \, U^c(\tfrac{1}{2},1) - \frac{1}{N_c^2} \, U^c(1,1) \right]
\end{aligned} \tag{8.105}$$

and

$$\begin{aligned}
\hat{\sigma}^{\text{SLL}}_{gg\to g}(Q_0) = -\hat{\sigma}_{gg\to g} \, \frac{32\pi^2}{\beta_0^3} \, N_c \, \Delta Y \int_1^{x_s} \frac{dx_2}{x_2} \, \ln\frac{x_s}{x_2} \int_1^{x_2} \frac{dx_1}{x_1} \\
\times \Bigg\{ \frac{6N_c^2}{N_c^2 - 1} \big[U^c(0,1) - U^c(\tfrac{1}{2},1) \big] \\
- \frac{(N_c - 2)(N_c + 3)}{2(N_c + 1)} \big[U^c(0,1) - U^c(v_3,1) \big] - \frac{N_c + 3}{N_c + 1} \big[U^c(0,1) - U^c(v_5,1) \big]
\end{aligned}$$

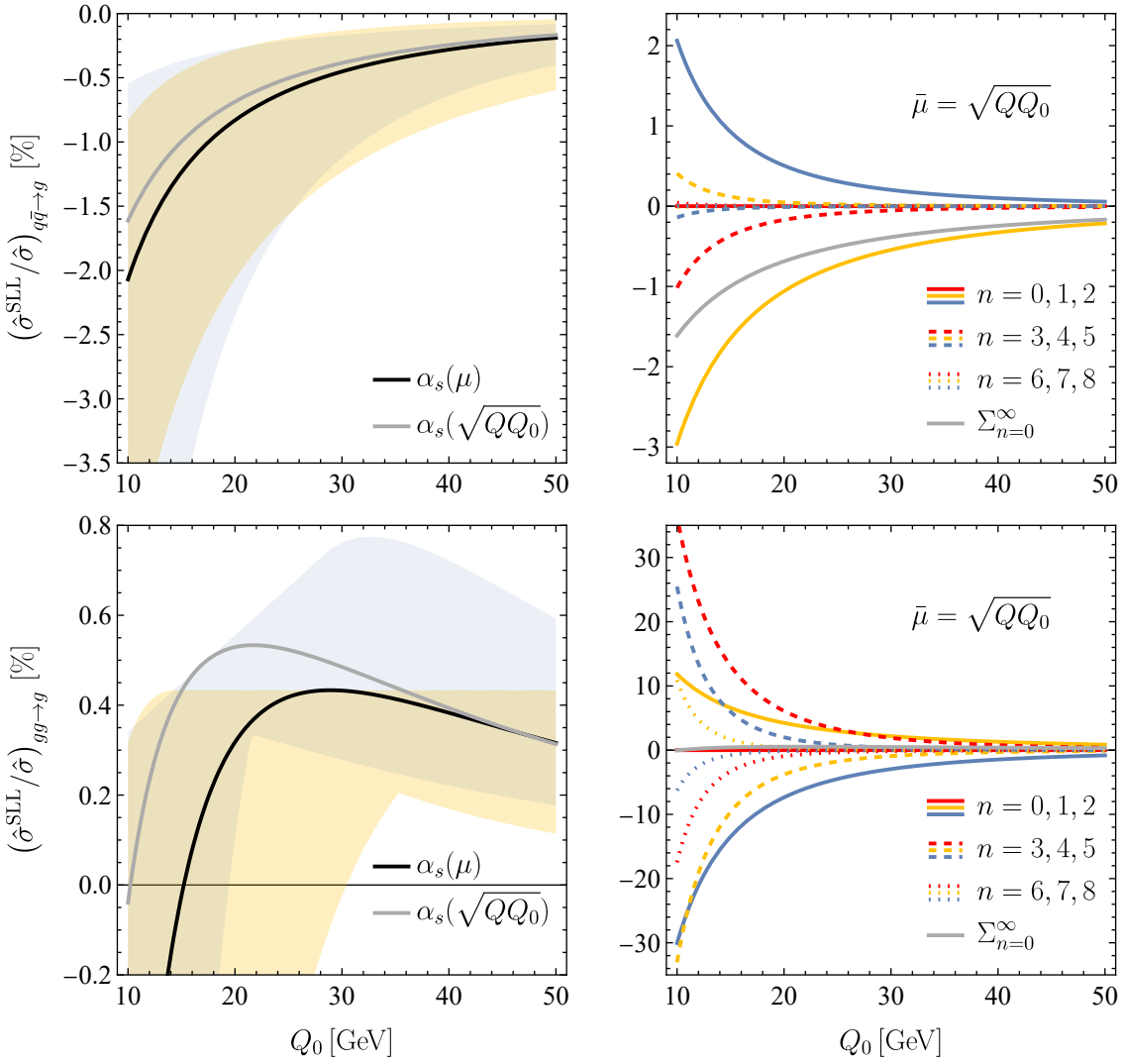

Figure 8.6: Numerical results for super-leading contributions to partonic $q\bar{q} \to g$ scattering (top row) and $gg \to g$ scattering (bottom row) as a function of the jet-veto scale Q_0. The color coding and input parameters are the same as in Figure 8.5. The terms with $n = 0$ vanish for $2 \to 1$ processes.

$$+ \frac{(N_c+2)(N_c-3)}{2(N_c-1)}\big[U^c(0,1) - U^c(v_4,1)\big] - \frac{N_c-3}{N_c-1}\big[U^c(0,1) - U^c(v_6,1)\big]\Big\}. \tag{8.106}$$

They fulfill the first sum rule in (8.103) and, therefore, the SLL contributions start at four-loop order. In Figure 8.6 these contributions are shown. The curves and bands have the same meaning as in Figure 8.5 and we observe several similarities. For $q\bar{q} \to g$ scattering, the absolute size of the SLLs can reach up to $\mathcal{O}(1\%)$ for small values of Q_0. The individual contributions in the $(3+n)$-th order in perturbation theory are of similar size with maxima at four- and five-loop order ($n = 1, 2$). Only moderate cancellations take place in this case. In contrast, for $gg \to g$ scattering the individual contributions are dominated by the five- to eight-loop order ($n = 2, 3, 4, 5$) and are more than an order of magnitude larger than the resummed contribution. However,

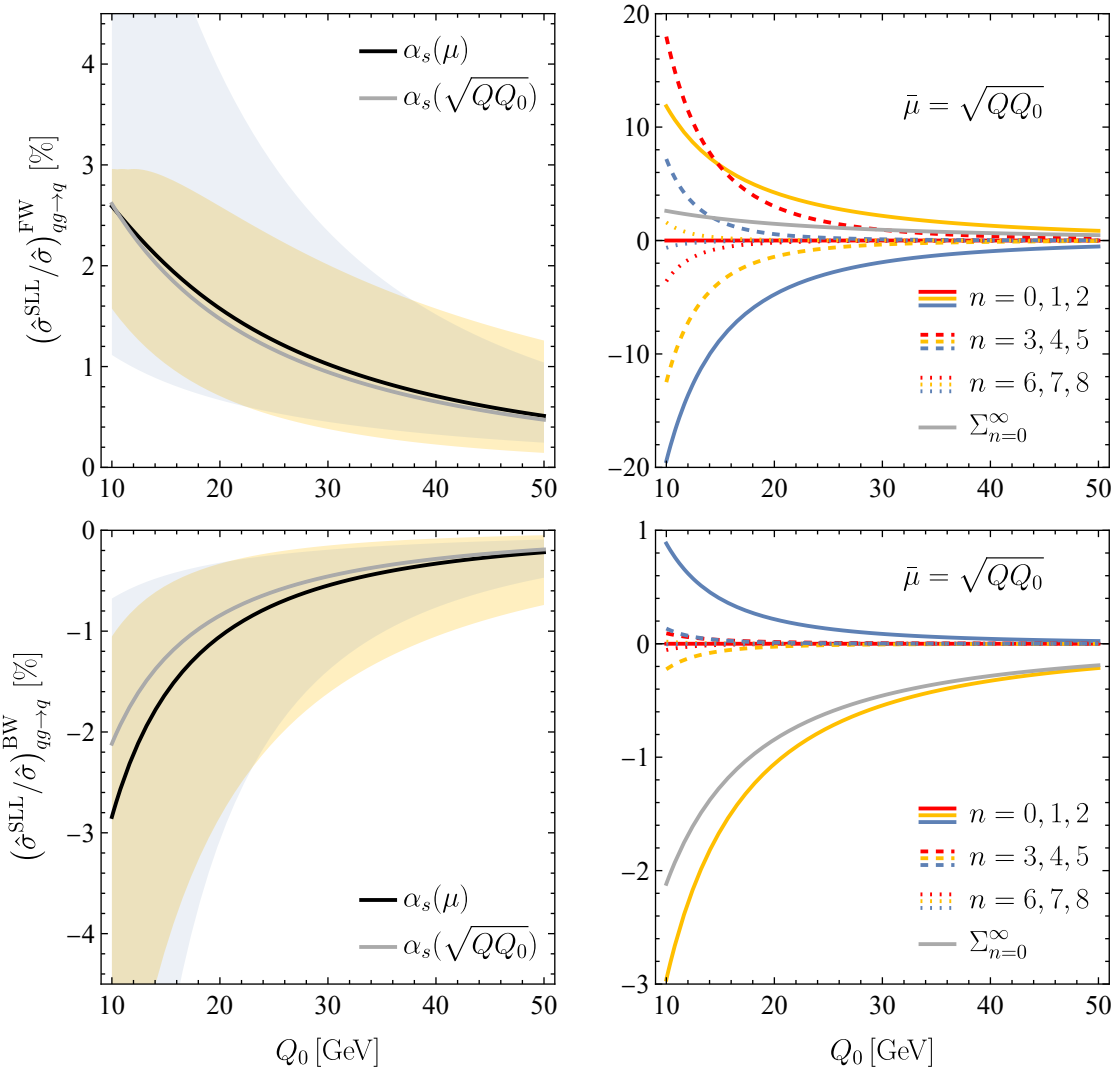

Figure 8.7: Numerical results for super-leading contributions to partonic $qg \to q$ forward (top row) and backward (bottom row) scattering as a function of the jet-veto scale Q_0. The color coding and input parameters are the same as in Figure 8.5. The terms with $n = 0$ vanish for $2 \to 1$ processes.

strong cancellations take place, reducing the absolute effect to at most $\pm 0.5\%$. Similar to $gg \to 0$, one can observe a sign change for jet-veto scale below $Q_0 \approx 15$ GeV. Comparing the diagonal SLL contribution for $2 \to 1$ scattering to the one of $2 \to 0$, we observe that the later is about a factor 3 smaller.

Considering the off-diagonal channel, i.e. $qg \to q$ scattering, we find in the forward limit

$$\hat{\sigma}^{\rm SLL,FW}_{qg\to q}(Q_0) = -\hat{\sigma}^{\rm FW}_{qg\to q}\,\frac{32\pi^2}{\beta_0^3}\,N_c\,\Delta Y \int_1^{x_s}\frac{dx_2}{x_2}\,\ln\frac{x_s}{x_2}\int_1^{x_2}\frac{dx_1}{x_1}$$
$$\times\left\{\frac{4N_c^2-2}{N_c^2-1}\left[U^c(0,1)-U^c(\tfrac{1}{2},1)\right]\right.$$

process	channels	forward	backward
$qq \to qq$	t, u	t	u
$gg \to gg$	$t, s, u, 4g$	t	u
$q\bar{q} \to gg$	t, s, u	t	u
$gg \to q\bar{q}$	t, s, u	t	u
$qq' \to qq'$	t	t	t
$q\bar{q} \to q'\bar{q}'$	s	s	s
$q\bar{q} \to q\bar{q}$	t, s	t	t, s
$qg \to qg$	t, s, u	t	u

Table 8.1: Contributions to partonic $2 \to 2$ scattering at tree level. The relevant color structures can be read off from the corresponding Feynman diagrams shown in Figure 8.8. The third (fourth) column shows the relevant contributions for (forward) backward scattering. Quarks q and q' have different flavor.

$$- \frac{N_c(N_c+3)}{2(N_c+1)} \big[U^c(0,1) - U^c(v_3,1)\big] + \frac{N_c(N_c-3)}{2(N_c-1)} \big[U^c(0,1) - U^c(v_4,1)\big] \Big\} \tag{8.107}$$

and in the backward case

$$\hat{\sigma}^{\text{SLL,BW}}_{qg\to q}(Q_0) = -\hat{\sigma}^{\text{BW}}_{qg\to q} \frac{32\pi^2}{\beta_0^3} N_c \Delta Y \int_1^{x_s} \frac{dx_2}{x_2} \ln\frac{x_s}{x_2} \int_1^{x_2} \frac{dx_1}{x_1} \times \big[2\, U^c(0,1) - 3\, U^c(\tfrac{1}{2},1) + U^c(1,1)\big] . \tag{8.108}$$

In both case, the cross section fulfills the first sum rule in (8.103) and, therefore, the SLLs again start at four-loop order. Figure 8.7 shows the SLL contribution to $qg \to q$ scattering for forward (top row) and backward (bottom row) scattering. Even though the resummed contributions are of similar size in both cases and reach $2-3\%$ for small jet-veto scales, there are two interesting differences. First, while in the forward case the individual contributions are large and strong cancellations take place, in the backward limit the second term in the perturbative expansion is already a factor 3 smaller than the first. One should thus compare the forward case to $gg \to g$ scattering and the backward one to $q\bar{q} \to g$, see Figure 8.6. Second, the cross section is enhanced by the SLLs for forward scattering but reduced in the backward case.

This example shows that in general SLLs can affect the differential cross section in a non-trivial way. Here, this dependence on the scattering kinematics is due to angular integral J_3 which differs between forward and backward scattering.

8.4.4 $2 \to 2$ Small-Angle Scattering Processes

For $2 \to 0$ and $2 \to 1$ scattering processes only one color structure contributes at tree level, simplifying the structure of the hard functions considerably. Turning to $2 \to 2$ scattering processes, this is no longer the case. In Table 8.1 we summarize the different channels, i.e. different color structures, contributing to tree-level QCD amplitudes. We observe that in most cases several color structures are relevant, providing a second

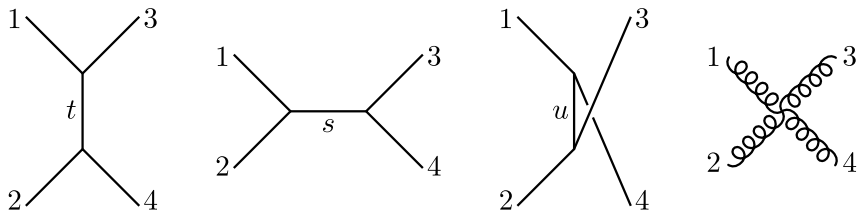

Figure 8.8: Generic Feynman diagrams contributing to partonic $2 \to 2$ scattering at tree level. Solid lines can represent (anti-)quarks or gluons.

source for the dependence of the SLLs on scattering kinematics. This effect is studied for $qq \to qq$ scattering in more detail in the next section.

For the moment, we restrict our analysis to small-angle scattering as in this case the amplitude is dominated by a single color structure, see the last two columns of Table 8.1. Applying color conservation $\boldsymbol{T}_1+\boldsymbol{T}_2+\boldsymbol{T}_3+\boldsymbol{T}_4 = 0$, one can show that except for $qg \to qg$ and $\bar{q}g \to \bar{q}g$ the angular integrals J_3 and J_4 only enter in the combination $(J_3 - J_4)$. As a result of this effect, the SLLs contribute equally to both forward and backward scattering for the processes listed in the upper portion of this table. The corresponding hard functions dominated by the t-channel diagrams in Figure 8.8 are

$$\begin{aligned}
\langle a_1, a_2, a_3, a_4 | \boldsymbol{\mathcal{H}}_{qq\to qq} | b_1, b_2, b_3, b_4 \rangle &= \langle \boldsymbol{\mathcal{H}}_{qq\to qq} \rangle \, \frac{2}{C_F N_c} \, t^a_{a_3 a_1} \, t^a_{a_4 a_2} \, t^b_{b_1 b_3} \, t^b_{b_2 b_4} \,, \\
\langle a_1, a_2, a_3, a_4 | \boldsymbol{\mathcal{H}}_{gg\to gg} | b_1, b_2, b_3, b_4 \rangle &= \langle \boldsymbol{\mathcal{H}}_{gg\to gg} \rangle \, \frac{1}{N_c^2(N_c^2-1)} \, f^{a_1 a_3 a} f^{a_2 a_4 a} f^{b_1 b_3 b} f^{b_2 b_4 b} \,, \\
\langle a_1, a_2, a_3, a_4 | \boldsymbol{\mathcal{H}}_{q\bar{q}\to gg} | b_1, b_2, b_3, b_4 \rangle &= \langle \boldsymbol{\mathcal{H}}_{q\bar{q}\to gg} \rangle \, \frac{1}{C_F^2 N_c} \, (t^{a_4} t^{a_3})_{a_2 a_1} (t^{b_3} t^{b_4})_{b_1 b_2} \,, \\
\langle a_1, a_2, a_3, a_4 | \boldsymbol{\mathcal{H}}_{gg\to q\bar{q}} | b_1, b_2, b_3, b_4 \rangle &= \langle \boldsymbol{\mathcal{H}}_{gg\to q\bar{q}} \rangle \, \frac{1}{C_F^2 N_c} \, (t^{a_1} t^{a_2})_{a_3 a_4} (t^{b_2} t^{b_1})_{b_4 b_3} \,,
\end{aligned} \tag{8.109}$$

In Figures 8.9 and 8.10 we show the contribution of the SLLs to the partonic cross section as a function of the jet-veto scale in these cases.

The SLL contribution for the processes in the lower portion of Table 8.1 differs between forward and backward scattering. For the first two of these processes this is due to the dependence on J_3 and J_4. The respective hard functions are

$$\langle a_1, a_2, a_3, a_4 | \boldsymbol{\mathcal{H}}_{q\bar{q}\to q'\bar{q}'} | b_1, b_2, b_3, b_4 \rangle = \langle \boldsymbol{\mathcal{H}}_{q\bar{q}\to q'\bar{q}'} \rangle \, \frac{2}{C_F N_c} \, t^a_{a_2 a_1} \, t^a_{a_3 a_4} \, t^b_{b_1 b_2} \, t^b_{b_4 b_3} \tag{8.110}$$

and $\boldsymbol{\mathcal{H}}_{qq'\to qq'} = \boldsymbol{\mathcal{H}}_{qq\to qq}$. For $q\bar{q} \to q\bar{q}$ and $qg \to qg$ also the color structures contributing to the hard functions deviate. We find in the forward limit

$$\begin{aligned}
\langle a_1, a_2, a_3, a_4 | \boldsymbol{\mathcal{H}}^{\mathrm{FW}}_{qg\to qg} | b_1, b_2, b_3, b_4 \rangle &= \langle \boldsymbol{\mathcal{H}}^{\mathrm{FW}}_{qg\to qg} \rangle \, \frac{1}{C_F N_c^2} \, f^{a_2 a_4 a} \, t^a_{a_3 a_1} \, f^{b_2 b_4 b} \, t^b_{b_1 b_3} \\
\langle a_1, a_2, a_3, a_4 | \boldsymbol{\mathcal{H}}^{\mathrm{FW}}_{q\bar{q}\to q\bar{q}} | b_1, b_2, b_3, b_4 \rangle &= \langle \boldsymbol{\mathcal{H}}^{\mathrm{FW}}_{q\bar{q}\to q\bar{q}} \rangle \, \frac{2}{C_F N_c} \, t^a_{a_3 a_1} \, t^a_{a_2 a_4} \, t^b_{b_1 b_3} \, t^b_{b_4 b_2}
\end{aligned} \tag{8.111}$$

and in the backward case

$$\langle a_1, a_2, a_3, a_4 | \boldsymbol{\mathcal{H}}^{\mathrm{BW}}_{qg\to qg} | b_1, b_2, b_3, b_4 \rangle = \langle \boldsymbol{\mathcal{H}}^{\mathrm{BW}}_{qg\to qg} \rangle \, \frac{1}{C_F^2 N_c} \, (t^{a_2} t^{a_4})_{a_3 a_1} \, (t^{b_4} t^{b_2})_{b_1 b_3} \,. \tag{8.112}$$

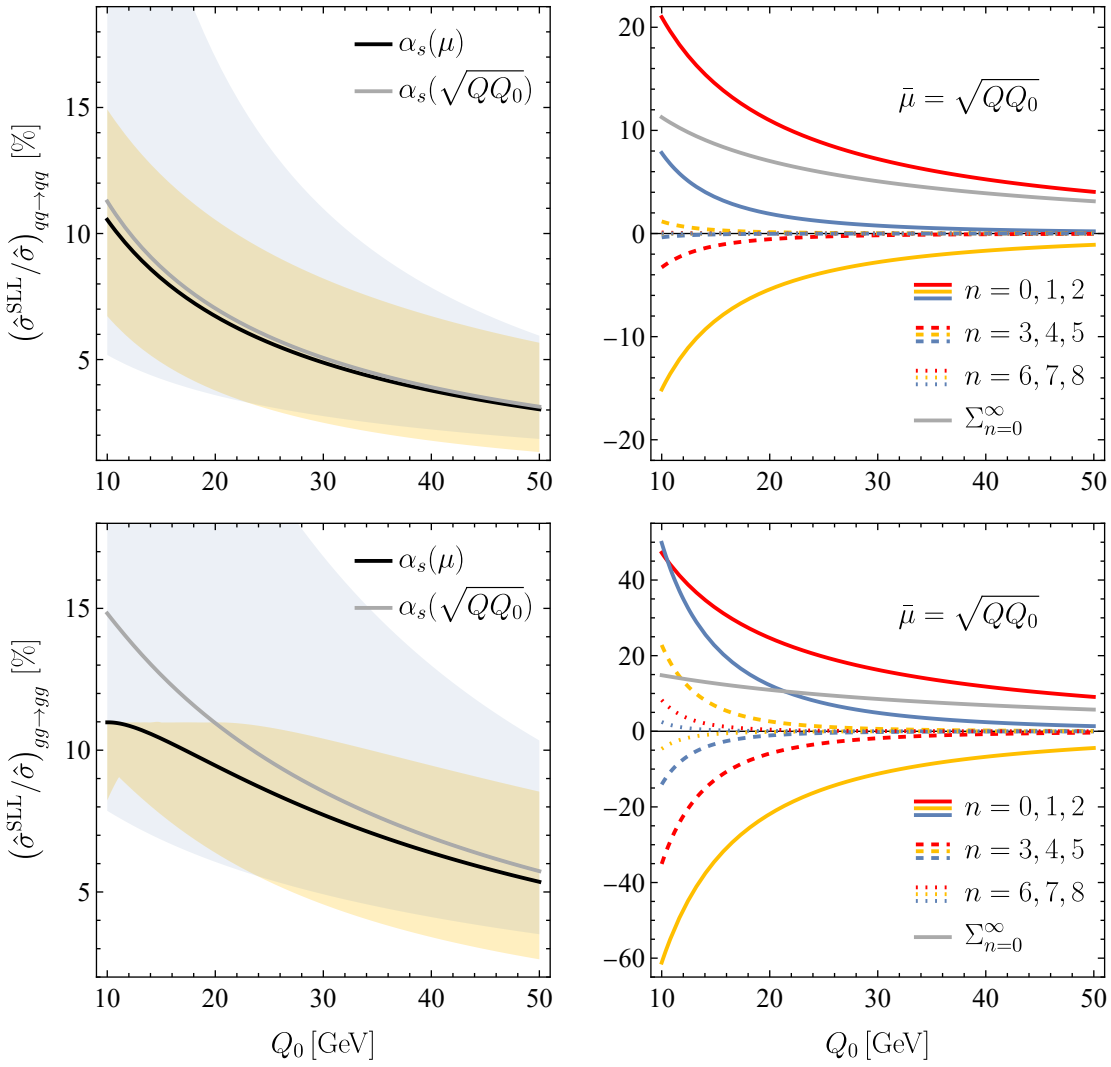

Figure 8.9: Numerical results for super-leading contributions to partonic $qq \to qq$ (top row) and $gg \to gg$ small-angle scattering (bottom row) as a function of the jet-veto scale Q_0. The color coding and input parameters are the same as in Figure 8.5.

The amplitude for $q\bar{q} \to q\bar{q}$ scattering does not simplify in the backward limit, since there is no u-channel diagram. Therefore, we exclude this case from our analysis. The SLL contributions in the forward and backward limit to the cross section are contrasted in Figures 8.11 and 8.12. As the hard function for $qq' \to qq'$ scattering is the same as for $qq \to qq$, the SLL contribution to this process can also be read off from the top row of Figure 8.9.

For all partonic $2 \to 2$ scattering processes, the corrections of the SLLs to the Born-level cross sections found after resummation are of $\mathcal{O}(15\%)$ for small jet-veto scales and should be included in future precision calculations of multi-jet LHC cross sections. The only exception is $q\bar{q} \to q'\bar{q}'$ scattering, shown in the middle rows in Figures 8.11 and 8.12, for which the SLL contribution amounts to just a few percent.

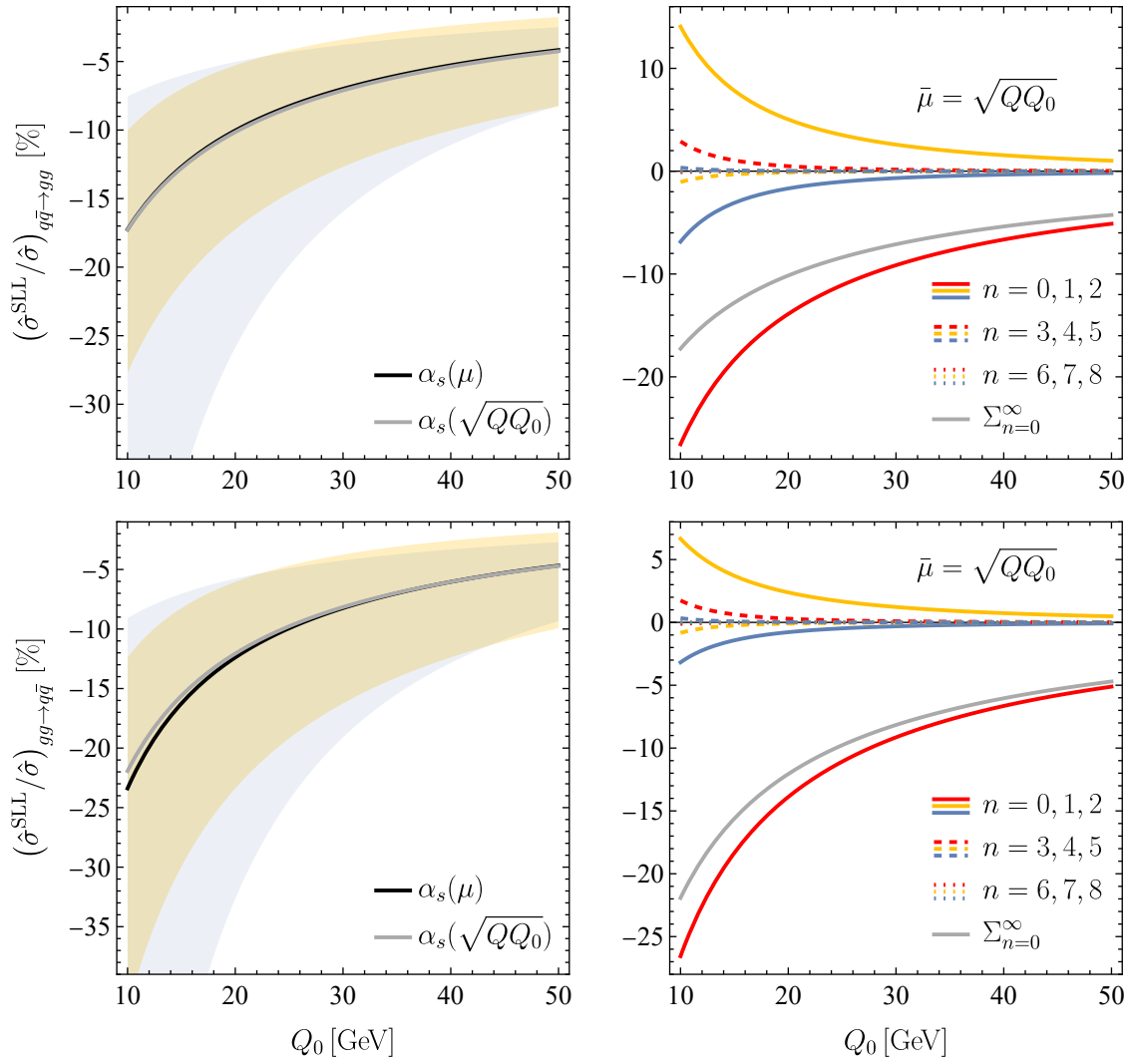

Figure 8.10: Numerical results for super-leading contributions to partonic $q\bar{q} \to gg$ (top row) and $gg \to q\bar{q}$ small-angle scattering (bottom row) as a function of the jet-veto scale Q_0. The color coding and input parameters are the same as in Figure 8.5.

By coincidence, the contribution to the cross section in this case

$$\begin{aligned}\hat{\sigma}^{\mathrm{SLL}}_{q\bar{q}\to q'\bar{q}'} = -\hat{\sigma}_{q\bar{q}\to q'\bar{q}'}\,\frac{32\pi^2}{\beta_0^3}\,N_c\int_1^{x_s}\frac{dx_2}{x_2}\,\ln\frac{x_s}{x_2}\int_1^{x_2}\frac{dx_1}{x_1}\\ \times\Bigg\{(J_4-J_3)\,\frac{N_c^2-4}{2N_c^2}\big[U^c(\tfrac{1}{2},1)-U^c(1,1)\big]\\ +J_{12}\bigg[\frac{2C_F}{N_c}\,U^c(0,1)-\frac{N_c^2-2}{N_c^2}\,U^c(\tfrac{1}{2},1)-\frac{1}{N_c^2}\,U^c(1,1)\bigg]\Bigg\}\end{aligned} \tag{8.113}$$

fulfills the first sum rule in (8.103) and, therefore, the $n = 0$ term in the perturbative expansion does not contribute. As this term always gives the dominant contribution for quark-initiated scattering processes, $q\bar{q} \to q'\bar{q}'$ scattering is comparable to the

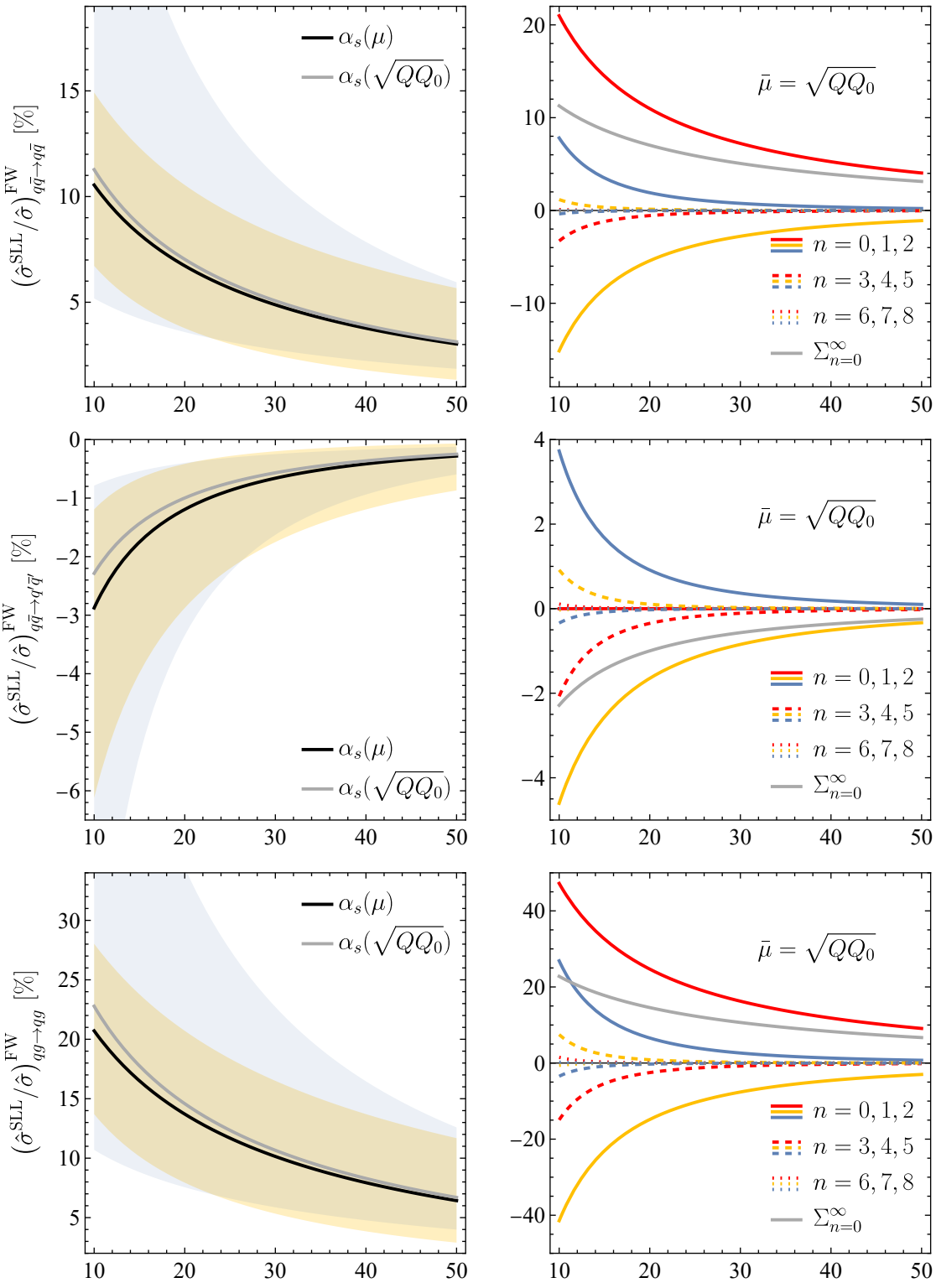

Figure 8.11: Numerical results for super-leading contributions to partonic $q\bar{q} \to q\bar{q}$ (top row), $q\bar{q} \to q'\bar{q}'$ (middle row), $qg \to qg$ (bottom row) forward scattering as a function of the jet-veto scale Q_0. The color coding and input parameters are the same as in Figure 8.5.

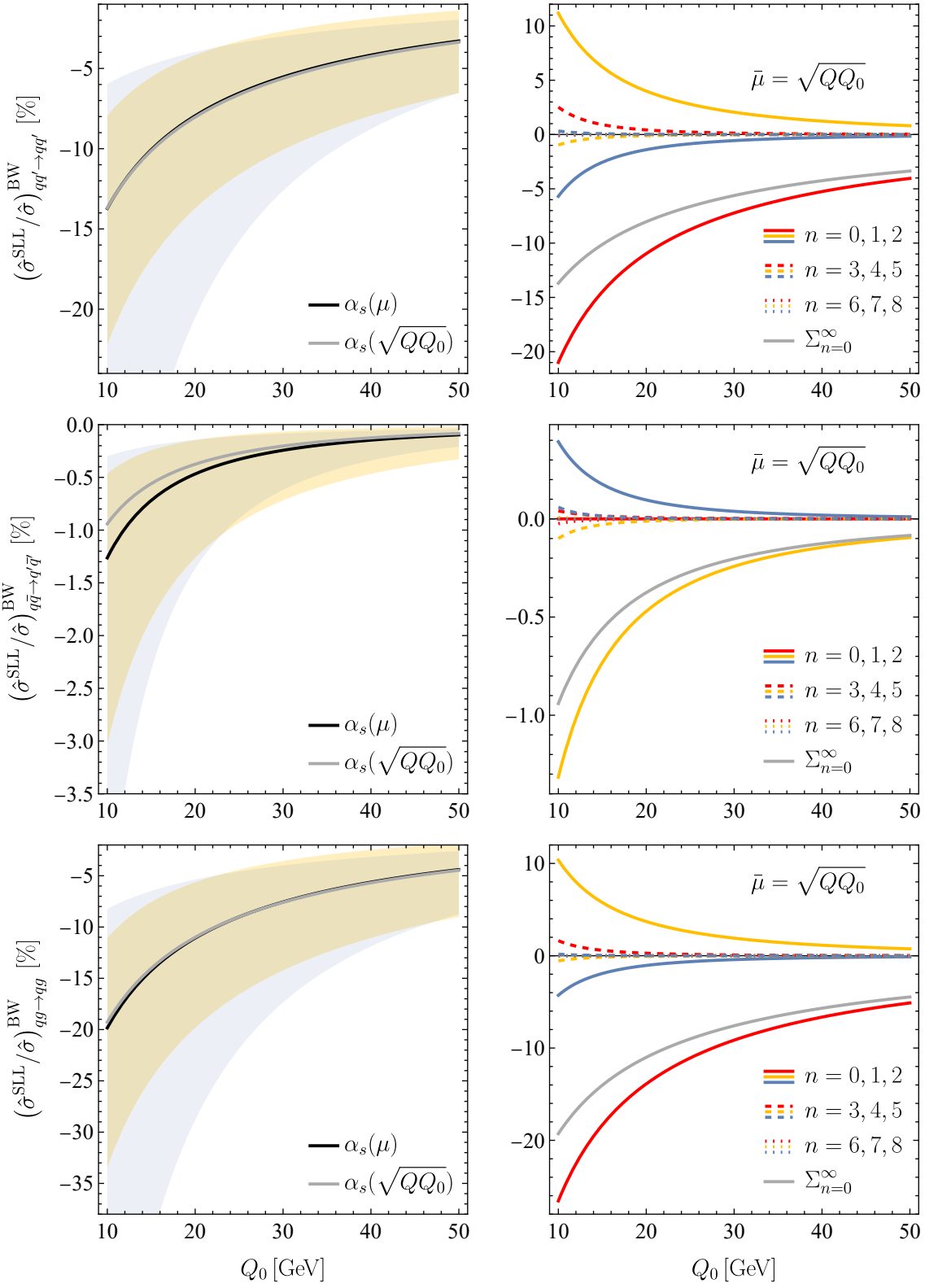

Figure 8.12: Numerical results for super-leading contributions to partonic $qq' \to qq'$ (top row), $q\bar{q} \to q'\bar{q}'$ (middle row), $qg \to qg$ (bottom row) backward scattering as a function of the jet-veto scale Q_0. The color coding and input parameters are the same as in Figure 8.5.

$2 \to 1$ processes in Figures 8.6 and 8.7. In the strict sense of the word, these $n = 0$ terms are not a "super-leading" effect, even though they result from two Glauber-gluon exchanges. For processes with gluons in the initial state the situation is different. While for $gg \to q\bar{q}$ scattering the higher individual contributions are small, for $qg \to qg$ and especially for $gg \to gg$ they give sizable corrections. The perturbative uncertainty (yellow bands) increases only slowly for decreasing Q_0 and on average is of magnitude $\pm 5\%$. In contrast, the scale uncertainty (blue bands) shows a strong dependence on the veto scale and becomes huge for small values of Q_0. The fixed coupling evaluated at the geometric mean $\bar{\mu} = \sqrt{QQ_0}$, however, provides a very good approximation to the RG-improved result for all processes except for $gg \to gg$. Comparing forward and backward scattering in Figures 8.11 and 8.12, we observe that the effect of the SLLs are of similar size in both cases but the sign can be different. The cancellations of individual terms is more pronounced for forward scattering.

8.4.5 Angular Dependence of $qq \to qq$ Scattering

Relinquishing the restriction on small-angle scattering or different flavors, several color structures contribute to most $2 \to 2$ partonic scattering processes. This yields a second source of dependence on the scattering kinematics for the SLLs, as in general different color structures can interfere.

To describe such scenarios, it is convenient to chose an orthonormal basis $\{|\mathcal{B}_I\rangle\}$ of color configurations and decompose the amplitude as

$$|\mathcal{M}_4\rangle = \sum_I \mathcal{M}_4^{(I)} |\mathcal{B}_I\rangle \,, \tag{8.114}$$

where the coefficients $\mathcal{M}_4^{(I)}$ are functions of the kinematic invariants. Sometimes, it is more convenient to work with non-orthogonal color structures, the generalization to this case is explained in Appendix A.5. The "unintegrated" hard function (7.39) can be expressed as a matrix in this basis

$$\left(\widetilde{\boldsymbol{\mathcal{H}}}_4\right)_{IJ} := \langle \mathcal{B}_I | \widetilde{\boldsymbol{\mathcal{H}}}_4 | \mathcal{B}_J \rangle = \mathcal{M}_4^{(I)} \, \mathcal{M}_4^{(J)*} \,. \tag{8.115}$$

The one- and two-loop hard functions for all $2 \to 2$ processes in QCD can be found in [111] and [112], respectively. Working in the partonic center-of-mass system, the simple kinematics for $2 \to 2$ scattering allow us to express the Born cross section (8.10) as

$$\left(\frac{d\hat{\sigma}}{dr}\right)_{2\to 2} = \frac{1}{16\pi\,\hat{s}} \left\langle \widetilde{\boldsymbol{\mathcal{H}}}_4 \, \mathbf{1} \right\rangle , \tag{8.116}$$

where $r = -\hat{t}/\hat{s} = \sin^2(\theta/2)$ and the phase-space constrains on the directions of parton 3 and 4 are implicitly understood. The trace computed in the basis $\{|\mathcal{B}_I\rangle\}$ yields

$$\left(\frac{d\hat{\sigma}}{dr}\right)_{2\to 2} = \frac{1}{16\pi\,\hat{s}} \frac{1}{\mathcal{N}_1 \mathcal{N}_2} \sum_I \sum_{\text{spins}} \left|\mathcal{M}_4^{(I)}\right|^2 , \tag{8.117}$$

with color- and spin-average factors $\mathcal{N}_i$ given in (7.10).

Similar to (8.116), one can determine the SLL contribution to the differential partonic cross section from (8.79). Expressing also the color structures as a matrix

$$\left(\boldsymbol{X}_i\right)_{IJ} \coloneqq \left\langle \mathcal{B}_I \middle| \boldsymbol{X}_i \middle| \mathcal{B}_J \right\rangle , \tag{8.118}$$

we find

$$\left(\frac{d\hat{\sigma}^{\text{SLL}}}{dr}\right)_{2\to 2} = \frac{1}{16\pi\,\hat{s}}\,\frac{1}{\mathcal{N}_1\mathcal{N}_2}\sum_{i=2}^{11}\sum_{I,J}\sum_{\text{spins}}\left(\widetilde{\boldsymbol{\mathcal{H}}}_4\right)_{IJ}\left(\boldsymbol{X}_i\right)_{JI}\varsigma_i^{\text{SLL}}(\mu_h,\mu_s)\,, \tag{8.119}$$

where $\mu_h \sim \sqrt{\hat{s}}$ and $\mu_s \sim Q_0$. The coefficient vectors for the color structures in RG-improved perturbation theory and for fixed coupling are given in (8.81) and (8.90), respectively.

Until now, most of the literature on SLLs studied processes involving a single color structure only, e.g. $qq' \to qq'$ scattering in Table 8.1. We analyze $qq \to qq$ scattering in the following, including the interference of two different color structures. They can be chosen as

$$\begin{aligned}\left\langle a_1,a_2,a_3,a_4 \middle| \mathcal{B}_1 \right\rangle &= \frac{1}{N_c}\,\delta_{a_3a_2}\,\delta_{a_4a_1}\,,\\ \left\langle a_1,a_2,a_3,a_4 \middle| \mathcal{B}_2 \right\rangle &= \frac{2}{\sqrt{N_c^2-1}}\,t^a_{a_3a_2}\,t^a_{a_4a_1}\,.\end{aligned} \tag{8.120}$$

The normalization factors are such that $\langle \mathcal{B}_I|\mathcal{B}_J\rangle = \delta_{IJ}$. For two-quark two-gluon and four-gluon scattering the basis is 3- and 9-dimensional, respectively, and can be found together with the associate hard functions in [112]. The matrix representations for the spin-averaged hard function (8.115) in this basis is

$$\begin{aligned}\frac{1}{4}\sum_{\text{spins}}\widetilde{\boldsymbol{\mathcal{H}}}_{qq\to qq} &= (4\pi\alpha_s)^2\,\frac{2C_F}{N_c r^2} \\ &\times\begin{pmatrix} N_c\,C_F(r^2-2r+2) & \frac{\sqrt{N_c^2-1}}{2}\left(\frac{r^3-3r^2+(N_c+4)r-2}{1-r}\right) \\ \frac{\sqrt{N_c^2-1}}{2}\left(\frac{r^3-3r^2+(N_c+4)r-2}{1-r}\right) & \frac{(N_c^2+1)r^4-4r^3+(N_c^2+2N_c+7)r^2-2(N_c+3)r+2}{2(1-r)^2}\end{pmatrix}.\end{aligned} \tag{8.121}$$

The ones for the color structures (8.118) can be found in Appendix A.5. The hard function is a symmetric 2×2 matrix, as QCD tree-level amplitudes do not contain any non-trivial phases. Therefore, the trace with the anti-symmetric color structure $\boldsymbol{X}_1$ vanishes, thereby confirming our previous findings.

In Figure 8.13 we show the contribution of the SLLs to the partonic $qq \to qq$ scattering cross section as a function of the jet rapidity $y_J \coloneqq y_3 = -y_4$ in the partonic center-of-mass system. The rapidity of parton 3 is related to the scattering angle by $y_3 = \ln\cot(\theta/2)$. The hard jets are restricted to lie outside the veto area (gray) of width $\Delta Y = 2$, i.e. $|y_J| > 1$. However, we plot the results for illustrative purposes also inside this region. The plot is obtained with fixed values $Q_0 = 25\,\text{GeV}$ of the jet-veto scale and the partonic center-of-mass energy $\sqrt{\hat{s}} = 1\,\text{TeV}$. The resummed effect of the SLLs shown in the left panel is of similar size ($\sim 6\%$) as for the small-angle limit, shown in the upper row of Figure 8.9. The right panel shows the summed contribution up to

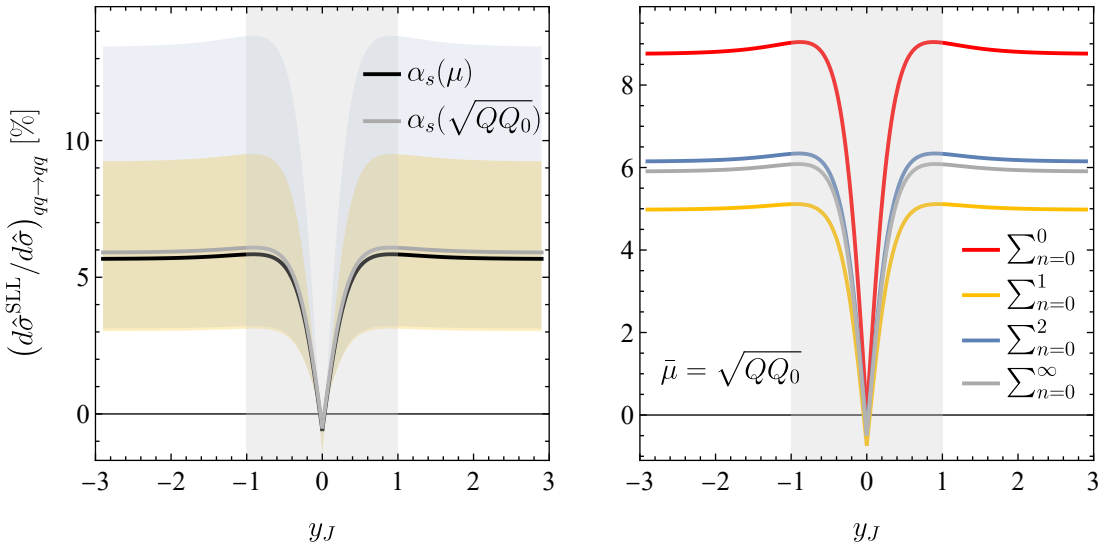

Figure 8.13: Numerical results for super-leading contributions to partonic $qq \to qq$ scattering as a function of the jet rapidity y_J, at fixed partonic center-of-mass energy $\sqrt{\hat{s}} = 1\,\mathrm{TeV}$ and jet-veto scale $Q_0 = 25\,\mathrm{GeV}$, and for a central rapidity gap with $\Delta Y = 2$ (gray area). The left plot shows the resummed contribution of the SLLs with a running coupling $\alpha_s(\mu)$ (black line) and for a fixed coupling $\alpha_s(\bar{\mu})$ with $\bar{\mu} = \sqrt{QQ_0}$ (gray line). The yellow and blue bands are obtained in the same way as in Figure 8.5. The right plot shows the contributions summed up to $(3+n)$-th order in perturbation theory for different values of n when working with a fixed coupling at $\bar{\mu} = \sqrt{QQ_0}$.

the $(3+n)$-th order in the fixed coupling approximation. As typical for quark-initiated processes, the exact result is approximate already well by summing $n \leq 2$.

Even though it is a small effect, the kinematic dependence on the SLL contributions on the jet rapidity is clearly visible in both plots. For processes where one can distinguish forward and backward scattering this effect is more pronounced. In order to perform a full phenomenological study of the SLLs, one needs to study the interference effects of different color structures for all relevant partonic processes and combine them with the PDFs, see (8.8).

Chapter 9

The Glauber Series

In the previous chapter, we have studied in detail the leading double-logarithmic corrections to gap-between-jet cross sections at hadron colliders, arising from the non-cancellation of soft+collinear singularities due to Glauber-gluon exchanges between initial-state partons. The contributions of these SLLs to the $2 \to M$ jet cross section is of the form

$$\sigma_{2\to M}^{\text{SLL}} \sim \frac{\alpha_s L_s}{\pi N_c} w_\pi \sum_{n=0}^{\infty} c_{1,n} w^{n+1} , \tag{9.1}$$

where the parameter w encodes the double logarithms L in the scale ratio and w_π contains the two Glauber phases $i\pi$ from the associated exchanges. Both parameters originate from the cusp logarithm $\ln[(-Q^2-i0)/Q_0^2] = 2L - i\pi$ and are defined in (8.66). Even though this effect formally starts at four-loop order ($n = 1$), for typical values, e.g. $Q = 1\,\text{TeV}$ and $Q_0 = 40\,\text{GeV}$, one finds $w \sim w_\pi = \mathcal{O}(1)$ and also the $n = 0$ term could be considered as "super-leading". Therefore, higher order Glauber-gluon exchanges lead to a more general series

$$\sigma_{2\to M}^{\text{SLL+G}} \sim \frac{\alpha_s L_s}{\pi N_c} \sum_{\ell=1}^{\infty} \sum_{n=0}^{\infty} c_{\ell,n} w_\pi^\ell w^{n+1} , \tag{9.2}$$

which is referred to as the *Glauber series* [1–3]. Here, ℓ denotes the number of Glauber pairs arising from Glauber-gluon exchanges.

The Glauber series is generated by the evolution operator for the hard function [3]

$$\begin{aligned} \boldsymbol{U}_{\text{SLL+G}}(\{\underline{n}\}, \mu_h, \mu_s) \coloneqq & \int_{\mu_s}^{\mu_h} \frac{d\mu_1}{\mu_1} \int_{\mu_s}^{\mu_1} \frac{d\mu_2}{\mu_2} \\ & \times \mathbf{P} \exp\left[\int_{\mu_1}^{\mu_h} \frac{d\mu}{\mu} \gamma_{\text{cusp}}\big(\alpha_s(\mu)\big) \Big(\boldsymbol{\Gamma}^c \ln \frac{\mu^2}{\mu_h^2} + \boldsymbol{V}^G \Big) \right] \gamma_{\text{cusp}}\big(\alpha_s(\mu_1)\big)\, \boldsymbol{V}^G \frac{\alpha_s(\mu_2)}{4\pi} \overline{\boldsymbol{\Gamma}} , \end{aligned} \tag{9.3}$$

where the path ordering is required as $\boldsymbol{V}^G$ and $\boldsymbol{\Gamma}^c$ do not commute and only acts on the exponential. Similar to the evolution operator for the SLLs (8.6), the rightmost factor needs to be $\boldsymbol{V}^G \overline{\boldsymbol{\Gamma}}$ to get a non-vanishing result under the color trace with the leading-order low-energy matrix element (7.20). In (9.3) even *and* odd numbers of Glauber operators are included. The latter become only relevant if the hard function itself yields a phases to get a real-valued contribution. In this case, the amplitude needs to be of the form $|\mathcal{M}_{2\to M}\rangle = |\mathcal{M}_{2\to M}^{(r)}\rangle + i|\mathcal{M}_{2\to M}^{(i)}\rangle$ where real and imaginary part have different color structure. In pure QCD this can only happen at loop level, but for electroweak amplitudes such phases can already appear at tree level through massive gauge bosons or Cabibbo–Kobayashi–Maskawa matrix elements [64]. Therefore, the SLLs and the Glauber series for these processes start already at three- and two-loop order, respectively. In the following, we thus include odd numbers of Glauber-operator insertions as well. The contribution of the Glauber series to the gap-between-jet cross

section is then obtained in the same way as for the SLLs, and reads

$$\sigma_{2\to M}^{\text{SLL+G}}(Q_0) = \sum_{\substack{\text{partonic}\\ \text{channels}}} \int d\xi_1\, d\xi_2\, f_1(\xi_1,\mu_s)\, f_2(\xi_2,\mu_s)\, \hat{\sigma}_{2\to M}^{\text{SLL+G}}(\xi_1,\xi_2,Q_0) \tag{9.4}$$

with partonic cross section

$$\hat{\sigma}_{2\to M}^{\text{SLL+G}}(\xi_1,\xi_2,Q_0) \coloneqq \left\langle \boldsymbol{\mathcal{H}}_{2\to M}(\{\underline{n}\},s,\xi_1,\xi_2,\mu_h)\, \boldsymbol{U}_{\text{SLL+G}}(\{\underline{n}\},\mu_h,\mu_s) \otimes \mathbf{1} \right\rangle, \tag{9.5}$$

where $\mu_s \sim Q_0$ and $\mu_h \sim Q$.

9.1 Color Basis

To evaluate the evolution operator (9.3) of the Glauber series under the trace, one needs to determine the action of the Glauber operator on all appearing color structures. By means of (8.27), it is thus necessary to calculate commutators with $\boldsymbol{T}_1 \cdot \boldsymbol{T}_2$. To understand the general mechanism behind this, we now look at generic color structures that can appear in the Glauber series [3].

Since the cusp anomalous dimension $\boldsymbol{\Gamma}^c$ and the Glauber operator $\boldsymbol{V}^G$ contain only initial-state generators and just one insertions of $\overline{\boldsymbol{\Gamma}}$ is relevant, there are two types of color structures that can appear

$$\begin{aligned} \boldsymbol{X}^{(\text{I})} &= \sum_{j>2} J_j\, \zeta \left(\boldsymbol{\mathcal{C}}_1\, \widetilde{\boldsymbol{\mathcal{C}}}_2 - \boldsymbol{\mathcal{C}}_2\, \widetilde{\boldsymbol{\mathcal{C}}}_1\right) \boldsymbol{T}_j\,, \\ \boldsymbol{X}^{(\text{II})} &= J_{12}\, \zeta \left(\boldsymbol{\mathcal{C}}_1\, \widetilde{\boldsymbol{\mathcal{C}}}_2 + \boldsymbol{\mathcal{C}}_2\, \widetilde{\boldsymbol{\mathcal{C}}}_1\right) \mathbf{1}_j\,, \end{aligned} \tag{9.6}$$

where we explicitly indicate the unit matrices for all final-state generators in the second type. Here, the objects $\boldsymbol{\mathcal{C}}_i$ and $\widetilde{\boldsymbol{\mathcal{C}}}_i$ are color-space matrices which contain products of color generators associated with parton i. The tilde indicates that these structures are not necessarily related by interchanging $1 \leftrightarrow 2$. One the one hand, they carry two *matrix* indices, i.e. anti-fundamental or fundamental indices if parton i is a quark or anti-quark, respectively, or adjoint indices if it is a gluon. On the other hand, they also carry an open *adjoint* index for each color generator. Whereas the matrix indices are to be contracted with the hard function under the color trace, the open adjoint indices are contracted with ζ, a color-space tensor of corresponding rank. For example, color structure $\boldsymbol{X}_1$ defined in (8.21) is of type (I) with

$$\zeta^{abc} = \frac{1}{2}\, i f^{abc}\,, \qquad \boldsymbol{\mathcal{C}}_1^a = \boldsymbol{T}_1^a\,, \qquad \widetilde{\boldsymbol{\mathcal{C}}}_2^b = \boldsymbol{T}_2^b\,, \tag{9.7}$$

where the third index of ζ is contracted with $\boldsymbol{T}_j^c$. As the cross section is invariant under $1 \leftrightarrow 2$, both types of color structures must be invariant as well. We have already seen above that $J_j \to -J_j$ and $J_{12} \to J_{12}$ under this exchange, which must be compensated by the color-space matrices.

A good choice for the structures $\boldsymbol{\mathcal{C}}_i$ and $\widetilde{\boldsymbol{\mathcal{C}}}_i$ are symmetrized products (8.34) of $SU(N_c)$ generators. Spelling out adjoint indices explicitly, they read

$$\boldsymbol{\mathcal{C}}_i^{(k)\,a_1\ldots a_k} = \left(\boldsymbol{T}_i^{a_1} \ldots \boldsymbol{T}_i^{a_k}\right)_+ \tag{9.8}$$

with $\boldsymbol{\mathcal{C}}_i^{(0)} = \mathbf{1}_i$. The open adjoint indices must be contracted with ζ, which can be constructed from all combinations of permutations of traces of fundamental generators

$$\begin{aligned} &\zeta^{(0)} = 1\,, \quad \zeta^{(2)\,a_1a_2} = \mathrm{tr}(t^{a_1}t^{a_2})\,, \quad \zeta^{(3)\,a_1a_2a_3} \in \left\{\mathrm{tr}(t^{a_1}t^{a_2}t^{a_3})\,, \mathrm{tr}(t^{a_1}t^{a_3}t^{a_2})\right\}, \\ &\zeta^{(4)\,a_1a_2a_3a_4} \in \left\{\mathrm{tr}(t^{a_1}t^{a_2}t^{a_3}t^{a_4}) + \text{perm.}\,, \mathrm{tr}(t^{a_1}t^{a_2})\,\mathrm{tr}(t^{a_3}t^{a_4}) + \text{perm.}\right\}. \end{aligned} \tag{9.9}$$

Note that there exists no $\zeta^{(1)}$ as generators are traceless. As in Chapter 8, we express these traces in the following through f- and d-symbols. The relevant relations are [108]

$$\begin{aligned} \mathrm{tr}(t^a t^b t^c) &= \frac{1}{4}(d^{abc} + if^{abc})\,, \\ \mathrm{tr}(t^a t^b t^c t^d) &= \frac{1}{4N_c}\,\delta^{ab}\delta^{cd} + \frac{1}{8}(d^{abe}d^{cde} - f^{abe}f^{cde} + if^{abe}d^{cde} + if^{cde}d^{abe})\,, \\ \mathrm{tr}(t^a t^b t^c t^d t^e) &= \frac{1}{8N_c}\,\delta^{cd}\,(d^{abe} + if^{abe}) + \frac{1}{8N_c}\,\delta^{ab}\,(d^{cde} + if^{cde}) \\ &\quad + \frac{1}{16}(d^{abf} + if^{abf})(d^{cdg} + if^{cdg})(d^{efg} + if^{efg})\,, \end{aligned} \tag{9.10}$$

which can be proven by applying (8.56).

From (9.6), it is easy to show that the cusp anomalous dimension $\boldsymbol{\Gamma}^c$ maps color structures with k adjoint indices (the rank of ζ) to color structures with again at most k adjoint indices. In other words, it does not increase the complexity. As a consequence, it is possible to find sets of color structures that are closed under repeated application of $\boldsymbol{\Gamma}^c$, e.g. $\{\boldsymbol{X}_2, \ldots, \boldsymbol{X}_{11}\}$ for the SLLs. Unfortunately, this is not possible for the Glauber operator as long as one works with initial-state generators of arbitrary representations. The Glauber operator acts as commutator and increases the complexity of color structures

$$\begin{aligned} &\zeta^{(k_1+k_2+\delta)}\left[\boldsymbol{T}_1\cdot\boldsymbol{T}_2, \boldsymbol{\mathcal{C}}_1^{(k_1)}\,\widetilde{\boldsymbol{\mathcal{C}}}_2^{(k_2)}\right] \\ &= \zeta^{(k_1+k_2+1+\delta)}\,\boldsymbol{\mathcal{C}}_1^{(k_1+1)}\,\widetilde{\boldsymbol{\mathcal{C}}}_2^{(k_2)} + \hat{\zeta}^{(k_1+k_2+1+\delta)}\,\boldsymbol{\mathcal{C}}_1^{(k_1)}\,\widetilde{\boldsymbol{\mathcal{C}}}_2^{(k_2+1)} + \ldots\,, \end{aligned} \tag{9.11}$$

where $\delta = 1$ ($\delta = 0$) for type I (II) structures and ellipsis denote terms that have at most $(k_1+k_2+\delta)$ adjoint indices. Therefore, it is not possible to construct a *finite* color basis valid for initial-state partons transforming under *any* representation. However, upon specifying a representation, one can always construct a finite basis, as is shown for the fundamental and adjoint representations below. This is a somewhat unexpected result, given the complexity of the color algebra in the adjoint representation, and allows one to access the all-order structure of the Glauber series.

9.1.1 Quark-Initiated Processes

We begin by constructing a color basis for processes with (anti-)quarks in the initial state. In this case, the color-space matrices in (9.6) can only be $\boldsymbol{\mathcal{C}}_i\,, \widetilde{\boldsymbol{\mathcal{C}}}_i \in \{\mathbf{1}_i, \boldsymbol{t}_i\}$ as products of (anti-)fundamental generators can always be reduced using the commutation and anti-commutation relation (8.56)

$$\boldsymbol{t}_i^a\,\boldsymbol{t}_i^b = \frac{1}{2}\left[\boldsymbol{t}_i^a, \boldsymbol{t}_i^b\right] + \frac{1}{2}\left\{\boldsymbol{t}_i^a, \boldsymbol{t}_i^b\right\} = \frac{1}{2N_c}\,\delta^{ab}\,\mathbf{1}_i + \frac{1}{2}\left(if^{abc} + \sigma_i d^{abc}\right)\boldsymbol{t}_i^c\,. \tag{9.12}$$

	$q\bar{q} \to 0$	$q\bar{q} \to g$	$qq' \to qq'$	$q\bar{q} \to q'\bar{q}'$	$q\bar{q}' \to q\bar{q}'$	$q\bar{q} \to gg$
$\boldsymbol{X}_1^q$	–	0	0	0	0	0
$\boldsymbol{X}_2^q$	–	0	0	$\mathcal{O}(1)$	$\mathcal{O}(1)$	0
$\boldsymbol{X}_3^q$	–	0	$\mathcal{O}(1)$	$\mathcal{O}(1)$	$\mathcal{O}(1/N_c^2)$	$\mathcal{O}(1)$
$\boldsymbol{X}_4^q$	$\mathcal{O}(1)$	$\mathcal{O}(1/N_c^2)$	$\mathcal{O}(1/N_c^2)$	$\mathcal{O}(1/N_c^2)$	$\mathcal{O}(1)$	$\mathcal{O}(1/N_c^4)$
$\boldsymbol{X}_5^q$	$\mathcal{O}(1)$	$\mathcal{O}(1)$	$\mathcal{O}(1)$	$\mathcal{O}(1)$	$\mathcal{O}(1)$	$\mathcal{O}(1)$

Table 9.1: Large-N_c counting of the traces $\langle \boldsymbol{\mathcal{H}}_{2\to M}\, \boldsymbol{X}_i^q \rangle$ for quark-initiated partonic (small-angle) scattering processes, where quarks q and q' have different flavors.

Therefore, we only need to consider color-space tensors ζ up to rank 3. They are

$$\zeta^{(0)} = 1\,, \quad \zeta^{(2)a_1a_2} = \delta^{a_1a_2}\,, \quad \zeta^{(3)a_1a_2a_3} \in \left\{ if^{a_1a_2a_3}\,, \sigma_1 d^{a_1a_2a_3}\,, \sigma_2 d^{a_1a_2a_3} \right\}, \tag{9.13}$$

where d-symbols always appear together with σ_i as evident from (9.12). Meeting also the symmetry constraints under the exchange $1 \leftrightarrow 2$, we find three structures of type I and two of type II [2, 4]

$$\begin{aligned}
\boldsymbol{X}_1^q &\coloneqq \sum_{j>2} J_j\, if^{abc}\, \boldsymbol{t}_1^a\, \boldsymbol{t}_2^b\, \boldsymbol{T}_j^c\,, & \boldsymbol{X}_4^q &\coloneqq \frac{1}{N_c}\, J_{12}\, \boldsymbol{t}_1 \cdot \boldsymbol{t}_2\,, \\
\boldsymbol{X}_2^q &\coloneqq \sum_{j>2} J_j\, (\sigma_1 - \sigma_2) d^{abc}\, \boldsymbol{t}_1^a\, \boldsymbol{t}_2^b\, \boldsymbol{T}_j^c\,, & \boldsymbol{X}_5^q &\coloneqq J_{12}\, \boldsymbol{1}\,. \\
\boldsymbol{X}_3^q &\coloneqq \frac{1}{N_c} \sum_{j>2} J_j \left(\boldsymbol{t}_1 - \boldsymbol{t}_2\right) \cdot \boldsymbol{T}_j\,,
\end{aligned} \tag{9.14}$$

Here, the factors $1/N_c$ are chosen such that the traces $\langle \boldsymbol{\mathcal{H}}_{2\to M}\, \boldsymbol{X}_i^q \rangle$ for all processes considered in Section 8.4 are at most of $\mathcal{O}(1)$ in the large-N_c expansion, see Table 9.1. Of course, it is possible to map the color structures describing the SLLs to this basis. One finds

$$\begin{aligned}
\boldsymbol{X}_1 &= \boldsymbol{X}_1^q & \boldsymbol{X}_6 &= -\frac{N_c^2-4}{2N_c^2}\, \sigma_1\sigma_2\, \boldsymbol{X}_4^q - \frac{N_c^2-1}{N_c^4}\, \boldsymbol{X}_5^q \\
\boldsymbol{X}_2 &= -\frac{1}{2}\, \boldsymbol{X}_2^q + \boldsymbol{X}_3^q & \boldsymbol{X}_7 &= \left(\frac{N_c^2-4}{N_c^2}\right)^2 \sigma_1\sigma_2\, \boldsymbol{X}_4^q \\
\boldsymbol{X}_3 &= \frac{N_c^2-4}{N_c^2}\, \boldsymbol{X}_2^q & \boldsymbol{X}_8 &= \frac{(N_c^2-4)(N_c^2-6)}{3N_c^4}\, \boldsymbol{X}_4^q \\
\boldsymbol{X}_4 &= \frac{1}{N_c^2}\left(\boldsymbol{X}_2^q - \boldsymbol{X}_3^q\right) & \boldsymbol{X}_9 &= \frac{N_c^2-4}{N_c^2}\, \sigma_1\sigma_2\, \boldsymbol{X}_4^q + \frac{N_c^2-1}{N_c^4}\, \boldsymbol{X}_5^q \\
\boldsymbol{X}_5 &= -\frac{N_c^2-1}{N_c^2}\, \boldsymbol{X}_3^q & \boldsymbol{X}_{10} &= \boldsymbol{X}_4^q \\
& & \boldsymbol{X}_{11} &= \boldsymbol{X}_5^q
\end{aligned} \tag{9.15}$$

In this case, the consistency relations (8.49) are clearly fulfilled and, therefore, the super-leading terms in N_c cancel for quark-initiated processes. Using this result, one can simplify the color trace (8.42) for the SLLs. The complicate dependence of the coefficients $c_i^{(r_1)}$ on the eigenvalues (8.48) mostly drops out and one is left with [73]

$$\begin{aligned} C^2_{r_1 r_2} = -16\pi^2\, N_c^{n+1} \Big[&- \frac{v_2^{r_1}}{2} \left\langle \boldsymbol{\mathcal{H}}_{2\to M}\, \boldsymbol{X}_2^q \otimes \mathbf{1} \right\rangle + v_1^{r_1} \left\langle \boldsymbol{\mathcal{H}}_{2\to M}\, \boldsymbol{X}_3^q \otimes \mathbf{1} \right\rangle \\ &+ 2\big(v_1^{r_1} - v_2^{r_1}\big) \left\langle \boldsymbol{\mathcal{H}}_{2\to M}\, \boldsymbol{X}_4^q \otimes \mathbf{1} \right\rangle + \frac{2C_F}{N_c} \big(v_0^{r_1} - v_1^{r_1}\big) \left\langle \boldsymbol{\mathcal{H}}_{2\to M}\, \boldsymbol{X}_5^q \otimes \mathbf{1} \right\rangle \Big] , \end{aligned} \tag{9.16}$$

where we used that $C_1 = C_2 = C_F$ in this case. Remarkably, only eigenvalues $v_0 = 0$, $v_1 = \frac{1}{2}$ and $v_2 = 1$ contribute for quark-initiated processes.

9.1.2 Gluon-Initiated Processes

For processes where both initial-state partons are gluons, the generators are given by the $SU(N_c)$ structure constant

$$\boldsymbol{T}_i = \boldsymbol{F}_i \,, \tag{9.17}$$

with $\boldsymbol{F}_i$ given in (8.55). There is no relation similar to (9.12) as anti-commutators of adjoint generators cannot be reduced. However, it is still possible to construct a finite color basis in this case. To simplify notation, we label the color-space-matrix part of the two generic color structures (9.6) as

$$\begin{aligned} &\text{type I:} \quad \boldsymbol{A}^{(j)} \coloneqq \zeta\big(\boldsymbol{\mathcal{C}}_1\, \widetilde{\boldsymbol{\mathcal{C}}}_2 - \boldsymbol{\mathcal{C}}_2\, \widetilde{\boldsymbol{\mathcal{C}}}_1\big) \boldsymbol{T}_j \,, \\ &\text{type II:} \quad \boldsymbol{S} \coloneqq \zeta\big(\boldsymbol{\mathcal{C}}_1\, \widetilde{\boldsymbol{\mathcal{C}}}_2 + \boldsymbol{\mathcal{C}}_2\, \widetilde{\boldsymbol{\mathcal{C}}}_1\big) \,, \end{aligned} \tag{9.18}$$

in the following. The $\boldsymbol{A}^{(j)}$ are anti-symmetric under the exchange $1 \leftrightarrow 2$ whereas the $\boldsymbol{S}$ are symmetric. The four matrix indices of these two structures are all adjoint. Factoring off the final-state generator $\boldsymbol{T}_j^c$ for $\boldsymbol{A}^{(j)}$, the two tensors

$$\begin{aligned} &\text{type I:} \quad \big\langle a_1, a_2 \big| \zeta\big(\boldsymbol{\mathcal{C}}_1\, \widetilde{\boldsymbol{\mathcal{C}}}_2 - \boldsymbol{\mathcal{C}}_2\, \widetilde{\boldsymbol{\mathcal{C}}}_1\big) \big| b_1, b_2, c \big\rangle \\ &\text{type II:} \quad \big\langle a_1, a_2 \big| \zeta\big(\boldsymbol{\mathcal{C}}_1\, \widetilde{\boldsymbol{\mathcal{C}}}_2 + \boldsymbol{\mathcal{C}}_2\, \widetilde{\boldsymbol{\mathcal{C}}}_1\big) \big| b_1, b_2 \big\rangle \end{aligned} \tag{9.19}$$

have five and four open indices, respectively. As all these open indices are adjoint, one possible basis choice are traces of generators in the fundamental representation, similar to (9.9) for ζ. Since the generators are traceless and normalized such that $\mathrm{tr}(t^a t^b) = \frac{1}{2}\,\delta^{ab}$, the only allowed tensors for type I consist of anti-symmetric (for $(a_1, b_1) \leftrightarrow (a_2, b_2)$) linear combinations of permutations of the traces

$$\mathrm{tr}(t^c\, t^{a_1}\, t^{a_2}\, t^{b_1}\, t^{b_2}) \quad \text{and} \quad \mathrm{tr}(t^c\, t^{a_1}\, t^{a_2})\, \delta^{b_1 b_2} \,. \tag{9.20}$$

To obtain a basis element $\boldsymbol{A}^{(j)}$, this linear combination is then multiplied by the left-over $\boldsymbol{T}_j^c$. Due to the cyclicity of the trace, there are $4! + \binom{5}{2}\, 2! = 44$ such permutations, 22 of which are anti-symmetric. For type II the allowed tensors are symmetric linear combinations of permutations of the traces

$$\mathrm{tr}(t^{a_1}\, t^{a_2}\, t^{b_1}\, t^{b_2}) \quad \text{and} \quad \delta^{a_1 a_2}\, \delta^{b_1 b_2} \,. \tag{9.21}$$

The 3! permutations of the first term allow for four symmetric linear combinations, together with the $\frac{1}{2}\binom{4}{2} = 3$ permutations of the second term which are already symmetric, yielding in total seven linearly independent $\boldsymbol{S}$ structures.

As linear combinations of (9.20) and (9.21) cannot be used within the color-space formalism straightforwardly, it is convenient to map them onto objects naturally appearing in the adjoint representation of the initial-state partons. Using (9.10), one can translate them to δ's, f- and d-symbols. Rearranging indices in such a way that (a_i, b_i) always appear together, the adjoint matrices

$$\left[\boldsymbol{\Delta}_i^{ab}\right]^{a_i b_i} := \delta^{aa_i}\delta^{bb_i} + \delta^{ba_i}\delta^{ab_i}\,, \qquad \left[\boldsymbol{\nabla}_i^{ab}\right]^{a_i b_i} := \delta^{aa_i}\delta^{bb_i} - \delta^{ba_i}\delta^{ab_i}\,, \tag{9.22}$$

together with $\mathbf{1}_i$, $\boldsymbol{F}_i$ and $\boldsymbol{D}_i$ naturally arise, see (8.55) for their definitions. They fulfill the important relations [108]

$$\begin{aligned} &\left[\boldsymbol{F}_i^a, \boldsymbol{F}_i^b\right] = i f^{abc}\boldsymbol{F}_i^c\,, && \boldsymbol{F}_i^a\boldsymbol{D}_i^b + \boldsymbol{F}_i^b\boldsymbol{D}_i^a = \boldsymbol{D}_i^a\boldsymbol{F}_i^b + \boldsymbol{D}_i^b\boldsymbol{F}_i^a = d^{abc}\boldsymbol{F}_i^c\,, \\ &\left[\boldsymbol{D}_i^a, \boldsymbol{D}_i^b\right] = i f^{abc}\boldsymbol{F}_i^c - \frac{2}{N_c}\boldsymbol{\nabla}_i^{ab}\,, && \left[\boldsymbol{F}_i^a, \boldsymbol{D}_i^b\right] = \left[\boldsymbol{D}_i^a, \boldsymbol{F}_i^b\right] = i f^{abc}\boldsymbol{D}_i^c\,, \end{aligned} \tag{9.23}$$

Commutators of these matrices can be reduced by applying (9.23), mimicking the properties of ordinary generators of $SU(N_c)$. However, it is in general not possible to simplify anti-commutators, resulting in a larger basis compared to the quark case. It is possible to remove one of the symmetric matrices as [108]

$$\boldsymbol{\Delta}_i^{ab} + \frac{N_c}{2}\left\{\boldsymbol{F}_i^a, \boldsymbol{F}_i^b\right\} + \frac{N_c}{2}\left\{\boldsymbol{D}_i^a, \boldsymbol{D}_i^b\right\} = 2\delta^{ab}\,\mathbf{1}_i + N_c\, d^{abc}\boldsymbol{D}_i^c\,. \tag{9.24}$$

In the following, we choose to remove $\left\{\boldsymbol{D}_i^a, \boldsymbol{D}_i^b\right\}$ using (9.24). As shown below, it suffices to consider the unit matrix $\mathbf{1}_i$, the two matrices $\boldsymbol{F}_i$ and $\boldsymbol{D}_i$ constructed from the structure constants together with $\boldsymbol{\Delta}_i$ and $\boldsymbol{\nabla}_i$ complemented by the two additional anti-commutators $\left\{\boldsymbol{F}_i^a, \boldsymbol{F}_i^b\right\}$ and $\left\{\boldsymbol{F}_i^a, \boldsymbol{D}_i^b\right\}$ to construct a basis for gluon-initiated process. Importantly, there is no need to include symmetrized products (8.34) with $k \geq 3$.

$\boldsymbol{A}^{(j)}$ structures: The third relation in (9.10) implies that we only need to consider color structures $\boldsymbol{A}^{(j)}$ containing at most three f- or d-symbols. In Table 9.2 all 26 such color structures are listed, sorted by the number of contracted indices, i.e. by the rank of ζ in (9.18). All other contractions either vanish by symmetry or can be reduced to those listed in the table. For the possible structures of $\boldsymbol{A}_3^{(j)}$-type *not* listed in Table 9.2, one can apply

$$\begin{aligned} &i f^{abc}\,\boldsymbol{\nabla}_i^{ab} = -2\boldsymbol{F}_i^c\,, && d^{abc}\left\{\boldsymbol{F}_i^a, \boldsymbol{F}_i^b\right\} = N_c\,\boldsymbol{D}_i^c\,, \\ &d^{abc}\,\boldsymbol{\Delta}_i^{ab} = 2\boldsymbol{D}_i^c\,, && d^{abc}\left\{\boldsymbol{F}_i^a, \boldsymbol{D}_i^b\right\} = \left(\frac{N_c^2 - 4}{N_c}\right)\boldsymbol{F}_i^c\,, \end{aligned} \tag{9.25}$$

to relate these operators to the $\boldsymbol{A}_2^{(j)}$. In principle, it is also possible to construct $\boldsymbol{A}_4^{(j)}$-type structures by contracting with $\zeta \in \{f^{abe}f^{cde}, d^{abe}d^{cde}, i f^{abe}d^{cde}\}$. However,

Two contracted indices		Four contracted indices	
$\boldsymbol{A}^{(j)}_{2,F}$	$\big(\boldsymbol{F}_1 - \boldsymbol{F}_2\big)\cdot\boldsymbol{T}_j$	$\boldsymbol{A}^{(j)}_{4,F,\Delta}$	$\big(\boldsymbol{F}_1^a\,\boldsymbol{\Delta}_2^{ab} - 1\leftrightarrow 2\big)\boldsymbol{T}_j^b$
$\boldsymbol{A}^{(j)}_{2,D}$	$\big(\boldsymbol{D}_1 - \boldsymbol{D}_2\big)\cdot\boldsymbol{T}_j$	$\boldsymbol{A}^{(j)}_{4,F,\nabla}$	$\big(\boldsymbol{F}_1^a\,\boldsymbol{\nabla}_2^{ab} - 1\leftrightarrow 2\big)\boldsymbol{T}_j^b$
		$\boldsymbol{A}^{(j)}_{4,F,FF}$	$\big(\boldsymbol{F}_1^a\,\{\boldsymbol{F}_2^a,\boldsymbol{F}_2^b\} - 1\leftrightarrow 2\big)\boldsymbol{T}_j^b$
Three contracted indices		$\boldsymbol{A}^{(j)}_{4,F,FD}$	$\big(\boldsymbol{F}_1^a\,\{\boldsymbol{F}_2^a,\boldsymbol{D}_2^b\} - 1\leftrightarrow 2\big)\boldsymbol{T}_j^b$
$\boldsymbol{A}^{(j)}_{3f,F,F}$	$if^{abc}\,\boldsymbol{F}_1^a\,\boldsymbol{F}_2^b\,\boldsymbol{T}_j^c$	$\boldsymbol{A}^{(j)}_{4,D,\Delta}$	$\big(\boldsymbol{D}_1^a\,\boldsymbol{\Delta}_2^{ab} - 1\leftrightarrow 2\big)\boldsymbol{T}_j^b$
$\boldsymbol{A}^{(j)}_{3f,D,D}$	$if^{abc}\,\boldsymbol{D}_1^a\,\boldsymbol{D}_2^b\,\boldsymbol{T}_j^c$	$\boldsymbol{A}^{(j)}_{4,D,\nabla}$	$\big(\boldsymbol{D}_1^a\,\boldsymbol{\nabla}_2^{ab} - 1\leftrightarrow 2\big)\boldsymbol{T}_j^b$
$\boldsymbol{A}^{(j)}_{3f,F,D}$	$if^{abc}\big(\boldsymbol{F}_1^a\boldsymbol{D}_2^b - \boldsymbol{F}_2^a\boldsymbol{D}_1^b\big)\boldsymbol{T}_j^c$	$\boldsymbol{A}^{(j)}_{4,D,FF}$	$\big(\boldsymbol{D}_1^a\,\{\boldsymbol{F}_2^a,\boldsymbol{F}_2^b\} - 1\leftrightarrow 2\big)\boldsymbol{T}_j^b$
$\boldsymbol{A}^{(j)}_{3d,F,D}$	$d^{abc}\big(\boldsymbol{F}_1^a\boldsymbol{D}_2^b - \boldsymbol{F}_2^a\boldsymbol{D}_1^b\big)\boldsymbol{T}_j^c$	$\boldsymbol{A}^{(j)}_{4,D,FD}$	$\big(\boldsymbol{D}_1^a\,\{\boldsymbol{F}_2^a,\boldsymbol{D}_2^b\} - 1\leftrightarrow 2\big)\boldsymbol{T}_j^b$

Five contracted indices			
$\boldsymbol{A}^{(j)}_{5f,\Delta,\Delta}$	$if^{abc}\,\boldsymbol{\Delta}_1^{ad}\,\boldsymbol{\Delta}_2^{bd}\,\boldsymbol{T}_j^c$		
$\boldsymbol{A}^{(j)}_{5f,\nabla,\nabla}$	$if^{abc}\,\boldsymbol{\nabla}_1^{ad}\,\boldsymbol{\nabla}_2^{bd}\,\boldsymbol{T}_j^c$		
$\boldsymbol{A}^{(j)}_{5f,\Delta,\nabla}$	$if^{abc}\big(\boldsymbol{\Delta}_1^{ad}\,\boldsymbol{\nabla}_2^{bd} - 1\leftrightarrow 2\big)\boldsymbol{T}_j^c$	$\boldsymbol{A}^{(j)}_{5d,\Delta,\nabla}$	$d^{abc}\big(\boldsymbol{\Delta}_1^{ad}\,\boldsymbol{\nabla}_2^{bd} - 1\leftrightarrow 2\big)\boldsymbol{T}_j^c$
$\boldsymbol{A}^{(j)}_{5f,\Delta,FF}$	$if^{abc}\big(\boldsymbol{\Delta}_1^{ad}\,\{\boldsymbol{F}_2^b,\boldsymbol{F}_2^d\} - 1\leftrightarrow 2\big)\boldsymbol{T}_j^c$	$\boldsymbol{A}^{(j)}_{5d,\Delta,FF}$	$d^{abc}\big(\boldsymbol{\Delta}_1^{ad}\,\{\boldsymbol{F}_2^b,\boldsymbol{F}_2^d\} - 1\leftrightarrow 2\big)\boldsymbol{T}_j^c$
$\boldsymbol{A}^{(j)}_{5f,\Delta,FD}$	$if^{abc}\big(\boldsymbol{\Delta}_1^{ad}\,\{\boldsymbol{F}_2^b,\boldsymbol{D}_2^d\} - 1\leftrightarrow 2\big)\boldsymbol{T}_j^c$	$\boldsymbol{A}^{(j)}_{5d,\Delta,FD}$	$d^{abc}\big(\boldsymbol{\Delta}_1^{ad}\,\{\boldsymbol{F}_2^b,\boldsymbol{D}_2^d\} - 1\leftrightarrow 2\big)\boldsymbol{T}_j^c$
$\boldsymbol{A}^{(j)}_{5f,\nabla,FF}$	$if^{abc}\big(\boldsymbol{\nabla}_1^{ad}\,\{\boldsymbol{F}_2^b,\boldsymbol{F}_2^d\} - 1\leftrightarrow 2\big)\boldsymbol{T}_j^c$	$\boldsymbol{A}^{(j)}_{5d,\nabla,FF}$	$d^{abc}\big(\boldsymbol{\nabla}_1^{ad}\,\{\boldsymbol{F}_2^b,\boldsymbol{F}_2^d\} - 1\leftrightarrow 2\big)\boldsymbol{T}_j^c$
$\boldsymbol{A}^{(j)}_{5f,\nabla,FD}$	$if^{abc}\big(\boldsymbol{\nabla}_1^{ad}\,\{\boldsymbol{F}_2^b,\boldsymbol{D}_2^d\} - 1\leftrightarrow 2\big)\boldsymbol{T}_j^c$	$\boldsymbol{A}^{(j)}_{5d,\nabla,FD}$	$d^{abc}\big(\boldsymbol{\nabla}_1^{ad}\,\{\boldsymbol{F}_2^b,\boldsymbol{D}_2^d\} - 1\leftrightarrow 2\big)\boldsymbol{T}_j^c$

Table 9.2: Possible anti-symmetric color structures featuring $\boldsymbol{T}_j$ for gluon-initiated processes.

contractions with two additional anti-commutators cannot contribute, as they already contain four f- or d-symbols and one can directly simplify

$$\begin{aligned}
f^{ace}f^{bde}\boldsymbol{\Delta}_i^{ab} &= \big\{\boldsymbol{F}_i^c,\boldsymbol{F}_i^d\big\}\,, & f^{ace}f^{bde}\boldsymbol{\nabla}_i^{ab} &= if^{cde}\boldsymbol{F}_i^e\,,\\
d^{ace}d^{bde}\boldsymbol{\Delta}_i^{ab} &= \big\{\boldsymbol{D}_i^c,\boldsymbol{D}_i^d\big\}\,, & d^{ace}d^{bde}\boldsymbol{\nabla}_i^{ab} &= if^{cde}\boldsymbol{F}_i^e - \frac{2}{N_c}\boldsymbol{\nabla}_i^{cd}\,,\\
if^{ace}d^{bde}\boldsymbol{\Delta}_i^{ab} &= if^{cde}\boldsymbol{D}_i^e\,, & if^{ace}d^{bde}\boldsymbol{\nabla}_i^{ab} &= \big\{\boldsymbol{F}_i^c,\boldsymbol{D}_i^d\big\}\,.
\end{aligned} \tag{9.26}$$

Recall that the anti-commutator $\big\{\boldsymbol{D}_i^c,\boldsymbol{D}_i^d\big\}$ can be eliminated by means of (9.24).

Following the argument around (9.20), there are only 22 linearly independent color structures of type I. Thus there exist non-trivial relations between the 26 structures listed in Table 9.2. They read

$$\begin{aligned}
\boldsymbol{A}^{(j)}_{5f,\nabla,FD} &= -\boldsymbol{A}^{(j)}_{4,F,FD}\,,\\
\boldsymbol{A}^{(j)}_{5d,\Delta,FF} &= \boldsymbol{A}^{(j)}_{4,D,FF}\,,\\
\boldsymbol{A}^{(j)}_{5f,\Delta,FD} &= 2\,\boldsymbol{A}^{(j)}_{3f,F,D} + \boldsymbol{A}^{(j)}_{5d,\nabla,FF}\,,
\end{aligned}$$

No contracted indices		Two contracted indices	
$\boldsymbol{S}_0$	$\mathbf{1}$	$\boldsymbol{S}_{2,F,F}$	$\boldsymbol{F}_1 \cdot \boldsymbol{F}_2$
		$\boldsymbol{S}_{2,D,D}$	$\boldsymbol{D}_1 \cdot \boldsymbol{D}_2$
		$\boldsymbol{S}_{2,F,D}$	$\boldsymbol{F}_1 \cdot \boldsymbol{D}_2 + \boldsymbol{F}_2 \cdot \boldsymbol{D}_1$

Four contracted indices			
$\boldsymbol{S}_{4,\Delta,\Delta}$	$\boldsymbol{\Delta}_1^{ab}\,\boldsymbol{\Delta}_2^{ab}$	$\boldsymbol{S}_{4,\Delta,FF}$	$\boldsymbol{\Delta}_1^{ab}\left\{\boldsymbol{F}_2^a,\boldsymbol{F}_2^b\right\} + \boldsymbol{\Delta}_2^{ab}\left\{\boldsymbol{F}_1^a,\boldsymbol{F}_1^b\right\}$
$\boldsymbol{S}_{4,\nabla,\nabla}$	$\boldsymbol{\nabla}_1^{ab}\,\boldsymbol{\nabla}_2^{ab}$	$\boldsymbol{S}_{4,\Delta,FD}$	$\boldsymbol{\Delta}_1^{ab}\left\{\boldsymbol{F}_2^a,\boldsymbol{D}_2^b\right\} + \boldsymbol{\Delta}_2^{ab}\left\{\boldsymbol{F}_1^a,\boldsymbol{D}_1^b\right\}$
		$\boldsymbol{S}_{4,\nabla,FD}$	$\boldsymbol{\nabla}_1^{ab}\left\{\boldsymbol{F}_2^a,\boldsymbol{D}_2^b\right\} + \boldsymbol{\nabla}_2^{ab}\left\{\boldsymbol{F}_1^a,\boldsymbol{D}_1^b\right\}$

Table 9.3: Possible symmetric color structures without $\boldsymbol{T}_j$ for gluon-initiated processes. Even though the individual terms in $\boldsymbol{S}_{4,\nabla,FD}$ are non-zero, they vanish in the symmetric combination (gray).

$$\boldsymbol{A}^{(j)}_{5d,\Delta,FD} = -\frac{8}{N_c}\,\boldsymbol{A}^{(j)}_{2,F} - 4\,\boldsymbol{A}^{(j)}_{3d,F,D} + \boldsymbol{A}^{(j)}_{4,F,FF} - \boldsymbol{A}^{(j)}_{4,D,FD} - \boldsymbol{A}^{(j)}_{5f,\nabla,FF}\,, \tag{9.27}$$

which can be used to reduce the full set to 22 basis structures. With the explicit basis at hand, we construct the isomorphism to the basis (9.20), for example

$$\begin{aligned}
\mathrm{tr}(t^c\,t^{a_1}\,t^{b_1}\,t^{a_2}\,t^{b_2}) - (1 \leftrightarrow 2) \quad &\Leftrightarrow \quad \frac{1}{8}\big(\boldsymbol{A}^{(j)}_{3f,F,F} + \boldsymbol{A}^{(j)}_{3f,D,D} - \boldsymbol{A}^{(j)}_{3f,F,D}\big)\,, \\
\mathrm{tr}(t^c\,t^{a_1}\,t^{b_1})\,\delta^{a_2b_2} - (1 \leftrightarrow 2) \quad &\Leftrightarrow \quad \frac{1}{4}\big(\boldsymbol{A}^{(j)}_{2,D} - \boldsymbol{A}^{(j)}_{2,F}\big)\,,
\end{aligned} \tag{9.28}$$

allowing us to express anti-symmetric linear combinations of traces of fundamental generators in terms of the basis structures listed in Table 9.2.

***S* structures:** Form the second relation in (9.10) it immediately follows that one only needs to consider $\boldsymbol{S}$ structures with up to two f- or d-symbols. There are eight such color structures, listed in Table 9.3, sorted by the number of contracted indices, i.e. by the rank of ζ in (9.18). All other contractions either vanish by symmetry or can be reduced to these, i.e. all possible $\boldsymbol{S}_3$-type structures can directly be reduced to $\boldsymbol{S}_2$ using (9.25). Since the basis of $\boldsymbol{S}$ structures contains only seven elements, as argued around (9.21), one non-trivial relation among the structures in Table 9.3 exist, we find

$$\boldsymbol{S}_{4,\Delta,FD} = 2\,\boldsymbol{S}_{2,F,D}\,. \tag{9.29}$$

Hence, one reduces the full set to seven basis structures. Again, it is possible to construct an isomorphism to the basis (9.21). For example,

$$\begin{aligned}
\mathrm{tr}(t^{a_1}\,t^{b_1}\,t^{a_2}\,t^{b_2}) \quad &\Leftrightarrow \quad \frac{1}{4N_c}\,\boldsymbol{S}_0 + \frac{1}{8}\big(\boldsymbol{S}_{2,F,F} + \boldsymbol{S}_{2,D,D} - \boldsymbol{S}_{2,F,D}\big)\,, \\
\delta^{a_1b_1}\,\delta^{a_2b_2} \quad &\Leftrightarrow \quad \frac{1}{4}\big(\boldsymbol{S}_{4,\Delta,\Delta} + \boldsymbol{S}_{4,\nabla,\nabla}\big)\,,
\end{aligned} \tag{9.30}$$

where both terms on the left-hand side are already symmetric under $1 \leftrightarrow 2$.

Remarkably, this construction yields a finite basis containing $22+7$ color structures for the infinite Glauber series of gluon-initiated processes. In the following, we choose the basis to be [3, 4]

$$
\begin{aligned}
\boldsymbol{X}_1^g &\coloneqq \sum_{j>2} J_j\, \boldsymbol{A}_{3f,F,F}^{(j)}\,, & \boldsymbol{X}_8^g &\coloneqq \frac{1}{N_c}\sum_{j>2} J_j\, \boldsymbol{A}_{2,F}^{(j)}\,, & \boldsymbol{X}_{15}^g &\coloneqq J_{12}\, \boldsymbol{S}_0\,,\\
\boldsymbol{X}_2^g &\coloneqq \sum_{j>2} J_j\, \boldsymbol{A}_{3f,D,D}^{(j)}\,, & \boldsymbol{X}_9^g &\coloneqq \sum_{j>2} J_j\, \boldsymbol{A}_{3d,F,D}^{(j)}\,, & \boldsymbol{X}_{16}^g &\coloneqq \frac{1}{N_c}\, J_{12}\, \boldsymbol{S}_{2,F,F}\,,\\
\boldsymbol{X}_3^g &\coloneqq \frac{1}{N_c}\sum_{j>2} J_j\, \boldsymbol{A}_{4,F,\nabla}^{(j)}\,, & \boldsymbol{X}_{10}^g &\coloneqq \frac{1}{N_c}\sum_{j>2} J_j\, \boldsymbol{A}_{4,F,\Delta}^{(j)}\,, & \boldsymbol{X}_{17}^g &\coloneqq \frac{1}{N_c}\, J_{12}\, \boldsymbol{S}_{2,D,D}\,,\\
\boldsymbol{X}_4^g &\coloneqq \frac{1}{N_c}\sum_{j>2} J_j\, \boldsymbol{A}_{5f,\Delta,\Delta}^{(j)}\,, & \boldsymbol{X}_{11}^g &\coloneqq \frac{1}{N_c^2}\sum_{j>2} J_j\, \boldsymbol{A}_{4,F,FF}^{(j)}\,, & \boldsymbol{X}_{18}^g &\coloneqq \frac{1}{N_c^2}\, J_{12}\, \boldsymbol{S}_{4,\Delta,\Delta}\,,\\
\boldsymbol{X}_5^g &\coloneqq \frac{1}{N_c^2}\sum_{j>2} J_j\, \boldsymbol{A}_{5f,\Delta,FF}^{(j)}\,, & \boldsymbol{X}_{12}^g &\coloneqq \frac{1}{N_c^2}\sum_{j>2} J_j\, \boldsymbol{A}_{4,D,FD}^{(j)}\,, & \boldsymbol{X}_{19}^g &\coloneqq \frac{1}{N_c}\, J_{12}\, \boldsymbol{S}_{4,\Delta,FF}\,,\\
\boldsymbol{X}_6^g &\coloneqq \frac{1}{N_c}\sum_{j>2} J_j\, \boldsymbol{A}_{5f,\nabla,\nabla}^{(j)}\,, & \boldsymbol{X}_{13}^g &\coloneqq \frac{1}{N_c}\sum_{j>2} J_j\, \boldsymbol{A}_{5f,\Delta,\nabla}^{(j)}\,, & \boldsymbol{X}_{20}^g &\coloneqq \frac{1}{N_c^2}\, J_{12}\, \boldsymbol{S}_{4,\nabla,\nabla}\,,\\
\boldsymbol{X}_7^g &\coloneqq \frac{1}{N_c^2}\sum_{j>2} J_j\, \boldsymbol{A}_{5d,\nabla,FD}^{(j)}\,, & \boldsymbol{X}_{14}^g &\coloneqq \frac{1}{N_c^2}\sum_{j>2} J_j\, \boldsymbol{A}_{5f,\nabla,FF}^{(j)}\,,
\end{aligned}
\tag{9.31}
$$

using (9.27) and (9.29). Ordering the the basis structures in this way and not assigning a label to the remaining $8+1$ structures turns out to be convenient. The factors $1/N_c$ are chosen such that the traces $\langle \boldsymbol{\mathcal{H}}_{2\to M}\, \boldsymbol{X}_i^g \rangle$ are at most of $\mathcal{O}(1)$ in the large-N_c expansion for the processes considered in Section 8.4. Mapping the eleven structures describing the SLLs to this basis, we find

$$
\begin{aligned}
\boldsymbol{X}_1 &= \boldsymbol{X}_1^g\,, & \boldsymbol{X}_6 &= -\frac{4}{N_c^2}\,\boldsymbol{X}_{15}^g - \frac{1}{2}\,\boldsymbol{X}_{17}^g - \frac{1}{2N_c^2}\,\boldsymbol{X}_{19}^g\,,\\
\boldsymbol{X}_2 &= 2\,\boldsymbol{X}_8^g + \frac{1}{2}\,\boldsymbol{X}_9^g + \boldsymbol{X}_{10}^g\,, & \boldsymbol{X}_7 &= \boldsymbol{X}_{17}^g\,,\\
\boldsymbol{X}_3 &= -\boldsymbol{X}_9^g\,, & \boldsymbol{X}_8 &= \frac{N_c^2-4}{3N_c^2}\,\boldsymbol{X}_{16}^g\,,\\
\boldsymbol{X}_4 &= -\boldsymbol{X}_{11}^g\,, & \boldsymbol{X}_9 &= \frac{4}{N_c^2}\,\boldsymbol{X}_{15}^g + \boldsymbol{X}_{17}^g + \boldsymbol{X}_{18}^g\,,\\
\boldsymbol{X}_5 &= -2\,\boldsymbol{X}_8^g\,, & \boldsymbol{X}_{10} &= \boldsymbol{X}_{16}^g\,,\\
& & \boldsymbol{X}_{11} &= \boldsymbol{X}_{15}^g\,.
\end{aligned}
\tag{9.32}
$$

In contrast to the case of quark-initiated processes not all basis structures are relevant for the SLLs. Clearly, the consistency relations (8.49) are fulfilled in this case and all the super-leading terms in N_c cancel for gluon-initiated processes.

9.1.3 Quark-Gluon-Initiated Processes

The third scenario relevant for QCD are processes initiated by one (anti-)quark and one gluon. Without loss of generality, we assume parton 1 to be the (anti-)quark, i.e.

$$\boldsymbol{T}_1^a = \boldsymbol{t}_1^a \qquad \text{and} \qquad \boldsymbol{T}_2^a = \boldsymbol{F}_2^a \,. \tag{9.33}$$

By making this choice, it is no longer possible to restrict the form of color structures by symmetry arguments under the exchange of parton 1 and 2. The color-space-matrix part of the generic color structures (9.6) thus only is

$$\begin{aligned} &\text{type I:} \quad \boldsymbol{O}^{(j)} \coloneqq \zeta\, \boldsymbol{\mathcal{C}}_1\, \widetilde{\boldsymbol{\mathcal{C}}}_2\, \boldsymbol{T}_j \,, \\ &\text{type II:} \quad \boldsymbol{O} \coloneqq \zeta\, \boldsymbol{\mathcal{C}}_1\, \widetilde{\boldsymbol{\mathcal{C}}}_2 \,. \end{aligned} \tag{9.34}$$

Employing (9.12) for parton 1, it is obvious that $\boldsymbol{\mathcal{C}}_1 \in \{\boldsymbol{1}_1\,, \boldsymbol{t}_1\}$. Distinguishing the case $\boldsymbol{\mathcal{C}}_1 = \boldsymbol{1}_1$ and $\boldsymbol{\mathcal{C}}_1^a = \boldsymbol{t}_1^a$ for both types of color structures, the tensors

$$\begin{aligned} &\text{type I:} \quad \big\langle a_2 \big| \zeta\, \widetilde{\boldsymbol{\mathcal{C}}}_2 \big| b_2, c \big\rangle \quad \text{and} \quad \big\langle a_2 \big| \zeta\, \widetilde{\boldsymbol{\mathcal{C}}}_2 \big| b_2, a, c \big\rangle \,, \\ &\text{type II:} \quad \big\langle a_2 \big| \zeta\, \widetilde{\boldsymbol{\mathcal{C}}}_2 \big| b_2 \big\rangle \quad \text{and} \quad \big\langle a_2 \big| \zeta\, \widetilde{\boldsymbol{\mathcal{C}}}_2 \big| b_2, a \big\rangle \,, \end{aligned} \tag{9.35}$$

have between two and four open adjoint indices. Similar to the gluonic case, we factor off $\boldsymbol{T}_j^c$ for the first type. A possible basis for the tensors of type I are linear combinations of permutations of

$$\mathrm{tr}(t^c\, t^{a_2}\, t^{b_2}) \quad \text{and} \quad \mathrm{tr}(t^c\, t^a\, t^{a_2}\, t^{b_2})\,,\, \delta^{ca}\, \delta^{a_2 b_2} \,, \tag{9.36}$$

for $\boldsymbol{\mathcal{C}}_1 = \boldsymbol{1}_1$ and $\boldsymbol{\mathcal{C}}_1^a = \boldsymbol{t}_1^a$, respectively. In total, there are $2! + 3! + \frac{1}{2}\binom{4}{2} = 11$ basis structures $\boldsymbol{O}^{(j)}$. For tensors of type II, the possible basis consists of the three elements

$$\delta^{a_2 b_2} \quad \text{and} \quad \mathrm{tr}(t^a\, t^{a_2}\, t^{b_2})\,,\, \mathrm{tr}(t^a\, t^{b_2}\, t^{a_2}) \,, \tag{9.37}$$

which combined with $\boldsymbol{1}_1$ and $\boldsymbol{t}_1^a$, respectively, yield 3 basis structures $\boldsymbol{S}$.

Again, the structures (9.36) and (9.37) are not suited to be used within the color-space formalism and are therefore mapped onto objects that naturally appear in this context. The obvious choices for $\boldsymbol{\mathcal{C}}_1$ are $\boldsymbol{1}_1$ and $\boldsymbol{t}_1^a$. For the color structure $\widetilde{\boldsymbol{\mathcal{C}}}_2$ of parton 2, we choose the same objects as in Section 9.1.2. Combining them to $\boldsymbol{O}^{(j)}$ and $\boldsymbol{O}$ color structures results in $11 + 3$ structures, listed in Table 9.4. For each d-symbol one includes a factor σ_1 (recall that $\sigma_1^2 = 1$), thus allowing for a simultaneous treatment of parton 1 being a quark or an anti-quark. By the same arguments as given in the previous section, no additional color structures are necessary. Therefore, the 14 color structures [3, 4]

$$\begin{aligned} \boldsymbol{X}_1^{qg} &\coloneqq \sum_{j>2} J_j\, \boldsymbol{O}_{3f,F}^{(j)} \,, & \boldsymbol{X}_4^{qg} &\coloneqq \frac{1}{N_c} \sum_{j>2} J_j\, \boldsymbol{O}_{2,F}^{(j)} \,, & \boldsymbol{X}_{12}^{qg} &\coloneqq J_{12}\, \boldsymbol{O}_0 \,, \\ \boldsymbol{X}_2^{qg} &\coloneqq \sum_{j>2} J_j\, \boldsymbol{O}_{3f,D}^{(j)} \,, & \boldsymbol{X}_5^{qg} &\coloneqq \frac{1}{N_c} \sum_{j>2} J_j\, \boldsymbol{O}_{2,T}^{(j)} \,, & \boldsymbol{X}_{13}^{qg} &\coloneqq \frac{1}{N_c}\, J_{12}\, \boldsymbol{O}_{2,F} \,, \end{aligned}$$

Two contracted indices		Three contracted indices		Four contracted indices	
$\boldsymbol{O}_{2,F}^{(j)}$	$\boldsymbol{F}_2 \cdot \boldsymbol{T}_j$	$\boldsymbol{O}_{3f,F}^{(j)}$	$if^{abc}\,\boldsymbol{t}_1^a\,\boldsymbol{F}_2^b\,\boldsymbol{T}_j^c$	$\boldsymbol{O}_{4,\Delta}^{(j)}$	$\boldsymbol{t}_1^a\,\boldsymbol{\Delta}_2^{ab}\,\boldsymbol{T}_j^b$
$\boldsymbol{O}_{2,D}^{(j)}$	$\sigma_1\,\boldsymbol{D}_2 \cdot \boldsymbol{T}_j$	$\boldsymbol{O}_{3f,D}^{(j)}$	$\sigma_1\,if^{abc}\,\boldsymbol{t}_1^a\,\boldsymbol{D}_2^b\,\boldsymbol{T}_j^c$	$\boldsymbol{O}_{4,\nabla}^{(j)}$	$\boldsymbol{t}_1^a\,\boldsymbol{\nabla}_2^{ab}\,\boldsymbol{T}_j^b$
$\boldsymbol{O}_{2,t}^{(j)}$	$\boldsymbol{t}_1 \cdot \boldsymbol{T}_j$	$\boldsymbol{O}_{3d,F}^{(j)}$	$\sigma_1\,d^{abc}\,\boldsymbol{t}_1^a\,\boldsymbol{F}_2^b\,\boldsymbol{T}_j^c$	$\boldsymbol{O}_{4,FF}^{(j)}$	$\boldsymbol{t}_1^a\,\{\boldsymbol{F}_2^a, \boldsymbol{F}_2^b\}\,\boldsymbol{T}_j^b$
		$\boldsymbol{O}_{3d,D}^{(j)}$	$d^{abc}\,\boldsymbol{t}_1^a\,\boldsymbol{D}_2^b\,\boldsymbol{T}_j^c$	$\boldsymbol{O}_{4,FD}^{(j)}$	$\sigma_1\,\boldsymbol{t}_1^a\,\{\boldsymbol{F}_2^a, \boldsymbol{D}_2^b\}\,\boldsymbol{T}_j^b$

No contracted indices		Two contracted indices	
$\boldsymbol{O}_0$	$\mathbf{1}$	$\boldsymbol{O}_{2,F}$	$\boldsymbol{t}_1 \cdot \boldsymbol{F}_2$
		$\boldsymbol{O}_{2,D}$	$\sigma_1\,\boldsymbol{t}_1 \cdot \boldsymbol{D}_2$

Table 9.4: Possible color structures with and without $\boldsymbol{T}_j$ for quark-gluon-initiated processes.

$$
\begin{aligned}
\boldsymbol{X}_3^{qg} &\coloneqq \frac{1}{N_c}\sum_{j>2} J_j\,\boldsymbol{O}_{4,\nabla}^{(j)}\,, & \boldsymbol{X}_6^{qg} &\coloneqq \sum_{j>2} J_j\,\boldsymbol{O}_{3d,F}^{(j)}\,, & \boldsymbol{X}_{14}^{qg} &\coloneqq \frac{1}{N_c}\,J_{12}\,\boldsymbol{O}_{2,D}\,,\\
& & \boldsymbol{X}_7^{qg} &\coloneqq \sum_{j>2} J_j\,\boldsymbol{O}_{3d,D}^{(j)}\,, & & \\
& & \boldsymbol{X}_8^{qg} &\coloneqq \frac{1}{N_c}\sum_{j>2} J_j\,\boldsymbol{O}_{4,\Delta}^{(j)}\,, & & \\
& & \boldsymbol{X}_9^{qg} &\coloneqq \frac{1}{N_c^2}\sum_{j>2} J_j\,\boldsymbol{O}_{4,FF}^{(j)}\,, & & \\
& & \boldsymbol{X}_{10}^{qg} &\coloneqq \frac{1}{N_c}\sum_{j>2} J_j\,\boldsymbol{O}_{2,D}^{(j)}\,, & & \\
& & \boldsymbol{X}_{11}^{qg} &\coloneqq \frac{1}{N_c^2}\sum_{j>2} J_j\,\boldsymbol{O}_{4,FD}^{(j)}\,, & & \qquad (9.38)
\end{aligned}
$$

are linearly independent and constitute a basis for the color algebra of (anti-)quark-gluon-initiated processes relevant for the Glauber series. The factors $1/N_c$ normalize the traces $\langle \boldsymbol{\mathcal{H}}_{2\to M}\,\boldsymbol{X}_i^{qg}\rangle$ to be at most of $\mathcal{O}(1)$ for all processes studied in Section 8.4. Restricting parton 1 to be a (anti-)quark and parton 2 to be a gluon, one can translate the SLL color structures to the above basis. We find

$$
\begin{aligned}
\boldsymbol{X}_1 &= \boldsymbol{X}_1^{qg}\,, & \boldsymbol{X}_6 &= \frac{2}{N_c^2}\,\boldsymbol{X}_{12}^{qg} + \frac{1}{2}\,\boldsymbol{X}_{14}^{qg}\,,\\
\boldsymbol{X}_2 &= \boldsymbol{X}_4^{qg} + 2\,\boldsymbol{X}_5^{qg} + \frac{1}{2}\,(\boldsymbol{X}_6^{qg} + \boldsymbol{X}_7^{qg}) + \boldsymbol{X}_8^{qg}\,, & \boldsymbol{X}_7 &= -\frac{N_c^2-4}{N_c^2}\,\boldsymbol{X}_{14}^{qg}\,,\\
\boldsymbol{X}_3 &= -\frac{N_c^2-4}{N_c^2}\,\boldsymbol{X}_6^{qg} - \boldsymbol{X}_7^{qg}\,, & \boldsymbol{X}_8 &= \frac{(N_c^2-4)(N_c^2-3)}{3N_c^4}\,\boldsymbol{X}_{13}^{qg}\,,
\end{aligned}
$$

$$\boldsymbol{X}_4 = -\frac{1}{N_c^2}\left(\boldsymbol{X}_4^{qg} + \boldsymbol{X}_6^{qg}\right) - \boldsymbol{X}_9^{qg}\,, \qquad \boldsymbol{X}_9 = -\frac{2}{N_c^2}\,\boldsymbol{X}_{12}^{qg} - \boldsymbol{X}_{14}^{qg}\,,$$
$$\boldsymbol{X}_5 = 2\left(\boldsymbol{X}_4^{qg} - \boldsymbol{X}_5^{qg}\right), \qquad \boldsymbol{X}_{10} = \boldsymbol{X}_{13}^{qg}\,,$$
$$\boldsymbol{X}_{11} = \boldsymbol{X}_{12}^{qg}\,, \tag{9.39}$$

where we used that $C_1 = C_F$ and $C_2 = C_A$. Similar to quark- and gluon-initiated processes, the consistency relations (8.49) are fulfilled and the super-leading terms in N_c also cancel for processes with one quark and one gluon in the initial state.

9.2 All-Order Structure

The all-order structure of the Glauber series can be obtained by expanding the path-ordered exponential in (9.3). Similar to the SLLs, we find that the relevant color trace is

$$C^l_{\{\underline{r}\}} \coloneqq \left\langle \boldsymbol{\mathcal{H}}_{2\to M}\,(\boldsymbol{\Gamma}^c)^{r_1}\,\boldsymbol{V}^G\,\ldots\,(\boldsymbol{\Gamma}^c)^{r_l}\,\boldsymbol{V}^G\,\overline{\boldsymbol{\Gamma}}\otimes\boldsymbol{1}\right\rangle, \tag{9.40}$$

where in total $n \coloneqq \sum_{i=1}^{l} r_i$ cusp anomalous dimensions $\boldsymbol{\Gamma}^c$ and l Glauber operators $\boldsymbol{V}^G$ are inserted. This color trace appears together with the iterated scale integrals

$$\begin{aligned} I^l_{\{\underline{r}\}}(\mu_h,\mu_s) \coloneqq \int_{\mu_s}^{\mu_h}\frac{d\mu_1}{\mu_1}\int_{\mu_s}^{\mu_1}\frac{d\mu_2}{\mu_2}\cdots\int_{\mu_s}^{\mu_{n+l}}\frac{d\mu_{n+l+1}}{\mu_{n+l+1}}\,\gamma_{\text{cusp}}\big(\alpha_s(\mu_1)\big)\,\ln\frac{\mu_1^2}{\mu_h^2}\,\ldots \\ \ldots\gamma_{\text{cusp}}\big(\alpha_s(\mu_{r_1})\big)\,\ln\frac{\mu_{r_1}^2}{\mu_h^2}\,\gamma_{\text{cusp}}\big(\alpha_s(\mu_{r_1+1})\big)\,\gamma_{\text{cusp}}\big(\alpha_s(\mu_{r_1+2})\big)\,\ln\frac{\mu_{r_1+2}^2}{\mu_h^2}\ldots \\ \ldots\gamma_{\text{cusp}}\big(\alpha_s(\mu_{n+l-1})\big)\,\ln\frac{\mu_{n+l-1}^2}{\mu_h^2}\,\gamma_{\text{cusp}}\big(\alpha_s(\mu_{n+l})\big)\,\frac{\alpha_s(\mu_{n+l+1})}{4\pi}\,. \end{aligned} \tag{9.41}$$

The integrals over μ_1 to μ_{r_1} and μ_{r_1+2} to $\mu_{r_1+r_2+1}$ of this expression result from the r_1 and r_2 insertions of $\boldsymbol{\Gamma}^c$ in (9.40) and so on. To calculate the contribution of the Glauber series to the partonic cross section, one would need to resum infinitely many infinite sums

$$\hat{\sigma}^{\text{SLL+G}}_{2\to M}(Q_0) = \sum_{l=1}^{\infty}\sum_{r_1=0}^{\infty}\cdots\sum_{r_l=0}^{\infty} I^l_{\{\underline{r}\}}(\mu_h,\mu_s)\,C^l_{\{\underline{r}\}}\,. \tag{9.42}$$

We avoid this problem in Section 9.3 by organizing the Glauber series in a more convenient way.

The scale integrals associated with the Glauber series can be evaluated in closed form when working with a fixed coupling $\alpha_s = \alpha_s(\bar{\mu})$ with reference scale $\bar{\mu}$. One finds [2]

$$\begin{aligned} I^l_{\{\underline{r}\}}(\mu_h,\mu_s)\Big|_{\text{fixed}} = \frac{\alpha_s}{4\pi}\,\gamma^{n+l}_{\text{cusp}}(\alpha_s)\,\frac{(-2)^n}{(2n+l+1)(2n+l)}\,L_s^{2n+l+1} \\ \times\prod_{k=1}^{l}\frac{(2\sum_{i=1}^{k-1}r_i+k-3)!!}{(2\sum_{i=1}^{k}r_i+k-1)!!}\,, \end{aligned} \tag{9.43}$$

where we define $(-2)!! \coloneqq (-1)!! \coloneqq 1$. For $l = 2$ this reduces to (8.58) for the SLLs. To show this, we change variables in (9.41) to $L_i = \ln(\mu_h/\mu_i)$ and invert the order of integration

$$\begin{aligned} I^l_{\{\underline{r}\}}(\mu_h,\mu_s)\Big|_{\text{fixed}} = \frac{\alpha_s}{4\pi}\,\gamma^{n+l}_{\text{cusp}}(\alpha_s)\,(-2)^n \int_0^{L_s} dL_{n+l+1}\cdots\int_0^{L_3} dL_2 \int_0^{L_2} dL_1 \\ \times \left(\prod_{i=1}^{r_1} L_i\right)\left(\prod_{i=r_1+2}^{r_1+r_2+1} L_i\right)\ldots\left(\prod_{i=r_1+\cdots+r_{l-1}+l}^{n+l-1} L_i\right). \end{aligned} \tag{9.44}$$

Concentrating on the integrals and performing the ones with the explicit logarithms yields

$$\prod_{i=1}^{l}\frac{1}{(2r_i)!!}\int_0^{L_s} dL_{l+1}\int_0^{L_{l+1}} dL_l\cdots\int_0^{L_2} dL_1\left(L_l^2-L_{l-1}^2\right)^{r_l}\ldots\left(L_2^2-L_1^2\right)^{r_2}L_1^{2r_1}, \tag{9.45}$$

where the integrals over L_i with $1 \le i \le l$ originate from the Glauber operators and the one over L_{l+1} from $\overline{\mathbf{\Gamma}}$. To solve these, we observe that for $k \le l$

$$\begin{aligned} &\int_0^{L_k} dL_{k-1}\left(L_k^2-L_{k-1}^2\right)^{r_k}\left(L_{k-1}\right)^{2\sum_{i=1}^{k-1}r_i+k-2} \\ &= (2r_k)!!\,\frac{\left(2\sum_{i=1}^{k-1}r_i+k-3\right)!!}{\left(2\sum_{i=1}^{k}r_i+k-1\right)!!}\left(L_k\right)^{2\sum_{i=1}^{k}r_i+k-1}. \end{aligned} \tag{9.46}$$

The integral over L_{k-1} thus increases the value of k in the exponent by one and leads to the prefactor. For $k = 1$ the second line is just $L_1^{2r_1}$ and we find

$$\begin{aligned} &\prod_{k=1}^{l}\frac{\left(2\sum_{i=1}^{k-1}r_i+k-3\right)!!}{\left(2\sum_{i=1}^{k}r_i+k-1\right)!!}\int_0^{L_s} dL_{l+1}\int_0^{L_{l+1}} dL_l\,L_l^{2n+l-1} \\ &= \frac{L_s^{2n+l+1}}{(2n+l+1)(2n+l)}\prod_{k=1}^{l}\frac{\left(2\sum_{i=1}^{k-1}r_i+k-3\right)!!}{\left(2\sum_{i=1}^{k}r_i+k-1\right)!!}. \end{aligned} \tag{9.47}$$

As we were not able to obtain a closed form expression for the iterated scale integrals with running coupling in the SLL case, there is no hope to achieve this for the Glauber series. Of course, one can calculate the integrals for l given values of r_i. However, this does not lead to any new insights and we spare the work.

Considering next the color trace (9.40), we can use the results from Section 8.1.1 and find for $l = 1$

$$C^1_{r_1} = 16i\pi\,N_c^{r_1}\left\langle \boldsymbol{\mathcal{H}}_{2\to M}\,\boldsymbol{X}_1\otimes\mathbf{1}\right\rangle. \tag{9.48}$$

As described above, the hard function $\boldsymbol{\mathcal{H}}_{2\to M}$ needs to contain a phase to yield a real-valued contribution. The result for the SLLs ($l = 2$) is given in (8.42) with $r = r_1$.

With the color bases from Section 9.1 at hand, the reduction of the color traces for higher l is now straightforward. One first computes the action of $\mathbf{\Gamma}^c$, according to (8.31) and (8.36) for basis structures with and without final-state generator, respectively, and $\boldsymbol{V}^G$, according to (8.27), on all basis structures and then expresses the reduced color traces as linear combinations of the basis structures with coefficients depending on l and $\{\underline{r}\}$.

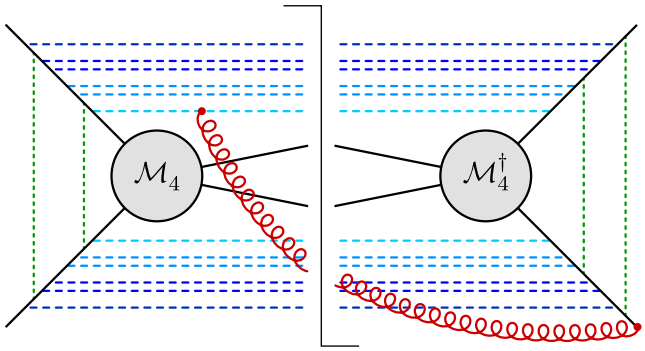

Figure 9.1: Example diagram for partonic $2 \to 2$ scattering giving rise to color structures with angular integral J_{12}. The colors have the same meaning as in Figure 8.2 but here four Glauber gluons are exchanged. Attachments to the later emissions (darker blue colors) do not contribute, as $\boldsymbol{V}^G$ maps color structures without final-state generators to zero.

9.2.1 Quark-Initiated Processes

Similar to (8.37) for the SLLs, it is convenient to define the matrix representations

$$\begin{aligned}\left\langle \boldsymbol{\mathcal{H}}\, \boldsymbol{\Gamma}^c \boldsymbol{X}_i^q \otimes \mathbf{1} \right\rangle &=: \sum_{\tilde{\imath}} \left\langle \boldsymbol{\mathcal{H}}\, \boldsymbol{X}_{\tilde{\imath}}^q \otimes \mathbf{1} \right\rangle N_c \left(\mathbb{\Gamma}^c\right)_{\tilde{\imath}i}\,, \\ \left\langle \boldsymbol{\mathcal{H}}\, \boldsymbol{V}^G \boldsymbol{X}_i^q \otimes \mathbf{1} \right\rangle &=: \sum_{\tilde{\imath}} \left\langle \boldsymbol{\mathcal{H}}\, \boldsymbol{X}_{\tilde{\imath}}^q \otimes \mathbf{1} \right\rangle i\pi N_c \left(\mathbb{V}^G\right)_{\tilde{\imath}i}\,,\end{aligned} \tag{9.49}$$

of cusp anomalous dimension and Glauber operator in the basis $\boldsymbol{X}^q := (\boldsymbol{X}_1^q, \dots, \boldsymbol{X}_5^q)$ for quark-initiated processes. Recall that the implicit sum over $j > 2$ is different between left- and right-hand side in the first equation as explained below (8.22). The explicit forms of these matrices read [2]

$$\mathbb{\Gamma}^c = \begin{pmatrix} 1 & 0 & 0 & 0 & 0 \\ 0 & 1 & 0 & 0 & 0 \\ 0 & 0 & \frac{1}{2} & 0 & 0 \\ 0 & 0 & -1 & 1 & 0 \\ 0 & 0 & -\frac{C_F}{N_c} & 0 & 0 \end{pmatrix}, \qquad \mathbb{V}^G = \begin{pmatrix} 0 & -2\delta_{q\bar{q}}\,\frac{N_c^2-4}{N_c^2} & \frac{4}{N_c^2} & 0 & 0 \\ -\frac{1}{2} & 0 & 0 & 0 & 0 \\ 1 & 0 & 0 & 0 & 0 \\ 0 & 0 & 0 & 0 & 0 \\ 0 & 0 & 0 & 0 & 0 \end{pmatrix}, \tag{9.50}$$

where $\delta_{q\bar{q}} := \frac{1}{4}(\sigma_1 - \sigma_2)^2$ equals 1 for the $q\bar{q}$ initial states, and 0 for qq or $\bar{q}\bar{q}$ initial states. The off-diagonal structure of $\mathbb{V}^G$ implies that different color structures contribute for even and odd values of l. Furthermore, the last two rows/columns are zero, i.e. the Glauber operator maps color structure without final-state generator to zero, reflecting that the soft gluon can only attach to the earliest collinear emission, see Figure 9.1.

Concluding from (8.18) that for quark-initiated processes

$$\left\langle \boldsymbol{\mathcal{H}}\, \boldsymbol{V}^G \overline{\boldsymbol{\Gamma}} \otimes \mathbf{1} \right\rangle = 16 i\pi \left\langle \boldsymbol{\mathcal{H}}\, \boldsymbol{X}_1^q \otimes \mathbf{1} \right\rangle = 16 i\pi \left\langle \boldsymbol{\mathcal{H}}\, \boldsymbol{X}^q \otimes \mathbf{1} \right\rangle \varsigma\,, \tag{9.51}$$

where $\varsigma := (1,0,0,0,0)^T$, the Glauber series can be studied completely in the color basis. We find for the color trace (9.40)

$$C_{\{\underline{r}\}}^l = 16\,(i\pi)^l\, N_c^{n+l-1} \left\langle \boldsymbol{\mathcal{H}}_{2\to M}\, \boldsymbol{X}^q \otimes \mathbf{1} \right\rangle \left[(\mathbb{\Gamma}^c)^{r_1}\, \mathbb{V}^G \, \dots \, (\mathbb{\Gamma}^c)^{r_{l-1}}\, \mathbb{V}^G\, (\mathbb{\Gamma}^c)^{r_l} \right] \varsigma\,. \tag{9.52}$$

The coefficients can be simplified as ς is an eigenvector of $\mathbb{\Gamma}^c$ with eigenvalue $v_2 = 1$ and as

$$\mathbb{V}^G \left(\mathbb{\Gamma}^c\right)^r \mathbb{V}^G \varsigma = \left[K_{12}\, v_2^r + \frac{4}{N_c^2}\, v_1^r\right] \varsigma \tag{9.53}$$

with $v_1 = \frac{1}{2}$ and

$$K_{12} \coloneqq (\sigma_1 - \sigma_2)^2\, \frac{N_c^2 - 4}{4N_c^2} = \frac{N_c^2 - 4}{N_c^2}\, \delta_{q\bar{q}}\,. \tag{9.54}$$

For even $l = 2\ell$, the color trace with simplified coefficients reads [2]

$$\begin{aligned} C_{\{\underline{r}\}}^{2\ell} = {} & \frac{16}{N_c} (-\pi^2)^\ell\, N_c^{n+2\ell} \prod_{i=2}^{\ell} \left[K_{12} + \frac{4}{N_c^2}\, v_1^{r_{2i-1}}\right] \\ & \times \Big[-\frac{v_2^{r_1}}{2} \left\langle \boldsymbol{\mathcal{H}}_{2\to M}\, \boldsymbol{X}_2^q \otimes \mathbf{1}\right\rangle + v_1^{r_1} \left\langle \boldsymbol{\mathcal{H}}_{2\to M}\, \boldsymbol{X}_3^q \otimes \mathbf{1}\right\rangle \\ & + 2\big(v_1^{r_1} - v_2^{r_1}\big) \left\langle \boldsymbol{\mathcal{H}}_{2\to M}\, \boldsymbol{X}_4^q \otimes \mathbf{1}\right\rangle + \frac{2C_F}{N_c} \big(v_0^{r_1} - v_1^{r_1}\big) \left\langle \boldsymbol{\mathcal{H}}_{2\to M}\, \boldsymbol{X}_5^q \otimes \mathbf{1}\right\rangle \Big]\,. \end{aligned} \tag{9.55}$$

Surprisingly, we recover the result (9.16) for the SLLs up to an additional prefactor. If $\delta_{q\bar{q}} = 0$, i.e. for qq or $\bar{q}\bar{q}$ scattering, this prefactor is suppressed in the large-N_c limit and, therefore, also the higher Glauber-operator insertions are suppressed in this limit. In contrast, for $q\bar{q}$ scattering this is not the case. Combining (9.55) with the iterated scale integrals (9.43) of the Glauber series, one obtains the contribution to the partonic cross section as series in w and w_π. However, deriving numerical predictions from this result is complicated as one needs to perform multiple infinite sums. For completeness, we mention that for odd $l = 2\ell - 1$ the color trace is

$$C_{\{\underline{r}\}}^{2\ell-1} = \frac{16i\pi}{N_c} (-\pi^2)^{\ell-1}\, N_c^{n+2\ell-1} \prod_{i=2}^{\ell} \left[K_{12} + \frac{4}{N_c^2}\, v_1^{r_{2i}}\right] \left\langle \boldsymbol{\mathcal{H}}_{2\to M}\, \boldsymbol{X}_1^q \otimes \mathbf{1}\right\rangle \tag{9.56}$$

which is just the result (9.48) for $l = 1$ with the same prefactor as for even l values. We note that in both cases the Glauber series is alternating in l. This statement also holds for gluon- and quark-gluon-initiated processes, as we show below.

9.2.2 Gluon-Initiated Processes

Table 9.5 summarizes how the basis structures constructed in Section 9.1 are related under the mapping of Glauber operators and cusp anomalous dimensions for gluon-initiated processes. Obviously, the basis structures in $\boldsymbol{X}^g \coloneqq (\boldsymbol{X}_1^g, \ldots, \boldsymbol{X}_{20}^g)$ are ordered such that the first seven structures emerge from an odd number of $\boldsymbol{V}^G$ insertions, see fifth column, and the remaining 14 from an even number, see fourth column.[1] Applying further insertions of $\boldsymbol{V}^G$ does not create new color structures. Besides these 20 basis structures there are nine structures which are not generated by the operators $\boldsymbol{V}^G$ and $\boldsymbol{\Gamma}^c$ in the color trace (shown in the right portion of the table). The reason is that for the gluon case the initial structure in (8.18) contains three f-symbols, and $\boldsymbol{V}^G$ as well

[1] Note that the operators from the first three columns are included in the fourth and fifth one as well.

$\boldsymbol{V}^G\,\overline{\boldsymbol{\Gamma}}$	$(\boldsymbol{V}^G)^2\,\overline{\boldsymbol{\Gamma}}$	$(\boldsymbol{V}^G)^3\,\overline{\boldsymbol{\Gamma}}$	$(\boldsymbol{V}^G)^4\,\overline{\boldsymbol{\Gamma}}$	$(\boldsymbol{V}^G)^5\,\overline{\boldsymbol{\Gamma}}$	never appear	
$\boldsymbol{X}_1^g$	$\boldsymbol{X}_8^g$	$\boldsymbol{X}_1^g$	$\boldsymbol{X}_8^g$	$\boldsymbol{X}_1^g$	$\boldsymbol{A}_{3f,F,D}^{(j)}$	$\boldsymbol{A}_{2,D}^{(j)}$
	$\boldsymbol{X}_9^g$	$\boldsymbol{X}_2^g$	$\boldsymbol{X}_9^g$	$\boldsymbol{X}_2^g$	$\boldsymbol{A}_{4,D,\nabla}^{(j)}$	$\boldsymbol{A}_{4,D,\Delta}^{(j)}$
	$\boldsymbol{X}_{10}^g$	$\boldsymbol{X}_3^g$	$\boldsymbol{X}_{10}^g$	$\boldsymbol{X}_3^g$	$\boldsymbol{A}_{5d,\Delta,\nabla}^{(j)}$	$\boldsymbol{A}_{4,D,FF}^{(j)}$
	$\boldsymbol{X}_{11}^g$	$\boldsymbol{X}_4^g$	$\boldsymbol{X}_{11}^g$	$\boldsymbol{X}_4^g$	$\boldsymbol{A}_{5d,\nabla,FF}^{(j)}$	$\boldsymbol{A}_{4,F,FD}^{(j)}$
		$\boldsymbol{X}_5^g$	$\boldsymbol{X}_{12}^g$	$\boldsymbol{X}_5^g$		
			$\boldsymbol{X}_{13}^g$	$\boldsymbol{X}_6^g$		
			$\boldsymbol{X}_{14}^g$	$\boldsymbol{X}_7^g$		
	$\boldsymbol{X}_{15}^g$		$\boldsymbol{X}_{15}^g$			$\boldsymbol{S}_{2,F,D}$
	$\boldsymbol{X}_{16}^g$		$\boldsymbol{X}_{16}^g$			
	$\boldsymbol{X}_{17}^g$		$\boldsymbol{X}_{17}^g$			
	$\boldsymbol{X}_{18}^g$		$\boldsymbol{X}_{18}^g$			
	$\boldsymbol{X}_{19}^g$		$\boldsymbol{X}_{19}^g$			
			$\boldsymbol{X}_{20}^g$			
$1+0$	$4+5$	$5+0$	$7+6$	$7+0$	$4+0$	$4+1$

Table 9.5: Color basis for gluon-initiated processes. The different columns list the basis structures appearing after given number of $\boldsymbol{V}^G$ insertions. Structures appearing for the first time are indicated in black, whereas structures that have appeared already before are indicated in gray. For a given number of Glauber operators, application of $\boldsymbol{\Gamma}^c$ does not create new structures containing $\boldsymbol{T}_j$ but does create the structures without $\boldsymbol{T}_j$ shown in the lower half. The one exception from this rule is $\boldsymbol{X}_{11}^g$, which only appears after applying $\boldsymbol{\Gamma}^c$ to $(\boldsymbol{V}^G)^2\,\overline{\boldsymbol{\Gamma}}$. The two last columns list $8+1$ basis structures that never appear starting out from (8.18).

as $\boldsymbol{\Gamma}^c$ contain two. Therefore, all structures with $\boldsymbol{T}_j$ can only contain an odd number of f-symbols, corresponding to the 14 operators listed in the left portion of Table 9.5. On the contrary, for the basis structure without final-state generator, $\boldsymbol{T}_j$ is replaced by an f-symbol, see (8.22), and consequently they must contain an even number.

Similar to (9.49) for quark-initiated processes, one can define matrix representations of the Glauber operator and the cusp anomalous dimension in the *physical*[2] basis $\boldsymbol{X}^g$. These 20×20 matrices can be decomposed as

$$\mathbb{I}^c = \begin{pmatrix} \tilde{\gamma}^{(j)} & 0_{7\times 7} & 0_{7\times 6} \\ 0_{7\times 7} & \gamma^{(j)} & 0_{7\times 6} \\ 0_{6\times 7} & \lambda & \gamma \end{pmatrix}, \qquad \mathbb{V}^G = \begin{pmatrix} 0_{7\times 7} & \tilde{\nu}^{(j)} & 0_{7\times 6} \\ \nu^{(j)} & 0_{7\times 7} & 0_{7\times 6} \\ 0_{6\times 7} & 0_{6\times 7} & 0_{6\times 6} \end{pmatrix}. \tag{9.57}$$

The simple form of $\mathbb{V}^G$ is the motivation for the ordering of the basis structures

[2]Physical in the sense that it only contains the $14+6$ color structures appearing in the Glauber series calculation and not the $8+1$ structures from the last two columns in Table 9.5.

in (9.31). Here the two $0_{7\times7}$ matrices on the diagonal reflect the fact that the structures with $\boldsymbol{T}_j$ can be split into two distinct subsets, each appearing only for an even or odd number of Glauber-operator insertions. The last six zero rows indicate that structures without final-state generator are mapped onto zero, similar to $\boldsymbol{X}_4^q$ and $\boldsymbol{X}_5^q$, whereas the two $0_{7\times6}$ matrices in the last column indicate that $\boldsymbol{V}^G$ does not create such structures at all. The positions of the non-zero entries in $\mathbb{\Gamma}^c$ indicate that the structures with $\boldsymbol{T}_j$ appearing for an odd number of $\boldsymbol{V}^G$ insertions do not mix with those appearing for an even number or with structures without final-state generator. Likewise, $\boldsymbol{\Gamma}^c$ can only map structures $\boldsymbol{X}_i^g$ with $i = 8,\dots,14$ onto structures $\boldsymbol{X}_i^g$ with $i > 14$. The submatrices of $\mathbb{\Gamma}^c$ and $\mathbb{V}^G$ have been calculated using `ColorMath` [113] and are given in Appendix A.6.

The reduced color trace can now be expressed as linear combinations of the basis structures $\boldsymbol{X}^g$ as in (9.52) with $\varsigma := (1,0,\dots,0)^T$ being a 20-component vector. Even though ς is an eigenvector of $\mathbb{\Gamma}^c$ irrespective of the nature of the initial-state partons, no relation similar to (9.53) holds for gluon-initiated processes. Therefore, the coefficients in the reduced color trace can only be determined by performing several matrix multiplications. One finds for even $l = 2\ell$

$$C_{\{\underline{r}\}}^{2\ell} = \frac{16}{N_c}(-\pi^2)^\ell\, N_c^{n+2\ell} \sum_{i=8}^{20} \left\langle \boldsymbol{\mathcal{H}}_{2\to M}\, \boldsymbol{X}_i^g \otimes \mathbf{1} \right\rangle c_i^{(\ell|\underline{r})} \tag{9.58}$$

and for odd $l = 2\ell - 1$

$$C_{\{\underline{r}\}}^{2\ell-1} = \frac{16i\pi}{N_c}(-\pi^2)^{\ell-1}\, N_c^{n+2\ell-1} \sum_{i=1}^{7} \left\langle \boldsymbol{\mathcal{H}}_{2\to M}\, \boldsymbol{X}_i^g \otimes \mathbf{1} \right\rangle \tilde{c}_i^{(\ell|\underline{r})}\,. \tag{9.59}$$

Here, the coefficient vectors are given by [3]

$$\begin{aligned}
c^{(\ell|\underline{r})}\Big|_{1-7} &:= \left(\prod_{i=2}^{\ell} \left(\tilde{\gamma}^{(j)}\right)^{r_{2i-3}} \tilde{\nu}^{(j)} \left(\gamma^{(j)}\right)^{r_{2i-2}} \nu^{(j)}\right) \varsigma\Big|_{1-7}\,,\\
c^{(\ell|\underline{r})}\Big|_{8-14} &:= \left(\gamma^{(j)}\right)^{r_1} \nu^{(j)} \left(\prod_{i=2}^{\ell} \left(\tilde{\gamma}^{(j)}\right)^{r_{2i-2}} \tilde{\nu}^{(j)} \left(\gamma^{(j)}\right)^{r_{2i-1}} \nu^{(j)}\right) \varsigma\Big|_{1-7}\,,\\
c^{(\ell|\underline{r})}\Big|_{15-20} &:= \tilde{\lambda}(r_1)\, \nu^{(j)} \left(\prod_{i=2}^{\ell} \left(\tilde{\gamma}^{(j)}\right)^{r_{2i-2}} \tilde{\nu}^{(j)} \left(\gamma^{(j)}\right)^{r_{2i-1}} \nu^{(j)}\right) \varsigma\Big|_{1-7}\,,
\end{aligned} \tag{9.60}$$

where the vectors are restricted to the components indicated by the subscript. Due to the simple form of $\mathbb{V}^G$, the complicate interplay of λ, γ and $\gamma^{(j)}$ in (9.57) is only relevant for the (3,2) entry of the block $(\mathbb{\Gamma}^c)^{r_1}$, which we denote by $\tilde{\lambda}(r_1)$.

To work out the contribution of the Glauber series to the partonic scattering cross section for gluon-initiated processes, one combines the reduced color traces with the iterated scale integrals (9.43). The situation here is even more complicated than for quark-initiated processes, as one not only needs to perform infinitely many infinite sums over $\{\underline{r}\}$ but also needs to determine the coefficients by multiple matrix products.

$\boldsymbol{V}^G\,\overline{\boldsymbol{\Gamma}}$	$(\boldsymbol{V}^G)^2\,\overline{\boldsymbol{\Gamma}}$	$(\boldsymbol{V}^G)^3\,\overline{\boldsymbol{\Gamma}}$	$(\boldsymbol{V}^G)^4\,\overline{\boldsymbol{\Gamma}}$
$\boldsymbol{X}_1^{qg}$	$\boldsymbol{X}_4^{qg}$	X_1^{qg}	X_4^{qg}
	$\boldsymbol{X}_5^{qg}$	$\boldsymbol{X}_2^{qg}$	X_5^{qg}
	$\boldsymbol{X}_6^{qg}$	$\boldsymbol{X}_3^{qg}$	X_6^{qg}
	$\boldsymbol{X}_7^{qg}$		X_7^{qg}
	$\boldsymbol{X}_8^{qg}$		X_8^{qg}
	$\boldsymbol{X}_9^{qg}$		X_9^{qg}
			$\boldsymbol{X}_{10}^{qg}$
			$\boldsymbol{X}_{11}^{qg}$
	$\boldsymbol{X}_{12}^{qg}$		X_{12}^{qg}
	$\boldsymbol{X}_{13}^{qg}$		X_{13}^{qg}
			$\boldsymbol{X}_{14}^{qg}$
$1+0$	$6+2$	$3+0$	$8+3$

Table 9.6: Color basis for quark-gluon-initiated processes. The columns and colors have the same meaning as in Table 9.5.

9.2.3 Quark-Gluon-Initiated Processes

For quark-gluon-initiated processes the action of Glauber operator and cusp anomalous dimension on the color basis $\boldsymbol{X}^{qg} \coloneqq (\boldsymbol{X}_1^{qg}, \ldots, \boldsymbol{X}_{14}^{qg})$ is sketched in Table 9.6. Similar to above, the order of the basis structures in (9.38) is chosen such that the first three elements emerge from an odd number of Glauber-operator insertions, see third column, whereas the remaining eleven structures contribute for even numbers, see fourth column. The insertion of five or more Glauber operators does not create any new structures. In contrast to the gluonic case, all $11+3$ basis structures constructed in Section 9.1 contribute to the Glauber series.

The 14×14 matrices representing $\boldsymbol{\Gamma}^c$ and $\boldsymbol{V}^G$ in the basis $\boldsymbol{X}^{qg}$, see (9.49) for their definition, can be decomposed as

$$\mathbb{\Gamma}^c = \begin{pmatrix} \tilde{\gamma}^{(j)} & 0_{3\times 8} & 0_{3\times 3} \\ 0_{8\times 3} & \gamma^{(j)} & 0_{8\times 3} \\ 0_{3\times 3} & \lambda & \gamma \end{pmatrix}, \qquad \mathbb{V}^G = \begin{pmatrix} 0_{3\times 3} & \tilde{\nu}^{(j)} & 0_{3\times 3} \\ \nu^{(j)} & 0_{8\times 8} & 0_{8\times 3} \\ 0_{3\times 3} & 0_{3\times 8} & 0_{3\times 3} \end{pmatrix}. \tag{9.61}$$

Here the positions of the non-zero submatrices reflect the same general properties as in (9.57) and they are given in Appendix A.7.

The reduced color trace for quark-gluon-initiated processes takes the form (9.58) and (9.59) for even and odd values of l, respectively. The coefficients are given in (9.60). Of course, for odd values only the first three color structures (components) and for even values the remaining eleven are relevant. The vector $\varsigma \coloneqq (1, 0, \ldots, 0)^T$ contains 14 components in this case.

9.3 Two Possible Expansions

We have seen in the previous section that the all-order structure of the Glauber series is very intricate. On the one hand, even in the fixed coupling approximation the iterated scale integrals (9.43) lead to a complicated ratio of double factorials. On the other hand, the coefficients of the basis structures in the reduced color trace (9.52) are not given by scalar functions but rather need to be determined through matrix multiplication. After combing these two results, one is left with infinitely many infinite sums that need to be performed in order to determine the contribution of the Glauber series to the partonic cross section. To circumvent dealing with this complicated structure, we discuss an alternative approach of how to organize the Glauber series in the following.

9.3.1 Expansion in $\boldsymbol{V}^G$

In the standard counting scheme $\alpha_s L_s = \mathcal{O}(1)$ it is convenient to expand the evolution operator (9.3) only in $\boldsymbol{V}^G$, while keeping the double logarithms exponentiated through (8.7). We then find a generalized version of (8.6) for the SLLs

$$\begin{aligned}\boldsymbol{U}^{(l)}_{\text{SLL}}(\{\underline{n}\},\mu_h,\mu_s) \coloneqq &\int_{\mu_s}^{\mu_h}\frac{d\mu_1}{\mu_1}\int_{\mu_s}^{\mu_1}\frac{d\mu_2}{\mu_2}\cdots\int_{\mu_s}^{\mu_l}\frac{d\mu_{l+1}}{\mu_{l+1}}\\ &\times\left[\prod_{i=1}^{l}\boldsymbol{U}^c(\mu_{i-1},\mu_i)\,\gamma_{\text{cusp}}\big(\alpha_s(\mu_i)\big)\,\boldsymbol{V}^G\right]\frac{\alpha_s(\mu_{l+1})}{4\pi}\,\overline{\boldsymbol{\Gamma}}\,,\end{aligned} \tag{9.62}$$

where $\mu_0 \coloneqq \mu_h$ and the terms in the product are ordered from left to right according to increasing values of i. The Glauber series is then obtained by summing all possible terms

$$\boldsymbol{U}_{\text{SLL+G}}(\{\underline{n}\},\mu_h,\mu_s) = \sum_{l=1}^{\infty}\boldsymbol{U}^{(l)}_{\text{SLL}}(\{\underline{n}\},\mu_h,\mu_s)\,. \tag{9.63}$$

From (9.62) it is evident that all double logarithms originate from multiple generalized Sudakov operators. It is straightforward to generalize this expressions to include multiple soft emissions, i.e. multiple insertions of $\overline{\boldsymbol{\Gamma}}$, as well as insertions of the collinear anomalous dimension (8.2). This provides a convenient RG-based framework to study subleading logarithmic corrections to non-global observables in future work.

In the following, we restrict the discussion to quark-initiated processes. However, a generalization to gluon- and quark-gluon-initiated processes is straightforward. Translating cusp anomalous dimension and Glauber operator to their matrix representations in the basis for quark-initiated processes, see (9.49), and using (9.51), we find for the contribution of the Glauber series to the partonic cross section [4]

$$\hat{\sigma}^{\text{SLL+G}}_{2\to M}(Q_0) = \sum_{l=1}^{\infty}\left\langle\boldsymbol{\mathcal{H}}_{2\to M}(\mu_h)\,\boldsymbol{X}^q\otimes\mathbf{1}\right\rangle\mathbb{U}^{(l)}_{\text{SLL}}(\mu_h,\mu_s)\,\varsigma\,, \tag{9.64}$$

where

$$\mathbb{U}^{(l)}_{\rm SLL}(\mu_h,\mu_s) \coloneqq 16(i\pi)^l\, N_c^{l-1} \int_{\mu_s}^{\mu_h}\frac{d\mu_1}{\mu_1}\int_{\mu_s}^{\mu_1}\frac{d\mu_2}{\mu_2}\cdots\int_{\mu_s}^{\mu_l}\frac{d\mu_{l+1}}{\mu_{l+1}}\,\mathbb{U}^c(\mu_h,\mu_1) \\ \times\left[\prod_{i=1}^{l-1}\gamma_{\rm cusp}\big(\alpha_s(\mu_i)\big)\,\mathbb{V}^G\,\mathbb{U}^c(\mu_i,\mu_{i+1})\right]\gamma_{\rm cusp}\big(\alpha_s(\mu_l)\big)\,\frac{\alpha_s(\mu_{l+1})}{4\pi}\,. \tag{9.65}$$

The matrix representation $\mathbb{U}^c(\mu_i,\mu_j)$ of the generalized Sudakov operator, defined in (8.77), takes for quark-initiated processes the form

$$\mathbb{U}^c(\mu_i,\mu_j) = \begin{pmatrix} U^c(1;\mu_i,\mu_j) & 0 & 0 & 0 & 0 \\ 0 & U^c(1;\mu_i,\mu_j) & 0 & 0 & 0 \\ 0 & 0 & U^c(\frac{1}{2};\mu_i,\mu_j) & 0 & 0 \\ 0 & 0 & 2\big[U^c(\frac{1}{2};\mu_i,\mu_j)-U^c(1;\mu_i,\mu_j)\big] & U^c(1;\mu_i,\mu_j) & 0 \\ 0 & 0 & \frac{2C_F}{N_c}\big[1-U^c(\frac{1}{2};\mu_i,\mu_j)\big] & 0 & 1 \end{pmatrix} \tag{9.66}$$

and all double-logarithmic effects are resummed into the scalar Sudakov factors (8.75) with eigenvalues $v_0=0$, $v_1=\frac{1}{2}$ and $v_2=2$.[3] It is instructive to explore the matrix structure of the result (9.65) in more detail, using that

$$\mathbb{V}^G\,\mathbb{U}^c(\mu_i,\mu_j) = \begin{pmatrix} 0 & -2\delta_{q\bar q}\,\frac{N_c^2-4}{N_c^2}\,U^c(1;\mu_i,\mu_j) & \frac{4}{N_c^2}\,U^c(\frac{1}{2};\mu_i,\mu_j) & 0 & 0 \\ -\frac{1}{2}\,U^c(1;\mu_i,\mu_j) & 0 & 0 & 0 & 0 \\ U^c(1;\mu_i,\mu_j) & 0 & 0 & 0 & 0 \\ 0 & 0 & 0 & 0 & 0 \\ 0 & 0 & 0 & 0 & 0 \end{pmatrix}. \tag{9.67}$$

As eigenvalue $v_0=0$ does not appear in this expression, it can only contribute through the leftmost factor $\mathbb{U}^c(\mu_h,\mu_1)$ in (9.65). The multiplication with the vector ς in (9.64) projects out the first column of the product of $(l-1)$ such matrices. It follows that for odd values of l, only the first component of the resulting vector is non-zero, while for even values of l, the first component vanishes but the remaining four components are non-zero. Using the fact that the vector ς is an eigenvector of $\mathbb{\Gamma}^c$ with eigenvalue $v_2=1$, which is true irrespective of the nature of the initial-state partons, see (8.74), the rightmost factor $\mathbb{U}^c(\mu_{l-1},\mu_l)$ always generates $U^c(1;\mu_{l-1},\mu_l)$. Note also that the (1,3) entry of the product $\mathbb{V}^G\,\mathbb{U}^c(\mu_i,\mu_j)$, which contains the only contribution corresponding to the eigenvalue $v_1=\frac{1}{2}$, vanishes in the large-N_c limit. In Section 9.5, we exploit this fact when treating higher-order terms in the Glauber series in the large-N_c approximation.

To calculate the coefficient vector $\mathbb{U}^{(l)}_{\rm SLL}(\mu_h,\mu_s)\,\varsigma$ in leading order RG-improved perturbation theory, we change variables in (9.65) to $x_i=\alpha_s(\mu_i)/\alpha_s(\mu_h)$ and use the one-loop approximation for the cusp anomalous dimension in the Glauber terms (with

[3] Remember, $U^c(0;\mu_i,\mu_j)=1$.

$\gamma_0 = 4$). Inverting also the order of integration, one finds

$$\begin{aligned}\mathbb{U}^{(l)}_{\rm SLL}(\mu_h,\mu_s) = (i\pi)^l\, N_c^{l-1}\,\frac{2^{l+3}}{\beta_0^{l+1}}\int_1^{x_s}\frac{dx_l}{x_l}\,\ln\frac{x_s}{x_l}\int_1^{x_l}\frac{dx_{l-1}}{x_{l-1}}\cdots\int_1^{x_2}\frac{dx_1}{x_1}\\ \times\,\mathbb{U}^c(\mu_h,\mu_1)\left[\prod_{i=1}^{l-1}\mathbb{V}^G\,\mathbb{U}^c(\mu_i,\mu_{i+1})\right],\end{aligned} \tag{9.68}$$

where the integral over x_{l+1} is already performed and the scalar Sudakov functions $U^c(v;\mu_i,\mu_j)$ expressed through the variables x_i, x_j can be found in (8.82). This formula accomplishes the resummation of the infinite series of terms involving l insertions of Glauber operators at leading order in RG-improved perturbation theory. For the first two terms, we find

$$\mathbb{U}^{(1)}_{\rm SLL}(\mu_h,\mu_s)\,\varsigma = \frac{16i\pi}{\beta_0^2}\int_1^{x_s}\frac{dx_1}{x_1}\,\ln\frac{x_s}{x_1}\,U^c(1,\mu_h,\mu_1)\,\varsigma\,, \tag{9.69}$$

where the right-hand side is proportional to the vector ς, i.e. only its first component is non-zero, and

$$\begin{aligned}\mathbb{U}^{(2)}_{\rm SLL}(\mu_h,\mu_s)\,\varsigma = -\frac{32\pi^2}{\beta_0^3}\,N_c\int_1^{x_s}\frac{dx_2}{x_2}\,\ln\frac{x_s}{x_2}\int_1^{x_2}\frac{dx_1}{x_1}\\ \times\begin{pmatrix}0\\ -\frac{1}{2}\,U^c(1;\mu_h,\mu_2)\\ U^c(\frac{1}{2},1;\mu_h,\mu_1,\mu_2)\\ 2\big[U^c(\frac{1}{2},1;\mu_h,\mu_1,\mu_2)-U^c(1;\mu_h,\mu_2)\big]\\ \frac{2C_F}{N_c}\big[U^c(1;\mu_1,\mu_2)-U^c(\frac{1}{2},1;\mu_h,\mu_1,\mu_2)\big]\end{pmatrix}.\end{aligned} \tag{9.70}$$

This result is equivalent to (8.81) for quark-initiated processes. Here, we have used the identities

$$U^c(1,1;\mu_h,\mu_1,\mu_2) = U^c(1;\mu_h,\mu_2)\,,\qquad U^c(0,1;\mu_h,\mu_1,\mu_2) = U^c(1;\mu_1,\mu_2)\,, \tag{9.71}$$

which follow from (8.76). As already explained above, the last eigenvalue always equals 1 and eigenvalue zero can only appear in the first entry. As we proceed to larger l values, we find

$$\begin{aligned}\mathbb{U}^{(3)}_{\rm SLL}(\mu_h,\mu_s)\,\varsigma = -\frac{64i\pi^3}{\beta_0^4}\,N_c^2\int_1^{x_s}\frac{dx_3}{x_3}\,\ln\frac{x_s}{x_3}\int_1^{x_3}\frac{dx_2}{x_2}\int_1^{x_2}\frac{dx_1}{x_1}\\ \times\Big[K_{12}\,U^c(1;\mu_h,\mu_3)+\tfrac{4}{N_c^2}\,U^c(1,\tfrac{1}{2},1;\mu_h,\mu_1,\mu_2,\mu_3)\Big]\varsigma\end{aligned} \tag{9.72}$$

and

$$\mathbb{U}^{(4)}_{\rm SLL}(\mu_h,\mu_s)\,\varsigma = \frac{128\pi^4}{\beta_0^5}\,N_c^3\int_1^{x_s}\frac{dx_4}{x_4}\,\ln\frac{x_s}{x_4}\int_1^{x_4}\frac{dx_3}{x_3}\int_1^{x_3}\frac{dx_2}{x_2}\int_1^{x_2}\frac{dx_1}{x_1} \tag{9.73}$$

$$\times \begin{pmatrix} 0 \\ -\frac{1}{2}\Big[K_{12}\,U^c(1;\mu_h,\mu_4) + \frac{4}{N_c^2}\,U^c(1,\frac{1}{2},1;\mu_h,\mu_2,\mu_3,\mu_4)\Big] \\ K_{12}\,U^c(\frac{1}{2},1;\mu_h,\mu_1,\mu_4) + \frac{4}{N_c^2}\,U^c(\frac{1}{2},1,\frac{1}{2},1;\mu_h,\mu_1,\mu_2,\mu_3,\mu_4) \\ 2\Big[K_{12}\,U^c(\frac{1}{2},1;\mu_h,\mu_1,\mu_4) + \frac{4}{N_c^2}\,U^c(\frac{1}{2},1,\frac{1}{2},1;\mu_h,\mu_1,\mu_2,\mu_3,\mu_4)\Big] \\ -2\Big[K_{12}\,U^c(1;\mu_h,\mu_4) + \frac{4}{N_c^2}\,U^c(1,\frac{1}{2},1;\mu_h,\mu_2,\mu_3,\mu_4)\Big] \\ \frac{2C_F}{N_c}\Big[K_{12}\,U^c(1;\mu_1,\mu_4) + \frac{4}{N_c^2}\,U^c(1,\frac{1}{2},1;\mu_1,\mu_2,\mu_3,\mu_4)\Big] \\ -\frac{2C_F}{N_c}\Big[K_{12}\,U^c(\frac{1}{2},1;\mu_h,\mu_1,\mu_4) + \frac{4}{N_c^2}\,U^c(\frac{1}{2},1,\frac{1}{2},1;\mu_h,\mu_1,\mu_2,\mu_3,\mu_4)\Big] \end{pmatrix},$$

with K_{12} defined in (9.54). In the all-order analysis (9.53), one finds the same behavior, the term with eigenvalue $v_1 = \frac{1}{2}$ instead of $v_2 = 1$ is suppressed in the large-N_c limit. The integrals over the x_i variables can be performed numerically without much effort.

Similar to the above discussion, one can derive the coefficient vectors for quark-gluon- and gluon-initiated processes. In the first case, the vector has 14 components and all eigenvalues in (8.48) together with

$$v_7 = \frac{3}{2} \tag{9.74}$$

contribute. In the latter case, the coefficient vector has 20 components and also the three eigenvalues

$$v_8 = 2\,, \qquad v_{9,10} = \frac{2N_c \pm 1}{N_c}\,, \tag{9.75}$$

where v_9 correspond to the plus sign, appear. In Section 9.6 we compare the contribution to the partonic $2 \to M$ cross section for different values of l.

9.3.2 Expansion in $\mathbf{\Gamma}^c$

As already discussed at the beginning of this chapter, for typical values of Q and Q_0 the two expansion parameters w and w_π are both of $\mathcal{O}(1)$. It is thus a priori not clear whether one should expand (9.3) in $\boldsymbol{V}^G$ or $\mathbf{\Gamma}^c$. Expanding in the latter, one finds [3]

$$\boldsymbol{U}_{\rm G}^{(n)}(\{\underline{n}\},\mu_h,\mu_s) \coloneqq \int_{\mu_s}^{\mu_h}\frac{d\mu_1}{\mu_1}\int_{\mu_s}^{\mu_1}\frac{d\mu_2}{\mu_2}\cdots\int_{\mu_s}^{\mu_{n+1}}\frac{d\mu_{n+2}}{\mu_{n+2}}\,\boldsymbol{U}^G(\mu_h,\mu_1) \tag{9.76}$$
$$\times\left[\prod_{i=1}^{n}\mathbf{\Gamma}^c\,\gamma_{\rm cusp}\big(\alpha_s(\mu_i)\big)\ln\frac{\mu_i^2}{\mu_h^2}\,\boldsymbol{U}^G(\mu_i,\mu_{i+1})\right]\gamma_{\rm cusp}\big(\alpha_s(\mu_{n+1})\big)\,\boldsymbol{V}^G\,\frac{\alpha_s(\mu_{n+2})}{4\pi}\,\overline{\mathbf{\Gamma}}\,,$$

where the Glauber operator is kept exponentiated through

$$\boldsymbol{U}^G(\mu_i,\mu_j) \coloneqq \exp\left[\boldsymbol{V}^G\int_{\mu_j}^{\mu_i}\frac{d\mu}{\mu}\,\gamma_{\rm cusp}\big(\alpha_s(\mu)\big)\right]. \tag{9.77}$$

By summing over the number of $\mathbf{\Gamma}^c$ insertions n, one recovers the evolution operator of the Glauber series

$$\boldsymbol{U}_{\text{SLL+G}}(\{\underline{n}\},\mu_h,\mu_s) = \sum_{n=0}^{\infty} \boldsymbol{U}_{\text{G}}^{(n)}(\{\underline{n}\},\mu_h,\mu_s)\,. \tag{9.78}$$

A similar strategy to include higher-order Glauber operators through exponentiation in parton showers was investigated in [53].

Similar to the discussion above, we restrict in the following to quark-initiated processes. The generalization to gluon- and quark-gluon-initiated processes is discussed at the end of this section. Expressing the evolution operator (9.76) in the color basis $\boldsymbol{X}^q$ for quark-initiated processes, one finds

$$\begin{aligned}\mathbb{U}_{\text{G}}^{(n)}(\mu_h,\mu_s) \coloneqq 16i\pi\, N_c^n \int_{\mu_s}^{\mu_h}\frac{d\mu_1}{\mu_1}\int_{\mu_s}^{\mu_1}\frac{d\mu_2}{\mu_2}\cdots\int_{\mu_s}^{\mu_{n+1}}\frac{d\mu_{n+2}}{\mu_{n+2}}\,\mathbb{U}^G(\mu_h,\mu_1)\\ \times\left[\prod_{i=1}^{n}\mathbb{\Gamma}^c\,\gamma_{\text{cusp}}\big(\alpha_s(\mu_i)\big)\ln\frac{\mu_i^2}{\mu_h^2}\,\mathbb{U}^G(\mu_i,\mu_{i+1})\right]\gamma_{\text{cusp}}\big(\alpha_s(\mu_{n+1})\big)\,\frac{\alpha_s(\mu_{n+2})}{4\pi}\,,\end{aligned} \tag{9.79}$$

where the matrix representation of $\boldsymbol{U}^G$ is

$$\mathbb{U}^G(\mu_i,\mu_j) \coloneqq \exp\left[i\pi\, N_c\,\mathbb{V}^G\int_{\mu_j}^{\mu_i}\frac{d\mu}{\mu}\,\gamma_{\text{cusp}}\big(\alpha_s(\mu)\big)\right]. \tag{9.80}$$

Due to the factor i in this definition, the matrix exponential can be expressed as linear combination of sines and cosines. We find

$$\begin{aligned}\mathbb{U}^G(\mu_i,\mu_j) = &\begin{pmatrix}0 & 0 & 0 & 0 & 0\\ 0 & \frac{4}{N_c^2v_\pi^2} & \frac{2}{N_c^2v_\pi^2} & 0 & 0\\ 0 & 2\big[v_\pi^2-\frac{4}{N_c^2}\big] & \big[v_\pi^2-\frac{4}{N_c^2}\big] & 0 & 0\\ 0 & 0 & 0 & 1 & 0\\ 0 & 0 & 0 & 0 & 1\end{pmatrix}\\ &+\cos u^G(v_\pi;\mu_i,\mu_j)\begin{pmatrix}1 & 0 & 0 & 0 & 0\\ 0 & \big[v_\pi^2-\frac{4}{N_c^2}\big] & -\frac{2}{N_c^2v_\pi^2} & 0 & 0\\ 0 & 2\big[\frac{4}{N_c^2}-v_\pi^2\big] & \frac{4}{N_c^2v_\pi^2} & 0 & 0\\ 0 & 0 & 0 & 0 & 0\\ 0 & 0 & 0 & 0 & 0\end{pmatrix}\\ &+i\sin u^G(v_\pi;\mu_i,\mu_j)\begin{pmatrix}0 & 2\big[\frac{4}{N_c^2}-v_\pi^2\big] & \frac{4}{N_c^2v_\pi} & 0 & 0\\ -\frac{1}{2v_\pi} & 0 & 0 & 0 & 0\\ \frac{1}{v_\pi} & 0 & 0 & 0 & 0\\ 0 & 0 & 0 & 0 & 0\\ 0 & 0 & 0 & 0 & 0\end{pmatrix},\end{aligned} \tag{9.81}$$

where all Glauber phases are contained in the scalar functions

$$u^G(v_\pi;\mu_i,\mu_j) \coloneqq v_\pi\,\pi\,N_c\int_{\mu_j}^{\mu_i}\frac{d\mu}{\mu}\,\gamma_{\text{cusp}}\big(\alpha_s(\mu)\big)\,. \tag{9.82}$$

The matrix $\mathbb{V}^G$ has only one (modulo a sign) non-vanishing eigenvalue v_π. It differs for qq or $\bar{q}\bar{q}$ and $q\bar{q}$ scattering

$$v_\pi = \begin{cases} \dfrac{2}{N_c} & \text{for } qq \text{ or } \bar{q}\bar{q} \text{ scattering,} \\ 1 & \text{for } q\bar{q} \text{ scattering.} \end{cases} \tag{9.83}$$

In the large-N_c limit, the matrix (9.80) becomes the unit matrix for qq and $\bar{q}\bar{q}$ scattering, reflecting the suppression of higher Glauber terms.

Similar to (9.68), we change variables in (9.79) to $x_i = \alpha_s(\mu_i)/\alpha_s(\mu_h)$ to determine the coefficient vector in RG-improved perturbation theory. Using the one-loop approximation in the Glauber terms (with $\gamma_0 = 4$) and keeping the two-loop expressions for the cusp anomalous dimension, we find

$$\begin{aligned}\mathbb{U}_{\text{G}}^{(n)}(\mu_h,\mu_s) = i\pi\,\frac{2^{n+4}}{\beta_0^{n+2}}\left[\frac{-4\pi N_c}{\beta_0\,\alpha_h}\right]^n \int_1^{x_s}\frac{dx_{n+1}}{x_{n+1}}\,\ln\frac{x_s}{x_{n+1}}\int_1^{x_{n+1}}\frac{dx_n}{x_n}\cdots\int_1^{x_2}\frac{dx_1}{x_1} \\ \times\,\mathbb{U}^G(\mu_h,\mu_1)\left[\prod_{i=1}^{n}\mathbb{\Gamma}^c\,\mathbb{U}^G(\mu_i,\mu_{i+1})\left(1-\frac{1}{x_i}\right)\right. \\ \left.\times\left\{1+\frac{\alpha_h}{4\pi}\left[\left(\frac{\gamma_1}{\gamma_0}-\frac{\beta_1}{\beta_0}\right)x_i+\frac{\beta_1}{\beta_0}\frac{x_i\,\ln x_i}{1-x_i}\right]\right\}\right]\end{aligned} \tag{9.84}$$

where we already performed the x_{n+2} integral and inverted the order of integration. As for the iterated scale integrals (8.63), it is important to keep the two-loop terms for cusp anomalous dimension and β-function to work at leading order in the strong coupling. The factor $i\pi$ originates from the rightmost insertion of a Glauber operator in (9.76). The scalar functions (9.82) are in this case given by

$$u^G(v_\pi;\mu_i,\mu_j) = \frac{\gamma_0\,v_\pi\,N_c}{2\beta_0}\,\ln\frac{x_j}{x_i}\,. \tag{9.85}$$

For the coefficient vector with $n = 0$ insertions of $\mathbf{\Gamma}^c$, the factor with the product over i is absent. After carrying out the x_1 integral, we find [2]

$$\begin{aligned}\mathbb{U}_{\text{G}}^{(0)}(\mu_h,\mu_s)\,\varsigma = \frac{8}{N_c\,\beta_0}\,\ln x_s\left\{\frac{i}{v_\pi}\left[\frac{1-\cos u^G(v_\pi;\mu_h,\mu_s)}{u^G(v_\pi;\mu_h,\mu_s)}\right]\varsigma\right. \\ \left.+\,\frac{1}{v_\pi^2}\left[\frac{\sin u^G(v_\pi;\mu_h,\mu_s)}{u^G(v_\pi;\mu_h,\mu_s)}-1\right]\begin{pmatrix}0\\-\frac{1}{2}\\1\\0\\0\end{pmatrix}\right\},\end{aligned} \tag{9.86}$$

where the term with the cosine only contributes if the hard function $\boldsymbol{\mathcal{H}}_{2\to M}$ contains a non-trivial phase. Including one insertion of the cusp anomalous dimension yields

$$\begin{aligned}\mathbb{U}_{\mathrm{G}}^{(1)}(\mu_h,\mu_s)\,\varsigma = -\frac{128\pi^2}{\beta_0^4\,\alpha_h}\,\frac{N_c}{v_\pi}\int_1^{x_s}\frac{dx_2}{x_2}\,\ln\frac{x_s}{x_2}\int_1^{x_2}\frac{dx_1}{x_1}\Bigg\{&\sin u^G(v_\pi;\mu_1,\mu_2)\begin{pmatrix}0\\ \frac{1}{2}\\ -\frac{1}{2}\\ 1\\ \frac{C_F}{N_c}\end{pmatrix}\\ -\Bigg[&\sin u^G(v_\pi;\mu_h,\mu_1)\,\cos u^G(v_\pi;\mu_1,\mu_2)-\left(1-\frac{2}{N_c^2 v_\pi^2}\right)\\ &\times\left[1-\cos u^G(v_\pi;\mu_h,\mu_1)\right]\sin u^G(v_\pi;\mu_1,\mu_2)\Bigg]\begin{pmatrix}0\\ -\frac{1}{2}\\ 1\\ 0\\ 0\end{pmatrix}\Bigg\}\\ +\ldots\,,\end{aligned} \tag{9.87}$$

where the ellipsis denote terms that only contribute if the hard function contains non-trivial phases. The two integrals can be performed numerically without much effort.

Generalizing the above derivation to processes with gluons in the initial state is complicated by the fact that in this case $\mathbb{V}^G$ has several non-vanishing eigenvalues. For gluon-initiated processes they are

$$v_\pi \in \left\{1\,,\frac{2}{N_c}\,,\frac{N_c+2}{N_c}\,,\frac{N_c-2}{N_c}\right\} \tag{9.88}$$

and for quark-gluon-initiated processes

$$v_\pi \in \left\{\frac{2}{N_c}\,,\frac{N_c+1}{N_c}\,,\frac{N_c-1}{N_c}\right\}. \tag{9.89}$$

The matrix (9.80) can then still be expressed as linear combinations of sines and cosines but one has to sum over all eigenvalues [3]

$$\begin{aligned}\mathbb{U}^G(\mu_i,\mu_j) = &\begin{pmatrix}\tilde{\mathcal{V}}_0 & 0 & 0\\ 0 & \mathcal{V}_0 & 0\\ 0 & 0 & 1\end{pmatrix}+\sum_{v_\pi}\cos u^G(v_\pi;\mu_i,\mu_j)\begin{pmatrix}\tilde{\mathcal{V}}_{v_\pi} & 0 & 0\\ 0 & \mathcal{V}_{v_\pi} & 0\\ 0 & 0 & 0\end{pmatrix}\\ &+i\sum_{v_\pi}\sin u^G(v_\pi;\mu_i,\mu_j)\begin{pmatrix}0 & \tilde{\mathcal{V}}'_{v_\pi} & 0\\ \mathcal{V}'_{v_\pi} & 0 & 0\\ 0 & 0 & 0\end{pmatrix},\end{aligned} \tag{9.90}$$

where the different submatrices can easily be derived from (9.57) and (9.61). With the explicit results at hand, one can straightforwardly derive the coefficient vector $\mathbb{U}_{\mathrm{G}}^{(n)}(\mu_h,\mu_s)\,\varsigma$ for partonic scattering processes with gluons in the initial state. In Section 9.6 we compare these results to the ones obtained by expanding in $\boldsymbol{V}^G$, i.e. by including all double logarithms.

9.4 Fixed-Coupling Results and Asymptotic Behavior

For the standard counting scheme $\alpha_s L_s = \mathcal{O}(1)$, the double logarithms are $\alpha_s L_s^2 \gg 1$ and, therefore, it is convenient to study the asymptotic behavior of the Glauber series in this limit. The large-w asymptotics of the SLLs are derived in Section 8.3 and one finds

$$\boldsymbol{U}_{\mathrm{SLL}}(\{\underline{n}\},\mu_h,\mu_s) \sim \frac{\alpha_s(\bar{\mu})\,L_s}{\pi\,N_c}\,w_\pi\,\ln(4w)\,. \tag{9.91}$$

In this section we generalize this analysis to the full Glauber series.

The result (9.65) provides a convenient framework for performing studies of the asymptotic behavior for $w \gg 1$, since it resums all double-logarithmic corrections. To study the large-w asymptotics, it is sufficient to evaluate the evolution operators with a fixed coupling $\alpha_s = \alpha_s(\bar{\mu})$, since the scale dependence of the running coupling is a single-logarithmic effect. Using also the one-loop approximation for the cusp anomalous dimension ($\gamma_0 = 4$), we find by changing variables to $L_i = \ln(\mu_h/\mu_i)$ and rescaling $L_i = z_i L_s$

$$\begin{aligned}\mathbb{U}^{(l)}_{\mathrm{SLL}}(\mu_h,\mu_s) = 4(i\pi)^l\,N_c^{l-1}\Big(\frac{\alpha_s}{\pi}\,L_s\Big)^{l+1}\int_0^1 dz_l\,(1-z_l)\int_0^{z_l} dz_{l-1}\cdots\int_0^{z_2} dz_1 \\ \times\,\mathbb{U}^c(\mu_h,\mu_1)\left[\prod_{i=1}^{l-1}\mathbb{V}^G\,\mathbb{U}^c(\mu_i,\mu_{i+1})\right].\end{aligned} \tag{9.92}$$

As in the first part of Section 9.3, we need to evaluate multi-dimensional integrals over concatenations of $U^c(v;\mu_i,\mu_j)$ with different eigenvalues. The last eigenvalue is 1 irrespective of the nature of the initial-state partons, since ς is eigenvector of $\mathbb{U}^c(\mu_i,\mu_j)$. We define the generalization of (8.85)

$$\begin{aligned}&\int_0^1 dz_l\,(1-z_l)\int_0^{z_l} dz_{l-1}\cdots\int_0^{z_2} dz_1\,U^c(v_{i_1},\dots,v_{i_{l-1}},1;\mu_h,\mu_1,\dots,\mu_l) \\ &=:\frac{1}{(l+1)!}\,\Sigma(v_{i_1},\dots,v_{i_{l-1}};w)\,,\end{aligned} \tag{9.93}$$

where the scalar evolution functions expressed through the variables z_i are given in (8.84). In the following, we collect explicit expressions for the coefficient vectors $\mathbb{U}^{(l)}_{\mathrm{SLL}}(\mu_h,\mu_s)\,\varsigma$ and the relevant functions as well as their asymptotic expansions. While individually the factors $U^c(v;\mu_i,\mu_j)$ in (9.93) exhibit exponential suppression, the additional scale integrals lead to a different functional dependence of the resummed expressions.

Case $l = 1$

For $l = 1$ the coefficient vector is given by

$$\mathbb{U}^{(1)}_{\mathrm{SLL}}(\mu_h,\mu_s)\,\varsigma = 2i\pi\Big(\frac{\alpha_s}{\pi}\,L_s\Big)^2\,\Sigma(w)\,\varsigma\,. \tag{9.94}$$

This formula holds for all types of processes, only the number of zero entries in the vector ς varies.[4] We find for $l = 1$ only one function

$$\Sigma(w) = \frac{\sqrt{\pi w}\,\mathrm{erf}\left(\sqrt{w}\right) + e^{-w} - 1}{w} = \frac{\sqrt{\pi}}{\sqrt{w}} - \frac{1}{w} + \mathcal{O}(e^{-w})\,, \tag{9.95}$$

where the last formula shows the complete asymptotic expansion for $w \gg 1$ up to exponentially small terms.

Case $l = 2$

The case $l = 2$ are the SLLs, which are studied in great detail in Chapter 8. If one is only interested in them, it suffices to consider the color structures $\{\boldsymbol{X}_1, \ldots, \boldsymbol{X}_{11}\}$ with coefficients (8.90) in the fixed coupling approximation. However, as this set is not appropriate to describe the entire Glauber series, one needs to work with the bases constructed in Section 9.1. For quark-initiated processes and for $l = 2$, the coefficient vector is given by

$$\mathbb{U}^{(2)}_{\mathrm{SLL}}(\mu_h, \mu_s)\,\varsigma = -\frac{2\pi^2}{3}\,N_c\left(\frac{\alpha_s}{\pi}\,L_s\right)^3 \begin{pmatrix} 0 \\ -\frac{1}{2}\,\Sigma(1;w) \\ \Sigma(\frac{1}{2};w) \\ 2\big[\Sigma(\frac{1}{2};w) - \Sigma(1;w)\big] \\ \frac{2C_F}{N_c}\big[\Sigma(0;w) - \Sigma(\frac{1}{2};w)\big] \end{pmatrix}. \tag{9.96}$$

Considering processes with gluons in the initial state, the results become quite lengthy and we do not show them explicitly. The three different Σ-functions as well as a form for generic eigenvalues $v > 0$ are given in (8.68) and (8.86). Their asymptotic form can be found in (8.92) and (8.93).

Case $l = 3$

For $l = 3$ Glauber-operator insertions, the coefficient vector is

$$\mathbb{U}^{(3)}_{\mathrm{SLL}}(\mu_h, \mu_s)\,\varsigma = -\frac{i\pi^3}{6}\,N_c^2\left(\frac{\alpha_s}{\pi}\,L_s\right)^4 \left[K_{12}\,\Sigma(1,1;w) + \tfrac{4}{N_c^2}\,\Sigma(1,\tfrac{1}{2};w)\right]\varsigma\,, \tag{9.97}$$

with K_{12} defined in (9.54). The only two functions relevant when considering quark-initiated processes are

$$\begin{aligned} \Sigma(1,1;w) &= 3\,\frac{\sqrt{\pi w}\,\mathrm{erf}\left(\sqrt{w}\right) + 2e^{-w} - 2}{w^2}\,, \\ \Sigma(1,\tfrac{1}{2};w) &= 12\int_0^1 dz\,(1-z)\,z^2\,e^{-z^2 w}\,{}_2F_2(1,1;\tfrac{3}{2},2;z^2\,\frac{w}{2})\,. \end{aligned} \tag{9.98}$$

[4] Recall, for quark-initiated process the vector ς has 5 entries, for quark-gluon-initiated processes 14 and for gluon-initiated process 20.

Their asymptotic expansions read

$$\begin{aligned}\Sigma(1,1;w) &= \frac{3\sqrt{\pi}}{w^{3/2}} - \frac{6}{w^2} + \mathcal{O}(e^{-w})\,,\\ \Sigma(1,\tfrac{1}{2};w) &= \frac{6\sqrt{\pi}\,\ln 2}{w^{3/2}} - \frac{3\pi}{w^2} + \mathcal{O}(e^{-\frac{w}{2}})\,.\end{aligned} \tag{9.99}$$

To obtain the second result, we have replaced the upper integration limit by infinity, using that the hypergeometric function behaves like ${}_2F_2(1,1;\frac{3}{2},2;y) \sim y^{-3/2}\,e^y$ for $y \to \infty$.

Case $l = 4$

Considering the second Glauber pair, i.e. the first corrections to the SLLs, the coefficient vector of the color basis $\boldsymbol{X}^q$ is given by

$$\mathbb{U}^{(4)}_{\text{SLL}}(\mu_h,\mu_s)\,\varsigma = \frac{\pi^4}{30}\,N_c^3\left(\frac{\alpha_s}{\pi}\,L_s\right)^5 \begin{pmatrix} 0 \\ -\frac{1}{2}\big[K_{12}\,\Sigma(1,1,1;w) + \frac{4}{N_c^2}\,\Sigma(1,1,\frac{1}{2};w)\big] \\ K_{12}\,\Sigma(\frac{1}{2},1,1;w) + \frac{4}{N_c^2}\,\Sigma(\frac{1}{2},1,\frac{1}{2};w) \\ 2\big[K_{12}\,\Sigma(\frac{1}{2},1,1;w) + \frac{4}{N_c^2}\,\Sigma(\frac{1}{2},1,\frac{1}{2};w)\big] \\ -2\big[K_{12}\,\Sigma(1,1,1;w) + \frac{4}{N_c^2}\,\Sigma(1,1,\frac{1}{2};w)\big] \\ \frac{2C_F}{N_c}\big[K_{12}\,\Sigma(0,1,1;w) + \frac{4}{N_c^2}\,\Sigma(0,1,\frac{1}{2};w)\big] \\ -\frac{2C_F}{N_c}\big[K_{12}\,\Sigma(\frac{1}{2},1,1;w) + \frac{4}{N_c^2}\,\Sigma(\frac{1}{2},1,\frac{1}{2};w)\big] \end{pmatrix}. \tag{9.100}$$

One encounters six functions, four of which can be expressed in closed form. They are

$$\begin{aligned}\Sigma(1,1,1;w) &= \frac{5}{2}\left[\frac{4+2e^{-w}}{w^2} - \frac{3\sqrt{\pi}\,\text{erf}\big(\sqrt{w}\big)}{w^{5/2}}\right],\\ \Sigma(\tfrac{1}{2},1,1;w) &= \frac{15\sqrt{2}}{2w^2}\left[2\sqrt{2} - 2\ln(1+\sqrt{2}) - 4i\pi\,T\left(\sqrt{2w},\frac{i}{\sqrt{2}}\right)\right]\\ &\quad - \frac{30\sqrt{\pi}}{w^{5/2}}\left[\text{erf}\big(\sqrt{w}\big) - \frac{1}{\sqrt{2}}\,\text{erf}\left(\sqrt{\frac{w}{2}}\right)\right],\\ \Sigma(0,1,1;w) &= \frac{15}{w^2} - \frac{15\sqrt{\pi}}{2w^{5/2}}\left[2\,\text{erf}\big(\sqrt{w}\big) - e^{-w}\,\text{erfi}\big(\sqrt{w}\big)\right],\\ \Sigma(1,1,\tfrac{1}{2};w) &= \frac{30\sqrt{2}}{w^2}\left[2\ln(1+\sqrt{2}) - \sqrt{2} + 4i\pi\,T\left(\sqrt{2w},\frac{i}{\sqrt{2}}\right)\right]\\ &\quad + \frac{30\sqrt{2\pi}}{w^{5/2}}\left[\frac{1}{\sqrt{2}}\,\text{erf}\big(\sqrt{w}\big) - \text{erf}\left(\sqrt{\frac{w}{2}}\right) + e^{-w}\,\text{erfi}\left(\sqrt{\frac{w}{2}}\right)\right].\end{aligned} \tag{9.101}$$

For the remaining two functions we have obtained one-dimensional integral representations

$$\Sigma(\tfrac{1}{2},1,\tfrac{1}{2};w) = \int_0^1 dz \left[\frac{\sqrt{\pi}}{\sqrt{w}}\, e^{\frac{w}{2}z^2}\left[\mathrm{erf}\left(\sqrt{w}\right) - \mathrm{erf}\left(\sqrt{w}\,z\right)\right] - \frac{2}{w}\, e^{-\frac{w}{2}}\, \sinh\left(\frac{w(1-z^2)}{2}\right)\right]$$
$$\times\, 30\, z^2\, {}_2F_2(1,1;\tfrac{3}{2},2;-\frac{1}{2}wz^2)\,,$$
$$\Sigma(0,1,\tfrac{1}{2};w) = \int_0^1 dz \left[\frac{\sqrt{\pi}}{w^{3/2}}\, e^{\frac{w}{2}z^2}\left[\mathrm{erf}\left(\sqrt{w}\right) - \mathrm{erf}\left(\sqrt{w}\,z\right)\right] - \frac{2}{w^2}\, e^{-\frac{w}{2}}\, \sinh\left(\frac{w(1-z^2)}{2}\right)\right]$$
$$\times\, 30\sqrt{2}\left[\ln(1+\sqrt{2}) + 2i\pi\left(T\left(\sqrt{w}\,z, i\sqrt{2}+0\right) - \frac{1}{4}\right)\right], \tag{9.102}$$

which can readily be evaluated numerically and the $i0$ prescription in the last line is need to regularize the pole at $t = i$ of (8.88).[5]

The asymptotic forms of these functions for $w \gg 1$ can be obtained by applying the method of regions [7] to the defining integrals (9.93). In general, these integrals receive contributions from the "soft" region $z_4 \sim w^{-1/2} \ll 1$ and the "hard" region $z_4 \sim 1$. However, we find that in the cases where all eigenvalues are non-zero the hard region gives rise to exponentially suppressed contributions, while for $v_{i_1} = 0$ it contributes terms starting at $\mathcal{O}(1/w^3)$, which are suppressed relative to the two leading terms scaling as $1/w^2$ and $1/w^{5/2}$, respectively.[6] It thus suffices to focus on the soft region, for which the upper limit on the integral over z_4 must be replaced by infinity. Introducing new integration variables via the substitutions $z_1 = t_1 z_2$, $z_2 = t_2 z_3$ and $z_3 = t_3 z_4$, and performing the integral over z_4, we then find up to higher-order terms

$$\Sigma(v_{i_1}, v_{i_2}, v_{i_3}; w)\Big|_{w\gg 1} = 60 \int_0^1 dt_1 \int_0^1 dt_2\, t_2 \int_0^1 dt_3\, t_3^2 \left[\frac{1}{w^2}\,\frac{1}{\Delta^2} - \frac{3\sqrt{\pi}}{4w^{5/2}}\,\frac{1}{\Delta^{5/2}}\right], \tag{9.103}$$

with

$$\Delta = v_{i_1} t_1^2 t_2^2 t_3^2 + v_{i_2}(1-t_1^2)\, t_2^2 t_3^3 + v_{i_3}(1-t_2^2)\, t_3^2 + (1-t_3^2)\,. \tag{9.104}$$

Performing the three parameter integrals for the cases of interest, we find the asymptotic forms

$$\Sigma(1,1,1;w) = \frac{10}{w^2} - \frac{15\sqrt{\pi}}{2w^{5/2}} + \mathcal{O}(e^{-w})\,,$$
$$\Sigma(\tfrac{1}{2},1,1;w) = \frac{15\left[2-\sqrt{2}\ln(1+\sqrt{2})\right]}{w^2} - \frac{15\sqrt{\pi}\,(2-\sqrt{2})}{w^{5/2}} + \mathcal{O}(e^{-\frac{w}{2}})\,,$$
$$\Sigma(0,1,1;w) = \frac{15}{w^2} - \frac{15\sqrt{\pi}}{w^{5/2}} + \mathcal{O}(w^{-3})\,,$$

[5] The sign of the $i0$ prescription and, therefore, the sign of the $\frac{1}{4}$ is opposite to the one used in our paper [4]. The current version is identical with the internal definition of `Mathematica` and allows for faster numerical evaluation.

[6] For $l = 2$ the hard region gives unsuppressed contributions for $v_{i_1} = 0$. This fact is responsible for the $\ln(4w)/w$ term and the absence of a term proportional to $w^{-3/2}$ in the expression for $\Sigma(0;w)$ in (8.93).

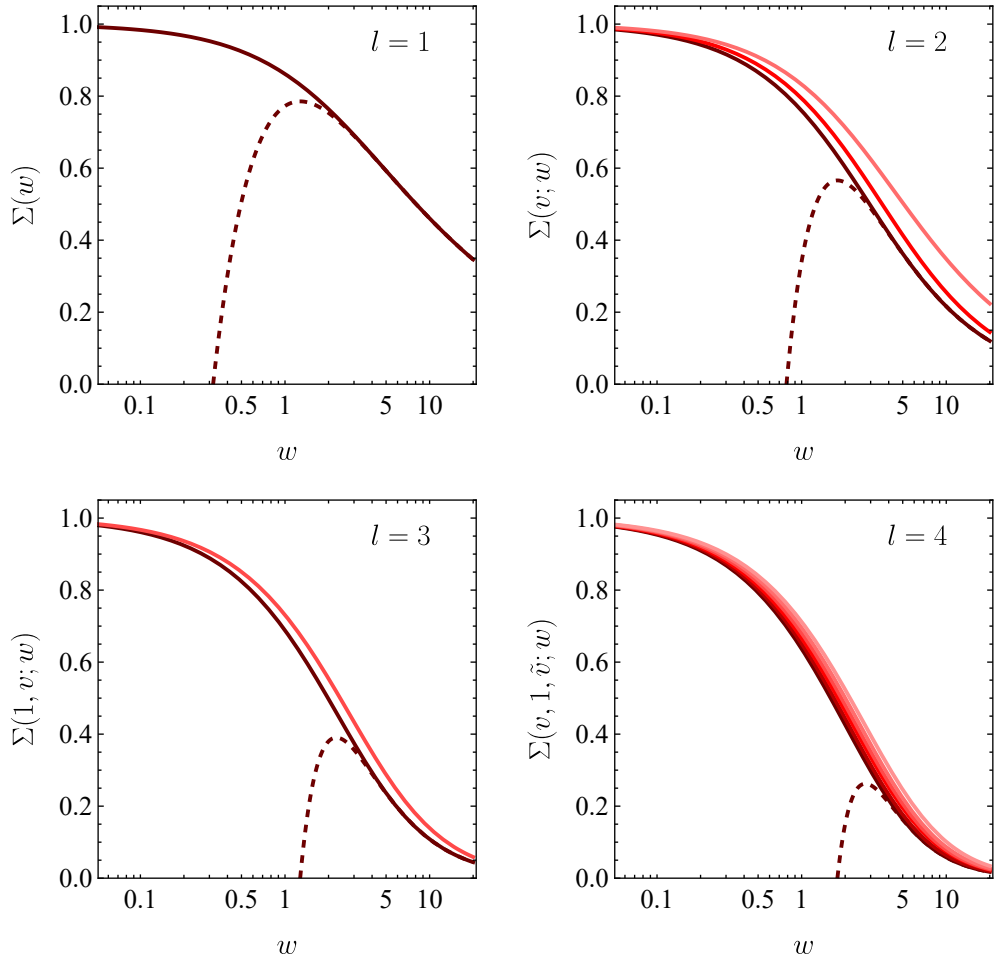

Figure 9.2: The Σ-functions for $l \leq 4$ are shown from bottom to top in each panel in the order in which they are presented in the text. The relevant eigenvalues are $v \in \{1, \frac{1}{2}, 0\}$ for $l = 2$, $v \in \{1, \frac{1}{2}\}$ for $l = 3$, and $(v, \tilde{v}) \in \{(1,1), (\frac{1}{2},1), (0,1), (1,\frac{1}{2}), (\frac{1}{2},\frac{1}{2}), (0,\frac{1}{2})\}$ for $l = 4$. The dashed lines show the asymptotic large-w behavior for the case of $\Sigma(1, \ldots, 1; w)$.

$$\Sigma(1,1,\tfrac{1}{2};w) = \frac{60}{w^2}\left[\sqrt{2}\ln(1+\sqrt{2}) - 1\right] - \frac{30\sqrt{\pi}\,(\sqrt{2}-1)}{w^{5/2}} + \mathcal{O}(e^{-\frac{w}{2}})\,,$$

$$\Sigma(\tfrac{1}{2},1,\tfrac{1}{2};w) = \frac{15\sqrt{2}}{w^2}\left[\frac{5\pi^2}{4} - \frac{3}{2}\ln^2 2 - 12\,\mathrm{Li}_2\big(\tfrac{1}{\sqrt{2}}\big)\right] - \frac{15\sqrt{2\pi}\,\ln 2}{w^{5/2}} + \mathcal{O}(e^{-\frac{w}{2}})\,,$$

$$\Sigma(0,1,\tfrac{1}{2};w) = \frac{30\ln^2(1+\sqrt{2})}{w^2} - \frac{30\sqrt{\pi}\,\ln(1+\sqrt{2})}{w^{5/2}} + \mathcal{O}(w^{-3})\,. \tag{9.105}$$

In Figure 9.2 we show the relevant functions Σ-functions for $l \leq 4$. As a representative example, the dashed line shows the asymptotic behavior for large w for the case of the function $\Sigma(1, \ldots, 1; w)$. We observe that for higher values of l, the asymptotic forms start providing a good approximation at increasingly larger w values. Note also that for given l the differences of two functions belonging to different eigenvalues v_i are much smaller than the individual functions. As a consequence, we find that the coefficients of the color operators $\boldsymbol{X}_4^q$ and $\boldsymbol{X}_5^q$ are considerably smaller in magnitude

than those of the operators $\boldsymbol{X}_2^q$ and $\boldsymbol{X}_3^q$, cf. (9.96) and (9.100).

All-order asymptotic behavior

The technique described for the case $l = 4$ can be straightforwardly extended to higher values of l. Focusing on the functions needed in (9.92), it follows that the leading asymptotic behavior for $w \gg 1$ is

$$\Sigma(v_{i_1}, \ldots, v_{i_{l-1}}; w) \sim \frac{1}{w^{l/2}}\,, \tag{9.106}$$

with the single exception that for $\Sigma(0; w)$ there is an extra factor $\ln w$ in the numerator, which for quark-initiated processes enters only in the fifth component of the evolution vector. For the generic case, we find [4]

$$\mathbb{U}_{\text{SLL}}^{(l)}(\mu_h, \mu_s) \sim \frac{(i\pi)^l}{(l+1)!}\, N_c^{l-1} \left(\frac{\alpha_s}{\pi}\, L_s\right)^{l+1} \frac{1}{w^{l/2}} = \frac{i^l}{(l+1)!}\, \frac{\alpha_s L_s}{\pi N_c}\, w_\pi^{l/2}\,. \tag{9.107}$$

Remarkably the dependence on w cancels in the asymptotic limit. In the conventional counting scheme $\alpha_s L_s = \mathcal{O}(1)$, where $w \sim 1/\alpha_s$ and $w_\pi \sim \alpha_s$, higher-order Glauber exchanges are parametrically suppressed in addition to the factorial suppression. It is thus to be expected that higher order Glauber terms yield considerably smaller contributions than the SLLs. Comparing numerical values, also the alternative counting scheme $\alpha_s L_s^2 = \mathcal{O}(1)$ can be justified. In this case higher-order terms in the Glauber series are even stronger suppressed.

9.5 Large-N_c Resummation

So far, our studies of the Glauber series relied on the expansion in either $\boldsymbol{V}^G$ or $\boldsymbol{\Gamma}^c$, see Section 9.3, or in both of these operators, see Section 9.2. We were able to determine the coefficients of the basis structures relevant for scattering processes in QCD in leading-order RG-improved perturbation theory for a given number l of Glauber-operator insertions or alternatively for a given number n of insertions of the cusp anomalous dimension. Furthermore, we determined the asymptotic behavior for $w \gg 1$ for all terms of the series in Section 9.4. However, we were not able to resum simultaneously in $\boldsymbol{V}^G$ and $\boldsymbol{\Gamma}^c$. In this section, we overcome this issue and perform a full resummation of the Glauber series for large N_c. As the Glauber series itself is subleading in $1/N_c$ compared to e.g. the NGLs, this corresponds to a resummation of next-to-leading terms in the large-N_c expansion of the respective cross section.

9.5.1 Quark-Initiated Processes

We begin by presenting the resummation of the Glauber series in the large-N_c limit for quark-initiated scattering processes [5]. In this limit, the contributions of higher-order Glauber-gluon exchanges simplify. In (9.72) and (9.73) only the terms proportional to K_{12} prevail and their prefactor simplifies to

$$K_{12} = \delta_{q\bar{q}} + \mathcal{O}(1/N_c^2)\,. \tag{9.108}$$

As the terms with unordered eigenvalues are subleading, it is possible to perform most of the integrals over the x_i, e.g.

$$\mathbb{U}^{(3)}_{\rm SLL}(\mu_h,\mu_s)\,\varsigma = \frac{16i\pi}{\beta_0^2}\int_1^{x_s}\frac{dx_3}{x_3}\,\ln\frac{x_s}{x_3}\,\delta_{q\bar q}\,\frac{1}{2!}\left(\frac{2i\pi N_c}{\beta_0}\,\ln x_3\right)^2 U^c(1;\mu_h,\mu_3)\,\varsigma + \dots\,, \tag{9.109}$$

where ellipsis denote subleading terms in the large-N_c expansion. The structure of this result is similar to $\mathbb{U}^{(1)}_{\rm SLL}(\mu_h,\mu_s)\,\varsigma$ in (9.69), aside from the additional factor in the integrand. At higher values of l, the feature remains, i.e. higher-order contributions in the Glauber series are absent for qq and $\bar q\bar q$ scattering.

For large N_c, the (1,3) entry of $\mathbb{V}^G$, given in (9.50), vanishes, leading to a substantial simplification. In this case, the relevant block in the Glauber series fulfills

$$\mathbb{V}^G\,\mathbb{U}^c(\mu_i,\mu_j) = \mathbb{V}^G\,U^c(1;\mu_i,\mu_j)\,, \tag{9.110}$$

where the structure of $\mathbb{U}^c(\mu_i,\mu_j)$ remains unchanged. Applying this important result leads to a simplified version of (9.68)

$$\begin{aligned}\mathbb{U}^{(l)}_{\rm SLL}(\mu_h,\mu_s)\,\varsigma = (i\pi)^l\,N_c^{l-1}\,\frac{2^{l+3}}{\beta_0^{l+1}}\int_1^{x_s}\frac{dx_l}{x_l}\,\ln\frac{x_s}{x_l}\int_1^{x_l}\frac{dx_{l-1}}{x_{l-1}}\cdots\int_1^{x_2}\frac{dx_1}{x_1}\\ \times\,\mathbb{U}^c(\mu_h,\mu_1)\big(\mathbb{V}^G\big)^{l-1}\,U^c(1;\mu_1,\mu_l)\,\varsigma\,.\end{aligned} \tag{9.111}$$

In the case of odd $l = 2\ell-1$, the remaining matrix structure simplifies as ς is an eigenvector of $(\mathbb{V}^G)^2$ with eigenvalue $\delta_{q\bar q}$. Exploiting further that $\mathbb{U}^c(\mu_h,\mu_1)\,\varsigma = U^c(1;\mu_h,\mu_1)\,\varsigma$, one can trivially perform the x_i-integrals for $i<l$, yielding

$$\begin{aligned}\mathbb{U}^{(2\ell-1)}_{\rm SLL}(\mu_h,\mu_s)\,\varsigma = 8\,\frac{(2i\pi)^{2\ell-1}}{\beta_0^{2\ell}}\,\frac{N_c^{2\ell-2}}{(2\ell-2)!}\,\delta_{q\bar q}^{\ell-1}\\ \times\int_1^{x_s}\frac{dx_l}{x_l}\,\ln\frac{x_s}{x_l}\;ln^{2\ell-2}x_l\,U^c(1;\mu_h,\mu_l)\,\varsigma\,.\end{aligned} \tag{9.112}$$

While for even $l=2\ell$ the vector ς is *not* an eigenvector of $(\mathbb{V}^G)^{2\ell-1}$, one can use

$$\big(\mathbb{V}^G\big)^{2\ell-1}\,\varsigma = \delta_{q\bar q}^{\ell-1}\,\mathbb{V}^G\,\varsigma \tag{9.113}$$

and perform the integrals over the x_i variables for $1<i<l$ to obtain

$$\begin{aligned}\mathbb{U}^{(2\ell)}_{\rm SLL}(\mu_h,\mu_s)\,\varsigma = 8\,\frac{(2i\pi)^{2\ell}}{\beta_0^{2\ell+1}}\,\frac{N_c^{2\ell-1}}{(2\ell-2)!}\,\delta_{q\bar q}^{\ell-1}\int_1^{x_s}\frac{dx_l}{x_l}\,\ln\frac{x_s}{x_l}\int_1^{x_l}\frac{dx_1}{x_1}\,\ln^{2\ell-2}\frac{x_l}{x_1}\\ \times\begin{pmatrix}0\\ -\frac{1}{2}\,U^c(1;\mu_h,\mu_l)\\ U^c(\frac{1}{2},1;\mu_h,\mu_1,\mu_l)\\ 2\big[U^c(\frac{1}{2},1;\mu_h,\mu_1,\mu_l)-U^c(1;\mu_h,\mu_l)\big]\\ \frac{2C_F}{N_c}\big[U^c(1;\mu_1,\mu_l)-U^c(\frac{1}{2},1;\mu_h,\mu_1,\mu_l)\big]\end{pmatrix}.\end{aligned} \tag{9.114}$$

Note that while the factor $\frac{2C_F}{N_c}$ in the last component of this expression should be replaced by 1 in the strict large-N_c limit, we prefer to keep it in its original form, as this ensures that the terms with $l = 2$, i.e. the SLLs, are reproduced exactly.

Resumming the Glauber series in the large-N_c limit is now straightforward. Keeping in mind that $\delta_{q\bar{q}}^{\ell-1} = 1$ for $\ell = 1$ also for qq and $\bar{q}\bar{q}$ scattering, we find for odd l

$$\sum_{\ell=1}^{\infty} \mathbb{U}_{\text{SLL}}^{(2\ell-1)}(\mu_h,\mu_s)\,\varsigma = \frac{16i\pi}{\beta_0^2}\int_1^{x_s}\frac{dx_2}{x_2}\,\ln\frac{x_s}{x_2}\,U^c(1;\mu_h,\mu_2) \times\left[1-2\delta_{q\bar{q}}\,\sin^2\left(\frac{\pi N_c}{\beta_0}\,\ln x_2\right)\right]\varsigma\,, \tag{9.115}$$

where the right-hand side is proportional to the vector ς, i.e. only its first component is non-zero. For even values of l, a double integral prevails as also the eigenvalues 0 and $\frac{1}{2}$ contribute. We find

$$\sum_{\ell=1}^{\infty} \mathbb{U}_{\text{SLL}}^{(2\ell)}(\mu_h,\mu_s)\,\varsigma = \frac{16\pi}{\beta_0^2}\,\frac{2\pi N_c}{\beta_0}\int_1^{x_s}\frac{dx_2}{x_2}\,\ln\frac{x_s}{x_2}\int_1^{x_2}\frac{dx_1}{x_1}\left[1-2\delta_{q\bar{q}}\,\sin^2\left(\frac{\pi N_c}{\beta_0}\,\ln\frac{x_2}{x_1}\right)\right] \times\begin{pmatrix} 0\\ \frac{1}{2}\,U^c(1;\mu_h,\mu_2)\\ -U^c(\frac{1}{2},1;\mu_h,\mu_1,\mu_2)\\ 2\big[U^c(1;\mu_h,\mu_2)-U^c(\frac{1}{2},1;\mu_h,\mu_1,\mu_2)\big]\\ \frac{2C_F}{N_c}\big[U^c(\frac{1}{2},1;\mu_h,\mu_1,\mu_2)-U^c(1;\mu_1,\mu_2)\big]\end{pmatrix}. \tag{9.116}$$

Combining (9.115) and (9.116) yields the resummed Glauber series in RG-improved perturbation theory, containing at most two scale integrals. In these expressions, the 1 inside the square brackets corresponds to the SLLs, whereas the term proportional to $\delta_{q\bar{q}}$ accounts for the effects of higher-order Glauber phases. It is therefore evident that the latter effects always reduce the contributions of the SLLs, albeit typically by a small amount, see Section 9.6. Note that for tree-level QCD processes, only an even number of Glauber-operator insertions contribute, as the cross section is real-valued. In general, however, the Glauber series contains both even and odd l values, where the latter are relevant e.g. for cross sections involving electroweak gauge bosons [64].

Fixed-Coupling Results and Asymptotic Behavior

The asymptotic behavior of the resummed Glauber series in the limit $\alpha_s L_s^2 \gg 1$ can be determined with the same techniques developed in Sections 8.3 and 9.4. Ignoring the running of the strong coupling, as it is a single-logarithmic effect, one can use

$$x_i = \frac{\alpha_s(\mu_i)}{\alpha_s(\mu_h)} \approx 1 + \frac{\beta_0\alpha_s L_s}{2\pi}\,z_i\,, \tag{9.117}$$

with fixed coupling $\alpha_s \equiv \alpha_s(\bar{\mu})$ evaluated at an intermediate scale $\bar{\mu} \in (\mu_s, \mu_h)$. The fixed coupling version of (9.115) reads

$$\sum_{\ell=1}^{\infty} \mathbb{U}_{\text{SLL}}^{(2\ell-1)}(\mu_h, \mu_s)\,\varsigma = \frac{4i\alpha_s L_s}{\pi N_c}\sqrt{w_\pi}\int_0^{\sqrt{w}} dy_2 \left(1-\frac{y_2}{\sqrt{w}}\right) e^{-y_2^2} \times \left[1-2\delta_{q\bar{q}}\,\sin^2\left(\frac{\sqrt{w_\pi}}{2}\,y_2\right)\right]\varsigma\,, \tag{9.118}$$

where we inserted (8.84) and rescaled $y_i \coloneqq \sqrt{w} z_i$. Its asymptotic behavior for $w \gg 1$ can be obtained by replacing the upper integration boundary on y_2 by infinity yielding

$$\sum_{\ell=1}^{\infty} \mathbb{U}_{\text{SLL}}^{(2\ell-1)}(\mu_h, \mu_s)\,\varsigma = \frac{2i\alpha_s L_s}{\pi N_c}\sqrt{w_\pi}\Bigg\{\sqrt{\pi}\big[1-\delta_{q\bar{q}}\big(1-e^{-\frac{w_\pi}{4}}\big)\big] - \frac{1}{\sqrt{w}}\left[1-\delta_{q\bar{q}}\sqrt{w_\pi}\,F\big(\tfrac{\sqrt{w_\pi}}{2}\big)\right] + \mathcal{O}(e^{-w})\Bigg\}\varsigma\,, \tag{9.119}$$

where the Dawson function is defined as

$$F(z) = e^{-z^2}\int_0^z dx\, e^{x^2} = \frac{\sqrt{\pi}}{2}\,e^{-z^2}\,\text{erfi}(z)\,. \tag{9.120}$$

For even values of l, we find working with a fixed coupling

$$\sum_{\ell=1}^{\infty} \mathbb{U}_{\text{SLL}}^{(2\ell)}(\mu_h, \mu_s)\,\varsigma = -\frac{4\alpha_s L_s}{\pi N_c}\,w_\pi \int_0^{\sqrt{w}} dy_2 \left(1-\frac{y_2}{\sqrt{w}}\right) e^{-y_2^2}\int_0^{y_2} dy_1 \times \left[1-2\delta_{q\bar{q}}\,\sin^2\left(\frac{\sqrt{w_\pi}}{2}\,(y_2-y_1)\right)\right] \begin{pmatrix} 0 \\ -\frac{1}{2} \\ e^{\frac{1}{2}y_1^2} \\ 2\big(e^{\frac{1}{2}y_1^2}-1\big) \\ \frac{2C_F}{N_c}\big(e^{y_1^2}-e^{\frac{1}{2}y_1^2}\big) \end{pmatrix}. \tag{9.121}$$

In almost all case it again suffices to replace the upper integration boundary on y_2 by infinity to obtain the asymptotic behavior. By the method of regions analysis in Section 9.4, the hard region only contributes for the last component in the term without the sine. For the three relevant integrals, we find

$$\begin{aligned} &\int_0^{\sqrt{w}} dy_2 \left(1-\frac{y_2}{\sqrt{w}}\right) e^{-y_2^2}\int_0^{y_2} dy_1 \left[1-2\delta_{q\bar{q}}\,\sin^2\left(\frac{\sqrt{w_\pi}}{2}\,(y_2-y_1)\right)\right] \\ &= \frac{1}{2}-\frac{\sqrt{\pi}}{4\sqrt{w}}-\delta_{q\bar{q}}\left[\frac{1}{2}-\frac{1}{\sqrt{w_\pi}}\,F\big(\tfrac{\sqrt{w_\pi}}{2}\big)-\frac{\sqrt{\pi}}{4\sqrt{w}}\Big(1-e^{-\frac{w_\pi}{4}}\Big)\right]+\mathcal{O}(e^{-w})\,, \end{aligned} \tag{9.122}$$

and

$$\begin{aligned}
&\int_0^{\sqrt{w}} dy_2 \left(1-\frac{y_2}{\sqrt{w}}\right) e^{-y_2^2} \int_0^{y_2} dy_1 \left[1-2\delta_{q\bar{q}}\,\sin^2\left(\frac{\sqrt{w_\pi}}{2}\,(y_2-y_1)\right)\right] e^{\frac{1}{2}y_1^2} \\
&= \frac{\ln(1+\sqrt{2})}{\sqrt{2}} - \frac{\sqrt{\pi}}{2\sqrt{2w}} - \delta_{q\bar{q}}\left[\frac{\ln(1+\sqrt{2})}{\sqrt{2}} + \sqrt{2}i\pi\, e^{\frac{w_\pi}{4}}\, T\big(\sqrt{w_\pi},\tfrac{i}{\sqrt{2}}\big)\right. \\
&\quad \left. + \frac{\pi\sqrt{w_\pi}}{4\sqrt{2w}}\, e^{\frac{w_\pi}{4}} \left(\mathrm{erf}\big(\tfrac{\sqrt{w_\pi}}{2}\big) - \mathrm{erf}\big(\tfrac{\sqrt{w_\pi}}{\sqrt{2}}\big)\right)\right] + \mathcal{O}(e^{-w/2})\,,
\end{aligned} \tag{9.123}$$

and

$$\begin{aligned}
&\int_0^{\sqrt{w}} dy_2 \left(1-\frac{y_2}{\sqrt{w}}\right) e^{-y_2^2} \int_0^{y_2} dy_1 \left[1-2\delta_{q\bar{q}}\,\sin^2\left(\frac{\sqrt{w_\pi}}{2}\,(y_2-y_1)\right)\right] e^{y_1^2} \\
&= \frac{\ln(4w)+\gamma_E-2}{4} - \delta_{q\bar{q}}\left[\frac{w_\pi}{8}\,{}_2F_2\big(1,1;\tfrac{3}{2},2;-\tfrac{w_\pi}{4}\big) - \frac{\pi\sqrt{w_\pi}}{8\sqrt{w}}\,\mathrm{erf}\big(\tfrac{\sqrt{w_\pi}}{2}\big)\right] + \mathcal{O}(w^{-1})\,.
\end{aligned} \tag{9.124}$$

In agreement with our findings in Section 9.4, it turns out that the dependence on the variable w of the Glauber series cancels in the asymptotic limit for all but the fifth component, which has a residual logarithmic dependence on w.

9.5.2 Gluons in the Initial State

There are two reasons why the resummation of the Glauber series for quark-initiated processes is particularly simple in the large-N_c limit. First, the relevant building block $\mathbb{V}^G\,\mathbb{U}^c(\mu_i,\mu_j)$ fulfills relation (9.110), allowing us to perform all except (at most) two scale integrals and to simplify the matrix structure in (9.68). Second, $\mathbb{\Gamma}^c$ remains diagonalizable in this limit. As soon as gluons are present in the initial state, these properties are lost, complicating the resummation [5].

The up to eleven different eigenvalues of $\mathbb{\Gamma}^c$, given in (8.48), (9.74) and (9.75), degenerate in the large-N_c limit to only five distinct ones

$$v_0 = 0\,, \qquad v_1 = \frac{1}{2}\,, \qquad v_2 = 1\,, \qquad v_7 = \frac{3}{2}\,, \qquad v_8 = 2\,, \tag{9.125}$$

where v_8 only contributes for gluon-initiated processes. As for quark-initiated processes, Sudakov factors with the eigenvalues v_0 and v_1 only arise from the last insertion of $\mathbb{U}^c(\mu_h,\mu_1)$ in (9.68). Therefore, the generalization of (9.110) reads[7]

$$\mathbb{V}^G\,\mathbb{U}^c(\mu_i,\mu_j) = \mathbb{V}_1^G\,U^c(1;\mu_i,\mu_j) + \mathbb{V}_{3/2}^G\,U^c(\tfrac{3}{2};\mu_i,\mu_j) + \mathbb{V}_2^G\,U^c(2;\mu_i,\mu_j)\,. \tag{9.126}$$

As ς is an eigenvector of $\mathbb{U}^c(\mu_i,\mu_j)$ with eigenvalue $U^c(1;\mu_i,\mu_j)$ irrespective of the nature of the initial-state partons, the coefficient matrices fulfill $\mathbb{V}_{3/2}^G\,\varsigma = \mathbb{V}_2^G\,\varsigma = 0$. For quark-gluon-initiated processes $\mathbb{V}_2^G = 0$ because the eigenvalue v_8 does not appear. Furthermore, the coefficient matrices satisfy

$$\mathbb{V}_1^G\,\mathbb{V}_{3/2}^G = 0\,, \qquad \mathbb{V}_{3/2}^G\,\mathbb{V}_2^G = 0\,, \qquad \mathbb{V}_1^G\,\mathbb{V}_2^G = 0\,, \qquad \mathbb{V}_2^G\,\mathbb{V}_1^G = 0\,, \tag{9.127}$$

[7] Note that $\mathbb{V}_2^G$ depends on μ_i,μ_j; however, this dependence is irrelevant as explained below (9.129).

ensuring that the eigenvalues (9.125) only appear strictly ordered in magnitude. The only exception is the first eigenvalue, which can take an arbitrary value.

There is one more subtlety that needs to be taken into account when dealing with gluons in the initial state. Since $\mathbb{\Gamma}^c$ is no longer diagonalizable once the large-N_c limit is taken, its matrix exponential $\mathbb{U}^c(\mu_i,\mu_j)$ with full N_c dependence contains terms of the form

$$N_c\big[U^c\big(\tfrac{3N_c+2}{2N_c};\mu_i,\mu_j\big)-U^c\big(\tfrac{3N_c-2}{2N_c};\mu_i,\mu_j\big)\big]=2\,I_h(\mu_i,\mu_j)\,U^c(\tfrac{3}{2};\mu_i,\mu_j)+\mathcal{O}(1/N_c^2)\,, \tag{9.128}$$

with the integral

$$I_h(\mu_i,\mu_j)\coloneqq N_c\int_{\mu_j}^{\mu_i}\frac{d\mu}{\mu}\,\gamma_{\text{cusp}}\big(\alpha_s(\mu)\big)\ln\frac{\mu^2}{\mu_h^2}\,, \tag{9.129}$$

which counts as $\mathcal{O}(1)$ in the large-N_c expansion. This effect arises for all N_c-dependent eigenvalues of $\mathbb{\Gamma}^c$, i.e. for $v_{3,4}$, $v_{5,6}$ and $v_{9,10}$. As consequence, the coefficient matrix $\mathbb{V}_2^G$ in (9.126) depends on μ_i,μ_j. Fortunately, this dependence drops out in the only relevant product $\mathbb{V}_2^G\,\mathbb{V}_{3/2}^G$. Therefore, we can treat $\mathbb{V}_2^G$ as scale-independent in the following. The coefficient matrix $\mathbb{V}_{3/2}^G$ does not depend on μ_i,μ_j at all.

Inserting the decomposition (9.126) in (9.68) and exploiting the properties of the coefficient matrices, one finds

$$\begin{aligned}\mathbb{U}_{\text{SLL}}^{(l)}(\mu_h,\mu_s)\,\varsigma=(i\pi)^l N_c^{l-1}\,\frac{2^{l+3}}{\beta_0^{l+1}}\int_1^{x_s}\frac{dx_l}{x_l}\ln\frac{x_s}{x_l}\int_1^{x_l}\frac{dx_{l-1}}{x_{l-1}}\dots\int_1^{x_2}\frac{dx_1}{x_1}\,\mathbb{U}^c(\mu_h,\mu_1)\\ \times\Big[\big(\mathbb{V}_1^G\big)^{l-1}U^c(1;\mu_1,\mu_l)+\sum_{i=2}^{l-1}\big(\mathbb{V}_{3/2}^G\big)^{i-1}\big(\mathbb{V}_1^G\big)^{l-i}U^c(\tfrac{3}{2},1;\mu_1,\mu_i,\mu_l)\\ +\sum_{j=3}^{l-1}\sum_{i=2}^{j-1}\big(\mathbb{V}_2^G\big)^{i-1}\big(\mathbb{V}_{3/2}^G\big)^{j-i}\big(\mathbb{V}_1^G\big)^{l-j}U^c(2,\tfrac{3}{2},1;\mu_1,\mu_i,\mu_j,\mu_l)\Big]\,\varsigma\,.\end{aligned} \tag{9.130}$$

The first term looks similar to the quark case (9.111). If $l\geq 2$, one can trivially perform all integrals except the ones over x_1 and x_l. For $l=1$ there is only one such integral, and one can use that $\mathbb{U}^c(\mu_h,\mu_1)\,\varsigma=U^c(1;\mu_h,\mu_1)\,\varsigma$. Combining these two cases, one obtains

$$\int_1^{x_l}\frac{dx_{l-1}}{x_{l-1}}\dots\int_1^{x_2}\frac{dx_1}{x_1}=\delta_{1l}+(1-\delta_{1l})\int_1^{x_l}\frac{dx_1}{x_1}\,\frac{1}{(l-2)!}\ln^{l-2}\frac{x_l}{x_1}\,. \tag{9.131}$$

For the second and third term in (9.130), also the integrals over x_i and x_i,x_j, respectively, are non-trivial. The remaining integrals evaluate to

$$\begin{aligned}\int_1^{x_l}\frac{dx_{l-1}}{x_{l-1}}\dots\int_1^{x_2}\frac{dx_1}{x_1}&=\int_1^{x_l}\frac{dx_i}{x_i}\int_1^{x_i}\frac{dx_1}{x_1}\,\frac{1}{(i-2)!}\ln^{i-2}\frac{x_i}{x_1}\,\frac{1}{(l-1-i)!}\ln^{l-1-i}\frac{x_l}{x_i}\,,\\ \int_1^{x_l}\frac{dx_{l-1}}{x_{l-1}}\dots\int_1^{x_2}\frac{dx_1}{x_1}&=\int_1^{x_l}\frac{dx_j}{x_j}\int_1^{x_j}\frac{dx_i}{x_i}\int_1^{x_i}\frac{dx_1}{x_1}\,\frac{1}{(i-2)!}\ln^{i-2}\frac{x_i}{x_1}\\ &\quad\times\frac{1}{(j-i-1)!}\ln^{j-i-1}\frac{x_j}{x_i}\,\frac{1}{(l-1-j)!}\ln^{l-1-j}\frac{x_l}{x_j}\,.\end{aligned} \tag{9.132}$$

Distinguishing the cases of even and odd l, one can calculate the matrix products in (9.130) and perform the sums over i, j, l, i.e. the resummation of the Glauber series.

For $l = 2\ell - 1$ odd, one finds for the matrix products

$$\begin{aligned}
\left(\mathbb{V}_1^G\right)^{2\ell-2} \varsigma &= \delta_{1\ell}\,\varsigma + (1-\delta_{1\ell})\,\varsigma_1\,, \\
\left(\mathbb{V}_{3/2}^G\right)^{i-1}\left(\mathbb{V}_1^G\right)^{2\ell-1-i} \varsigma &= (1+\delta_{i,2\ell-2})\,\varsigma_{3/2}\,, \\
\left(\mathbb{V}_2^G\right)^{i-1}\left(\mathbb{V}_{3/2}^G\right)^{j-i}\left(\mathbb{V}_1^G\right)^{2\ell-1-j} \varsigma &= (1+\delta_{j,2\ell-2})\,\varsigma_2\,.
\end{aligned} \tag{9.133}$$

The ς vectors differ between quark-gluon and gluon-initiated processes and are given in Appendices A.6 and A.7, respectively. Combining this with (9.131) and (9.132), the coefficient vector of the basis structures can be expressed as

$$\begin{aligned}
\sum_{\ell=1}^{\infty} \mathbb{U}_{\text{SLL}}^{(2\ell-1)}(\mu_h,\mu_s)\,\varsigma = \frac{16i\pi}{\beta_0^2}\int_1^{x_s}\frac{dx_4}{x_4}\,\ln\frac{x_s}{x_4}\Bigg\{ & U^c(1;\mu_h,\mu_4)\,\varsigma \\
& - \frac{2\pi N_c}{\beta_0}\int_1^{x_4}\frac{dx_1}{x_1}\,U^c(1;\mu_1,\mu_4)\,\sin\left(\frac{2\pi N_c}{\beta_0}\,\ln\frac{x_4}{x_1}\right)\mathbb{U}^c(\mu_h,\mu_1)\,\varsigma_1 \\
& - \left(\frac{2\pi N_c}{\beta_0}\right)^2\int_1^{x_4}\frac{dx_2}{x_2}\int_1^{x_2}\frac{dx_1}{x_1}\,U^c(\tfrac{3}{2},1;\mu_1,\mu_2,\mu_4) \\
& \qquad \times\left[\cos\left(\frac{2\pi N_c}{\beta_0}\,\ln\frac{x_4}{x_1}\right)+\cos\left(\frac{2\pi N_c}{\beta_0}\,\ln\frac{x_2}{x_1}\right)\right]\mathbb{U}^c(\mu_h,\mu_1)\,\varsigma_{3/2} \\
& + \left(\frac{2\pi N_c}{\beta_0}\right)^3\int_1^{x_4}\frac{dx_3}{x_3}\int_1^{x_3}\frac{dx_2}{x_2}\int_1^{x_2}\frac{dx_1}{x_1}\,U^c(2,\tfrac{3}{2},1;\mu_1,\mu_2,\mu_3,\mu_4) \\
& \qquad \times\left[\sin\left(\frac{2\pi N_c}{\beta_0}\,\ln\frac{x_4}{x_1}\right)+\sin\left(\frac{2\pi N_c}{\beta_0}\,\ln\frac{x_3}{x_1}\right)\right]\mathbb{U}^c(\mu_h,\mu_1)\,\varsigma_2\Bigg\}.
\end{aligned} \tag{9.134}$$

After carrying out the last products $\mathbb{U}^c(\mu_h,\mu_1)\,\varsigma_i$, it is possible to combine some terms by integrating over x_1. However, these simplifications are not universal and are performed separately for quark-gluon and gluon-initiated processes in Appendices A.6 and A.7, respectively.

For $l = 2\ell$ even, the matrix products evaluate to

$$\begin{aligned}
\left(\mathbb{V}_1^G\right)^{2\ell-1} \varsigma &= \delta_{1\ell}\,\tilde{\varsigma} + (1-\delta_{1\ell})\,\tilde{\varsigma}_1\,, \\
\left(\mathbb{V}_{3/2}^G\right)^{i-1}\left(\mathbb{V}_1^G\right)^{2\ell-i} \varsigma &= (1+\delta_{i,2\ell-1})\,\tilde{\varsigma}_{3/2}\,, \\
\left(\mathbb{V}_2^G\right)^{i-1}\left(\mathbb{V}_{3/2}^G\right)^{j-i}\left(\mathbb{V}_1^G\right)^{2\ell-j} \varsigma &= (1+\delta_{j,2\ell-1})\,\tilde{\varsigma}_2\,.
\end{aligned} \tag{9.135}$$

The $\tilde{\varsigma}$ vectors are also given in Appendices A.6 and A.7. Performing the sums over i, j, ℓ in (9.130) results in

$$\sum_{\ell=1}^{\infty} \mathbb{U}_{\text{SLL}}^{(2\ell)}(\mu_h,\mu_s)\,\varsigma = -\frac{16\pi}{\beta_0^2}\int_1^{x_s}\frac{dx_4}{x_4}\,\ln\frac{x_s}{x_4}\left\{\frac{2\pi N_c}{\beta_0}\int_1^{x_4}\frac{dx_1}{x_1}\,U^c(1;\mu_1,\mu_4)\,\mathbb{U}^c(\mu_h,\mu_1)\,\tilde{\varsigma}\right.$$

$$
\begin{aligned}
&- \frac{2\pi N_c}{\beta_0} \int_1^{x_4} \frac{dx_1}{x_1}\, U^c(1;\mu_1,\mu_4)\, 2\,\sin^2\left(\frac{\pi N_c}{\beta_0}\,\ln\frac{x_4}{x_1}\right) \mathbb{U}^c(\mu_h,\mu_1)\,\tilde{\varsigma}_1 \\
&- \left(\frac{2\pi N_c}{\beta_0}\right)^2 \int_1^{x_4} \frac{dx_2}{x_2} \int_1^{x_2} \frac{dx_1}{x_1}\, U^c(\tfrac{3}{2},1;\mu_1,\mu_2,\mu_4) \\
&\qquad \times \left[\sin\left(\frac{2\pi N_c}{\beta_0}\,\ln\frac{x_4}{x_1}\right) + \sin\left(\frac{2\pi N_c}{\beta_0}\,\ln\frac{x_2}{x_1}\right)\right] \mathbb{U}^c(\mu_h,\mu_1)\,\tilde{\varsigma}_{3/2} \\
&- \left(\frac{2\pi N_c}{\beta_0}\right)^3 \int_1^{x_4} \frac{dx_3}{x_3} \int_1^{x_3} \frac{dx_2}{x_2} \int_1^{x_2} \frac{dx_1}{x_1}\, U^c(2,\tfrac{3}{2},1;\mu_1,\mu_2,\mu_3,\mu_4) \\
&\qquad \times \left[\cos\left(\frac{2\pi N_c}{\beta_0}\,\ln\frac{x_4}{x_1}\right) + \cos\left(\frac{2\pi N_c}{\beta_0}\,\ln\frac{x_3}{x_1}\right)\right] \mathbb{U}^c(\mu_h,\mu_1)\,\tilde{\varsigma}_2\Big\}.
\end{aligned}
\tag{9.136}
$$

After the products $\mathbb{U}^c(\mu_h,\mu_1)\,\varsigma_i$ are carried out, the result becomes very lengthy and contains terms proportional to $I_h(\mu_h,\mu_1)$ by the mechanism described in (9.128). As its construction is straightforward, we do not show the expression explicitly.

With (9.134) and (9.136) we extended the large-N_c resummation of the Glauber series to processes with gluons in the initial state. It is remarkable that the resummed series can be expressed through simple trigonometric functions and an at most four-fold integral. In analogy to the previous section, these equations may now be used to determine the large-w asymptotics by restricting to the fixed-coupling approximation (9.117). Here, we omit a detailed discussion due to the complexity of the resulting expressions, which involve four-fold integrals that are no longer amenable to straightforward analytical evaluation. The qualitative dependence on the parameter w, however, is similar to the one for quark-initiated processes, i.e. the leading term is constant up to logarithmic corrections.

9.6 Numerical Estimates

In Section 8.4 we have seen that SLLs give sizable contributions to the partonic cross section for $2 \to 2$ scattering processes. For small values of the jet-veto scale Q_0, they are of $\mathcal{O}(15\%)$ and, therefore, should be included in future precision calculations. In contrast, for $2 \to 0$ and $2 \to 1$ scattering, i.e. for the production of electroweak gauge bosons with no or a single jet, the SLLs play a minor role. Higher order Glauber-gluon exchanges are parametrically suppressed, cf. the discussion at the end of Section 9.4, but the associated expansion parameter w_π is numerically of similar size as w. Therefore, we examine the numerical impact of including higher terms in the Glauber series on partonic $2 \to 0$, $2 \to 1$, and $2 \to 2$ scattering cross sections in the following.

As we were not able to expressed the resummed Glauber series with full N_c dependence in closed form or as simple integral representation, we employed two different expansions in Section 9.3. In Figure 9.3 we compare the convergence of the expansion (9.62) in $\boldsymbol{V}^G$, which resums all double logarithms, to the one (9.76) in $\boldsymbol{\Gamma}^c$, which resums all Glauber phases, in RG-improved perturbation theory. Here and in the following plots, we identify $\mu_s = Q_0$ and $\mu_h = \sqrt{\hat{s}} = 1\,\text{TeV}$ and use a central rapidity gap with $\Delta Y = 2$. Analyzing different $2 \to 2$ small-angle scattering processes, we conclude

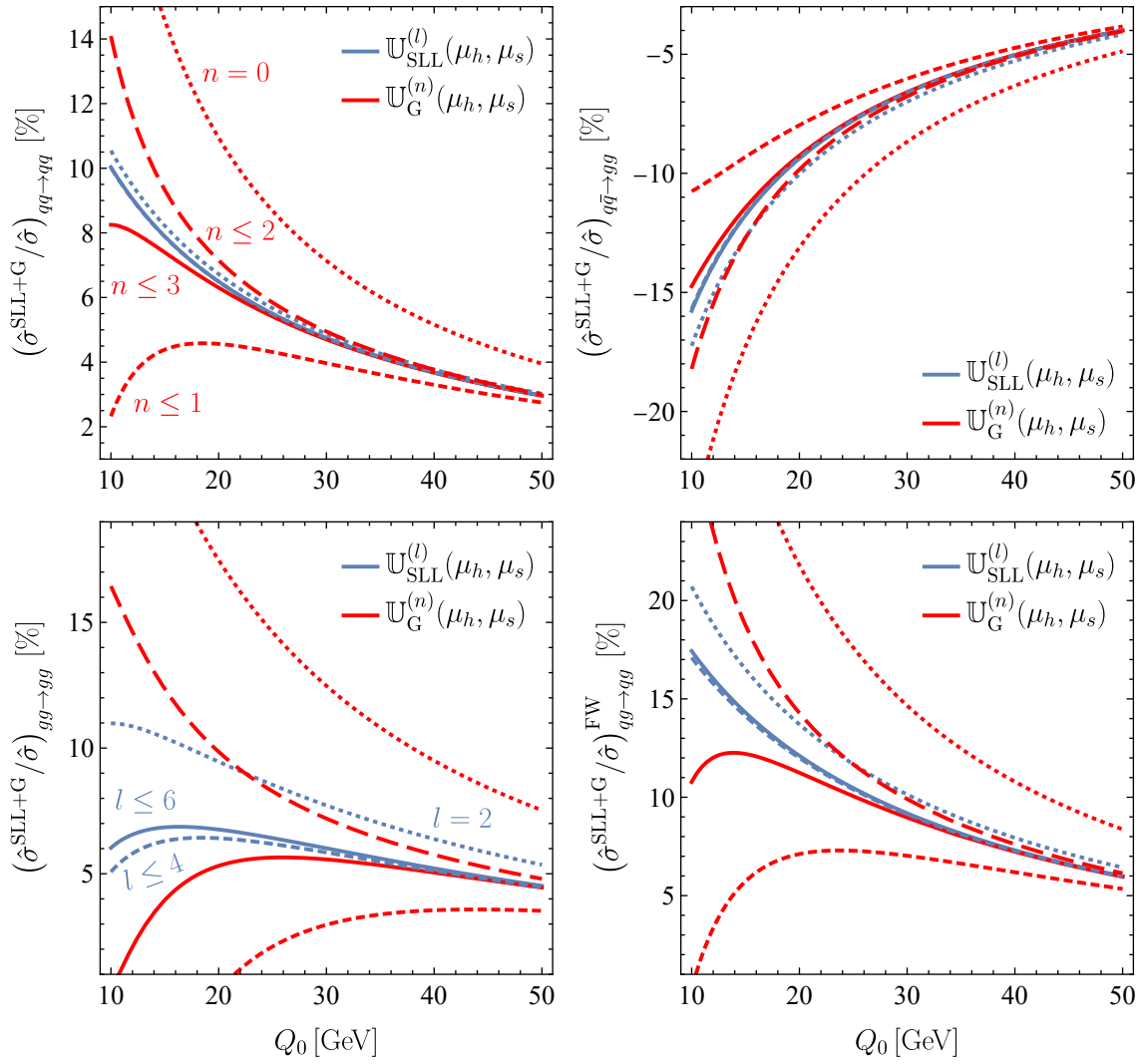

Figure 9.3: Comparison of the expansions in $\boldsymbol{V}^G$ (blue lines) and in $\boldsymbol{\Gamma}^c$ (red lines) of the Glauber series in RG-improved perturbation theory. The plots show the contributions to $qq \to qq$ (upper left), $q\bar{q} \to gg$ (upper right), $gg \to gg$ (lower left), and $qg \to qg$ (lower right) small-angle scattering as a function of the jet-veto scale Q_0, at fixed partonic center-of-mass energy $\sqrt{\hat{s}} = 1\,\mathrm{TeV}$ and for a central rapidity gap with $\Delta Y = 2$. The individual contributions are indicated in all plots with the same line style and labeled in the left panels.

that the expansion in $\boldsymbol{V}^G$ converges significantly faster. The difference between the sum of the first two ($l \le 4$) and first three terms ($l \le 6$) of this expansion is very small over the full range of Q_0 values. Remember that for QCD Born processes only even numbers of Glauber-operator insertions contribute. The expansion in $\boldsymbol{\Gamma}^c$ converges slower. While for larger values of Q_0 the difference between the curves with $n \le 2$ and $n \le 3$ is also very small, for small values of the veto scale the double logarithms give the dominant contribution and the difference is still significant, especially for processes with gluons in the initial state. As the rate of convergence depends on the process-independent coefficients of the basis structures, these observations remain valid for

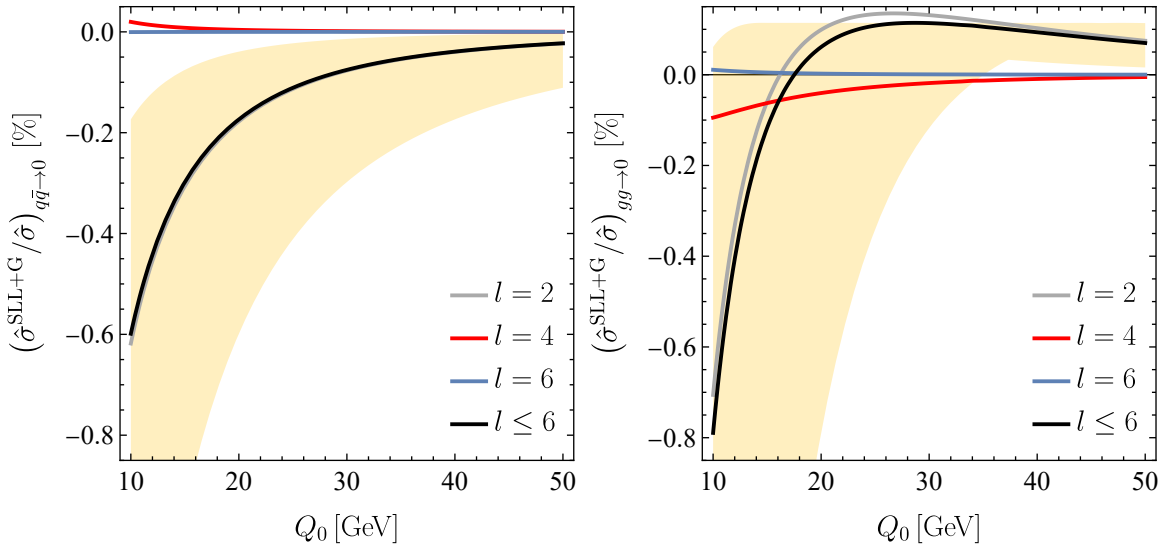

Figure 9.4: Numerical results for the Glauber-series contribution to partonic $2 \to 0$ scattering in RG-improved perturbation theory as a function of the jet-veto scale Q_0, at fixed partonic center-of-mass energy $\sqrt{\hat{s}} = 1\,\mathrm{TeV}$ and for a central rapidity gap with $\Delta Y = 2$. The left plot shows the effect for $q\bar{q} \to 0$ and the right for $gg \to 0$ scattering. The individual contributions of the first three Glauber pairs are shown in gray ($l = 2$, SLLs), red ($l = 4$), and blue ($l = 6$). The sum of all these contributions is indiacte by the black curve. The perturbative uncertainties indicated by the yellow bands are obtained from the variation of the soft scale μ_s by a factor of 2 about its default value.

other scattering processes. Therefore, we analyze the contributions of the Glauber series in the following only in the first expansion. We include up to $l = 6$ Glauber-operator insertions, since the integrals associated with even higher l are numerically hard to evaluate.

9.6.1 $2 \to 0$ Scattering Processes

First, we concentrate on $2 \to 0$ scattering processes, i.e. processes relevant for the production of one or several electroweak bosons at hadron colliders via $q\bar{q}$ scattering or gluon fusion. The respective hard functions are given in (8.100). Evaluating the traces $\langle \boldsymbol{\mathcal{H}}_{q\bar{q}\to 0}\, \boldsymbol{X}^q \rangle$ and $\langle \boldsymbol{\mathcal{H}}_{gg\to 0}\, \boldsymbol{X}^g \rangle$ and combining them with the coefficient vector (9.68), determined in RG-improved perturbation theory, one can analyze the contribution of the Glauber series to the partonic cross section for different values of l. In Figure 9.4 we show the individual contributions for $l = 2, 4, 6$ (gray, red, blue lines) and the summed result (black lines) as a function of the jet-veto scale. The yellow band estimates the perturbative uncertainty and is obtained by varying the soft scale between $Q_0/2 < \mu_s < 2Q_0$. While for $q\bar{q} \to 0$ all higher Glauber pairs give a negligibly small contribution, the $l = 4$ term for $gg \to 0$ gives a sizable contribution compared to the one of the SLLs ($l = 2$). However, the overall magnitude is still very small in both cases and the Glauber series effects the cross sections for electroweak boson production without additional jets only insignificantly.

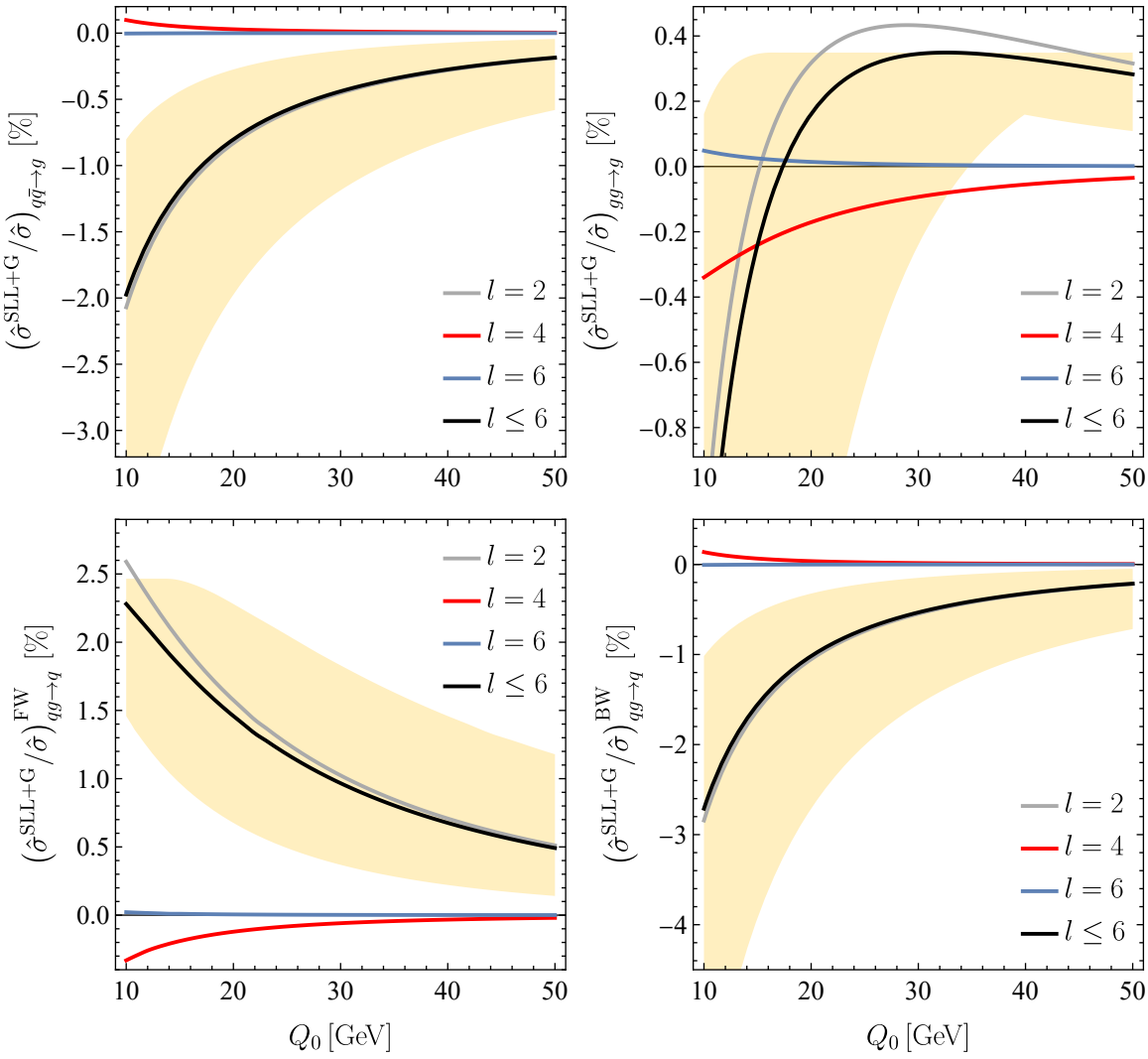

Figure 9.5: Numerical results for the Glauber-series contribution to partonic $2 \to 1$ scattering. The plots show $q\bar{q} \to g$ (upper left), $gg \to g$ (upper right), and $qg \to q$ (bottom row) scattering. The color coding and input parameters are the same as in Figure 9.4.

9.6.2 $2 \to 1$ Scattering Processes

Next, we analyze the impact of the Glauber series on processes like $pp \to H + \text{jet}$ or $pp \to V + \text{jet}$. The hard functions for the three relevant partonic scattering processes $q\bar{q} \to g$, $gg \to g$, and $qg \to q$ are given in (8.104). The contribution of the Glauber series to the cross sections for $2 \to 1$ scattering as a function of the jet-veto scale is shown in Figure 9.5. For processes with quarks in the initial state the total contribution is of $\mathcal{O}(1\%)$, but higher Glauber pairs again give negligibly small contributions. Considering $gg \to g$ scattering, the second Glauber pair ($l = 4$) gives a sizable contribution compared to the SLLs, especially for small values of Q_0. However, the overall effect in this case is small. We note once again that the Glauber series effects the dependence on the scattering kinematics, i.e. the effect for $qg \to q$ differs between forward and backward scattering in sign and magnitude.

9.6.3 $2 \to 2$ Small-Angle Scattering Processes

For $2 \to 2$ scattering processes, we restrict our analysis to small-angle scattering and do not consider interference effects between different color structures. The hard functions for these types of processes can be found in Section 8.4.4. Figure 9.6 shows the Glauber-series contribution to the partonic cross section for six different $2 \to 2$ small-angle scattering processes as a function of the jet-veto scale. For the three depicted quark-initiated processes $qq \to qq$, $q\bar{q} \to q'\bar{q}'$, and $q\bar{q} \to gg$ higher Glauber pairs yield insignificantly small effects. The $l = 4$ contribution (red lines) is already an order of magnitude smaller than the one of the SLLs ($l = 2$, gray lines) and the $l = 6$ curve (blue lines) is indistinguishable from the zero line. A similar statement holds for $gg \to q\bar{q}$ scattering shown in lower right panel. The situation is completely different for $gg \to gg$ scattering, the effect of the second Glauber pair ($l = 4$) reaches -6% for small values of Q_0 and thereby reduces the effect of the SLLs by about a factor 2. The third Glauber pair ($l = 6$) only contributes for very small veto scales in this case. For $qg \to qg$ scattering, the $l = 4$ contribution is still sizable but the significant part of the Glauber-series contribution is due to the SLLs.

In summary, including the full Glauber series always reduces the effect of the SLLs on the partonic scattering cross section, as they are the first term in an alternating series, cf. Section 9.2. However, higher Glauber pairs suffer from a strong factorial suppression, due to the iterated scale integrals, and can be neglected for quark-initiated processes. For processes with gluons in the initial state it suffices to consider also the second Glauber pair ($l = 4$).

Lastly, in Figure 9.7 we compare the in the large-N_c limit resummed Glauber series (red lines) to the SLLs only (gray lines) and the up to $l = 6$ summed result (black lines), which numerically is close to the resummed result with full N_c dependence as we have seen above. We show the effect to the partonic cross section for four different $2 \to 2$ small-angle scattering processes as a function of the jet-veto scale. The red line for the two quark-initiated processes is dashed to allow it to be distinguished from the other lines. As higher terms in the Glauber series are absent in the large-N_c limit for qq and $\bar{q}\bar{q}$ scattering, see (9.116), the gray and red curve lie perfectly on top of each other for $qq \to qq$ scattering.[8] For $q\bar{q} \to gg$ and $qg \to qg$ scattering, the large-N_c approximation works very well as indicated by the close alignment of the red and black curves. In contrast, for $gg \to gg$ scattering the large-N_c approximation is less accurate but can be improved by including the SLLs with full N_c dependence (red dotted line). This is not surprising, as we have seen in the center left panel of Figure 9.6 that the effect of higher Glauber pairs is most pronounced in this case.

[8] Remember that we did not replace $\frac{2C_F}{N_c} \to 1$ in (9.116), as would be demanded in the strict large-N_c limit, thus capturing the contribution of the SLLs completely.

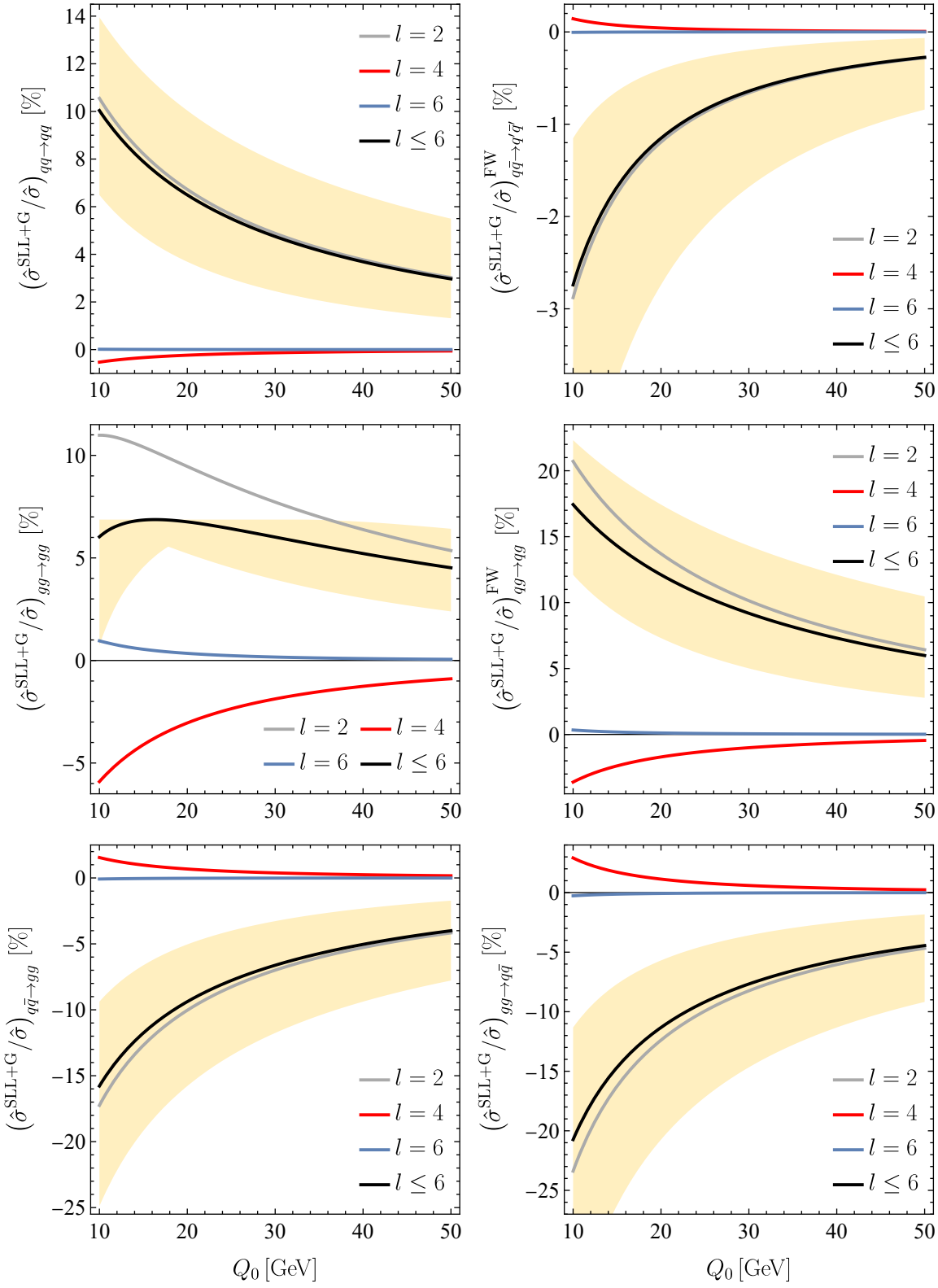

Figure 9.6: Numerical results for the Glauber-series contribution to partonic $2 \to 2$ scattering. The plots show $qq \to qq$ (UL), $q\bar{q} \to q'\bar{q}'$ (UR), $gg \to gg$ (CL), $qg \to qg$ (CR), $q\bar{q} \to gg$ (LL), and $gg \to q\bar{q}$ (LR) small-angle scattering. The color coding and input parameters are the same as in Figure 9.4.

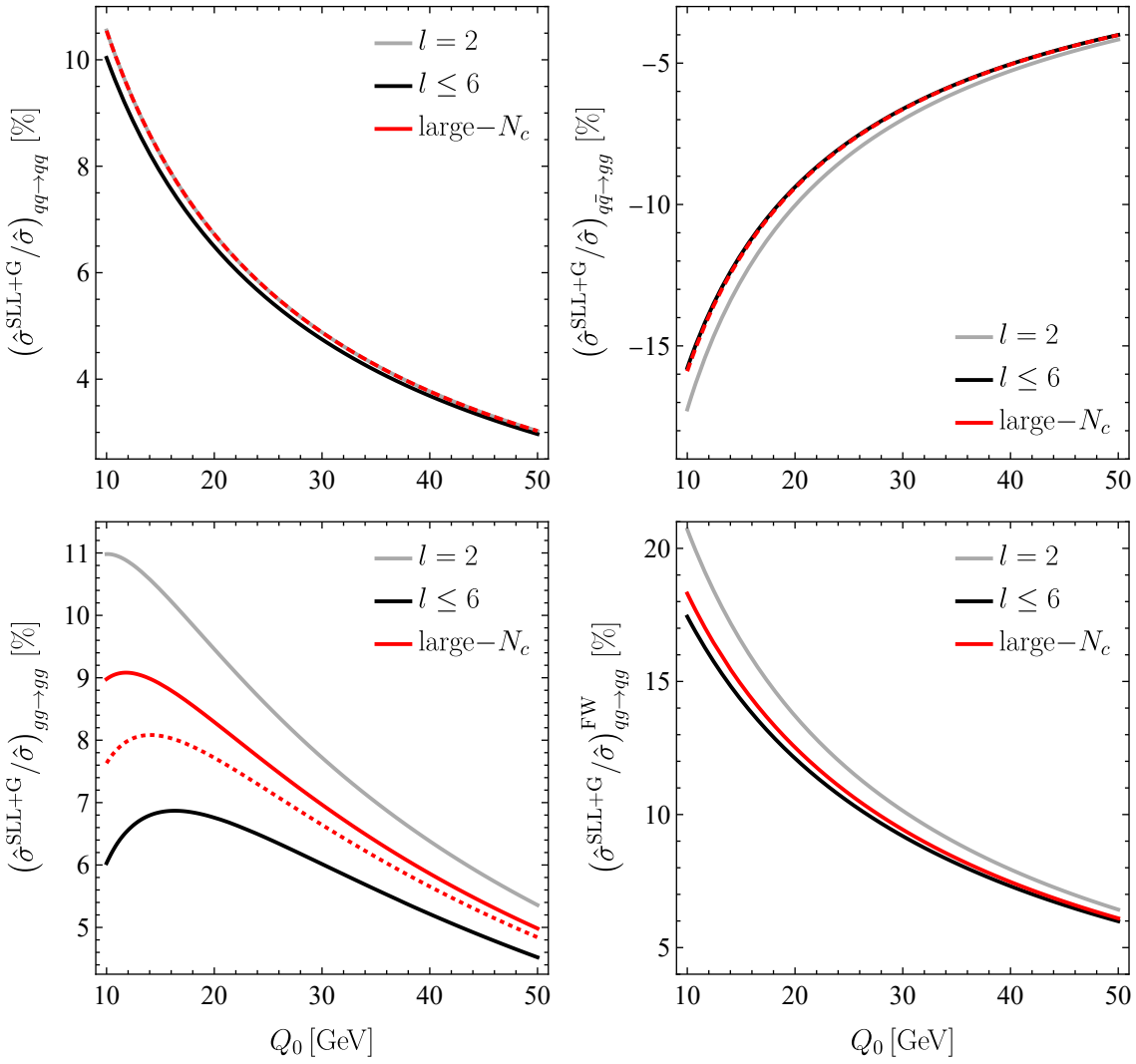

Figure 9.7: Comparison of the Glauber series resummed in the large-N_c limit (red lines) to the SLLs (gray lines) and summed result for $l \leq 6$ (black lines). The plots show the same processes with the same input parameters as in Figure 9.3. The red dotted line in the lower left panel shows the in the large-N_c limit resummed result but with full N_c dependence of the SLLs.

Chapter 10

Conclusion

In this part, we have derived a factorization theorem for gap-between-jet cross sections at hadron colliders. It consists of two parts: a hard function $\boldsymbol{\mathcal{H}}_m$ encoding the high-energy physics at the scale $\mu_h \sim Q$, and a low-energy matrix element $\boldsymbol{\mathcal{W}}_m$ encoding perturbative soft and collinear dynamics associated with the low scale $\mu_s \sim Q_0$, as well as non-perturbative physics. Both objects are matrices in color and multiplicity space. The RG evolution of the hard function from μ_h down to μ_s is governed by an anomalous dimensions matrix $\boldsymbol{\Gamma}^H$ in this space. We have extracted the one-loop form of $\boldsymbol{\Gamma}^H$, which splits into a collinear and a soft part. The former describes a modified DGLAP evolution of the parton distribution functions, as real and virtual part have a different color structure. The latter takes into account soft and soft+collinear emissions from the hard partons as the cancellation of the associated singularities is spoiled by complex Glauber phases. They arise from factorization breaking Glauber-gluon exchanges between initial-state partons.

By solving the RG equation of the hard function, one can resum all large logarithms in the scale ratio $Q/Q_0 \gg 1$. The leading double-logarithmic corrections are obtained by including one soft emission operator $\overline{\boldsymbol{\Gamma}}$ and two Glauber operators $\boldsymbol{V}^G$ alongside an arbitrary number of soft+collinear anomalous dimensions $\boldsymbol{\Gamma}^c$. We have extended the resummation of these super-leading logarithms (SLLs) for quark-initiated processes in [73] to processes with initial-state partons transforming under an arbitrary representation. Working with a fixed strong coupling, the resummed SLLs can be expressed through Kampé de Fériet functions depending on the parameter $w \sim \alpha_s L^2$ containing the double logarithms. Even though the SLLs are obtained from an evolution operator expressed through generalized Sudakov exponentials, their asymptotic behavior for $w \gg 1$ is proportional to $\ln w$ and, therefore, they are not suppressed. Generalizing the resummation to RG-improved perturbation theory, we reduced the result to a simple two-fold integral over generalized Sudakov functions. A detailed numerical analysis for partonic $2 \to M$ scattering processes with $M \leq 2$ revealed that individual contributions in a fixed-order expansion can be huge, especially for gluon-initiated processes, and significant cancellations in the alternating series take place. Resummation is therefore crucial to obtain reliable predictions. For $2 \to 1$ scattering, the first term in the fixed-order expansion vanishes and the SLLs start at four-loop order. For $2 \to 0$ scattering, the second term also vanishes and SLLs arise first one order higher. As higher order contributions are numerically suppressed in these cases, the SLLs play only a subdominant role for Higgs-boson or vector-boson production with a single or no jet. In contrast, for $2 \to 2$ scattering the resummed SLLs can amount for $\mathcal{O}(15\%)$ corrections relative to the Born cross section. Formally, they also start at four-loop order in this case, but the three-loop term contributes significantly as well. For $2 \to 2$ scattering processes different color structures interfere and thereby the SLLs also change the shape of the differential cross section. We discussed this feature exemplary for $qq \to qq$ scattering. The perturbative uncertainty, estimated by varying the soft scale about a factor 2, is of $\mathcal{O}(1)$ and thus the study of subleading

logarithmic corrections is of major importance.

As a first subleading logarithmic correction, we included alongside with the double logarithms an arbitrary number l of Glauber-gluon exchanges. Each of them results in a factor $i\pi$, which numerically is of similar size as the large logarithm. This Glauber series can then be expanded in the two parameters w and $w_\pi \sim \alpha_s \pi^2$, where the $l = 2$ term is just the SLLs. We found that it alternates in both parameters and starts at three-loop order. To determine the all-order structure and perform a (partial) resummation, we developed three color bases. For quark-initiated processes this basis contains 5, for gluon-initiated 20 and for quark-gluon-initiated 14 elements. The elements are constructed from initial-state generators $\boldsymbol{t}_i$ in the fundamental representation and adjoint generators/matrices $\boldsymbol{F}_i$, $\boldsymbol{D}_i$, $\boldsymbol{\Delta}_i$ and $\boldsymbol{\nabla}_i$. Translating the relevant operators to matrices $\mathbb{V}^G$ and $\mathbb{\Gamma}^c$ in one of these bases, we were able to resum either all Glauber phases or all double logarithms for a given number of $\boldsymbol{\Gamma}^c$ and $\boldsymbol{V}^G$ insertions, respectively. Exploiting the latter expansion and working in a fixed coupling approximation, it is possible to determine the large-w asymptotic of the Glauber series. We found that higher terms are parametrically suppressed compared to the SLLs. It turns out that higher order terms in this series are also suppressed numerically. Studying various $2 \to M$ partonic scattering processes for $M \leq 2$ showed that it is always sufficient to truncate after $l = 4$ Glauber-operator insertions, for quark-initiated processes one only needs to consider the SLLs ($l = 2$). Working in the large-N_c approximation, we resummed the Glauber series, which itself is subleading in $1/N_c$, to all orders. The result can be expressed as an at most two-, three- or four-fold integral over generalized Sudakov functions for quark-, quark-gluon- or gluon-initiated processes. From a purely phenomenological point of view, however, a better approximation is obtained by working with the truncated series with full N_c dependence. From a conceptual point of view in contrast, it is remarkable that the resummation of the Glauber series is possible in the large-N_c limit. This suggests that the treatment of non-global logarithms at hadron colliders simplifies in our framework within this limit.

Appendix I

A.3 Color-Helicity-Space Formalism

The amplitude for partonic $1 + 2 \to 3 \dots m$ scattering depends on the colors $\{a_i\}$, spins $\{s_i\}$ and momenta $\{\underline{p}\}$ of all involved partons. It is convenient to introduce an orthonormal basis in color-helicity space $|a_1, \dots, a_m; s_1, \dots, s_m\rangle$ and define a vector in this space with coefficients given by the amplitude [78, 79]

$$\big|\mathcal{M}_m(\{\underline{p}\})\big\rangle \coloneqq \sum_{\{a_i\}} \sum_{\{s_i\}} \big[\mathcal{M}_m(\{\underline{p}\})\big]^{a_1 \dots a_m}_{s_1 \dots s_m} \big|a_1, \dots, a_m; s_1, \dots, s_m\big\rangle \,. \tag{A.3.1}$$

In the following discussion, we omit the momentum dependence to increase readability. The scalar product of this vector with itself is

$$\big\langle \mathcal{M}_m \big| \mathcal{M}_m \big\rangle = \mathcal{N}_1 \mathcal{N}_2 \sum_{\text{spin/color}} |\mathcal{M}_m|^2 \,, \tag{A.3.2}$$

where on the right-hand side one sums (averages) over final-state (initial-state) colors and spins. The factors $\mathcal{N}_i$ for the initial-state partons are canceled by the ones contained in the definition of the trace $\langle \dots \rangle$ in (7.1).

The emission of a gluon from parton i is described by the color charge operator $\boldsymbol{T}_i$. If the color of the emitted gluon is a, its action on the color space is defined by

$$\big\langle a_1, \dots, a_m, a \big| \boldsymbol{T}_i \big| b_1, \dots, b_m \big\rangle \coloneqq \delta^{a_1 b_1} \dots \big[\boldsymbol{T}_i^a\big]^{a_i b_i} \dots \delta^{a_m b_m} \,, \tag{A.3.3}$$

where the non-trivial matrix elements are given by

$$\big[\boldsymbol{T}_i^a\big]^{a_i b_i} = \begin{cases} t^a_{a_i b_i} & \text{for } i \text{ (initial-state) final-state (anti-)quark,} \\ -t^a_{b_i a_i} & \text{for } i \text{ (final-state) initial-state (anti-)quark,} \\ -i f^{a a_i b_i} & \text{for } i \text{ gluon.} \end{cases} \tag{A.3.4}$$

If parton i is an (anti)-quark, the generators are also denoted by $\boldsymbol{t}_i$. Since the low-energy matrix element (7.16) is a unit matrix in helicity space and we are mainly interested in the soft RG evolution (7.63), we concentrate primarily on the color space properties in this work. As we often omit the m-dimensional basis vectors in the main text, it is convenient to define $\boldsymbol{T}_i^a \coloneqq \langle a | \boldsymbol{T}_i$. These generators fulfill the usual $SU(N_c)$ commutation relation separately for each parton

$$\big[\boldsymbol{T}_i^a, \boldsymbol{T}_j^b\big] = i f^{abc}\, \boldsymbol{T}_i^c\, \delta_{ij} \,. \tag{A.3.5}$$

Introducing the notation $\boldsymbol{T}_i \cdot \boldsymbol{T}_j \coloneqq \sum_a \boldsymbol{T}_i^a\, \boldsymbol{T}_j^a$, one finds $\boldsymbol{T}_i \cdot \boldsymbol{T}_i = C_i\, \mathbf{1}$, where

$$C_i = \begin{cases} C_F = \frac{N_c^2 - 1}{2 N_c} & \text{for } i \text{ (anti-)quark,} \\ C_A = N_c & \text{for } i \text{ gluon.} \end{cases} \tag{A.3.6}$$

By definition, the vector $|\mathcal{M}_m\rangle$ is a color-singlet state and thus *color conservation* is [78, 79]

$$\sum_{i=1}^{m} \boldsymbol{T}_i^a \left|\mathcal{M}_m\right\rangle = 0\,. \tag{A.3.7}$$

Similar to gluon emissions, the emission of a quark can be described by the color charge operator $\boldsymbol{T}_i$, see the two middle splittings in Figure 7.4. However, due to the change in the partonic configuration in this case, one needs to consider all partons in the splitting $i \to P + j$. The color structure in (7.56) describing the splitting $q \to g + q$ is defined by

$$\left\langle a_1, \ldots, a_i, \ldots, a_m, a_j \middle| \boldsymbol{\mathcal{C}}_{q\to g} \middle| b_1, \ldots, b_P, \ldots, b_m \right\rangle \coloneqq T_F^{-\frac{1}{2}}\, \delta^{a_1 b_1} \ldots \left[\boldsymbol{T}_j^{b_P}\right]^{a_j a_i} \ldots \delta^{a_m b_m}\,, \tag{A.3.8}$$

where a_i, a_j and b_P are the colors of the quarks and gluon, respectively. In this work we use $T_F = \frac{1}{2}$. For the splitting $g \to q + \bar{q}$ it is

$$\left\langle a_1, \ldots, a_i, \ldots, a_m, a_j \middle| \boldsymbol{\mathcal{C}}_{g\to q} \middle| b_1, \ldots, b_P, \ldots, b_m \right\rangle \coloneqq C_F^{-\frac{1}{2}}\, \delta^{a_1 b_1} \ldots \left[\boldsymbol{T}_j^{a_i}\right]^{a_j b_P} \ldots \delta^{a_m b_m}\,, \tag{A.3.9}$$

where a_i, a_j and b_P are the colors of gluon, anti-quark and quark, respectively. For completeness, we mention $\boldsymbol{\mathcal{C}}_{i\to P} \coloneqq C_i^{-1/2}\, \boldsymbol{T}_i$ if parton i and P are both (anti-)quarks or both gluons, see (A.3.3). These color structures are normalized such that

$$\boldsymbol{\mathcal{C}}_{i\to P}^{\dagger}\, \boldsymbol{\mathcal{C}}_{i\to P} = \mathbf{1}\,. \tag{A.3.10}$$

Physically, they map an amplitude $|\mathcal{M}_m\rangle$ with initial-state parton P to an amplitude $|\mathcal{M}_{m+1}\rangle$ with parton P replaced by i and additional final-state parton j in color space.

In the hard function, the amplitude vector (A.3.1) is squared as a density matrix, thus the emission of a parton changes the color structure on both sides. For a gluon emission, we introduce the $\circ$ symbol defined by

$$\boldsymbol{\mathcal{H}}_m\, \boldsymbol{T}_{i,L} \circ \boldsymbol{T}_{j,R} \coloneqq \boldsymbol{T}_i^{a_k}\, \boldsymbol{\mathcal{H}}_m\, \boldsymbol{T}_j^{b_k}\,, \tag{A.3.11}$$

where a_k (b_k) is the color index of the emitted gluon in the (conjugate) amplitude. Here, the color basis on the left-hand side includes an additional $\langle a_k|$ ($|b_k\rangle$) for the (conjugate) amplitude contained in the definition of $\boldsymbol{T}_i^{a_k}$ ($\boldsymbol{T}_j^{b_k}$) on the right-hand side. Using the $\circ$ symbol, one can rewrite the action of the splitting amplitudes as

$$\delta_{iP}\, \boldsymbol{\mathcal{C}}_{i\to P}\, \boldsymbol{\mathcal{H}}_m\, \boldsymbol{\mathcal{C}}_{i\to P}^{\dagger} = \boldsymbol{\mathcal{H}}_m\, \frac{1}{C_i}\, \boldsymbol{T}_{i,L} \circ \boldsymbol{T}_{i,R} \tag{A.3.12}$$

for the case that parton i and P are the same.

A.4 Heavy Quark Threshold

The perturbative expansion coefficients of the cusp anomalous dimension (7.32) and the QCD β-function (8.62) at one- and two-loop order are given by [114]

$$\begin{aligned} \gamma_0 &= 4\,, & \gamma_1 &= 4\left[\left(\frac{67}{9} - \frac{\pi^2}{3}\right) C_A - \frac{20}{9}\, T_F n_f\right], \\ \beta_0 &= \frac{11}{3}\, C_A - \frac{4}{3}\, T_F n_f\,, & \beta_1 &= \frac{34}{3}\, C_A^2 - \frac{20}{3}\, C_A T_F n_f - 4 C_F T_F n_f\,. \end{aligned} \tag{A.4.1}$$

For $N_c = 3$ colors and $n_f = 5$ active light quark flavors one has $\frac{\beta_1}{\beta_0} = \frac{116}{23} \approx 5.043$ and $\frac{\gamma_1}{\gamma_0} = \frac{151}{9} - \pi^2 \approx 6.908$. We have used these values along with the two-loop expression for the running coupling and starting value $\alpha_s^{(5)}(m_Z) = 0.118$, when deriving our numerical results.

In the realistic scenario where the interval (μ_s, μ_h) contains the top-quark threshold $\mu_t \sim m_t$, one should in principle not work with a fixed value $n_f = 5$ but instead adjust the number of light quark flavors as a function of the scale. For instance, for the scale integrals over the cusp anomalous dimension in (8.6) one should replace

$$\begin{aligned}
&\int_{\mu_j}^{\mu_i} \frac{d\mu}{\mu}\, \gamma_{\rm cusp}\big(\alpha_s(\mu)\big) \\
&\to \int_{\alpha_s(\mu_j)}^{\alpha_s(\mu_i)} d\alpha\, \frac{\gamma_{\rm cusp}^{(5)}(\alpha)}{\beta^{(5)}(\alpha)}\,; && \mu_j < \mu_i < \mu_t\,, \\
&\to \int_{\alpha_s(\mu_j)}^{\alpha_s(\mu_t)} d\alpha\, \frac{\gamma_{\rm cusp}^{(5)}(\alpha)}{\beta^{(5)}(\alpha)} + \int_{\alpha_s(\mu_t)}^{\alpha_s(\mu_i)} d\alpha\, \frac{\gamma_{\rm cusp}^{(6)}(\alpha)}{\beta^{(6)}(\alpha)}\,; && \mu_j < \mu_t < \mu_i\,, \\
&\to \int_{\alpha_s(\mu_j)}^{\alpha_s(\mu_i)} d\alpha\, \frac{\gamma_{\rm cusp}^{(6)}(\alpha)}{\beta^{(6)}(\alpha)}\,; && \mu_t < \mu_j < \mu_i\,,
\end{aligned} \tag{A.4.2}$$

where the superscripts denote the value of n_f for the various integrals. The running of the strong coupling also depends on the value of n_f, as described by the relation $d\alpha_s/d\ln\mu = \beta^{(n_f)}(\alpha_s)$. Note that at two-loop order the coupling is continuous at the quark threshold, such that $\alpha_s^{(5)}(\mu_t) = \alpha_s^{(6)}(\mu_t)$. For simplicity, we refrain from adding a superscript on the running coupling itself, i.e. we use $\alpha_s(\mu) := \alpha_s^{(n_f)}(\mu)$.

For the generalized Sudakov operator $\boldsymbol{U}^c(\mu_i, \mu_j)$ in (8.7) and the associated scalar functions $U^c(v; \mu_i, \mu_j)$ in (8.75) the situation is more complicated, because the relevant scale integral $I_h(\mu_i, \mu_j)$, defined in (9.129), with $\mu_h > \mu_i > \mu_j$ includes a logarithm $\ln(\mu^2/\mu_h^2)$ of the hard scale. Eliminating the scale μ in favor of the running coupling $\alpha_s(\mu)$, and distinguishing the different scale hierarchies, we obtain

$$\begin{aligned}
&I_h(\mu_i, \mu_j) \\
&\to 2N_c \int_{\alpha_s(\mu_j)}^{\alpha_s(\mu_i)} d\alpha\, \frac{\gamma_{\rm cusp}^{(5)}(\alpha)}{\beta^{(5)}(\alpha)} \left[\int_{\alpha_s(\mu_h)}^{\alpha_s(\mu_t)} \frac{d\alpha'}{\beta^{(6)}(\alpha')} + \int_{\alpha_s(\mu_t)}^{\alpha} \frac{d\alpha'}{\beta^{(5)}(\alpha')} \right]; && \mu_j < \mu_i < \mu_t\,, \\
&\to 2N_c \int_{\alpha_s(\mu_j)}^{\alpha_s(\mu_t)} d\alpha\, \frac{\gamma_{\rm cusp}^{(5)}(\alpha)}{\beta^{(5)}(\alpha)} \left[\int_{\alpha_s(\mu_h)}^{\alpha_s(\mu_t)} \frac{d\alpha'}{\beta^{(6)}(\alpha')} + \int_{\alpha_s(\mu_t)}^{\alpha} \frac{d\alpha'}{\beta^{(5)}(\alpha')} \right] \\
&\qquad + 2N_c \int_{\alpha_s(\mu_t)}^{\alpha_s(\mu_i)} d\alpha\, \frac{\gamma_{\rm cusp}^{(6)}(\alpha)}{\beta^{(6)}(\alpha)} \int_{\alpha_s(\mu_h)}^{\alpha} \frac{d\alpha'}{\beta^{(6)}(\alpha')}\,; && \mu_j < \mu_t < \mu_i\,, \\
&\to 2N_c \int_{\alpha_s(\mu_j)}^{\alpha_s(\mu_i)} d\alpha\, \frac{\gamma_{\rm cusp}^{(6)}(\alpha)}{\beta^{(6)}(\alpha)} \int_{\alpha_s(\mu_h)}^{\alpha} \frac{d\alpha'}{\beta^{(6)}(\alpha')}\,; && \mu_t < \mu_j < \mu_i\,.
\end{aligned} \tag{A.4.3}$$

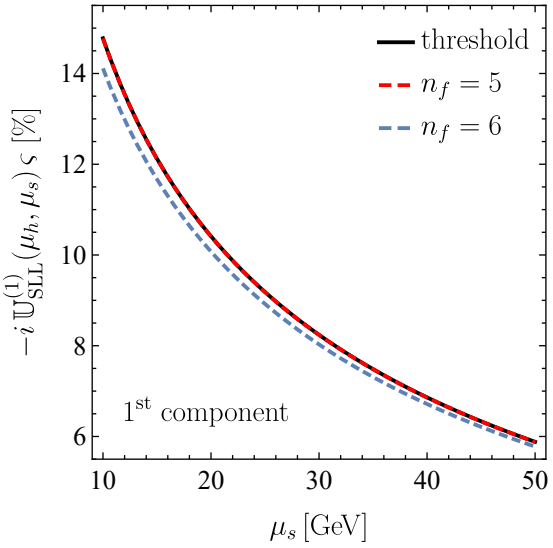

Figure A.1: Numerical results for the evolution vector $\mathbb{U}^{(1)}_{\text{SLL}}(\mu_h,\mu_s)\,\varsigma$ for quark-initiated processes. We show the first component for threshold matching (black line), $\alpha_s^{(5)}(\mu)$ (red line) and $\alpha_s^{(6)}(\mu)$ (blue line). The results are obtained with $\mu_h = 1\,\text{TeV}$ and threshold $\mu_t = m_t = 175\,\text{GeV}$.

Expanding the QCD β-function and the cusp anomalous dimension, it is straightforward to derive from these results the generalization of the expression (8.82) for the various scale hierarchies.

Numerically, it turns out that the effect of accounting for the top-quark threshold is very small. For example, Figure A.1 shows $\mathbb{U}^{(1)}_{\text{SLL}}(\mu_h,\mu_s)\,\varsigma$ as a function of μ_s for the default choices $\mu_h = 1\,\text{TeV}$ and $\mu_t = m_t = 175\,\text{GeV}$.

A.5 Matrix Representations for $qq \to qq$

At the beginning of Section 8.4.5, we introduced an orthonormal basis to decompose the scattering amplitude. Even though this is always possible, it turns out to be more convenient to decompose the amplitude in a non-orthogonal basis $\{|\mathcal{D}_I\rangle\}$ in some cases. The non-trivial scalar products of the basis elements are collected in the Gram matrix

$$\boldsymbol{G}_{IJ} = \langle \mathcal{D}_I | \mathcal{D}_J \rangle\,, \tag{A.5.1}$$

which allows one to write the completeness relation

$$\mathbf{1} = \sum_{I,J} |\mathcal{D}_I\rangle \left(\boldsymbol{G}^{-1}\right)_{IJ} \langle \mathcal{D}_J|\,. \tag{A.5.2}$$

The trace of the "unintegrated" hard function with a color structure in (8.79) can now be expressed as

$$\langle \widetilde{\boldsymbol{\mathcal{H}}}_4\, \boldsymbol{X}_i \rangle = \sum_{I,J,K,L} \left(\boldsymbol{G}^{-1}\right)_{IJ} \langle \mathcal{D}_J | \widetilde{\boldsymbol{\mathcal{H}}}_4 | \mathcal{D}_K \rangle \left(\boldsymbol{G}^{-1}\right)_{KL} \langle \mathcal{D}_L | \boldsymbol{X}_i | \mathcal{D}_I \rangle\,, \tag{A.5.3}$$

where we dropped the spin sum and average factors contained in $\langle \ldots \rangle$ on the right-hand side. It is thus convenient to define as matrix representation of the hard function

$$\left(\widetilde{\boldsymbol{\mathcal{H}}}_4\right)_{IJ} \coloneqq \sum_{K,L} \left(\boldsymbol{G}^{-1}\right)_{IK} \left\langle \mathcal{D}_K \middle| \widetilde{\boldsymbol{\mathcal{H}}}_4 \middle| \mathcal{D}_L \right\rangle \left(\boldsymbol{G}^{-1}\right)_{LJ} = \mathcal{M}_4^{(I)}\, \mathcal{M}_4^{(J)*} \tag{A.5.4}$$

and generalize (8.118) to

$$\left(\boldsymbol{X}_i\right)_{IJ} \coloneqq \left\langle \mathcal{D}_I \middle| \boldsymbol{X}_i \middle| \mathcal{D}_J \right\rangle . \tag{A.5.5}$$

The trace (A.5.3) can then be calculated by

$$\left\langle \widetilde{\boldsymbol{\mathcal{H}}}_4\, \boldsymbol{X}_i \right\rangle = \sum_{I,J} \left(\widetilde{\boldsymbol{\mathcal{H}}}_4\right)_{IJ} \left(\boldsymbol{X}_i\right)_{JI} . \tag{A.5.6}$$

To determine the differential Born cross section (8.116) one replaces the matrix representation of the color structure by the Gram matrix.

Considering $qq \to qq$ scattering as in Section 8.4.5, we choose the orthogonal basis [112]

$$\left\langle a_1, a_2, a_3, a_4 \middle| \mathcal{D}_1 \right\rangle = \delta_{a_3 a_2}\, \delta_{a_4 a_1} , \qquad \left\langle a_1, a_2, a_3, a_4 \middle| \mathcal{D}_2 \right\rangle = t^a_{a_3 a_2}\, t^a_{a_4 a_1} \tag{A.5.7}$$

to avoid the appearance of normalization factors in (8.121). Color structure $\boldsymbol{X}_{11}$ is by definition proportional to the Gram matrix, in this basis one finds

$$\boldsymbol{X}_{11} = J_{12}\, \boldsymbol{G} = J_{12} \begin{pmatrix} N_c^2 & 0 \\ 0 & \frac{C_F N_c}{2} \end{pmatrix} . \tag{A.5.8}$$

The spin-averaged hard function is [112]

$$\begin{aligned} \frac{1}{4} \sum_{\text{spins}} \widetilde{\boldsymbol{\mathcal{H}}}_{qq\to qq} &= (4\pi\alpha_s)^2\, \frac{2C_F}{N_c^2\, r^2} \\ &\times \begin{pmatrix} C_F(r^2 - 2r + 2) & \frac{r^3 - 3r^2 + (N_c+4)r - 2}{1-r} \\ \frac{r^3 - 3r^2 + (N_c+4)r - 2}{1-r} & \frac{(N_c^2+1)r^4 - 4r^3 + (N_c^2+2N_c+7)r^2 - 2(N_c+3)r + 2}{C_F\,(1-r)^2} \end{pmatrix} . \end{aligned} \tag{A.5.9}$$

The matrix representations of the remaining color structures relevant for the SLLs read

$$\begin{aligned} \boldsymbol{X}_1 &= J_{43}\, \frac{C_F N_c^2}{4} \begin{pmatrix} 0 & 1 \\ -1 & 0 \end{pmatrix} , & \boldsymbol{X}_6 &= J_{12}\, \frac{C_F}{N_c} \begin{pmatrix} -2 & -\frac{N_c^2-4}{4N_c} \\ -\frac{N_c^2-4}{4N_c} & -\frac{N_c^2+2}{4N_c^2} \end{pmatrix} , \\ \boldsymbol{X}_2 &= J_{43}\, \frac{C_F}{2} \begin{pmatrix} -2N_c & 1 \\ 1 & C_F \end{pmatrix} , & \boldsymbol{X}_7 &= J_{12}\, \frac{C_{3F}}{N_c^2} \begin{pmatrix} 0 & \frac{N_c^2-4}{N_c} \\ \frac{N_c^2-4}{N_c} & -\frac{N_c^2-4}{N_c^2} \end{pmatrix} , \\ \boldsymbol{X}_3 &= \begin{pmatrix} 0 & 0 \\ 0 & 0 \end{pmatrix} , & \boldsymbol{X}_8 &= J_{12}\, \frac{C_{3F}}{N_c^2} \begin{pmatrix} 0 & \frac{N_c^2-6}{3N_c} \\ \frac{N_c^2-6}{3N_c} & -\frac{N_c^2-6}{3N_c^2} \end{pmatrix} , \\ \boldsymbol{X}_4 &= J_{43}\, \frac{C_F}{2N_c^2} \begin{pmatrix} 2N_c & -1 \\ -1 & -C_F \end{pmatrix} , & \boldsymbol{X}_9 &= J_{12}\, \frac{C_F}{N_c} \begin{pmatrix} 2 & \frac{N_c^2-4}{2N_c} \\ \frac{N_c^2-4}{2N_c} & \frac{3}{2N_c^2} \end{pmatrix} , \\ \boldsymbol{X}_5 &= J_{43}\, \frac{C_F^2}{N_c} \begin{pmatrix} 2N_c & -1 \\ -1 & -C_F \end{pmatrix} , & \boldsymbol{X}_{10} &= J_{12}\, \frac{C_F}{N_c} \begin{pmatrix} 0 & \frac{N_c}{2} \\ \frac{N_c}{2} & -\frac{1}{2} \end{pmatrix} , \end{aligned} \tag{A.5.10}$$

with $J_{43} \coloneqq (J_4 - J_3)$ and $C_{3F} = \frac{N_c^2-4}{2N_c} C_F$ is the cubic Casimir of the fundamental representation [108]. We note that all matrices above except for $\boldsymbol{X}_1$ are symmetric.

A.6 Gluon-Initiated Processes

As the color basis (9.31) for gluon-initiated scattering processes contains 20 elements, matrix representations and coefficient vectors in the basis are large objects. In this appendix, we give the most important quantities relevant for the computations in the main text.

For the matrix representations (9.57) of $\mathbf{\Gamma}^c$ and $\boldsymbol{V}^G$, one finds

$$\tilde{\gamma}^{(j)} = \begin{pmatrix} 1 & 0 & \frac{2}{N_c^2} & 0 & 0 & \frac{2}{N_c^2} & \frac{2}{N_c^2} \\ 0 & 1 & 0 & 0 & -\frac{2}{N_c^2} & 0 & 0 \\ 0 & 0 & \frac{3}{2} & 0 & 0 & 0 & \frac{2}{N_c^2} \\ 0 & 0 & 0 & 2 & -\frac{4}{N_c^2} & 0 & 0 \\ 0 & 0 & 0 & -1 & 2 & 0 & 0 \\ 0 & 0 & 0 & 0 & 0 & 2 & 0 \\ 0 & 0 & 0 & 0 & 0 & 0 & 2 \end{pmatrix}, \qquad \gamma^{(j)} = \begin{pmatrix} \frac{1}{2} & 0 & 0 & -\frac{2}{N_c^2} & 0 & 0 & \frac{6}{N_c^2} \\ 0 & 1 & 0 & -\frac{1}{2N_c^2} & \frac{1}{2N_c^2} & 0 & \frac{3}{2N_c^2} \\ 0 & 0 & \frac{3}{2} & -\frac{1}{N_c^2} & 0 & 0 & \frac{1}{N_c^2} \\ 0 & 0 & -1 & \frac{3}{2} & 0 & 1 & 0 \\ 0 & 0 & 0 & 0 & \frac{3}{2} & 0 & \frac{1}{2} \\ 0 & 0 & 0 & 0 & 0 & 2 & -\frac{1}{N_c^2} \\ 0 & 0 & 0 & 0 & 0 & -1 & 2 \end{pmatrix},$$

$$\gamma = \begin{pmatrix} 0 & 0 & 0 & 0 & -\frac{16}{N_c^2} & 0 \\ 0 & 1 & 0 & 0 & 0 & \frac{4}{N_c^2} \\ 0 & 0 & 1 & 0 & -4 & 0 \\ 0 & 0 & 0 & 2 & -4 & 0 \\ 0 & 0 & 0 & -\frac{1}{N_c^2} & 2 & 0 \\ 0 & 0 & 0 & 0 & 0 & 2 \end{pmatrix}, \qquad \lambda = \begin{pmatrix} -1 & 0 & -\frac{4}{N_c^2} & -\frac{2}{N_c^2} & 0 & 0 & \frac{4}{N_c^2} \\ -1 & 0 & -4 & 1 & \frac{2}{N_c^2} & -2 & \frac{6}{N_c^2} \\ 0 & 0 & -1 & 0 & -1 & 0 & 1 \\ 0 & 0 & -1 & \frac{1}{2} & 0 & 0 & 1 \\ 0 & 0 & \frac{1}{4} & -\frac{1}{2N_c^2} & 0 & \frac{1}{2} & 0 \\ 0 & 0 & 0 & 0 & \frac{1}{2} & 0 & -\frac{3}{2} \end{pmatrix}, \tag{A.6.1}$$

and

$$\nu^{(j)} = \begin{pmatrix} 2 & 0 & 0 & 0 & \frac{4}{N_c^2} & 0 & -\frac{8}{N_c^2} \\ \frac{1}{2} & -\frac{1}{2} & 0 & 0 & \frac{1}{N_c^2} & 0 & -\frac{3}{N_c^2} \\ 1 & 0 & -1 & 0 & -\frac{2}{N_c^2} & 0 & 0 \\ 0 & 0 & -1 & -1 & 0 & 1 & 0 \\ 0 & 0 & 0 & 0 & 1 & 0 & -1 \\ 0 & 0 & 0 & \frac{1}{2} & -\frac{2}{N_c^2} & \frac{1}{2} & -\frac{2}{N_c^2} \\ 0 & 0 & 1 & -1 & 1 & 1 & -1 \end{pmatrix}, \quad \tilde{\nu}^{(j)} = \begin{pmatrix} \frac{4}{N_c^2} & \frac{N_c^2-8}{N_c^2} & \frac{2}{N_c^2} & \frac{1}{N_c^2} & -\frac{1}{N_c^2} & 0 & -\frac{2}{N_c^2} \\ 0 & -1 & 0 & -\frac{1}{N_c^2} & \frac{1}{N_c^2} & 0 & 0 \\ 0 & -1 & -1 & 0 & 0 & 0 & \frac{4}{N_c^2} \\ 0 & 0 & 0 & -\frac{2}{N_c^2} & 0 & 1 & 0 \\ 0 & 0 & -1 & 0 & 0 & 0 & \frac{1}{2} \\ 0 & 0 & 0 & 0 & -\frac{2}{N_c^2} & 1 & \frac{2}{N_c^2} \\ 0 & 0 & 0 & 0 & 0 & 0 & -\frac{1}{2} \end{pmatrix}, \tag{A.6.2}$$

respectively. Resumming the Glauber series in the large-N_c limit, one needs to apply

powers of $\mathbb{V}_i^G$ to ς in (9.130). For odd l values, we find

$$\begin{aligned}
\varsigma_1 &= \frac{1}{2}\,(1,-1,-1,0,0,0,0,\dots)^T\,,\\
\varsigma_{3/2} &= \frac{1}{2}\,(0,0,-1,0,-1,0,0,\dots)^T\,,\\
\varsigma_2 &= \frac{1}{4}\,(0,0,0,0,-1,0,1,\dots)^T\,,
\end{aligned} \tag{A.6.3}$$

where we show only the first seven components being relevant in this case. For even l values, the relevant components 8 to 14 of these vectors are

$$\begin{aligned}
\tilde{\varsigma} &= \frac{1}{2}\,(\dots,4,1,2,0,0,0,0,\dots)^T\,,\\
\tilde{\varsigma}_1 &= \frac{1}{2}\,(\dots,2,1,1,0,0,0,0,\dots)^T\,,\\
\tilde{\varsigma}_{3/2} &= \frac{1}{2}\,(\dots,0,0,1,1,0,0,-1,\dots)^T\,,\\
\tilde{\varsigma}_2 &= \frac{1}{2}\,(\dots,0,0,0,0,-1,0,-1,\dots)^T\,.
\end{aligned} \tag{A.6.4}$$

Performing the products $\mathbb{U}^c(\mu_h,\mu_1)\,\varsigma_i$ in (9.134), the dependence on μ_1 cancels for some terms and one can combine them by evaluating the x_1-integral with terms with one integral less. The simplified result reads

$$\begin{aligned}
\sum_{\ell=1}^{\infty}\mathbb{U}_{\rm SLL}^{(2\ell-1)}(\mu_h,\mu_s)\,\varsigma = \frac{16i\pi}{\beta_0^2}\int_1^{x_s}\frac{dx_3}{x_3}\,\ln\frac{x_s}{x_3}\Bigg\{&U^c(1;\mu_h,\mu_3)\\
&\times\left[\cos^2\left(\frac{\pi N_c}{\beta_0}\,\ln x_3\right)(1,0,0,0,0,0,0,\dots)^T\right.\\
&\left.+\sin^2\left(\frac{\pi N_c}{\beta_0}\,\ln x_3\right)(0,1,0,0,0,0,0,\dots)^T\right]\\
+\frac{\pi N_c}{\beta_0}\int_1^{x_3}\frac{dx_1}{x_1}\,&U^c(\tfrac{3}{2},1;\mu_h,\mu_1,\mu_3)\\
&\times\left[\sin\left(\frac{2\pi N_c}{\beta_0}\,\ln x_3\right)+\sin\left(\frac{2\pi N_c}{\beta_0}\,\ln x_1\right)\right](0,0,1,0,0,0,0,\dots)^T\\
+\left(\frac{\pi N_c}{\beta_0}\right)^2\int_1^{x_3}\frac{dx_2}{x_2}\int_1^{x_2}\frac{dx_1}{x_1}\,&U^c(2,\tfrac{3}{2},1;\mu_h,\mu_1,\mu_2,\mu_3)\\
\times\Bigg(\left[\cos\left(\frac{2\pi N_c}{\beta_0}\,\ln\frac{x_3}{x_1}\right)+\cos\left(\frac{2\pi N_c}{\beta_0}\,\ln\frac{x_2}{x_1}\right)\right]&(0,0,0,0,1,0,1,\dots)^T\\
+\left[\cos\left(\frac{2\pi N_c}{\beta_0}\,\ln x_3\right)+\cos\left(\frac{2\pi N_c}{\beta_0}\,\ln x_2\right)\right]&(0,0,0,0,1,0,-1,\dots)^T\Bigg)\Bigg\}.
\end{aligned} \tag{A.6.5}$$

In contrast to (9.116) for quark-initiated processes, we here work in the strict large-N_c limit. This proves to be convenient as then there is no term with a fourfold integral.

A.7 Quark-Gluon-Initiated Processes

Similar to Appendix A.6, this appendix lists the relevant matrix representations and coefficient vectors for quark-gluon-initiated processes in the basis (9.38).

For the matrix representations (9.61) of $\mathbf{\Gamma}^c$ and $\boldsymbol{V}^G$, one finds

$$\tilde{\gamma}^{(j)} = \begin{pmatrix} 1 & 0 & \frac{1}{N_c^2} \\ 0 & 1 & 0 \\ 0 & 0 & \frac{3}{2} \end{pmatrix}, \qquad \gamma^{(j)} = \begin{pmatrix} \frac{1}{2} & 0 & 0 & 0 & 0 & 0 & 0 & 0 \\ 0 & \frac{1}{2} & 0 & 0 & 0 & -\frac{2}{N_c^2} & 0 & 0 \\ 0 & 0 & 1 & 0 & 0 & 0 & 0 & -\frac{1}{2N_c^2} \\ 0 & 0 & 0 & 1 & 0 & -\frac{1}{2N_c^2} & 0 & 0 \\ 0 & 0 & 0 & 0 & \frac{3}{2} & -\frac{1}{N_c^2} & 0 & 0 \\ 0 & 0 & 0 & 0 & -1 & \frac{3}{2} & 0 & 0 \\ 0 & 0 & 0 & 0 & 0 & 0 & \frac{1}{2} & 0 \\ 0 & 0 & 0 & 0 & 0 & 0 & 0 & \frac{3}{2} \end{pmatrix},$$

$$\gamma = \begin{pmatrix} 0 & 0 & 0 \\ 0 & 1 & 0 \\ 0 & 0 & 1 \end{pmatrix}, \qquad \lambda = \begin{pmatrix} \frac{1}{2} & -\frac{C_F}{2N_c} & 0 & 0 & -\frac{1}{2N_c^2} & -\frac{1}{2N_c^2} & 0 & 0 \\ \frac{1}{2} & -\frac{1}{2} & 0 & 0 & -2 & \frac{1}{2} & 0 & 0 \\ 0 & 0 & 0 & 0 & 0 & 0 & \frac{1}{2} & -\frac{1}{2} \end{pmatrix}, \tag{A.7.1}$$

and

$$\nu^{(j)} = \begin{pmatrix} -1 & 0 & \frac{2}{N_c^2} \\ 2 & 0 & 0 \\ -\frac{1}{2} & \frac{1}{2} & \frac{2}{N_c^2} \\ \frac{1}{2} & -\frac{1}{2} & 0 \\ 1 & 0 & -1 \\ 0 & 0 & -1 \\ 0 & -1 & 0 \\ 0 & 0 & -1 \end{pmatrix}, \quad \tilde{\nu}^{(j)} = \begin{pmatrix} -\frac{2}{N_c^2} & \frac{2}{N_c^2} & -\frac{N_c^2-4}{2N_c^2} & \frac{N_c^2-8}{2N_c^2} & \frac{1}{N_c^2} & \frac{1}{2N_c^2} & 0 & -\frac{1}{2N_c^2} \\ 0 & 0 & \frac{1}{2} & -\frac{N_c^2-4}{2N_c^2} & -\frac{1}{N_c^2} & -\frac{1}{2N_c^2} & -\frac{2}{N_c^2} & \frac{1}{2N_c^2} \\ 0 & 0 & 0 & -1 & -1 & 0 & 0 & -\frac{1}{N_c^2} \end{pmatrix}, \tag{A.7.2}$$

respectively. Resummig the Glauber series in the large-N_c limit, one finds after carrying out the matrix products in (9.130) for odd l values

$$\begin{aligned} \varsigma_1 &= \frac{1}{2}\,(1, -1, -1, \dots)^T, \\ \varsigma_{3/2} &= \frac{1}{2}\,(0, 0, -1, \dots)^T, \end{aligned} \tag{A.7.3}$$

where we only show the first three components relevant for an odd number of Glauber-

operator insertions, and for even l values

$$\begin{aligned}\tilde{\varsigma} &= \frac{1}{2}\,(\ldots,-2,4,-1,1,2,0,0,0,0,0,0)^T,\\ \tilde{\varsigma}_1 &= \frac{1}{2}\,(\ldots,-1,2,-1,1,1,0,1,0,0,0,0)^T,\\ \tilde{\varsigma}_{3/2} &= \frac{1}{2}\,(\ldots,0,0,0,0,1,1,0,1,0,0,0)^T,\end{aligned} \tag{A.7.4}$$

where we dropped the first three components as they are irrelevant. Since eigenvalue $v_8 = 2$ does not appear for quark-gluon-initiated processes, i.e. $\mathbb{V}_2^G = 0$, one finds $\varsigma_2 = \tilde{\varsigma}_2 = 0$.

Performing the products $\mathbb{U}^c(\mu_h,\mu_1)\,\varsigma_i$ in (9.134), the dependence on μ_1 cancels for some terms and one can combine them by evaluating the x_1-integral with terms with one integral less. The simplified result reads

$$\begin{aligned}\sum_{\ell=1}^{\infty}\mathbb{U}_{\text{SLL}}^{(2\ell-1)}(\mu_h,\mu_s)\,\varsigma = \frac{16i\pi}{\beta_0^2}\int_1^{x_s}\frac{dx_2}{x_2}\,\ln\frac{x_s}{x_2}\Bigg\{&U^c(1;\mu_h,\mu_2)\\ &\times\left[\cos^2\left(\frac{\pi N_c}{\beta_0}\,\ln x_2\right)\begin{pmatrix}1\\0\\0\\\vdots\end{pmatrix}+\sin^2\left(\frac{\pi N_c}{\beta_0}\,\ln x_2\right)\begin{pmatrix}0\\1\\0\\\vdots\end{pmatrix}\right]\\ +\frac{\pi N_c}{\beta_0}\int_1^{x_2}\frac{dx_1}{x_1}\,&U^c(\tfrac{3}{2},1;\mu_h,\mu_1,\mu_2)\\ &\times\left[\sin\left(\frac{2\pi N_c}{\beta_0}\,\ln x_2\right)+\sin\left(\frac{2\pi N_c}{\beta_0}\,\ln x_1\right)\right]\begin{pmatrix}0\\0\\1\\\vdots\end{pmatrix}\Bigg\}.\end{aligned} \tag{A.7.5}$$

Similar to (A.6.5), we here work in the strict large-N_c limit as then there is no term with a threefold integral.

Part II

Weak Annihilation Amplitudes in Non-Leptonic B-Meson Decays

Chapter 11

Leading-Power Factorization

The flavor sector of the SM is an excellent place to search for new physics. However, theoretical predictions have to catch up to the increasing experimental accuracy to allow for potential new discoveries. Predictions for exclusive non-leptonic B-meson decay rates suffer from large uncertainties due to the lack of a consistent treatment for power corrections in $\Lambda_{\rm QCD}/m_b$. The QCD factorization approach does not account for weak annihilation contributions as they are a next-to-leading power (NLP) effect. These contributions suffer from *endpoint-divergent convolution integrals* breaking the factorization. It is convenient to study them in the SCET framework as decay products and spectator quark can be described by collinear and soft modes, respectively. The power counting parameter in this case is $\lambda := (\Lambda_{\rm QCD}/m_b)^{1/2}$.[1] Improving the understanding of weak annihilation amplitudes and endpoint-divergent convolution integrals is also crucial to understand the underlying power expansion of SCET.

11.1 Weak Effective Hamiltonian

The highest relevant scales in B-meson decays are the B-meson mass, $m_B \approx 5.3\,\text{GeV}$, and the b-quark mass, $m_b \approx 4.2\,\text{GeV}$. Their difference is consider to be $\mathcal{O}(\lambda^2)$. It is therefore convenient to integrate out all heavier SM particles, i.e. top quark, W, Z and Higgs boson, in the standard EFT approach. This results in new four-fermion and additional two-quark one-photon/gluon interactions encoded in the so-called *weak effective Hamiltonian* [115]. The relevant part for the study of non-leptonic B-meson decays is

$$\mathcal{H}_{\rm eff} = \frac{G_F}{\sqrt{2}} \sum_{q=u,c} \lambda_q \left[C_1 Q_1^q + C_2 Q_2^q + \sum_{i=3}^{10} C_i Q_i + C_{7\gamma} Q_{7\gamma} + C_{8g} Q_{8g} \right] + \text{h.c.}\,, \tag{11.1}$$

where $\frac{G_F}{\sqrt{2}} = \frac{g^2}{8M_W^2}$ is the Fermi constant with M_W the W-boson mass and g the weak-interaction coupling constant. The products of CKM matrix elements are denoted by $\lambda_q = V_{qb}V_{qd}^*$ and fulfill the unitarity relation $\lambda_u + \lambda_c + \lambda_t = 0$.

The current-current operators $Q_{1,2}^q$ arise from integrating out the W boson and are given by

$$Q_1^q = \big(\bar{q}b\big)_{V-A} \big(\bar{d}q\big)_{V-A}\,, \qquad Q_2^q = \big(\bar{q}^i b^j\big)_{V-A} \big(\bar{d}^j q^i\big)_{V-A}\,, \tag{11.2}$$

with $(\bar{q}_1 q_2)_{V\pm A} = \bar{q}_1 \gamma^\mu (1 \pm \gamma_5) q_2$ and i, j being color indices. The QCD penguin operators $Q_{3,\dots,6}$ originate from integrating out the W boson and the top quark, they read

$$\begin{aligned} Q_3 &= \big(\bar{d}b\big)_{V-A} \sum_q \big(\bar{q}q\big)_{V-A}\,, & Q_4 &= \big(\bar{d}^i b^j\big)_{V-A} \sum_q \big(\bar{q}^j q^i\big)_{V-A}\,, \\ Q_5 &= \big(\bar{d}b\big)_{V-A} \sum_q \big(\bar{q}q\big)_{V+A}\,, & Q_6 &= \big(\bar{d}^i b^j\big)_{V-A} \sum_q \big(\bar{q}^j q^i\big)_{V+A}\,, \end{aligned} \tag{11.3}$$

[1] Soft and (anti-)collinear modes have virtuality $p^2 \sim \Lambda_{\rm QCD}^2$.

where a summation over $q = u, d, s, c, b$ is implied. Integrating out also the Z boson, one finds the electroweak penguin operators $Q_{7,\dots,10}$ defined as

$$\begin{aligned} Q_7 &= \frac{3}{2}\,(\bar{d}b)_{V-A} \sum_q e_q\,(\bar{q}q)_{V-A}\,, \qquad Q_8 = \frac{3}{2}\,(\bar{d}^i b^j)_{V-A} \sum_q e_q\,(\bar{q}^j q^i)_{V-A}\,, \\ Q_9 &= \frac{3}{2}\,(\bar{d}b)_{V-A} \sum_q e_q\,(\bar{q}q)_{V+A}\,, \qquad Q_{10} = \frac{3}{2}\,(\bar{d}^i b^j)_{V-A} \sum_q e_q\,(\bar{q}^j q^i)_{V+A}\,, \end{aligned} \tag{11.4}$$

where e_q is the electric charge of quark q. The electromagnetic $Q_{7\gamma}$ and chromomagnetic Q_{8g} dipole operators arise by the same mechansim as the penguin operators but with a mass insertion for the b-quark. They are given by

$$Q_{7\gamma} = \frac{e}{8\pi^2}\, m_b\, \bar{d}\sigma_{\mu\nu}(1+\gamma_5)\, b\, F^{\mu\nu}_{\rm QED}\,, \qquad Q_{8g} = \frac{g_s}{8\pi^2}\, m_b\, \bar{d}\sigma_{\mu\nu}(1+\gamma_5)\, F^{\mu\nu}\, b\,, \tag{11.5}$$

with $\sigma^{\mu\nu} = \frac{i}{2}[\gamma^\mu, \gamma^\nu]$. The QCD field strength tensor is given below (3.1) and the one of QED is defined similarly. The weak effective Hamiltonian for non-leptonic B_s meson decays is obtained by replacing $d \to s$ in the above expressions.

Both the operators Q_i^q, Q_i and the Wilson coefficients C_i in (11.1) depend on the renormalization scale μ. The latter are calculated at a high scale $\mu \sim M_W$ and evolved down to $\mu \sim m_b$ by solving their RG equations. At the low scale, coefficient C_1 is numerically most relevant [116]. The primary challenge in calculating non-leptonic decay amplitudes lies in evaluating the hadronic matrix elements of the local operators present in the effective Hamiltonian.

11.2 QCD Factorization

The QCD factorization approach developed by Beneke, Buchalla, Neubert and Sachrajda (BBNS) in the seminal papers [116–120] provides a systematic theoretical framework for calculating these matrix elements in the heavy-quark limit, i.e. at leading power in λ. For an exclusive decay $B \to M_1\, M_2$ into two light mesons M_1, M_2 the amplitude factorizes as

$$\begin{aligned} \big\langle M_1\, M_2 \big| Q_i \big| B \big\rangle = &\sum_{j=+,0,T} F_j^{B\to M_1}(m_2^2) \int_0^1 dy\, T_{ij}^{\rm I}(y)\, f_2\, \phi_2(y) + (1 \leftrightarrow 2) \\ &+ \int_0^1 d\xi\, dx\, dy\, T_i^{\rm II}(\xi, x, y)\, f_B\, \Phi_B(\xi)\, f_1\, \phi_1(x)\, f_2\, \phi_2(y)\,, \end{aligned} \tag{11.6}$$

where the decay constant and leading-twist light-cone distribution amplitude (LCDA) of the B-meson in QCD are denoted by f_B and Φ_B, respectively. The LCDA is defined by the non-local matrix element

$$\big\langle 0 \big| \bar{d}(tn)\,[tn, 0]\, \frac{\not{n}}{2}\, \gamma_5\, b(0) \big| \bar{B}(p) \big\rangle = i f_B\, \frac{n\cdot p}{2} \int_0^1 d\xi\, e^{-i\xi t n\cdot p}\, \Phi_B(\xi)\,, \tag{11.7}$$

where $[tn, 0]$ denotes a finite-distance Wilson line, and the decay constant by the local limit $t \to 0$. Furthermore, m_i is the mass, f_i the decay constant and ϕ_i the

leading-twist LCDA of meson M_i. More details on their definition can be found in Appendix A.8. The $B \to M_i$ form factors are denoted by $F_j^{B\to M_i}$ and their definitions can be found in [118]. For completeness we mention that if meson M_1 is heavy, only the first term in (11.6) contributes.

The factorization formula (11.6) disentangles the non-perturbative hadronic dynamics – in form of decay constants, form factors and LCDAs – from the hard-scattering kernels $T_{ij}^{\rm I}$ and $T_i^{\rm II}$, which are, in principle, calculable to all orders in perturbation theory. The matrix elements are described in terms of convolutions of these hard-scattering kernels with the LCDAs.

SCET Formulation

SCET has been developed as an EFT for processes involving highly energetic light particles, with particular focus on B-meson decays [12–15, 20]. Proofs of QCD factorization in exclusive B decays using this framework have been presented for the radiative modes $B^- \to \gamma\ell^-\bar\nu_\ell$ in [121, 122] and $\bar B \to \bar K^*\gamma$ in [24].

We now explain how the leading power factorization formula (11.6) for non-leptonic decays translates to SCET, starting for simplicity with the heavy-to-light form factors. By performing a two-step matching, they can be factorized as [11]

$$F_j^{B\to M} = H_j\,\zeta^{B\to M} + \tilde f_B\,\phi_B^+ \star T_j \star f_M\,\phi_M\,, \tag{11.8}$$

where $\tilde f_B$ and ϕ_B^+ denote the B-meson decay constant and leading-twist LCDA defined in HQET, see Appendix A.8. The LCDAs are convoluted with the hard-scattering kernels T_j as indicated by the $\star$ symbol. The universal soft-overlap part of the form factors is denoted by $\zeta^{B\to M}$ and the hard functions H_j are matching coefficients from the matching QCD $\to$ SCET-1. The relevant SCET-1 operators for the first and second term in (11.8) are of the form

$$O_1^\pm = \big[\bar\chi_{hc}\,(1\pm\gamma_5)\,b_v\big]\,, \qquad O_2^\pm = \frac{1}{m_b}\big[\bar\chi_{hc}\,\not{\mathcal{A}}_{hc}^\perp\,(1\pm\gamma_5)\,b_v\big]\,, \tag{11.9}$$

respectively. Hard-collinear fields are displaced in $\bar n$ direction and the flavors of the quarks depend on the heavy-to-light transition under consideration. The correct mass dimension of operator $O_2^\pm$ is ensured by the factor $1/m_b$. To describe decays in transverse polarized vector mesons, one needs to add extra $\gamma_\perp$ to these operators.

The matrix element $\langle M|O_1^\pm|B\rangle$ defines $\zeta^{B\to M}$. Technically, this object needs to be treated in SCET(hc,c,s).[2] Matching the second operator on SCET-2 as explained in Section 4.2 yields an operator with two collinear, one soft, and the HQET b-quark field. The coefficients T_j can thus be decomposed into hard functions convoluted with jet functions, both calculable in perturbation theory. In the absence of leading-power interactions between different sectors in SCET-2, the transition matrix element can finally be factorized, yielding the LCDAs for the two mesons.

[2] Factorizing it further introduces several new non-perturbative functions and leads to endpoint-divergent convolution integrals [123, 124].

Similar to the form factor, one can perform a two-step matching for the full weak effective Hamiltonian (11.1). In SCET-1, one finds two types of operators that contribute at leading power. They read [125]

$$\begin{aligned} O_1^{\pm} &= \left[\bar{\mathcal{X}}_{hc}\, \bar{n}\!\!\!/ (1-\gamma_5) b_v\right] \left[\bar{\mathcal{X}}_{\overline{hc}}\, n\!\!\!/ (1\pm\gamma_5)\mathcal{X}_{\overline{hc}}\right], \\ O_2^{\pm} &= \frac{1}{m_b}\left[\bar{\mathcal{X}}_{hc}\, \mathcal{A}_{hc}^{\perp}\, \bar{n}\!\!\!/ (1+\gamma_5) b_v\right] \left[\bar{\mathcal{X}}_{\overline{hc}}\, n\!\!\!/ (1\pm\gamma_5)\mathcal{X}_{\overline{hc}}\right], \end{aligned} \tag{11.10}$$

where (anti-)hard-collinear fields are displaced along $\bar{n}$ (n). We do not show different color and flavor structures. For decays including transverse polarized vector mesons, one needs to include extra $\gamma_\perp$.

The leading-power factorization theorem for weak effective operators reads [21, 22]

$$\begin{aligned} \left\langle M_1 M_2 \middle| Q_i \middle| B \right\rangle &= \zeta^{B\to M_1}(m_2^2) \int_0^1 dy\, T_i^{\mathrm{I}}(y)\, f_2 \phi_2(y) + (1 \leftrightarrow 2) \\ &\quad + \int_0^\infty \frac{d\omega}{\omega} \int_0^1 dx\, dy\, T_i^{\mathrm{II}}(\omega, x, y)\, \tilde{f}_B \phi_B^+(\omega)\, f_1 \phi_1(x)\, f_2 \phi_2(y)\,. \end{aligned} \tag{11.11}$$

The first line originates from matching the anti-hard-collinear sector of $O_1^{\pm}$ trivially on SCET-2 and translating the hard-collinear sector to the heavy-to-light soft-overlap form factor. Matching both sectors of $O_2^{\pm}$, one obtains SCET-2 operators of $\mathcal{O}(\lambda^{12})$ in the power expansion. Evaluating their matrix elements yields the contribution with three LCDAs in the second line. The kernels T_i^{I} and T_i^{II} can also be decomposed in hard and jet functions. By factoring out $1/\omega$ in the second line, we ensure that the coefficients T_i^{II} only dependent logarithmically on the small variable $\omega \sim \lambda^2$, which can be interpreted as the momentum fraction of the B-meson carried by the light spectator quark. As it was pointed out in [126], this factorization formula is equivalent to (11.6).[3]

11.3 Weak Annihilation

Besides the form factor and hard-scattering contributions in the first and second line of (11.6), respectively, there is a third class which contributes at leading order in α_s to the decay amplitude. This so-called weak annihilation contribution arises from diagrams in which the soft spectator quark participates in the weak effective vertex.[4] The leading power diagrams studied by BBNS are shown in Figure 11.1. Their contribution to the amplitude is of the form [116]

$$\left\langle M_1 M_2 \middle| Q_i \middle| B \right\rangle \sim f_B f_1 f_2 \int_0^1 dx\, dy \left[\frac{1}{\bar{x}^2 y} + \frac{1}{y(1-x\bar{y})}\right] \phi_1(x)\, \phi_2(y) \tag{11.12}$$

for operators Q_i with Dirac structure $(V-A)\otimes(V-A)$. The first and second term arise from diagrams (a) and (b) in Figure 11.1, respectively, whereas the contributions of diagrams (c) and (d) cancel in this case. Here and in the following, we use the abbreviations $\bar{y} = 1-y$ and $\bar{x} = 1-x$.

[3] This conclusion was under debate, see also [127, 128].

[4] Weak annihilation contributions to semileptonic decays are studied in [129].

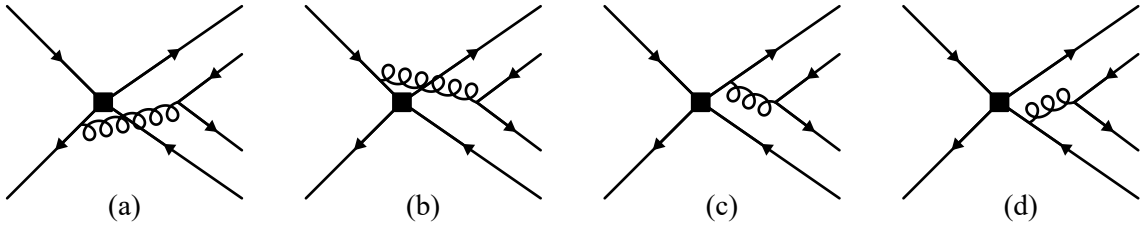

Figure 11.1: Leading power weak annihilation contributions studied by BBNS.

From the asymptotic form of the light-meson LCDA $\phi_1(x) \sim x\bar{x}$, it is obvious that the convolution integral over the momentum fraction x diverges in the endpoint $x \to 1$ for the first term in (11.12). This endpoint divergence clearly breaks factorization of soft and collinear physics. However, comparing the SCET version (11.11) of the leading power factorization formula to the weak annihilation contribution (11.12), we note that there is no factor $1/\omega \sim \lambda^{-2}$ in the latter. It is therefore evident, that weak annihilation contributions are NLP in the λ expansion [116, 118].[5] Even over 20 years after the QCD factorization approach has been developed, it is still an open question whether a more general factorization framework can be established, in which power-suppressed contributions to non-leptonic two-body decay amplitudes of B mesons can be treated consistently.

In the following, we establish such a NLP factorization theorem. For concreteness, we focus on the two-body decay mode $\bar{B}^0 \to K^+K^-$, which is a pure weak annihilation channel. At the valence-quark level, the flavor structure of this decay is $(\bar{d}b) \to (\bar{u}s) + (\bar{s}u)$, i.e. the quark flavors in initial and final state are different and hence both valence quarks of the B meson need to be annihilated. Our discussion is general enough that it can be applied to other two-body decay modes (also those which are not pure annihilation modes) in a straightforward way. The majority of this part is dedicated to the successive matching of the weak effective Hamiltonian from QCD $\to$ SCET-1 $\to$ SCET-2. In Chapters 12 and 13 the two matching steps are presented in detail. The matrix elements of the relevant operators are then evaluated in Chapter 14, before we discuss the cancellation of endpoint divergences in Chapter 15. We conclude in Chapter 16.

[5] To arrive at this conclusion, one has to take into account that $f_B \sim \tilde{f}_B$ and that the B-meson LCDA ϕ_B^+ is normalized to 1.

Chapter 12

Matching onto SCET-1

The weak effective Hamiltonian (11.1) provides an effective description of weak-interaction processes for scales above the b-quark and below the W-boson mass. At the hard scale $\mu_h \sim m_b$, this Hamiltonian is matched onto SCET, which is the appropriate EFT describing b-quark decay processes into light quarks and gauge bosons, which can either be soft (with energies of order $\Lambda_{\rm QCD}$) or collinear (carry large energies of order m_b in one direction). As described in Section 4.2, this matching is performed in two steps:

(1) At the scale $\mu_h \sim m_b$ hard modes, with momenta and virtualities of order m_b, are integrated out and the theory is matched onto SCET-1. The Wilson coefficients arising in this first matching step are called hard functions, and they depend on the scales m_b and $2E_i \sim m_b$, where E_i denote the energies of the light final-state mesons M_i in the rest frame of the B meson.

(2) After the effective theory SCET-1 has been evolved down to the intermediate jet scale $\mu_j \sim \sqrt{m_b \Lambda_{\rm QCD}}$, the (anti-)hard-collinear modes are integrated out and one matches to the final effective theory SCET-2. The Wilson coefficients arising in this second matching step, called jet functions, depend on the scales $\sqrt{2E_i \Lambda_{\rm QCD}}$. The low-energy hadronic matrix elements remaining in SCET-2 capture all long-distance hadronic dynamics in the decay process.

In our discussion we closely follow the two-step matching procedure presented in [11, 23, 24]. Focusing on the decay $\bar{B}^0 \to K^+K^-$, we choose the directions of the K^- and K^+ mesons to be n and $\bar{n}$, respectively. The relevant Lagrangian is given by the sum of SCET-1 Lagrangian (3.11) and HQET Lagrangian (5.7). We express the operators in the EFT through hard-collinear building blocks (3.3) and ordinary soft fields to ensure hard-collinear gauge invariance. The form of these operators is restricted by RPI type (III), see (3.6). Since we are only concerned with the leading contribution to weak annihilation amplitudes, types (I) and (II) are not relevant for the present discussion.

Whenever a SCET-1 operator contains $N_{hc} > 1$ fields in the hard-collinear sector, these fields share the large component $\bar{n} \cdot p_{hc}$ of the total hard-collinear momentum. Since the large components of hard-collinear momenta are always positive, we assign variables $\tilde{y}_i \in (0,1)$ with $i = 1, \ldots, N_{hc}$ to the fields, which specify the fraction of the large moment component carried by the individual fields. Specifically, we define [130]

$$\phi^i_{hc\,(\tilde{y}_i)} \coloneqq \delta\left(\tilde{y}_i - \frac{\bar{n}\cdot\mathcal{P}^i_{hc}}{\bar{n}\cdot\mathcal{P}_{hc}}\right)\phi^i_{hc}\,, \tag{12.1}$$

where the label operator $\bar{n}\cdot\mathcal{P}_{hc}$ projects out the large component of the total hard-collinear momentum carried by an operator, whereas the label operator $\bar{n}\cdot\mathcal{P}^i_{hc}$ projects out the large component of the hard-collinear momentum carried by a given hard-collinear field ϕ^i_{hc}. These label operators are nothing but ordinary derivative operators

$\bar{n}\cdot\partial_{hc}$ acting on the product of all hard-collinear fields or a single field ϕ^i_{hc}, respectively. The hard functions and operator matrix elements depend on the variables $\{y_i\}$, and in the effective Lagrangian one must integrate over these variables. The condition $\sum_i \bar{n}\cdot\mathcal{P}^i_{hc} = \bar{n}\cdot\mathcal{P}_{hc}$ implies that one of these integrations is trivial, since the last δ function can be rewritten as

$$\delta\left(\tilde{y}_{N_{hc}} - \frac{\bar{n}\cdot\mathcal{P}^{N_{hc}}_{hc}}{\bar{n}\cdot\mathcal{P}_{hc}}\right) = \delta\left(1 - \sum_{i=1}^{N_{hc}} \tilde{y}_i\right). \tag{12.2}$$

In a completely analogous way, we introduce momentum-fraction variables $\tilde{x}_i \in (0,1)$ with $i = 1,\ldots,N_{\overline{hc}}$ and define fields $\phi^i_{\overline{hc}\,(\tilde{x}_i)}$ in the anti-hard-collinear sector.

Following [24], we use a generic notation to indicate the Dirac structures that can occur in the various operators. The Dirac basis is spanned by the 16 matrices

$$1\,,\quad \gamma_5\,,\quad \gamma_\perp^\mu\,,\quad \gamma_\perp^\mu\gamma_5\,,\quad \not{n}\,,\quad \not{n}\gamma_5\,,\quad \not{n}\gamma_\perp^\mu\,,\quad \not{\bar{n}}\,,\quad \not{\bar{n}}\gamma_5\,,\quad \not{\bar{n}}\gamma_\perp^\mu\,,\quad \not{n}\not{\bar{n}}\,,\quad [\gamma_\perp^\mu,\gamma_\perp^\nu]\,, \tag{12.3}$$

where the transverse Lorentz indices can take two distinct values. We express all SCET operators in terms of fermion fields with definite chirality (left- or right-handed), and hence there is no need to write out additional factors of γ_5. We thus define the sets

$$\Gamma' = \left\{1, \gamma_\perp^\mu\right\}, \tag{12.4}$$

as well as

$$\Gamma = \left\{1, \gamma_\perp^\mu, \not{n}, \not{n}\gamma_\perp^\mu, \not{\bar{n}}, \not{\bar{n}}\gamma_\perp^\mu, \not{n}\not{\bar{n}}, [\gamma_\perp^\mu,\gamma_\perp^\nu]\right\}. \tag{12.5}$$

The different quark bilinears we encounter in our analysis are then of the form

$$\bar{\mathcal{X}}_{hc}\,\not{\bar{n}}\,\Gamma'(1\pm\gamma_5)\,\mathcal{X}_{hc}\,, \qquad\qquad \bar{\mathcal{X}}_{\overline{hc}}\,\Gamma'(1\pm\gamma_5)\,\mathcal{X}_{hc}\,, \tag{12.6}$$

and

$$\bar{\mathcal{X}}_{hc}\,\not{\bar{n}}\,\Gamma'(1\pm\gamma_5)\,b_v\,, \qquad\qquad \bar{\mathcal{X}}_{hc}\,\Gamma'(1\pm\gamma_5)\,b_v\,, \tag{12.7}$$

and similarly for bilinears in which hard-collinear and anti-hard-collinear fields are interchanged (in which case one must replace $\bar{n}\to n$). Lorentz invariance requires that all open transverse Lorentz indices in the SCET operators are contracted using the symbols (we use the convention $\epsilon^{0123} = -1$)

$$\eta_\perp^{\mu\nu} = \eta^{\mu\nu} - \frac{n^\mu\bar{n}^\nu + \bar{n}^\mu n^\nu}{2}\,, \qquad\qquad \epsilon_\perp^{\mu\nu} = \frac{1}{2}\,\epsilon^{\mu\nu\alpha\beta}\,\bar{n}_\alpha\,n_\beta\,. \tag{12.8}$$

When $\epsilon_\perp$ is contracted with a Dirac matrix next to a (anti-)hard-collinear spinor, it can be traded for $\eta_\perp$ using the relations [123]

$$i\epsilon_\perp^{\mu\nu}\gamma_{\perp\nu}\not{n} = \eta_\perp^{\mu\nu}\gamma_{\perp\nu}\gamma_5\not{n} = \gamma_\perp^\mu\gamma_5\not{n}\,, \qquad -i\epsilon_\perp^{\mu\nu}\gamma_{\perp\nu}\not{\bar{n}} = \eta_\perp^{\mu\nu}\gamma_{\perp\nu}\gamma_5\not{\bar{n}} = \gamma_\perp^\mu\gamma_5\not{\bar{n}}\,, \tag{12.9}$$

which hold in four spacetime dimensions. A corollary of these relations are the identities

$$\begin{aligned}
&\not{n}\gamma_\perp^\mu(1\mp\gamma_5)\otimes\not{\bar{n}}\gamma_{\perp\mu}(1\pm\gamma_5) = 0\,,\\
&\not{\bar{n}}\gamma_\perp^\mu(1\pm\gamma_5)\otimes\not{\bar{n}}\gamma_{\perp\mu}(1\pm\gamma_5) = 0\,,\\
&\not{n}\gamma_\perp^\mu(1\pm\gamma_5)\otimes\not{n}\gamma_{\perp\mu}(1\pm\gamma_5) = 0\,,
\end{aligned} \tag{12.10}$$

which can be used to eliminate certain operators involving four or more fermion fields from the operator basis. Note also that there is no need to allow for the commutator $[\gamma_\perp^\mu, \gamma_\perp^\nu]$ next to a (anti-)hard-collinear spinor, because of the identities [123]

$$\gamma_\perp^\mu \gamma_\perp^\nu \not{n} = \left(\eta_\perp^{\mu\nu} - i\epsilon_\perp^{\mu\nu}\gamma_5\right)\not{n}\,, \qquad \gamma_\perp^\mu \gamma_\perp^\nu \not{\bar{n}} = \left(\eta_\perp^{\mu\nu} + i\epsilon_\perp^{\mu\nu}\gamma_5\right)\not{\bar{n}}\,. \tag{12.11}$$

The Dirac structure in the most general soft-quark bilinear is spanned by the matrices $\Gamma(1 \pm \gamma_5)$.

Expressions for Feynman diagrams in the full theory also contain the heavy-quark momentum $p_b = m_b v + k$, see (5.1). In general, gluon attachments on the incoming b-quark line yields structures of the form

$$\frac{\not{p}_b + \not{q}_n + m_b}{(p_b + q_n)^2 - m_b^2}\,\gamma^{\mu_n} \cdots \frac{\not{p}_b + \not{q}_1 + m_b}{(p_b + q_1)^2 - m_b^2}\,\gamma^{\mu_1}\, u_b(p_b)\,. \tag{12.12}$$

The denominators take the form $2m_b v \cdot (q_i + k) + (q_i + k)^2$. In the numerators, all factors of m_b can be moved next to the b-quark spinor, where they can be replaced by $m_b u_b(p_b) = (m_b \not{v} + \not{k})u_b(p_b)$, assuming that the heavy quark is on-shell, which can always be done in matching calculations. Using momentum conservation, we then replace $m_b v = p_{K^+} + p_{K^-} - k'$, where k' is another soft momentum. Once this is done, the b-quark mass m_b and the 4-velocity v do not enter the SCET operators and matching coefficients.

12.1 Four-Quark Operators

From the structure of the operators in the weak effective Hamiltonian (11.1), it follows that the simplest SCET-1 operators contain four quark fields carrying the flavor quantum numbers of $(\bar{d}b)(\bar{u}u)$ or $(\bar{d}b)(\bar{s}s)$. We choose the reference vectors n and $\bar{n}$ such that the final-state meson K^+ is made up of anti-collinear partons, containing u and $\bar{s}$ as valence quarks. The final-state meson K^- consist of collinear partons, containing s and $\bar{u}$ as valence quarks. Since the original operators Q_i^q and Q_i have mass dimension $D = 6$, we need to construct operators with the same mass dimension in the effective theory. For four-quark operators containing a $(\bar{u}u)$ pair, the three possibilities are

$$\begin{aligned}
O^u_{4,hc,r}(\{\underline{\tilde{y}}\},\mu) &= \left[\bar{\mathcal{X}}^{(d)}_{hc(\tilde{y}_1)}\gamma_{\perp\mu}(1-\gamma_5)b_v\right]\left[\bar{\mathcal{X}}^{(u)}_{\overline{hc}}\,\gamma_\perp^\mu(1-\gamma_5)\mathcal{X}^{(u)}_{hc(\tilde{y}_2)}\right], \\
O^u_{4,\overline{hc},r}(\{\underline{\tilde{x}}\},\mu) &= \left[\bar{\mathcal{X}}^{(d)}_{\overline{hc}(\tilde{x}_2)}\gamma_{\perp\mu}(1-\gamma_5)b_v\right]\left[\bar{\mathcal{X}}^{(u)}_{\overline{hc}(\tilde{x}_1)}\gamma_\perp^\mu(1+\gamma_5)\mathcal{X}^{(u)}_{hc}\right], \\
O^{\pm,u}_{4,s,r}(\mu) &= \left[\bar{q}_s^{(d)}\gamma_{\perp\mu}(1-\gamma_5)b_v\right]\left[\bar{\mathcal{X}}^{(u)}_{\overline{hc}}\,\gamma_\perp^\mu(1\pm\gamma_5)\mathcal{X}^{(u)}_{hc}\right],
\end{aligned} \tag{12.13}$$

where we indicate the quark flavors using superscripts, except for the b-quark. The colored subscripts $(\tilde{y}_i)$ and $(\tilde{x}_i)$ denote the fractions of the total large momentum components $\bar{n}\cdot p_{hc}$ and $n \cdot p_{\overline{hc}}$ carried by the corresponding fields, see Figure 12.1. We denote the collection of these variables by $\{\underline{\tilde{y}}\}$ and $\{\underline{\tilde{x}}\}$. The operators depend on these variables, and they also depend on the renormalization scale μ, as indicated. The third operator is color-marked in gray to indicate that it does not contribute at leading power, see (12.17). Analogous operators in which the two transverse Dirac matrices

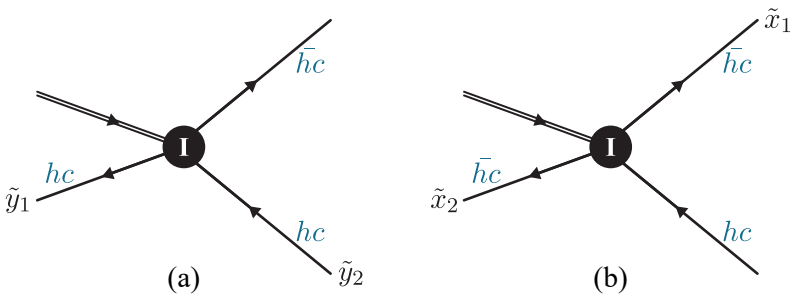

Figure 12.1: Choice of the momentum variables in the SCET-1 four-quark operators $O^u_{4,hc,r}$ (left) and $O^u_{4,\overline{hc},r}$ (right).

are contracted with the $\epsilon_\perp$ symbol can be ignored, because they can be reduced to the above operators using the relations (12.9). Note also that the variants of the first two operators in which the second quark bilinear contains fields with opposite chirality vanish due to the identities in (12.10).

Our labeling of the operators is such that the first superscript ($\pm$), if present, refers to the choices $(1 \pm \gamma_5)$ in the second quark bilinear, whereas the second superscript ($q = u, s$) indicates the flavor content $(\bar{d}b)(\bar{q}q)$ of the operator. The first subscript (here 4) shows the number of fermion fields of an operator, while the second subscript (hc, $\overline{hc}$, s) refers to the SCET field used for the $\bar{d}$-quark. The two up-quark fields carry large energy along the directions n and $\bar{n}$, because they end up in the mesons K^- and K^+. The down-quark field eventually (after matching onto SCET-2) ends up as the soft spectator quark inside the $\bar{B}^0$ meson.

In fixing the Dirac structure of the operators, we have taken into account that the $\bar{d}$-quark in the weak effective Hamiltonian (11.1) is always left-handed, whereas the two up-type quarks have the same chirality. This requires the presence of a matrix $\gamma_\perp$ between the spinors of the second quark bilinear, and Lorentz invariance then requires that the first bilinear also contains such a matrix. Additional insertions of $\not{n}$ or $\not{\bar{n}}$ are then not allowed in the first bilinear, since they would violate boost invariance.

The last subscript (r) refers to the color structure of an operator. For simplicity of the notation we do not write out the color indices of the various quark fields explicitly, but it is understood that in all cases the SCET operators are of the form

$$O^u_{4,hc,r}(\{\underline{\tilde{y}}\},\mu) = \big[\bar{\mathcal{X}}^{(d)\,i_1}_{hc(\tilde{y}_1)}\gamma_{\perp\mu}(1-\gamma_5)b_v^{j_1}\big]\big[\bar{\mathcal{X}}^{(u)\,i_2}_{\overline{hc}}\gamma_\perp^\mu(1-\gamma_5)\mathcal{X}^{(u)\,j_2}_{hc(\tilde{y}_2)}\big]\big[T_{(r)}\big]^{i_1\,i_2}_{j_1\,j_2}\,, \quad (12.14)$$

and similarly for the other operators. The fact that the SCET operators are overall color singlets implies that each color index j_i transforming in the fundamental representation of $SU(N_c)$ must be contracted with an index i_i transforming in the anti-fundamental representation. In the present case, there are two possible index contractions, namely

$$\big[T_{(1)}\big]^{i_1\,i_2}_{j_1\,j_2} = \delta^{i_1 j_1}\,\delta^{i_2 j_2}\,, \qquad \big[T_{(2)}\big]^{i_1\,i_2}_{j_1\,j_2} = \delta^{i_1 j_2}\,\delta^{i_2 j_1}\,. \quad (12.15)$$

They correspond to the familiar color structures, where the two quark bilinears carry color indices $[ii][jj]$ or $[ij][ji]$, respectively.

SCET-1 field	SCET-2 fields	power counting
$\mathcal{X}_{hc}^{(u)}$	$\mathcal{X}_{c}^{(u)}$	λ^2
$\mathcal{A}_{hc}^{\perp}$	$\mathcal{A}_{c}^{\perp}$	λ^2
$\bar{\mathcal{X}}_{hc}^{(d)}$	$\bar{q}_s^{(d)}\mathcal{A}_{c}^{\perp}$	λ^3
$\mathcal{A}_{hc}^{\perp}$	$\bar{\mathcal{X}}_{c}^{(s)}q_s^{(s)}$	λ^3
$\bar{\mathcal{X}}_{hc}^{(d)}$	$(\bar{\mathcal{X}}_{c}^{(s)}q_s^{(s)})\,\bar{q}_s^{(d)}$	λ^4
$\mathcal{X}_{hc}^{(u)}$	$\mathcal{X}_{c}^{(u)}(\bar{\mathcal{X}}_{c}^{(s)}q_s^{(s)})$	λ^5

Table 12.1: Relevant matching relations for hard-collinear quark and gluon fields onto collinear and soft fields in SCET-2 [11, 23, 24]. In the last relation, one has the freedom to add one of the objects $\partial_\perp$, $\mathcal{A}_c^\perp$ or $A_s^\perp$ without encountering a further power suppression. In all other cases, adding extra fields implies a higher-order scaling with λ. The non-trivial matching relations are visualized in Figure 12.2.

It is instructive to explore how the four-quark operators in (12.13) can be matched onto SCET-2 operators containing (at least) two soft quarks for the initial-state $\bar{B}^0$-meson, two collinear quarks for the final-state K^- meson and two anti-collinear quarks for the final-state K^+ meson. While this matching is discussed in detail in Chapter 13, we now briefly sketch the outcome of this discussion. The relevant branchings and their scaling with λ are shown in Table 12.1. For the first operator, we find that the matching relation giving rise to the lowest power of λ is

$$O^u_{4,hc,r} = \big[\,\bar{\mathcal{X}}^{(d)}_{hc}\,\gamma_{\perp\mu}(1-\gamma_5)\,b_v\big]\big[\,\bar{\mathcal{X}}^{(u)}_{\overline{hc}}\,\gamma_\perp^\mu(1-\gamma_5)\,\mathcal{X}^{(u)}_{hc}\,\big] \sim \lambda^{14}\,, \tag{12.16}$$

$$\bar{\mathcal{X}}^{(d)}_{hc} \to (\bar{\mathcal{X}}^{(s)}_{c} q^{(s)}_s)\,\bar{q}^{(d)}_s \sim\lambda^4 \qquad \bar{\mathcal{X}}^{(u)}_{\overline{hc}} \to (\bar{q}^{(s)}_s \mathcal{X}^{(s)}_{\bar{c}})\,\bar{\mathcal{X}}^{(u)}_{\bar{c}} \sim\lambda^5 \qquad \mathcal{X}^{(u)}_{hc} \to \mathcal{X}^{(u)}_{c} \sim\lambda^2$$

and in complete analogy one finds that $O^u_{4,\overline{hc},r}$ is also $\mathcal{O}(\lambda^{14})$. For the third operator, on the other hand, the matching relation with the lowest power of λ reads

$$O^{\pm,u}_{4,s,r} = \big[\bar{q}^{(d)}_s\gamma_{\perp\mu}(1-\gamma_5)\,b_v\big]\big[\,\bar{\mathcal{X}}^{(u)}_{\overline{hc}}\,\gamma_\perp^\mu(1\pm\gamma_5)\,\mathcal{X}^{(u)}_{hc}\,\big] \sim \lambda^{16}\,. \tag{12.17}$$

$$\bar{q}^{(d)}_s \sim\lambda^3 \qquad \bar{\mathcal{X}}^{(u)}_{\overline{hc}} \to (\bar{q}^{(s)}_s \mathcal{X}^{(s)}_{\bar{c}})\,\bar{\mathcal{X}}^{(u)}_{\bar{c}} \sim\lambda^5 \qquad \mathcal{X}^{(u)}_{hc} \to \mathcal{X}^{(u)}_{c}(\bar{\mathcal{X}}^{(s)}_{c} q^{(s)}_s) \sim\lambda^5$$

We show below that SCET-2 operators with power counting λ^{14} are indeed the leading-power operators contributing to weak-annihilation amplitudes. It follows that the operator $O^{\pm,u}_{4,s,r}$ does not contribute at leading power, and we therefore ignore it from now on. Note that in the matching onto SCET-2 the SCET-1 four-quark operators map onto eight-quark operators of the type (we suppress Dirac structures and color indices for simplicity)

$$\big[\bar{q}^{(d)}_s\ldots b_v\;\bar{q}^{(s)}_s\ldots q^{(s)}_s\big]\big[\bar{\mathcal{X}}^{(u)}_{\bar{c}}\ldots\mathcal{X}^{(s)}_{\bar{c}}\big]\big[\bar{\mathcal{X}}^{(s)}_{c}\ldots\mathcal{X}^{(u)}_{c}\big]\,, \tag{12.18}$$

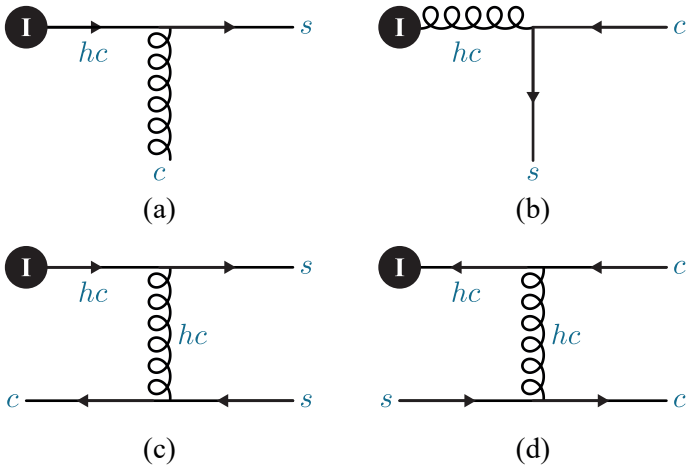

Figure 12.2: Feynman diagrams contributing at tree level to the non-trivial matching for hard-collinear quark and gluon fields onto collinear and soft fields in SCET-2, see Table 12.1. Similar to the last diagram, there are additional $\mathcal{O}(\lambda^5)$ contributions with soft or collinear gluons attached.

and not six-quark operators, as one would naively expect. The hadronic matrix elements of these operators involve so far unknown higher-order distribution amplitudes of the B meson.

In complete analogy with (12.13), for operators containing an $(\bar{s}s)$ pair we define

$$\begin{aligned} O^{s}_{4,\overline{hc},r}(\{\underline{\tilde{x}}\},\mu) &= \left[\bar{\mathcal{X}}^{(d)}_{\overline{hc}(\tilde{x}_1)}\gamma_{\perp\mu}(1-\gamma_5)b_v\right]\left[\bar{\mathcal{X}}^{(s)}_{hc}\gamma^{\mu}_{\perp}(1-\gamma_5)\mathcal{X}^{(s)}_{\overline{hc}(\tilde{x}_2)}\right], \\ O^{s}_{4,hc,r}(\{\underline{\tilde{y}}\},\mu) &= \left[\bar{\mathcal{X}}^{(d)}_{hc(\tilde{y}_2)}\gamma_{\perp\mu}(1-\gamma_5)b_v\right]\left[\bar{\mathcal{X}}^{(s)}_{hc(\tilde{y}_1)}\gamma^{\mu}_{\perp}(1+\gamma_5)\mathcal{X}^{(s)}_{\overline{hc}}\right]. \end{aligned} \tag{12.19}$$

Note that the final-state s-quark is now hard-collinear, while the $\bar{s}$-quark is anti-hard-collinear. We have written these operators in such an order that they are obtained from the operators in (12.13) making the replacements $u \leftrightarrow s$, $hc \leftrightarrow \overline{hc}$, $n \leftrightarrow \bar{n}$, and $\tilde{x}_i \leftrightarrow \tilde{y}_i$. The Wilson coefficients of these operators are later derived by making these replacements.

12.2 Four-Quark Operators with an Additional Gluon

It turns out that SCET-1 operators containing an additional (anti-)hard-collinear gluon field can give rise to SCET-2 operators of the same order in power counting as those descending from the operators in (12.13). We therefore define the boost-invariant operators

$$O^{\pm,u}_{4g,\overline{hc},r}(\{\underline{\tilde{x}},\underline{\tilde{y}}\},\mu) = \frac{1}{n\cdot\mathcal{P}_{\overline{hc}}}\left[\bar{\mathcal{X}}^{(d)}_{\overline{hc}(\tilde{x}_2)}\not{n}(1-\gamma_5)b_v\right]\left[\bar{\mathcal{X}}^{(u)}_{\overline{hc}(\tilde{x}_1)}\mathcal{A}^{\perp}_{hc(\tilde{y}_1)}(1\pm\gamma_5)\mathcal{X}^{(u)}_{hc(\tilde{y}_2)}\right],$$

$$O^{\pm,u}_{4g,hc,r}(\{\underline{\tilde{y}}\},\mu) = \frac{1}{\bar{n}\cdot\mathcal{P}_{hc}}\left[\bar{\mathcal{X}}^{(d)}_{hc(\tilde{y}_1)}\not{\bar{n}}(1-\gamma_5)b_v\right]\left[\bar{\mathcal{X}}^{(u)}_{\overline{hc}}\mathcal{A}^{\perp}_{hc(\tilde{y}_3)}(1\pm\gamma_5)\mathcal{X}^{(u)}_{hc(\tilde{y}_2)}\right],$$

$$O^{\pm,u}_{4g,s\bar{n},r}(\{\underline{\tilde{y}}\},\mu) = \frac{1}{\bar{n}\cdot\mathcal{P}_{hc}}\left[\bar{q}^{(d)}_{s}\not{\bar{n}}(1-\gamma_5)b_v\right]\left[\bar{\mathcal{X}}^{(u)}_{\overline{hc}}\mathcal{A}^{\perp}_{hc(\tilde{y}_1)}(1\pm\gamma_5)\mathcal{X}^{(u)}_{hc(\tilde{y}_2)}\right],$$

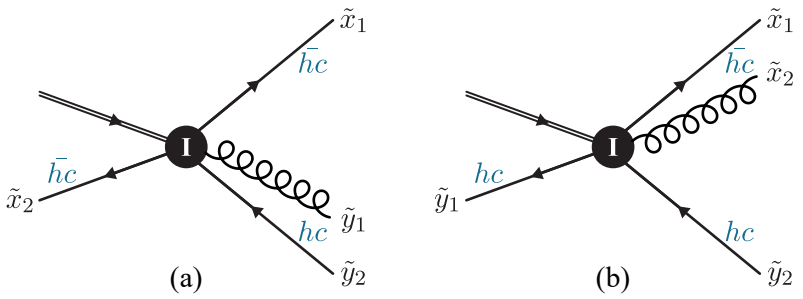

Figure 12.3: Choice of the momentum variables in the SCET-1 four-quark operators $O^{\pm,u}_{4g,\overline{hc},r}$ (left) and $O^{\pm,u}_{4\bar{g},hc,r}$ (right) with an additional (anti-)hard-collinear gluon.

$$O^{\pm,u}_{4g,s\,n,r}(\{\underline{\tilde{y}}\},\mu) = \frac{1}{n\cdot\mathcal{P}_{\overline{hc}}}\left[\bar{q}_s^{(d)}\not{n}(1-\gamma_5)b_v\right]\left[\bar{\mathcal{X}}^{(u)}_{\overline{hc}}\mathcal{A}^{\perp}_{hc(\tilde{y}_1)}(1\pm\gamma_5)\mathcal{X}^{(u)}_{hc(\tilde{y}_2)}\right], \tag{12.20}$$

where the color marking indicates that only the first operator matches on leading-power SCET-2 operators. The subscript $4g$ means that the operators contain four fermion fields and a hard-collinear gluon field. Note that the second operator contains three fields in the hard-collinear sector, and hence it is necessary to introduce two independent momentum-fraction variables $\tilde{y}_1$ and $\tilde{y}_2$. We also define analogous operators with a subscript $4\bar{g}$, in which the hard-collinear gluon field $\mathcal{A}^{\perp}_{hc}$ is replaced by the anti-hard-collinear field $\mathcal{A}^{\perp}_{\overline{hc}}$. The only relevant operator of this type is

$$O^{\pm,u}_{4\bar{g},hc,r}(\{\underline{\tilde{x}},\underline{\tilde{y}}\},\mu) = \frac{1}{\bar{n}\cdot\mathcal{P}_{hc}}\left[\bar{\mathcal{X}}^{(d)}_{hc(\tilde{y}_1)}\not{\bar{n}}(1-\gamma_5)b_v\right]\left[\bar{\mathcal{X}}^{(u)}_{\overline{hc}(\tilde{x}_1)}\mathcal{A}^{\perp}_{\overline{hc}(\tilde{x}_2)}(1\pm\gamma_5)\mathcal{X}^{(u)}_{hc(\tilde{y}_2)}\right]. \tag{12.21}$$

Our choice of momentum fractions in the operators $O^{\pm,u}_{4g,\overline{hc},r}$ and $O^{\pm,u}_{4\bar{g},hc,r}$ is illustrated in Figure 12.3. In the last two operators in (12.20) we add a label n or $\bar{n}$ next to the symbol s indicating a soft down-quark field. This label shows whether the soft quark field is followed by $\not{n}$ or $\not{\bar{n}}$. The fact that the two up-type quarks must have the same chirality requires the presence of $\gamma_\perp$ in the second quark bilinear, and the transverse index on this structure must be contracted with the transverse index on the gluon field. As mentioned earlier, contractions with $\epsilon_\perp$ can always be eliminated using the relations (12.9).

The product of fields in each operator in (12.20) has mass dimension $D = 7$, and to ensure that the effective Lagrangian has mass dimension $D = 6$ requires that each operator must contain an inverse large derivative acting on the (anti-)hard-collinear fields. Which of the two options $\bar{n}\cdot\partial_{hc}$ or $n\cdot\partial_{\overline{hc}}$ applies is determined by boost invariance. Note that the corresponding momentum components $\bar{n}\cdot p_{hc} \sim m_b$ and $n\cdot p_{\overline{hc}} \sim m_b$ are the large components of the (anti-)hard-collinear momenta, and it is natural that the corresponding inverse derivative operators appear after the matching to SCET-1. If an operator contains more than one (anti-)hard-collinear field, then these derivatives can act on any one (or any combination) of these fields. In (12.20) we have introduced the label operators $\bar{n}\cdot\mathcal{P}_{hc}$ and $n\cdot\mathcal{P}_{\overline{hc}}$, which project out the large component of the total (anti-)hard-collinear momentum carried by an operator. In

our case this is the component $\bar{n}\cdot p_{K^-}$ or $n\cdot p_{K^+}$ of one of the momenta of the final-state mesons. The dependence on the momentum fractions carried by the individual fields is contained in the Wilson coefficients multiplying the operators in the effective Lagrangian.

As before, the subscript r on the operators labels the different color structures. Writing out color indices explicitly, the operators in (12.20) take the form

$$\begin{aligned} O^{\pm,u}_{4g,\overline{hc},r}(\{\underline{\tilde{x}},\underline{\tilde{y}}\},\mu) = \frac{1}{n\cdot\mathcal{P}_{\overline{hc}}}\,\big[\bar{\mathcal{X}}^{(d)\,i_1}_{\overline{hc}(\tilde{x}_2)}\,\not{n}(1-\gamma_5)\,b_v^{j_1}\big] \\ \times\,\big[\bar{\mathcal{X}}^{(u)\,i_2}_{\overline{hc}(\tilde{x}_1)}\,(\mathcal{A}^{\perp a}_{hc(\tilde{y}_1)})^{j_2\,i_3}\,(1\pm\gamma_5)\,\mathcal{X}^{(u)\,j_3}_{hc(\tilde{y}_2)}\big]\,\big[T_{(r)}\big]^{i_1\,i_2\,i_3}_{j_1\,j_2\,j_3}\,, \end{aligned} \tag{12.22}$$

and similarly for the other operators. A basis of color tensors is given by

$$\begin{aligned} \big[T_{(1)}\big]^{i_1\,i_2\,i_3}_{j_1\,j_2\,j_3} &= \delta^{i_1 j_1}\,\delta^{i_2 j_2}\,\delta^{i_3 j_3}\,, & \big[T_{(2)}\big]^{i_1\,i_2\,i_3}_{j_1\,j_2\,j_3} &= \delta^{i_1 j_3}\,\delta^{i_2 j_2}\,\delta^{i_3 j_1}\,, \\ \big[T_{(3)}\big]^{i_1\,i_2\,i_3}_{j_1\,j_2\,j_3} &= \delta^{i_1 j_2}\,\delta^{i_2 j_3}\,\delta^{i_3 j_1}\,, & \big[T_{(4)}\big]^{i_1\,i_2\,i_3}_{j_1\,j_2\,j_3} &= \delta^{i_1 j_2}\,\delta^{i_2 j_1}\,\delta^{i_3 j_3}\,, \\ \big[T_{(5)}\big]^{i_1\,i_2\,i_3}_{j_1\,j_2\,j_3} &= \delta^{i_1 j_1}\,\delta^{i_2 j_3}\,\delta^{i_3 j_2}\,, & \big[T_{(6)}\big]^{i_1\,i_2\,i_3}_{j_1\,j_2\,j_3} &= \delta^{i_1 j_3}\,\delta^{i_2 j_1}\,\delta^{i_3 j_2}\,. \end{aligned} \tag{12.23}$$

Note that index contractions with the symbols $\epsilon^{i_1 i_2 i_3}$ and $\epsilon^{j_1 j_2 j_3}$ do not arise in QCD. Taking into account that $SU(N_c)$ generators are traceless, we find that the structures $T_{(5)}$ and $T_{(6)}$ give rise to vanishing operators in (12.22).

Let us again explore how the operators in (12.20) can be matched onto SCET-2 operators containing (at least) two soft quarks for the initial-state $\bar{B}^0$-meson, two collinear quarks for the final-state K^- meson and two anti-collinear quarks for the final-state K^+ meson. Using the matching relations summarized in Table 12.1, we find that the relations giving rise to the lowest power of λ are

$$O^{\pm,u}_{4g,\overline{hc},r} = \frac{1}{n\cdot\mathcal{P}_{\overline{hc}}}\,\big[\underset{\substack{\downarrow\\(\bar{q}_s^{(s)}\mathcal{X}^{(s)}_{\overline{c}})\,\bar{q}_s^{(d)}\\ \sim\lambda^4}}{\bar{\mathcal{X}}^{(d)}_{\overline{hc}}}\,\not{n}(1-\gamma_5)\,\underset{\sim\lambda^3}{b_v}\big]\,\big[\underset{\substack{\swarrow\\ \bar{\mathcal{X}}^{(u)}_{\overline{c}}\\ \sim\lambda^2}}{\bar{\mathcal{X}}^{(u)}_{\overline{hc}}}\,\underset{\substack{\downarrow\\ \bar{\mathcal{X}}^{(s)}_{c}q_s^{(s)}\\ \sim\lambda^3}}{\mathcal{A}^{\perp}_{hc}}\,(1\pm\gamma_5)\,\underset{\substack{\downarrow\\ \mathcal{X}^{(u)}_{c}\\ \sim\lambda^2}}{\mathcal{X}^{(u)}_{hc}}\big] \sim\lambda^{14}\,, \tag{12.24}$$

but

$$\begin{aligned} O^{\pm,u}_{4g,hc,r} &= \frac{1}{\bar{n}\cdot\mathcal{P}_{hc}}\,\big[\underset{\substack{\downarrow\\(\bar{\mathcal{X}}^{(s)}_{c}q_s^{(s)})\,\bar{q}_s^{(d)}\\ \sim\lambda^4}}{\bar{\mathcal{X}}^{(d)}_{hc}}\,\not{\bar{n}}(1-\gamma_5)\,\underset{\sim\lambda^3}{b_v}\big]\,\big[\underset{\substack{\downarrow\\(\bar{q}_s^{(s)}\mathcal{X}^{(s)}_{\overline{c}})\,\bar{\mathcal{X}}^{(u)}_{\overline{c}}\\ \sim\lambda^5}}{\bar{\mathcal{X}}^{(u)}_{\overline{hc}}}\,\underset{\substack{\searrow\\ \not{\mathcal{A}}^{\perp}_{c}\\ \sim\lambda^2}}{\mathcal{A}^{\perp}_{hc}}\,(1\pm\gamma_5)\,\underset{\substack{\downarrow\\ \mathcal{X}^{(u)}_{c}\\ \sim\lambda^2}}{\mathcal{X}^{(u)}_{hc}}\big] \sim\lambda^{16}\,, \\ O^{\pm,u}_{4g,hc,r} &= \frac{1}{\bar{n}\cdot\mathcal{P}_{hc}}\,\big[\underset{\substack{\downarrow\\ \bar{q}_s^{(d)}\mathcal{A}^{\perp}_{c}\\ \sim\lambda^3}}{\bar{\mathcal{X}}^{(d)}_{hc}}\,\not{\bar{n}}(1-\gamma_5)\,\underset{\sim\lambda^3}{b_v}\big]\,\big[\underset{\substack{\downarrow\\(\bar{q}_s^{(s)}\mathcal{X}^{(s)}_{\overline{c}})\,\bar{\mathcal{X}}^{(u)}_{\overline{c}}\\ \sim\lambda^5}}{\bar{\mathcal{X}}^{(u)}_{\overline{hc}}}\,\underset{\substack{\searrow\\ \bar{\mathcal{X}}^{(s)}_{c}q_s^{(s)}\\ \sim\lambda^3}}{\mathcal{A}^{\perp}_{hc}}\,(1\pm\gamma_5)\,\underset{\substack{\downarrow\\ \mathcal{X}^{(u)}_{c}\\ \sim\lambda^2}}{\mathcal{X}^{(u)}_{hc}}\big] \sim\lambda^{16}\,. \end{aligned} \tag{12.25}$$

Similarly, one finds that the leading SCET-2 operators deriving from the operators $O_{4g,s\bar{n},r}$ and $O_{4g,sn,r}$ scale like λ^{16}. Hence, only the first operator in (12.20) contributes at leading power in λ.

As mentioned earlier, the corresponding operators containing an $(\bar{s}s)$ pair instead of the $(\bar{u}u)$ pair can be constructed from the operators in (12.20) and (12.21) by making the replacements $u \leftrightarrow s$, $hc \leftrightarrow \overline{hc}$, $n \leftrightarrow \bar{n}$, and $\tilde{x}_i \leftrightarrow \tilde{y}_i$. This yields

$$\begin{aligned} O^{\pm,s}_{4\bar{g},hc,r}(\{\underline{\tilde{x}},\underline{\tilde{y}}\},\mu) &= \frac{1}{\bar{n}\cdot\mathcal{P}_{hc}}\left[\bar{\mathcal{X}}^{(d)}_{hc(\tilde{y}_2)}\,\bar{n}\!\!\!/\,(1-\gamma_5)\,b_v\right]\left[\bar{\mathcal{X}}^{(s)}_{hc(\tilde{y}_1)}\mathcal{A}^{\perp}_{\overline{hc}(\tilde{x}_1)}(1\pm\gamma_5)\,\mathcal{X}^{(s)}_{\overline{hc}(\tilde{x}_2)}\right], \\ O^{\pm,s}_{4g,\overline{hc},r}(\{\underline{\tilde{x}},\underline{\tilde{y}}\},\mu) &= \frac{1}{n\cdot\mathcal{P}_{\overline{hc}}}\left[\bar{\mathcal{X}}^{(d)}_{\overline{hc}(\tilde{x}_1)}\,n\!\!\!/\,(1-\gamma_5)\,b_v\right]\left[\bar{\mathcal{X}}^{(s)}_{hc(\tilde{y}_1)}\mathcal{A}^{\perp}_{hc(\tilde{y}_2)}(1\pm\gamma_5)\,\mathcal{X}^{(s)}_{\overline{hc}(\tilde{x}_2)}\right]. \end{aligned} \tag{12.26}$$

The different color structures of these operators are defined as

$$\begin{aligned} O^{\pm,s}_{4\bar{g},hc,r}(\{\underline{\tilde{x}},\underline{\tilde{y}}\},\mu) &= \frac{1}{\bar{n}\cdot\mathcal{P}_{hc}}\left[\bar{\mathcal{X}}^{(d)\,i_1}_{hc(\tilde{y}_2)}\,\bar{n}\!\!\!/\,(1-\gamma_5)\,b_v^{j_1}\right] \\ &\quad\times\left[\bar{\mathcal{X}}^{(s)\,i_2}_{hc(\tilde{y}_1)}(\mathcal{A}^{\perp a}_{\overline{hc}(\tilde{x}_1)})^{j_2\,i_3}(1\pm\gamma_5)\,\mathcal{X}^{(s)\,j_3}_{\overline{hc}(\tilde{x}_2)}\right]\left[T_{(r)}\right]^{i_1\,i_2\,i_3}_{j_1\,j_2\,j_3}, \end{aligned} \tag{12.27}$$

where the color tensors are the same as in (12.23).

This exhausts the list of four-quark operators which need to be retained in SCET-1. Operators containing a soft gluon field $A_s^\perp$ or a $\partial_\perp$ derivative instead of the (anti-)hard-collinear gluon field in (12.20) do not contribute at leading order to the weak annihilation amplitudes, because after matching onto SCET-2 they give rise to scaling relations analogous to that shown in the first line of (12.25). Similarly, operators with two (anti-)hard-collinear gluon fields give rise to subleading power SCET-2 operators. The same remark holds for four-quark operators containing more than one (anti-)hard-collinear gluon field, because any additional field counts at least $\mathcal{O}(\lambda^2)$.

12.3 Six-Quark Operators

The hard-scattering contributions to the weak annihilation amplitudes shown in Section 11.3 correspond to SCET-1 operators containing six quark fields, one for each valence quark of the initial- and final-state mesons. We thus define the boost-invariant operators

$$\begin{aligned} O^{\pm}_{6,s\bar{n},r}(\{\underline{\tilde{x}},\underline{\tilde{y}}\},\mu) &= \frac{1}{n\cdot\mathcal{P}_{\overline{hc}}\,(\bar{n}\cdot\mathcal{P}_{hc})^2}\left[\bar{q}_s^{(d)}\,\bar{n}\!\!\!/\,(1-\gamma_5)\,b_v\right] \\ &\quad\times\left[\bar{\mathcal{X}}^{(u)}_{\overline{hc}(\tilde{x}_1)}\,n\!\!\!/\,(1\pm\gamma_5)\,\mathcal{X}^{(s)}_{\overline{hc}(\tilde{x}_2)}\right]\left[\bar{\mathcal{X}}^{(s)}_{hc(\tilde{y}_1)}\,\bar{n}\!\!\!/\,(1\pm\gamma_5)\,\mathcal{X}^{(u)}_{hc(\tilde{y}_2)}\right], \\ O^{\pm}_{6,sn,r}(\{\underline{\tilde{x}},\underline{\tilde{y}}\},\mu) &= \frac{1}{(n\cdot\mathcal{P}_{\overline{hc}})^2\,\bar{n}\cdot\mathcal{P}_{hc}}\left[\bar{q}_s^{(d)}\,n\!\!\!/\,(1-\gamma_5)\,b_v\right] \\ &\quad\times\left[\bar{\mathcal{X}}^{(u)}_{\overline{hc}(\tilde{x}_1)}\,n\!\!\!/\,(1\pm\gamma_5)\,\mathcal{X}^{(s)}_{\overline{hc}(\tilde{x}_2)}\right]\left[\bar{\mathcal{X}}^{(s)}_{hc(\tilde{y}_1)}\,\bar{n}\!\!\!/\,(1\pm\gamma_5)\,\mathcal{X}^{(u)}_{hc(\tilde{y}_2)}\right], \\ O^{\pm}_{6,hc,r}(\{\underline{\tilde{x}},\underline{\tilde{y}}\},\mu) &= \frac{1}{n\cdot\mathcal{P}_{\overline{hc}}\,(\bar{n}\cdot\mathcal{P}_{hc})^2}\left[\bar{\mathcal{X}}^{(d)}_{hc(\tilde{y}_3)}\,\bar{n}\!\!\!/\,(1-\gamma_5)\,b_v\right] \\ &\quad\times\left[\bar{\mathcal{X}}^{(u)}_{\overline{hc}(\tilde{x})}\,n\!\!\!/\,(1\pm\gamma_5)\,\mathcal{X}^{(s)}_{\overline{hc}}\right]\left[\bar{\mathcal{X}}^{(s)}_{hc(\tilde{y}_1)}\,\bar{n}\!\!\!/\,(1\pm\gamma_5)\,\mathcal{X}^{(u)}_{hc(\tilde{y}_2)}\right], \end{aligned}$$

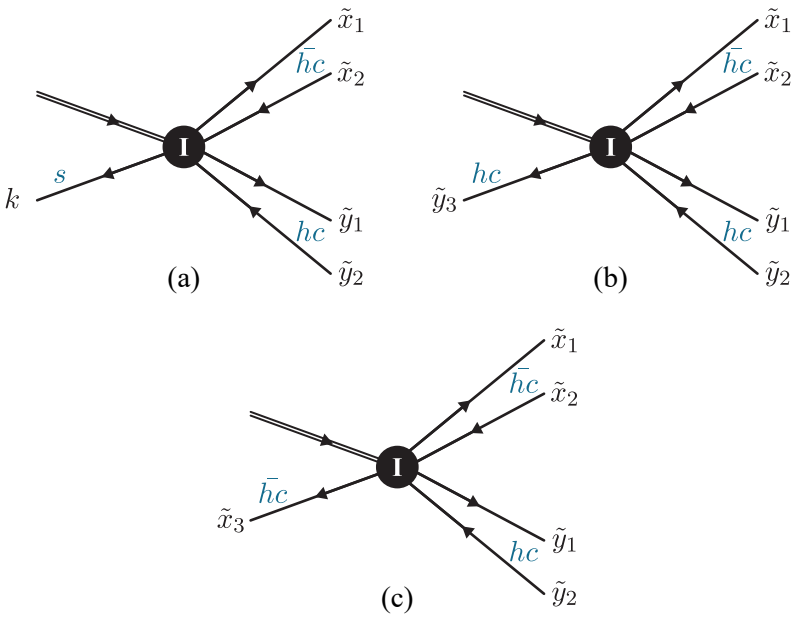

Figure 12.4: Choice of the momentum variables in the SCET-1 six-quark operators $O^{\pm}_{6,s\bar{n},r}$ and $O^{\pm}_{6,sn,r}$ (left), $O^{\pm}_{6,hc,r}$ (right), and $O^{\pm}_{6,\overline{hc},r}$ (bottom).

$$O^{\pm}_{6,\overline{hc},r}(\{\underline{\tilde{x}},\underline{\tilde{y}}\},\mu) = \frac{1}{(n\cdot\mathcal{P}_{\overline{hc}})^2\,\bar{n}\cdot\mathcal{P}_{hc}}\left[\bar{\mathcal{X}}^{(d)}_{\overline{hc}(\tilde{x}_3)}\,\not{n}(1-\gamma_5)\,b_v\right] \times\left[\bar{\mathcal{X}}^{(u)}_{\overline{hc}(\tilde{x}_1)}\,\not{n}(1\pm\gamma_5)\,\mathcal{X}^{(s)}_{\overline{hc}(\tilde{x}_2)}\right]\left[\bar{\mathcal{X}}^{(s)}_{hc(\tilde{y}_1)}\,\not{\bar{n}}(1\pm\gamma_5)\,\mathcal{X}^{(u)}_{hc(\tilde{y}_2)}\right], \quad (12.28)$$

where one must choose the same sign in the last two quark bilinears in each operator. The reason is that the two up quarks must have the same chirality and the same is true for the two strange quarks. One pair is produced from the chiral weak currents in the weak effective Hamiltonian (11.1), while the other pair is generated from QCD interactions, which preserve chirality in the limit where the light quark masses are neglected. The six fermion fields in each operator have mass dimension $D = 9$, and ensuring mass dimension $D = 6$ requires the presence of three inverse large derivatives. As before, we implement them using label operators. Which derivatives must be chosen is dictated by boost invariance. Once again, it is understood that the derivatives can act on any field (or any combination of fields) in the relevant sectors, and the Wilson coefficients of the operators contain the dependence on the momentum fractions carried by these fields. Our choice of momentum fractions in the various six-quark operators is illustrated in Figure 12.4.

In principle, one could consider an analogous set of six-quark operators containing an additional pair of transverse Dirac matrices $\gamma_\perp$. The above argument that the two up quarks must have the same chirality and the two strange quarks must have the same chirality, while the chiralities of each pair can be different, requires that the transverse Dirac matrices must be inserted in the last two quark bilinears, giving rise to the structure

$$\not{n}\gamma^\mu_\perp(1\mp\gamma_5)\otimes\not{\bar{n}}\gamma_{\perp\mu}(1\pm\gamma_5)\,. \quad (12.29)$$

However, any operator containing this structure vanishes according to (12.10).

As throughout this thesis, the subscript r on the operators labels the different color structures. Writing out color indices explicitly, the first operator in (12.28) takes the form

$$O^{\pm}_{6,s\bar{n},r}(\{\underline{\tilde{x}},\underline{\tilde{y}}\},\mu) = \frac{1}{n\cdot\mathcal{P}_{\overline{hc}}\,(\bar{n}\cdot\mathcal{P}_{hc})^2}\,\big[\bar{q}_s^{(d)\,i_1}\,\bar{\not{n}}(1-\gamma_5)\,b_v^{j_1}\big]\big[\bar{\mathcal{X}}^{(u)\,i_2}_{\overline{hc}(\tilde{x}_1)}\,\not{n}(1\pm\gamma_5)\,\mathcal{X}^{(s)\,j_2}_{\overline{hc}(\tilde{x}_2)}\big] \\ \times\big[\bar{\mathcal{X}}^{(s)\,i_3}_{hc(\tilde{y}_1)}\,\bar{\not{n}}(1\pm\gamma_5)\,\mathcal{X}^{(u)\,j_3}_{hc(\tilde{y}_2)}\big]\big[T_{(r)}\big]^{i_1\,i_2\,i_3}_{j_1\,j_2\,j_3}\,, \tag{12.30}$$

with basis color structures defined in (12.23). The color structure of the remaining operators can be written in an analogous form. Finally, note that we have omitted the superscript $q = u, s$ on the six-quark operators, because under the replacements $u \leftrightarrow s$, $hc \leftrightarrow \overline{hc}$, $n \leftrightarrow \bar{n}$, $\tilde{x}_i \leftrightarrow \tilde{y}_i$, and $(i_2, j_2) \leftrightarrow (i_3, j_3)$ the operators map onto themselves. They therefore receive matching contributions from operators in the full theory with flavor structures $(\bar{d}b)(\bar{u}u)$ and $(\bar{d}b)(\bar{s}s)$.

The only possibility to match the operators (12.28) to leading power SCET-2 operators is by trivial matching, see Table 12.1. Therefore, six-quark operators containing additional $\partial_\perp$ derivatives do not contribute at leading power to weak annihilation amplitudes.

12.4 Comments on the Structure of the Operators

The SCET-1 operators collected above have different power counting in λ. Yet, they give rise to contributions of the same (leading) power after they have been matched onto the relevant SCET-2 operators. This is discussed in detail in Chapter 13. Operators with more fields cannot contribute by the same argument given at the end of Section 12.3.

For the SCET-1 operators constructed in this chapter, it is understood that all fields are evaluated at the spacetime point $z = 0$ after the derivatives have been carried out. Alternatively, one can work with operators in which the hard-collinear fields are displaced from $z = 0$ by a light-like distance $s_i\bar{n}$, whereas the anti-hard-collinear fields are displaced by a light-like distance $t_i n$, see Section 7.1. The inverse derivatives can then be generated by integrals over the parameters s_i and t_i, e.g.

$$\int_{-\infty}^{0} dt\,\phi_{hc}(t\bar{n}) = \int_{-\infty}^{0} dt\,e^{-it\,(i\bar{n}\cdot\partial+i0)}\,\phi_{hc}(z)\Big|_{z=0} = \frac{i}{i\bar{n}\cdot\partial+i0}\,\phi_{hc}(0) \tag{12.31}$$

for a generic hard-collinear field ϕ_{hc}. Here, the $i0$ prescription is needed to make the integral well defined. The two formulations are therefore equivalent.

While our focus in the discussion above has been on the construction of boost-invariant operators, it is more conventional to collect the inverse (anti-)hard-collinear derivatives in the hard matching coefficients, which are encountered when the weak effective Hamiltonian (11.1) is matched onto SCET-1. When this is done, only the products of the hard functions with the corresponding SCET-1 operators are boost invariant. Note that, beyond tree-level in QCD interactions, boost invariance allows for logarithmic corrections to the above expressions of the form

$$\ln^n\left[\frac{\bar{n}\cdot\partial_{hc}\,n\cdot\partial_{\overline{hc}}}{\mu^2}\right], \tag{12.32}$$

where μ denotes the renormalization scale. These terms govern the scale dependence of the hard coefficient functions.

12.5 Tree-Level Matching Results

We now illustrate the general results described above with an explicit matching calculation, focusing on four-quark operators and working at tree level in QCD interactions.[1] In this approximation, we only need to keep the terms in the weak effective Hamiltonian (11.1) with flavor structures $(\bar{d}b)(\bar{u}u)$ or $(\bar{d}b)(\bar{s}s)$, corresponding to the flavors of four of the valence quarks in the $\bar{B}^0 \to K^+K^-$ process. Using a Fierz transformation for the operators Q_1^q and Q_2^q, and defining the new operators

$$\mathcal{Q}_1^{\pm,q} = \big(\bar{d}b\big)_{V-A}\big(\bar{q}q\big)_{V\pm A}\,, \qquad \mathcal{Q}_2^{\pm,q} = \big(\bar{d}^i b^j\big)_{V-A}\big(\bar{q}^j q^i\big)_{V\pm A}\,, \tag{12.33}$$

we find that at a hard matching scale $\mu_h \sim m_b$

$$\mathcal{H}_{\text{eff}} = \sum_{q=u,s}\sum_{r=1,2}\Big[\mathcal{C}_r^{-,q}(\mu_h)\,\mathcal{Q}_r^{-,q}(\mu_h) + \mathcal{C}_r^{+,q}(\mu_h)\,\mathcal{Q}_r^{+,q}(\mu_h)\Big] + \dots\,, \tag{12.34}$$

where ellipsis represent terms which do not contribute to weak annihilation amplitudes at tree level. Exploiting the unitarity of the CKM matrix, we find for the matching coefficients

$$\begin{aligned}
\mathcal{C}_1^{-,q}(\mu_h) &= \frac{G_F}{\sqrt{2}}\Big[\lambda_u\,C_2(\mu_h)\,\delta^{qu} - \lambda_t\,C_3(\mu_h) - \lambda_t\,C_7(\mu_h)\Big]\,,\\
\mathcal{C}_2^{-,q}(\mu_h) &= \frac{G_F}{\sqrt{2}}\Big[\lambda_u\,C_1(\mu_h)\,\delta^{qu} - \lambda_t\,C_4(\mu_h) - \lambda_t\,C_8(\mu_h)\Big]\,,\\
\mathcal{C}_1^{+,q}(\mu_h) &= -\frac{G_F}{\sqrt{2}}\,\lambda_t\Big[C_5(\mu_h) + C_9(\mu_h)\Big]\,,\\
\mathcal{C}_2^{+,q}(\mu_h) &= -\frac{G_F}{\sqrt{2}}\,\lambda_t\Big[C_6(\mu_h) + C_{10}(\mu_h)\Big]\,.
\end{aligned} \tag{12.35}$$

Note that the coefficients $\mathcal{C}_i^{+,q}$ are independent of the flavor q and only $\mathcal{C}_2^{-,u}$ depends on the largest Wilson coefficient C_1.

In the remainder of this section, we present the tree-level matching relations obtained when the weak effective Hamiltonian (12.34) is matched onto SCET-1 at a scale of order $\mu_h \sim m_b$. In general, the resulting weak Lagrangian in SCET-1 takes the generic form

$$\mathcal{L}_{\text{eff}}^{\text{SCET}-1} = -\sum_n H_n(\mu) \star O_n(\mu)\,, \tag{12.36}$$

where we refer to the Wilson coefficients as hard functions H_n, and the relevant operators O_n have been defined in the previous sections. The global minus sign arises from translating the weak effective Hamiltonian to a weak effective Lagrangian. Recall that both the hard functions and the operators depend on the momentum fractions $\tilde{x}_i$ and

[1] The Wilson coefficient of the chromomagnetic dipole operator Q_{8g} in the weak effective Hamiltonian is relatively small and, therefore, ignored in the following.

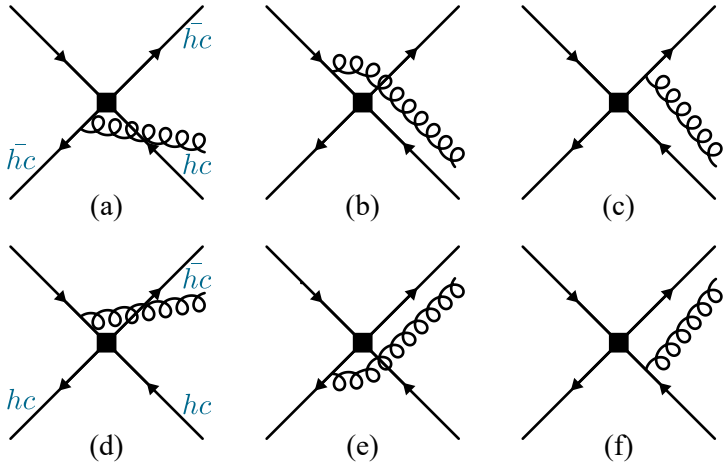

Figure 12.5: Feynman diagrams contributing to the matching coefficients of the SCET-1 four-quark operators with an additional hard-collinear (top row) or anti-hard-collinear (bottom row) gluon. The definition of the momentum-fraction variables is illustrated in Figure 12.3.

$\tilde{y}_i$ carried by the various (anti-)hard-collinear fields. If $N_{hc} > 1$ and/or $N_{\overline{hc}} > 1$, one needs to integrate over these variables with measure

$$\left(\prod_{i=1}^{N_{hc}} \int_0^1 d\tilde{y}_i\right)\left(\prod_{j=1}^{N_{\overline{hc}}} \int_0^1 d\tilde{x}_j\right), \tag{12.37}$$

which is indicated in (12.36) by the $\star$ symbol.

12.5.1 Four-Quark Operators

The tree-level matching conditions are trivial in this case, because the weak effective Hamiltonian (12.34) consists of four-quark operators. We obtain

$$\begin{aligned} H^u_{4,hc,r}(\{\tilde{y}_i\},\mu_h) &= \mathcal{C}_r^{-,u}(\mu_h)\,, \qquad H^s_{4,hc,r}(\{\tilde{y}_i\},\mu_h) = \mathcal{C}_r^{+,s}(\mu_h)\,, \\ H^u_{4,\overline{hc},r}(\{\tilde{x}_i\},\mu_h) &= \mathcal{C}_r^{+,u}(\mu_h)\,, \qquad H^s_{4,\overline{hc},r}(\{\tilde{x}_i\},\mu_h) = \mathcal{C}_r^{-,s}(\mu_h)\,, \end{aligned} \tag{12.38}$$

for $r = 1, 2$. Starting at one-loop order, a dependence on the momentum-fraction variables $\tilde{x}_i$ and $\tilde{y}_i$ would arise.

12.5.2 Four-Quark Operators with an Additional Gluon

The tree-level Feynman diagrams contributing to these matching relations are shown in Figure 12.5. In evaluating these diagrams we make frequent use of the relations (12.9) and (12.11), which can be used to simplify the Dirac algebra and bring the result into a form which corresponds to matrix elements of the basis operators defined in Section 12.2. For the Wilson coefficients of the operators containing a hard-collinear

gluon field, defined in (12.20) and (12.26), we find

$$\begin{aligned}
H^{-,u}_{4g,\overline{hc},1}(\{\tilde{\underline{x}},\tilde{\underline{y}}\},\mu_h) &= -\frac{1}{\tilde{x}_1}\,\mathcal{C}_1^{-,u}(\mu_h)\,, & H^{+,u}_{4g,\overline{hc},1}(\{\tilde{\underline{x}},\tilde{\underline{y}}\},\mu_h) &= -\frac{1}{\tilde{x}_1}\,\mathcal{C}_1^{+,u}(\mu_h)\,,\\
H^{-,u}_{4g,\overline{hc},2}(\{\tilde{\underline{x}},\tilde{\underline{y}}\},\mu_h) &= -\frac{1}{\tilde{x}_1}\,\mathcal{C}_2^{-,u}(\mu_h)\,, & H^{+,u}_{4g,\overline{hc},2}(\{\tilde{\underline{x}},\tilde{\underline{y}}\},\mu_h) &= -\frac{\tilde{x}_2}{\tilde{x}_1}\,\mathcal{C}_2^{+,u}(\mu_h)\,,\\
H^{-,u}_{4g,\overline{hc},3}(\{\tilde{\underline{x}},\tilde{\underline{y}}\},\mu_h) &= \frac{1}{\tilde{x}_2}\,\mathcal{C}_1^{-,u}(\mu_h)\,, & H^{+,u}_{4g,\overline{hc},3}(\{\tilde{\underline{x}},\tilde{\underline{y}}\},\mu_h) &= \mathcal{C}_1^{+,u}(\mu_h)\,,\\
H^{-,u}_{4g,\overline{hc},4}(\{\tilde{\underline{x}},\tilde{\underline{y}}\},\mu_h) &= \frac{1}{\tilde{x}_2}\,\mathcal{C}_2^{-,u}(\mu_h)\,, & H^{+,u}_{4g,\overline{hc},4}(\{\tilde{\underline{x}},\tilde{\underline{y}}\},\mu_h) &= 0\,.
\end{aligned} \tag{12.39}$$

Since we are working at tree level, there cannot be a dependence on $\tilde{y}_2$. The dependence on $\tilde{y}_1$ always cancels between numerator and denominator. In an analogous way, we obtain for the Wilson coefficients of the operators containing an anti-hard-collinear gluon field, defined in (12.21) and (12.26), the expressions

$$\begin{aligned}
H^{-,u}_{4\bar{g},hc,1}(\{\tilde{\underline{x}},\tilde{\underline{y}}\},\mu_h) &= \frac{1}{\tilde{y}_2}\,\mathcal{C}_1^{-,u}(\mu_h)\,, & H^{+,u}_{4\bar{g},hc,1}(\{\tilde{\underline{x}},\tilde{\underline{y}}\},\mu_h) &= \frac{1}{\tilde{y}_2}\,\mathcal{C}_1^{+,u}(\mu_h)\,,\\
H^{-,u}_{4\bar{g},hc,2}(\{\tilde{\underline{x}},\tilde{\underline{y}}\},\mu_h) &= \mathcal{C}_2^{-,u}(\mu_h)\,, & H^{+,u}_{4\bar{g},hc,2}(\{\tilde{\underline{x}},\tilde{\underline{y}}\},\mu_h) &= 0\,,\\
H^{-,u}_{4\bar{g},hc,3}(\{\tilde{\underline{x}},\tilde{\underline{y}}\},\mu_h) &= \mathcal{C}_1^{-,u}(\mu_h)\,, & H^{+,u}_{4\bar{g},hc,3}(\{\tilde{\underline{x}},\tilde{\underline{y}}\},\mu_h) &= \frac{1}{\tilde{y}_1}\,\mathcal{C}_1^{+,u}(\mu_h)\,,\\
H^{-,u}_{4\bar{g},hc,4}(\{\tilde{\underline{x}},\tilde{\underline{y}}\},\mu_h) &= \frac{1}{\tilde{y}_2}\,\mathcal{C}_2^{-,u}(\mu_h)\,, & H^{+,u}_{4\bar{g},hc,4}(\{\tilde{\underline{x}},\tilde{\underline{y}}\},\mu_h) &= \frac{1}{\tilde{y}_1\tilde{y}_2}\,\mathcal{C}_2^{+,u}(\mu_h)\,.
\end{aligned} \tag{12.40}$$

In all cases, the Wilson coefficients of the operators containing an $(\bar{s}s)$ pair are obtained from the coefficients of operators containing an $(\bar{u}u)$ pair by making the replacements $u \leftrightarrow s$, $hc \leftrightarrow \overline{hc}$, $n \leftrightarrow \bar{n}$, and $\tilde{x}_i \leftrightarrow \tilde{y}_i$ everywhere. The coefficients $H^{\pm,s}_{4g,\overline{hc},r}$ are thus obtained from $H^{\pm,u}_{4\bar{g},hc,r}$, and the coefficients $H^{\pm,s}_{4\bar{g},hc,r}$ are derived from $H^{\pm,u}_{4g,\overline{hc},r}$.

12.5.3 Six-Quark Operators

In the derivation of the matching coefficients for the six-quark operators we make frequent use of Fierz identities to reorder the hard-collinear and anti-hard-collinear quark fields. For hard-collinear fields the relevant identities are (with correlated signs) [123]

$$\begin{aligned}
\big[\bar{\mathcal{X}}_{hc}(1\pm\gamma_5)\Gamma_1\psi_1\big]\big[\bar{\psi}_2\,\Gamma_2(1\mp\gamma_5)\mathcal{X}_{hc}\big] &= -\big[\bar{\mathcal{X}}_{hc}\,\frac{\bar{n}\!\!\!/}{2}(1\mp\gamma_5)\mathcal{X}_{hc}\big]\big[\bar{\psi}_2\,\Gamma_2\,\frac{n\!\!\!/}{2}(1\pm\gamma_5)\,\Gamma_1\psi_1\big]\,,\\
\big[\bar{\mathcal{X}}_{hc}(1\pm\gamma_5)\Gamma_1\psi_1\big]\big[\bar{\psi}_2\,\Gamma_2(1\pm\gamma_5)\mathcal{X}_{hc}\big] &= -\big[\bar{\mathcal{X}}_{hc}\,\frac{\bar{n}\!\!\!/}{2}\gamma_\perp^\alpha(1\pm\gamma_5)\mathcal{X}_{hc}\big]\big[\bar{\psi}_2\,\Gamma_2\gamma_{\perp\alpha}\,\frac{n\!\!\!/}{2}\,\Gamma_1\psi_1\big]\,,
\end{aligned} \tag{12.41}$$

where ψ_1 and ψ_2 denote generic (in our case soft and anti-hard-collinear) spinor fields, and the Dirac matrices Γ_1 and Γ_2 can be arbitrary. Analogous relations (with n and $\bar{n}$ interchanged) hold for anti-hard-collinear fields. We also use the relation

$$\gamma_\perp^\mu\gamma_\perp^\alpha\gamma_{\perp\mu} = 0\,, \tag{12.42}$$

which holds in four spacetime dimensions. The color indices on the various quark fields can be rearranged using the color Fierz identity

$$(t^a)^{ij}\,(t^a)^{kl} = \frac{1}{2}\left(\delta^{il}\,\delta^{kj} - \frac{1}{N_c}\,\delta^{ij}\,\delta^{kl}\right). \tag{12.43}$$

In this way, we obtain for the Wilson coefficients of the operators containing a soft spectator quark followed by $\not{n}$

$$\begin{aligned}
H^-_{6,s\bar{n},1}(\{\underline{\tilde{x}},\underline{\tilde{y}}\},\mu_h) &= \frac{\pi\,\alpha_h}{2}\left[\frac{1}{\tilde{y}_1\tilde{x}_2}\,\mathcal{C}_1^{-,u}(\mu_h) - \frac{1}{\tilde{x}_1\tilde{y}_2}\,\mathcal{C}_1^{-,s}(\mu_h)\right],\\
H^-_{6,s\bar{n},2}(\{\underline{\tilde{x}},\underline{\tilde{y}}\},\mu_h) &= \frac{\pi\,\alpha_h}{2}\left[\frac{1}{\tilde{y}_1(\tilde{x}_2+\tilde{x}_1\tilde{y}_1)}\,\mathcal{C}_2^{-,u}(\mu_h) + \frac{1}{\tilde{x}_1\tilde{y}_2^2}\,\mathcal{C}_2^{-,s}(\mu_h)\right],\\
H^-_{6,s\bar{n},3}(\{\underline{\tilde{x}},\underline{\tilde{y}}\},\mu_h) &= \frac{\pi\,\alpha_h}{2}\left[\frac{1}{\tilde{y}_1(\tilde{x}_2+\tilde{x}_1\tilde{y}_1)}\,\mathcal{C}_1^{-,u}(\mu_h) - \frac{1}{N_c}\,\frac{\tilde{y}_1}{\tilde{x}_1\tilde{y}_2^2}\,\mathcal{C}_2^{-,s}(\mu_h)\right],\\
H^-_{6,s\bar{n},4}(\{\underline{\tilde{x}},\underline{\tilde{y}}\},\mu_h) &= \frac{\pi\,\alpha_h}{2}\left[\frac{1}{\tilde{y}_1\tilde{x}_2}\,\mathcal{C}_2^{-,u}(\mu_h) - \frac{1}{\tilde{x}_1\tilde{y}_2}\,\mathcal{C}_2^{-,s}(\mu_h)\right],\\
H^-_{6,s\bar{n},5}(\{\underline{\tilde{x}},\underline{\tilde{y}}\},\mu_h) &= -\frac{\pi\,\alpha_h}{2N_c}\left[\frac{1}{\tilde{y}_1}\left(\frac{1}{\tilde{x}_2+\tilde{x}_1\tilde{y}_1}+\frac{1}{\tilde{x}_2}\right)\mathcal{C}_1^{-,u}(\mu_h) + \frac{\tilde{y}_1}{\tilde{x}_1\tilde{y}_2^2}\,\mathcal{C}_1^{-,s}(\mu_h)\right],\\
H^-_{6,s\bar{n},6}(\{\underline{\tilde{x}},\underline{\tilde{y}}\},\mu_h) &= \frac{\pi\,\alpha_h}{2}\left[-\frac{1}{N_c}\,\frac{1}{\tilde{y}_1}\left(\frac{1}{\tilde{x}_2+\tilde{x}_1\tilde{y}_1}+\frac{1}{\tilde{x}_2}\right)\mathcal{C}_2^{-,u}(\mu_h) + \frac{1}{\tilde{x}_1\tilde{y}_2^2}\,\mathcal{C}_1^{-,s}(\mu_h)\right],
\end{aligned} \tag{12.44}$$

and

$$\begin{aligned}
H^+_{6,s\bar{n},1}(\{\underline{\tilde{x}},\underline{\tilde{y}}\},\mu_h) &= \frac{\pi\,\alpha_h}{2}\left[\frac{1}{\tilde{y}_1\tilde{x}_2}\,\mathcal{C}_1^{+,u}(\mu_h) - \frac{1}{\tilde{x}_1\tilde{y}_2}\,\mathcal{C}_1^{+,s}(\mu_h)\right],\\
H^+_{6,s\bar{n},2}(\{\underline{\tilde{x}},\underline{\tilde{y}}\},\mu_h) &= 0\,,\\
H^+_{6,s\bar{n},3}(\{\underline{\tilde{x}},\underline{\tilde{y}}\},\mu_h) &= \frac{\pi\,\alpha_h}{2}\left[\frac{1}{\tilde{y}_1^2\tilde{x}_2}\,\mathcal{C}_1^{+,u}(\mu_h) - \frac{1}{N_c}\,\frac{1}{\tilde{y}_2}\left(\frac{1}{\tilde{x}_1+\tilde{x}_2\tilde{y}_2}-\frac{1}{\tilde{x}_1}\right)\mathcal{C}_2^{+,s}(\mu_h)\right],\\
H^+_{6,s\bar{n},4}(\{\underline{\tilde{x}},\underline{\tilde{y}}\},\mu_h) &= \frac{\pi\,\alpha_h}{2}\left[\frac{1+\tilde{y}_1}{\tilde{y}_1^2\tilde{x}_2}\,\mathcal{C}_2^{+,u}(\mu_h) + \frac{1}{\tilde{y}_2}\left(\frac{1}{\tilde{x}_1+\tilde{x}_2\tilde{y}_2}-\frac{1}{\tilde{x}_1}\right)\mathcal{C}_2^{+,s}(\mu_h)\right],\\
H^+_{6,s\bar{n},5}(\{\underline{\tilde{x}},\underline{\tilde{y}}\},\mu_h) &= -\frac{\pi\,\alpha_h}{2N_c}\left[\frac{1+\tilde{y}_1}{\tilde{y}_1^2\tilde{x}_2}\,\mathcal{C}_1^{+,u}(\mu_h) + \frac{1}{\tilde{y}_2}\left(\frac{1}{\tilde{x}_1+\tilde{x}_2\tilde{y}_2}-\frac{1}{\tilde{x}_1}\right)\mathcal{C}_1^{+,s}(\mu_h)\right],\\
H^+_{6,s\bar{n},6}(\{\underline{\tilde{x}},\underline{\tilde{y}}\},\mu_h) &= \frac{\pi\,\alpha_h}{2}\left[-\frac{1}{N_c}\,\frac{1+\tilde{y}_1}{\tilde{y}_1^2\tilde{x}_2}\,\mathcal{C}_2^{+,u}(\mu_h) + \frac{1}{\tilde{y}_2(\tilde{x}_1+\tilde{x}_2\tilde{y}_2)}\,\mathcal{C}_1^{+,s}(\mu_h)\right],
\end{aligned} \tag{12.45}$$

where we use the abbreviation $\alpha_h = \alpha_s(\mu_h)$. The Wilson coefficients for operators with soft spectator followed by $\not{n}$ are

$$H^-_{6,sn,1}(\{\underline{\tilde{x}},\underline{\tilde{y}}\},\mu_h) = \frac{\pi\,\alpha_h}{2}\left[-\frac{1}{\tilde{y}_1\tilde{x}_2}\,\mathcal{C}_1^{-,u}(\mu_h) + \frac{1}{\tilde{x}_1\tilde{y}_2}\,\mathcal{C}_1^{-,s}(\mu_h)\right],$$

$$
\begin{aligned}
H^-_{6,sn,2}(\{\tilde{\underline{x}},\tilde{\underline{y}}\},\mu_h) &= \frac{\pi\alpha_h}{2}\bigg[-\frac{1}{\tilde{y}_1\tilde{x}_2}\,\mathcal{C}_2^{-,u}(\mu_h)+\frac{1}{\tilde{x}_1\tilde{y}_2}\,\mathcal{C}_2^{-,s}(\mu_h)\bigg]\,,\\
H^-_{6,sn,3}(\{\tilde{\underline{x}},\tilde{\underline{y}}\},\mu_h) &= \frac{\pi\alpha_h}{2}\bigg[\frac{1}{\tilde{y}_1\tilde{x}_2^2}\,\mathcal{C}_1^{-,u}(\mu_h)-\frac{1}{N_c}\,\frac{1}{\tilde{x}_1}\bigg(\frac{1}{\tilde{y}_2+\tilde{x}_1\tilde{y}_1}+\frac{1}{\tilde{y}_2}\bigg)\mathcal{C}_2^{-,s}(\mu_h)\bigg]\,,\\
H^-_{6,sn,4}(\{\tilde{\underline{x}},\tilde{\underline{y}}\},\mu_h) &= \frac{\pi\alpha_h}{2}\bigg[\frac{1}{\tilde{y}_1\tilde{x}_2^2}\,\mathcal{C}_2^{-,u}(\mu_h)+\frac{1}{\tilde{x}_1(\tilde{y}_2+\tilde{x}_1\tilde{y}_1)}\,\mathcal{C}_2^{-,s}(\mu_h)\bigg],\\
H^-_{6,sn,5}(\{\tilde{\underline{x}},\tilde{\underline{y}}\},\mu_h) &= -\frac{\pi\alpha_h}{2N_c}\bigg[\frac{\tilde{x}_1}{\tilde{y}_1\tilde{x}_2^2}\,\mathcal{C}_1^{-,u}(\mu_h)+\frac{1}{\tilde{x}_1}\bigg(\frac{1}{\tilde{y}_2+\tilde{x}_1\tilde{y}_1}+\frac{1}{\tilde{y}_2}\bigg)\mathcal{C}_1^{-,s}(\mu_h)\bigg]\,,\\
H^-_{6,sn,6}(\{\tilde{\underline{x}},\tilde{\underline{y}}\},\mu_h) &= \frac{\pi\alpha_h}{2}\bigg[-\frac{1}{N_c}\,\frac{\tilde{x}_1}{\tilde{y}_1\tilde{x}_2^2}\,\mathcal{C}_2^{-,u}(\mu_h)+\frac{1}{\tilde{x}_1(\tilde{y}_2+\tilde{x}_1\tilde{y}_1)}\,\mathcal{C}_1^{-,s}(\mu_h)\bigg]\,,
\end{aligned}
\tag{12.46}
$$

and

$$
\begin{aligned}
H^+_{6,sn,1}(\{\tilde{\underline{x}},\tilde{\underline{y}}\},\mu_h) &= \frac{\pi\alpha_h}{2}\bigg[-\frac{1}{\tilde{y}_1\tilde{x}_2}\,\mathcal{C}_1^{+,u}(\mu_h)+\frac{1}{\tilde{x}_1\tilde{y}_2}\,\mathcal{C}_1^{+,s}(\mu_h)\bigg]\,,\\
H^+_{6,sn,2}(\{\tilde{\underline{x}},\tilde{\underline{y}}\},\mu_h) &= \frac{\pi\alpha_h}{2}\bigg[\frac{1}{\tilde{x}_2}\bigg(\frac{1}{\tilde{y}_1+\tilde{x}_2\tilde{y}_2}-\frac{1}{\tilde{y}_1}\bigg)\mathcal{C}_2^{+,u}(\mu_h)+\frac{1+\tilde{x}_1}{\tilde{x}_1^2\tilde{y}_2}\,\mathcal{C}_2^{+,s}(\mu_h)\bigg]\,,\\
H^+_{6,sn,3}(\{\tilde{\underline{x}},\tilde{\underline{y}}\},\mu_h) &= \frac{\pi\alpha_h}{2}\bigg[\frac{1}{\tilde{x}_2(\tilde{y}_1+\tilde{x}_2\tilde{y}_2)}\,\mathcal{C}_1^{+,u}(\mu_h)-\frac{1}{N_c}\,\frac{1+\tilde{x}_1}{\tilde{x}_1^2\tilde{y}_2}\,\mathcal{C}_2^{+,s}(\mu_h)\bigg]\,,\\
H^+_{6,sn,4}(\{\tilde{\underline{x}},\tilde{\underline{y}}\},\mu_h) &= 0\,,\\
H^+_{6,sn,5}(\{\tilde{\underline{x}},\tilde{\underline{y}}\},\mu_h) &= -\frac{\pi\alpha_h}{2N_c}\bigg[\frac{1}{\tilde{x}_2}\bigg(\frac{1}{\tilde{y}_1+\tilde{x}_2\tilde{y}_2}-\frac{1}{\tilde{y}_1}\bigg)\mathcal{C}_1^{+,u}(\mu_h)+\frac{1+\tilde{x}_1}{\tilde{x}_1^2\tilde{y}_2}\,\mathcal{C}_1^{+,s}(\mu_h)\bigg]\,,\\
H^+_{6,sn,6}(\{\tilde{\underline{x}},\tilde{\underline{y}}\},\mu_h) &= \frac{\pi\alpha_h}{2}\bigg[-\frac{1}{N_c}\,\frac{1}{\tilde{x}_2}\bigg(\frac{1}{\tilde{y}_1+\tilde{x}_2\tilde{y}_2}-\frac{1}{\tilde{y}_1}\bigg)\mathcal{C}_2^{+,u}(\mu_h)+\frac{1}{\tilde{x}_1^2\tilde{y}_2}\,\mathcal{C}_1^{+,s}(\mu_h)\bigg]\,.
\end{aligned}
\tag{12.47}
$$

The coefficients for the six-quark operators with (anti-)hard-collinear spectator are given in Appendix A.9. As we show below, they only contribute to decay amplitudes of B^* mesons.

Chapter 13

Matching onto SCET-2

Below the intermediate jet scale QCD is described by SCET-2, see Chapter 4. The Lagrangian of this theory is given by the sum of (4.5) and (5.7) in our case and does not contain interaction terms including fields from different sectors at leading power.[1]

While the power counting in λ is not preserved in the matching from SCET-1 to SCET-2, the mass dimension of the operators *is* conserved in this step. Given the generic structure of the SCET-1 operators,

$$O_{\text{SCET}-1} \sim [\text{soft fields}] \times [\overline{hc} \text{ fields}] \times [hc \text{ fields}]\,, \tag{13.1}$$

it is important to note that the blocks of hard-collinear and anti-hard-collinear fields can be matched onto SCET-2 separately, while the soft fields are matched onto themselves, i.e.

$$\begin{aligned} [hc \text{ fields}] &\to [\text{collinear fields}] \times [\text{soft fields}]\,, \\ [\overline{hc} \text{ fields}] &\to [\text{anti-collinear fields}] \times [\text{soft fields}]\,, \\ [\text{soft fields}] &\to [\text{soft fields}]\,. \end{aligned} \tag{13.2}$$

In the matching $[hc] \to [c] \times [s]$ the collinear bracket cannot be empty by momentum conservation, and the soft bracket cannot be empty as soon as there are at least two particles in the final state. The detailed form of these matching relations have been studied in [11, 24]. As described in Section 4.2, hard-collinear fields can be integrated out at tree level by solving their classical equations of motion, using a systematic expansion in powers of λ [11]. Alternatively, one can construct the relevant relations by constructing the most general set of boost-invariant operators built out of collinear and soft fields with the correct quantum numbers [24]. The second method also works beyond tree level, but in order to fix the Wilson coefficients of the various operators explicit matching calculations are required.

13.1 Multipole Expansion and Soft Decoupling

So far we have omitted the spacetime dependence of the various component fields in the SCET-1 operators. For the purposes of the following discussion, it is instructive to be more general. Without loss of generality, we evaluate the local operators in the weak effective Hamiltonian (11.1) at the spacetime point $z = 0$. As mentioned earlier, however, the operators built out of effective fields in SCET-1 are in general non-local operators. Hard-collinear fields live at positions along the $\bar{n}$ light cone, e.g. $\mathcal{X}_{hc}(s_1\bar{n})$ and $\mathcal{A}_{hc}^{\perp}(s_2\bar{n})$ etc., with $\mathcal{O}(\lambda^0)$ parameters s_i. The reason is that expanding these non-local fields generates unsuppressed derivatives $\bar{n} \cdot \partial_{hc}$. Likewise, anti-hard-collinear fields live at positions along the n light cone, e.g. $\mathcal{X}_{\overline{hc}}(t_1 n)$ and $\mathcal{A}_{\overline{hc}}^{\perp}(t_2 n)$.

[1] At higher orders in power counting, effective interactions connecting collinear and soft fields can be induced by integrating out hard-collinear field [11]. These interactions play no role for our analysis.

Before matching onto SCET-2, it is convenient to perform the decoupling transformation to get rid of leading-power interactions between (anti-)hard-collinear and soft fields. As explained in Appendix A.2, the soft Wilson lines introduced during this decoupling are evaluated at z_- (z_+) in the (anti-)hard-collinear sector. In other words, when the decoupling is performed in the SCET-1 operators defined in Chapter 12, the soft Wilson lines all live at $z = 0$. Therefore, we suppress spacetime point arguments $z = 0$ in the following. Due to the decoupling, soft fields only appear as gauge invariant building blocks defined in (4.9) and for the HQET field we define

$$\mathcal{H}_{v,n} := S_n^\dagger\, b_v\,. \tag{13.3}$$

Similar building blocks defined with $n \to \bar{n}$ arise for the anti-hard-collinear sector.

In the next step, the decoupled (anti-)hard-collinear fields are matched onto (anti-) collinear and soft fields in SCET-2. In these matching relations, the soft fields are integrated over light-like directions. This non-locality of the soft fields is related to the fact that the components $n \cdot p_{hc}$ and $n \cdot p_s$ are of similar size [11]. In the spirit of (12.31), we do not work with fields displaced along the light cone but prefer to use inverse derivatives acting on soft fields. Therefore, we define

$$\phi_{s,n\,(\omega)} := \delta(\omega - in\cdot\partial_s)\,\phi_{s,n}\,, \qquad \phi_{s,\bar{n}\,(\bar{\omega})} := \delta(\bar{\omega} - i\bar{n}\cdot\partial_s)\,\phi_{s,\bar{n}}\,. \tag{13.4}$$

RPI requires ω ($\bar{\omega}$) to behave like n ($\bar{n}$) under boosts in this relation. The change in mass dimension of the soft fields can be ignored, as the δ functions are compensated by integrals over ω and $\bar{\omega}$ in the effective Lagrangian. The jet functions and soft matrix elements depend on these variables.

13.2 Six-Quark Operators

We begin with the first two six-quark SCET-1 operators given in (12.28), which contain all the six quarks needed as constituents of the final-state mesons. Therefore, the leading contributions after the matching to SCET-2 are obtained by implementing the trivial matching relations, in which all (anti-)hard-collinear quark fields are mapped onto the corresponding (anti-)collinear fields. Using a less trivial matching relation for the (anti-)hard-collinear quark fields gives rise to power-suppressed SCET-2 operators.

Since fields of different type in SCET-2 do not interact, hadronic matrix elements of such operators can be non-vanishing only if the fields of each type are in a color-singlet state. Performing the decoupling transformation first and employing the trivial matching relations (4.12) afterwards, we find for the collinear bracket

$$\begin{aligned}
&\bar{\mathcal{X}}_{hc}^{(s)\,i_3}(s_1\bar{n})\,\bar{n}\!\!\!/\,(1\pm\gamma_5)\,\mathcal{X}_{hc}^{(u)\,j_3}(s_2\bar{n})\\
&= \bar{\mathcal{X}}_{hc}^{(s)(0)\,k_3}(s_1\bar{n})\big(S_n^\dagger\big)^{k_3 i_3}\,\bar{n}\!\!\!/\,(1\pm\gamma_5)\big(S_n\big)^{j_3 l_3}\mathcal{X}_{hc}^{(u)(0)\,l_3}(s_2\bar{n})\\
&\to \bar{\mathcal{X}}_{c}^{(s)\,k_3}(s_1\bar{n})\big(S_n^\dagger\big)^{k_3 i_3}\,\bar{n}\!\!\!/\,(1\pm\gamma_5)\big(S_n\big)^{j_3 l_3}\mathcal{X}_{c}^{(u)\,l_3}(s_2\bar{n})\\
&\to \frac{\delta^{j_3 i_3}}{N_c}\,\big[\bar{\mathcal{X}}_{c}^{(s)}(s_1\bar{n})\,\bar{n}\!\!\!/\,(1\pm\gamma_5)\,\mathcal{X}_{c}^{(u)}(s_2\bar{n})\big]\,,
\end{aligned} \tag{13.5}$$

where we projected onto a color-singlet state in the last line and a sum over color indices on the quark fields is understood. Recall that our notation is such that we do not display spacetime arguments $z = 0$. We find that the (unitary) soft Wilson lines from the decoupling transformation cancel out. Similarly, the anti-collinear bracket becomes

$$\bar{\mathcal{X}}^{(u)\,i_2}_{\overline{hc}}(t_1 n)\,\not{n}(1\pm\gamma_5)\,\mathcal{X}^{(s)\,j_2}_{\overline{hc}}(t_2 n) \to \frac{\delta^{j_2 i_2}}{N_c}\left[\bar{\mathcal{X}}^{(u)}_{\bar{c}}(t_1 n)\,\not{n}(1\pm\gamma_5)\,\mathcal{X}^{(s)}_{\bar{c}}(t_2 n)\right]. \tag{13.6}$$

Projecting also the soft quark fields on a color-singlet state, we finally obtain for $O^{\pm}_{6,s\bar{n},r}$

$$\begin{aligned}&\frac{1}{N_c^3}\,\delta^{j_1 i_1}\,\delta^{j_2 i_2}\,\delta^{j_3 i_3}\left[T_{(r)}\right]^{i_1\,i_2\,i_3}_{j_1\,j_2\,j_3}\left[\bar{q}^{(d)}_s\,\bar{\not{n}}(1-\gamma_5)\,b_v\right]\\ &\times\left[\bar{\mathcal{X}}^{(u)}_{\bar{c}}(t_1 n)\,\not{n}(1\pm\gamma_5)\,\mathcal{X}^{(s)}_{\bar{c}}(t_2 n)\right]\left[\bar{\mathcal{X}}^{(s)}_{c}(s_1\bar{n})\,\bar{\not{n}}(1\pm\gamma_5)\,\mathcal{X}^{(u)}_{c}(s_2\bar{n})\right],\end{aligned} \tag{13.7}$$

which is of $\mathcal{O}(\lambda^{14})$. This defines the leading power for SCET-2 operators describing weak-annihilation amplitudes. For $O^{\pm}_{6,sn,r}$ one just has to replace $\bar{\not{n}} \to \not{n}$ in the first bracket. The projected color structures evaluate to

$$\frac{1}{N_c^3}\,\delta^{j_1 i_1}\,\delta^{j_2 i_2}\,\delta^{j_3 i_3}\left[T_{(r)}\right]^{i_1\,i_2\,i_3}_{j_1\,j_2\,j_3} = \begin{cases} 1\,; & r = 1\,,\\ \frac{1}{N_c}\,; & r = 2,4,5\,,\\ \frac{1}{N_c^2}\,; & r = 3,6\,. \end{cases} \tag{13.8}$$

The purpose of keeping the momentum arguments of the fields explicit was to demonstrate that the cancellation of soft Wilson lines works out even if the various (anti-) hard-collinear fields live at different spacetime points. At this point we can switch back to momentum space, as we have done in Chapter 12.

It follows from this discussion that at the intermediate jet scale μ_j the twelve six-quark SCET-1 operators $O^{\pm}_{6,s\bar{n},r}$ and $O^{\pm}_{6,sn,r}$ (with $r = 1,\dots,6$) in (12.28) match onto only two SCET-2 operators, which we define as

$$\begin{aligned}\mathcal{O}^{\pm}_{6,\bar{n}}(\{\underline{x},\underline{y}\},\mu) &= \frac{1}{n\cdot\mathcal{P}_{\bar{c}}\,(\bar{n}\cdot\mathcal{P}_c)^2}\left[\bar{\mathcal{Q}}^{(d)}_{s,\bar{n}}\,\bar{\not{n}}(1-\gamma_5)\,\mathcal{H}_{v,\bar{n}}\right]\\ &\quad\times\left[\bar{\mathcal{X}}^{(u)}_{\bar{c}(x_1)}\,\not{n}(1\pm\gamma_5)\,\mathcal{X}^{(s)}_{\bar{c}(x_2)}\right]\left[\bar{\mathcal{X}}^{(s)}_{c(y_1)}\,\bar{\not{n}}(1\pm\gamma_5)\,\mathcal{X}^{(u)}_{c(y_2)}\right],\\ \mathcal{O}^{\pm}_{6,n}(\{\underline{x},\underline{y}\},\mu) &= \frac{1}{(n\cdot\mathcal{P}_{\bar{c}})^2\,\bar{n}\cdot\mathcal{P}_c}\left[\bar{\mathcal{Q}}^{(d)}_{s,n}\,\not{n}(1-\gamma_5)\,\mathcal{H}_{v,n}\right]\\ &\quad\times\left[\bar{\mathcal{X}}^{(u)}_{\bar{c}(x_1)}\,\not{n}(1\pm\gamma_5)\,\mathcal{X}^{(s)}_{\bar{c}(x_2)}\right]\left[\bar{\mathcal{X}}^{(s)}_{c(y_1)}\,\bar{\not{n}}(1\pm\gamma_5)\,\mathcal{X}^{(u)}_{c(y_2)}\right].\end{aligned} \tag{13.9}$$

Here we include in the soft brackets two Wilson lines in order to get the soft building blocks (4.9) and (13.3). They are chosen such that $\bar{\mathcal{Q}}^{(d)}_{s,n}$ ($\bar{\mathcal{Q}}^{(d)}_{s,\bar{n}}$) is followed by $\not{n}$ ($\bar{\not{n}}$) as for the four-quark operators, see below. For these operators the soft fields are *not* displaced along the light cone, and, therefore, the B meson is just described by the decay constant $\tilde{f}_B$ in the amplitude. The momentum fractions $\{\underline{x},\underline{y}\}$ are chosen similar to Figure 12.4a.

For the remaining two operators in (12.28), we need to match the (anti-)hard-collinear down-quark field onto a soft down-quark field plus other fields, containing

SCET-1 field	SCET-2 fields	power counting	relevance
$\mathcal{X}_{hc}^{(q)}$	$\mathcal{A}_c^\perp + \mathcal{Q}_{s,n}^{(q)}$	λ^3	✓
$\mathcal{X}_{hc}^{(q)}$	$\mathcal{Q}_{s,n}^{(q)} + \bar{\mathcal{X}}_c^{(q')} + \mathcal{Q}_{s,n}^{(q')}$	λ^4	✓
$\mathcal{X}_{hc}^{(q)}$	$\mathcal{Q}_{s,n}^{(q)} + \bar{\mathcal{Q}}_{s,n}^{(q')} + \mathcal{X}_c^{(q')}$	λ^4	✓

Table 13.1: Matching relations for a hard-collinear quark onto a soft quark of the same flavor plus other partons [11, 24].

at least one (anti-)collinear field. The possible matching relations arising a different orders in power counting are shown in Table 13.1. We are only interest in the $\mathcal{O}(\lambda^3)$ matching relation shown in the first line of the table, because when combined with the trivial matching relations for all other (anti-)hard-collinear fields this yields operators of $\mathcal{O}(\lambda^{14})$. Using higher-order matching relations for any of the fields gives rise to power-suppressed SCET-2 operators. Boost invariance uniquely fixes the structure of the matching relation for the decoupled down-quark field. At tree level, see Figure 12.2, it reads [11]

$$\bar{\mathcal{X}}_{hc}^{(d)(0)} \to \frac{1}{in\cdot\partial_s}\,\bar{\mathcal{Q}}_{s,n}^{(d)}\,\mathcal{A}\!\!\!/_c^\perp\,\frac{\bar{n}\!\!\!/}{2}\,. \tag{13.10}$$

An analogous relation holds in the anti-hard-collinear sector.[2]

Performing the decoupling transformation and projecting onto color-singlet states in this case is more involved. For $O_{6,hc,r}^{\pm}$ the anti-collinear bracket yields the same result as (13.6) but the collinear bracket becomes (omitting all spacetime arguments)

$$\begin{aligned}
&\bar{\mathcal{X}}_{hc}^{(s)i_3}\,\bar{n}\!\!\!/\,(1\pm\gamma_5)\,\mathcal{X}_{hc}^{(u)j_3} \\
&\to \bar{\mathcal{X}}_c^{(s)k_3}\big(S_n^\dagger\big)^{k_3 i_3}\big(\mathcal{A}_{c,\mu}^\perp\big)^{l_1 k_1}\bar{n}\!\!\!/\,(1\pm\gamma_5)\big(S_n\big)^{j_3 l_3}\mathcal{X}_c^{(u)l_3} \\
&\to \frac{1}{N_c^2-1}\Big(\big(S_n^\dagger\big)^{l_1 i_3}\big(S_n\big)^{j_3 k_1} - \frac{1}{N_c}\delta^{j_3 i_3}\,\delta^{l_1 k_1}\Big)\,\big[\bar{\mathcal{X}}_c^{(s)}\,\mathcal{A}_{c,\mu}^\perp\,\bar{n}\!\!\!/\,(1\pm\gamma_5)\,\mathcal{X}_c^{(u)}\big]\,,
\end{aligned} \tag{13.11}$$

where a sum over color indices on the quark and gluon fields is understood. Combining this with the soft bracket yields

$$\begin{aligned}
&\frac{1}{N_c(N_c^2-1)}\,\delta^{j_2 i_2}\Big(\big(S_n^\dagger\big)^{l_1 i_3}\big(S_n\big)^{j_3 k_1} - \frac{1}{N_c}\delta^{j_3 i_3}\,\delta^{l_1 k_1}\Big)\,\big[T_{(r)}\big]_{j_1 j_2 j_3}^{i_1 i_2 i_3} \\
&\times\,\big[\bar{\mathcal{Q}}_{s,n}^{(d)l_1}\big(S_n^\dagger\big)^{k_1 i_1}\gamma_\perp^\mu\,n\!\!\!/\,\bar{n}\!\!\!/\,(1-\gamma_5)\,b_v^{j_1}\big] \\
&= \big[\bar{q}_s^{(d)}\,\gamma_\perp^\mu\,n\!\!\!/\,\bar{n}\!\!\!/\,(1-\gamma_5)\,b_v\big]\begin{cases}\frac{1}{N_c}\,; & r=2\,,\\ \frac{1}{N_c^2}\,; & r=3,6\,,\\ 0\,; & r=1,4,5\,.\end{cases}
\end{aligned} \tag{13.12}$$

[2] At the same order one can construct operators given by the same expressions times arbitrary powers of the boost-invariant ratio $(n\cdot A_s/n\cdot\partial_s)$. However, all of these terms are already taken into account by working with the gauge-invariant building block $\mathcal{A}_{s,n}$.

SCET-1 field	SCET-2 fields	power counting	relevance
$\mathcal{A}_{hc}^{\perp}$	$\mathcal{A}_{c}^{\perp}$	λ^2	
$\mathcal{A}_{hc}^{\perp}$	$\bar{\mathcal{X}}_{c}^{(q)} + \mathcal{Q}_{s,n}^{(q)}$	λ^3	✓
$\mathcal{A}_{hc}^{\perp}$	$\bar{\mathcal{Q}}_{s,n}^{(q)} + \mathcal{X}_{c}^{(q)}$	λ^3	✓

Table 13.2: Matching relations for a hard-collinear gluon [11, 24].

Again the soft Wilson lines from the decoupling cancel. A similar derivation holds for $O_{6,\overline{hc},r}^{\pm}$ and we find only two SCET-2 operators

$$\begin{aligned}
\mathcal{O}_{6c}^{\pm}(\omega, \{\underline{x}, \underline{y}\}, \mu) &= \frac{1}{n\cdot\mathcal{P}_{\bar{c}}\,(\bar{n}\cdot\mathcal{P}_c)^2}\left[\bar{\mathcal{Q}}_{s,n\,(\omega)}^{(d)}\,\gamma_{\perp\mu}\,\bar{n}\!\!\!/\,n\!\!\!/\,(1-\gamma_5)\,\mathcal{H}_{v,n}\right] \\
&\quad\times\left[\bar{\mathcal{X}}_{\bar{c}(x_1)}^{(u)}\,n\!\!\!/\,(1\pm\gamma_5)\,\mathcal{X}_{\bar{c}(x_2)}^{(s)}\right]\left[\bar{\mathcal{X}}_{c(y_1)}^{(s)}\,\mathcal{A}_{c(y_3)}^{\perp\mu}\,\bar{n}\!\!\!/\,(1\pm\gamma_5)\,\mathcal{X}_{c(y_2)}^{(u)}\right], \\
\mathcal{O}_{6\bar{c}}^{\pm}(\bar{\omega}, \{\underline{x}, \underline{y}\}, \mu) &= \frac{1}{(n\cdot\mathcal{P}_{\bar{c}})^2\,\bar{n}\cdot\mathcal{P}_c}\left[\bar{\mathcal{Q}}_{s,\bar{n}\,(\bar{\omega})}^{(d)}\,\gamma_{\perp\mu}\,n\!\!\!/\,\bar{n}\!\!\!/\,(1-\gamma_5)\,\mathcal{H}_{v,\bar{n}}\right] \\
&\quad\times\left[\bar{\mathcal{X}}_{\bar{c}(x_1)}^{(u)}\,\mathcal{A}_{\bar{c}(x_3)}^{\perp\mu}\,n\!\!\!/\,(1\pm\gamma_5)\,\mathcal{X}_{\bar{c}(x_2)}^{(s)}\right]\left[\bar{\mathcal{X}}_{c(y_1)}^{(s)}\,\bar{n}\!\!\!/\,(1\pm\gamma_5)\,\mathcal{X}_{c(y_2)}^{(u)}\right].
\end{aligned} \tag{13.13}$$

These operators are not boost invariant and have mass dimension $D = 7$. Boost invariance and mass dimension $D = 6$ are restored when combined with the Wilson coefficients which contain the inverse derivative from (13.10). For our decay of interest $\bar{B}^0 \to K^+K^-$, these operators do not contribute, as they describe B^*-meson decays.

13.3 Four-Quark Operators with an Additional Gluon

Let us next discuss the matching for the SCET-1 four-quark operators in (12.20), (12.21) and (12.26), which contain an additional gluon field. If the (anti-)hard-collinear gluon field would simply be matched onto the corresponding (anti-)collinear gluon field, then these operators are suppressed by two powers in λ relative to the six-quark SCET-2 operators discussed above. Hence, we need to invoke a non-trivial matching relation for the gluon field, in which it splits up into a quark pair. Possible matching relations contributing at different orders in power counting are shown in Table 13.2. The leading contributions including a quark pair arise at $\mathcal{O}(\lambda^3)$. At tree-level, see Figure 12.2, it is given by [11]

$$\mathcal{A}_{hc,\mu}^{(0)\perp} \to 4\pi\,\alpha_s\,\frac{1}{(in\cdot\partial_s)(i\bar{n}\cdot\partial_c)}\sum_q\left[\bar{\mathcal{X}}_c^{(q)}\,\gamma_{\perp\mu}\,t^a\,\mathcal{Q}_{s,n}^{(q)} + \text{h.c.}\right]t^a\,. \tag{13.14}$$

Besides this, the (anti-)hard-collinear down quark must match onto a soft down quark together with an (anti-)collinear strange-quark for SCET-1 operators with $(\bar{u}u)$ pair and an up-quark for operators with $(\bar{s}s)$ pair, respectively. According to Table 13.1 the leading contribution in this case is of $\mathcal{O}(\lambda^4)$. At tree-level, see Figure 12.2, the

matching relation reads [11]

$$\bar{\mathcal{X}}^{(d)(0)}_{hc} \to 2\pi\alpha_s \frac{1}{in\cdot\partial_s}\,\bar{\mathcal{Q}}^{(d)}_{s,n}\,\gamma_\perp^\mu \not{n}\, t^a \frac{1}{(in\cdot\partial_s)(i\bar{n}\cdot\partial_c)} \sum_q \left[\bar{\mathcal{X}}^{(q)}_c \gamma_{\perp\mu} t^a\, \mathcal{Q}^{(q)}_{s,n} + \text{h.c.}\right]. \quad (13.15)$$

Of course, similar relations to (13.14) and (13.15) in the anti-collinear sector exist.

To get a leading power contribution from the operators $O^{+,q}_{4g,\overline{hc},r}$ we then match the decoupled hard-collinear gluon according to (13.14), the anti-hard-collinear down quark according to (13.15) and the two (anti-)hard-collinear quarks with flavor $q = u, s$ trivially onto SCET-2 fields. Applying the Fierz transformations (12.41) twice, we can combine (anti-)collinear and soft fields to spinor bilinears. Projecting onto color-singlet states in the (anti-)collinear bracket and combining the result with the soft bracket, we find that one pair $S^\dagger_{\bar{n}} S_n$ does not cancel out. We end up with the following eight-quark SCET-2 operators

$$\begin{aligned}
\mathcal{O}^s_{8,\perp\bar{n},r} &= \frac{1}{(n\cdot\mathcal{P}_{\bar{c}})^2\,\bar{n}\cdot\mathcal{P}_c}\left[\bar{\mathcal{Q}}^{(d)}_{s,\bar{n}(\bar{\omega})}\,\gamma_{\perp\mu}\not{\bar{n}}\not{n}(1-\gamma_5)\,\mathcal{H}_{v,\bar{n}}\right]\left[\bar{\mathcal{Q}}^{(s)}_{s,\bar{n}(\bar{\rho})}\,\not{\bar{n}}\not{n}\gamma_\perp^\mu(1+\gamma_5)\,S^\dagger_{\bar{n}}S_n\,\mathcal{Q}^{(s)}_{s,n(\rho)}\right] \\
&\quad\times\left[\bar{\mathcal{X}}^{(u)}_{\bar{c}(x_1)}\not{n}(1+\gamma_5)\,\mathcal{X}^{(s)}_{\bar{c}(x_2)}\right]\left[\bar{\mathcal{X}}^{(s)}_{c(y_1)}\not{\bar{n}}(1+\gamma_5)\,\mathcal{X}^{(u)}_{c(y_2)}\right], \\
\mathcal{O}^u_{8,\perp\bar{n},r} &= \frac{1}{(n\cdot\mathcal{P}_{\bar{c}})^2\,\bar{n}\cdot\mathcal{P}_c}\left[\bar{\mathcal{Q}}^{(d)}_{s,\bar{n}(\bar{\omega})}\,\gamma_{\perp\mu}\not{\bar{n}}\not{n}(1-\gamma_5)\,\mathcal{H}_{v,\bar{n}}\right]\left[\bar{\mathcal{Q}}^{(u)}_{s,n(\rho)}\,S^\dagger_n S_{\bar{n}}\not{n}\not{\bar{n}}\gamma_\perp^\mu(1-\gamma_5)\,\mathcal{Q}^{(u)}_{s,\bar{n}(\bar{\rho})}\right] \\
&\quad\times\left[\bar{\mathcal{X}}^{(u)}_{\bar{c}(x_1)}\not{n}(1-\gamma_5)\,\mathcal{X}^{(s)}_{\bar{c}(x_2)}\right]\left[\bar{\mathcal{X}}^{(s)}_{c(y_1)}\not{\bar{n}}(1-\gamma_5)\,\mathcal{X}^{(u)}_{c(y_2)}\right]. \qquad (13.16)
\end{aligned}$$

The superscript $q = u, s$ specifies whether the operator contains an additional $(\bar{u}u)$ or $(\bar{s}s)$ soft quark pair. The subscript $\perp\bar{n}$ indicates that the spectator down quark is followed by $\gamma_\perp\not{\bar{n}}$. The choice of momentum variables is illustrated in Figure 13.1. These operators have mass dimension $D = 9$ and are not boost invariant. However, the correct mass dimension and boost invariance are restored after combining with the Wilson coefficients. Applying the same procedure to the operators $O^{-,q}_{4\bar{g},hc,r}$, we find

$$\begin{aligned}
\mathcal{O}^s_{8,\perp n,r} &= \frac{1}{n\cdot\mathcal{P}_{\bar{c}}\,(\bar{n}\cdot\mathcal{P}_c)^2}\left[\bar{\mathcal{Q}}^{(d)}_{s,n(\omega)}\,\gamma_{\perp\mu}\not{n}\not{\bar{n}}(1-\gamma_5)\,\mathcal{H}_{v,n}\right]\left[\bar{\mathcal{Q}}^{(s)}_{s,\bar{n}(\bar{\rho})}\,S^\dagger_{\bar{n}}S_n\,\not{\bar{n}}\not{n}\gamma_\perp^\mu(1-\gamma_5)\,\mathcal{Q}^{(s)}_{s,n(\rho)}\right] \\
&\quad\times\left[\bar{\mathcal{X}}^{(u)}_{\bar{c}(x_1)}\not{n}(1-\gamma_5)\,\mathcal{X}^{(s)}_{\bar{c}(x_2)}\right]\left[\bar{\mathcal{X}}^{(s)}_{c(y_1)}\not{\bar{n}}(1-\gamma_5)\,\mathcal{X}^{(u)}_{c(y_2)}\right], \\
\mathcal{O}^u_{8,\perp n,r} &= \frac{1}{n\cdot\mathcal{P}_{\bar{c}}\,(\bar{n}\cdot\mathcal{P}_c)^2}\left[\bar{\mathcal{Q}}^{(d)}_{s,n(\omega)}\,\gamma_{\perp\mu}\not{n}\not{\bar{n}}(1-\gamma_5)\,\mathcal{H}_{v,n}\right]\left[\bar{\mathcal{Q}}^{(u)}_{s,n(\rho)}\,\not{n}\not{\bar{n}}\gamma_\perp^\mu(1+\gamma_5)\,S^\dagger_n S_{\bar{n}}\,\mathcal{Q}^{(u)}_{s,\bar{n}(\bar{\rho})}\right] \\
&\quad\times\left[\bar{\mathcal{X}}^{(u)}_{\bar{c}(x_1)}\not{n}(1+\gamma_5)\,\mathcal{X}^{(s)}_{\bar{c}(x_2)}\right]\left[\bar{\mathcal{X}}^{(s)}_{c(y_1)}\not{\bar{n}}(1+\gamma_5)\,\mathcal{X}^{(u)}_{c(y_2)}\right]. \qquad (13.17)
\end{aligned}$$

After projecting onto color-singlet states in the (anti-)collinear brackets, two possible color structures $r = \text{i}, \text{ii}$ in the soft sector remain. For $\mathcal{O}^u_{8,\perp\bar{n},r}$, they are

$$\left[\bar{\mathcal{Q}}^{(d)\,i_1}_{s,\bar{n}}\,\gamma_{\perp\mu}\not{\bar{n}}\not{n}(1-\gamma_5)\,\mathcal{H}^{j_1}_{v,\bar{n}}\right]\left[\bar{\mathcal{Q}}^{(s)\,i_2}_{s,\bar{n}}\,\not{\bar{n}}\not{n}\gamma_\perp^\mu(1+\gamma_5)\left(S^\dagger_{\bar{n}}S_n\,\mathcal{Q}^{(s)}_{s,n}\right)^{j_2}\right]\left[T_{(r)}\right]^{i_1\,i_2}_{j_1\,j_2}, \quad (13.18)$$

with

$$\left[T_{(\text{i})}\right]^{i_1\,i_2}_{j_1\,j_2} = \delta^{i_1 j_1}\,\delta^{i_2 j_2}, \qquad \left[T_{(\text{ii})}\right]^{i_1\,i_2}_{j_1\,j_2} = (t^a)^{i_1 j_1}\,(t^a)^{i_2 j_2}. \quad (13.19)$$

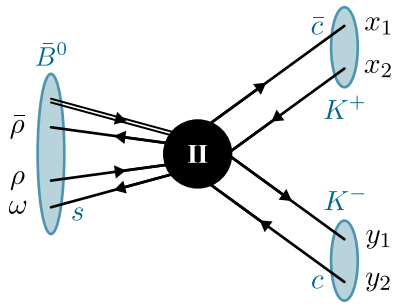

Figure 13.1: Choice of the momentum variables in the SCET-2 eight-quark operators.

And similar for the other operators. It proves to be convenient to choose these color structures instead of the ones defined in (12.15). They are related by the color Fierz relation (12.43).

The four leading power operators originating from $O^{-,q}_{4g,\overline{hc},r}$ are

$$\begin{aligned}
\mathcal{O}^{s,\perp}_{8,\perp\bar{n},r} &= \frac{1}{(n\cdot\mathcal{P}_{\bar{c}})^2\,\bar{n}\cdot\mathcal{P}_c}\left[\bar{\mathcal{Q}}^{(d)}_{s,\bar{n}(\bar{\omega})}\,\gamma_{\perp\mu}\vec{\not{n}}\not{n}(1-\gamma_5)\,\mathcal{H}_{v,\bar{n}}\right]\left[\bar{\mathcal{Q}}^{(s)}_{s,\bar{n}(\bar{\rho})}\,\vec{\not{n}}\not{n}(1-\gamma_5)\,S^\dagger_{\bar{n}}S_n\,\mathcal{Q}^{(s)}_{s,n(\rho)}\right]\\
&\quad\times\left[\bar{\mathcal{X}}^{(u)}_{\bar{c}(x_1)}\,\not{n}\gamma^\mu_\perp(1+\gamma_5)\,\mathcal{X}^{(s)}_{\bar{c}(x_2)}\right]\left[\bar{\mathcal{X}}^{(s)}_{c(y_1)}\,\vec{\not{n}}(1-\gamma_5)\,\mathcal{X}^{(u)}_{c(y_2)}\right],\\
\mathcal{O}^{u,\perp}_{8,\perp\bar{n},r} &= \frac{1}{(n\cdot\mathcal{P}_{\bar{c}})^2\,\bar{n}\cdot\mathcal{P}_c}\left[\bar{\mathcal{Q}}^{(d)}_{s,\bar{n}(\bar{\omega})}\,\gamma_{\perp\mu}\vec{\not{n}}\not{n}(1-\gamma_5)\,\mathcal{H}_{v,\bar{n}}\right]\left[\bar{\mathcal{Q}}^{(u)}_{s,n}\,S^\dagger_nS_{\bar{n}}\,\not{n}\vec{\not{n}}(1-\gamma_5)\,\mathcal{Q}^{(u)}_{s,\bar{n}}\right]\\
&\quad\times\left[\bar{\mathcal{X}}^{(u)}_{\bar{c}(x_1)}\,\not{n}\gamma^\mu_\perp(1+\gamma_5)\,\mathcal{X}^{(s)}_{\bar{c}(x_2)}\right]\left[\bar{\mathcal{X}}^{(s)}_{c(y_1)}\,\vec{\not{n}}(1+\gamma_5)\,\mathcal{X}^{(u)}_{c(y_2)}\right]
\end{aligned}\tag{13.20}$$

and the ones from $O^{+,q}_{4\bar{g},hc,r}$ are

$$\begin{aligned}
\mathcal{O}^{s,\perp}_{8,\perp n,r} &= \frac{1}{n\cdot\mathcal{P}_{\bar{c}}\,(\bar{n}\cdot\mathcal{P}_c)^2}\left[\bar{\mathcal{Q}}^{(d)}_{s,n(\omega)}\,\gamma_{\perp\mu}\not{n}\vec{\not{n}}(1-\gamma_5)\,\mathcal{H}_{v,n}\right]\left[\bar{\mathcal{Q}}^{(s)}_{s,\bar{n}(\bar{\rho})}\,S^\dagger_{\bar{n}}S_n\,\vec{\not{n}}\not{n}(1-\gamma_5)\,\mathcal{Q}^{(s)}_{s,n(\rho)}\right]\\
&\quad\times\left[\bar{\mathcal{X}}^{(u)}_{\bar{c}(x_1)}\,\not{n}(1+\gamma_5)\,\mathcal{X}^{(s)}_{\bar{c}(x_2)}\right]\left[\bar{\mathcal{X}}^{(s)}_{c(y_1)}\,\vec{\not{n}}\gamma^\mu_\perp(1+\gamma_5)\,\mathcal{X}^{(u)}_{c(y_2)}\right],\\
\mathcal{O}^{u,\perp}_{8,\perp n,r} &= \frac{1}{n\cdot\mathcal{P}_{\bar{c}}\,(\bar{n}\cdot\mathcal{P}_c)^2}\left[\bar{\mathcal{Q}}^{(d)}_{s,n(\omega)}\,\gamma_{\perp\mu}\not{n}\vec{\not{n}}(1-\gamma_5)\,\mathcal{H}_{v,n}\right]\left[\bar{\mathcal{Q}}^{(u)}_{s,n}\,\not{n}\vec{\not{n}}(1-\gamma_5)\,S^\dagger_nS_{\bar{n}}\,\mathcal{Q}^{(u)}_{s,\bar{n}}\right]\\
&\quad\times\left[\bar{\mathcal{X}}^{(u)}_{\bar{c}(x_1)}\,\not{n}(1-\gamma_5)\,\mathcal{X}^{(s)}_{\bar{c}(x_2)}\right]\left[\bar{\mathcal{X}}^{(s)}_{c(y_1)}\,\vec{\not{n}}\gamma^\mu_\perp(1+\gamma_5)\,\mathcal{X}^{(u)}_{c(y_2)}\right].
\end{aligned}\tag{13.21}$$

The superscript $\perp$ indicates that these operators only contribute to B^*-meson decays. The color structure of the soft brackets is similar to (13.18), i.e. the soft Wilson lines belong to the soft quark field standing close by. We do not consider these operators in the following.

13.4 Four-Quark Operators

The matching relations for the four-quark operators listed in (12.13) and (12.19) are more involved. These operators do not contain the pair of strange or up quarks needed to form the final-state kaons, respectively, and hence this pair must be generated in

SCET-1 field	SCET-2 fields	power counting	relevance
$\mathcal{X}_{hc}^{(q)}$	$\mathcal{X}_{c}^{(q)}$	λ^2	✓
$\mathcal{X}_{hc}^{(q)}$	$\mathcal{X}_{c}^{(q)} + \mathcal{A}_{s,n}^{\perp}$	λ^4	
$\mathcal{X}_{hc}^{(q)}$	$\mathcal{X}_{c}^{(q)} + \bar{n}\cdot\mathcal{A}_{s,n}$	λ^4	
$\mathcal{X}_{hc}^{(q)}$	$\mathcal{X}_{c}^{(q)} + \mathcal{A}_{c}^{\perp} + \mathcal{A}_{s,n}^{\perp}$	λ^4	
$\mathcal{X}_{hc}^{(q)}$	$\mathcal{X}_{c}^{(q)} + \mathcal{A}_{s,n}^{\perp} + \mathcal{A}_{s,n}^{\perp}$	λ^4	
$\mathcal{X}_{hc}^{(q)}$	$\mathcal{X}_{c}^{(q)} + \bar{\mathcal{Q}}_{s,n}^{(q')} + \mathcal{Q}_{s,n}^{(q')}$	λ^4	
$\mathcal{X}_{hc}^{(q)}$	$\mathcal{X}_{c}^{(q)} + \bar{\mathcal{X}}_{c}^{(q')} + \mathcal{Q}_{s,n}^{(q')}$	λ^5	✓
$\mathcal{X}_{hc}^{(q)}$	$\mathcal{X}_{c}^{(q)} + \bar{\mathcal{Q}}_{s,n}^{(q')} + \mathcal{X}_{c}^{(q')}$	λ^5	✓
$\mathcal{X}_{hc}^{(q)}$	$\mathcal{X}_{c}^{(q)} + \bar{\mathcal{X}}_{c}^{(q')} + \mathcal{Q}_{s,n}^{(q')} + \mathcal{A}_{c}^{\perp}$	λ^5	✓
$\mathcal{X}_{hc}^{(q)}$	$\mathcal{X}_{c}^{(q)} + \bar{\mathcal{Q}}_{s,n}^{(q')} + \mathcal{X}_{c}^{(q')} + \mathcal{A}_{c}^{\perp}$	λ^5	✓
$\mathcal{X}_{hc}^{(q)}$	$\mathcal{X}_{c}^{(q)} + \bar{\mathcal{X}}_{c}^{(q')} + \mathcal{Q}_{s,n}^{(q')} + \mathcal{A}_{s,n}^{\perp}$	λ^5	✓
$\mathcal{X}_{hc}^{(q)}$	$\mathcal{X}_{c}^{(q)} + \bar{\mathcal{Q}}_{s,n}^{(q')} + \mathcal{X}_{c}^{(q')} + \mathcal{A}_{s,n}^{\perp}$	λ^5	✓

Table 13.3: Matching relations for a hard-collinear quark onto a collinear quark of the same flavor plus other partons [11, 24].

the matching onto SCET-2. Moreover, each of these operators contains either only one hard-collinear or one anti-hard-collinear quark field and, therefore, this quark has to match at least onto two (anti-)collinear quarks in SCET-2. According to Table 13.3, the leading such contribution is of $\mathcal{O}(\lambda^5)$, see also Figure 12.2, and contains also contributions with additional soft or (anti-)collinear gluons. The explicit expression is rather lengthy and can be found in eq. (45) of [11]. In order to get a leading power contribution the remaining up or strange quark in the opposite sector has to match trivially whereas the down quark has to generate the missing strange or up quark to form a kaon, respectively. The leading contribution with the correct field content is (13.15).

First, let us consider $O_{4,hc,r}^{u}$. After performing the decoupling transformation, matching the down quark according to (13.15), applying the Fierz transformation (12.41) once and projecting onto a color-singlet state in the collinear bracket, we define the operator

$$\begin{aligned}\widehat{\mathcal{O}}_{6,n,r}^{u} = \frac{1}{\bar{n}\cdot\mathcal{P}_c}\big[\bar{\mathcal{Q}}_{s,n(\omega)}^{(d)}\,\bar{n}\!\!\!/(1-\gamma_5)\,\mathcal{H}_{v,n}\big]\big[\bar{\mathcal{X}}_{\overline{hc}}^{(u)(0)}S_{\bar{n}}^{\dagger}S_n\,\bar{n}\!\!\!/(1-\gamma_5)\mathcal{Q}_{s,n(\rho)}^{(s)}\big] \\ \times\big[\bar{\mathcal{X}}_{c(y_1)}^{(s)}\,n\!\!\!/(1-\gamma_5)\,\mathcal{X}_{c(y_2)}^{(u)}\big]\,.\end{aligned} \tag{13.22}$$

Note that we dropped two soft inverse derivatives, which would restore boost invariance and the correct mass dimension. Strictly speaking, this operator is defined in SCET(hc,c,s) as it contains both (anti-)hard-collinear and (anti-)collinear fields, we

indicate this by the hat. The color structure of the first two brackets is

$$\left[\bar{Q}^{(d)\,i_1}_{s,n}\,\not{n}(1-\gamma_5)\,\mathcal{H}^{j_1}_{v,n}\right]\left[\left(\bar{\mathcal{X}}^{(u)(0)}_{\overline{hc}}S^\dagger_{\bar{n}}S_n\right)^{i_2}\not{n}(1-\gamma_5)Q^{(s)\,j_2}_{s,n}\right]\left[T_{(r)}\right]^{i_1\,i_2}_{j_1\,j_2}\,, \tag{13.23}$$

with $T_{(r)}$ defined in (13.19).

For the second four-quark SCET-1 operator $O^u_{4,\overline{hc},r}$, one follows the same steps and defines at an intermediate stage

$$\begin{aligned}\widehat{\mathcal{O}}^u_{6,\bar{n},r} = \frac{1}{n\cdot\mathcal{P}_{\bar{c}}}&\left[\bar{Q}^{(d)}_{s,\bar{n}(\bar{\omega})}\,\not{\bar{n}}(1-\gamma_5)\,\mathcal{H}_{v,\bar{n}}\right]\left[\bar{Q}^{(s)}_{s,\bar{n}(\bar{\rho})}\,\not{\bar{n}}(1+\gamma_5)\,S^\dagger_{\bar{n}}S_n\,\mathcal{X}^{(u)(0)}_{hc}\right]\\ &\times\left[\bar{\mathcal{X}}^{(u)}_{\bar{c}(x_1)}\,\not{n}(1+\gamma_5)\,\mathcal{X}^{(s)}_{\bar{c}(x_2)}\right].\end{aligned} \tag{13.24}$$

Its color structure is similar to (13.23).

Matching the remaining (anti-)hard-collinear quarks in (13.22) and (13.24) at $\mathcal{O}(\lambda^5)$ onto SCET-2, we find several operators containing eight quarks as well as operators containing an additional soft or (anti-)collinear gluon. It is convenient to apply a Fierz transformation (12.41) to bring the matching relations in the form

$$\bar{\mathcal{X}}^{(u)(0)}_{\overline{hc}}\to\left[\bar{\mathcal{X}}^{(u)}_{\bar{c}}\ldots\mathcal{X}^{(s)}_{\bar{c}}\right]\bar{Q}^{(s)}_{s,\bar{n}}\ldots\,,\qquad \mathcal{X}^{(u)(0)}_{hc}\to\ldots Q^{(s)}_{s,n}\left[\bar{\mathcal{X}}^{(s)}_{c}\ldots\mathcal{X}^{(u)}_{c}\right] \tag{13.25}$$

and already perform the color-singlet projection in the (anti-)collinear bracket. If the matching relation does include an additional gluon, this projection works as in (13.11) otherwise as in (13.6).

Finally, the simplest eight-quark operators are

$$\begin{aligned}\mathcal{O}^s_{8,n,r} = \frac{1}{(n\cdot\mathcal{P}_{\bar{c}})^2\,\bar{n}\cdot\mathcal{P}_c}&\left[\bar{Q}^{(d)}_{s,n(\omega)}\,\not{n}(1-\gamma_5)\,\mathcal{H}_{v,n}\right]\left[\bar{Q}^{(s)}_{s,\bar{n}(\bar{\rho})}\,S^\dagger_{\bar{n}}S_n\,\not{n}(1-\gamma_5)\,Q^{(s)}_{s,n(\rho)}\right]\\ &\times\left[\bar{\mathcal{X}}^{(u)}_{\bar{c}(x_1)}\,\not{n}(1-\gamma_5)\,\mathcal{X}^{(s)}_{\bar{c}(x_2)}\right]\left[\bar{\mathcal{X}}^{(s)}_{c(y_1)}\,\not{\bar{n}}(1-\gamma_5)\,\mathcal{X}^{(u)}_{c(y_2)}\right],\\ \mathcal{O}^s_{8,\bar{n},r} = \frac{1}{n\cdot\mathcal{P}_{\bar{c}}\,(\bar{n}\cdot\mathcal{P}_c)^2}&\left[\bar{Q}^{(d)}_{s,\bar{n}(\bar{\omega})}\,\not{\bar{n}}(1-\gamma_5)\,\mathcal{H}_{v,\bar{n}}\right]\left[\bar{Q}^{(s)}_{s,\bar{n}(\bar{\rho})}\,\not{\bar{n}}(1+\gamma_5)\,S^\dagger_{\bar{n}}S_n\,Q^{(s)}_{s,n(\rho)}\right]\\ &\times\left[\bar{\mathcal{X}}^{(u)}_{\bar{c}(x_1)}\,\not{n}(1+\gamma_5)\,\mathcal{X}^{(s)}_{\bar{c}(x_2)}\right]\left[\bar{\mathcal{X}}^{(s)}_{c(y_1)}\,\not{\bar{n}}(1+\gamma_5)\,\mathcal{X}^{(u)}_{c(y_2)}\right].\end{aligned} \tag{13.26}$$

The two possible color structures $r=\mathrm{i},\mathrm{ii}$ in the soft bracket are the same as in (13.18) and the choice of momentum variables is visualized in Figure 13.1. The second type of eight-quark operators contains also a derivative $\partial_\perp$ in the numerator acting on (anti-)collinear fields,

$$\begin{aligned}\mathcal{O}^s_{8\bar{\partial},n,r} = \frac{1}{(n\cdot\mathcal{P}_{\bar{c}})^2\,\bar{n}\cdot\mathcal{P}_c}&\left[\bar{Q}^{(d)}_{s,n(\omega)}\,\not{n}(1-\gamma_5)\,\mathcal{H}_{v,n}\right]\left[\bar{Q}^{(s)}_{s,\bar{n}(\bar{\rho})}\,S^\dagger_{\bar{n}}S_n\,\not{\bar{n}}\not{n}(1-\gamma_5)\,Q^{(s)}_{s,n(\rho)}\right]\\ &\times\left[\bar{\mathcal{X}}^{(u)}_{\bar{c}(x_1)}\,\not{n}\,i\partial\!\!\!/_{\bar{c}\perp}(1+\gamma_5)\,\mathcal{X}^{(s)}_{\bar{c}(x_1)}\right]\left[\bar{\mathcal{X}}^{(s)}_{c(y_1)}\,\not{\bar{n}}(1-\gamma_5)\,\mathcal{X}^{(u)}_{c(y_2)}\right],\\ \mathcal{O}^s_{8\partial,\bar{n},r} = \frac{1}{n\cdot\mathcal{P}_{\bar{c}}\,(\bar{n}\cdot\mathcal{P}_c)^2}&\left[\bar{Q}^{(d)}_{s,\bar{n}(\bar{\omega})}\,\not{\bar{n}}(1-\gamma_5)\,\mathcal{H}_{v,\bar{n}}\right]\left[\bar{Q}^{(s)}_{s,\bar{n}(\bar{\rho})}\,\not{\bar{n}}\not{n}(1-\gamma_5)\,S^\dagger_{\bar{n}}S_n\,Q^{(s)}_{s,n(\rho)}\right]\\ &\times\left[\bar{\mathcal{X}}^{(u)}_{\bar{c}(x_1)}\,\not{n}(1+\gamma_5)\,\mathcal{X}^{(s)}_{\bar{c}(x_2)}\right]\left[\bar{\mathcal{X}}^{(s)}_{c(y_1)}\,\not{\bar{n}}\,i\partial\!\!\!/_{c\perp}(1+\gamma_5)\,\mathcal{X}^{(u)}_{c(y_2)}\right].\end{aligned} \tag{13.27}$$

These operators have mass dimension $D = 10$ which is reduced to $D = 6$ after combining with the Wilson coefficients. In principal, there are also operators containing a soft derivative in the numerator but applying the soft equations of motion,

$$\bar{n}\!\!\!/ n\!\!\!/ \, i\partial\!\!\!/_\perp \mathcal{Q}^{(s)}_{s,n} = -2in\cdot\partial\, \bar{n}\!\!\!/ \, \mathcal{Q}^{(s)}_{s,n} - \bar{n}\!\!\!/ n\!\!\!/ \, \mathcal{A}\!\!\!/^\perp_{s,n} \mathcal{Q}^{(s)}_{s,n}\,, \tag{13.28}$$

they can be reduced to the operators (13.26) and operators containing eight quarks and an additional soft gluon, see (13.30) below.

Besides operators containing only eight quarks, there are ones with an additional (anti-)collinear gluon. They read

$$\begin{aligned}
\mathcal{O}^s_{8\bar{c},n,r} &= \frac{1}{(n\cdot\mathcal{P}_{\bar{c}})^2\,\bar{n}\cdot\mathcal{P}_c}\big[\bar{\mathcal{Q}}^{(d)}_{s,n(\omega)}\, n\!\!\!/(1-\gamma_5)\,\mathcal{H}_{v,n}\big]\big[\bar{\mathcal{Q}}^{(s)}_{s,\bar{n}(\bar{\rho})}\, S^\dagger_{\bar{n}} S_n\, \bar{n}\!\!\!/ n\!\!\!/(1-\gamma_5)\,\mathcal{Q}^{(s)}_{s,n(\rho)}\big] \\
&\quad\times\big[\bar{\mathcal{X}}^{(u)}_{\bar{c}(x_1)}\, n\!\!\!/\, \mathcal{A}\!\!\!/^\perp_{\bar{c}(x_3)}(1+\gamma_5)\,\mathcal{X}^{(s)}_{\bar{c}(x_2)}\big]\big[\bar{\mathcal{X}}^{(s)}_{c(y_1)}\, \bar{n}\!\!\!/(1-\gamma_5)\,\mathcal{X}^{(u)}_{c(y_2)}\big]\,, \\
\mathcal{O}^s_{8c,\bar{n},r} &= \frac{1}{n\cdot\mathcal{P}_{\bar{c}}\,(\bar{n}\cdot\mathcal{P}_c)^2}\big[\bar{\mathcal{Q}}^{(d)}_{s,\bar{n}(\bar{\omega})}\, \bar{n}\!\!\!/(1-\gamma_5)\,\mathcal{H}_{v,\bar{n}}\big]\big[\bar{\mathcal{Q}}^{(s)}_{s,\bar{n}(\bar{\rho})}\, \bar{n}\!\!\!/ n\!\!\!/(1-\gamma_5)\, S^\dagger_{\bar{n}} S_n\, \mathcal{Q}^{(s)}_{s,n(\rho)}\big] \\
&\quad\times\big[\bar{\mathcal{X}}^{(u)}_{\bar{c}(x_1)}\, n\!\!\!/(1+\gamma_5)\,\mathcal{X}^{(s)}_{\bar{c}(x_2)}\big]\big[\bar{\mathcal{X}}^{(s)}_{c(y_1)}\, \bar{n}\!\!\!/\, \mathcal{A}\!\!\!/^\perp_{c(y_3)}(1+\gamma_5)\,\mathcal{X}^{(u)}_{c(y_2)}\big]\,.
\end{aligned} \tag{13.29}$$

The last type of leading power SCET-2 operators contains eight quarks and an additional soft gluon

$$\begin{aligned}
\mathcal{O}^s_{8s,n,r} &= \frac{1}{(n\cdot\mathcal{P}_{\bar{c}})^2\,\bar{n}\cdot\mathcal{P}_c}\big[\bar{\mathcal{Q}}^{(d)}_{s,n(\omega)}\, n\!\!\!/(1-\gamma_5)\,\mathcal{H}_{v,n}\big]\big[\bar{\mathcal{Q}}^{(s)}_{s,\bar{n}(\bar{\rho})}\, \mathcal{A}\!\!\!/^\perp_{s,\bar{n}(\bar{\sigma})}\, S^\dagger_{\bar{n}} S_n\, \bar{n}\!\!\!/ n\!\!\!/(1-\gamma_5)\,\mathcal{Q}^{(s)}_{s,n(\rho)}\big] \\
&\quad\times\big[\bar{\mathcal{X}}^{(u)}_{\bar{c}(x_1)}\, n\!\!\!/(1-\gamma_5)\,\mathcal{X}^{(s)}_{\bar{c}(x_2)}\big]\big[\bar{\mathcal{X}}^{(s)}_{c(y_1)}\, \bar{n}\!\!\!/(1-\gamma_5)\,\mathcal{X}^{(u)}_{c(y_2)}\big]\,, \\
\mathcal{O}^s_{8s,\bar{n},r} &= \frac{1}{n\cdot\mathcal{P}_{\bar{c}}\,(\bar{n}\cdot\mathcal{P}_c)^2}\big[\bar{\mathcal{Q}}^{(d)}_{s,\bar{n}(\bar{\omega})}\, \bar{n}\!\!\!/(1-\gamma_5)\,\mathcal{H}_{v,\bar{n}}\big]\big[\bar{\mathcal{Q}}^{(s)}_{s,\bar{n}(\bar{\rho})}\, \bar{n}\!\!\!/ n\!\!\!/\, S^\dagger_{\bar{n}} S_n\, \mathcal{A}\!\!\!/^\perp_{s,n(\sigma)}(1+\gamma_5)\,\mathcal{Q}^{(s)}_{s,n(\rho)}\big] \\
&\quad\times\big[\bar{\mathcal{X}}^{(u)}_{\bar{c}(x_1)}\, n\!\!\!/(1+\gamma_5)\,\mathcal{X}^{(s)}_{\bar{c}(x_2)}\big]\big[\bar{\mathcal{X}}^{(s)}_{c(y_1)}\, \bar{n}\!\!\!/(1+\gamma_5)\,\mathcal{X}^{(u)}_{c(y_2)}\big]\,.
\end{aligned} \tag{13.30}$$

As evident from (13.22) and (13.24), there are only two possible color structures $r = \mathrm{i}, \mathrm{ii}$ for these operators

$$\begin{aligned}
&\big[\bar{\mathcal{Q}}^{(d)\,i_1}_{s,n}\, n\!\!\!/(1-\gamma_5)\,\mathcal{H}^{j_1}_{v,n}\big]\big[\big(\bar{\mathcal{Q}}^{(s)}_{s,\bar{n}}\, \mathcal{A}\!\!\!/^\perp_{s,\bar{n}}\, S^\dagger_{\bar{n}} S_n\big)^{i_2}\, \bar{n}\!\!\!/ n\!\!\!/(1-\gamma_5)\,\mathcal{Q}^{(s)\,j_2}_{s,n}\big]\,\big[T_{(r)}\big]^{i_1\,i_2}_{j_1\,j_2}\,, \\
&\big[\bar{\mathcal{Q}}^{(d)\,i_1}_{s,\bar{n}}\, \bar{n}\!\!\!/(1-\gamma_5)\,\mathcal{H}^{j_1}_{v,\bar{n}}\big]\big[\bar{\mathcal{Q}}^{(s)\,i_2}_{s,\bar{n}}\, \bar{n}\!\!\!/ n\!\!\!/(1-\gamma_5)\big(S^\dagger_{\bar{n}} S_n\, \mathcal{A}\!\!\!/^\perp_{s,n}\, \mathcal{Q}^{(s)}_{s,n}\big)^{j_2}\big]\,\big[T_{(r)}\big]^{i_1\,i_2}_{j_1\,j_2}\,,
\end{aligned} \tag{13.31}$$

with $T_{(r)}$ given in (13.19). The choice of momentum variables for eight-quark operator with additional gluon is illustrated in Figure 13.2. If one would also consider B^*-meson decays, one would find 16 additional leading power operators originating from four-quark SCET-1 operators with $(\bar{u}u)$ pair.

SCET-1 four-quark operators with $(\bar{s}s)$ pair (12.19) match on SCET-2 operators containing eight quarks (and additional gluons) with a $(\bar{u}u)$ soft quark pair. For

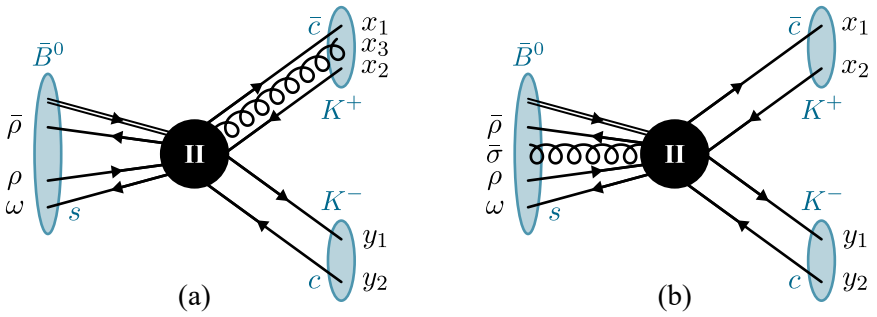

Figure 13.2: Choice of the momentum variables in the SCET-2 eight-quark operators with additional gluon $\mathcal{O}^s_{8\bar{c},n,r}$ (left) and $\mathcal{O}^s_{8s,n,r}$ (right).

example, the analog of (13.26) is

$$\begin{aligned}\mathcal{O}^u_{8,n,r} &= \frac{1}{(n\cdot\mathcal{P}_{\bar{c}})^2\,\bar{n}\cdot\mathcal{P}_c}\left[\bar{\mathcal{Q}}^{(d)}_{s,n(\omega)}\,\not{n}(1-\gamma_5)\,\mathcal{H}_{v,n}\right]\left[\bar{\mathcal{Q}}^{(u)}_{s,n(\rho)}\,\not{n}(1+\gamma_5)\,S_n^\dagger S_{\bar{n}}\,\mathcal{Q}^{(u)}_{s,\bar{n}(\bar{\rho})}\right]\\ &\quad\times\left[\bar{\mathcal{X}}^{(u)}_{\bar{c}(x_1)}\,\not{n}(1+\gamma_5)\,\mathcal{X}^{(s)}_{\bar{c}(x_2)}\right]\left[\bar{\mathcal{X}}^{(s)}_{c(y_1)}\,\not{\bar{n}}(1+\gamma_5)\,\mathcal{X}^{(u)}_{c(y_2)}\right],\\ \mathcal{O}^u_{8,\bar{n},r} &= \frac{1}{n\cdot\mathcal{P}_{\bar{c}}\,(\bar{n}\cdot\mathcal{P}_c)^2}\left[\bar{\mathcal{Q}}^{(d)}_{s,\bar{n}(\bar{\omega})}\,\not{\bar{n}}(1-\gamma_5)\,\mathcal{H}_{v,\bar{n}}\right]\left[\bar{\mathcal{Q}}^{(u)}_{s,n(\rho)}\,S_n^\dagger S_{\bar{n}}\,\not{\bar{n}}(1-\gamma_5)\,\mathcal{Q}^{(u)}_{s,\bar{n}(\bar{\rho})}\right]\\ &\quad\times\left[\bar{\mathcal{X}}^{(u)}_{\bar{c}(x_1)}\,\not{n}(1-\gamma_5)\,\mathcal{X}^{(s)}_{\bar{c}(x_2)}\right]\left[\bar{\mathcal{X}}^{(s)}_{c(y_1)}\,\not{\bar{n}}(1-\gamma_5)\,\mathcal{X}^{(u)}_{c(y_2)}\right].\end{aligned}\tag{13.32}$$

In general, the eight-quark operators with $(\bar{u}u)$ soft quark pair are obtained by making the replacements $u\leftrightarrow s$, $c\leftrightarrow\bar{c}$, $n\leftrightarrow\bar{n}$, $x_i\leftrightarrow y_i$, $\omega\leftrightarrow\bar{\omega}$, $\rho\leftrightarrow\bar{\rho}$, and $\sigma\leftrightarrow\bar{\sigma}$ everywhere.

13.5 Tree-Level Matching Results

In this section, we present the tree-level matching relations obtained when the weak effective SCET-1 Lagrangian (12.36) is matched onto SCET-2 at a scale $\mu_j\sim\sqrt{m_b\Lambda_{\rm QCD}}$. In general, the resulting weak Lagrangian in SCET-2 takes the generic form

$$\mathcal{L}^{\rm SCET-2}_{\rm eff} = -\sum_m D_m(\mu)\star\mathcal{O}_m(\mu)\,,\tag{13.33}$$

where the relevant operators $\mathcal{O}_m$ have been defined in the previous sections. The Wilson coefficients D_m of the full matching can be decomposed as

$$D_m(\mu) = \sum_n J_{m,n}(\mu)\star H_n(\mu)\star\bar{J}_{m,n}(\mu)\,.\tag{13.34}$$

The jet functions $J_{m,n}$ and $\bar{J}_{m,n}$ originate from matching SCET-1 to SCET-2 in the hard-collinear and anti-collinear sector, respectively, and the hard functions H_n are the ones from the matching QCD to SCET-1, see Section 12.5. The sum over n includes all SCET-1 operators that match onto the given SCET-2 operator $\mathcal{O}_m$. Working at tree level, only one SCET-1 operator (with different color structures) contributes to the matching for a given SCET-2 operator. This simplifies the structure of the jet functions considerably. We give their explicit expressions in Appendix A.10.

The hard functions depend only on the momentum fractions $\tilde{x}_i$ and $\tilde{y}_i$ of the various (anti-)hard-collinear fields. The jet functions depend also on the momentum fraction x_i and y_i of the (anti-)collinear fields. Therefore, the symbols $\star$ in (13.34) indicate that one needs to integrate over the momentum fractions of the (anti-)hard-collinear fields with measure

$$\left(\prod_{i=1}^{N_{hc}}\int_0^1 d\tilde{y}_i\right)\left(\prod_{j=1}^{N_{\overline{hc}}}\int_0^1 d\tilde{x}_j\right). \tag{13.35}$$

Here N_{hc} ($N_{\overline{hc}}$) denotes the number of (anti-)hard-collinear fields in SCET-1 operator O_n. Similar to (12.36), these integrals are only present if $N_{hc} > 1$ and/or $N_{\overline{hc}} > 1$. As we work at tree level, the jet functions contain δ functions and these integrals can be performed trivially. The symbol $\star$ in (13.33) indicates that one also needs to integrate over the momentum fractions of the (anti-)collinear fields and the soft momenta with measure

$$\left(\prod_{i=1}^{N_c}\int_0^1 dy_i\right)\left(\prod_{j=1}^{N_{\bar{c}}}\int_0^1 dx_j\right)\left(\prod_{k=1}^{N_s}\int_{-\infty}^{\infty} d\omega_k\right), \tag{13.36}$$

where N_c ($N_{\bar{c}}$) is the number of (anti-)collinear fields and N_s the number of light soft fields in SCET-2 operator $\mathcal{O}_m$. In the following, N_c as number of collinear fields does not appear anymore and, therefore, it cannot be confused with number of colors. In general, the soft variables $\{\underline{\omega}\} = \{\omega, \bar{\omega}, \dots\}$ need to be integrate in $(-\infty, \infty)$ as soft momenta are not conserved in HQET and SCET.

Below we list the full tree-level Wilson coefficients for the operators defined in the previous sections. However, we restrict to operators relevant for $\bar{B}^0 \to K^+K^-$ and do not include the coefficients relevant for B^*-meson decays.

13.5.1 Six-Quark Operators

For SCET-2 operators containing six quarks (13.9), the jet functions are trivial and their full Wilson coefficients (13.34) are given by linear combinations of $H^{\pm}_{6,s\bar{n},r}$ and $H^{\pm}_{6,sn,r}$. Taking into account the factors from the color singlet projection in (13.8), we find

$$\begin{aligned}
D^{+}_{6,\bar{n}}(\{\underline{x},\underline{y}\},\mu_j) = \frac{C_F}{N_c}\,\pi\,\alpha_j\Bigg\{&+\frac{1}{y_1x_2}\,\mathcal{C}_1^{+,u}(\mu_j)+\frac{1}{x_2}\left(\frac{1}{y_1^2}+\frac{1}{y_1}\right)\frac{\mathcal{C}_2^{+,u}(\mu_j)}{N_c}\\
&-\frac{1}{y_2x_1}\,\mathcal{C}_1^{+,s}(\mu_j)+\frac{1}{y_2}\left(\frac{1}{x_1+x_2y_2}-\frac{1}{x_1}\right)\frac{\mathcal{C}_2^{+,s}(\mu_j)}{N_c}\Bigg\},\\
D^{-}_{6,\bar{n}}(\{\underline{x},\underline{y}\},\mu_j) = \frac{C_F}{N_c}\,\pi\,\alpha_j\Bigg\{&+\frac{1}{y_1x_2}\,\mathcal{C}_1^{-,u}(\mu_j)+\frac{1}{y_1}\left(\frac{1}{x_2}+\frac{1}{x_2+y_1x_1}\right)\frac{\mathcal{C}_2^{-,u}(\mu_j)}{N_c}\\
&-\frac{1}{y_2x_1}\,\mathcal{C}_1^{-,s}(\mu_j)+\frac{1}{x_1}\left(\frac{1}{y_2^2}-\frac{1}{y_2}\right)\frac{\mathcal{C}_2^{-,s}(\mu_j)}{N_c}\Bigg\},
\end{aligned}$$

$$
\begin{aligned}
D^{+}_{6,n}(\{\underline{x},\underline{y}\},\mu_j) &= \frac{C_F}{N_c}\,\pi\alpha_j\bigg\{-\frac{1}{y_1x_2}\,\mathcal{C}_1^{+,u}(\mu_j)+\frac{1}{x_2}\left(\frac{1}{y_1+y_2x_2}-\frac{1}{y_1}\right)\frac{\mathcal{C}_2^{+,u}(\mu_j)}{N_c}\\
&\qquad+\frac{1}{y_2x_1}\,\mathcal{C}_1^{+,s}(\mu_j)+\frac{1}{y_2}\left(\frac{1}{x_1^2}+\frac{1}{x_1}\right)\frac{\mathcal{C}_2^{+,s}(\mu_j)}{N_c}\bigg\},\\
D^{-}_{6,n}(\{\underline{x},\underline{y}\},\mu_j) &= \frac{C_F}{N_c}\,\pi\alpha_j\bigg\{-\frac{1}{y_1x_2}\,\mathcal{C}_1^{-,u}(\mu_j)+\frac{1}{y_1}\left(\frac{1}{x_2^2}-\frac{1}{x_2}\right)\frac{\mathcal{C}_2^{-,u}(\mu_j)}{N_c}\\
&\qquad+\frac{1}{y_2x_1}\,\mathcal{C}_1^{-,s}(\mu_j)+\frac{1}{x_1}\left(\frac{1}{y_2}+\frac{1}{y_2+y_1x_1}\right)\frac{\mathcal{C}_2^{-,s}(\mu_j)}{N_c}\bigg\},
\end{aligned}
\tag{13.37}
$$

with abbreviation $\alpha_j=\alpha_s(\mu_j)$. We show below that the matrix elements of $\mathcal{O}^{\pm}_{6,\bar n}$ and $\mathcal{O}^{\pm}_{6,n}$ evaluate to the same expressions. Therefore, one has to add up the corresponding Wilson coefficients and finds that $\mathcal{Q}_1^{\pm,q}$ does not contribute to six-quark SCET-2 operators.

13.5.2 Eight-Quark Operators

For eight-quark operators (13.16) and (13.17) originating from SCET-1 operators with four quarks and additional gluon, the full Wilson coefficients at tree level are

$$
\begin{aligned}
D^{s}_{8,\perp\bar n,\mathrm{i}}(\{\underline{x},\underline{y},\underline{\omega}\},\mu_j) &= -\frac{1}{8N_c^2}\,\pi^2\alpha_j^2\,\frac{1}{\bar\rho(\bar\rho+\bar\omega)\rho}\,\frac{1}{y_1x_1x_2}\\
&\quad\times\left\{\frac{C_F}{N_c}\,x_1\,\mathcal{C}_1^{+,u}(\mu_j)+\frac{C_F}{N_c^2}\,x_2\,\mathcal{C}_2^{+,u}(\mu_j)\right\},\\
D^{s}_{8,\perp\bar n,\mathrm{ii}}(\{\underline{x},\underline{y},\underline{\omega}\},\mu_j) &= +\frac{1}{8N_c^2}\,\pi^2\alpha_j^2\,\frac{1}{\bar\rho(\bar\rho+\bar\omega)\rho}\,\frac{1}{y_1x_1x_2}\\
&\quad\times\left\{2\left(C_F+\frac{x_1}{N_c}\right)\mathcal{C}_1^{+,u}(\mu_j)+\frac{N_c^2+1}{N_c^2}\,x_2\,\mathcal{C}_2^{+,u}(\mu_j)\right\},\\
D^{s}_{8,\perp n,\mathrm{i}}(\{\underline{x},\underline{y},\underline{\omega}\},\mu_j) &= -\frac{1}{8N_c^2}\,\pi^2\alpha_j^2\,\frac{1}{\rho(\rho+\omega)\bar\rho}\,\frac{1}{y_1y_2x_2}\\
&\quad\times\left\{\frac{C_F}{N_c}\,y_2\,\mathcal{C}_1^{-,u}(\mu_j)+\frac{C_F}{N_c^2}\big(2C_F\,N_c\,y_2-1\big)\mathcal{C}_2^{-,u}(\mu_j)\right\},\\
D^{s}_{8,\perp n,\mathrm{ii}}(\{\underline{x},\underline{y},\underline{\omega}\},\mu_j) &= -\frac{1}{8N_c^2}\,\pi^2\alpha_j^2\,\frac{1}{\rho(\rho+\omega)\bar\rho}\,\frac{1}{y_1y_2x_2}\\
&\quad\times\left\{2\left(C_F+\frac{N_c^2-2}{2N_c}\,y_2\right)\mathcal{C}_1^{-,u}(\mu_j)+\left(4C_F^2\,y_2+\frac{1}{N_c^2}\right)\mathcal{C}_2^{-,u}(\mu_j)\right\}.
\end{aligned}
\tag{13.38}
$$

Note that the Wilson coefficients of the operator $\mathcal{O}^{s}_{8,\perp\bar n,r}$ ($\mathcal{O}^{s}_{8,\perp n,r}$) depend on the hard functions $\mathcal{C}^{+,u}_{r'}$ ($\mathcal{C}^{-,u}_{r'}$) with opposite flavor superscript. As in general they are integrated over the entire real axis, the $i0$ prescription of the soft variables can be relevant, see e.g. [131]. However, in our case it is always the same $\omega-i0$, $\bar\omega-i0$ and so on.

The full Wilson coefficients for the SCET(hc,c,s) operators (13.22) and (13.24) are at tree level given by

$$\begin{aligned}
\widehat{D}^u_{6,n,\mathrm{i}} &= \pi\,\alpha_j\,\frac{1}{\rho(\rho+\omega)}\,\frac{1}{y_1}\,\frac{C_F}{N_c^2}\,\mathcal{C}_2^{-,u}(\mu_j)\,,\\
\widehat{D}^u_{6,n,\mathrm{ii}} &= \pi\,\alpha_j\,\frac{1}{\rho(\rho+\omega)}\,\frac{1}{y_1}\left[\frac{1}{N_c}\,\mathcal{C}_1^{-,u}(\mu_j)+\frac{2C_F}{N_c}\,\mathcal{C}_2^{-,u}(\mu_j)\right],\\
\widehat{D}^u_{6,\bar{n},\mathrm{i}} &= \pi\,\alpha_j\,\frac{1}{\bar{\rho}(\bar{\rho}+\bar{\omega})}\,\frac{1}{x_2}\,\frac{C_F}{N_c^2}\,\mathcal{C}_2^{+,u}(\mu_j)\,,\\
\widehat{D}^u_{6,\bar{n},\mathrm{ii}} &= \pi\,\alpha_j\,\frac{1}{\bar{\rho}(\bar{\rho}+\bar{\omega})}\,\frac{1}{x_2}\left[\frac{1}{N_c}\,\mathcal{C}_1^{+,u}(\mu_j)-\frac{1}{N_c^2}\,\mathcal{C}_2^{+,u}(\mu_j)\right].
\end{aligned}\tag{13.39}$$

Matching also the remaining (anti-)hard-collinear up-quark field to SCET-2, we find for the Wilson coefficients of the eight-quark operators (13.26)

$$\begin{aligned}
D^s_{8,n,\mathrm{i}}(\{\underline{x},\underline{y},\underline{\omega}\},\mu_j) &= +\frac{2C_F^2}{N_c^3}\,\pi^2\alpha_j^2\,\frac{1}{\rho(\rho+\omega)\bar{\rho}}\,\frac{1+x_2}{y_1\,x_2^2}\,\mathcal{C}_2^{-,u}(\mu_j)\,,\\
D^s_{8,n,\mathrm{ii}}(\{\underline{x},\underline{y},\underline{\omega}\},\mu_j) &= +\frac{2C_F}{N_c^2}\,\pi^2\alpha_j^2\,\frac{1}{\rho(\rho+\omega)\bar{\rho}}\,\frac{1+x_2}{y_1\,x_2^2}\left[\mathcal{C}_1^{-,u}(\mu_j)+2C_F\,\mathcal{C}_2^{-,u}(\mu_j)\right],\\
D^s_{8,\bar{n},\mathrm{i}}(\{\underline{x},\underline{y},\underline{\omega}\},\mu_j) &= -\frac{2C_F^2}{N_c^3}\,\pi^2\alpha_j^2\,\frac{1}{\bar{\rho}(\bar{\rho}+\bar{\omega})\rho}\,\frac{1+y_1}{y_1^2\,x_2}\,\mathcal{C}_2^{+,u}(\mu_j)\,,\\
D^s_{8,\bar{n},\mathrm{ii}}(\{\underline{x},\underline{y},\underline{\omega}\},\mu_j) &= -\frac{2C_F}{N_c^2}\,\pi^2\alpha_j^2\,\frac{1}{\bar{\rho}(\bar{\rho}+\bar{\omega})\rho}\,\frac{1+y_1}{y_1^2\,x_2}\left[\mathcal{C}_1^{+,u}(\mu_j)-\frac{1}{N_c}\,\mathcal{C}_2^{+,u}(\mu_j)\right]
\end{aligned}\tag{13.40}$$

and for the ones with additional derivatives (13.27)

$$\begin{aligned}
D^s_{8\bar{\partial},n,\mathrm{i}}(\{\underline{x},\underline{y},\underline{\omega}\},\mu_j) &= +\frac{C_F^2}{N_c^3}\,\pi^2\alpha_j^2\,\frac{1}{\rho(\rho+\omega)\bar{\rho}^2}\,\frac{1}{y_1\,x_1\,x_2^2}\,\mathcal{C}_2^{-,u}(\mu_j)\,,\\
D^s_{8\bar{\partial},n,\mathrm{ii}}(\{\underline{x},\underline{y},\underline{\omega}\},\mu_j) &= +\frac{C_F}{N_c^2}\,\pi^2\alpha_j^2\,\frac{1}{\rho(\rho+\omega)\bar{\rho}^2}\,\frac{1}{y_1\,x_1\,x_2^2}\left[\mathcal{C}_1^{-,u}(\mu_j)+2C_F\,\mathcal{C}_2^{-,u}(\mu_j)\right],\\
D^s_{8\partial,\bar{n},\mathrm{i}}(\{\underline{x},\underline{y},\underline{\omega}\},\mu_j) &= -\frac{C_F^2}{N_c^3}\,\pi^2\alpha_j^2\,\frac{1}{\bar{\rho}(\bar{\rho}+\bar{\omega})\rho^2}\,\frac{1}{y_1^2\,y_2\,x_2}\,\mathcal{C}_2^{+,u}(\mu_j)\,,\\
D^s_{8\partial,\bar{n},\mathrm{ii}}(\{\underline{x},\underline{y},\underline{\omega}\},\mu_j) &= -\frac{C_F}{N_c^2}\,\pi^2\alpha_j^2\,\frac{1}{\bar{\rho}(\bar{\rho}+\bar{\omega})\rho^2}\,\frac{1}{y_1^2\,y_2\,x_2}\left[\mathcal{C}_1^{+,u}(\mu_j)-\frac{1}{N_c}\,\mathcal{C}_2^{+,u}(\mu_j)\right].
\end{aligned}\tag{13.41}$$

The Wilson coefficients for the eight-quark operators with $(\bar{u}u)$ soft quark pair, i.e. for $\mathcal{O}^u_{8,\perp\bar{n},r}$ and $\mathcal{O}^u_{8,\perp n,r}$ as well as $\mathcal{O}^u_{8,\bar{n},r}$ and $\mathcal{O}^u_{8,n,r}$, are obtained by making the replacements $u\leftrightarrow s$, $c\leftrightarrow\bar{c}$, $n\leftrightarrow\bar{n}$, $x_i\leftrightarrow y_i$, $\omega\leftrightarrow\bar{\omega}$, and $\rho\leftrightarrow\bar{\rho}$ everywhere. For the operators with an additional derivative, $\mathcal{O}^u_{8\partial,\bar{n},r}$ and $\mathcal{O}^u_{8\bar{\partial},n,r}$, one also needs to replace $\partial\leftrightarrow\bar{\partial}$.

13.5.3 Eight-Quark Operators with an Additional Gluon

For the operators with eight quarks and additional (anti-)collinear gluon (13.29) or with an additional soft gluon (13.30), the full Wilson coefficients are at tree level given

by

$$
\begin{aligned}
D^s_{8\bar{c},n,\mathrm{i}}(\{\underline{x},\underline{y},\underline{\omega}\},\mu_j) &= -\frac{1}{2N_c^2}\,\pi^2\alpha_j^2\,\frac{1}{\rho(\rho+\omega)\bar{\rho}^2}\,\frac{1}{y_1(x_2+x_3)^2} \\
&\quad\times\left[\frac{x_3}{x_2}-1+\frac{2}{N_c^2}-\frac{2C_F}{N_c}\frac{(x_2+x_3)^2}{x_2(x_1+x_3)}\right]\mathcal{C}_2^{-,u}(\mu_j)\,, \\
D^s_{8\bar{c},n,\mathrm{ii}}(\{\underline{x},\underline{y},\underline{\omega}\},\mu_j) &= -\frac{1}{2N_c}\,\pi^2\alpha_j^2\,\frac{1}{\rho(\rho+\omega)\bar{\rho}^2}\,\frac{1}{y_1(x_2+x_3)^2} \\
&\quad\times\left[\frac{x_3}{x_2}-1+\frac{2}{N_c^2}-\frac{2C_F}{N_c}\frac{(x_2+x_3)^2}{x_2(x_1+x_3)}\right]\left[\mathcal{C}_1^{-,u}(\mu_j)+2C_F\,\mathcal{C}_2^{-,u}(\mu_j)\right], \\
D^s_{8c,\bar{n},\mathrm{i}}(\{\underline{x},\underline{y},\underline{\omega}\},\mu_j) &= +\frac{C_F}{2N_c^2}\,\pi^2\alpha_j^2\,\frac{1}{\bar{\rho}(\bar{\rho}+\bar{\omega})\rho^2}\,\frac{1}{(y_1+y_3)^2x_2} \\
&\quad\times\left[\frac{y_3}{y_1}-1+\frac{2}{N_c^2}-\frac{2C_F}{N_c}\frac{(y_1+y_3)^2}{y_1(y_2+y_3)}\right]\mathcal{C}_2^{+,u}(\mu_j)\,, \\
D^s_{8c,\bar{n},\mathrm{ii}}(\{\underline{x},\underline{y},\underline{\omega}\},\mu_j) &= +\frac{1}{2N_c}\,\pi^2\alpha_j^2\,\frac{1}{\bar{\rho}(\bar{\rho}+\bar{\omega})\rho^2}\,\frac{1}{(y_1+y_3)^2x_2} \\
&\quad\times\left[\frac{y_3}{y_1}-1+\frac{2}{N_c^2}-\frac{2C_F}{N_c}\frac{(y_1+y_3)^2}{y_1(y_2+y_3)}\right]\left[\mathcal{C}_1^{+,u}(\mu_j)-\frac{1}{N_c}\,\mathcal{C}_2^{+,u}(\mu_j)\right]
\end{aligned}
\tag{13.42}
$$

and

$$
\begin{aligned}
D^s_{8s,n,\mathrm{i}}(\{\underline{x},\underline{y},\underline{\omega}\},\mu_j) &= -\frac{1}{2N_c^2}\,\pi^2\alpha_j^2\,\frac{1}{\rho(\rho+\omega)(\bar{\rho}+\bar{\sigma})^2}\,\frac{1}{y_1x_2^2} \\
&\quad\times\left[\left(1-\frac{2C_F}{N_c}\,x_2\right)\frac{\bar{\sigma}}{\bar{\rho}}+\frac{1}{N_c^2}\right]\mathcal{C}_2^{-,u}(\mu_j)\,, \\
D^s_{8s,n,\mathrm{ii}}(\{\underline{x},\underline{y},\underline{\omega}\},\mu_j) &= -\frac{1}{2N_c}\,\pi^2\alpha_j^2\,\frac{1}{\rho(\rho+\omega)(\bar{\rho}+\bar{\sigma})^2}\,\frac{1}{y_1x_2^2} \\
&\quad\times\left[\left(1-\frac{2C_F}{N_c}\,x_2\right)\frac{\bar{\sigma}}{\bar{\rho}}+\frac{1}{N_c^2}\right]\left[\mathcal{C}_1^{-,u}(\mu_j)+2C_F\,\mathcal{C}_2^{-,u}(\mu_j)\right], \\
D^s_{8s,\bar{n},\mathrm{i}}(\{\underline{x},\underline{y},\underline{\omega}\},\mu_j) &= -\frac{C_F}{2N_c^2}\,\pi^2\alpha_j^2\,\frac{1}{\bar{\rho}(\bar{\rho}+\bar{\omega})(\rho+\sigma)^2}\,\frac{1}{y_1^2x_2} \\
&\quad\times\left[\left(1-\frac{2C_F}{N_c}\,y_1\right)\frac{\sigma}{\rho}+\frac{1}{N_c^2}\right]\mathcal{C}_2^{+,u}(\mu_j)\,, \\
D^s_{8s,\bar{n},\mathrm{ii}}(\{\underline{x},\underline{y},\underline{\omega}\},\mu_j) &= -\frac{1}{2N_c}\,\pi^2\alpha_j^2\,\frac{1}{\bar{\rho}(\bar{\rho}+\bar{\omega})(\rho+\sigma)^2}\,\frac{1}{y_1^2x_2} \\
&\quad\times\left[\left(1-\frac{2C_F}{N_c}\,y_1\right)\frac{\sigma}{\rho}+\frac{1}{N_c^2}\right]\left[\mathcal{C}_1^{+,u}(\mu_j)-\frac{1}{N_c}\,\mathcal{C}_2^{+,u}(\mu_j)\right],
\end{aligned}
\tag{13.43}
$$

respectively. Similar to above, the Wilson coefficients for the operators with $(\bar{u}u)$ soft quark pair are obtained by replacing $u \leftrightarrow s$, $c \leftrightarrow \bar{c}$, $n \leftrightarrow \bar{n}$, $x_i \leftrightarrow y_i$, $\omega \leftrightarrow \bar{\omega}$, $\rho \leftrightarrow \bar{\rho}$, and $\sigma \leftrightarrow \bar{\sigma}$ in these expressions.

Chapter 14

Weak Annihilation Amplitudes

In this chapter, we determine the matrix elements $\langle K^+K^-|\mathcal{Q}_r^{\pm,q}|\bar{B}^0\rangle$ for the operators defined in (12.33) in terms of convolutions over Wilson coefficients with LCDAs and generalized soft functions for the B meson. The appearing endpoint divergences of weak annihilation amplitudes are discussed in detail in Chapter 15.

The relevant operators obtained after matching on SCET-2 are of the from

$$\mathcal{O}_{\text{SCET}-2} \sim [\text{soft fields}] \times [\bar{c}\text{ fields}] \times [c\text{ fields}]\,. \tag{14.1}$$

As interactions between different modes in SCET-2 are power suppressed, it is possible to factorize the matrix elements as

$$\big\langle K^+K^-\big|\mathcal{O}_{\text{SCET}-2}\big|\bar{B}^0\big\rangle \sim \big\langle 0\big|\text{soft fields}\big|\bar{B}^0\big\rangle\big\langle K^+\big|\bar{c}\text{ fields}\big|0\big\rangle\big\langle K^-\big|c\text{ fields}\big|0\big\rangle\,. \tag{14.2}$$

This factorization for an individual operator actually works to all orders in λ as the subleading soft-collinear interaction terms in the Lagrangian (4.5) only contribute for scattering processes of the form $s+c \to s+c$ but not for $s+s \to c+c$ studied here [11]. However, at subleading power new operators contribute. Many of the factorized matrix elements can be evaluated straightforwardly in terms of LCDAs and decay constants. Translating the (anti-)collinear fields with colored momentum-fraction subscript to position space, e.g.

$$\mathcal{X}^{(u)}_{c(y_2)} = \bar{n}\cdot p_{K^-}\int\frac{dt}{2\pi}\,\mathcal{X}_c(t\bar{n})\,e^{-iy_2t\bar{n}\cdot p_{K^-}}\,, \tag{14.3}$$

one can easily convince oneself that the standard (anti-)collinear brackets are

$$\begin{aligned}
\frac{1}{\bar{n}\cdot\mathcal{P}_c}\big\langle K^-\big|\bar{\mathcal{X}}^{(s)}_{c(y_1)}\,\bar{n}\!\!\!/(1\pm\gamma_5)\,\mathcal{X}^{(u)}_{c(y_2)}\big|0\big\rangle &= \mp if_K\,\phi_K(y_1)\,\delta(1-y_1-y_2)\,,\\
\frac{1}{n\cdot\mathcal{P}_{\bar{c}}}\big\langle K^+\big|\bar{\mathcal{X}}^{(u)}_{\bar{c}(x_1)}\,n\!\!\!/(1\pm\gamma_5)\,\mathcal{X}^{(s)}_{\bar{c}(x_2)}\big|0\big\rangle &= \mp if_K\,\phi_K(x_1)\,\delta(1-x_1-x_2)\,,
\end{aligned} \tag{14.4}$$

i.e. the leading-twist light meson LCDAs, see Appendix A.8 for their definitions.

14.1 Six-Quark Contributions

The soft bracket for the six-quark operators (13.9) is local and simply evaluates to the HQET decay constant

$$\begin{aligned}
\big\langle 0\big|\,\bar{\mathcal{Q}}^{(d)}_{s,\bar{n}}\,\bar{n}\!\!\!/(1-\gamma_5)\mathcal{H}_{v,\bar{n}}\big|\bar{B}^0\big\rangle &= -i\tilde{f}_B\,\sqrt{m_B}\,\bar{n}\cdot v\,,\\
\big\langle 0\big|\,\bar{\mathcal{Q}}^{(d)}_{s,n}\,n\!\!\!/(1-\gamma_5)\mathcal{H}_{v,n}\big|\bar{B}^0\big\rangle &= -i\tilde{f}_B\,\sqrt{m_B}\,n\cdot v\,.
\end{aligned} \tag{14.5}$$

Replacing the QCD eigenstate with the leading order HQET one yields a factor $\sqrt{m_B}$. Applying momentum conservation in the first line, one can replace $m_B\,\bar{n}\cdot v$ with the

large component of p_{K^-} and cancel the remaining label operator in (13.9). A similar relation holds also for the second line. Combing this with (14.4) yields the useful result

$$\left\langle \mathcal{O}^{\pm}_{6,\bar n} \right\rangle = \left\langle \mathcal{O}^{\pm}_{6,n} \right\rangle . \tag{14.6}$$

Here and in the following, we use the shorthand notation $\langle \ldots \rangle := \langle K^+K^-| \ldots |\bar B^0\rangle$. Adding up the associated Wilson coefficients $D^{\pm}_{6,\bar n}$ and $D^{\pm}_{6,n}$ in (13.37), we find that all contributions proportional to $\mathcal{C}_1^{\pm,q}$ cancel, i.e.

$$\left\langle \mathcal{Q}_1^{\pm,q} \right\rangle_{\text{6-quark}} \to 0 . \tag{14.7}$$

For the operators with color structure $[ij][ji]$, the six-quark contributions read

$$\left\langle \mathcal{Q}_2^{+,u} \right\rangle_{\text{6-quark}} \to \frac{C_F}{N_c^2}\,\pi\alpha_s\, i f_B f_K^2 \int_0^1 dx\, dy \left[\frac{1}{\bar x y^2} + \frac{1}{\bar x(1-x\bar y)}\right] \phi_K(x)\,\phi_K(y) \tag{14.8}$$

and

$$\left\langle \mathcal{Q}_2^{-,u} \right\rangle_{\text{6-quark}} \to \frac{C_F}{N_c^2}\,\pi\alpha_s\, i f_B f_K^2 \int_0^1 dx\, dy \left[\frac{1}{\bar x^2 y} + \frac{1}{y(1-x\bar y)}\right] \phi_K(x)\,\phi_K(y) , \tag{14.9}$$

where we replaced the HQET decay constant with the one defined in full QCD, cf. (A.8.7). Similar relations for $\mathcal{Q}_2^{\pm,s}$ are obtained by replacing $x \leftrightarrow y$ in the above expressions. With (14.7–14.9) we have recovered the result (11.12) obtained in the QCD factorization approach. Clearly, the convolution integrals in (14.8) and (14.9) suffer from endpoint divergences for $y \to 0$ and $x \to 1$, respectively, as the leading-twist LCDAs for the kaons vanish only linearly in the endpoints, see Appendix A.8.

14.2 Eight-Quark Contributions

In SCET-2, there are two different eight-quark operators contributing to weak annihilation amplitudes. First, we concentrate on $\mathcal{O}^q_{8,\perp\bar n,r}$ and $\mathcal{O}^q_{8,\perp n,r}$, originating from four quark SCET-1 operators with additional gluon. We restrict our discussion to the case $q = s$, i.e. the weak effective operators $\mathcal{Q}_r^{\pm,u}$, applying the usual replacement rules one can obtain the results for $\mathcal{Q}_r^{\pm,s}$.

The collinear and anti-collinear brackets just yield the leading-twist LCDAs for the kaons in this case. In the soft bracket, one encounters so far unknown four-quark contributions to the B meson. Therefore, we define four soft functions by

$$\begin{aligned}
&\left\langle 0\middle| \bar{\mathcal{Q}}^{(s)}_{s,\bar n}(t_2\bar n)\, \bar n\!\!\!/ n\!\!\!/ \gamma_\perp^\mu (1+\gamma_5)\, S_{\bar n}^\dagger S_n\, \mathcal{Q}^{(s)}_{s,n}(sn)\; \bar{\mathcal{Q}}^{(d)}_{s,\bar n}(t_1\bar n)\, \gamma_{\perp\mu}\bar n\!\!\!/ n\!\!\!/ (1-\gamma_5)\, \mathcal{H}_{v,\bar n} \middle| \bar B_v \right\rangle \\
&=: i\tilde f_B \int d\bar\omega\, d\rho\, d\bar\rho\, e^{-i(\bar\omega t_1 + \bar\rho t_2 + \rho s)}\, \phi^\perp_{4B,r}(\bar\omega,\rho,\bar\rho) , \\
&\left\langle 0\middle| \bar{\mathcal{Q}}^{(s)}_{s,\bar n}(t\bar n)\, S_{\bar n}^\dagger S_n\, \bar n\!\!\!/ n\!\!\!/ \gamma_\perp^\mu (1-\gamma_5)\, \mathcal{Q}^{(s)}_{s,n}(s_2 n)\; \bar{\mathcal{Q}}^{(d)}_{s,n}(s_1 n)\, \gamma_{\perp\mu} n\!\!\!/ \bar n\!\!\!/ (1-\gamma_5)\, \mathcal{H}_{v,n} \middle| \bar B_v \right\rangle \\
&=: i\tilde f_B \int d\omega\, d\rho\, d\bar\rho\, e^{-i(\bar\rho t + \omega s_1 + \rho s_2)}\, \bar\phi^\perp_{4B,r}(\omega,\rho,\bar\rho) ,
\end{aligned} \tag{14.10}$$

where the HQET fields and the soft Wilson lines are evaluated at $z = 0$. The subscript $r = \mathrm{i}, \mathrm{ii}$ refers to the two different color structures in (13.18) and the superscript $\perp$ indicates that both quark billinears contain a $\gamma_\perp$. RPI dictates that $\phi^\perp_{4B,r}$ ($\bar\phi^\perp_{4B,r}$) transforms as n ($\bar n$) under boosts. It is important to note that the HQET matrix elements contain soft fields displaced in both light-cone directions. Therefore, not all distances of two fields are light like and we do *not* call them LCDAs. Similar soft functions depending on two light-cone directions appear when including QED corrections [131] and in the context of long-distance penguin contributions to $\bar B \to \gamma\gamma$ decays [132, 133].[1] In contrast to the standard LCDAs, the support of these functions extends to negative values for the variables $\{\underline{\omega}\}$ [131].

Combining the expressions for the matrix elements in terms of LCDAs, soft functions and the Wilson coefficients in (13.38), we find

$$\begin{aligned}\big\langle \mathcal{Q}_1^{+,u}\big\rangle^\perp_{\text{8-quark}} \to -\frac{1}{8N_c^2}\,\pi^2\alpha_s^2\, i f_B f_K^2 \int_0^1 \frac{dy}{y}\,\phi_K(y)\int_0^1 \frac{dx}{x\bar x}\,\phi_K(x)\int \frac{d\bar\omega\, d\rho\, d\bar\rho}{\bar\rho(\bar\rho+\bar\omega)\rho}\,\frac{1}{n\cdot v}\\ \times\left[2\left(C_F+\frac{x}{N_c}\right)\phi^\perp_{4B,\mathrm{ii}}(\bar\omega,\rho,\bar\rho)-\frac{C_F}{N_c}\,x\,\phi^\perp_{4B,\mathrm{i}}(\bar\omega,\rho,\bar\rho)\right]\end{aligned} \tag{14.11}$$

and

$$\begin{aligned}\big\langle \mathcal{Q}_1^{-,u}\big\rangle^\perp_{\text{8-quark}} \to +\frac{1}{8N_c^2}\,\pi^2\alpha_s^2\, i f_B f_K^2 \int_0^1 \frac{dx}{\bar x}\,\phi_K(x)\int_0^1 \frac{dy}{y\bar y}\,\phi_K(y)\int \frac{d\omega\, d\rho\, d\bar\rho}{\rho(\rho+\omega)\bar\rho}\,\frac{1}{\bar n\cdot v}\\ \times\left[2\left(C_F+\frac{N_c^2-2}{2N_c}\,\bar y\right)\bar\phi^\perp_{4B,\mathrm{ii}}(\omega,\rho,\bar\rho)+\frac{C_F}{N_c}\,\bar y\,\bar\phi^\perp_{4B,\mathrm{i}}(\omega,\rho,\bar\rho)\right]\end{aligned} \tag{14.12}$$

for weak effective operators with color structure $[ii][jj]$. The factors $n\cdot v$ and $\bar n\cdot v$ could be remove by defining boost-invariant soft variables.[2] The corresponding relations for the ones with $[ij][ji]$ read

$$\begin{aligned}\big\langle \mathcal{Q}_2^{+,u}\big\rangle^\perp_{\text{8-quark}} \to -\frac{1}{8N_c^2}\,\pi^2\alpha_s^2\, i f_B f_K^2 \int_0^1 \frac{dy}{y}\,\phi_K(y)\int_0^1 \frac{dx}{x}\,\phi_K(x)\int \frac{d\bar\omega\, d\rho\, d\bar\rho}{\bar\rho(\bar\rho+\bar\omega)\rho}\,\frac{1}{n\cdot v}\\ \times\left[\frac{N_c^2+1}{N_c^2}\,\phi^\perp_{4B,\mathrm{ii}}(\bar\omega,\rho,\bar\rho)-\frac{C_F}{N_c^2}\,\phi^\perp_{4B,\mathrm{i}}(\bar\omega,\rho,\bar\rho)\right]\end{aligned} \tag{14.13}$$

and

$$\begin{aligned}\big\langle \mathcal{Q}_2^{-,u}\big\rangle^\perp_{\text{8-quark}} \to +\frac{1}{8N_c^2}\,\pi^2\alpha_s^2\, i f_B f_K^2 \int_0^1 \frac{dx}{\bar x}\,\phi_K(x)\int_0^1 \frac{dy}{y\bar y}\,\phi_K(y)\int \frac{d\omega\, d\rho\, d\bar\rho}{\rho(\rho+\omega)\bar\rho}\,\frac{1}{\bar n\cdot v}\\ \times\left[\left(4C_F^2\,\bar y+\frac{1}{N_c^2}\right)\bar\phi^\perp_{4B,\mathrm{ii}}(\omega,\rho,\bar\rho)+\frac{C_F}{N_c^2}\big(2C_F N_c\,\bar y-1\big)\,\bar\phi^\perp_{4B,\mathrm{i}}(\omega,\rho,\bar\rho)\right].\end{aligned} \tag{14.14}$$

Obviously, the convolution integrals in the collinear and anti-collinear momentum fractions are finite. Answering this question for the soft variables $\{\underline{\omega}\}$ is more complicated

[1] Slightly simpler soft functions depending on both light-cone directions also arise in collider physics [134, 135].

[2] In the B-meson rest frame, these factors are absent as $2\,v = n + \bar n$.

because the new functions $\phi^{\perp}_{4B,r}$ and $\bar\phi^{\perp}_{4B,r}$ are completely unknown in the literature. Defined in terms of fields displaced in both light-cone directions, it is unclear whether one can analyze them using conformal symmetry arguments [136]. Nevertheless, applying such arguments suggests that

$$\phi^{\perp}_{4B,r}(\bar\omega,\rho,\bar\rho)\sim\bar\omega\,\rho\,\bar\rho\,,\qquad \bar\phi^{\perp}_{4B,r}(\omega,\rho,\bar\rho)\sim\omega\,\rho\,\bar\rho\,, \tag{14.15}$$

for small values of $\{\underline{\omega}\}$, leading to the conclusion that the soft convolution integrals are well defined at the origin. Since these integrals extend over the entire real axis, they can also be treated as Cauchy integrals. However, this does not necessarily guarantee the existence of inverse moments [131]. We come back to the question of existence of convolution integrals in the next chapter.

The second eight-quark contribution (with additional gluons) originates from SCET-1 operators with only four quarks. It is convenient to study their effect in terms of the SCET(hc,c,s) operators (13.22) and (13.24). For the weak effective operators with color structure $[ii][jj]$, their contributions are

$$\begin{aligned}\big\langle\mathcal{Q}_1^{+,u}\big\rangle_{\text{8-quark}} \to{}& -\frac{1}{N_c}\,\pi\alpha_s\,if_K\int_0^1\frac{dx}{\bar x}\,\phi_K(x)\int\frac{d\bar\omega\,d\bar\rho}{\bar\rho(\bar\rho+\bar\omega)}\\ &\times\big\langle K^-\big|\bar{\mathcal{Q}}^{(s)}_{s,\bar n\,(\bar\rho)}\,\bar{\not n}(1+\gamma_5)\,t^a\,S^\dagger_{\bar n}S_n\,\mathcal{X}^{(u)(0)}_{hc}\;\bar{\mathcal{Q}}^{(d)}_{s,\bar n\,(\bar\omega)}\,t^a\,\bar{\not n}(1-\gamma_5)\,\mathcal{H}_{v,\bar n}\big|\bar B^0\big\rangle\end{aligned} \tag{14.16}$$

and

$$\begin{aligned}\big\langle\mathcal{Q}_1^{-,u}\big\rangle_{\text{8-quark}} \to{}& +\frac{1}{N_c}\,\pi\alpha_s\,if_K\int_0^1\frac{dy}{y}\,\phi_K(y)\int\frac{d\omega\,d\rho}{\rho(\rho+\omega)}\\ &\times\big\langle K^+\big|\bar{\mathcal{X}}^{(u)(0)}_{\overline{hc}}S^\dagger_{\bar n}S_n\,t^a\,\not n(1-\gamma_5)\mathcal{Q}^{(s)}_{s,n\,(\rho)}\;\bar{\mathcal{Q}}^{(d)}_{s,n\,(\omega)}\,t^a\,\not n(1-\gamma_5)\,\mathcal{H}_{v,n}\big|\bar B^0\big\rangle\,.\end{aligned} \tag{14.17}$$

The contributions for the ones with $[ij][ji]$ read

$$\begin{aligned}\big\langle\mathcal{Q}_2^{+,u}\big\rangle_{\text{8-quark}} \to{}& -\pi\alpha_s\,if_K\int_0^1\frac{dx}{\bar x}\,\phi_K(x)\int\frac{d\bar\omega\,d\bar\rho}{\bar\rho(\bar\rho+\bar\omega)}\\ &\times\bigg[\frac{C_F}{N_c^2}\big\langle K^-\big|\bar{\mathcal{Q}}^{(s)}_{s,\bar n\,(\bar\rho)}\,\bar{\not n}(1+\gamma_5)\,S^\dagger_{\bar n}S_n\,\mathcal{X}^{(u)(0)}_{hc}\;\bar{\mathcal{Q}}^{(d)}_{s,\bar n\,(\bar\omega)}\,\bar{\not n}(1-\gamma_5)\,\mathcal{H}_{v,\bar n}\big|\bar B^0\big\rangle\\ &-\frac{1}{N_c^2}\big\langle K^-\big|\bar{\mathcal{Q}}^{(s)}_{s,\bar n\,(\bar\rho)}\,\bar{\not n}(1+\gamma_5)\,t^a\,S^\dagger_{\bar n}S_n\,\mathcal{X}^{(u)(0)}_{hc}\;\bar{\mathcal{Q}}^{(d)}_{s,\bar n\,(\bar\omega)}\,t^a\,\bar{\not n}(1-\gamma_5)\,\mathcal{H}_{v,\bar n}\big|\bar B^0\big\rangle\bigg]\end{aligned} \tag{14.18}$$

and

$$\begin{aligned}\big\langle\mathcal{Q}_2^{-,u}\big\rangle_{\text{8-quark}} \to{}& +\pi\alpha_s\,if_K\int_0^1\frac{dy}{y}\,\phi_K(y)\int\frac{d\omega\,d\rho}{\rho(\rho+\omega)}\\ &\times\bigg[\frac{C_F}{N_c^2}\big\langle K^+\big|\bar{\mathcal{X}}^{(u)(0)}_{\overline{hc}}S^\dagger_{\bar n}S_n\,\not n(1-\gamma_5)\mathcal{Q}^{(s)}_{s,n\,(\rho)}\;\bar{\mathcal{Q}}^{(d)}_{s,n\,(\omega)}\,\not n(1-\gamma_5)\,\mathcal{H}_{v,n}\big|\bar B^0\big\rangle\\ &+\frac{2C_F}{N_c}\big\langle K^+\big|\bar{\mathcal{X}}^{(u)(0)}_{\overline{hc}}S^\dagger_{\bar n}S_n\,t^a\,\not n(1-\gamma_5)\mathcal{Q}^{(s)}_{s,n\,(\rho)}\;\bar{\mathcal{Q}}^{(d)}_{s,n\,(\omega)}\,t^a\,\not n(1-\gamma_5)\,\mathcal{H}_{v,n}\big|\bar B^0\big\rangle\bigg]\,.\end{aligned} \tag{14.19}$$

As discussed in Chapter 13, the up-quark fields are matched onto SCET-2 at $\mathcal{O}(\lambda^5)$ yielding leading- and subleading-twist LCDAs for the kaon and new four- and five-particle soft functions for the B meson. However, the cancellation of endpoint divergences is more transparent expressing our results through the matrix elements $\langle K^\pm|\ldots|\bar{B}^0\rangle$, which can be considered as "non-local form factors". The convolution integrals over the (anti-)collinear momentum fractions in (14.16–14.19) are well-defined. In the next chapter, we explain why the soft convolution integrals of these form factors must diverge for $\rho \to -\infty$ and $\bar{\rho} \to -\infty$ when their color structure is $[ii][jj]$, while remaining finite otherwise.

Chapter 15

Endpoint Divergences

The factorization of soft and collinear physics at NLP in the λ expansion is often spoiled by endpoint divergent convolution integrals. In our case, the six-quark contributions to the factorization of the matrix elements for $\mathcal{Q}_2^{\pm,q}$ in (14.8) and (14.9) indeed diverge. However, in the sum of all contributions the endpoint divergences have to cancel as observables are finite. The *refactorization-based subtraction* (RBS) scheme developed in the seminal papers [137,138] allows for a consistent treatment of endpoint divergences and thereby the establishment of NLP factorization theorems. It has been successfully applied to collider physics [137–142] and only recently also to inclusive and exclusive B-meson decay amplitudes [143–145]. In this chapter, we show how the RBS scheme is applied to exclusive non-leptonic weak annihilation amplitudes.

15.1 Finite Contributions

It is easy to decide whether convolution integrals in the (anti-)collinear momentum fractions are finite, as the behavior of the relevant LCDAs in the endpoints is well known. In contrast, the endpoint behavior of the generalized soft functions and non-local form factors is completely unknown and, therefore, determining the existence of the convolution integrals in the soft variables $\{\underline{\omega}\}$ is more complicated.

Nevertheless, the requirement that in the sum of the six-quark and the two different eight-quark contributions all endpoint divergences have to cancel separately for all weak effective operators allows one to identify finite contributions. As the matrix element for $\mathcal{Q}_1^{+,u}$ does not receive any contributions from six-quark operators, one can conclude from comparing (14.11) and (14.16) that

$$\int \frac{d\bar{\omega}\, d\rho d\bar{\rho}}{\bar{\rho}(\bar{\rho}+\bar{\omega})\rho}\, \phi_{4B,\mathrm{ii}}^{\perp}(\bar{\omega},\rho,\bar{\rho}) = \text{finite}\,. \tag{15.1}$$

A cancellation of divergences cannot occur as the soft function is multiplied with different independent hadronic quantities, i.e. the integrals over x differ. Similarly, comparing (14.13) to (14.8) and (14.18), we conclude that also for the second color structure

$$\int \frac{d\bar{\omega}\, d\rho d\bar{\rho}}{\bar{\rho}(\bar{\rho}+\bar{\omega})\rho}\, \phi_{4B,\mathrm{i}}^{\perp}(\bar{\omega},\rho,\bar{\rho}) = \text{finite}\,. \tag{15.2}$$

Repeating the analysis for the operators $\mathcal{Q}_r^{-,u}$ with $r = 1,2$, it is possible to show that for all eight-quark contributions with $\gamma_\perp$ in the soft brackets the soft convolution integrals are finite, i.e.

$$\left\langle \mathcal{Q}_r^{\pm,u} \right\rangle_{\text{8-quark}}^{\perp} \to \text{finite}\,. \tag{15.3}$$

Exploiting once more that the operators $\mathcal{Q}_1^{\pm,u}$ do not receive any six-quark contributions, we can directly conclude that also

$$\left\langle \mathcal{Q}_1^{\pm,u} \right\rangle_{\text{8-quark}} \to \text{finite}\,. \tag{15.4}$$

Of course, this implies that the convolutions over the non-local form factors with color structure $[t^a][t^a]$ in (14.16) and (14.17) are finite. As the soft variables are integrated over the entire real axis, the notion of an endpoint becomes complicated. Here, "finite" always refers to the integrals being well-defined.

15.2 Cancellation of Singularities

From the discussion in the previous section, it is obvious that the only divergent contributions from soft convolution integrals are

$$\int \frac{d\bar\omega\, d\bar\rho}{\bar\rho(\bar\rho+\bar\omega)} \left\langle K^-\middle|\bar Q^{(s)}_{s,\bar n\,(\bar\rho)}\, \bar{\not n}(1+\gamma_5)\, S_{\bar n}^\dagger S_n\, \mathcal{X}^{(u)(0)}_{hc}\; \bar Q^{(d)}_{s,\bar n\,(\bar\omega)}\, \bar{\not n}(1-\gamma_5)\, \mathcal{H}_{v,\bar n}\middle|\bar B^0\right\rangle \tag{15.5}$$

and in the opposite sector

$$\int \frac{d\omega\, d\rho}{\rho(\rho+\omega)} \left\langle K^+\middle|\bar{\mathcal{X}}^{(u)(0)}_{\overline{hc}}\, S_{\bar n}^\dagger S_n\, \not n(1-\gamma_5) Q^{(s)}_{s,n\,(\rho)}\; \bar Q^{(d)}_{s,n\,(\omega)}\, \not n(1-\gamma_5)\, \mathcal{H}_{v,n}\middle|\bar B^0\right\rangle . \tag{15.6}$$

We can conclude even further that their divergences have to cancel with the ones of the six-quark contributions in (14.8) and (14.9), respectively. In the following, we restrict the discussion to the operator $\mathcal{Q}_2^{+,u}$. The results for $\mathcal{Q}_2^{-,u}$ can be obtained by replacing $y \to \bar x$ and $\bar\rho \to \rho$.

Heuristically, this cancellation can be understood as follows. In the endpoints, the momentum of one of the K^- constituents becomes soft, i.e. $y \sim \lambda^2$, and, by momentum conservation, the other constituent hard-collinear. From the definition of the kaon LCDA in this limit

$$\frac{1}{\bar n\cdot\mathcal{P}_c} \left\langle K^-\middle|\underbrace{\bar Q^{(s)}_{s,n}(0)}_{\sim\lambda^3}\, \bar{\not n}\,\gamma_5\, \mathcal{X}^{(u)(0)}_{hc}(t\bar n)\middle|0\right\rangle = -i\underbrace{f_K}_{\sim\lambda^2} \int_0^1 \underbrace{dy}_{\sim\lambda^2}\, e^{i\bar y t\bar n\cdot p}\, 6\underbrace{y\bar y}_{\sim\lambda^2} , \tag{15.7}$$

one can infer that the combination of the hard-collinear field and the kaon state must be of $\mathcal{O}(\lambda^3)$ in the power expansion. There are two options to achieve this:

(1) The counting of the kaon state is the standard one, i.e. λ^{-2}, and, therefore, the hard-collinear field counts as λ^5. This is precisely the same power at which this field in (15.5) is eventually matched onto SCET-2, cf. the discussion below (13.24). A graphical illustration of the endpoint configuration in this case is shown in Figure 15.1.

(2) The hard-collinear field counts canonically as λ, whereas the kaon state in the endpoint counts as λ^2. In this case, one should, of course, count the field and the state in (15.5) similarly.

Using the first option, the kaon consists of collinear fields only and the power suppression in the endpoint arises from an $\mathcal{O}(\lambda^5)$ splitting of the hard-collinear field, see Table 13.3. Equivalently, one can consider the kaon in the endpoint as being build up from soft and hard-collinear fields, resulting in a power suppression of the state. On a technical level, the matrix element on the left-hand side of (15.7) implicitly contains

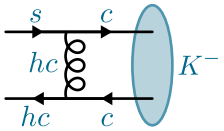

Figure 15.1: Endpoint configuration of the kaon consisting of collinear fields only.

two insertions of subleading power Lagrangians, yielding an $\mathcal{O}(\lambda^4)$ suppression. They can either be combined with the hard-collinear field (option 1) or with the kaon state (option 2). The cancellation of the endpoint divergences can then take place in both cases because of the refactorization condition

$$[\![D^+_{6,\bar{n}}]\!](x,y) = (\bar{n}\cdot p_{K^-})^2\,[\![\widehat{D}^s_{6,\bar{n},\mathrm{i}}]\!](x;\bar{\omega},\bar{\rho})\,, \tag{15.8}$$

which is fulfilled if one identifies $\bar{\rho} \equiv -y\,\bar{n}\cdot p_{K^-}$. Remember that all soft momenta are chosen to be incoming. Here and in the following, $[\![f]\!]$ denotes the leading terms of f in the limit $y \to 0$ and $\bar{\rho} \to -\infty$, respectively [137].

On the technical level, one has to rearrange contributions in

$$\begin{aligned}\left\langle \mathcal{Q}_2^{+,u}\right\rangle \to &\int_0^1 dx\,dy\, D^+_{6,\bar{n}}(x,y)\left\langle \mathcal{O}^+_{6,\bar{n}}\right\rangle(x,y)\\ &+\int_0^1 dx\int d\bar{\omega}\,d\bar{\rho}\,\widehat{D}^s_{6,\bar{n},\mathrm{i}}(x;\bar{\omega},\bar{\rho})\left\langle \widehat{\mathcal{O}}_{6,\bar{n},\mathrm{i}}\right\rangle(x;\bar{\omega},\bar{\rho})+\dots\,,\end{aligned} \tag{15.9}$$

where ellipsis denote terms free of endpoint divergences and we already performed some of the integrals over momentum fractions using the δ functions in (14.4). In a slight abuse of notation, we denote the coefficients of $\mathcal{C}_2^{+,u}$ in (13.37–13.39) also as $D^+_{6,\bar{n}}$, $D^+_{6,n}$, etc. To regularize the endpoint divergence for $\bar{\rho} \to -\infty$, we subtracted from the second line of (15.9)

$$\int_0^1 dx\int d\bar{\omega}\,d\bar{\rho}\,[\![\widehat{D}^s_{6,\bar{n},\mathrm{i}}]\!](x;\bar{\omega},\bar{\rho})\,[\![\left\langle \widehat{\mathcal{O}}_{6,\bar{n},\mathrm{i}}\right\rangle]\!](x;\bar{\omega},\bar{\rho})\,\theta(-\Lambda-\bar{\rho})\,, \tag{15.10}$$

where Λ is some arbitrary cutoff. In this limit, the up- and strange-quark fields in (15.5) become collinear – gauge invariance is ensured by the $S^\dagger_{\bar{n}}S_n$ Wilson line pair – and one can factorize the non-local form factor into the leading-twist kaon LCDA and an B-meson-to-vacuum matrix element. However, as the Wilson coefficient $\widehat{D}^s_{6,\bar{n},\mathrm{i}}$ is independent of $\bar{\omega}$ in the endpoint, performing the associated integral moves the down-quark field to zero and this matrix element simply evaluates to the decay constant, see (14.5). These observations can be summarized in a second refactorization condition

$$\int d\bar{\omega}\,[\![\left\langle \widehat{\mathcal{O}}_{6,\bar{n},\mathrm{i}}\right\rangle]\!](x;\bar{\omega},\bar{\rho}) = \bar{n}\cdot p_{K^-}\,[\![\left\langle \mathcal{O}^+_{6,\bar{n}}\right\rangle]\!](x,y)\,, \tag{15.11}$$

with $\bar{\rho} \equiv -y\,\bar{n}\cdot p_{K^-}$. Adding back the expression (15.10) to the first line of (15.9), one also regularizes the endpoint divergence for $y \to 0$. To demonstrate this, one can use

the two refactorization conditions (15.8) and (15.11) to rewrite

$$\begin{aligned}
&\int d\bar\omega\, d\bar\rho\, \big[\!\big[\widehat D^s_{6,\bar n,\mathrm{i}}\big]\!\big](x;\bar\omega,\bar\rho)\,\big[\!\big[\langle\widehat{\mathcal O}_{6,\bar n,\mathrm{i}}\rangle\big]\!\big](x;\bar\omega,\bar\rho)\,\theta(-\Lambda-\bar\rho)\\
&= \left(\int_{\Lambda/\bar n\cdot p_{K^-}}^{\infty} dy - \underbrace{\int_0^\infty dy}_{=0}\right)\big[\!\big[D^+_{6,\bar n}\big]\!\big](x,y)\,\big[\!\big[\langle\mathcal O^+_{6,\bar n}\rangle\big]\!\big](x,y)\\
&= -\int_0^{\Lambda/\bar n\cdot p_{K^-}} dy\,\big[\!\big[D^+_{6,\bar n}\big]\!\big](x,y)\,\big[\!\big[\langle\mathcal O^+_{6,\bar n}\rangle\big]\!\big](x,y)\,.
\end{aligned}\tag{15.12}$$

Here, the integral over $y\in(0,\infty)$ in the second line vanishes in dimensional regularization, due to scalelessness. In deriving the factorization theorem, we work with bare fields. From the last line, it is obvious that the natural choice is $\Lambda=\bar n\cdot p_{K^-}=m_b$. In this case, the factorization theorem for $\mathcal Q_2^{+,u}$ reads

$$\begin{aligned}
\big\langle\mathcal Q_2^{+,u}\big\rangle \to{}& \int_0^1 dx\,dy\, D^+_{6,n}(x,y)\,\langle\mathcal O^+_{6,n}\rangle(x,y)\\
&+\int_0^1 dx\,dy\,\Big\{D^+_{6,\bar n}(x,y)\,\langle\mathcal O^+_{6,\bar n}\rangle(x,y) - \big[\!\big[D^+_{6,\bar n}\big]\!\big](x,y)\,\big[\!\big[\langle\mathcal O^+_{6,\bar n}\rangle\big]\!\big](x,y)\Big\}\\
&+\int_0^1 dx\,dy\int d\bar\omega\,d\rho\,d\bar\rho\sum_{r=\mathrm{i,ii}} D^s_{8,\perp\bar n,r}(x,y;\bar\omega,\rho,\bar\rho)\,\big\langle\mathcal O_{8,\perp\bar n,r}\big\rangle(x,y;\bar\omega,\rho,\bar\rho)\\
&+\int_0^1 dx\int d\bar\omega\,d\bar\rho\,\Big\{\widehat D^s_{6,\bar n,\mathrm{i}}(x;\bar\omega,\bar\rho)\,\big\langle\widehat{\mathcal O}_{6,\bar n,\mathrm{i}}\big\rangle(x;\bar\omega,\bar\rho)\\
&\qquad\qquad - \big[\!\big[\widehat D^s_{6,\bar n,\mathrm{i}}\big]\!\big](x;\bar\omega,\bar\rho)\,\big[\!\big[\langle\widehat{\mathcal O}_{6,\bar n,\mathrm{i}}\rangle\big]\!\big](x;\bar\omega,\bar\rho)\,\theta(-m_b-\bar\rho)\Big\}\\
&+\int_0^1 dx\int d\bar\omega\,d\bar\rho\,\widehat D^s_{6,\bar n,\mathrm{ii}}(x;\bar\omega,\bar\rho)\,\big\langle\widehat{\mathcal O}_{6,\bar n,\mathrm{ii}}\big\rangle(x;\bar\omega,\bar\rho)\,.
\end{aligned}\tag{15.13}$$

Each individual integral is well defined and no endpoint singularities spoil factorization. In order to avoid creating artificial power-suppressed terms, it is convenient to split for explicit calculations [137]

$$\begin{aligned}
&\int d\bar\rho\,\Big\{\widehat D^s_{6,\bar n,\mathrm{i}}(\bar\rho)\,\big\langle\widehat{\mathcal O}_{6,\bar n,\mathrm{i}}\big\rangle(\bar\rho) - \big[\!\big[\widehat D^s_{6,\bar n,\mathrm{i}}\big]\!\big](\bar\rho)\,\big[\!\big[\langle\widehat{\mathcal O}_{6,\bar n,\mathrm{i}}\rangle\big]\!\big](\bar\rho)\,\theta(-m_b-\bar\rho)\Big\}\\
&=\int_{-\Lambda_{\mathrm{QCD}}}^{\infty} d\bar\rho\,\widehat D^s_{6,\bar n,\mathrm{i}}(\bar\rho)\,\big\langle\widehat{\mathcal O}_{6,\bar n,\mathrm{i}}\big\rangle(\bar\rho) + \int_{-m_b}^{-\Lambda_{\mathrm{QCD}}} d\bar\rho\,\big[\!\big[\widehat D^s_{6,\bar n,\mathrm{i}}\big]\!\big](\bar\rho)\,\big[\!\big[\langle\widehat{\mathcal O}_{6,\bar n,\mathrm{i}}\rangle\big]\!\big](\bar\rho)\\
&\qquad+\int_{-\infty}^{-\Lambda_{\mathrm{QCD}}} d\bar\rho\,\Big\{\widehat D^s_{6,\bar n,\mathrm{i}}(\bar\rho)\,\big\langle\widehat{\mathcal O}_{6,\bar n,\mathrm{i}}\big\rangle(\bar\rho) - \big[\!\big[\widehat D^s_{6,\bar n,\mathrm{i}}\big]\!\big](\bar\rho)\,\big[\!\big[\langle\widehat{\mathcal O}_{6,\bar n,\mathrm{i}}\rangle\big]\!\big](\bar\rho)\Big\}\,,
\end{aligned}\tag{15.14}$$

where we dropped irrelevant arguments to increase readability. All of the three integrals have homogeneous power counting and in the sum the dependence on Λ_{QCD} cancels out. It is thus also possible to choose a different parameter of $\mathcal O(\Lambda_{\mathrm{QCD}})$.

Similar to the soft-overlap contribution $\zeta^{B\to M}$ of the heavy-to-light form factors, the operators $\widehat{\mathcal{O}}_{6,\bar{n},r}$ are defined in SCET(hc,c,s). Matching the remaining hard-collinear field at power λ^5 on SCET-2, one again finds several endpoint divergent convolution integrals over leading- *and* subleading-twist LCDAs for the kaon. In complete analogy to the form factor, they have to cancel with divergences in soft convolutions. These cancellations are very intricate and still not fully understood, see [123, 146, 147] for different approaches. For weak annihilation amplitudes, the situation is even more complicated as the involved soft functions describe so far unknown four- and five-particle contributions to the B meson. Similar to the soft functions defined in (14.10), they contain soft fields displaced in both light-cone directions complicating the analysis significantly. The study of these objects is left for future work. However, when working with the SCET(hc,c,s) operators, all contributions in (15.13) are finite.

Chapter 16

Summary

In this part, we systematically matched the operators of the weak effective Hamiltonian relevant for non-leptonic B-meson decays onto SCET-2. For concreteness, we focused on the pure annihilation channel $\bar{B}^0 \to K^+K^-$. In the first step, these four-quark operators were matched from QCD onto SCET-1 by integrating out hard modes with virtuality m_b^2. We identified three distinct classes of SCET-1 operators: operators containing only four quarks, four quarks with an additional gluon, and six-quark operators. At tree level, the Wilson coefficients of the first class are trivial, containing only the Wilson coefficients of the weak effective operators. For the other two classes, the Wilson coefficients depend on the momentum fractions carried by the various hard-collinear and anti-hard-collinear fields, reflecting the non-locality of these operators.

Even though the SCET-1 operators do have different power counting, they contribute at the same power after being matched onto SCET-2 at an intermediate scale of virtuality $\Lambda_{\text{QCD}}\, m_b$. The six-quark operators already contain all the necessary quark flavors to form the three mesons. Therefore, all (anti-)hard-collinear fields are matched trivially, i.e. they are replaced by (anti-)collinear fields, resulting in SCET-2 operators of $\mathcal{O}(\lambda^{14})$. Since the four-quark and four-quark operators with an additional gluon lack the constituent quarks for the final-state mesons, some of their SCET-1 fields are matched non-trivially onto SCET-2. As a result, they contribute through eight-quark and eight-quark operators with an additional gluon. The jet functions from this second matching step depend on the momentum fractions of the various (anti-)hard-collinear and (anti-)collinear fields, as well as the light-cone components of the soft field momenta. We have calculated these functions at tree level for all relevant operators.

When calculating the $\langle K^+K^-|\ldots|\bar{B}^0\rangle$ matrix elements, we recovered the well-known BBNS results from the six-quark SCET-2 operators, expressed as convolutions over the leading-twist LCDAs of the kaons. These results contain endpoint divergences arising from (anti-)collinear momentum fractions tending to zero. The matrix elements of the eight-quark operators (with an additional gluon) evaluate to convolutions over both leading- and subleading-twist LCDAs for the light mesons, as well as convolutions over previously unknown four- and five-particle soft functions for the B meson. The defining matrix elements of these functions involve soft fields displaced along both light-cone directions, significantly complicating their analysis. The existence of the soft convolution integrals thus presents an intricate issue.

In the endpoint region of the six-quark contributions, one of the kaon constituents becomes soft while the other becomes (anti-)hard-collinear. This makes it convenient to match only one sector of the SCET-1 four-quark operators onto SCET-2. The resulting operators contain six fields, and their matrix elements evaluate to non-local $\bar{B}^0 \to K^\pm$ form factors. From the consistency requirement that all endpoint divergences must cancel individually for a given weak effective operator, we can determine which soft convolution integrals in this framework are well-defined. Notably, all convolution integrals over soft functions from SCET-1 four-quark operators with

an additional gluon are finite. By refactorizing the non-local form factors in divergent convolutions, we demonstrate the cancellation of all endpoint divergences, thereby establishing a subleading-power factorization theorem for weak-annihilation decay amplitudes *without* introducing new modes in the EFT. Deducing phenomenological implications is complicated because weak annihilation amplitudes depend on several unknown hadronic quantities. This challenge will be addressed in future work. However, if the remaining (anti-)hard-collinear field is also matched onto SCET-2, new endpoint-divergent convolution integrals emerge which have to cancel separately.

Parenthetically, we note that the authors of [148] regularize the endpoint divergences in non-leptonic weak annihilation amplitudes by employing kernels with inhomogeneous power counting. Although we reproduce their results within the lowest-lying-state approximation[1], their approach sacrifices one of the key advantages of SCET by not utilizing homogeneous objects. As a consequence, they need to perform a λ expansion after the convolution integrals are evaluated and fail to identify eight-quark contributions arising from SCET-1 four-quark operators with an additional gluon. Moreover, their method cannot be generalized to higher powers in this expansion, limiting its applicability.

[1] In [148] this is referred to as "ground-state factorization approximation" and simply means inserting a vacuum $|0\rangle\langle 0|$ in (14.10), (15.5) and (15.6).

Appendix II

A.8 Light-Cone Distribution Amplitudes

LCDAs play an important role in many exclusive hard processes and are crucial ingredients of factorization theorems in B physics. In this appendix, we give the definitions relevant for decays into pseudoscalar mesons.

Light Mesons

For light mesons, one can define them in full QCD [149] or equivalently in SCET-2 [23]. Expressed through the collinear gauge invariant building blocks (4.8), the defining relation of the twist-2 LCDA reads

$$\langle M(p)|\bar{\mathcal{X}}_c(0)\,\frac{\bar{n}\!\!\!/}{2}\,\gamma_5\,\mathcal{X}_c(t\bar{n})|0\rangle = -if_M\,\frac{\bar{n}\cdot p}{2}\int_0^1 dy\,e^{i\bar{y}t\bar{n}\cdot p}\,\phi_M(y)\,. \tag{A.8.1}$$

The decay constant f_M is defined by the local limit $t\to 0$, i.e. the LCDA is normalized to 1.

Three new LCDAs arise at twist-3, which are connected through the equations of motion. The 3-particle LCDA is defined in full QCD in terms of the field strength tensor $F^{\mu\nu}$. In SCET-2, this definition translates to

$$\begin{aligned}&\langle M(p)|\bar{\mathcal{X}}_c(0)\,\frac{\bar{n}\!\!\!/}{2}\,\gamma_5\,\mathcal{A}_c^\perp(s\bar{n})\,\mathcal{X}_c(t\bar{n})|0\rangle\\ &= (d-2)\,if_{3M}\,\frac{\bar{n}\cdot p}{2}\int\mathcal{D}y\,e^{i(y_2\,t+y_3\,s)\bar{n}\cdot p}\,\frac{\phi_{3M}(y_1,y_2,y_3)}{y_3}\,,\end{aligned} \tag{A.8.2}$$

where the integral measure is defined as

$$\int\mathcal{D}y \coloneqq \int_0^1 dy_1\,dy_2\,dy_3\,\delta(1-y_1-y_2-y_3)\,. \tag{A.8.3}$$

Turning the field strength tensor to the collinear building blocks yields an inverse derivative which is responsible for the factor $1/y_3$ on the right-hand side. The remaining twist-3 LCDAs ϕ_σ and ϕ_P are defined similar to (A.8.1) but with a different Dirac structure, see e.g. [149]. They do not appear directly in our calculations. However, ϕ_σ appears through the matrix element of the eight-quark operators with additional derivatives in the numerator (13.27). One finds [146]

$$\begin{aligned}\langle M(p)|\bar{\mathcal{X}}_c(0)\,\frac{\bar{n}\!\!\!/}{2}\,\gamma_5\,i\partial\!\!\!/_\perp\,\mathcal{X}_c(t\bar{n})|0\rangle &= (d-2)\,\frac{\bar{n}\cdot p}{2}\int_0^1 dy\,e^{i\bar{y}t\bar{n}\cdot p}\\ &\times\left[\frac{if_M\,\mu_M}{2d-2}\,\phi_\sigma(y)+if_{3M}\int\mathcal{D}y\,\frac{\phi_{3M}(y_1,y_2,y_3)}{y_3^2}\,\big(\theta(y_3-y)-\theta(\bar{y}-y_3)\big)\right],\end{aligned} \tag{A.8.4}$$

with $\bar{y}=1-y$ and $\mu_M=m_M^2/(m_q+m_{\bar{q}})$.

To determine whether a term contributing to weak-annihilation decay amplitudes suffers from endpoint divergences for small momentum fractions or not, it is crucial to know how the various LCDAs behave in these endpoints. The endpoint behavior can be determined applying conformal symmetry arguments, one finds for the relevant LCDAs [149]

$$\phi_M(y) \approx 6y\bar{y}\,, \qquad \phi_\sigma(y) \approx 6y\bar{y}\,, \qquad \phi_{3M}(y_1,y_2,y_3) \approx 360 y_1 y_2 y_3^2\,. \tag{A.8.5}$$

Heavy Mesons

In full QCD there is no distinction between heavy and light mesons. Therefore, the leading-twist B-meson LCDA in (11.7) is defined similarly to the one for light mesons. In contrast, in HQET the leading-twist B-meson LCDAs is defined by [150, 151]

$$\langle 0|\,\bar{\mathcal{Q}}_{s,n}(tn)\,\frac{\not{n}}{2}\,\gamma_5\,\mathcal{H}_{v,n}(0)\,|\bar{B}_v\rangle = i\tilde{f}_B\,\frac{n\cdot v}{2}\int_0^\infty d\omega\, e^{-i\omega t}\phi_B^+(\omega)\,, \tag{A.8.6}$$

where we use the soft gauge invariant building blocks (4.9). As the heavy quark mass is $m_b \to \infty$ in HQET, the momentum fraction carried by the spectator quark needs to be integrated up to infinity. The HQET decay constant $\tilde{f}_B$ is related to the physical decay constant f_B by [152]

$$f_B\sqrt{m_B} = \tilde{f}_B(\mu)\left[1 + \frac{C_F\,\alpha_s(\mu)}{4\pi}\left(\frac{3}{2}\ln\frac{m_B^2}{\mu^2} - 2\right) + \mathcal{O}(\alpha_s^2)\right]. \tag{A.8.7}$$

Similarly, it is possible to match the QCD LCDA (11.7) onto HQET [153].

A.9 Hard Functions for Six-Quark Operators

The Wilson coefficients of the six-quark operators with hard-collinear spectator, defined in (12.28), are given by

$$H^-_{6,hc,1}(\{\underline{\tilde{x}},\underline{\tilde{y}}\},\mu_h) = \frac{\pi\alpha_h}{2}\left[\frac{1}{\tilde{y}_1\tilde{x}_2(1-\tilde{y}_3)}\,\mathcal{C}_1^{-,u}(\mu_h) - \frac{1}{\tilde{x}_1\tilde{y}_2(1-\tilde{y}_3)}\,\mathcal{C}_1^{-,s}(\mu_h)\right],$$

$$H^-_{6,hc,2}(\{\underline{\tilde{x}},\underline{\tilde{y}}\},\mu_h) = \frac{\pi\alpha_h}{2}\left[\frac{1}{\tilde{y}_1(\tilde{x}_2+\tilde{x}_1\tilde{y}_1)}\,\mathcal{C}_2^{-,u}(\mu_h) + \frac{1}{\tilde{x}_1\tilde{y}_2(\tilde{y}_2+\tilde{y}_3)}\,\mathcal{C}_2^{-,s}(\mu_h)\right],$$

$$H^-_{6,hc,3}(\{\underline{\tilde{x}},\underline{\tilde{y}}\},\mu_h) = \frac{\pi\alpha_h}{2}\left[\frac{1}{\tilde{y}_1(\tilde{x}_2+\tilde{x}_1\tilde{y}_1)}\,\mathcal{C}_1^{-,u}(\mu_h)\right.$$
$$\left. - \frac{1}{N_c}\,\frac{\tilde{y}_1-\tilde{y}_3}{\tilde{x}_1\tilde{y}_2(\tilde{y}_2+\tilde{y}_3)(1-\tilde{y}_3)}\,\mathcal{C}_2^{-,s}(\mu_h)\right],$$

$$H^-_{6,hc,4}(\{\underline{\tilde{x}},\underline{\tilde{y}}\},\mu_h) = \frac{\pi\alpha_h}{2}\left[\frac{1}{\tilde{y}_1\tilde{x}_2(1-\tilde{y}_3)}\,\mathcal{C}_2^{-,u}(\mu_h) - \frac{1}{\tilde{x}_1\tilde{y}_2(1-\tilde{y}_3)}\,\mathcal{C}_2^{-,s}(\mu_h)\right],$$

$$H^-_{6,hc,5}(\{\underline{\tilde{x}},\underline{\tilde{y}}\},\mu_h) = -\frac{\pi\alpha_h}{2N_c}\left[\frac{1}{\tilde{y}_1}\left(\frac{1}{\tilde{x}_2+\tilde{x}_1\tilde{y}_1} + \frac{1}{\tilde{x}_2(1-\tilde{y}_3)}\right)\mathcal{C}_1^{-,u}(\mu_h)\right.$$
$$\left. + \frac{\tilde{y}_1-\tilde{y}_3}{\tilde{x}_1\tilde{y}_2(\tilde{y}_2+\tilde{y}_3)(1-\tilde{y}_3)}\,\mathcal{C}_1^{-,s}(\mu_h)\right],$$

$$H^{-}_{6,hc,6}(\{\underline{\tilde{x}},\underline{\tilde{y}}\},\mu_h) = \frac{\pi\alpha_h}{2}\Bigg[-\frac{1}{N_c}\frac{1}{\tilde{y}_1}\bigg(\frac{1}{\tilde{x}_2+\tilde{x}_1\tilde{y}_1}+\frac{1}{\tilde{x}_2(1-\tilde{y}_3)}\bigg)\mathcal{C}_2^{-,u}(\mu_h) + \frac{1}{\tilde{x}_1\tilde{y}_2(\tilde{y}_2+\tilde{y}_3)}\,\mathcal{C}_1^{-,s}(\mu_h)\Bigg], \tag{A.9.1}$$

and

$$H^{+}_{6,hc,1}(\{\underline{\tilde{x}},\underline{\tilde{y}}\},\mu_h) = \frac{\pi\alpha_h}{2}\Bigg[\frac{1}{\tilde{y}_1\tilde{x}_2(1-\tilde{y}_3)}\,\mathcal{C}_1^{+,u}(\mu_h) - \frac{1}{\tilde{x}_1\tilde{y}_2(1-\tilde{y}_3)}\,\mathcal{C}_1^{+,s}(\mu_h)\Bigg],$$

$$H^{+}_{6,hc,2}(\{\underline{\tilde{x}},\underline{\tilde{y}}\},\mu_h) = 0\,,$$

$$H^{+}_{6,hc,3}(\{\underline{\tilde{x}},\underline{\tilde{y}}\},\mu_h) = \frac{\pi\alpha_h}{2}\Bigg[\frac{1}{\tilde{y}_1\tilde{x}_2(\tilde{y}_1+\tilde{y}_3)}\,\mathcal{C}_1^{+,u}(\mu_h) - \frac{1}{N_c}\frac{1}{\tilde{y}_2}\bigg(\frac{1}{\tilde{x}_1+\tilde{x}_2\tilde{y}_2}-\frac{1}{\tilde{x}_1(1-\tilde{y}_3)}\bigg)\mathcal{C}_2^{+,s}(\mu_h)\Bigg],$$

$$H^{+}_{6,hc,4}(\{\underline{\tilde{x}},\underline{\tilde{y}}\},\mu_h) = \frac{\pi\alpha_h}{2}\Bigg[\frac{1+\tilde{y}_1}{\tilde{y}_1\tilde{x}_2(\tilde{y}_1+\tilde{y}_3)(1-\tilde{y}_3)}\,\mathcal{C}_2^{+,u}(\mu_h) + \frac{1}{\tilde{y}_2}\bigg(\frac{1}{\tilde{x}_1+\tilde{x}_2\tilde{y}_2}-\frac{1}{\tilde{x}_1(1-\tilde{y}_3)}\bigg)\mathcal{C}_2^{+,s}(\mu_h)\Bigg],$$

$$H^{+}_{6,hc,5}(\{\underline{\tilde{x}},\underline{\tilde{y}}\},\mu_h) = -\frac{\pi\alpha_h}{2N_c}\Bigg[\frac{1+\tilde{y}_1}{\tilde{y}_1\tilde{x}_2(\tilde{y}_1+\tilde{y}_3)(1-\tilde{y}_3)}\,\mathcal{C}_1^{+,u}(\mu_h) + \frac{1}{\tilde{y}_2}\bigg(\frac{1}{\tilde{x}_1+\tilde{x}_2\tilde{y}_2}-\frac{1}{\tilde{x}_1(1-\tilde{y}_3)}\bigg)\mathcal{C}_1^{+,s}(\mu_h)\Bigg],$$

$$H^{+}_{6,hc,6}(\{\underline{\tilde{x}},\underline{\tilde{y}}\},\mu_h) = \frac{\pi\alpha_h}{2}\Bigg[-\frac{1}{N_c}\frac{1+\tilde{y}_1}{\tilde{y}_1\tilde{x}_2(\tilde{y}_1+\tilde{y}_3)(1-\tilde{y}_3)}\,\mathcal{C}_2^{+,u}(\mu_h) + \frac{1}{\tilde{y}_2(\tilde{x}_1+\tilde{x}_2\tilde{y}_2)}\,\mathcal{C}_1^{+,s}(\mu_h)\Bigg]. \tag{A.9.2}$$

The Wilson coefficients of the six-quark operators with anti-hard-collinear spectator, defined in (12.28), are given by

$$H^{-}_{6,\overline{hc},1}(\{\underline{\tilde{x}},\underline{\tilde{y}}\},\mu_h) = \frac{\pi\alpha_h}{2}\Bigg[-\frac{1}{\tilde{y}_1\tilde{x}_2(1-\tilde{x}_3)}\,\mathcal{C}_1^{-,u}(\mu_h) + \frac{1}{\tilde{x}_1\tilde{y}_2(1-\tilde{x}_3)}\,\mathcal{C}_1^{-,s}(\mu_h)\Bigg],$$

$$H^{-}_{6,\overline{hc},2}(\{\underline{\tilde{x}},\underline{\tilde{y}}\},\mu_h) = \frac{\pi\alpha_h}{2}\Bigg[-\frac{1}{\tilde{y}_1\tilde{x}_2(1-\tilde{x}_3)}\,\mathcal{C}_2^{-,u}(\mu_h) + \frac{1}{\tilde{x}_1\tilde{y}_2(1-\tilde{x}_3)}\,\mathcal{C}_2^{-,s}(\mu_h)\Bigg],$$

$$H^{-}_{6,\overline{hc},3}(\{\underline{\tilde{x}},\underline{\tilde{y}}\},\mu_h) = \frac{\pi\alpha_h}{2}\Bigg[\frac{1}{\tilde{y}_1\tilde{x}_2(\tilde{x}_2+\tilde{x}_3)}\,\mathcal{C}_1^{-,u}(\mu_h) - \frac{1}{N_c}\frac{1}{\tilde{x}_1}\bigg(\frac{1}{\tilde{y}_2+\tilde{x}_1\tilde{y}_1}+\frac{1}{\tilde{y}_2(1-\tilde{x}_3)}\bigg)\mathcal{C}_2^{-,s}(\mu_h)\Bigg],$$

$$H^{-}_{6,\overline{hc},4}(\{\underline{\tilde{x}},\underline{\tilde{y}}\},\mu_h) = \frac{\pi\alpha_h}{2}\Bigg[\frac{1}{\tilde{y}_1\tilde{x}_2(\tilde{x}_2+\tilde{x}_3)}\,\mathcal{C}_2^{-,u}(\mu_h) + \frac{1}{\tilde{x}_1(\tilde{y}_2+\tilde{x}_1\tilde{y}_1)}\,\mathcal{C}_2^{-,s}(\mu_h)\Bigg],$$

$$
\begin{aligned}
H^{-}_{6,\overline{hc},5}(\{\underline{\tilde{x}},\underline{\tilde{y}}\},\mu_h) &= -\frac{\pi\alpha_h}{2N_c}\bigg[\frac{\tilde{x}_1-\tilde{x}_3}{\tilde{y}_1\tilde{x}_2(\tilde{x}_2+\tilde{x}_3)(1-\tilde{x}_3)}\,\mathcal{C}_1^{-,u}(\mu_h)\\
&\qquad + \frac{1}{\tilde{x}_1}\bigg(\frac{1}{\tilde{y}_2+\tilde{x}_1\tilde{y}_1}+\frac{1}{\tilde{y}_2(1-\tilde{x}_3)}\bigg)\mathcal{C}_1^{-,s}(\mu_h)\bigg]\,,\\
H^{-}_{6,\overline{hc},6}(\{\underline{\tilde{x}},\underline{\tilde{y}}\},\mu_h) &= \frac{\pi\alpha_h}{2}\bigg[-\frac{1}{N_c}\,\frac{\tilde{x}_1-\tilde{x}_3}{\tilde{y}_1\tilde{x}_2(\tilde{x}_2+\tilde{x}_3)(1-\tilde{x}_3)}\,\mathcal{C}_2^{-,u}(\mu_h)\\
&\qquad + \frac{1}{\tilde{x}_1(\tilde{y}_2+\tilde{x}_1\tilde{y}_1)}\,\mathcal{C}_1^{-,s}(\mu_h)\bigg]\,,
\end{aligned}
\tag{A.9.3}
$$

and

$$
\begin{aligned}
H^{+}_{6,\overline{hc},1}(\{\underline{\tilde{x}},\underline{\tilde{y}}\},\mu_h) &= \frac{\pi\alpha_h}{2}\bigg[-\frac{1}{\tilde{y}_1\tilde{x}_2(1-\tilde{x}_3)}\,\mathcal{C}_1^{+,u}(\mu_h)+\frac{1}{\tilde{x}_1\tilde{y}_2(1-\tilde{x}_3)}\,\mathcal{C}_1^{+,s}(\mu_h)\bigg]\,,\\
H^{+}_{6,\overline{hc},2}(\{\underline{\tilde{x}},\underline{\tilde{y}}\},\mu_h) &= \frac{\pi\alpha_h}{2}\bigg[\frac{1}{\tilde{x}_2}\bigg(\frac{1}{\tilde{y}_1+\tilde{x}_2\tilde{y}_2}-\frac{1}{\tilde{y}_1(1-\tilde{x}_3)}\bigg)\mathcal{C}_2^{+,u}(\mu_h)\\
&\qquad + \frac{1+\tilde{x}_1}{\tilde{x}_1\tilde{y}_2(\tilde{x}_1+\tilde{x}_3)(1-\tilde{x}_3)}\,\mathcal{C}_2^{+,s}(\mu_h)\bigg]\,,\\
H^{+}_{6,\overline{hc},3}(\{\underline{\tilde{x}},\underline{\tilde{y}}\},\mu_h) &= \frac{\pi\alpha_h}{2}\bigg[\frac{1}{\tilde{x}_2(\tilde{y}_1+\tilde{x}_2\tilde{y}_2)}\,\mathcal{C}_1^{+,u}(\mu_h)\\
&\qquad - \frac{1}{N_c}\,\frac{1+\tilde{x}_1}{\tilde{x}_1\tilde{y}_2(\tilde{x}_1+\tilde{x}_3)(1-\tilde{x}_3)}\,\mathcal{C}_2^{+,s}(\mu_h)\bigg]\,,\\
H^{+}_{6,\overline{hc},4}(\{\underline{\tilde{x}},\underline{\tilde{y}}\},\mu_h) &= 0\,,\\
H^{+}_{6,\overline{hc},5}(\{\underline{\tilde{x}},\underline{\tilde{y}}\},\mu_h) &= -\frac{\pi\alpha_h}{2N_c}\bigg[\frac{1}{\tilde{x}_2}\bigg(\frac{1}{\tilde{y}_1+\tilde{x}_2\tilde{y}_2}-\frac{1}{\tilde{y}_1(1-\tilde{x}_3)}\bigg)\mathcal{C}_1^{+,u}(\mu_h)\\
&\qquad + \frac{1+\tilde{x}_1}{\tilde{x}_1\tilde{y}_2(\tilde{x}_1+\tilde{x}_3)(1-\tilde{x}_3)}\,\mathcal{C}_1^{+,s}(\mu_h)\bigg]\,,\\
H^{+}_{6,\overline{hc},6}(\{\underline{\tilde{x}},\underline{\tilde{y}}\},\mu_h) &= \frac{\pi\alpha_h}{2}\bigg[-\frac{1}{N_c}\,\frac{1}{\tilde{x}_2}\bigg(\frac{1}{\tilde{y}_1+\tilde{x}_2\tilde{y}_2}-\frac{1}{\tilde{y}_1(1-\tilde{x}_3)}\bigg)\mathcal{C}_2^{+,u}(\mu_h)\\
&\qquad + \frac{1}{\tilde{x}_1\tilde{y}_2(\tilde{x}_1+\tilde{x}_3)}\,\mathcal{C}_1^{+,s}(\mu_h)\bigg]\,.
\end{aligned}
\tag{A.9.4}
$$

As a cross check, we note that

$$
\lim_{\tilde{x}_3,\tilde{y}_3\to 0} H^{\pm}_{6,hc,r} = H^{\pm}_{6,s\bar{n},r}\,, \qquad \lim_{\tilde{x}_3,\tilde{y}_3\to 0} H^{\pm}_{6,\overline{hc},r} = H^{\pm}_{6,sn,r}\,. \tag{A.9.5}
$$

A.10 Jet Functions

In general, for a given SCET-2 operator $\mathcal{O}_m$ several SCET-1 operator O_n contribute to the matching. The jet functions $J_{m,n}$ and $\bar{J}_{m,n}$ in (13.34) can be considered as vectors in the space of SCET-1 operators. In the following, we give the expressions obtained by tree-level matching.

Six-Quark Operators

For the six-quark SCET-2 operators $\mathcal{O}^{\pm}_{6,\bar{n}}$ and $\mathcal{O}^{\pm}_{6,n}$ only the six-quark SCET-1 operators contribute to the matching. Taking the factors from the color singlet projection (13.8) into account, we find for the jet functions

$$\begin{aligned} J^{\pm}_{6,\bar{n}}(\{\underline{\tilde{y}},\underline{y}\},\mu_j) = J^{\pm}_{6,n}(\{\underline{\tilde{y}},\underline{y}\},\mu_j) = \delta(y_1-\tilde{y}_1)\,\delta(y_2-\tilde{y}_2) \begin{pmatrix} 1 \\ \frac{1}{N_c} \\ \frac{1}{N_c^2} \\ \frac{1}{N_c} \\ \frac{1}{N_c} \\ \frac{1}{N_c^2} \end{pmatrix}, \\ \bar{J}^{\pm}_{6,\bar{n}}(\{\underline{\tilde{x}},\underline{x}\},\mu_j) = \bar{J}^{\pm}_{6,n}(\{\underline{\tilde{x}},\underline{x}\},\mu_j) = \delta(x_1-\tilde{x}_1)\,\delta(x_2-\tilde{x}_2) \begin{pmatrix} 1 \\ 1 \\ 1 \\ 1 \\ 1 \\ 1 \end{pmatrix}, \end{aligned} \tag{A.10.1}$$

where the r-th entry of the vectors gives the contribution of SCET-1 operator $O^{\pm}_{6,s\bar{n},r}$ and $O^{\pm}_{6,sn,r}$, respectively. We decided to put all color factors in the jet functions and not in the anti-jet functions. However, this is a choice and one could distribute them differently.

Eight-Quark Operators

For the eight-quark SCET-2 operators $\mathcal{O}^{s}_{8,\perp\bar{n},r}$ and $\mathcal{O}^{s}_{8,\perp n,r}$ only the four-quark SCET-1 operators with additional gluon contribute to the matching. We find for the jet functions of $\mathcal{O}^{s}_{8,\perp\bar{n},r}$

$$\begin{aligned} J^{s}_{8,\perp\bar{n},\mathrm{i}}(\{\underline{\tilde{y}},\underline{y},\underline{\omega}\},\mu_j) = -4\pi\alpha_j\,\frac{1}{\rho y_1}\,\delta(y_1-\tilde{y}_1)\,\delta(y_2-\tilde{y}_2)\Big(-\frac{1}{32}\Big) \begin{pmatrix} 0 \\ -\frac{C_F}{2N_c^4} \\ \frac{C_F}{2N_c^3} \\ \frac{C_F^2}{N_c^3} \end{pmatrix}, \\ J^{s}_{8,\perp\bar{n},\mathrm{ii}}(\{\underline{\tilde{y}},\underline{y},\underline{\omega}\},\mu_j) = -4\pi\alpha_j\,\frac{1}{\rho y_1}\,\delta(y_1-\tilde{y}_1)\,\delta(y_2-\tilde{y}_2)\Big(-\frac{1}{32}\Big) \begin{pmatrix} \frac{C_F}{N_c^2} \\ \frac{N_c^2+1}{2N_c^4} \\ -\frac{1}{N_c^3} \\ -\frac{C_F}{N_c^3} \end{pmatrix}, \end{aligned} \tag{A.10.2}$$

where the r-th entry shows the contribution of $O^{+,u}_{4g,\overline{hc},r}$. Again, we decided to put all color factors together with a factor $-1/32$ from simplifications in the jet and not in

the anti-jet functions. Therefore, the anti-jet functions are independent of the color structure and read

$$\bar{J}^s_{8,\perp\bar{n},r}(\{\underline{\tilde{x}},\underline{x},\underline{\omega}\},\mu_j) = -2\pi\alpha_j\,\frac{1}{\bar{\rho}(\bar{\rho}+\bar{\omega})x_2}\,\delta(x_1-\tilde{x}_1)\,\delta(x_2-\tilde{x}_2)\begin{pmatrix}1\\1\\1\\1\end{pmatrix}. \tag{A.10.3}$$

For the operators $\mathcal{O}^s_{8,\perp n,r}$, we have

$$J^s_{8,\perp n,r}(\{\underline{\tilde{y}},\underline{y},\underline{\omega}\},\mu_j) = -2\pi\alpha_j\,\frac{1}{\rho(\rho+\omega)y_1}\,\delta(y_1-\tilde{y}_1)\,\delta(y_2-\tilde{y}_2)\begin{pmatrix}1\\1\\1\\1\end{pmatrix}, \tag{A.10.4}$$

where the r-th entry shows the contribution of $O^{-,u}_{4\bar{g},hc,r}$. For symmetry reason, we put the color factors together with the factor $-1/32$ in the anti-jet functions. They are

$$\begin{aligned}
\bar{J}^s_{8,\perp n,\mathrm{i}}(\{\underline{\tilde{x}},\underline{x},\underline{\omega}\},\mu_j) &= -4\pi\alpha_j\,\frac{1}{\bar{\rho}x_2}\,\delta(x_1-\tilde{x}_1)\,\delta(x_2-\tilde{x}_2)\Big(-\frac{1}{32}\Big)\begin{pmatrix}0\\ \frac{C_F^2}{N_c^3}\\ \frac{C_F}{2N_c^3}\\ \frac{C_F}{2N_c^4}\end{pmatrix},\\
\bar{J}^s_{8,\perp n,\mathrm{ii}}(\{\underline{\tilde{x}},\underline{x},\underline{\omega}\},\mu_j) &= -4\pi\alpha_j\,\frac{1}{\bar{\rho}x_2}\,\delta(x_1-\tilde{x}_1)\,\delta(x_2-\tilde{x}_2)\Big(-\frac{1}{32}\Big)\begin{pmatrix}\frac{C_F}{N_c^2}\\ \frac{2C_F^2}{N_c^2}\\ \frac{N_c^2-2}{2N_c^3}\\ \frac{1}{2N_c^4}\end{pmatrix}.
\end{aligned} \tag{A.10.5}$$

As the four-quark SCET-1 operators contain only one (anti-)hard-collinear field, there is a canonical way to distribute color factors between jet and anti-jet functions. For the eight-quark SCET-2 operators $\mathcal{O}^s_{8,n,r}$, we choose

$$\begin{aligned}
J^s_{8,n,1}(\{\underline{\tilde{y}},\underline{y},\underline{\omega}\},\mu_j) &= \pi\alpha_j\,\frac{1}{\rho(\rho+\omega)y_1}\,\delta(y_1-\tilde{y}_1)\,\delta(y_2-\tilde{y}_2)\begin{pmatrix}-\frac{1}{2N_c^2}\\ 0\end{pmatrix},\\
J^s_{8,n,2}(\{\underline{\tilde{y}},\underline{y},\underline{\omega}\},\mu_j) &= \pi\alpha_j\,\frac{1}{\rho(\rho+\omega)y_1}\,\delta(y_1-\tilde{y}_1)\,\delta(y_2-\tilde{y}_2)\begin{pmatrix}\frac{1}{2N_c}\\ \frac{C_F}{N_c}\end{pmatrix}
\end{aligned} \tag{A.10.6}$$

and

$$\bar{J}^s_{8,n,r}(\{\underline{x},\underline{\omega}\},\mu_j) = +\frac{C_F}{N_c}\,2\pi\alpha_j\,\frac{1+x_2}{\bar{\rho}x_2^2}\begin{pmatrix}1\\1\end{pmatrix}, \tag{A.10.7}$$

where the r-th entry shows the contribution of $O^u_{4,hc,r}$. For $\mathcal{O}^s_{8,\bar{n},r}$ we have

$$J^s_{8,\bar{n},r}(\{\underline{y},\underline{\omega}\},\mu_j) = -\frac{C_F}{N_c}\,2\pi\alpha_j\,\frac{1+y_1}{\rho y_1^2}\begin{pmatrix}1\\1\end{pmatrix} \tag{A.10.8}$$

and

$$\begin{aligned}\bar{J}^s_{8,\bar{n},1}(\{\tilde{\underline{x}},\underline{x},\underline{\omega}\},\mu_j) &= \pi\alpha_j\,\frac{1}{\bar{\rho}(\bar{\rho}+\bar{\omega})x_2}\,\delta(x_1-\tilde{x}_1)\,\delta(x_2-\tilde{x}_2)\begin{pmatrix}-\frac{1}{2N_c^2}\\ +\frac{1}{2N_c}\end{pmatrix},\\ \bar{J}^s_{8,\bar{n},2}(\{\tilde{\underline{x}},\underline{x},\underline{\omega}\},\mu_j) &= \pi\alpha_j\,\frac{1}{\bar{\rho}(\bar{\rho}+\bar{\omega})x_2}\,\delta(x_1-\tilde{x}_1)\,\delta(x_2-\tilde{x}_2)\begin{pmatrix}+\frac{1}{2N_c}\\ -\frac{1}{2N_c^2}\end{pmatrix},\end{aligned} \tag{A.10.9}$$

where the r-th entry shows the contribution of $O^u_{4,\overline{hc},r}$. For eight-quark SCET-2 operators with additional derivatives $\mathcal{O}^s_{8\bar{\partial},n,r}$ and $\mathcal{O}^s_{8\partial,\bar{n},r}$, the same SCET-1 operators contribute. The associated jet functions are

$$J^s_{8\bar{\partial},n,r} = J^s_{8,n,r}\,,\qquad \bar{J}^s_{8\bar{\partial},n,r}(\{\underline{x},\underline{\omega}\},\mu_j) = +\frac{C_F}{N_c}\,\pi\alpha_j\,\frac{1}{\bar{\rho}^2\,x_1\,x_2^2}\begin{pmatrix}1\\1\end{pmatrix} \tag{A.10.10}$$

and

$$\bar{J}^s_{8\partial,\bar{n},r} = \bar{J}^s_{8,\bar{n},r}\,,\qquad J^s_{8\partial,\bar{n},r}(\{\underline{y},\underline{\omega}\},\mu_j) = -\frac{C_F}{N_c}\,\pi\alpha_j\,\frac{1}{\rho^2\,y_1^2\,y_2}\begin{pmatrix}1\\1\end{pmatrix}. \tag{A.10.11}$$

These results match the ones obtained in [123]. The jet functions for the operators with $(\bar{u}u)$ soft quark pair are obtained by replacing $u \leftrightarrow s$, $c \leftrightarrow \bar{c}$, $n \leftrightarrow \bar{n}$, $x_i \leftrightarrow y_i$, $\omega \leftrightarrow \bar{\omega}$, $\rho \leftrightarrow \bar{\rho}$, and $\partial \leftrightarrow \bar{\partial}$ in the above expressions.

Eight-Quark Operators with an Additional Gluon

The SCET-2 operators with eight quarks and additional (anti-)collinear gluon $\mathcal{O}^s_{8\bar{c},n,r}$ and $\mathcal{O}^s_{8c,\bar{n},r}$ also originate from the four-quark SCET-1 operators. Their jet functions read

$$J^s_{8\bar{c},n,r} = J^s_{8,n,r}\,, \tag{A.10.12}$$

$$\bar{J}^s_{8\bar{c},n,r}(\{\underline{x},\underline{\omega}\},\mu_j) = -\frac{\pi\alpha_j}{2}\,\frac{1}{\bar{\rho}^2\,(x_2+x_3)^2}\left[\frac{x_3}{x_2}-1+\frac{2}{N_c^2}-\frac{2C_F}{N_c}\frac{(x_2+x_3)^2}{x_2(x_1+x_3)}\right]\begin{pmatrix}1\\1\end{pmatrix}$$

and

$$\bar{J}^s_{8c,\bar{n},r} = \bar{J}^s_{8,\bar{n},r}\,, \tag{A.10.13}$$

$$J^s_{8c,\bar{n},r}(\{\underline{y},\underline{\omega}\},\mu_j) = +\frac{\pi\alpha_j}{2}\,\frac{1}{\rho^2\,(y_1+y_3)^2}\left[\frac{y_3}{y_1}-1+\frac{2}{N_c^2}-\frac{2C_F}{N_c}\frac{(y_1+y_3)^2}{y_1(y_2+y_3)}\right]\begin{pmatrix}1\\1\end{pmatrix}.$$

The last type of SCET-2 operators that originate from the four-quark SCET-1 operators are the ones with additional soft gluon. The jet functions of $\mathcal{O}^s_{8s,n,r}$ and $\mathcal{O}^s_{8s,\bar{n},r}$ read

$$\begin{aligned}J^s_{8s,n,r} &= J^s_{8,n,r}\,,\\ \bar{J}^s_{8s,n,r}(\{\underline{x},\underline{\omega}\},\mu_j) &= -\frac{\pi\alpha_j}{2}\,\frac{1}{(\bar{\rho}+\bar{\sigma})^2x_2^2}\left[\left(1-\frac{2C_F}{N_c}\,x_2\right)\frac{\bar{\sigma}}{\bar{\rho}}+\frac{1}{N_c^2}\right]\begin{pmatrix}1\\1\end{pmatrix}\end{aligned} \tag{A.10.14}$$

and

$$\bar{J}^s_{8s,\bar{n},r} = \bar{J}^s_{8,\bar{n},r}\,,$$
$$J^s_{8s,\bar{n},r}(\{\underline{y},\underline{\omega}\},\mu_j) = -\frac{\pi\alpha_j}{2}\,\frac{1}{(\rho+\sigma)^2\,y_1^2}\left[\left(1-\frac{2C_F}{N_c}\,y_1\right)\frac{\sigma}{\rho}+\frac{1}{N_c^2}\right]\begin{pmatrix}1\\1\end{pmatrix}, \tag{A.10.15}$$

respectively. These results again match the ones obtain in [123]. The jet functions for the operators with $(\bar{u}u)$ soft quark pair are obtained by replacing $u \leftrightarrow s$, $c \leftrightarrow \bar{c}$, $n \leftrightarrow \bar{n}$, $x_i \leftrightarrow y_i$, $\omega \leftrightarrow \bar{\omega}$, $\rho \leftrightarrow \bar{\rho}$, and $\sigma \leftrightarrow \bar{\sigma}$ in the above expressions.

Epilogue

Chapter 17

Precision is Key

In the absence of any direct hints to new physics, it has become clear that precision may be the key to discovery. This thesis advances the understanding of non-global jet observables at hadron colliders and weak annihilation B-meson decay amplitudes, leading to more precise theoretical predictions.

In Part I, we derived a factorization theorem for non-global observables at hadron colliders and used it to resum the leading double-logarithmic corrections, the super-leading logarithms (SLLs), appearing in the perturbative expansion of $2 \to M$ jet cross sections. Furthermore, we extended our analysis to include a first class of subleading logarithmic corrections arising from multiple Glauber-gluon exchanges. A detailed conclusion can be found in Chapter 10.

As the theoretical uncertainties of jet observables are the limiting factor in collider experiments, it is of major importance to reduce them by improving our understanding of (subleading) logarithmic corrections. However, including multiple Glauber-gluon exchanges is only a first step in achieving single-logarithmic accuracy for non-global observables at hadron colliders. One needs to allow for multiple soft emissions, i.e. insertions of $\overline{\mathbf{\Gamma}}$, as well and also has to consider the purely collinear part $\mathbf{\Gamma}_i^C$ of the anomalous dimension. As a next step, it would be worthwhile to study a second soft emission as this will produce the first true non-global logarithm (NGL). The methods developed in this thesis (exponentiating double logarithms, constructing color bases) provide a good tool for analyzing this case. Studying the interplay of SLLs and NGLs could reveal interesting new features of non-global observables and will reduce the perturbative uncertainties.

In Part II, we established a subleading power factorization theorem for exclusive non-leptonic B-meson decay amplitudes. By performing a systematic two-step matching of the weak effective Hamiltonian to the relevant effective theory, SCET-2, we discovered several so far unknown eight-quark operators (with additional gluon). We were able to demonstrate the cancellation of endpoint divergences between six-quark and "form-factor-type" contributions. An overview of our results can be found in Chapter 16.

Studying the new soft functions arising from the eight-quark operators in more detail will be a crucial next step to include subleading power corrections to theoretical predictions for non-leptonic two-body B-meson decay rates. Since the soft physics they describe is non-perturbative, one method to study them is to determine their renormalization group evolution, which can be calculated in perturbation theory. Including subleading power effects to decay rates is important to enhance the accuracy of theoretical predictions and allows one to distinguish new physics from Standard Model contributions.

In conclusion, this work contributes to the ongoing effort of applying SCET to high-energy collider physics and B-meson decay processes, highlighting the critical role of factorization in improving the theoretical understanding of precision observables, which is essential for the advancement of particle physics.

Bibliography

[1] T. Becher, M. Neubert, D.Y. Shao and M. Stillger, *Factorization of non-global LHC observables and resummation of super-leading logarithms*, *JHEP* **12** (2023) 116 [2307.06359].

[2] P. Böer, M. Neubert and M. Stillger, *Glauber phases in non-global LHC observables: resummation for quark-initiated processes*, *JHEP* **10** (2023) 075 [2307.11089].

[3] P. Böer, P. Hager, M. Neubert, M. Stillger and X. Xu, *Glauber phases in non-global LHC observables: resummation for gluon-initiated processes*, *JHEP* **02** (2024) 109 [2311.18811].

[4] P. Böer, P. Hager, M. Neubert, M. Stillger and X. Xu, *Renormalization-group improved resummation of super-leading logarithms*, *JHEP* **08** (2024) 035 [2405.05305].

[5] P. Böer, P. Hager, M. Neubert, M. Stillger and X. Xu, *Resummation of Glauber phases in non-global LHC observables for large N_c*, *JHEP* **08** (2024) 036 [2407.01691].

[6] P. Böer, M. Neubert and M. Stillger, *in preparation*, .

[7] M. Beneke and V.A. Smirnov, *Asymptotic expansion of Feynman integrals near threshold*, *Nucl. Phys. B* **522** (1998) 321 [hep-ph/9711391].

[8] Y. Ma, *Identifying regions in wide-angle scattering via graph-theoretical approaches*, 2312.14012.

[9] T. Becher, A. Broggio and A. Ferroglia, *Introduction to Soft-Collinear Effective Theory*, vol. 896, Springer (2015), 10.1007/978-3-319-14848-9, [1410.1892].

[10] I.Z. Rothstein and I.W. Stewart, *An Effective Field Theory for Forward Scattering and Factorization Violation*, *JHEP* **08** (2016) 025 [1601.04695].

[11] M. Beneke and T. Feldmann, *Factorization of heavy to light form-factors in soft collinear effective theory*, *Nucl. Phys. B* **685** (2004) 249 [hep-ph/0311335].

[12] C.W. Bauer, S. Fleming, D. Pirjol and I.W. Stewart, *An Effective field theory for collinear and soft gluons: Heavy to light decays*, *Phys. Rev. D* **63** (2001) 114020 [hep-ph/0011336].

[13] C.W. Bauer, D. Pirjol and I.W. Stewart, *Soft collinear factorization in effective field theory*, *Phys. Rev. D* **65** (2002) 054022 [hep-ph/0109045].

[14] M. Beneke, A.P. Chapovsky, M. Diehl and T. Feldmann, *Soft collinear effective theory and heavy to light currents beyond leading power*, *Nucl. Phys. B* **643** (2002) 431 [hep-ph/0206152].

[15] M. Beneke and T. Feldmann, *Multipole expanded soft collinear effective theory with non-abelian gauge symmetry*, *Phys. Lett. B* **553** (2003) 267 [hep-ph/0211358].

[16] T. Becher, M. Neubert and G. Xu, *Dynamical Threshold Enhancement and Resummation in Drell-Yan Production*, *JHEP* **07** (2008) 030 [0710.0680].

[17] P. Böer and P. Hager, *On the gauge-invariance of SCET beyond leading power*, *JHEP* **08** (2023) 197 [2306.12412].

[18] M. Beneke, P. Hager and R. Szafron, *Soft-collinear gravity beyond the leading power*, *JHEP* **03** (2022) 080 [2112.04983].

[19] A.V. Manohar, T. Mehen, D. Pirjol and I.W. Stewart, *Reparameterization invariance for collinear operators*, *Phys. Lett. B* **539** (2002) 59 [hep-ph/0204229].

[20] R.J. Hill and M. Neubert, *Spectator interactions in soft collinear effective theory*, *Nucl. Phys. B* **657** (2003) 229 [hep-ph/0211018].

[21] J. Chay and C. Kim, *Nonleptonic B decays into two light mesons in soft collinear effective theory*, *Nucl. Phys. B* **680** (2004) 302 [hep-ph/0301262].

[22] C.W. Bauer, D. Pirjol, I.Z. Rothstein and I.W. Stewart, $B \to M_1 M_2$*: Factorization, charming penguins, strong phases, and polarization*, *Phys. Rev. D* **70** (2004) 054015 [hep-ph/0401188].

[23] R.J. Hill, T. Becher, S.J. Lee and M. Neubert, *Sudakov resummation for subleading SCET currents and heavy-to-light form-factors*, *JHEP* **07** (2004) 081 [hep-ph/0404217].

[24] T. Becher, R.J. Hill and M. Neubert, *Factorization in* $B \to V\gamma$ *decays*, *Phys. Rev. D* **72** (2005) 094017 [hep-ph/0503263].

[25] M. Beneke, P. Böer, J.-N. Toelstede and K.K. Vos, *QED factorization of non-leptonic B decays*, *JHEP* **11** (2020) 081 [2008.10615].

[26] M. Beneke, M. Garny, R. Szafron and J. Wang, *Anomalous dimension of subleading-power N-jet operators*, *JHEP* **03** (2018) 001 [1712.04416].

[27] H. Georgi, *An Effective Field Theory for Heavy Quarks at Low-energies*, *Phys. Lett. B* **240** (1990) 447.

[28] M. Neubert, *Heavy quark symmetry*, *Phys. Rept.* **245** (1994) 259 [hep-ph/9306320].

[29] N. Isgur and M.B. Wise, *Weak Decays of Heavy Mesons in the Static Quark Approximation*, *Phys. Lett. B* **232** (1989) 113.

[30] N. Isgur and M.B. Wise, *WEAK TRANSITION FORM-FACTORS BETWEEN HEAVY MESONS*, *Phys. Lett. B* **237** (1990) 527.

[31] E. Eichten and B.R. Hill, *Static effective field theory: $1/m$ corrections*, *Phys. Lett. B* **243** (1990) 427.

[32] A.F. Falk, M. Neubert and M.E. Luke, *The Residual mass term in the heavy quark effective theory*, *Nucl. Phys. B* **388** (1992) 363 [hep-ph/9204229].

[33] M. Beneke, A. Broggio, S. Jaskiewicz and L. Vernazza, *Threshold factorization of the Drell-Yan process at next-to-leading power*, *JHEP* **07** (2020) 078 [1912.01585].

[34] G.F. Sterman and S. Weinberg, *Jets from Quantum Chromodynamics*, *Phys. Rev. Lett.* **39** (1977) 1436.

[35] M. Dasgupta and G.P. Salam, *Resummation of nonglobal QCD observables*, *Phys. Lett. B* **512** (2001) 323 [hep-ph/0104277].

[36] A. Banfi, G. Marchesini and G. Smye, *Away from jet energy flow*, *JHEP* **08** (2002) 006 [hep-ph/0206076].

[37] J. Jalilian-Marian, A. Kovner, A. Leonidov and H. Weigert, *The BFKL equation from the Wilson renormalization group*, *Nucl. Phys. B* **504** (1997) 415 [hep-ph/9701284].

[38] H. Weigert, *Unitarity at small Bjorken x*, *Nucl. Phys. A* **703** (2002) 823 [hep-ph/0004044].

[39] E. Ferreiro, E. Iancu, A. Leonidov and L. McLerran, *Nonlinear gluon evolution in the color glass condensate. 2.*, *Nucl. Phys. A* **703** (2002) 489 [hep-ph/0109115].

[40] I. Balitsky, *Operator expansion for high-energy scattering*, *Nucl. Phys. B* **463** (1996) 99 [hep-ph/9509348].

[41] Y.V. Kovchegov, *Unitarization of the BFKL pomeron on a nucleus*, *Phys. Rev. D* **61** (2000) 074018 [hep-ph/9905214].

[42] H. Weigert, *Non-global jet evolution at finite N_c*, *Nucl. Phys. B* **685** (2004) 321 [hep-ph/0312050].

[43] Y. Hatta and T. Ueda, *Resummation of non-global logarithms at finite N_c*, *Nucl. Phys. B* **874** (2013) 808 [1304.6930].

[44] Y. Hagiwara, Y. Hatta and T. Ueda, *Hemisphere jet mass distribution at finite N_c*, *Phys. Lett. B* **756** (2016) 254 [1507.07641].

[45] Y. Hatta and T. Ueda, *Non-global logarithms in hadron collisions at $N_c = 3$*, *Nucl. Phys. B* **962** (2021) 115273 [2011.04154].

[46] M. De Angelis, J.R. Forshaw and S. Plätzer, *Resummation and Simulation of Soft Gluon Effects beyond Leading Color*, *Phys. Rev. Lett.* **126** (2021) 112001 [2007.09648].

[47] S. Plätzer, *Summing Large-N Towers in Colour Flow Evolution*, *Eur. Phys. J. C* **74** (2014) 2907 [1312.2448].

[48] Z. Nagy and D.E. Soper, *Effects of subleading color in a parton shower*, *JHEP* **07** (2015) 119 [1501.00778].

[49] R. Ángeles Martínez, M. De Angelis, J.R. Forshaw, S. Plätzer and M.H. Seymour, *Soft gluon evolution and non-global logarithms*, *JHEP* **05** (2018) 044 [1802.08531].

[50] Z. Nagy and D.E. Soper, *Parton showers with more exact color evolution*, *Phys. Rev. D* **99** (2019) 054009 [1902.02105].

[51] Z. Nagy and D.E. Soper, *Effect of color on rapidity gap survival*, *Phys. Rev. D* **100** (2019) 074012 [1905.07176].

[52] J.R. Forshaw, J. Holguin and S. Plätzer, *Parton branching at amplitude level*, *JHEP* **08** (2019) 145 [1905.08686].

[53] Z. Nagy and D.E. Soper, *Exponentiating virtual imaginary contributions in a parton shower*, *Phys. Rev. D* **100** (2019) 074005 [1908.11420].

[54] S. Höche and D. Reichelt, *Numerical resummation at subleading color in the strongly ordered soft gluon limit*, *Phys. Rev. D* **104** (2021) 034006 [2001.11492].

[55] J.R. Forshaw, J. Holguin and S. Plätzer, *Building a consistent parton shower*, *JHEP* **09** (2020) 014 [2003.06400].

[56] K. Hamilton, R. Medves, G.P. Salam, L. Scyboz and G. Soyez, *Colour and logarithmic accuracy in final-state parton showers*, *JHEP* **03** (2021) 041 [2011.10054].

[57] M. Balsiger, T. Becher and D.Y. Shao, *NLL′ resummation of jet mass*, *JHEP* **04** (2019) 020 [1901.09038].

[58] A. Banfi, F.A. Dreyer and P.F. Monni, *Next-to-leading non-global logarithms in QCD*, *JHEP* **10** (2021) 006 [2104.06416].

[59] A. Banfi, F.A. Dreyer and P.F. Monni, *Higher-order non-global logarithms from jet calculus*, *JHEP* **03** (2022) 135 [2111.02413].

[60] T. Becher, N. Schalch and X. Xu, *Resummation of Next-to-Leading Nonglobal Logarithms at the LHC*, *Phys. Rev. Lett.* **132** (2024) 081602 [2307.02283].

[61] S. Ferrario Ravasio, K. Hamilton, A. Karlberg, G.P. Salam, L. Scyboz and G. Soyez, *Parton Showering with Higher Logarithmic Accuracy for Soft Emissions*, *Phys. Rev. Lett.* **131** (2023) 161906 [2307.11142].

[62] M. van Beekveld, S. Ferrario Ravasio, G.P. Salam, A. Soto-Ontoso, G. Soyez and R. Verheyen, *PanScales parton showers for hadron collisions: formulation and fixed-order studies*, *JHEP* **11** (2022) 019 [2205.02237].

[63] S. Catani, D. de Florian and G. Rodrigo, *Space-like (versus time-like) collinear limits in QCD: Is factorization violated?*, *JHEP* **07** (2012) 026 [1112.4405].

[64] J.R. Forshaw, M.H. Seymour and A. Siodmok, *On the Breaking of Collinear Factorization in QCD*, *JHEP* **11** (2012) 066 [1206.6363].

[65] M.D. Schwartz, K. Yan and H.X. Zhu, *Collinear factorization violation and effective field theory*, *Phys. Rev. D* **96** (2017) 056005 [1703.08572].

[66] J.R. Forshaw, A. Kyrieleis and M.H. Seymour, *Super-leading logarithms in non-global observables in QCD*, *JHEP* **08** (2006) 059 [hep-ph/0604094].

[67] J.R. Forshaw, A. Kyrieleis and M.H. Seymour, *Super-leading logarithms in non-global observables in QCD: Colour basis independent calculation*, *JHEP* **09** (2008) 128 [0808.1269].

[68] J. Keates and M.H. Seymour, *Super-leading logarithms in non-global observables in QCD: Fixed order calculation*, *JHEP* **04** (2009) 040 [0902.0477].

[69] J. Forshaw, J. Keates and S. Marzani, *Jet vetoing at the LHC*, *JHEP* **07** (2009) 023 [0905.1350].

[70] T. Becher, M. Neubert, L. Rothen and D.Y. Shao, *Effective Field Theory for Jet Processes*, *Phys. Rev. Lett.* **116** (2016) 192001 [1508.06645].

[71] T. Becher, M. Neubert, L. Rothen and D.Y. Shao, *Factorization and Resummation for Jet Processes*, *JHEP* **11** (2016) 019 [1605.02737].

[72] T. Becher and J. Haag, *Factorization and resummation for sequential recombination jet cross sections*, *JHEP* **01** (2024) 155 [2309.17355].

[73] T. Becher, M. Neubert and D.Y. Shao, *Resummation of Super-Leading Logarithms*, *Phys. Rev. Lett.* **127** (2021) 212002 [2107.01212].

[74] M. Balsiger, T. Becher and D.Y. Shao, *Non-global logarithms in jet and isolation cone cross sections*, *JHEP* **08** (2018) 104 [1803.07045].

[75] C.W. Bauer and M.D. Schwartz, *Improving jet distributions with effective field theory*, *Phys. Rev. Lett.* **97** (2006) 142001 [hep-ph/0604065].

[76] C.W. Bauer and M.D. Schwartz, *Event Generation from Effective Field Theory*, *Phys. Rev. D* **76** (2007) 074004 [hep-ph/0607296].

[77] M. Beneke, M. Garny, R. Szafron and J. Wang, *Anomalous dimension of subleading-power N-jet operators. Part II*, *JHEP* **11** (2018) 112 [1808.04742].

[78] S. Catani and M.H. Seymour, *The Dipole formalism for the calculation of QCD jet cross-sections at next-to-leading order*, *Phys. Lett. B* **378** (1996) 287 [hep-ph/9602277].

[79] S. Catani and M.H. Seymour, *A General algorithm for calculating jet cross-sections in NLO QCD*, *Nucl. Phys. B* **485** (1997) 291 [hep-ph/9605323].

[80] J.R. Forshaw and J. Holguin, *Coulomb gluons will generally destroy coherence*, *JHEP* **12** (2021) 084 [2109.03665].

[81] T. Becher and M. Neubert, *On the Structure of Infrared Singularities of Gauge-Theory Amplitudes*, *JHEP* **06** (2009) 081 [0903.1126].

[82] ATLAS collaboration, *Measurement of dijet production with a veto on additional central jet activity in pp collisions at $\sqrt{s} = 7$ TeV using the ATLAS detector*, *JHEP* **09** (2011) 053 [1107.1641].

[83] ATLAS collaboration, *Measurements of jet vetoes and azimuthal decorrelations in dijet events produced in pp collisions at $\sqrt{s} = 7$ TeV using the ATLAS detector*, *Eur. Phys. J. C* **74** (2014) 3117 [1407.5756].

[84] J.C. Collins, D.E. Soper and G.F. Sterman, *All Order Factorization for Drell-Yan Cross-sections*, *Phys. Lett. B* **134** (1984) 263.

[85] J.C. Collins, D.E. Soper and G.F. Sterman, *Soft Gluons and Factorization*, *Nucl. Phys. B* **308** (1988) 833.

[86] J.C. Collins, D.E. Soper and G.F. Sterman, *Factorization of Hard Processes in QCD*, *Adv. Ser. Direct. High Energy Phys.* **5** (1989) 1 [hep-ph/0409313].

[87] T. Becher, P. Hager, S. Jaskiewicz, M. Neubert and D. Schwienbacher, *Factorization restoration through Glauber gluons*, 2408.10308.

[88] C.W. Bauer, B.O. Lange and G. Ovanesyan, *On Glauber modes in Soft-Collinear Effective Theory*, *JHEP* **07** (2011) 077 [1010.1027].

[89] J.R. Gaunt, *Glauber Gluons and Multiple Parton Interactions*, *JHEP* **07** (2014) 110 [1405.2080].

[90] M. Zeng, *Drell-Yan process with jet vetoes: breaking of generalized factorization*, *JHEP* **10** (2015) 189 [1507.01652].

[91] P. Bijl, S. Niedenzu and W.J. Waalewijn, *Probing factorization violation with vector angularities*, *Phys. Rev. D* **109** (2024) 014011 [2307.02521].

[92] T. Becher and M. Neubert, *Drell-Yan Production at Small q_T, Transverse Parton Distributions and the Collinear Anomaly*, *Eur. Phys. J. C* **71** (2011) 1665 [1007.4005].

[93] J.-Y. Chiu, A. Jain, D. Neill and I.Z. Rothstein, *A Formalism for the Systematic Treatment of Rapidity Logarithms in Quantum Field Theory*, *JHEP* **05** (2012) 084 [1202.0814].

[94] T. Becher and M. Neubert, *Infrared singularities of scattering amplitudes in perturbative QCD*, *Phys. Rev. Lett.* **102** (2009) 162001 [0901.0722].

[95] E. Gardi and L. Magnea, *Factorization constraints for soft anomalous dimensions in QCD scattering amplitudes*, *JHEP* **03** (2009) 079 [0901.1091].

[96] L.J. Dixon, E. Gardi and L. Magnea, *On soft singularities at three loops and beyond*, *JHEP* **02** (2010) 081 [0910.3653].

[97] V. Ahrens, M. Neubert and L. Vernazza, *Structure of Infrared Singularities of Gauge-Theory Amplitudes at Three and Four Loops*, *JHEP* **09** (2012) 138 [1208.4847].

[98] T. Becher and M. Neubert, *Infrared singularities of scattering amplitudes and N^3LL resummation for n-jet processes*, *JHEP* **01** (2020) 025 [1908.11379].

[99] S. Catani and M. Grazzini, *The soft gluon current at one loop order*, *Nucl. Phys. B* **591** (2000) 435 [hep-ph/0007142].

[100] C. Duhr and T. Gehrmann, *The two-loop soft current in dimensional regularization*, *Phys. Lett. B* **727** (2013) 452 [1309.4393].

[101] L.J. Dixon, E. Herrmann, K. Yan and H.X. Zhu, *Soft gluon emission at two loops in full color*, *JHEP* **05** (2020) 135 [1912.09370].

[102] T. Becher, T. Rauh and X. Xu, *Two-loop anomalous dimension for the resummation of non-global observables*, *JHEP* **08** (2022) 134 [2112.02108].

[103] S. Catani, D. de Florian and G. Rodrigo, *The Triple collinear limit of one loop QCD amplitudes*, *Phys. Lett. B* **586** (2004) 323 [hep-ph/0312067].

[104] S. Catani and M. Grazzini, *Infrared factorization of tree level QCD amplitudes at the next-to-next-to-leading order and beyond*, *Nucl. Phys. B* **570** (2000) 287 [hep-ph/9908523].

[105] G. Altarelli and G. Parisi, *Asymptotic Freedom in Parton Language*, *Nucl. Phys. B* **126** (1977) 298.

[106] V.N. Gribov and L.N. Lipatov, *Deep inelastic e p scattering in perturbation theory*, *Sov. J. Nucl. Phys.* **15** (1972) 438.

[107] Y.L. Dokshitzer, *Calculation of the Structure Functions for Deep Inelastic Scattering and e+ e- Annihilation by Perturbation Theory in Quantum Chromodynamics.*, *Sov. Phys. JETP* **46** (1977) 641.

[108] H.E. Haber, *Useful relations among the generators in the defining and adjoint representations of SU(N)*, *SciPost Phys. Lect. Notes* **21** (2021) 1 [1912.13302].

[109] M. Neubert, *Renormalization-group improved calculation of the $B \to X_s\gamma$ branching ratio*, *Eur. Phys. J. C* **40** (2005) 165 [hep-ph/0408179].

[110] K.G. Chetyrkin, J.H. Kuhn and M. Steinhauser, *RunDec: A Mathematica package for running and decoupling of the strong coupling and quark masses*, *Comput. Phys. Commun.* **133** (2000) 43 [hep-ph/0004189].

[111] R. Kelley and M.D. Schwartz, *1-loop matching and NNLL resummation for all partonic 2 to 2 processes in QCD*, *Phys. Rev. D* **83** (2011) 045022 [1008.2759].

[112] A. Broggio, A. Ferroglia, B.D. Pecjak and Z. Zhang, *NNLO hard functions in massless QCD*, *JHEP* **12** (2014) 005 [1409.5294].

[113] M. Sjödahl, *ColorMath - A package for color summed calculations in SU(N_c)*, *Eur. Phys. J. C* **73** (2013) 2310 [1211.2099].

[114] I.A. Korchemskaya and G.P. Korchemsky, *On lightlike Wilson loops*, *Phys. Lett. B* **287** (1992) 169.

[115] G. Buchalla, A.J. Buras and M.E. Lautenbacher, *Weak decays beyond leading logarithms*, *Rev. Mod. Phys.* **68** (1996) 1125 [hep-ph/9512380].

[116] M. Beneke, G. Buchalla, M. Neubert and C.T. Sachrajda, *QCD factorization in $B \to \pi K, \pi\pi$ decays and extraction of Wolfenstein parameters*, *Nucl. Phys. B* **606** (2001) 245 [hep-ph/0104110].

[117] M. Beneke, G. Buchalla, M. Neubert and C.T. Sachrajda, *QCD factorization for $B \to \pi\pi$ decays: Strong phases and CP violation in the heavy quark limit*, *Phys. Rev. Lett.* **83** (1999) 1914 [hep-ph/9905312].

[118] M. Beneke, G. Buchalla, M. Neubert and C.T. Sachrajda, *QCD factorization for exclusive, nonleptonic B meson decays: General arguments and the case of heavy light final states*, *Nucl. Phys. B* **591** (2000) 313 [hep-ph/0006124].

[119] M. Beneke and M. Neubert, *Flavor singlet B decay amplitudes in QCD factorization*, *Nucl. Phys. B* **651** (2003) 225 [hep-ph/0210085].

[120] M. Beneke and M. Neubert, *QCD factorization for $B \to PP$ and $B \to PV$ decays*, *Nucl. Phys. B* **675** (2003) 333 [hep-ph/0308039].

[121] E. Lunghi, D. Pirjol and D. Wyler, *Factorization in leptonic radiative $B \to \gamma e \nu$ decays*, *Nucl. Phys. B* **649** (2003) 349 [hep-ph/0210091].

[122] S.W. Bosch, R.J. Hill, B.O. Lange and M. Neubert, *Factorization and Sudakov resummation in leptonic radiative B decay*, *Phys. Rev. D* **67** (2003) 094014 [hep-ph/0301123].

[123] B.O. Lange and M. Neubert, *Factorization and the soft overlap contribution to heavy to light form-factors*, *Nucl. Phys. B* **690** (2004) 249 [hep-ph/0311345].

[124] T. Becher, R.J. Hill and M. Neubert, *Soft collinear messengers: A New mode in soft collinear effective theory*, *Phys. Rev. D* **69** (2004) 054017 [hep-ph/0308122].

[125] M. Beneke, *Soft-collinear factorization in B decays*, *Nucl. Part. Phys. Proc.* **261-262** (2015) 311 [1501.07374].

[126] M. Beneke, G. Buchalla, M. Neubert and C.T. Sachrajda, *Comment on "$B \to M_1 M_2$: Factorization, charming penguins, strong phases, and polarization"*, *Phys. Rev. D* **72** (2005) 098501 [hep-ph/0411171].

[127] C.W. Bauer, D. Pirjol, I.Z. Rothstein and I.W. Stewart, *On differences between SCET and QCDF for $B \to \pi\pi$ decays*, *Phys. Rev. D* **72** (2005) 098502 [hep-ph/0502094].

[128] M. Beneke, G. Buchalla, M. Neubert and C.T. Sachrajda, *Penguins with Charm and Quark-Hadron Duality*, *Eur. Phys. J. C* **61** (2009) 439 [0902.4446].

[129] Y.-K. Huang, Y.-L. Shen, C. Wang and Y.-M. Wang, *Next-to-Leading-Order Weak Annihilation Correction to Rare $B \to \{K, \pi\}\,\ell^+\ell^-$ Decays*, 2403.11258.

[130] S. Alte, M. König and M. Neubert, *Effective Field Theory after a New-Physics Discovery*, *JHEP* **08** (2018) 095 [1806.01278].

[131] M. Beneke, P. Böer, J.-N. Toelstede and K.K. Vos, *Light-cone distribution amplitudes of heavy mesons with QED effects*, *JHEP* **08** (2022) 020 [2204.09091].

[132] Q. Qin, Y.-L. Shen, C. Wang and Y.-M. Wang, *Deciphering the Long-Distance Penguin Contribution to $\bar{B}_{d,s} \to \gamma\gamma$ Decays*, *Phys. Rev. Lett.* **131** (2023) 091902 [2207.02691].

[133] Y.-K. Huang, Y. Ji, Y.-L. Shen, C. Wang, Y.-M. Wang and X.-C. Zhao, *Renormalization-Group Evolution for the Bottom-Meson Soft Function*, 2312.15439.

[134] Z.L. Liu, B. Mecaj, M. Neubert, X. Wang and S. Fleming, *Renormalization and Scale Evolution of the Soft-Quark Soft Function*, *JHEP* **07** (2020) 104 [2005.03013].

[135] M. Beneke, Y. Ji and X. Wang, *Renormalization of the next-to-leading-power $\gamma\gamma \to h$ and $gg \to h$ soft quark functions*, *JHEP* **05** (2024) 246 [2403.17738].

[136] V.M. Braun, Y. Ji and A.N. Manashov, *Higher-twist B-meson Distribution Amplitudes in HQET*, *JHEP* **05** (2017) 022 [1703.02446].

[137] Z.L. Liu and M. Neubert, *Factorization at subleading power and endpoint-divergent convolutions in $h \to \gamma\gamma$ decay*, *JHEP* **04** (2020) 033 [1912.08818].

[138] Z.L. Liu, B. Mecaj, M. Neubert and X. Wang, *Factorization at subleading power and endpoint divergences in $h \to \gamma\gamma$ decay. Part II. Renormalization and scale evolution*, *JHEP* **01** (2021) 077 [2009.06779].

[139] Z.L. Liu, B. Mecaj, M. Neubert and X. Wang, *Factorization at subleading power, Sudakov resummation, and endpoint divergences in soft-collinear effective theory*, *Phys. Rev. D* **104** (2021) 014004 [2009.04456].

[140] Z.L. Liu, M. Neubert, M. Schnubel and X. Wang, *Factorization at next-to-leading power and endpoint divergences in $gg \to h$ production*, *JHEP* **06** (2023) 183 [2212.10447].

[141] M. Beneke, M. Garny, S. Jaskiewicz, J. Strohm, R. Szafron, L. Vernazza et al., *Next-to-leading power endpoint factorization and resummation for off-diagonal "gluon" thrust*, *JHEP* **07** (2022) 144 [2205.04479].

[142] G. Bell, P. Böer and T. Feldmann, *Muon-electron backward scattering: a prime example for endpoint singularities in SCET*, *JHEP* **09** (2022) 183 [2205.06021].

[143] T. Feldmann, N. Gubernari, T. Huber and N. Seitz, *Contribution of the electromagnetic dipole operator O_7 to the $\bar{B}_s \to \mu^+\mu^-$ decay amplitude*, *Phys. Rev. D* **107** (2023) 013007 [2211.04209].

[144] C. Cornella, M. König and M. Neubert, *Structure-dependent QED effects in exclusive B decays at subleading power*, *Phys. Rev. D* **108** (2023) L031502 [2212.14430].

[145] T. Hurth and R. Szafron, *Refactorisation in subleading $\bar{B} \to X_s\gamma$*, *Nucl. Phys. B* **991** (2023) 116200 [2301.01739].

[146] P. Böer, *QCD Factorisation in Exclusive Semileptonic B Decays New Applications and Resummation of Rapidity Logarithms*, Ph.D. thesis, Siegen U., 2018.

[147] P. Böer, G. Bell, T. Feldmann, D. Horstmann and V. Shtabovenko, *Soft-overlap contribution to $B_c \to \eta_c$ form factors: diagrammatic resummation of double logarithms*, *PoS* **RADCOR2023** (2024) 086 [2309.08410].

[148] C.-D. Lü, Y.-L. Shen, C. Wang and Y.-M. Wang, *Shedding new light on weak annihilation B-meson decays*, *Nucl. Phys. B* **990** (2023) 116175 [2202.08073].

[149] V.M. Braun and I.E. Filyanov, *Conformal Invariance and Pion Wave Functions of Nonleading Twist*, *Z. Phys. C* **48** (1990) 239.

[150] A.G. Grozin and M. Neubert, *Asymptotics of heavy meson form-factors*, *Phys. Rev. D* **55** (1997) 272 [hep-ph/9607366].

[151] B.O. Lange and M. Neubert, *Renormalization group evolution of the B meson light cone distribution amplitude*, *Phys. Rev. Lett.* **91** (2003) 102001 [hep-ph/0303082].

[152] E. Eichten and B.R. Hill, *An Effective Field Theory for the Calculation of Matrix Elements Involving Heavy Quarks*, *Phys. Lett. B* **234** (1990) 511.

[153] M. Beneke, G. Finauri, K.K. Vos and Y. Wei, *QCD light-cone distribution amplitudes of heavy mesons from boosted HQET*, *JHEP* **09** (2023) 066 [2305.06401].

Acknowledgments

The acknowledgments have been removed from the electronic publication of this dissertation for privacy reasons.